
# Estudio de los Fenómenos de Transporte Termo-Hidrodinámicos de No Equilibrio en Mezclas Líquidas

David Alonso de Mezquia González

Mondragon Goi Eskola Politeknikoa

Dpto. de Mecánica y Producción Industrial

Arrasate-Mondragon, 21 de diciembre de 2012


# Estudio de los Fenómenos de Transporte Termo-Hidrodinámicos de No Equilibrio en Mezclas Líquidas

David Alonso de Mezquia González

dirigida por:

Mohammed Mounir Bou-Ali Saidi
Dpto. de Mecánica y Producción Industrial, Mondragon Unibertsitatea

*para la obtención del grado de Doctor*
*bajo el programa de doctorado de la Universidad de Mondragon*
*Comportamiento Mecánico y de Materiales.*

Arrasate-Mondragon, 21 de diciembre de 2012

**Keywords:** Difusión, Termodifusión, Mezclas Multicomponente, Propiedades de Transporte

# Abstract

In this doctoral thesis, an experimental study on the transport properties on liquid mixtures has been conducted. The molecular diffusion coefficient, thermodiffusion coefficient and Soret coefficient of several mixtures have been analyzed. The molecular diffusion coefficient has been measured by the sliding symmetric tubes technique, while the thermodiffusion coefficient has been determined using the thermogravitational technique. The Soret coefficient, on the other hand, has been calculated using the data obtained with these two experimental techniques.

Different types of mixtures have been analyzed using these techniques. On the one hand, several binary mixtures, specifically mixtures of hydrocarbons, aqueous mixtures and polymer mixtures, have been studied. In the group of hydrocarbon mixtures, the thermodiffusion, molecular diffusion and Soret coefficients at 25 °C of three equimolar and equimass normal alkane series have been determined (49 binary mixtures). The analysis of the obtained data has been used to develop three correlations for the prediction of the transport properties of the binary mixtures composed by these components. The first of these expressions, is a quantitative correlation which is used for the determination of the thermodiffusion coefficient in normal alkane binary mixtures at any concentration. The second quantitative correlation developed, does the same thing but with the molecular diffusion coefficient, using the data of the molecular mass difference of the components and the dynamic viscosity of the mixture. The experimental data obtained for the Soret coefficient has been used to develop another quantitative correlation for the determination of this coefficient.

In the case of aqueous mixtures, measurements of the transport properties in water-isopropanol mixture in the whole range of concentration at 25 °C have been carried out. The experimental analysis of this mixture has also been done by other laboratories (*Service de Chimie physique E.P.* and *Microgravity Resesarch Center*, both from university of Brussels, and *Department of Physics* from university of Bayreuth), both in ground and microgravity conditions. The results obtained in this international collaboration work, can be considered as a consistent reference data for the mixtures which present a sign change in the Soret coefficient over their concentration range.

For polymer mixtures, a combination of the sliding symmetric tubes and the gravimetric techniques has been used to study the water-polyacrylamide binary system in collaboration with FAST laboratory of *Pierre et Marie Curie* university. The analysis carried out using these two techniques has allowed the determination of the molecular diffusion coefficient of the mixture throughout the concentration range of the three regimes that can be found in this mixture: concentrated, diluted and semi-diluted.

Additionally, measurements of the thermodiffusion coefficient in ternary hydrocarbon mixtures have been done. Two of these mixtures (tetrahydronaphthalene-isobutylbenzene-*n*dodecane and toluene-*n*hexane-*n*dodecane) at several concentrations and 25 °C have been analyzed. The data measured has been used to analyze and check the reliability degree of a correlation developed in a previous work. This correlation is able to predict the thermodiffusion coefficient in ternary mixtures using the data of their corresponding binary mixtures.

# Resumen

En esta tesis doctoral se ha llevado a cabo un estudio experimental sobre las propiedades de trasporte en mezclas líquidas. Se ha determinado el coeficiente de difusión molecular, coeficiente de termodifusión y coeficiente Soret en diferentes sistemas. El coeficiente de difusión molecular ha sido medido por medio de la técnica de los tubos simétricos deslizantes, mientras que el coeficiente de termodifusión se ha determinado utilizando la técnica termogravitacional. El coeficiente Soret, por otra parte, se ha calculado utilizando los datos obtenidos mediante las dos técnicas anteriores.

De este modo, se han estudiado varias mezclas binarias, concretamente mezclas de hidrocarburos, mezclas acuosas y mezclas de polímeros. En el caso de las mezclas compuestas de hidrocarburos, se han analizado tres series equimolares y equimásicas de alcanos normales (49 mezclas binarias), de las cuales se han determinado los coeficientes de termodifusión, difusión molecular y Soret a 25 °C. El análisis de los datos obtenidos ha permitido desarrollar tres correlaciones para la predicción de las propiedades de transporte en las mezclas binarias de estos compuestos. Por un lado, se ha desarrollado una correlación cuantitativa para el coeficiente de termodifusión, la cual permite la determinación de este coeficiente a cualquier concentración. También se ha desarrollado otra correlación cuantitativa la cual permite hacer lo propio para la determinación del coeficiente de difusión molecular en estas mezclas a partir de los datos de la diferencia de masa molecular y viscosidad dinámica. Por su parte, los resultados experimentales obtenidos para el coeficiente Soret en mezclas binarias de alcanos normales han permitido desarrollar otra correlación cuantitativa para la determinación de este coeficiente.

En el caso de las mezclas acuosas, se han realizado mediciones de las propiedades de transporte en la mezcla de agua-isopropanol en todo el rango de concentración a 25 °C. El análisis experimental de esta mezcla, también ha sido realizado por otros laboratorios (*Service de Chimie physique E.P.* y *Microgravity Resesarch Center*, ambos de la universidad Libre de Bruselas y *Department of Physics* de la universidad de Bayreuth), tanto en condiciones terrestres como de microgravedad. Los resultados obtenidos en este trabajo de colaboración internacional, pueden considerarse como una referencia sólida, fundamentalmente para el caso de las mezclas que presentan un cambio de signo del coeficiente Soret a lo largo del rango de concentración.

En las mezclas de polímeros, se ha analizado el sistema binario agua-poliacrilamida utilizando tanto la técnica de los tubos simétricos deslizantes como la técnica gravimétrica, en colaboración con el laboratorio FAST de la universidad *Pierre et Marie Curie*. El análisis conjunto mediante estas dos técnicas ha permitido la determinación del coeficiente de difusión molecular a lo largo del rango de concentración en los tres regímenes que presenta esta mezcla: diluido, semi-diluido y concentrado.

Adicionalmente, se han realizado medidas del coeficiente de termodifusión en mezclas ternarias de hidrocarburos. Se han estudiado dos mezclas ternarias (tetrahidronaftalina-isobutilbenceno-*n*dodecano y tolueno-*n*hexano-*n*dodecano) a diferentes concentraciones y una temperatura de 25 °C. Los resultados obtenidos han permitido analizar y comprobar el grado de fiabilidad de la correlación desarrollada en un trabajo anterior, la cual permite la predicción del coeficiente de termodifusión en mezclas ternarias a partir de los datos de las correspondientes mezclas binarias.

# Laburpena

Doktoretza-tesi honetan nahasketa likidoen garraio-ezaugarri buruzko azterketa esperimentala egin da. Sistema ezberdinetako difusio-molekular, termodifusio eta Soret koefizienteak aztertu dira. Difusio-molekular koefizientea, hodi simetriko irristakor teknikarekin neurtu da. Termodifusio koefizientea, beste aldean, teknika termograbitazioarekin neurtu da, Soret koefizientea, beste bi teknikekin lortutako datuekin kalkulatuz.

Nahasketa desberdinak ikertu izan dira teknika hauek erabiliz. Alde batean likido-nahaste bitarrak aztertu dira. Hauen artean hidrokarburoen nahasketak, ur-nahasketak eta polimeroen nahasketak aurkitzen dira. Hidrokarburoen nahasketen kasuan, hiru alkano serie ekimolar eta hiru alkano serie ekimasikoen termodifusio, difusio-molekular eta Soret koefizienteak 25 gradutara zehaztu dira (49 nahaste bitarrak). Lortutako datuak aztertuz, konposatu hauen garraio-ezaugarriak iragartzeko hiru korrelazio garatu dira. Lehenengo korrelazio kuantitatiboa, hidrokarburoen nahasketa bitarretan edozein kontzentrazioetan termodifusio koefizientea zehazteko aukera ematen du. Garatutako bigarren korrelazio kuantitatiboa gauza berdina egiten du baina difusio-molekular koefizientearekin, nahasketaren biskositate eta bere konposatuen masa molekularren diferentzien datuak erabiliz. Soret koefizientean lortutako emaitz esperimentalak, bestalde, koefiziente hau zehazteko beste korrelazio kuantitatibo bat garatzeko erabili dira.

Ur-nahasketen kasuan, ura eta isopropanolen arteko nahasketako garraio-propietateak kontzentrazio tarte osoan ikertu dira. Nahasketa hau beste laborategi batzuetan ere esperimentalki ikertu da (*Service de Chimie physique E.P.* eta *Microgravity Resesarch Center*, biak Brusela-ko unibertsitatekoak eta *Department of Physics* Bayreuth-eko unibertsitatekoa), lur eta mikrograbitate kondizioetan. Nazioarteko mailan egindako ikerketa honetan lortutako emaitzak erreferentzia bezala hartu ahal dira, Soret koefizientean zeinu aldaketa daukaten nahasketetan.

Polimero nahasketetan, ura-poliakrilamida sisteman, hodi simetriko irristakor eta grabimetriko tekniken konbinazioa erabiliz, difusio-molekular koefizientea neurtu da. Analisi hau *Pierre et Marie Curie* unibertsiteko FAST taldearekin egindako elkar lana izan da. Bi teknika hauen konbinazioa erabiliz, nahasketa honen difusio-molekular koefizienteak kontzentrazio tarte guztietan, nahasketa honek daukadan hiru erregimenetan (kontzentratua, diluitua eta semi-diluitua) neurtu dira.

Hidrokarburoen nahasketa hirutarretan ere termodifusio koefizientea neurtu da. Mota honetako bi nahasketa kontzentrazio desberdinetan 25 gradutara aztertu dira (tetrahidronaftalina-isobutilbencenoa-*n*dodekanoa eta toluenoa-*n*hexanoa-*n*dodekanoa). Lortutako emaitzak, lehen egindako beste lana baten garatutako korrelazioaren portaera aztertzeko erabili dira. Korrelazio hau, nahaste bitarren datuak erabiliz, nahasketa hirutarretako termodifusio koefizientea kalkulatzeko erabiltzen da.

## Agradecimientos

Llegados a este momento, en el cual el final de esta tesis se ve tan próximo, uno echa la vista atrás y ve, que aunque parezca mentira, han pasado ya cuatro años desde su comienzo. Han sido cuatro años muy intensos, llenos de grandes momentos, y en los que he tenido la suerte de coincidir con grandes personas. He de admitir que no todo ha sido siempre fácil, pero el gran ambiente que he encontrado siempre a mi alrededor, ha facilitado enormemente las cosas. Mi principal intención con estas líneas es intentar agradecer a todas estas personas el haberme ayudado durante estos cuatro años. Espero no olvidarme de nadie, y sé que será difícil, pero espero ser capaz de expresar en lo que sigue mi agradecimiento a todos ellos.

En primer lugar me gustaría agradecer a mi director de tesis, Mounir, por su dedicación y su interés diario durante todos estos años. Si no fuera por él, muy probablemente nada de esto hubiera sido posible. Gracias por todo Mounir.

Lo siguiente es agradecer el apoyo recibido por parte de mi familia y amigos, y en especial de mis padres. Ellos siempre han estado allí, y siempre he sabido que puedo contar con ellos, lo que sinceramente, en muchos momentos ha sido fundamental. Siempre os agradeceré vuestro apoyo incondicional y vuestra paciencia conmigo.

También me gustaría agradecer a todos los miembros del grupo de Fluidos, por su ayuda en todo momento. El buen ambiente que he encontrado siempre, así como la cercanía de todos será algo que siempre recordaré. He aprendido mucho de todos vosotros, tanto a nivel personal como profesional, y por ello os estoy agradecido. Les doy las gracias a Pedro, y en especial a Pablo, por todo lo que me han enseñado sobre las diferentes instalaciones y su manipulación. También les agradezco profundamente a las diferentes personas que han pasado por el laboratorio a lo largo de estos años, y con los que más tiempo he pasado: Alain, Andoni, Aitziber, Veci, Jon, Joanes, Izaro, Estela, Miren, Karmele, Iker, etc., ha sido un placer trabajar con todos vosotros y siempre os estaré agradecido por toda vuestra ayuda.

Me gustaría también agradecer a los catedráticos de la de la UPV, Joseba Madariaga y Carlos Santamaría por todo lo que me han ayudado, y por sus enseñanzas. Sin duda su cercanía y saber hacer han sido de gran ayuda para mí, y he aprendido mucho de ellos.

En estas líneas quiero acordarme también de todos los compañeros doctorandos. En especial de aquellos con los que he tenido más relación como Alain, Quintana, Joanes, Javi, Pablo, Haritz, Jokin, Ione, Alaitz, Nuria, Nagore... . He aprendido mucho de vosotros, y las experiencias compartidas y los momentos que hemos pasado juntos son inolvidables.

No me puedo olvidar del resto de gente de Eskola que también me ha ayudado a lo largo de este tiempo. La gente del taller, la gente del departamento de compras, del almacén, biblioteca, organización académica, seguridad, etc. Se agradece vuestra cercanía y vuestro saber hacer. Sin vuestra colaboración mucho del trabajo realizado a lo largo de esta tesis habría sido imposible.

También me gustaría agradecer a toda esa gente con la que he tenido el privilegio de comer y de compartir cafes durante estos años. Esos momentos de desconexión y de disfrute han sido fundamentales y las muchas risas, inquietudes e historias que hemos compartido han supuesto la contrapartida perfecta para esos momentos de saturación mental.

Por último me gustaría agradecer a Mondragon Goi Eskola Politeknikoa por la ayuda recibida, la cual ha hecho posible la realización de esta tesis.

# Índice general

# Nomenclatura

| | |
|---|---|
| $\alpha$ | Coeficiente de expansión térmica, $K^{-1}$ |
| $\beta$ | Coeficiente de expansión másica |
| $\delta M$ | Masa reducida |
| $\mu$ | Viscosidad dinámica, $Pa/s$ |
| $\nu$ | Viscosidad cinemática, $m^2/s$ |
| $\overline{\mu}$ | Viscosidad dinámica de las mezclas a concentración equimasica, $Pa \cdot s$ |
| $\overline{\varphi}_p$ | Concentración volumétrica de polímero |
| $\overline{c^{up/bot}}$ | Concentración másica media del componente más denso en el tubo superior/inferior en la instalación SST |
| $\rho$ | Densidad de la mezcla, $kg \cdot m^3$ |
| $\mathbf{D}_T^i$ | Coeficiente fenomenológico de termodifusión del componente $i$ en una mezcla multicomponente, $m^2/s \cdot K$ |
| $A$ | Factor de calibración, $kg/m^3 \cdot s$ |
| $B$ | Factor de calibración, $kg/m^3$ |
| $c_i^{up/bot}$ | Concentración másica inicial del componente más denso en el tubo superior/inferior en la instalación SST |
| $c_i$ | Concentración másica del componente $i$ en la mezcla |
| $D$ | Coeficiente de difusión molecular, $m^2/s$ |
| $D_i^0$ | Coeficiente de difusión propio del componente $i$, $m^2/s$ |

| | |
|---|---|
| $D^0_{Ti}$ | Valor límite del coeficiente de termodifusión del componente $i$, $\mathrm{m}^2/\mathrm{s} \cdot \mathrm{K}$ |
| $D_T$ | Coeficiente de termodifusión, $m^2/s \cdot K$ |
| $g$ | Aceleración de la gravedad, $m/s^2$ |
| $J$ | Flujo de materia, $kg/m^2 \cdot s$ |
| $k'_i$ | Coeficiente de calibración del plano correspondiente al índice de refracción |
| $k_i$ | Coeficiente de calibración del plano correspondiente a la densidad, $kg/m^3$ |
| $L$ | Longitud, $m$ |
| $L_x$ | Profundidad del gap de la columna termogravitacional, $m$ |
| $L_y$ | Anchura del gap de la columna termogravitacional, $m$ |
| $L_z$ | Altura del gap de la columna termogravitacional, $m$ |
| $m_i$ | Masa del componente $i$ en la mezcla, $kg$ |
| $M_T$ | Masa total de la mezcla, $kg$ |
| $P$ | Período de vibración, $s$ |
| $S_T$ | Coeficiente Soret, $K^{-1}$ |
| $T$ | Temperatura, °C |
| $t$ | Tiempo, $s$ |
| $x_i$ | Concentración molar del componente $i$ en la mezcla |

# Capítulo 1

# Introducción

La difusión es un fenómeno de transporte de materia que se produce tanto en sólidos, como en líquidos, como en gases. Este transporte de materia puede generarse por varias causas: un gradiente de concentración, un gradiente de temperatura y/o un gradiente de presión. Este fenómeno tiene influencia en diferentes campos, y cada día son más las aplicaciones donde se demuestra que la difusión es un fenómeno a tener en cuenta [1, 2]. De hecho, existe a día de hoy un creciente interés en esta temática, tanto a nivel experimental como analítico y numérico [3, 4].

Por ello, el objetivo general de esta tesis doctoral ha sido el análisis experimental mediante diferentes técnicas (técnica termogravitacional y técnica *sliding symmetric tubes*) para determinar los coeficientes de difusión molecular, difusión térmica y Soret, en diversas mezclas líquidas tanto binarias como ternarias. Los resultados obtenidos en este estudio, darán respuesta a la gran demanda de datos experimentales que son necesarios para el avance en el estudio y comprensión de este fenómeno.

## 1.1. Estado del arte

Un gradiente de temperatura en el seno de una mezcla líquida provoca una separación de sus componentes, efecto conocido como difusión térmica o termodifusión. Esta separación, causa a su vez un gradiente de concentración, el cual genera un flujo de materia en sentido contrario debido a la difusión molecular. La relación existente entre estos dos efectos se conoce como efecto Soret o efecto Ludwig-Soret.

Estos fenómenos de transporte de masa ya habían generado interés desde el siglo XIX, cuando C. Soret [5, 6, 7] y C. Ludwig [8] observaron, de forma independiente cómo, en disoluciones salinas bajo un gradiente de temperatura, la sal se concentraba en la zona más fría. En reconocimiento a estos esfuerzos iniciales es por lo que

actualmente se conoce a la separación que se produce en el seno de una mezcla al verse sometida a un gradiente de temperatura como efecto Soret o Ludwig-Soret. Desde entonces han sido muchos los estudios realizados sobre el efecto Soret, aunque aún a día de hoy, sigue sin ser un fenómeno completamente comprendido [2, 9, 10].

### 1.1.1. Aplicaciones del Efecto Soret

Conforme se han realizado avances en el campo industrial, se ha podido comprobar cómo el efecto Soret tiene influencia en un gran número de procesos naturales e industriales. Así por ejemplo, uno de los campos en los que se han generado un mayor número de trabajos relacionados con este fenómeno, ha sido en los hidrocarburos [11, 12, 13, 14, 15, 16, 17]. La principal razón de este interés radica en la influencia que tiene el efecto Soret en los pozos petrolíferos [18, 19, 20], siendo uno de los factores que afecta a la distribución de los componentes en estos, debido a los gradientes de temperatura generados en función de la profundidad. Conocer la distribución de los componentes en los pozos petrolíferos es fundamental para la optimización de la explotación de los mismos [21, 22].

Así mismo, y relacionado con este ámbito, se ha visto como el efecto Soret también se manifiesta en el transporte de hidrocarburos y gases condensados [23, 24]. Especialmente en las deposiciones de cera en los conductos de las refinerías y en las tuberías de transporte, obstruyéndolas e impidiendo su correcto funcionamiento. Con el fin de optimizar este proceso se hace interesante modelar el proceso de formación de la cera. Es en este punto donde el efecto Soret hace su aparición, teniendo influencia en los modelos elaborados para optimizar el transporte de hidrocarburos [24, 25].

En el caso de las explotaciones petrolíferas, y con el fin de obtener un mayor rendimiento de los pozos petrolíferos y aumentar su vida útil, se inyecta $CO_2$ en los mismos (Figura 1.1). Éste, se mezcla con el contenido del pozo mejorando sus características termodinámicas (menor viscosidad, mayor volumen, etc.), reduciendo el esfuerzo necesario para su extracción y rentabilizando su producción. Una vez extraído el crudo del pozo, se separa el $CO_2$ contenido en el fluido, obteniendo de este modo el producto final deseado. Es en estos procesos de mezclado y separación en los que se necesita conocer las propiedades de transporte de los diferentes componentes [26, 27].

Otro punto de interés se encuentra en los procesos de captura y retención de $CO_2$. Gran parte de la energía que se consume en el mundo, está generada por combustibles fósiles (gas natural, petróleo y carbón). Esto libera en la atmósfera gran cantidad de $CO_2$, lo que, de acuerdo con [28], afecta negativamente sobre el cambio climático.

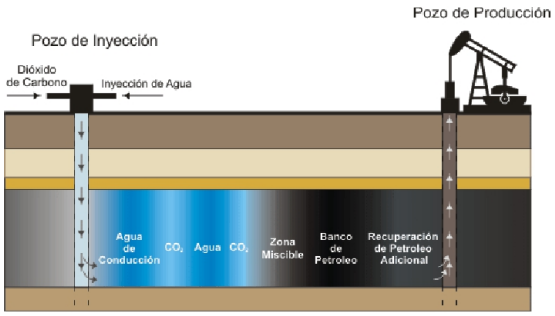


Figura 1.1: Esquema del sistema de inyección de $CO_2$ en los pozos petrolíferos para aumentar su productividad.

Con el fin de reducir la cantidad de $CO_2$ en la atmósfera, se han propuesto diferentes métodos [29] como la retención de $CO_2$ en plantas o su acumulación en el océano (Figura 1.2). Sin embargo, a día de hoy, la opción que parece con mayores perspectivas de futuro es la captura y posterior retención geológica del $CO_2$. En esta técnica, se utilizan diferentes procesos de separación y almacenamiento para la retención de $CO_2$ en las plantas térmicas de generación de energía. Posteriormente este $CO_2$ es inyectado en reservas agotadas de petróleo o de gas para su almacenamiento [30]. El aumento de la eficiencia y eficacia de ambos procesos pasa por el conocimiento de las propiedades de transporte, las cuales están relacionadas con el efecto Soret de los componentes.

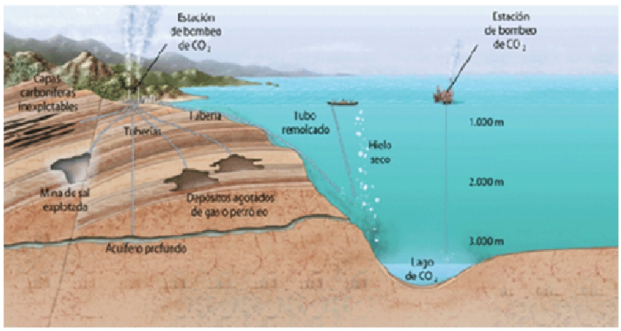


Figura 1.2: Representación de los diferentes métodos para el almacenamiento de $CO_2$.

También se ha mostrado el rol del efecto Soret en la modificación de la concentración de los componentes atrapados en el hielo (Figura 1.3) a diferentes profundidades en las zonas árticas [31]. Mediante el análisis de estos cambios de concentración, se puede determinar el registro del cambio climático a lo largo de la vida de nuestro planeta [32].

Figura 1.3: Bloques de hielo extraídos para el estudio del cambio climático.

En el campo de la generación de energía también se señala al efecto Soret como un mecanismo a tener en cuenta para optimizar el funcionamiento de sistemas como los estanques solares o *solar ponds* (Figura 1.4) [33, 34], así como en el caso de las torres solares (Figura 1.5). En estas instalaciones se tiene una torre, en cuya base se instalan unos cristales que causan un efecto invernadero. Esto crea que el aire en la base de la torre se caliente, generando un flujo por difusión en su interior que provoca el movimiento de unas turbinas y por consiguiente, la generación de energía [35].

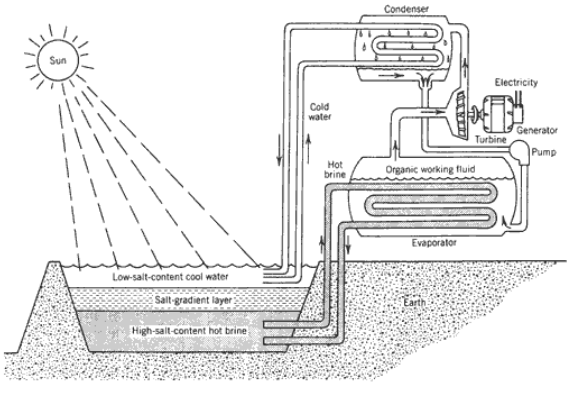


Figura 1.4: Esquema de la generación de energía mediante piscina solar.

En las centrales nucleares el efecto Soret también tiene importancia en la modelización de la retención de las moléculas de tritio en el reactor [36]. Además se ha demostrado su influencia en etapas posteriores de este proceso en las que se ha descubierto que el efecto Soret tiene importancia en el proceso de almacenaje de los residuos derivados de la generación de energía nuclear [37].

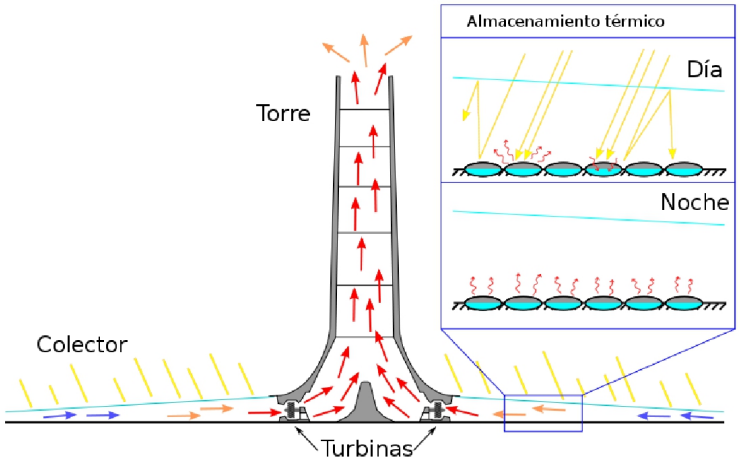


Figura 1.5: Imagen de la torre solar y esquema de su funcionamiento.

También se está estudiando la influencia del efecto Soret en las aleaciones fundidas y en las aleaciones de metales y semiconductores. En estos sistemas, debido a los gradientes de temperatura, se producen transportes de materia que provocan enriquecimientos de materiales en ciertas zonas del sistema. Este efecto es aprovechado en diferentes procesos industriales, como la fabricación de materiales dopados [38] o la fabricación de arrays de tres dimensiones en semiconductores [39].

Otros procesos en los cuales se atribuye importancia al efecto Soret son los procesos de separación de isótopos [40] y los procesos de deposición química [41, 42, 43], así como la caracterización de polímeros mediante la técnica *field flow fractionation* [44, 45, 46]. En cuanto a las aplicaciones industriales, se ha podido apreciar cómo el efecto Soret también tiene influencia en los fluidos magnetoreológicos [47, 48], los cuales generan interés en el sector de la automoción (sistema de amortiguación), la disipación de calor o el sellado dinámico [49].

En el campo de la biología también se ha podido comprobar la influencia de este efecto y sus posibles aplicaciones. Así por ejemplo, en [50], se demuestra cómo el efecto Soret pudo ser la causa de la acumulación de protobiomoléculas que al interactuar entre ellas sentaron las bases del origen de la vida. Hoy en día, se sigue utilizando este efecto en diversos dispositivos de separación de células y estudio del ADN [2, 51]. Adicionalmente, la termodifusión se presenta como un método revolucionario para procesos de separación en mezclas biológicas [52].

### 1.1.2. Estudio del Efecto Soret

Se ha organizado este apartado de análisis del estado del arte del efecto Soret de acuerdo con sus dos ámbitos de trabajo. Por un lado se presentan los resultados y los avances logrados en la parte del desarrollo analítico y numérico y por otro lado los progresos realizados a nivel experimental en cuanto a técnicas y métodos de análisis. A continuación se presenta un resumen de los diferentes avances que se han logrado hasta día de hoy en cada campo.

#### Estudios Teóricos y Numéricos

Con respecto a los estudios teóricos del efecto Soret, existen gran cantidad de modelos cuyo fin es predecir el comportamiento termohidrodinámico en mezclas líquidas. Sin embargo, tal y como ha quedado reflejado en [2], existen una gran cantidad de estudios que carecen de una teoría unificada para explicar este fenómeno. De hecho, se considera el efecto Soret, como el único mecanismo de transporte hidrodinámico que carece de una explicación física simple [9]. Esto, ha causado que se hayan desarrollado multitud de modelos basados en diferentes teorías. Esta diferenciación se ve acentuada por el hecho de que cada sistema estudiado se ve sometido a diferentes efectos. Así por ejemplo, la modelización de sistemas de hidrocarburos, con moléculas lineales y de anillos, difiere de la de sistemas de coloides, en los que uno de los compuestos es de tamaño mucho mayor que el otro [1], o de la de mezclas asociativas, que presentan efectos químicos que pueden provocar cambios de signo en algunas de sus propiedades en función de la concentración [53]. Esto hace que un modelo cuyo rendimiento es bueno para un tipo de mezclas, pierda efectividad al utilizarlo en otro tipo de mezclas.

Se pueden clasificar los modelos desarrollados hasta la fecha en dos grupos: modelos dinámicos o cinéticos y modelos estáticos. Entre los modelos estáticos se encuentran los de Kempers [54, 55], Haase [56] o Firoozabadi *et al.* [57, 58]. En el grupo de los modelos dinámicos se incluyen el de Drickamer *et al.* [59], o su versión modificada de Eslamian y Saghir [60]. También se puede encontrar en este grupo el modelo de Bringuier [61].

Se ha comprobado cómo los modelos estáticos tienen buena capacidad de predicción en mezclas críticas y a altas presiones. Sin embargo, al estudiar mezclas a presiones más cercanas a la atmosférica, la capacidad de predicción de los modelos dinámicos parece prevalecer [2].

Otra posible clasificación que se puede realizar es dependiendo de si los modelos necesitan parámetros de ajuste o no. Algunos de los modelos, precisan de algún parámetro de ajuste, como los de Drickamer y Rutherford y sus sucesores [59, 62,

63, 64], el de Firoozabadi [57, 58] o el de Mortimer y Eyring [65]. En el otro grupo se encuentran modelos como el de Haase [56] o Kempers [54, 55], los cuales no necesitan de parámetro de ajuste alguno. En esta clasificación, se ha podido comprobar cómo los modelos que necesitan un parámetro de ajuste están, en general, en mejor acuerdo con los resultados experimentales. Sin embargo, estos modelos son criticados ya que no existe un método universal y standard para la determinación de estos parámetros [2].

Una tercera forma de clasificar los modelos, es en función del tipo de aproximación que se utilice. De este modo, la mayoría de los modelos se pueden clasificar según tres aproximaciones: hidrodinámica, termodinámica de no equilibrio o teoría cinética. Los modelos basados en la aproximación hidrodinámica, como los de Semenov y Schimpf [66], o el de Brenner [67], son mayormente utilizados para modelizar procesos termoforéticos, asumiendo que existen partículas en un solvente, el cual es tratado como un medio continuo [2]. En los modelos basados en la termodinámica de no equilibrio (Eslamian-Saghir [60], Prigogine [68] o Artola *et al.* [69]), se precisa determinar la entalpía o calor de transporte. Los modelos de Bringuier [61] o Kincaid [70], forman parte de los que utilizan la teoría cinética. En este caso, aunque las expresiones analíticas obtenidas son muy robustas, tienen implícitas una serie de asunciones para su resolución, como la colisión elástica de las partículas, en el caso de Bringuier [61], o las esferas duras, en el caso de Kincaid [70].

Cabe destacar que existen otros tipos de modelos que se desmarcan de las clasificaciones anteriores, como el modelo de Shapiro [71], el cual usa la teoría de las fluctuaciones, o el modelo de Morozov [72], basado en mecánica estadística.

Otra de las opciones de analizar la interacción molecular debido al efecto Soret, es mediante las simulaciones que utilizan la dinámica molecular (MD). Una de las opciones es computar los coeficientes fenomenológicos de Onsager utilizando la dinámica molecular de equilibrio (EMD)[73, 74]. Otra opción es el uso del método de la dinámica molecular de no equilibrio (NEMD) [75, 76, 77]. Esta metodología ha demostrado su validez para determinar el efecto Soret en mezclas binarias [78, 79, 80, 81].

Por su parte, también se ha realizado un enorme esfuerzo para avanzar en la simplificación del proceso mediante el desarrollo de varias correlaciones basadas en datos experimentales, las cuales permiten la obtención de los coeficientes de termodifusión y difusión molecular en mezclas binarias y ternarias a partir de las propiedades de dichas mezclas [17, 82, 83, 84]. Estas correlaciones han mostrado ser de gran utilidad para el avance en los modelos de predicción basados en la dinámica molecular [85].

**Estudios Experimentales**

Desde el descubrimiento del efecto Soret en el siglo XIX, se han desarrollado diferentes técnicas experimentales para su análisis. En la mayoría de las técnicas, el objetivo es determinar dos de los coeficientes de transporte, obteniendo el tercero mediante la expresión (1.1).

$$S_T = \frac{D_T}{D} \tag{1.1}$$

Las técnicas experimentales utilizadas para medir estos coeficientes se pueden clasificar en función de su afinidad con respecto al efecto de la convección. Se tienen técnicas que utilizan métodos convectivos y técnicas en las que este efecto es perjudicial para el proceso de análisis experimental (sistemas no convectivos).

Entre los métodos no convectivos se encuentran técnicas como la célula de Soret clásica [86, 87]. En esta técnica, se introduce la mezcla a estudiar entre dos placas horizontales de un material conductor del calor, unidas por unas paredes de un material aislante. Enfriando la placa inferior y calentando la superior, se genera un gradiente de temperatura, el cual genera la separación de los componentes de la mezcla. Mediante análisis de muestras, más usualmente, a través de métodos ópticos, se determina el cambio de concentración que se ha dado en la mezcla, pudiendo obtener el coeficiente Soret mediante la expresión (1.2).

$$\Delta c = -S_T c_0 (1 - c_0) \Delta T \tag{1.2}$$

Normalmente, al someter a una mezcla binaria a un gradiente de temperatura, el componente con mayor densidad se dirige hacia la zona fría [88], mientras que el otro componente se dirige a la zona caliente. Esto se conoce como efecto Soret positivo. Sin embargo hay ciertas mezclas, como las mezclas asociativas, en que bajo ciertas condiciones ocurre el efecto opuesto, es decir, el componente más denso se dirige hacia la zona caliente. Este efecto se conoce como Soret negativo.

En mezclas con Soret negativo, en la célula de Soret clásica, se genera convección, creando inestabilidades e impidiendo una correcta medición del coeficiente Soret. En este tipo de mezclas, se recomienda trabajar con la configuración Rayleigh-Benard [89] o en condiciones geométricas específicas. En esta configuración, la cual se encuentra dentro del grupo de técnicas convectivas, se modifica la dirección del gradiente de temperatura, siendo la zona inferior la de mayor temperatura. Bajo ciertas condiciones técnicas, se consigue estabilizar el sistema, haciendo posible la obtención del coeficiente Soret negativo en este tipo de mezclas.

Una técnica de medición del coeficiente Soret basada en la célula de Soret clásica, es la técnica *optical beam deflection* [90, 91]. Esta técnica (Figura 1.6) también consta de una célula con dos placas horizontales mantenidas a diferente temperatura. Con el fin de obtener un mejor control del gradiente de temperatura aplicado, el sistema posee unos elementos Peltier controlados mediante un sistema proporcional integral derivativo (PID). Esta técnica utiliza un sistema óptico de medición para la determinación del cambio de concentración que se da en la mezcla. Para ello, se hace pasar un rayo láser por la mezcla cuando esta se encuentra homogeneizada y en ausencia de gradiente de temperatura. Al aplicar el gradiente de temperatura, los componentes de la mezcla se redistribuyen, creando un gradiente de concentración. Esta variación de la concentración causa un cambio en el índice de refracción de la muestra. Comparando el cambio en el índice de refracción con respecto al estado inicial se puede obtener el cambio de concentración que se da en la mezcla, lo que a su vez permite obtener sus coeficientes de transporte.

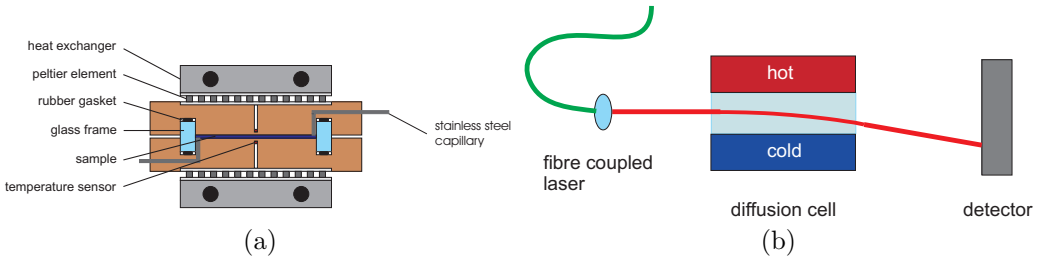


Figura 1.6: Técnica *optical beam deflection* (OBD) (a) Esquema de la célula; (b) Diagrama de la refracción del rayo dentro de la célula.

Una de las ventajas que tiene este sistema de análisis es que permite estudiar el cambio de concentración de los componentes tanto en el estado transitorio como en el estacionario. Gracias a esto, mediante esta técnica se pueden obtener el coeficiente de difusión molecular, termodifusión y Soret de la mezcla contenida en el interior de la célula.

Uno de los puntos más sensibles de esta técnica, y que comparten muchas de las técnicas basadas en métodos ópticos de medición, es que precisan de los denominados factores de contraste. Estos factores corresponden al cambio en el índice de refracción de la mezcla en función de la concentración ($\partial n/\partial c$) y de la temperatura ($\partial n/\partial T$). Estos factores deben de ser lo suficientemente sensibles y precisos, para no inducir errores en la medida. En ciertas mezclas y a ciertas concentraciones estos factores de contraste pueden perder sensibilidad, imposibilitando una correcta medición en

algún rango de concentración del sistema estudiado, tal y como sucede en la mezcla agua-etanol [91].

La técnica *optical digital interferometry* [92] utiliza también una célula de aspecto similar a la célula de Soret clásica (Figura 1.7). Al igual que en el caso de la técnica OBD, el gradiente de temperatura en la mezcla es generado de forma externa por medio de elementos Peltier.

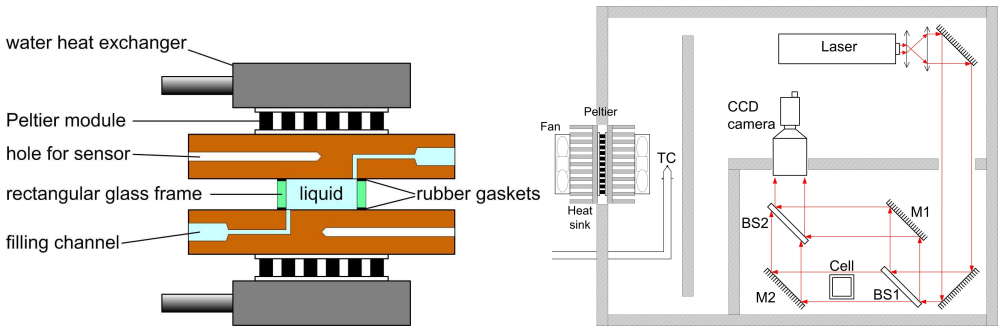


(a) (b)

Figura 1.7: Técnica *optical digital interferometry* (ODI) (a) Esquema de la célula; (b) Diagrama de todo el dispositivo ODI.

El sistema de análisis, aun siendo óptico también, varía con respecto al anterior. En este caso, la medición del cambio de concentración se lleva a cabo por medio de un interferómetro del tipo Mach-Zehnder. En esta técnica, se tiene un láser, el cual se divide en dos, haciendo que pase uno de ellos a través de la célula. Posteriormente los dos rayos vuelven a converger formando un interferograma (Figura 1.8) que es recogido por una cámara con un dispositivo *charge-coupled device* (CCD). Mediante el análisis de estos interferogramas se obtiene el perfil de concentración de los componentes a lo largo de la célula, necesario para la determinación del coeficiente Soret. Recientemente, se está trabajando en sistemas que proporcionan dos interferogramas en dos direcciones perpendiculares [93], los cuales permiten obtener superficies de concentración dentro de la célula (Figura 1.8).

Otra técnica basada en métodos ópticos para la determinación de la concentración en la mezcla de estudio es la técnica *thermal diffusion forced Rayleigh scattering* (TDFRS) [94, 95]. En esta técnica también se dispone de una célula donde se introduce la muestra, pero a diferencia de las técnicas ópticas anteriores, el gradiente de temperatura es generado en el seno de la mezcla. En este dispositivo (ver figura 1.9), se dispone de dos rayos láser de diferentes longitudes de onda. Uno de ellos se utiliza para generar el gradiente de temperatura en la mezcla. Para ello, el láser se divide en

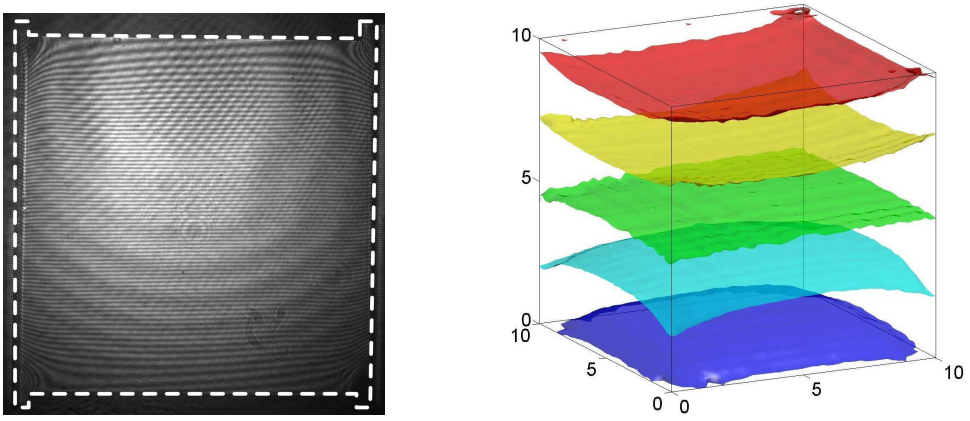


(a) (b)

Figura 1.8: Resultados de interferometría mediante la técnica *optical digital interferometry* (ODI) (a) Patrón de interferencia debido a la separación de los componentes en la célula; (b) distribución de las superficies de igual concentración a lo largo del volumen de la célula.

dos haces de igual intensidad. Uno de estos haces se desfasa con respecto al otro y se hacen converger ambos en la mezcla. Esto genera una rejilla de intensidad de luz en la mezcla. A la mezcla de estudio se le añade una pequeña cantidad de tinte, el cual hace que la rejilla de intensidad del rayo sea absorbida por la mezcla convirtiéndose en una rejilla de temperatura. Unas franjas están a mayor temperatura que las otras, lo que provoca el efecto Soret en la mezcla. Esto causa un cambio de concentración en la mezcla que es medido utilizando el segundo láser del dispositivo.

Esta técnica determina tanto el coeficiente Soret como el coeficiente de difusión molecular de la mezcla, obteniéndose posteriormente el coeficiente de termodifusión mediante la expresión (1.1).

El principal inconveniente de esta técnica es la necesidad de la adición del tinte. Se ha podido comprobar cómo el efecto de este tinte puede tener influencia en los resultados obtenidos [96]. Por esta razón se ha desarrollado una versión de este dispositivo denominada *infrared thermal diffusion forced Rayleigh scattering* (IR-TDFRS) [97], en el cual se ha modificado la longitud de onda del láser de escritura, con el fin de que su intensidad pueda ser absorbida por la mezcla de estudio sin necesidad del tinte.

Otra de las técnica ópticas que se han desarrollado para la medición del coeficiente Soret es la técnica *thermal lens* [98]. El principio básico de este método consiste en

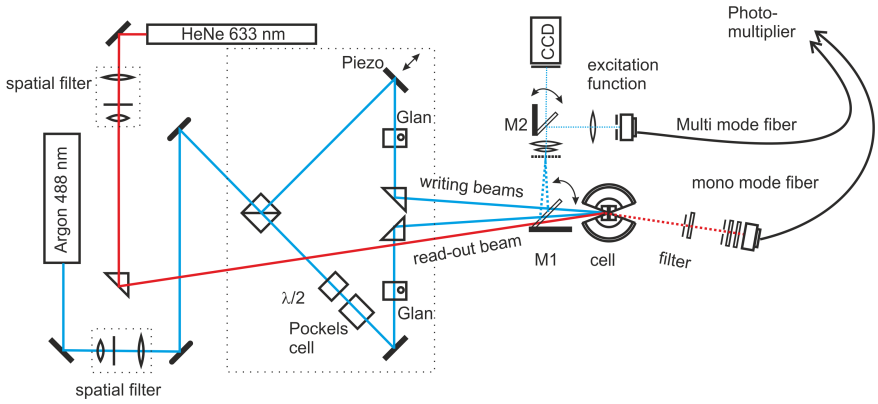


Figura 1.9: Esquema de la técnica *thermal diffusion forced Rayleigh scattering* (TDFRS).

la medición de la cantidad de calor depositado en un medio después de un proceso de absorción de luz. Esta técnica (Figura 1.10) utiliza un rayo láser, el cual es el encargado tanto de calentar la muestra como de medir el cambio de concentración en la misma mediante un detector.

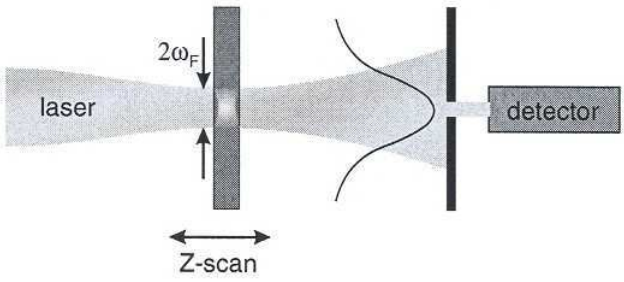


Figura 1.10: Esquema del dispositivo *thermal lens*.

La técnica de la célula de termodifusión de dos cámaras [99, 100], tiene una estructura basada en dos células rectangulares conectadas (Figura 1.11). Las dos cámaras están conectadas por un estrecho canal equipado con una válvula de paso. Al comienzo del experimento, y estando la mezcla homogénea en las dos cámaras, se calienta una de las cámaras para generar un transporte de masa. Cuando se alcanza el estado estacionario se cierra la válvula, deteniendo de este modo el proceso termodifusivo. Analizando muestras de ambas cámaras, se obtiene la concentración en cada una de ellas, lo que junto con el dato de la concentración inicial, permite obtener

el coeficiente Soret de la mezcla. Existen diferentes versiones de este aparato [101] en las que se conectan varias de estas cámaras con el fin de aumentar la separación de los componentes.

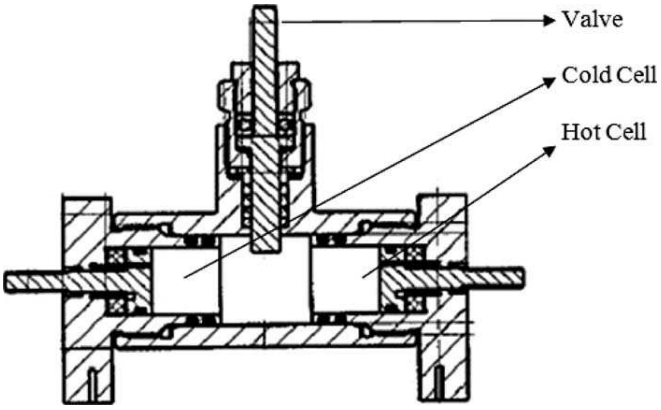


Figura 1.11: Esquema de la célula de termodifusión de dos cámaras. La célula de la figura está diseñada para medidas a altas presiones.

La técnica termogravitacional, a diferencia de las técnicas anteriores y a excepción de la técnica de la célula de Rayleigh, aprovecha las corrientes convectivas para amplificar la separación entre los extremos de la columna termogravitacional (para más información ver sección 2.4). También se ha mostrado que la separación entre los extremos de la columna puede aumentarse en función del grado de inclinación de la columna [102, 103].

Existen dos procesos de medición mediante la columna termogravitacional. En el primero de ellos se realiza un análisis del régimen transitorio. Este análisis, se puede hacer por medio de extracciones en las columnas, con las que se consigue determinar el coeficiente de difusión molecular [104, 105], o mediante un análisis utilizando velocimetría láser. Este análisis permite obtener el coeficiente Soret a partir de los cambios en las amplitudes de convección [106].

El segundo de los procesos consiste en la determinación de la separación de los componentes de la mezcla una vez se ha alcanzado el estado estacionario por medio de extracciones a diferentes alturas de la columna, utilizando estos datos para la determinación del coeficiente de termodifusión [106]. Para poder obtener el coeficiente Soret en este caso, los resultados obtenidos mediante la columna termogravitacional se complementan con los obtenidos mediante otras técnicas desarrolladas para la determinación del coeficiente de difusión molecular, como pueden ser la técnica *sliding symmetric tubes* [84] (para más información ver sección 2.5), la técnica

*open endend capillary* [106] o alguna de las técnicas anteriormente descritas que proporcione medidas de este coeficiente.

La principal ventaja que ofrece la técnica termogravitacional, además de no verse perjudicada por la convección provocada por la gravedad, es que no precisa de un conocimiento preciso del gradiente de temperatura aplicado, ya que este únicamente afecta a la velocidad de separación de los componentes y no a la separación en el estado estacionario. Como contrapartida, en esta técnica pueden aparecer inestabilidades no deseadas al tratar con mezclas de Soret negativo [107]. Sin embargo, bajo ciertas condiciones se ha conseguido establecer el gradiente de densidad adverso en este tipo de mezclas, al menos para las columnas de configuración cilíndrica [108, 109].

### Evolución del Estudio del Efecto Soret

En la actualidad se están realizando avances en diferentes campos. A continuación se van a citar algunos de los más notables, principalmente en el campo experimental.

El efecto Soret en mezclas binarias ha sido ampliamente estudiado, y existen varias teorías capaces de describir con un alto grado de fiabilidad el comportamiento de estas mezclas [58, 60, 61, 110]. Hasta la fecha, son también muchos los datos experimentales disponibles en este campo, incluso se han realizado medidas mediante varias técnicas en mezclas binarias [91, 92, 111, 112, 113, 114, 115, 116], las cuales muestran el gran acuerdo entre las diferentes técnicas experimentales y sirven de referencia para nuevos dispositivos. A su vez, se están realizando esfuerzos en el campo de las mezclas asociativas, ya que presentan un cambio en el signo del coeficiente Soret que pocos modelos teóricos son capaces de predecir [2]. Es por ello que se están realizando nuevas medidas experimentales mediante diferentes técnicas en estas mezclas [93], con el fin de conseguir una buena caracterización de las mismas.

Sin embargo, todavía es necesario aumentar la cantidad de datos experimentales en la bibliografía disponible en mezclas liquidas, especialmente en lo referente a datos experimentales en mezclas multicomponentes. Existen algunos modelos teóricos capaces de predecir las propiedades de transporte en mezclas multicomponentes [54, 117, 118], pero son pocos los datos experimentales disponibles para su validación [16, 17, 119, 120, 121, 122]. Incluso todavía son pocas las técnicas experimentales capaces de llevar a cabo medidas en este tipo de mezclas, y los resultados obtenidos mediante las mismas no están del todo en acuerdo.

Una de las primeras técnicas en proporcionar datos experimentales del coeficiente de termodifusión en mezclas ternarias fue la técnica termogravitacional [17, 119, 120]. Utilizando un sistema de análisis basado en dos propiedades independientes del fluido (densidad e índice de refracción), se puede determinar la concentración de cada

componente en una mezcla ternaria, lo que permite obtener el coeficiente de termodifusión de los componentes de la mezcla [123]. Utilizando esta técnica se han realizado mediciones en mezclas ternarias de hidrocarburos como son tetrahidronaftalina-isobutilbenceno-*n*dodecano y tetrahidronaftalina-isobutilbenceno-*n*decano.

Otra de las técnicas con las que se han obtenido resultados experimentales en mezclas ternarias es la técnica *optical beam deflection* [122]. Para ello, se ha incorporado a esta técnica otro láser de una longitud de onda diferente. Esto permite obtener dos medidas independientes del índice de refracción, y por ende de la concentración de los componentes. Esta técnica se ha utilizado para realizar medidas en dos mezclas ternarias compuestas por tetrahidronaftalina-isobutilbenceno-*n*dodecano y metilnaftalina-*n*octano-*n*decano.

La técnica de la célula de termodifusión de dos cámaras también ha sido utilizada para realizar medidas en mezclas ternarias y cuaternarias [16, 121]. Las mezclas ternarias que han sido analizadas mediante esta técnica han sido las compuestas por metano, butano y *n*-dodecano, y tetrahidonaftalina, isobutilbenceno y *n*-dodecano y la mezcla cuaternaria de los compuestos tetrahidronaftalina, isobutilbenceno, *n*-dodecano y cis,1,2-dimetilciclohexano. Estas mediciones se han llevado a cabo en un entorno de microgravedad, y a altas presiones.

Como se puede apreciar en la bibliografía, los datos experimentales disponibles no son cuantiosos, y son pocos también los sistemas estudiados. Únicamente para la mezcla tetrahidronaftalina, isobutilbenceno y *n*-dodecano se puede realizar una comparación, e incluso en esta mezcla, las únicas medidas realizadas en condiciones similares son las obtenidas mediante la técnica termogravitacional y la técnica *optical beam deflection*. No obstante, los resultados obtenidos tampoco son concluyentes. Paralelamente se han desarrollado nuevas correlaciones capaces de determinar los coeficientes de termodifusión en estas mezclas [17], sin embargo, aunque pueden ayudar a aclarar las dudas en este campo, todavía requieren de más datos experimentales para su comprobación.

Con el fin de verificar los datos experimentales disponibles se están realizando mediciones en un entorno de microgravedad. Al realizar los experimentos en el espacio, se minimiza el efecto de la gravedad la cual genera la convección. Existen diferentes plataformas en las que es posible realizar estos experimentos, como el satélite FOTON o la Estación Espacial Internacional (ISS). Se han llevado a cabo experimentos en estas instalaciones [16, 121, 124, 125, 126, 127], analizando diferentes tipos de mezclas. El análisis de los resultados obtenidos ha generado otra discusión en este tipo de experimentos, relacionada con la influencia en los mismos de las vibraciones [128, 129] y de la influencia de los *g-jitters* [130]. Estos son pequeñas perturbaciones gravitatorias generadas por la actividad en la instalación espacial. A pesar de los

prometedores resultados obtenidos, todavía hay un debate en la comunidad científica sobre la necesidad de estos experimentos y si los resultados obtenidos compensan su elevado coste.

En este marco, hay proyectos como el DCMIX, en el que varios laboratorios están colaborando con el fin de llevar a cabo mediciones tanto en mezclas binarias como ternarias en la ISS por medio de técnicas ópticas. Las mediciones llevadas a cabo en el espacio van a ser contrastadas con las realizadas en los diferentes laboratorios. Concretamente se van a utilizar métodos ópticos (como la *optical beam deflection*) y métodos que no se ven afectados por la convección (columna termogravitacional). El fin de estas medidas es obtener unos valores que sirvan de referencia para mezclas ternarias, lo que permitirá avanzar tanto a nivel teórico como experimental en el estudio de las mismas.

Otros esfuerzos en la investigación del efecto Soret están dedicados a su estudio a altas presiones. Parte del interés en este estudio se debe a su influencia en la distribución de los componentes en los pozos petrolíferos [18, 19, 20, 21, 22]. En los pozos, los componentes están sometidos a grandes presiones, sin embargo, la mayoría de los datos experimentales en la bibliografía son a presión atmosférica. Aunque existen trabajos teóricos que pronuncian la capacidad de predecir las propiedades de transporte a altas presiones, no son muchos los datos experimentales con los que se pueden contrastar las predicciones de los modelos. Por ello, se están desarrollando nuevos dispositivos para avanzar en el estudio experimental de este tipo de mezclas [16, 131, 132].

Como se puede ver son muchos los campos, tanto experimentales como analíticos, con relación al efecto Soret en los que se está trabajando, y son muchas todavía las cuestiones en las que no se ha alcanzado un acuerdo unánime. El trabajo realizado en esta tesis pretende corroborar el avance en estos campos y especialmente en el estudio de los fenómenos de transporte termo-hidrodinámicos de no equilibrio en mezclas líquidas.

## 1.2. Objetivos

El objetivo de esta tesis aborda un problema muy complejo y al mismo tiempo transcendental para la generación de nuevos conocimientos en el campo de las propiedades de transporte. En concreto, los resultados obtenidos en esta tesis doctoral ayudarán, en su medida, a resolver los problemas relacionados con los fenómenos de transporte de mezclas líquidas, y permitirán mejorar los formalismos de predicción.

Con el fin de cumplir este objetivo, se han propuesto los siguientes objetivos parciales desglosados para esta tesis doctoral:

1. Determinar las propiedades termofísicas en mezclas líquidas.
2. Determinar el coeficiente de termodifusión ($D_T$) en mezclas líquidas binarias.
3. Determinar el coeficiente de termodifusión ($D_T$) en mezclas líquidas ternarias.
4. Determinar el coeficiente de difusión molecular ($D$) en mezclas líquidas binarias.
5. Determinar el coeficiente Soret ($S_T$) en mezclas líquidas binarias.
6. Desarrollar nuevas correlaciones fenomenológicas cuantitativas para predecir los coeficientes de difusión molecular, termodifusión y coeficiente Soret en mezclas binarias y ternarias.

En la figura 1.12 se muestra un diagrama de flujo con los objetivos parciales de esta tesis doctoral. El estudio de los fenómenos de transporte en esta tesis, se divide en el análisis de mezclas binarias y ternarias de las que se determinan los diferentes coeficientes de transporte. Los resultados obtenidos permitirán el desarrollo de nuevas relaciones fenomenológicas.

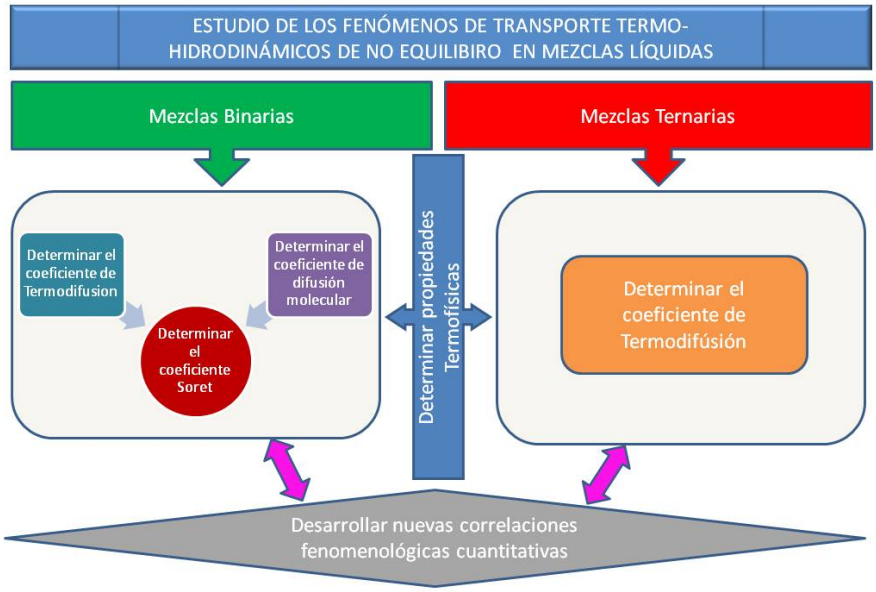


Figura 1.12: Diagrama de flujo de los objetivos parciales para la consecución del objetivo general de esta tesis doctoral.

En definitiva, la finalidad de esta tesis doctoral es avanzar en el desarrollo de nuevas metodologías experimentales y de nuevas relaciones fenomenológicas con el fin de lograr avanzar en la compresión de los fenómenos de transporte termo-hidrodinámicos de no equilibrio en mezclas líquidas.

# Capítulo 2

# Metodología

La realización de esta tesis doctoral ha requerido la utilización de diversos dispositivos, los cuales se han utilizado en la parte experimental de su desarrollo. En esta sección se van a describir los diferentes equipos y las metodologías utilizadas.

Cabe destacar que parte de los dispositivos utilizados, más concretamente las columnas termogravitacionales y la instalación *sliding symmetric tubes*, han sido desarrollados y construidos íntegramente en Mondragon Goi Eskola Politeknikoa (MGEP). Este hecho ha permitido realizar un análisis más profundo de estas instalaciones y de los procesos físicos que son la base de su funcionamiento. Además, se han identificado las variables más importantes a tener en cuenta a la hora de construir un dispositivo y de diseñar el procedimiento experimental, lo cual ha influido en la metodología a seguir durante los experimentos.

## 2.1. Preparación de Muestras

Uno de los factores decisivos a la hora de determinar una propiedad o parámetro físico es la composición de las mezclas estudiadas. Ha quedado demostrado cómo las propiedades de transporte de las mezclas líquidas se ven influenciadas por la composición de sus componentes [11, 83, 133]. Es por ello, que se considera que esta actividad es de vital importancia en los procesos de medición.

En este caso, las mezclas se han elaborado según su concentración másica, utilizando balanzas digitales de alta precisión. En el laboratorio de Mecánica de Fluidos de MGEP se dispone de dos balanzas (Figura 2.1), de las cuales se utiliza una u otra dependiendo de la cantidad de mezcla a preparar. En caso de necesitar cantidades de fluido superiores a 200 cc, se utiliza la balanza digital GRAM VSI 4500, la cual posee una resolución de 10 mg y tiene un fondo de escala de 4500 g. En el caso de

necesitar una menor cantidad de muestra, se trabaja con la balanza digital GRAM VXI 310, la cual tiene una resolución de 0.1 mg y un fondo de escala de 310 g.

(a) (b)

Figura 2.1: Balanzas digitales disponibles en el laboratorio de Mecánica de Fluidos: (a) Balanza digital GRAM VSI 4500; (b) Balanza digital GRAM VXI 310.

El procedimiento a seguir para la elaboración de las mezclas, tanto binarias como ternarias, consiste en añadir a la mezcla los componentes correspondientes en orden decreciente de densidad. Conociendo la concentración másica de cada uno de los componentes en la mezcla, se añaden las masas correspondientes, las cuales se calculan por medio de la ecuación (2.1).

$$M_T = \frac{m_i}{c_i} \qquad i = 1, 2, 3 \tag{2.1}$$

## 2.2. Medida de la densidad e índice de refracción

Para la medición de la densidad de los líquidos se ha utilizado un densímetro de tubo vibrante Anton Paar 5000 (Figura 2.2). Este aparato es capaz de determinar la densidad de un fluido con una resolución de $10^{-6}$ gr/$cm^3$ y una precisión de $5 \cdot 10^{-6}$ gr/$cm^3$, requiriendo para ello una cantidad aproximada de 1.5 cc. El control de la temperatura del fluido de análisis en este dispositivo se realiza mediante unos

elementos Peltier, los cuales permiten obtener un control de la temperatura con una resolución de $10^{-3}$ °C.

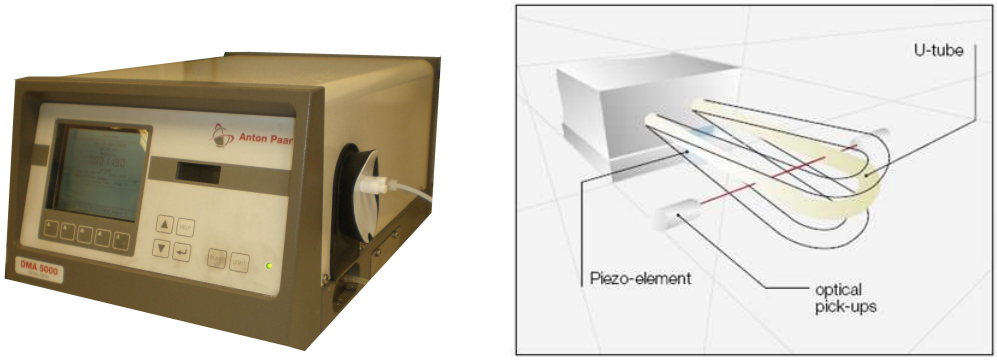


(a) (b)

Figura 2.2: Densímetro Anton Paar DMA 5000 utilizado para la determinación de la densidad de los fluidos (a) Imagen del dispositivo y (b) esquema de su funcionamiento.

Este dispositivo utiliza el principio del cuerpo vibrante. Según este principio, el periodo de vibración de un cuerpo es inversamente proporcional a su densidad. Esta relación se puede representar mediante la expresión (2.2).

$$\rho = A \cdot P^2 + B \tag{2.2}$$

Por lo tanto, obteniendo los factores $A$ y $B$ en la ecuación (2.2) se puede obtener la densidad a partir del periodo de vibración del cuerpo.

El densímetro DMA 5000 está provisto de un tubo de cuarzo en forma de U (Figura 2.2), el cual se hace vibrar mediante un excitador piezoeléctrico. La vibración del tubo es medida mediante unos acelerómetros ópticos con los que se determina el periodo de vibración del tubo.

En este caso, la determinación de los factores $A$ y $B$ en la ecuación (2.2) se realiza mediante la medida del período de vibración del tubo con dos fluidos de densidad conocida, en este caso aire y agua bidestilada. Esto permite crear un sistema de ecuaciones en las que las únicas incógnitas son estos dos factores. Cabe comentar que con el fin de evitar errores en la medición de la densidad de los fluidos, el proceso de calibración se ha realizado de forma sistemática mensualmente.

La medición del índice de refracción se ha realizado mediante el uso de un refractómetro Anton Paar RXA 156. Este aparato, el cual posee un láser de una lon-

gitud de onda de 589.3±0.1 nm, tiene una repetibilidad en la medida del índice de refracción de $2 \cdot 10^{-5}$ nD con una resolución de la temperatura de 0.01 °C.

La principal ventaja que proporcionan estos aparatos, densímetro y refractómetro, además de la gran precisión en las medidas que realizan, radica en que son capaces de trabajar conjuntamente y de realizar una medida simultánea (Figura 2.3), lo que a su vez aumenta la precisión de los resultados obtenidos para la densidad e índice de refracción.


Figura 2.3: Conjunto de densímetro Anton Paar DMA 5000 y refractómetro Anton Paar RXA 156 en su configuración para la realización de medidas simultáneas de la densidad e índice de refracción.

### 2.2.1. Determinación del coeficiente de expansión térmica

Entre las propiedades de los fluidos que se determinan utilizando los dispositivos anteriores, se encuentra el coeficiente de expansión térmica ($\alpha$). Este coeficiente representa el cambio de volumen que se da en los fluidos debido a un cambio en su temperatura, viniendo determinado por la expresión (2.3).

$$\alpha = -\frac{1}{\rho} \cdot \frac{\partial \rho}{\partial T} \tag{2.3}$$

Para el cálculo del coeficiente de expansión térmica, se determina la densidad de una mezcla a una concentración dada, a intervalos de 0.5 °C, en un rango de temperatura de ± 1 °C alrededor de la temperatura de estudio.

Tal y como se puede apreciar en la figura 2.4, el cambio de densidad en las mezclas en función de la temperatura tiene un comportamiento lineal, por lo que obteniendo la pendiente de esta recta, se puede calcular el coeficiente de expansión térmica de la mezcla mediante la expresión (2.3).

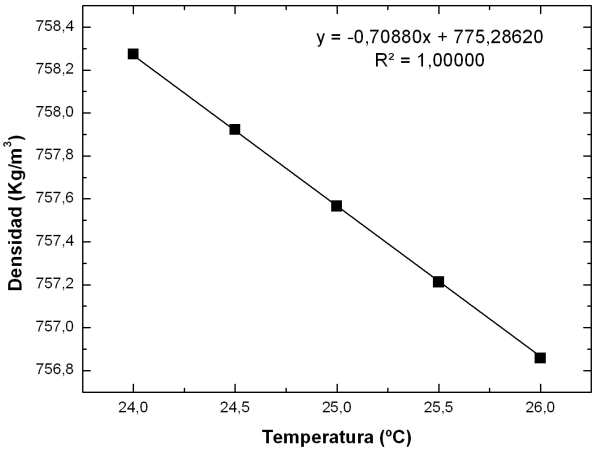


Figura 2.4: Cambio de densidad en función de la temperatura para la mezcla $nC_{12}$-$nC_{16}$ a una temperatura media de 25 °C y una concentración másica del 50 %.

### 2.2.2. Determinación del coeficiente de expansión másica

Otra de las propiedades de las mezclas a determinar es el coeficiente de expansión másica. Este coeficiente determina el cambio de volumen en la mezcla en función de la concentración de los componentes de la misma. Este coeficiente se define mediante la ecuación (2.4).

$$\beta = \frac{1}{\rho} \cdot \frac{\partial \rho}{\partial c} \tag{2.4}$$

En mezclas binarias, este coeficiente proporciona una relación entre la densidad de la mezcla y la concentración. Para la obtención de este coeficiente se preparan 5 muestras de concentración conocida, estando su concentración alrededor de la concentración de la mezcla de estudio ($c_0 \pm 2\,\%$). Determinando la densidad de estas muestras, se puede obtener una relación entre la densidad y la concentración de los componentes de la mezcla, tal y como se muestra en la figura 2.5.

Al realizar las muestras a una concentración muy cercana a la concentración de estudio, se asegura que la relación entre la densidad y la concentración tenga un comportamiento lineal. De esta manera se puede calcular el coeficiente de expansión másica mediante la expresión (2.4) utilizando la pendiente de la ecuación de la recta obtenida.

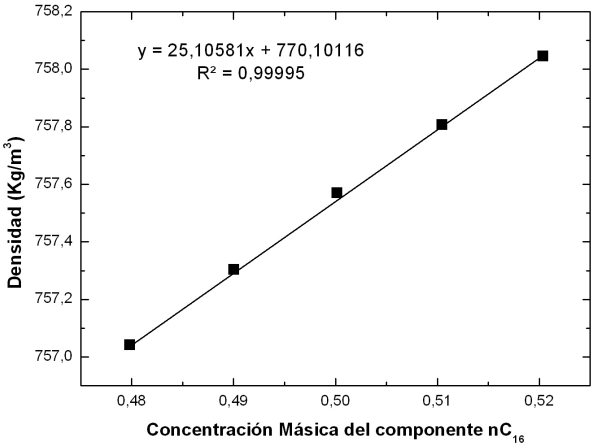


Figura 2.5: Cambio de densidad en función de la concentración para la mezcla $nC_{12}$-$nC_{16}$ a una temperatura media de 25 °C y una concentración másica del 50 %.

### 2.2.3. Calibración en mezclas ternarias

A la hora de realizar medidas de las propiedades de transporte, uno de los factores que hay que determinar es la concentración de cada componente en las mezclas analizadas. Existen varios métodos de análisis para la determinación de la concentración de los componentes en mezclas líquidas. En esta tesis doctoral, se ha utilizado la medida de la densidad y/o el índice de refracción, dependiendo de las mezclas analizadas.

En las mezclas binarias, la concentración de los componentes se consigue por medio del coeficiente de expansión másica (ver sección 2.2.2), es decir, mediante un análisis basado en la medida de la densidad.

En cuanto a las mezclas ternarias, este procedimiento no es suficiente, y se hace necesaria la elaboración de una calibración más extensa basada en la medida de la densidad y el índice de refracción de la muestra. Además, considerando que la suma de las concentraciones de los componentes de la mezcla debe ser igual a la unidad, se genera el sistema de ecuaciones (2.5), (2.6) y (2.7).

$$1 = c_i + c_j + c_k \tag{2.5}$$

$$\rho = k_0 \cdot c_i + k_1 \cdot c_j + k_2 \cdot c_k \tag{2.6}$$

$$nD = k'_0 \cdot c_i + k'_1 \cdot c_j + k'_2 \cdot c_k \tag{2.7}$$

Por lo tanto, obteniendo los coeficientes $k$ y $k'$ de estas ecuaciones, se puede obtener la concentración de los componentes de una mezcla ternaria a partir de la medida de su densidad y de su índice de refracción. Para la obtención de estos coeficientes, se elaboran dos planos de calibración, uno correspondiente a la densidad y otro al índice de refracción.

Para la construcción de estos planos se preparan un total de 25 muestras de concentración conocida, en las que se varía la concentración de cada uno de los tres componentes, de manera que se encuentren alrededor de la concentración de la mezcla de estudio. Estos planos se pueden ver en la figura 2.6.

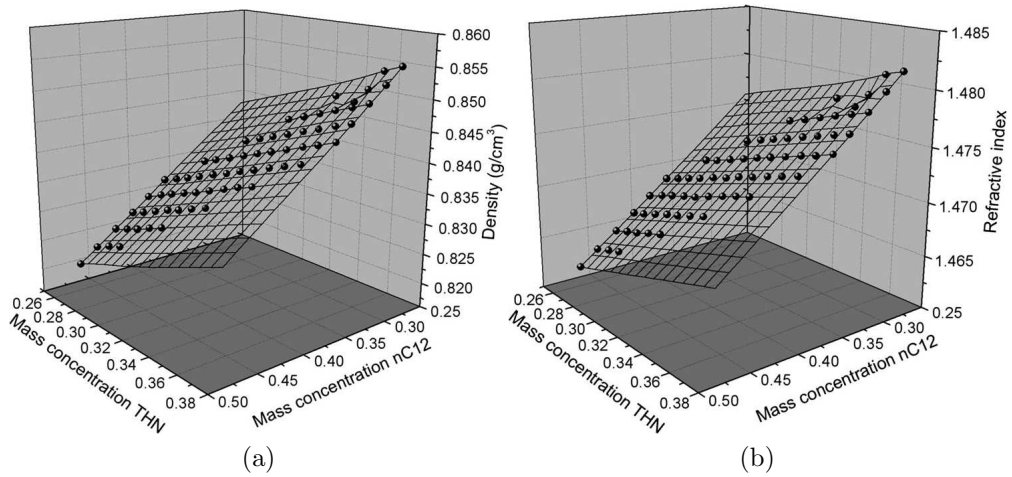


(a) (b)

Figura 2.6: Planos de calibración correspondientes a la densidad (a) e índice de refracción (b) elaborados para la mezcla ternaria THN-IBB-$nC_{12}$ a una concentración másica 1:1:1 y una temperatura media de 25 °C.

Una vez determinados los planos, se utiliza el método de los mínimos cuadrados para obtener los coeficientes de calibración $k$ y $k'$. Mediante los coeficientes obtenidos, se comprueba la calidad de la calibración realizada, recalculando la concentración de las 25 muestras utilizadas en este procedimiento. Analizando las diferencias entre los datos experimentales y calculados se aprecia la calidad de la calibración.

## 2.3. Medida de la Viscosidad

Otra de las propiedades de los fluidos que se ha determinado a lo largo de esta tesis, ha sido la viscosidad de las mezclas. Para determinar esta propiedad se dispone

en el laboratorio de Mecánica de Fluidos de MGEP de dos viscosímetros. Ambos se basan en el mismo principio, la Ley de Stoke de caída de un cuerpo sumergido en un fluido. Esta Ley relaciona el tiempo de caída de un cuerpo sumergido en un fluido con la viscosidad dinámica del fluido mediante la ecuación (2.8).

$$\mu = K \cdot (\rho_b - \rho_l) \cdot \Delta t \tag{2.8}$$

donde $\rho_b$ y $\rho_l$ denotan las densidades del cuerpo en caída y del fluido en el que está sumergido respectivamente. La variable $K$, es una constante de calibración, la cual se determina mediante la realización experimental de medidas en fluidos de viscosidad conocida.

### 2.3.1. Viscosímetro de caída de bola HAAKE

Uno de los aparatos de los que se dispone para la determinación de la viscosidad de los fluidos, es un viscosímetro HAAKE de caída de bola (Figura 2.7). Mediante este dispositivo se puede determinar la viscosidad dinámica de mezclas líquidas con una repetibilidad superior al 99 %.

(a) (b)

Figura 2.7: Viscosímetro HAAKE de caída de bola. (a) Imagen del dispositivo y (b) diferentes bolas disponibles para el viscosímetro.

El rango de utilización de este dispositivo varía dependiendo del cuerpo en caída de su interior. En este caso el dispositivo posee un conjunto de seis bolas diferentes con las que se consiguen mediciones en fluidos en el rango de viscosidades de 0.2-75000 $mPa \cdot s$.

El control de la temperatura en este dispositivo se realiza mediante la circulación de agua alrededor de la cavidad de ensayo por medio de un baño termostático, el cual tiene una precisión de 0.1 °C.

### 2.3.2. Microviscosímetro de caída de bola Anton Paar AMVn

La viscosidad de las mezclas estudiadas se ha medido adicionalmente con un microviscosímetro de caída de bola Anton Paar AMVn (Figura 2.8). Este dispositivo permite la determinación de la viscosidad dinámica en líquidos con un error en la determinación del tiempo de caída de la bola inferior a 0.002 $s$. El control de la temperatura del fluido en este dispositivo se realiza mediante unos elementos Peltier integrados en el dispositivo que permiten un ajuste de la temperatura con una precisión de 0.05 °C.

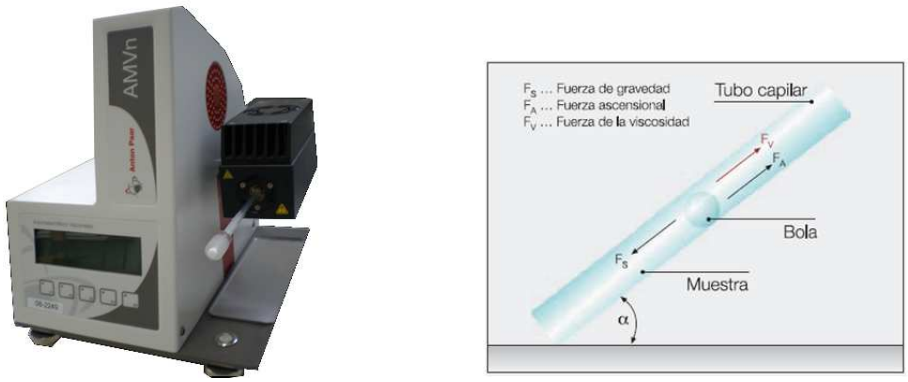


(a) (b)

Figura 2.8: Viscosímetro Anton Paar AMVn (a) Imagen del dispositivo; (b) Representación del principio de caída de bola para la medida de la viscosidad dinámica mediante este dispositivo.

Mediante este dispositivo se puede determinar la viscosidad dinámica de fluidos de diferentes rangos de viscosidades (0.3-10000 $mPa \cdot s$). Para un correcto proceso de medición, se deben ajustar dos parámetros del mismo. Por un lado se debe seleccionar el tubo capilar adecuado y por otro las dimensiones del cuerpo de caída.

En esta tesis doctoral se ha utilizado un único capilar, el cual es adecuado para mediciones en fluidos comprendidos en un rango de viscosidad entre 0.3 y 10 $mPa \cdot s$. Para optimizar la medida de la viscosidad con este capilar, se ajusta el tiempo de caída del cuerpo variando el ángulo en el que se realiza la medición.

## 2.4. Medida del coeficiente de termodifusión ($D_T$)

El coeficiente de termodifusión de las mezclas estudiadas se ha determinado mediante la técnica termogravitacional. En esta técnica se introduce la mezcla de estudio entre dos superficies paralelas que se encuentran a diferentes temperaturas. Debido a esta diferencia de temperatura entre las dos paredes, se genera un flujo debido a la termodifusión ($J_{DT}$), el cual produce la separación horizontal de los componentes de la mezcla. Esta separación genera, a su vez, un flujo de difusión ($J_D$), que tiende a mezclar otra vez los componentes de la mezcla. La separación horizontal de los componentes de la mezcla, genera diferencias de densidad horizontal en el espacio de trabajo, lo cual provoca un flujo convectivo debido a la presencia del campo gravitatorio. La combinación de estos tres efectos da lugar a una separación vertical amplificada entre los extremos de la columna. Estos efectos se pueden ver representados en la figura 2.9.

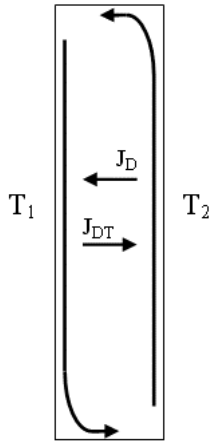


Figura 2.9: Representación de los diferentes flujos que se producen bajo el efecto termogravitacional.

El análisis de la diferencia de concentración en el estado estacionario que se genera a lo largo de la columna permite la determinación del coeficiente de termodifusión. Para ello se utiliza la expresión (2.9), que ya ha sido ampliamente estudiada en la bibliografía [102, 106, 134], y que se basa en la teoría para gases de Furry, Jones y Onsager [135], que posteriormente fue extendida a disoluciones concentradas por Majumdar [136].

$$\Delta c_i = -\frac{504 L_z}{g L_x^4} \frac{D_T^i \nu}{\alpha} c_i c_j \tag{2.9}$$

En el laboratorio de Mecánica de Fluidos de MGEP se dispone en estos momentos de tres instalaciones termogravitacionales, siendo dos de ellas de configuración paralelepípeda y una de configuración cilíndrica. Hay que señalar que la columna termogravitacional cilíndrica tiene la característica de poder trabajar con fluidos a presiones de hasta 500 bar [137].

### 2.4.1. Columnas Termogravitacionales Planas

Como se ha comentado anteriormente, en el laboratorio de Mecánica de Fluidos de MGEP se dispone de dos columnas termogravitacionales de configuración plana. Las dos columnas termogravitacionales planas (Figura 2.10) han sido diseñadas y construidas íntegramente en MGEP [138]. A su vez, se ha considerado en el diseño de una de estas dos columna la posibilidad de trabajar tanto como columna termogravitacional como célula elemental, cambiando su posición de trabajo de vertical a horizontal [138].

Figura 2.10: Instalación termogravitacional plana.

Las columnas planas están compuestas por dos placas paralelas de aluminio. Se ha utilizado el aluminio ya que éste posee buenas propiedades de conducción térmica y presenta una buena resistencia a la corrosión. Estas placas poseen una cavidad interior por la que circula agua procedente de dos baños termostáticos con el fin de generar el gradiente de temperatura necesario para la realización del ensayo.

La plancha que hace de separador entre las dos placas, fría y caliente, es de Ketron Peek-1000. Este material posee buenas propiedades mecánicas así como una

conductividad térmica muy baja, con lo que el fluido a analizar queda únicamente sometido a un gradiente de temperatura horizontal a lo largo del gap.

Una de las columnas planas posee unas medidas efectivas del gap de trabajo de 500 mm de altura, 50 mm de ancho y una distancia entre la pared fría y caliente de 1 mm. Mediante esta relación de aspecto se considera que la columna opera dentro de los límites de validez de la teoría F.J.O. [139, 140].

La segunda columna termogravitacional plana (Figura 2.10), también construida en MGEP, es muy similar a la anterior. Geométricamente, tanto la anchura del gap como su espesor son idénticos (50x1 mm). La principal diferencia entre ambas columnas radica en que la longitud de esta segunda columna es mayor. En este caso la longitud de la cavidad del gap alcanza los 980 mm. Este cambio afecta principalmente a la separación de los componentes dentro de la columna; aumenta la sensibilidad de medición de la separación estacionaria a lo largo de la columna y por lo tanto, se reducen los errores a la hora de la determinación de la distribución de los componentes. Esto es especialmente importante en las mezclas ternarias, donde la separación de algunos de los componentes es reducida.

Para conseguir la temperatura deseada en cada pared de las columnas, se utilizan dos baños termostáticos de la marca Julabo (Figura 2.11). Estos baños hacen circular agua bidestilada, por los canales dispuestos en las placas de las columnas. Los baños son capaces de controlar la temperatura del fluido en circulación con una precisión de 0.01 °C. La temperatura conseguida en las placas se determina por medio de una sonda Pt 100. Esto permite un control tanto horizontal como vertical del gradiente de temperatura que se encuentra en el interior del gap con una precisión de alrededor de 0.1 °C.

(a) (b)

Figura 2.11: Baño termostáticos (a) Julabo y (b) Lauda utilizados para generar el gradiente de temperatura en las columnas termogravitacionales.

### 2.4.2. Columna Termogravitacional Cilíndrica

Adicionalmente a las dos columnas termogravitacionales planas, se dispone en el laboratorio de Mecánica de Fluidos de MGEP de una columna termogravitacional de configuración cilíndrica (Figura 2.12). La columna, que ha sido diseñada y fabricada en MGEP [141], está formada por dos cilindros de acero inoxidable concéntricos los cuales tienen una separación entre ellos de 1 mm, en la cual se aloja la mezcla de fluidos de estudio.

Figura 2.12: Instalación termogravitacional cilíndrica de MGEP.

Para conseguir la temperatura deseada en estos cilindros se hace circular una corriente de agua por su interior con la ayuda de unos baños termostáticos Lauda (Figura 2.11). Debido a la mayor masa y superficie de contacto de estos cilindros, los baños utilizados para atemperar los cilindros son de mayor tamaño que en el caso de las columnas planas.

La principal cualidad de esta columna es que puede realizar ensayos tanto a presión atmosférica como a altas presiones (hasta 500 bar) [132]. La columna posee cinco puntos de extracción a diferentes alturas para la extracción de muestras de su interior.

El principio de funcionamiento de esta columna es idéntico al de las columnas termogravitacionales planas. Además, la relación de radios de curvatura (radio de curvatura= 0.99), hace a efectos prácticos que las superficies se asemejen a dos planos paralelos.

## 2.5. Medida del coeficiente de difusión molecular ($D$)

La determinación del coeficiente de difusión molecular se ha realizado mediante la técnica *sliding symmetric tubes* (SST) [84]. Esta técnica fue desarrollada para suplir las carencias que se observaban en la técnica *open ended capillary* (OEC) [106] que se había utilizado hasta entonces en MGEP. Las ventajas de esta técnica incluyen una reducción de la cantidad de fluido utilizado, permitiendo, a su vez, la realización de ensayos en mezclas altamente volátiles de una forma más precisa y económica.

La técnica *sliding symmetric tubes* consiste en una serie de conjuntos compuestos por dos tubos idénticos (Figura 2.13). Estos conjuntos tienen dos posiciones: tubos separados y tubos enfrentados. En la posición de tubos separados el contenido de ambos tubos se encuentra aislado el uno del otro, mientras que en la posición de tubos enfrentados, los dos tubos se encuentran conectados.

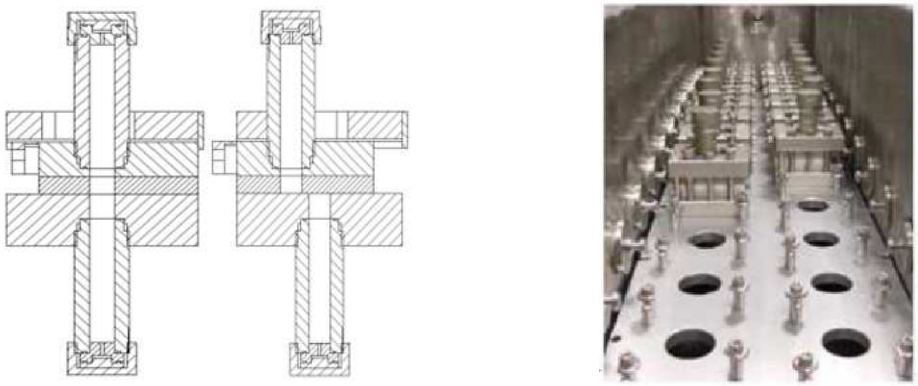

(a) (b)

Figura 2.13: Instalación *sliding symmetric tubes* (a) Representación de los conjuntos utilizados y (b) Colocación de los conjuntos en el baño para su atemperamiento.

En la realización de un ensayo se utilizan típicamente diez de estos conjuntos. Partiendo de estos conjuntos en su posición de tubos separados, se introduce en cada uno de ellos la mezcla a estudiar con una pequeña diferencia de concentración ($c_0 \pm 3\,\%$). Es decir, si se pretende determinar el coeficiente de difusión molecular de una mezcla al 50 % en fracción másica de cada componente, se prepara una muestra con un 47 % de concentración másica del componente más denso y otra muestra con un 53 % de concentración másica del componente más denso. La cantidad necesaria

aproximada de cada muestra es de unos 50 cc de mezcla para un ensayo utilizando 10 conjuntos. La mezcla con una mayor densidad se introduce en el tubo inferior, mientras que la mezcla menos densa se introduce en el tubo superior. De esta forma, se evita la aparición del fenómeno de la convección.

Los conjuntos son introducidos en su posición de tubos separados en un baño con agua (Figura 2.13) para que la mezcla en su interior alcance la temperatura de ensayo. La temperatura del agua del baño se controla mediante un baño de circulación, el cual permite obtener una precisión de 0,01 °C. Cuando los tubos se han atemperado, se cambian todos los conjuntos de la posición de tubos separados a la posición de tubos enfrentados permitiendo así que aparezca la difusión molecular entre los líquidos contenidos en los dos tubos.

Cada ciertos periodos de tiempo, se vuelve a cambiar la posición de los tubos en cada conjunto, deteniendo de esta forma el intercambio de masa entre los dos tubos. Estos conjuntos se extraen del baño y se analiza la composición en cada uno de los dos tubos. Esto permite conocer el cambio de concentración de cada componente en cada tubo en función del tiempo (Figura 2.14), y por lo tanto, utilizando las ecuaciones (2.10) y (2.11) se puede obtener el coeficiente de difusión molecular de la mezcla [84].

El tiempo total del ensayo varía en función del valor del coeficiente de difusión molecular de la mezcla, aunque para las mezclas estudiadas en esta tesis doctoral se encuentra entre 120h y 216h.

$$\overline{c^{up}}(t) - \frac{c_i^{up} + c_i^{bot}}{2} = \frac{8}{\pi^2}\left(c_i^{up} - \frac{c_i^{up} + c_i^{bot}}{2}\right)\sum_{n=0}^{\infty}\frac{e^{-\left(n+\frac{1}{2}\right)^2\frac{\pi^2}{L^2}Dt}}{(2n+1)^2} \tag{2.10}$$

$$\overline{c^{bot}}(t) - \frac{c_i^{up} + c_i^{bot}}{2} = -\frac{8}{\pi^2}\left(c_i^{up} - \frac{c_i^{up} + c_i^{bot}}{2}\right)\sum_{n=0}^{\infty}\frac{e^{-\left(n+\frac{1}{2}\right)^2\frac{\pi^2}{L^2}Dt}}{(2n+1)^2} \tag{2.11}$$

Para resolver las ecuaciones (2.10) y (2.11) se utiliza el método de los mínimos cuadrados mediante el programa de cálculo matemático *Matlab*. Con el fin de facilitar el uso de este programa para el cálculo del coeficiente de difusión molecular, se ha desarrollado una "GUI"de *Matlab* (Figura 2.14) que hace más sencillo su uso.

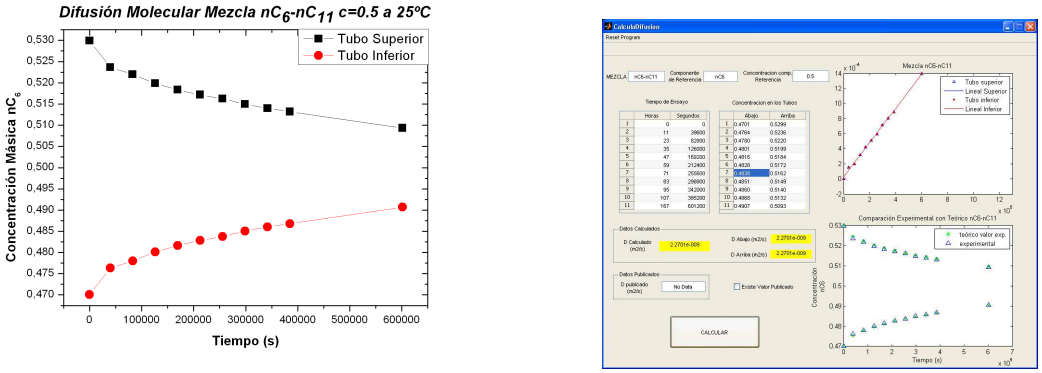


(a) (b)

Figura 2.14: Cambio de concentración másica del componente $nC_6$ en los tubos superior e inferior de la instalación SST en función del tiempo para la mezcla *n*hexano-*n*undecano al 50$wt\,\%$ y a una temperatura de 25 °C (a) y GUI del programa *Matlab* utilizada para el cálculo del coeficiente de difusión molecular (b).

## 2.6. Medida del coeficiente Soret ($S_T$)

La determinación del coeficiente Soret ($S_T$) se ha realizado de forma indirecta, por lo que se utilizan los valores experimentales obtenidos para los coeficientes de termodifusión, mediante la instalación termogravitacional, y molecular, por medio de la técnica *sliding symmetric tubes*, utilizando posteriormente la expresión (1.1) para calcular el coeficiente Soret de la mezcla estudiada.

# Capítulo 3

# Resultados

En esta sección se van a presentar los resultados obtenidos durante la elaboración de esta tesis doctoral, relacionados con la medida del coeficiente de termodifusión ($D_T$), coeficiente de difusión molecular ($D$) y coeficiente Soret ($S_T$) en diferentes tipos de mezclas. Por un lado se van a presentar los resultados obtenidos en mezclas de hidrocarburos, en las cuales se han estudiado tanto mezclas binarias como mezclas ternarias. Adicionalmente también se presentan los resultados derivados del estudio de mezclas acuosas y mezclas de polímeros.

Cabe mencionar que muchos de los resultados presentados han sido publicado en revistas indexadas. Estos trabajos se han adjuntado en los apéndices para facilitar la comprensión y para completar la información proporcionada en este apartado.

## 3.1. Mezclas de Hidrocarburos

Uno de los tipos de compuestos que se han estudiado a lo largo de esta tesis han sido los hidrocarburos. Por un lado se han realizado análisis de los coeficientes de difusión molecular, termodifusión y Soret de series de mezclas binarias de estos compuestos, y por otra parte, se ha llevado a cabo un análisis en varias mezclas ternarias más enfocado en la determinación del coeficiente de termodifusión de los compuestos de esta familia.

### 3.1.1. Mezclas Binarias de Alcanos Normales

Un primer estudio dentro del grupo de los hidrocarburos, se ha realizado en la familia de los alcanos normales. Estos compuestos forman cadenas lineales de carbonos e hidrógenos, cuya longitud va variando. Así por ejemplo el *n*-pentano forma

una cadena de 5 carbonos, mientras que el *n*-dodecano posee una cadena compuesta por 12 carbonos. Estos elementos forman parte del crudo, y su configuración los hace apropiados para la modelización y el estudio del efecto Soret en estos sistemas. Los compuestos analizados de esta familia y algunas de sus propiedades se pueden ver en la tabla 3.1.

Tabla 3.1: Propiedades físicas de los alcanos normales a una temperatura de $T = 25$ °C.

| Componente | $\rho$ (kg/m$^3$) | $\mu \times 10^{-3}$ (Pa · s) | M (amu) | $I_x$ (amu $\mathring{A}^2$) | $I_y$ (amu $\mathring{A}^2$) | $I_z$ (amu $\mathring{A}^2$) |
|---|---|---|---|---|---|---|
| *n*-pentano ($nC_5$) | 621.770 | 0.224 | 72.15 | 30.634 | 250.028 | 264.696 |
| *n*-hexano ($nC_6$) | 655.120 | 0.300 | 86.18 | 35.785 | 426.917 | 443.541 |
| *n*-heptano ($nC_7$) | 679.780 | 0.387 | 100.20 | 43.334 | 667.452 | 688.432 |
| *n*-octano ($nC_8$) | 698.760 | 0.508 | 114.23 | 48.760 | 989.298 | 1012.510 |
| *n*-nonano ($nC_9$) | 713.960 | 0.665 | 128.25 | 55.947 | 1397.630 | 1424.830 |
| *n*-decano ($nC_{10}$) | 726.090 | 0.838 | 142.28 | 61.534 | 1908.410 | 1938.010 |
| *n*-undecano ($nC_{11}$) | 736.740 | 1.098 | 156.30 | 68.520 | 2528.110 | 2561.500 |
| *n*-dodecano ($nC_{12}$) | 745.150 | 1.383 | 170.34 | 74.215 | 3271.710 | 3307.600 |
| *n*-tridecano ($nC_{13}$) | 752.890 | 1.724 | 184.36 | 81.074 | 4146.460 | 4186.020 |
| *n*-tetradecano ($nC_{14}$) | 759.340 | 2.128 | 198.39 | 86.845 | 5166.710 | 5208.850 |
| *n*-pentadecano ($nC_{15}$) | 765.360 | 2.570 | 212.42 | 93.614 | 6340.250 | 6385.960 |
| *n*-hexadecano ($nC_{16}$) | 770.210 | 3.032 | 226.45 | 99.442 | 7680.940 | 7729.290 |
| *n*-heptadecano ($nC_{17}$) | 774.520 | 3.690 | 240.46 | 106.145 | 9197.020 | 9248.880 |

**Resultados de las Propiedades de Transporte**

El estudio de los alcanos normales se ha centrado en tres series de estos componentes, en las que se ha seleccionado uno de estos elementos como referencia, combinándose posteriormente con el resto de alcanos. Las series seleccionadas han sido $nC_6$-$nC_i$ ($i$=6, 7, 8,..., 18 ), $nC_{10}$-$nC_i$ ($i$=5, 6, 7, 14,..., 20) y $nC_{12}$-$nC_i$ ($i$=5,..., 9, 16, 17, 18). Estas series han sido estudiadas a una temperatura media de $T = 25$ °C tanto a una concentración equimásica como a una concentración equimolar de sus componentes.

El coeficiente de termodifusión de algunas de las mezclas de estas series ya había sido presentado en trabajos anteriores [82, 142, 143]. En esta tesis se han completado los valores para este coeficiente en estas series, añadiendo los valores obtenidos en la

medición del coeficiente de difusión molecular. Esto ha permitido a su vez, determinar el coeficiente Soret de estas mezclas. Los resultados obtenidos en la medición de los coeficientes de difusión molecular y termodifusión, así como de sus propiedades termofísicas, se muestran en las tablas 3.2, 3.3, 3.4, 3.5, 3.6 y 3.7.

Tabla 3.2: Propiedades medidas de la serie $nC_6$-$nC_i$ a una concentración másica de 0.50 y a una temperatura de $T = 25$ °C.

| Mezcla, $c$ =0.5 | $\mu \times 10^{-3}$ (Pa · s) | $\alpha \times 10^{5}$ ($K^{-1}$) | $\beta \times 10^{2}$ | $\rho$ (kg/m$^3$) | $D \times 10^{-9}$ (m$^2$/s) | $D_T \times 10^{-12}$ (m$^2$/s · K) |
|---|---|---|---|---|---|---|
| $nC_{10}$-$nC_6$ | 0.470 | 1.199 | 0.103 | 689.823 | 2.53 | 6.71 |
| $nC_{11}$-$nC_6$ | 0.531 | 1.178 | 0.118 | 694.886 | 2.27 | 6.65 |
| $nC_{12}$-$nC_6$ | 0.558 | 1.159 | 0.128 | 698.803 | 2.09 | 7.45 |
| $nC_{13}$-$nC_6$ | 0.610 | 1.142 | 0.139 | 702.374 | 1.96 | 7.57 |
| $nC_{14}$-$nC_6$ | 0.656 | 1.132 | 0.147 | 705.405 | 1.76 | 7.95 |
| $nC_{15}$-$nC_6$ | 0.694 | 1.120 | 0.155 | 708.106 | 1.62 | 8.28 |
| $nC_{16}$-$nC_6$ | 0.745 | 1.110 | 0.161 | 710.322 | 1.54 | 8.37 |
| $nC_{17}$-$nC_6$ | 0.774 | 1.106 | 0.167 | 712.325 | 1.46 | 8.57 |
| $nC_{18}$-$nC_6$ | 0.827 | 1.090 | 0.172 | 714.123 | 1.39 | 8.90 |

Tabla 3.3: Propiedades medidas de la serie $nC_6$-$nC_i$ a una concentración molar de 0.50 y a una temperatura de $T = 25$ °C. * Datos obtenidos de la Ref. [82].

| Mezcla, $x$ =0.5 | $\mu \times 10^{-3}$ (Pa · s) | $\alpha \times 10^{5}$ ($K^{-1}$) | $\beta \times 10^{2}$ | $\rho$ (kg/m$^3$) | $D \times 10^{-9}$ (m$^2$/s) | $D_T \times 10^{-12}$ (m$^2$/s · K) |
|---|---|---|---|---|---|---|
| $nC_{10}$-$nC_6$ | 0.538 | 1.159 | 0.103 | 698.508 | 2.53 | 6.08* |
| $nC_{11}$-$nC_6$ | 0.623 | 1.124 | 0.117 | 706.712 | 2.14 | 6.40 |
| $nC_{12}$-$nC_6$ | 0.730 | 1.098 | 0.129 | 713.792 | 1.93 | 6.45* |
| $nC_{13}$-$nC_6$ | 0.831 | 1.068 | 0.139 | 720.307 | 1.67 | 6.61 |
| $nC_{14}$-$nC_6$ | 0.945 | 1.047 | 0.148 | 726.124 | 1.54 | 6.68* |
| $nC_{15}$-$nC_6$ | 1.108 | 1.025 | 0.155 | 731.762 | 1.48 | 6.47 |
| $nC_{16}$-$nC_6$ | 1.260 | 1.009 | 0.162 | 736.556 | 1.26 | 6.38* |
| $nC_{17}$-$nC_6$ | 1.432 | 0.991 | 0.169 | 741.007 | 1.24 | 6.10 |
| $nC_{18}$-$nC_6$ | 1.715 | 0.976 | 0.174 | 745.086 | 1.12 | 5.90* |

Tabla 3.4: Propiedades medidas de la serie $nC_{10}$-$nC_i$ a una concentración másica de 0.50 y a una temperatura de $T = 25$ °C. * Datos obtenidos de la Ref. [142].

| Mezcla, $c$ =0.5 | $\mu \times 10^{-3}$ (Pa · s) | $\alpha \times 10^{5}$ ($K^{-1}$) | $\beta \times 10^{2}$ | $\rho$ (kg/m$^3$) | $D \times 10^{-9}$ (m$^2$/s) | $D_T \times 10^{-12}$ (m$^2$/s · K) |
|---|---|---|---|---|---|---|
| $nC_{10}$-$nC_5$ | 0.399 | 1.288 | 0.157 | 672.306 | 3.03 | 9.24* |
| $nC_{10}$-$nC_6$ | 0.470 | 1.200 | 0.103 | 689.823 | 2.54 | 6.71* |
| $nC_{10}$-$nC_7$ | 0.563 | 1.141 | 0.066 | 702.601 | 2.09 | 4.37* |
| $nC_{14}$-$nC_{10}$ | 1.293 | 0.983 | 0.045 | 742.526 | 0.91 | 2.25 |
| $nC_{15}$-$nC_{10}$ | 1.397 | 0.974 | 0.052 | 745.446 | 0.82 | 2.39* |
| $nC_{16}$-$nC_{10}$ | 1.515 | 0.967 | 0.059 | 747.768 | 0.76 | 2.47* |
| $nC_{17}$-$nC_{10}$ | 1.634 | 0.958 | 0.065 | 749.893 | 0.70 | 2.53* |
| $nC_{18}$-$nC_{10}$ | 1.778 | 0.951 | 0.070 | 751.756 | 0.66 | 2.56* |
| $nC_{20}$-$nC_{10}$ | 2.102 | 0.944 | 0.078 | 754.988 | - | 2.65* |

Tabla 3.5: Propiedades medidas de la serie $nC_{10}$-$nC_i$ a una concentración molar de 0.50 y a una temperatura de $T = 25$ °C. * Datos obtenidos de la Ref. [82]; [a] Determinado con la correlación del coeficiente de difusión molecular en [84]; [b] Determinado con la correlación del coeficiente de termodifusión en [82].

| Mezcla, $x$ =0.5 | $\mu \times 10^{-3}$ (Pa · s) | $\alpha \times 10^{5}$ ($K^{-1}$) | $\beta \times 10^{2}$ | $\rho$ (kg/m$^3$) | $D \times 10^{-9}$ (m$^2$/s) | $D_T \times 10^{-12}$ (m$^2$/s · K) |
|---|---|---|---|---|---|---|
| $nC_{10}$-$nC_5$ | 0.486 | 1.203 | 0.155 | 689.961 | 2.96 | 8.78* |
| $nC_{10}$-$nC_6$ | 0.538 | 1.159 | 0.103 | 698.508 | 2.53 | 6.08* |
| $nC_{10}$-$nC_7$ | 0.608 | 1.122 | 0.066 | 706.677 | 2.07 | 3.90* |
| $nC_{14}$-$nC_{10}$ | 1.410 | 0.976 | 0.044 | 745.410 | 0.88[a] | 1.84[b] |
| $nC_{15}$-$nC_{10}$ | 1.582 | 0.960 | 0.052 | 749.433 | 0.78 | 2.15* |
| $nC_{16}$-$nC_{10}$ | 1.762 | 0.952 | 0.059 | 752.850 | 0.72 | 2.23* |
| $nC_{17}$-$nC_{10}$ | 2.009 | 0.939 | 0.064 | 756.111 | 0.70 | 2.29* |
| $nC_{18}$-$nC_{10}$ | 2.255 | 0.928 | 0.069 | 759.213 | 0.61 | 2.38* |

Tabla 3.6: Propiedades medidas de la serie $nC_{12}$-$nC_i$ a una concentración másica de 0.50 y a una temperatura de $T = 25$ °C. * Datos obtenidos de la Ref. [143].

| Mezcla, $c$ =0.5 | $\mu \times 10^{-3}$ (Pa · s) | $\alpha \times 10^{5}$ ($K^{-1}$) | $\beta \times 10^{2}$ | $\rho$ (kg/m$^3$) | $D \times 10^{-9}$ (m$^2$/s) | $D_T \times 10^{-12}$ (m$^2$/s · K) |
|---|---|---|---|---|---|---|
| $nC_{12}$-$nC_5$ | 0.455 | 1.247 | 0.181 | 680.928 | 2.57 | 10.94* |
| $nC_{12}$-$nC_6$ | 0.558 | 1.159 | 0.128 | 698.803 | 2.09 | 7.45* |
| $nC_{12}$-$nC_7$ | 0.682 | 1.102 | 0.092 | 711.767 | 1.70 | 5.15* |
| $nC_{12}$-$nC_8$ | 0.807 | 1.060 | 0.062 | 721.447 | 1.49 | 3.39* |
| $nC_{12}$-$nC_9$ | 0.945 | 1.030 | 0.043 | 729.407 | 1.24 | 2.15* |
| $nC_{16}$-$nC_{12}$ | 2.034 | 0.936 | 0.033 | 757.548 | 0.59 | 1.21 |
| $nC_{17}$-$nC_{12}$ | 2.232 | 0.930 | 0.039 | 759.557 | 0.55 | 1.27* |
| $nC_{18}$-$nC_{12}$ | 2.395 | 0.932 | 0.044 | 761.665 | 0.50 | 1.49* |

Tabla 3.7: Propiedades medidas de la serie $nC_{12}$-$nC_i$ a una concentración molar de 0.50 y a una temperatura de $T = 25$ °C. * Datos obtenidos de la Ref. [82]; [a] Determinado con la correlación del coeficiente de difusión molecular en [84]; [b] Determinado con la correlación del coeficiente de termodifusión en [82].

| Mezcla, $x$ =0.5 | $\mu \times 10^{-3}$ (Pa · s) | $\alpha \times 10^{5}$ ($K^{-1}$) | $\beta \times 10^{2}$ | $\rho$ (kg/m$^3$) | $D \times 10^{-9}$ (m$^2$/s) | $D_T \times 10^{-12}$ (m$^2$/s · K) |
|---|---|---|---|---|---|---|
| $nC_{12}$-$nC_5$ | 0.671 | 1.126 | 0.180 | 706.503 | 2.20 | 8.81* |
| $nC_{12}$-$nC_6$ | 0.730 | 1.098 | 0.129 | 713.792 | 1.93 | 6.45* |
| $nC_{12}$-$nC_7$ | 0.807 | 1.066 | 0.092 | 720.338 | 1.70 | 4.74* |
| $nC_{12}$-$nC_8$ | 0.892 | 1.043 | 0.064 | 726.279 | 1.45 | 3.23* |
| $nC_{12}$-$nC_9$ | 0.992 | 1.021 | 0.043 | 731.708 | 1.26 | 2.15* |
| $nC_{16}$-$nC_{12}$ | 2.113 | 9.300 | 0.033 | 759.300 | 0.58[a] | 1.16[b] |
| $nC_{17}$-$nC_{12}$ | 2.389 | 0.922 | 0.039 | 759.557 | 0.54 | 1.29* |
| $nC_{18}$-$nC_{12}$ | 2.665 | 0.909 | 0.044 | 761.665 | 0.48 | 1.33* |

**Comparación de los resultados experimentales con los obtenidos utilizando análisis numérico**

Los resultados obtenidos han permitido realizar diferentes análisis. Así por ejemplo, se ha realizado una comparación para la serie $nC_6$-$nC_i$ en concentración equimásica, entre los datos experimentales y los obtenidos mediante cálculos basados en la termodinámica de no equilibrio y llevados a cabo por el grupo del Prof. Saghir de la universidad de Rayerson (apéndice D).

Este grupo ha utilizado para el cálculo del coeficiente de termodifusión un modelo basado en la termodinámica de no equilibrio, el cual considera la energía del efecto viscoso para obtener los coeficientes fenomenológicos necesarios en la aplicación de este tipo de modelos. Adicionalmente, el modelo utilizado, requiere valores del coeficiente de difusión molecular para llevar a cabo el cálculo. Con el fin de analizar la influencia de los valores proporcionados de este coeficiente al modelo, se han computado valores del coeficiente de termodifusión utilizando los datos experimentales obtenidos del coeficiente de difusión molecular ($D_T^{NE1}$) y los datos estimados mediante el modelo propuesto en [144] ($D_T^{NE2}$).

Los datos obtenidos para los coeficientes de termodifusión y difusión molecular han sido utilizados para la determinación del coeficiente Soret mediante la ecuación (1.1). Se han calculado diferentes valores de este coeficiente en función del método de obtención de los coeficientes $D_T$ y $D$. De este modo se tiene el coeficiente $S_T^{exp}$, el cual ha sido determinado utilizando únicamente datos experimentales. El coeficiente $S_T^{NE1}$, por otro lado, ha sido calculado utilizando los datos experimentales del coeficiente $D$ y los valores numéricos $D_T^{NE1}$ del coeficiente de termodifusión. Finalmente, el coeficiente $S_T^{NE2}$ ha sido determinado íntegramente utilizando datos obtenidos mediante modelos de predicción. La figura 3.1, muestra una comparación de los resultados obtenidos para el coeficiente de difusión molecular y el coeficiente Soret determinados mediante los diferentes métodos. Los valores negativos del coeficiente Soret en esta figura se deben a que se considera el componente $nC_6$ como componente de referencia.

Los resultados obtenidos muestran cómo en el caso del coeficiente de difusión molecular, los valores experimentales obtenidos para este coeficiente están en gran acuerdo con los determinados mediante el modelo de predicción en [144], con desviaciones por debajo del 5 %. Estos resultados han servido para comprobar cómo pequeñas variaciones en el valor del coeficiente $D$, no tienen un gran impacto en los valores calculados del coeficiente $D_T$, al menos para la serie de alcanos normales $nC_6$-$nC_i$ (i=10, 11,..., 18) analizada.

La comparación entre los datos experimentales del coeficiente Soret y los obtenidos mediante los diferentes modelos de predicción muestran un buen acuerdo. Sin

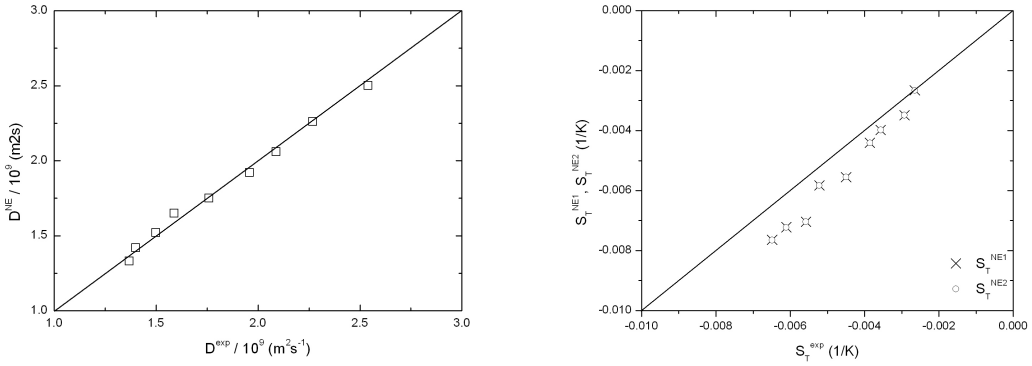


(a) (b)

Figura 3.1: Resultados obtenidos para la serie $nC_6$-$nC_i$ (i=10, 11,..., 18) a fracción másica de 0.5 y a una temperatura media de $T = 25$ °C. (a) Comparación de los valores del coeficiente de difusión molecular determinados experimentalmente y mediante la expresión (17) del apéndice D (b) Comparación de los valores del coeficiente Soret determinados experimentalmente ($S_T^{exp} = D_T^{exp}/D^{exp}$) y mediante el modelo de predicción ($S_T^{NE1} = D_T^{NE1}/D^{exp}$; $S_T^{NE2} = D_T^{NE2}/D^{NE}$).

embargo se puede apreciar como las diferencias entre los datos obtenidos aumentan al aumentar la masa molecular de la mezcla. Esto puede ser un indicador de que la diferencia de la masa molecular de los componentes de las mezclas debe de ser representada de forma más agresiva en los modelos.

### Correlación para el coeficiente de termodifusión $D_T$

Los datos experimentales obtenidos en las series estudiadas, han sido utilizados adicionalmente para la elaboración de correlaciones de predicción de las propiedades de transporte. Estas correlaciones son importantes ya que permiten la estimación de los valores de estas propiedades sin la necesidad de la realización de experimentos.

Así mismo, los resultados experimentales obtenidos a lo largo de esta tesis, han sido utilizados en el desarrollo de tres nuevas correlaciones. Una de estas correlaciones ha sido elaborada para la determinación del coeficiente de termodifusión en mezclas binarias de alcanos normales para cualquier concentración (apéndice B), mientras que la segunda correlación hace lo propio con el coeficiente de difusión molecular (apéndice E). Por último, se ha desarrollado otra nueva correlación para la determinación del coeficiente Soret en las mezclas binarias de alcanos normales a cualquier

concentración (apéndice I).

La correlación desarrollada para el coeficiente de termodifusión, se basa en la relación determinada en mezclas equimolares, entre la diferencia de masa molecular de los componentes de la mezcla y la separación determinada de los mismos dentro de la columna termogravitacional. Utilizando esta relación, en [82] se obtiene una correlación para la determinación del coeficiente de termodifusión en mezclas equimolares de alcanos normales. Esta correlación se ha extendido a mezclas binarias de alcanos normales en todo el rango de concentración.

Para ello, se ha observado que la correlación en [82] permite deducir que existe una proporcionalidad entre la variación de masa de los componentes de la mezcla y el factor $(D_T c_1 c_2 \mu/\alpha)$. La figura 3.2 muestra la relación existente entre estos factores para diferentes mezclas de alcanos a concentraciones molares de $x = 0{,}20$, $x = 0{,}30$, $x = 0{,}40$ y $x = 0{,}80$. Tal y como se puede ver en esta figura 3.2, en todos los casos se cumple que existe una regresión lineal entre estos factores, que viene dada por la expresión (3.1), en la que el parámetro $k$, únicamente depende de la concentración molar de los componentes de la mezcla.

$$\frac{D_T c_1 c_2 \mu}{\alpha} = k(x_1)\Delta M \tag{3.1}$$

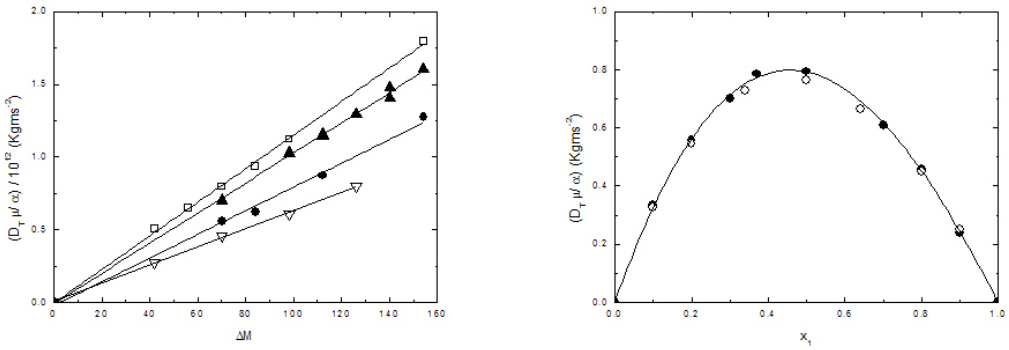


(a) (b)

Figura 3.2: Variación del factor $(D_T c_1 c_2 \mu/\alpha)$ en función de la diferencia de masa molecular de los componentes para diferentes mezclas de alcanos normales para las concentraciones molares de (•) $x = 0{,}20$, (▲) $x = 0{,}30$, (□) $x = 0{,}40$ y (▽) $x = 0{,}80$ (a) y en función de la concentración molar para las mezclas (•) $nC_{12}$-$nC_7$ y (○) $nC_{10}$-$nC_5$ (b).

Con el fin de obtener una expresión que permita calcular el coeficiente $k$ en la ecuación (3.1), se han realizado medidas del coeficiente de termodifusión en la serie $nC_{12}$-$nC_7$ a diferentes concentraciones másicas. Utilizando los datos obtenidos, se ha representado el factor $(D_T c_1 c_2 \mu/\alpha)$, en función de la concentración molar de la mezcla (Figura 3.2). Adicionalmente, en esta figura se han introducido también los datos obtenidos de [142], correspondientes a la mezcla $nC_{10}$-$nC_5$, cuya diferencia de masa entre los componentes es prácticamente idéntica a la de la mezcla $nC_{12}$-$nC_7$, pudiendo, de este modo, comprobar que los datos de ambas mezclas se ajustan en la misma curva. La ecuación de esta curva de ajuste, divida entre la diferencia de masa molecular de los componentes de la mezcla, corresponde a la expresión que define el parámetro $k$. En este caso, la expresión obtenida viene dada por la ecuación (3.2).

$$k(x_1) = (5{,}34x_1 - 7{,}00x_1^2 + 1{,}65x_1^3)10^{-11} \tag{3.2}$$

Por lo tanto, teniendo en cuenta el desarrollo anterior, se puede obtener la expresión (3.3), la cual permite obtener el coeficiente de termodifusión en mezclas binarias de alcanos normales a partir de los datos de la masa molecular de los componentes, el coeficiente de expansión másica y la viscosidad dinámica de la mezcla junto con las concentraciones molar y másica de los componentes en la mezcla. En la figura 3.3 se muestra una comparación del coeficiente de termodifusión determinado experimentalmente y mediante la expresión (3.3). Tal y como se puede apreciar, el acuerdo entre los datos experimentales y los determinados utilizando la correlación (3.3) es muy bueno, con errores por debajo del 5 %.

$$D_T c_1 c_2 = k(x_1)(M_1 - M_2)\frac{\alpha}{\mu} \tag{3.3}$$

Adicionalmente, la expresión (3.3) puede ser adaptada para su uso en la región diluida de las mezclas binarias de alcanos normales, es decir, cuando la concentración de uno de los componentes de la mezcla tiende a cero. El objetivo de esta adaptación es la comparación de la correlación desarrollada con las teorías [67, 135, 139, 145] y los resultados experimentales [146] disponibles en la literatura. Para ello, si se toma el componente 2 como solvente y el 1 como soluto ($M_1 > M_2$), se puede obtener la expresión (3.4), para el cálculo del coeficiente de termodifusión propio del componente 2.

$$D_T(x_1 \to 0) = 5{,}34 \times 10^{-11}\frac{\alpha_2}{\mu_2}M_2\left(1 - \frac{M_2}{M_1}\right) \tag{3.4}$$

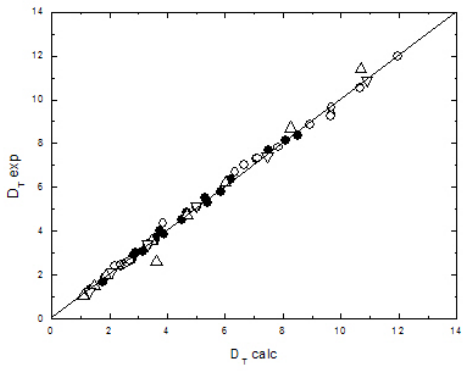


Figura 3.3: Comparación de los datos del coeficiente de termodifusión determinados experimentalmente y mediante la correlación (3.3) para las mezclas de alcanos normales a una temperatura de $T = 25$ °C.

Mientras que el calculo del coeficiente de termodifusión propio del componente 1, se realiza a partir de la expresión (3.5).

$$D_T(x_2 \to 0) = 3{,}71 \times 10^{-11} \frac{\alpha_1}{\mu_1} M_1 \left( \frac{M_1}{M_2} - 1 \right) \tag{3.5}$$

En estas expresiones se puede ver como el coeficiente de termodifusión es dependiente del ration $(\alpha/\mu)$, lo cual ya había sido reflejado en las teorías de Semenov y Shimpf [145] y de Brenner [67]. Por otra parte, la dependencia de este coeficiente con el inverso de la viscosidad ya había sido observada experimentalmente en [147].

Adicionalmente, se ha comprobado la dependencia del coeficiente de termodifusión con la concentración másica de los componentes de la mezcla. Para ello, se han representado los valores del coeficiente de termodifusión de las series $nC_{12}$-$nC_7$ y $nC_{10}$-$nC_5$ en función de la masa molecular de sus componentes. Tal y como se puede apreciar en la figura 3.4, los datos se ajustan a una línea, con lo que se puede escribir la ecuación (3.6) para definir el coeficiente de termodifusión en estas mezclas.

$$D_T = c_1 D_T(c_2 \to 0) + c_2 D_T(c_1 \to 0) \tag{3.6}$$

Según la expresión (3.6), el coeficiente de termodifusión de las mezclas de alcanos normales se puede calcular en todo el rango de concentración a partir de los valores del coeficiente de termodifusión propio de los componentes de la mezcla, los cuales pueden ser calculados utilizando las expresiones (3.4) y (3.5). Con el fin de comprobar

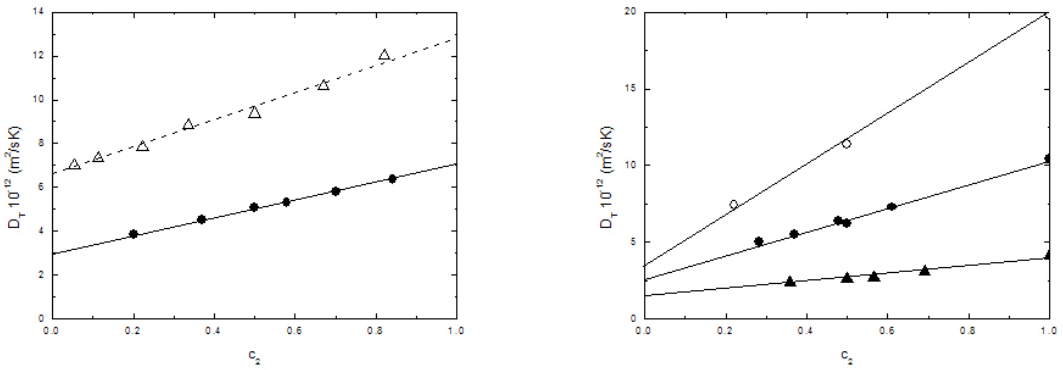


(a) (b)

Figura 3.4: Valor del coeficiente de termodifusión (a) en función de la concentración másica de los componentes para las mezclas (•) $nC_{12}$-$nC_7$ y (△) $nC_{10}$-$nC_5$ y (b) en función de la concentración másica de los componentes para las mezclas de alcanos normales (○) $nC_{18}$-$nC_5$, (•) $nC_{18}$-$nC_7$ y (△) $nC_{18}$-$nC_{10}$, calculados utilizando la expresión (3.6).

la validez de la expresión (3.6) se ha calculando el coeficiente de termodifusión de varias mezclas (Figura 3.4), pudiendo comprobar, en todos los casos, que la diferencia entre los datos experimentales y los determinados mediante la expresión (3.6) se encuentran por debajo del 5 %.

### Correlación para el coeficiente de difusión molecular $D$

La segunda correlación desarrollada está enfocada en la determinación del coeficiente de difusión molecular en mezclas binarias de alcanos normales (apéndice E). En este desarrollo se han utilizado los resultados obtenidos del coeficiente de difusión molecular de las series $nC_6$-$nC_i$, $nC_{10}$-$nC_i$ y $nC_{12}$-$nC_i$ a una concentración másica de 0.50 de sus componentes. Adicionalmente, se han estudiado las mezclas $nC_{12}$-$nC_6$, $nC_{12}$-$nC_7$ y $nC_{12}$-$nC_8$ en todo el rango de concentración. Los resultados obtenidos en estas mezclas se presentan en la tabla 3.8.

Los resultados obtenidos en las mezclas equimásicas, muestran cómo existe una relación entre el coeficiente de difusión molecular de dichas mezclas y la viscosidad de las mismas. En la figura 3.5, se ha representado el coeficiente de difusión molecular de estas mezcla en función del inverso de su viscosidad dinámica. En todos los casos se ha podido comprobar cómo los datos obtenidos ajustan a una línea que pasa por

Tabla 3.8: Valores del coeficiente de difusión molecular de mezclas binarias de alcanos normales en función de la concentración másica de sus componentes. $D$ corresponde a los valores experimentales y $D_{calc}$ corresponde a los valores calculados mediante la correlación en [84].

| Mezcla | $c_1$ | $D \times 10^{-9}$ ($m^2/s$) | $D_{calc} \times 10^{-9}$ ($m^2/s$) | Dif. (%) |
|---|---|---|---|---|
| $nC_{12}$-$nC_6$ | 0.18 | 2.48 | 2.55 | -3.0 |
| | 0.46 | 2.24 | 2.17 | 3.1 |
| | 0.50 | 2.13 | 2.11 | 0.7 |
| | 0.66 | 1.93 | 1.88 | 2.2 |
| | 0.82 | 1.72 | 1.67 | 2.9 |
| | 0.95 | 1.51 | 1.49 | 1.0 |
| $nC_{12}$-$nC_7$ | 0.16 | 2.09 | 2.04 | 2.6 |
| | 0.42 | 1.84 | 1.80 | 2.2 |
| | 0.50 | 1.70 | 1.73 | -1.7 |
| | 0.63 | 1.64 | 1.61 | 1.6 |
| | 0.80 | 1.48 | 1.46 | 1.2 |
| | 0.94 | 1.37 | 1.33 | 2.9 |
| $nC_{12}$-$nC_8$ | 0.10 | 1.70 | 1.69 | 0.6 |
| | 0.40 | 1.56 | 1.52 | 2.5 |
| | 0.50 | 1.49 | 1.46 | 2.0 |
| | 0.80 | 1.25 | 1.28 | -2.4 |

el origen, cuya pendiente toma el valor de $k$ =1.18×$10^{-12}$ $kgm/s^2$. Por lo tanto, para las mezclas equimolares de alcanos normales, se puede escribir el coeficiente de difusión molecular en función de la viscosidad dinámica de las mezclas mediante la expresión (3.7).

$$D = k\frac{1}{\overline{\mu}} \tag{3.7}$$

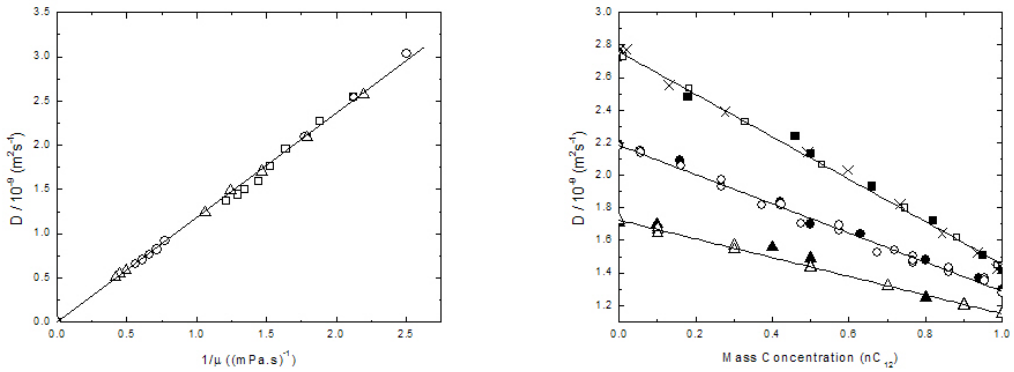


(a) (b)

Figura 3.5: Valores del coeficiente de difusión molecular en función del inverso de la viscosidad dinámica de las mezclas para las series de alcanos normales (□) $nC_6$-$nC_i$, (○) $nC_{10}$-$nC_i$ y (△) $nC_{12}$-$nC_i$ (a) y en función de la concentración másica de los componentes para las mezclas de alcanos normales medidas en este trabajo (■) $nC_{12}$-$nC_6$, (●) $nC_{12}$-$nC_7$, (▲) $nC_{12}$-$nC_8$ y en la bibliografía (□) $nC_{12}$-$nC_6$ en [148], (×) $nC_{12}$-$nC_6$ en [149] , (◯) $nC_{12}$-$nC_7$ en [150] y (△) $nC_{12}$-$nC_8$ en [151] (b).

En cuanto al coeficiente de difusión molecular en función de la concentración, en la literatura se sugiere que este coeficiente es lineal en función de la concentración másica de los componentes [151]. Para comprobar esto, se han graficado los datos disponibles de las series $nC_{12}$-$nC_6$, $nC_{12}$-$nC_7$ y $nC_{12}$-$nC_8$, junto con los disponibles en la literatura para estas mismas series [148, 149, 150, 151] en función de la concentración másica de sus componentes. Tal y como se puede apreciar en la figura 3.5, para todas las series analizadas se comprueba que los datos del coeficiente de difusión molecular se ajustan a una recta definida por la ecuación (3.8).

$$D = c_2 D_1^0 + c_1 D_2^0 \tag{3.8}$$

Adicionalmente, un análisis de estos datos (ver tabla 3.9), muestra que la relación existente entre los coeficientes de difusión propios de los componentes es equiparable a la relación entre sus masas moleculares (ecuación (3.9)).

$$\frac{D_1^0}{D_2^0} = \frac{M_1}{M_2} \tag{3.9}$$

Tabla 3.9: Valores del coeficiente de difusión molecular propio y de las masas moleculares de mezclas binarias de alcanos normales. Datos obtenidos de las Ref. [150] y Ref. [152].

| Mezcla | $D_1^0 \times 10^{-9}$ ($m^2/s$) | $D_2^0 \times 10^{-9}$ ($m^2/s$) | $D_1^0/D_2^0$ | $M_1/M_2$ | $\delta$ (%) |
|---|---|---|---|---|---|
| $nC_{16}$-$nC_6$ | 2.21 | 0.85 | 2.60 | 2.62 | 0.7 |
| $nC_{12}$-$nC_6$ | 2.74 | 1.42 | 1.93 | 1.97 | 2.5 |
| $nC_{12}$-$nC_7$ | 2.19 | 1.30 | 1.69 | 1.70 | 0.6 |
| $nC_{12}$-$nC_8$ | 1.71 | 1.15 | 1.49 | 1.49 | 0.0 |
| $nC_{16}$-$nC_{12}$ | 0.67 | 0.49 | 1.36 | 1.33 | -2.2 |
| $nC_7$-$nC_8$ | 2.80 | 2.43 | 1.15 | 1.14 | -1.7 |

A partir de los resultados obtenidos en las ecuaciones (3.7), (3.8) y (3.9), se puede deducir la expresión (3.10), la cual permite obtener el coeficiente de difusión molecular en mezclas de alcanos normales a cualquier concentración a partir de los datos de las masas moleculares de los componentes de la mezcla, su concentración y la viscosidad de la mezcla a una concentración másica de 0.50. Los datos experimentales para el coeficiente de difusión molecular se han comparado con los obtenidos mediante esta correlación, encontrando para todos los casos, tanto para los datos experimentales determinados en este trabajo (Tabla 3.8) como para los disponibles en la bibliografía (Figura 3.6), diferencias por debajo del 4 %.

$$D = \frac{2k}{\overline{\mu}} \left( \frac{M_1 c_2 + M_2 c_1}{M_1 + M_2} \right) \tag{3.10}$$

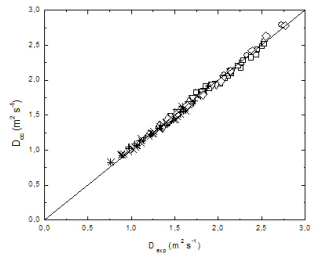

Figura 3.6: Comparación de los datos del coeficiente de difusión molecular para las mezclas de alcanos normales (□) $nC_{10}$-$nC_7$ (Ref. [150]), (○) $nC_{12}$-$nC_6$ (Ref. [148]), (◊) $nC_{12}$-$nC_6$ (Ref. [149]), (▽) $nC_{12}$-$nC_7$ (Ref. [150]), (△) $nC_{12}$-$nC_8$ (Ref. [151]), (+) $nC_{14}$-$nC_7$ (Ref. [150]), (×) $nC_{14}$-$nC_8$ (Ref. [150]), (∗) $nC_{16}$-$nC_7$ (Ref. [148]), y los determinados para estas mezclas utilizando la correlación (3.10).

### Correlación para el coeficiente Soret $S_T$

Tal y como se ha comentado en la sección 1, el efecto Soret tiene gran importancia en numerosos fenómenos. Por ello, el análisis de este fenómeno y la determinación precisa de este coeficiente ha alcanzado un renovado interés.

Para el caso de las mezclas gaseosas y a bajas presiones, resulta que el factor de difusión térmica ($\alpha_T = S_T \cdot T$) es casi independiente de la composición. La teoría cinética de gases predice que el valor de $\alpha_T$ está ligado a las masas moleculares o a la relación de tamaños entre las especies de la mezcla.

En el desarrollo llevado a cabo en diversos estudios [70, 135], se encontró que se puede desarrollar el factor $\alpha_T$ en potencias de la masa reducida de los componentes de la mezcla, siendo los coeficientes de estas expresiones independientes de la concentración, pero estando influenciados por la densidad.

Mientras que en el caso de las mezclas líquidas, también se han desarrollado análisis del coeficiente Soret en [153, 154], basados en la suposición de que el efecto Soret en mezclas binarias es un factor que depende de contribuciones como la masa molecular y la inercia. Utilizando estas premisas, en [153], se llega a la expresión (3.11) para la determinación del coeficiente Soret en mezclas binarias, especialmente en mezclas isotópicas.

$$S_T = S_T^0 + a_M \delta M + b_I \delta I \tag{3.11}$$

Donde $\delta M = (M_1 - M_2)/(M_1 + M_2)$ y $\delta I = (I_1 - I_2)/(I_1 + I_2)$. En esta expresión, los coeficientes $a_M$ y $b_I$ se obtienen de un proceso de ajuste por medio de los datos experimentales. El factor $S_T^0$, se obtiene de forma análoga, siendo, adicionalmente,

dependiente de la concentración de los componentes. En [154], se realiza una variación en la expresión (3.11), donde se sustituyen los términos $\delta M$ y $\delta I$, por la diferencia de masa e inercia respectivamente, tal y como se muestra en la expresión (3.12).

$$S_T = S_T^0 + a_M \Delta M + b_I \Delta I \tag{3.12}$$

Con el fin de comprobar estas teorías para otras mezclas, se ha analizado el rendimiento de la expresión (3.12) para las series equimolares $nC_6$-$nC_i$, $nC_{10}$-$nC_i$, $nC_{12}$-$nC_i$ de alcanos normales. Se han obtenido los coeficientes correspondiente a cada una de las series, tal y como se aprecia en la tabla 3.10, aplicándolos posteriormente a su serie correspondiente y al resto de series analizadas. En las figuras 3.7, 3.8 y 3.9 se presentan los resultados obtenidos para cada una de las tres series de alcanos normales estudiadas.

Tabla 3.10: Valores de los parámetros $S_T^0$, $a_M$ y $b_I$ en la expresión (3.12) para las mezclas $nC_6$-$nC_i$, $nC_{10}$-$nC_i$ y $nC_{12}$-$nC_i$.

| Mezcla | $S_T^0 \times 10^{-3}$ ($K^{-1}$) | $a_M \times 10^{-3}$ ($K^{-1}$ $amu^{-1}$) | $b_I \times 10^{-3}$ ($K^{-1}$ $amu^{-1}$ $\mathring{A}^{-2}$) |
|---|---|---|---|
| $nC_6$-$nC_i$ | 1.68 | 7.44 | 3.55 |
| $nC_{10}$-$nC_i$ | -0.36 | -4.67 | 6.35 |
| $nC_{12}$-$nC_i$ | -0.24 | 4.07 | 2.99 |

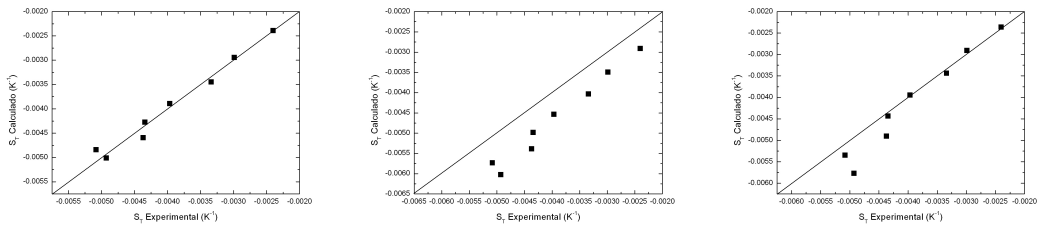


(a) (b) (c)

Figura 3.7: Comparación entre los datos experimentales y los determinados mediante la ecuación (3.12) en [154] para el coeficiente Soret en mezclas binarias de alcanos normales equimolares de la serie $nC_6$-$nC_i$ (a) Usando los datos de ajuste de la serie $nC_6$-$nC_i$; (b) Usando los datos de ajuste de la serie $nC_{10}$-$nC_i$; (c) Usando los datos de ajuste de la serie $nC_{12}$-$nC_i$.

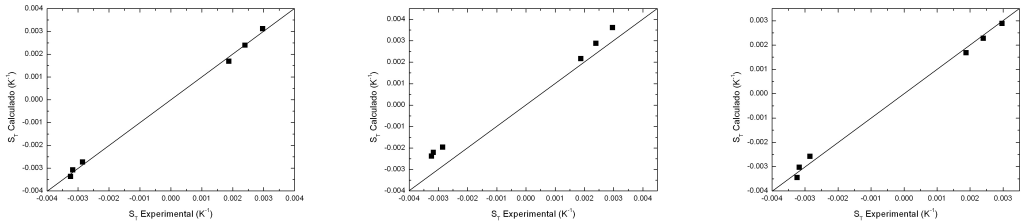


(a) (b) (c)

Figura 3.8: Comparación entre los datos experimentales y los determinados mediante la ecuación (3.12) en [154] para el coeficiente Soret en mezclas binarias de alcanos normales equimolares de la serie $nC_{10}$-$nC_i$ (a) Usando los datos de ajuste de la serie $nC_{10}$-$nC_i$; (b) Usando los datos de ajuste de la serie $nC_6$-$nC_i$; (c) Usando los datos de ajuste de la serie $nC_{12}$-$nC_i$.

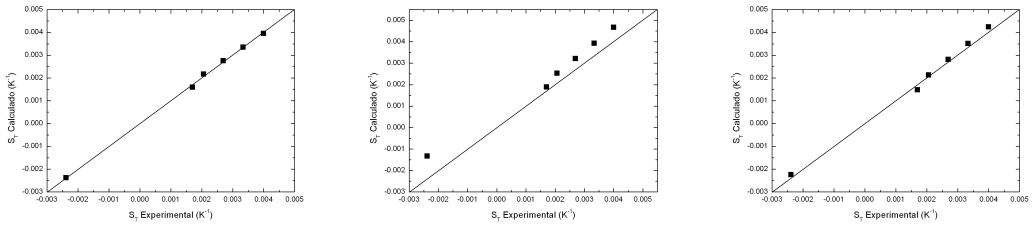


(a) (b) (c)

Figura 3.9: Comparación entre los datos experimentales y los determinados mediante la ecuación (3.12) en [154] para el coeficiente Soret de mezclas binarias de alcanos normales equimolares de la serie $nC_{12}$-$nC_i$ (a) Usando los datos de ajuste de la serie $nC_{12}$-$nC_i$; (b) Mezcla $nC_{10}$-$nC_i$; (c) Usando los datos de ajuste de la serie $nC_{10}$-$nC_i$.

Se ha podido comprobar cómo en general, la capacidad de predicción de la expresión (3.12) es buena, pero se aprecia que al aplicar estos coeficientes a otras series la calidad de predicción de las expresiones disminuye. Cabe mencionar que recientemente en [155], se ha presentado otra nueva versión de esta expresión.

**Correlación para el coeficiente Soret $S_T$ en mezclas de alcanos normales**

En [80], por otro lado, se estudió la influencia de las masas de los componentes sobre el factor de difusión térmica. Se realizaron simulaciones numéricas en mezclas binarias de esferas de Lennard-Jones en un rango de estados termodinámicos extenso y se dedujo que, para mezclas equimoleculares, la relación entre el factor de difusión térmica y el cociente entre la diferencia de masas y la suma de masas (masa reducida) se mantiene aproximadamente constante en todos los estados analizados. Además encontraron que esta relación depende fuertemente de la densidad de la mezcla.

A la vista de los resultados encontrados en estos trabajos, en lo que sigue se va desarrollar una correlación del coeficiente Soret que puede predecir la magnitud de este coeficiente para cualquier concentración. Para ello se hará uso de los datos experimentales del coeficiente Soret obtenidos en este trabajo y calculados a partir de los valores obtenidos del coeficiente de difusión molecular y termodifusión en mezclas binarias de alcanos normales.

Para ello, en primer lugar se van a estudiar las mezclas equimolares de estos compuestos. En la tabla 3.11 se muestran los valores experimentales para el coeficiente Soret obtenidos para las series $nC_6$-$nC_i$, $nC_{10}$-$nC_i$ y $nC_{12}$-$nC_i$ de estos compuestos, a una concentración molar de 0.50 y a una temperatura de $T = 25$ °C.

En la figura 3.10, se muestran los valores del coeficiente Soret en estas series de alcanos normales en función del factor $\rho^4 \delta M$. Los valores del coeficiente Soret pueden ajustarse a una curva de segundo grado, por medio de la ecuación (3.13).

$$S_T = 46{,}44(\rho^4 \delta M)[1 - 1{,}57(\rho^4 \delta M)] \tag{3.13}$$

donde $\delta M = (M_1 - M_2)/(M_1 + M_2)$. En la tabla 3.11, se muestran las diferencias entre los valores experimentales y los determinados por medio de la expresión (3.13). Tal y como se puede apreciar, el acuerdo entre ambos valores es excelente.

En consecuencia, puede concluirse que para una mezcla binaria equimolar de alcanos normales, el coeficiente Soret puede calcularse exclusivamente si se conoce la densidad de la mezcla.

Una vez analizado el caso de las mezclas equimolares, se ha estudiado la dependencia del coeficiente Soret con la composición de las mezclas binarias de alcanos normales. Para ello se han examinado las series binarias $nC_{12}$-$nC_6$, $nC_{12}$-$nC_7$, $nC_{12}$-$nC_8$ y $nC_{10}$-$nC_5$ en todo el rango de concentración. Los valores del coeficiente Soret para estas mezclas se muestran en la tabla 3.12. Para la determinación del coeficiente Soret, en el caso de la mezcla $nC_{12}$-$nC_6$ los datos del coeficiente de difusión molecular y del coeficiente de termodifusión han sido determinados experimentalmente en

Tabla 3.11: Comparación entre los valores experimentales y los calculados con la correlación (3.13) para el coeficiente Soret en las series binarias de alcanos normales $nC_6$-$nC_i$, $nC_{10}$-$nC_i$ y $nC_{12}$-$nC_i$ a una concentración molar de 0.50 y a una temperatura de $T = 25$ °C.

| Mezcla, $x$ =0.5 | $S_T^{Exp} \times 10^{-3}$ ($K^{-1}$) | $S_T^{Calc} \times 10^{-3}$ ($K^{-1}$) | $\delta$( %) |
|---|---|---|---|
| Serie $nC_6$-$nC_i$; $x = 0{,}5$ | | | |
| $nC_{10}$-$nC_6$ | 2.40 | 2.47 | -2.5 |
| $nC_{11}$-$nC_6$ | 2.99 | 2.97 | 0.7 |
| $nC_{12}$-$nC_6$ | 3.34 | 3.43 | -2.5 |
| $nC_{13}$-$nC_6$ | 3.96 | 3.84 | 3.0 |
| $nC_{14}$-$nC_6$ | 4.34 | 4.21 | 2.9 |
| $nC_{15}$-$nC_6$ | 4.37 | 4.56 | -4.1 |
| $nC_{16}$-$nC_6$ | 5.06 | 4.86 | 4.2 |
| $nC_{17}$-$nC_6$ | 4.92 | 5.13 | -4.1 |
| $nC_{18}$-$nC_6$ | 5.27 | 5.38 | -2.0 |
| Serie $nC_{10}$-$nC_i$; $x = 0{,}5$ | | | |
| $nC_{10}$-$nC_5$ | 2.97 | 3.04 | -2.5 |
| $nC_{10}$-$nC_6$ | 2.40 | 2.47 | -2.5 |
| $nC_{10}$-$nC_7$ | 1.88 | 1.87 | 0.6 |
| $nC_{14}$-$nC_{10}$ | 2.09 | 2.17 | -3.7 |
| $nC_{15}$-$nC_{10}$ | 2.76 | 2.61 | 5.5 |
| $nC_{16}$-$nC_{10}$ | 3.10 | 3.01 | 2.8 |
| Serie $nC_{12}$-$nC_i$; $x = 0{,}5$ | | | |
| $nC_{12}$-$nC_5$ | 4.00 | 3.94 | 1.6 |
| $nC_{12}$-$nC_6$ | 3.34 | 3.43 | -2.5 |
| $nC_{12}$-$nC_7$ | 2.79 | 2.89 | -3.4 |
| $nC_{12}$-$nC_8$ | 2.23 | 2.33 | -4.3 |
| $nC_{12}$-$nC_9$ | 1.71 | 1.76 | -2.9 |
| $nC_{16}$-$nC_{12}$ | 2.00 | 2.02 | -0.1 |
| $nC_{17}$-$nC_{12}$ | 2.39 | 2.40 | -0.4 |
| $nC_{18}$-$nC_{12}$ | 2.77 | 2.81 | -1.4 |

esta tesis, al igual que los valores del coeficiente de difusión molecular de las mezclas $nC_{12}$-$nC_7$ y $nC_{12}$-$nC_8$. Los datos del coeficiente de termodifusión de la serie $nC_{10}$-$nC_5$ han sido determinados experimentalmente en [142] y [83] respectivamente. Los

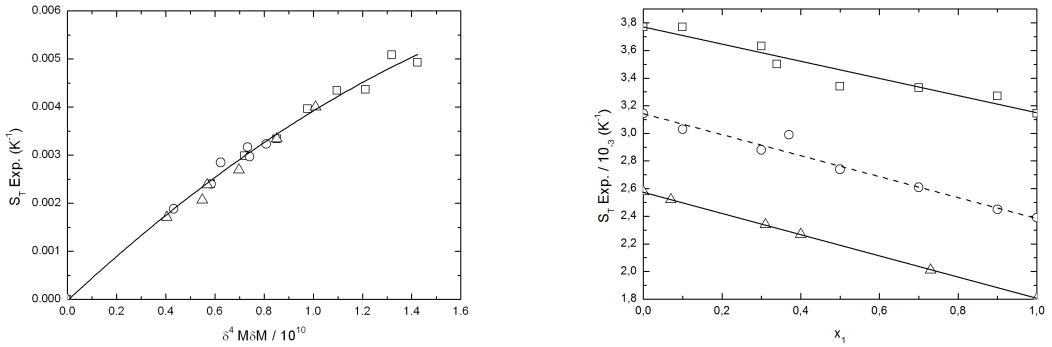


(a) (b)

Figura 3.10: Datos experimentales del coeficiente Soret en función del parámetro $\rho^4 \delta M$ para las series de alcanos normales equimolares (□) $nC_6$-$nC_i$, (○) $nC_{10}$-$nC_i$ y (△) $nC_{12}$-$nC_i$ (a) y en función de la concentración molar para las series de alcanos normales (□) $nC_{12}$-$nC_6$, (○) $nC_{12}$-$nC_7$ y (△) $nC_{12}$-$nC_8$ a una temperatura media de 25 °C (b).

valores utilizados para el coeficiente de termodifusión de las series $nC_{12}$-$nC_6$ y $nC_{12}$-$nC_8$, y de difusión molecular de la serie $nC_{10}$-$nC_5$ y $nC_{12}$-$nC_7$ han sido calculados utilizando las correlaciones (3.3), desarrollada en [83], y (3.10), desarrollada en [84], respectivamente.

En la figura 3.10, se representa el valor del coeficiente Soret de estas mezclas en función de la concentración molar de las mezclas. Tal y como se puede apreciar, el valor del coeficiente Soret depende linealmente de la fracción molar de la mezcla.

Adicionalmente en la tabla 3.13 se muestran los valores obtenidos del coeficiente Soret en las series de alcanos normales equimásicas. Para la determinación del coeficiente Soret de estas mezclas se han utilizado los valores del coeficiente de difusión molecular y termodifusión presentados en la sección 3.1.1 de este documento.

Tabla 3.12: Comparación entre los valores experimentales y los calculados con la correlación (3.26) para el coeficiente Soret en los sistemas $nC_{12}$-$nC_6$, $nC_{12}$-$nC_7$, $nC_{12}$-$nC_8$ y $nC_{10}$-$nC_5$ en todo el rango de concentración y a una temperatura de $T = 25$ °C. * Datos obtenidos de la Ref. [142]; † Datos obtenidos de la Ref. [83]; [a] Determinados con la correlación (3.10) en [84]; [b] Determinados con la correlación (3.3) en [83].

| Mezcla | $x_1$ | $D_T \times 10^{-12}$ $(m^2/s \cdot \mathrm{K})$ | $D \times 10^{-9}$ $(m^2/s)$ | $S_T^{Exp} \times 10^{-3}$ $(\mathrm{K}^{-1})$ | $S_T^{Calc} \times 10^{-3}$ $(\mathrm{K}^{-1})$ | $\delta(\%)$ |
|---|---|---|---|---|---|---|
| $nC_{12}$-$nC_6$ | 0.10 | 9.14 | 2.48 | 3.69 | 3.70 | -0.4 |
| ($\lambda$=0.100) | 0.30 | 7.62 | 2.24 | 3.40 | 3.56 | -4.5 |
| | 0.34 | 7.45 | 2.13 | 3.50 | 3.54 | 1.1 |
| | 0.50 | 6.45 | 1.93 | 3.34 | 3.45 | -2.5 |
| | 0.70 | 5.37 | 1.72 | 3.12 | 3.21 | -5.1 |
| | 0.90 | 4.50 | 1.51 | 2.98 | 3.15 | -5.3 |
| $nC_{12}$-$nC_7$ | 0.10 | 6.34† | 2.09 | 3.03 | 3.22 | -5.8 |
| ($\lambda$=0.144) | 0.30 | 5.30† | 1.84 | 2.88 | 3.05 | -5.6 |
| | 0.37 | 5.08† | 1.70 | 2.99 | 2.99 | 0.0 |
| | 0.50 | 4.74† | 1.70 | 2.79 | 2.89 | -3.4 |
| | 0.70 | 3.86† | 1.48 | 2.61 | 2.72 | -4.1 |
| | 0.90 | 3.35† | 1.37 | 2.45 | 2.55 | -4.3 |
| $nC_{12}$-$nC_8$ | 0.07 | 4.34[b] | 1.70 | 2.55 | 2.67 | -4.4 |
| ($\lambda$=0.171) | 0.31 | 3.62[b] | 1.56 | 2.32 | 2.48 | -6.4 |
| | 0.40 | 3.39[b] | 1.49 | 2.28 | 2.41 | -5.5 |
| | 0.50 | 3.23 | 1.45 | 2.23 | 2.33 | -4.3 |
| | 0.73 | 2.64[b] | 1.25 | 2.11 | 2.15 | 1.5 |
| $nC_{10}$-$nC_5$ | 0.10 | 11.90* | 3.75[a] | 3.17 | 3.14 | 1.0 |
| ($\lambda$=0.041) | 0.20 | 10.36* | 3.36[a] | 3.08 | 3.12 | -1.1 |
| | 0.34 | 9.37* | 3.03 | 3.09 | 3.08 | 0.4 |
| | 0.50 | 8.76* | 2.96 | 2.96 | 3.04 | -2.7 |
| | 0.64 | 7.56* | 2.48[a] | 3.05 | 3.01 | 1.4 |
| | 0.80 | 6.92* | 2.20[a] | 3.15 | 2.97 | 6.0 |

Tabla 3.13: Comparación entre los valores experimentales y los calculados con la correlación (3.26) para el coeficiente Soret en las series de alcanos normales $nC_6$-$nC_i$, $nC_{10}$-$nC_i$ y $nC_{12}$-$nC_i$ a una concentración másica de 0.50 y a una temperatura de $T = 25$ °C.

| Mezcla, $c$ =0.5 | $x_1$ | $\lambda$ | $S_T^{Exp} \times 10^{-3}$ ($K^{-1}$) | $S_T^{Calc} \times 10^{-3}$ ($K^{-1}$) | $\delta$( %) |
|---|---|---|---|---|---|
| Serie $nC_6$-$nC_i$; $c = 0{,}5$ | | | | | |
| $nC_{10}$-$nC_6$ | 0.38 | 0.085 | 2.65 | 2.52 | 5.4 |
| $nC_{11}$-$nC_6$ | 0.36 | 0.099 | 2.93 | 3.05 | -4.0 |
| $nC_{12}$-$nC_6$ | 0.34 | 0.100 | 3.56 | 3.54 | 0.8 |
| $nC_{13}$-$nC_6$ | 0.32 | 0.102 | 3.86 | 3.98 | -3.0 |
| $nC_{14}$-$nC_6$ | 0.30 | 0.108 | 4.52 | 4.40 | 2.7 |
| $nC_{15}$-$nC_6$ | 0.29 | 0.105 | 5.11 | 4.76 | 7.4 |
| $nC_{16}$-$nC_6$ | 0.28 | 0.097 | 5.44 | 5.07 | 7.2 |
| $nC_{17}$-$nC_6$ | 0.26 | 0.108 | 5.87 | 5.40 | 8.7 |
| Serie $nC_{10}$-$nC_i$; $c = 0{,}5$ | | | | | |
| $nC_{10}$-$nC_5$ | 0.34 | 0.041 | 3.05 | 3.08 | -1.1 |
| $nC_{10}$-$nC_6$ | 0.38 | 0.085 | 2.64 | 2.52 | 5.0 |
| $nC_{10}$-$nC_7$ | 0.41 | 0.130 | 2.09 | 1.92 | 9.1 |
| $nC_{16}$-$nC_{10}$ | 0.39 | 0.192 | 3.35 | 3.14 | 6.5 |
| Serie $nC_{12}$-$nC_i$; $c = 0{,}5$ | | | | | |
| $nC_{12}$-$nC_5$ | 0.30 | 0.056 | 4.26 | 4.03 | 5.6 |
| $nC_{12}$-$nC_6$ | 0.34 | 0.100 | 3.56 | 3.54 | 0.8 |
| $nC_{12}$-$nC_7$ | 0.37 | 0.144 | 3.03 | 2.99 | 1.2 |
| $nC_{12}$-$nC_8$ | 0.40 | 0.171 | 2.28 | 2.41 | -5.5 |
| $nC_{12}$-$nC_9$ | 0.43 | 0.178 | 1.73 | 1.80 | -3.7 |
| $nC_{16}$-$nC_{12}$ | 0.43 | 0.178 | 2.05 | 2.07 | -0.9 |
| $nC_{17}$-$nC_{12}$ | 0.41 | 0.188 | 2.32 | 2.48 | -6.3 |

El siguiente paso en el desarrollo de la correlación ha sido el análisis de la dependencia del coeficiente Soret con la masa reducida de los componentes y la fracción molar de la mezcla. Para ello, se parte de la relación (3.6), la cual se deduce de los resultados obtenidos en la sección 3.1.1 de este documento y que se refiere a la linealidad que presenta el coeficiente de termodifusión en función de la concentración másica.

En la expresión (3.6) se puede sustituir la concentración másica por la concentración molar de la mezcla, obteniendo de este modo la ecuación (3.14).

$$D_T = \frac{D^0_{T1} M_2 x_2 + D^0_{T2} M_1 x_1}{M_1 x_1 + M_2 x_2} = D_T(x_1) \tag{3.14}$$

Por otro lado, también se ha deducido que el coeficiente de difusión molecular es lineal en función de la concentración másica de los componentes de la mezcla (ecuación (3.8)). Por lo tanto haciendo un desarrollo análogo al del caso del coeficiente de termodifusión se obtiene la expresión (3.15) para este coeficiente.

$$D = D^0_1 c_2 + D^0_2 c_1 = \frac{D^0_1 M_2 x_2 + D^0_2 M_1 x_1}{M_1 x_1 + M_2 x_2} = D(x_1) \tag{3.15}$$

Por consiguiente, a partir de las expresiones (3.14) y (3.15) el coeficiente Soret puede definirse por medio de la ecuación (3.16).

$$S_T(x_1) = \frac{D_T}{D} = \frac{D^0_{T1} M_2 x_2 + D^0_{T2} M_1 x_1}{D^0_1 M_2 x_2 + D^0_2 M_1 x_1} \tag{3.16}$$

En la sección 3.1.1 ya se dedujo la similitud entre los valores de la relación de masas moleculares de los componentes de una mezcla y la relación de los coeficientes de difusión propios de la mezcla. Introduciendo los términos $S^0_{T1} = D^0_{T1}/D^0_1$ y $S^0_{T2} = D^0_{T2}/D^0_2$ junto con la relación $x_1 + x_2 = 1$, se obtiene la expresión (3.17).

$$S_T(x_1) = S^0_{T1} x_2 + S^0_{T2} x_1 \tag{3.17}$$

La expresión (3.17) reafirma la linealidad del coeficiente Soret con la fracción molar de la mezcla, ya observada en los datos experimentales (Figura 3.10). Adicionalmente, aplicando esta ecuación a mezclas equimolares se obtiene la expresión (3.18).

$$S_T(x = 0{,}5) = \frac{S^0_{T1} + S^0_{T2}}{2} = \overline{S_T} \tag{3.18}$$

Debido a la linealidad puesta de manifiesto previamente (Figura 3.10), los valores límites del coeficiente Soret para $x = 0$ y $x = 1$ toman la forma:

$$S_{T1}^0 = \overline{S_T} + \Delta S_T \tag{3.19}$$

$$S_{T2}^0 = \overline{S_T} - \Delta S_T \tag{3.20}$$

$$\Delta S_T = \frac{S_{T1}^0 - S_{T2}^0}{2} \tag{3.21}$$

De las expresiones anteriores se puede obtener lo siguiente:

$$S_T(x_1) = \overline{S_T} + \Delta S_T(x_2 - x_1) = \overline{S_T}\ \left[1 - \frac{\Delta S_T}{\overline{S_T}}(x_1 - x_2)\right] \tag{3.22}$$

donde se puede deducir que:

$$S_T(x_1) = \overline{S_T}\ \left[1 - \frac{S_{T1}^0 - S_{T2}^0}{S_{T1}^0 + S_{T2}^0}(x_1 - x_2)\right] \tag{3.23}$$

y por lo tanto:

$$S_T(x_1) = \overline{S_T}\ \left[1 - \frac{\frac{S_{T1}^0}{S_{T2}^0} - 1}{\frac{S_{T1}^0}{S_{T2}^0} + 1}(x_1 - x_2)\right] \tag{3.24}$$

Teniendo en cuenta que:

$$\frac{S_{T1}^0}{S_{T2}^0} = \frac{D_2^0}{D_1^0}\frac{D_{T1}^0}{D_{T2}^0} = \frac{M_2}{M_1}\frac{D_{T1}^0}{D_{T2}^0} \tag{3.25}$$

En consecuencia se puede definir la expresión (3.26), para la determinación del coeficiente Soret en función de la concentración molar.

$$S_T(x_1) = \overline{S_T}[1 - \lambda(x_1 - x_2)] \tag{3.26}$$

donde $\lambda$ se define mediante la expresión (3.27):

$$\lambda = \frac{D_{T1}^0 M_2 - D_{T2}^0 M_1}{D_{T1}^0 M_2 + D_{T2}^0 M_1} \tag{3.27}$$

Recordando que $\overline{S_T}$ es una función cuadrática de la densidad, se puede introducir la expresión (3.13) en la ecuación (3.26), consiguiendo la siguiente expresión:

$$S_T(x_1) = 46{,}44\rho^4\delta M[1 - 1{,}57\rho^4\delta M][1 - \lambda(x_1 - x_2)] \tag{3.28}$$

En secciones anteriores de esta tesis se han obtenido dos expresiones, (3.4) y (3.5), las cuales permiten la determinación de los valores límites del coeficiente de termodifusión a partir de los valores de la masa molecular de los componentes de la mezcla y del coeficiente de expansión térmica y viscosidad dinámica de los componentes puros. Por lo tanto, se puede determinar el coeficiente Soret en una mezcla binaria de alcanos normales a cualquier concentración a partir de los datos de la viscosidad dinámica y el coeficiente de expansión térmica de los componentes puros de la mezcla y de la densidad de la mezcla equimolar de los mismos.

En las tablas 3.12 y 3.13, se muestra la diferencia entre los valores experimentales obtenidos para el coeficiente Soret en las mezclas binarias de alcanos analizadas y los valores obtenidos mediante la correlación propuesta. Tal y como se puede ver, el acuerdo entre los datos obtenidos es razonablemente bueno, con una diferencia menor al error experimental estimado para los resultados experimentales del coeficiente Soret.

### 3.1.2. Mezclas Multicomponentes

El estudio de las mezclas compuestas de hidrocarburos realizado durante esta tesis, se ha completado mediante el análisis del coeficiente de difusión térmica de mezclas multicomponentes. En este caso, junto con los alcanos normales, caracterizados por ser componentes lineales, se han estudiado compuestos formados por un anillo (isobutilbenceno y tolueno), y dos anillos (tetrahidronaftalina). Esto permite una mejor modelización de los distintos componentes que se pueden encontrar en los pozos petrolíferos.

Las mediciones se han realizado en mezclas ternarias de estos componentes a diferentes concentraciones de los mismos. Adicionalmente, con el fin de obtener una mayor comprensión del fenómeno de la termodifusión en mezclas ternarias, se ha analizado también el coeficiente de termodifusión de las correspondientes mezclas binarias.

En el caso de las mezclas ternarias, mediante la técnica termogravitacional se determina el coeficiente $\mathbf{D}_T^i$, el cual se refiere al coeficiente fenomenológico de termodifusión del componente $i$ en una mezcla multicomponente.

Los sistemas estudiados en mezclas ternarias han sido dos: tetrahidronaftalina-isobutilbenceno-*n*dodecano (THN-IBB-$nC_{12}$) y tolueno-*n*hexano-*n*dodecano (Tol-$nC_6$-$nC_{12}$). A continuación se van a presentar los resultados obtenidos en cada uno de estos dos sistemas.

**Sistema THN-IBB-$nC_{12}$**

La mezcla THN-IBB-$nC_{12}$ es la que más ampliamente ha sido estudiada de las dos mezclas ternarias analizadas durante esta tesis, ya que esta mezcla representa una buena caracterización de las mezclas multicomponentes en los pozos petrolíferos. Recientemente se ha comenzado una colaboración entre varios de grupos de investigación a escala internacional dentro del marco del proyecto DCMIX de la Agencia Espacial Europea (ESA), para la caracterización por medio de diversas técnicas de esta mezcla. Los experimentos que se van a llevar a cabo incluyen medidas en el espacio en un entorno de microgravedad, y experimentos en condiciones terrestres por medio de diferentes técnicas, como la técnica termogravitacional o la técnica *Optical Beam Deflection*, entre otras.

De acuerdo con el proyecto DCMIX, se han obtenido los primeros resultados de microgravedad. Aún no se han podido analizar la totalidad de los resultados obtenidos, pero los datos preliminares recopilados son prometedores. En la figura 3.11 se puede ver un ejemplo de los datos obtenidos.

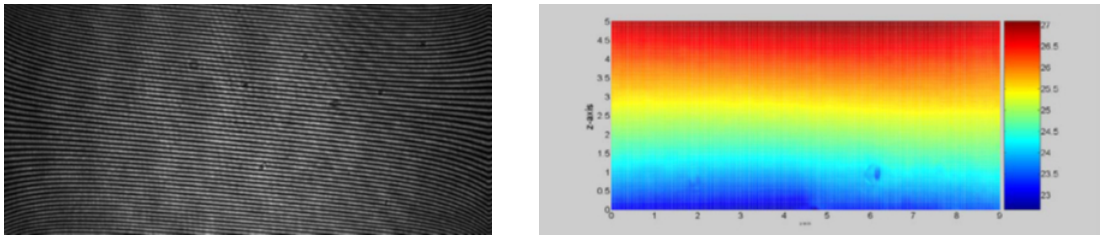

(a) (b)

Figura 3.11: Interferogramas obtenidos de los ensayos de microgravedad dentro del proyecto DCMIX (a) Imagen de la franja de interferencias y (b) Perfil de temperaturas dentro de la célula.

En Mondragon Goi Eskola Politeknikoa se ha contribuido a este proyecto mediante la medición del coeficiente de termodifusión de las mezclas que van a ser objeto de estudio por medio de tres columnas termogravitacionales, dos de configuración plana y otra de configuración cilíndrica (apéndice J). Las concentraciones másicas de las mezclas ternarias, así como de sus correspondientes mezclas binarias se pueden ver en la tabla 3.14. Estas concentraciones de las mezclas ternarias son las que se han definido en el proyecto DCMIX.

La tabla 3.15 muestra los resultados obtenidos a una temperatura de 25 °C en la medida de la densidad, el coeficiente de expansión térmica, el coeficiente de expansión

Tabla 3.14: Concentración másica de cada uno de los componentes en las mezclas ternarias estudiadas y en sus correspondientes mezclas binarias.

| Mezcla | Concentración Másica | | |
|---|---|---|---|
| | THN | IBB | $nC_{12}$ |
| I | 0.1000 | 0.1000 | 0.8000 |
| I.1 | 0.5000 | 0.5000 | 0 |
| I.2 | 0.1111 | 0 | 0.8888 |
| I.3 | 0 | 0.1111 | 0.8888 |
| II | 0.1000 | 0.8000 | 0.1000 |
| II.1 | 0.1111 | 0.8888 | 0 |
| II.2 | 0.5000 | 0 | 0.5000 |
| II.3 | 0 | 0.8888 | 0.1111 |
| III | 0.8000 | 0.1000 | 0.1000 |
| III.1 | 0.8888 | 0.1111 | 0 |
| III.2 | 0.8888 | 0 | 0.1111 |
| III.3 | 0 | 0.5000 | 0.5000 |
| IV | 0.4500 | 0.1000 | 0.4500 |
| IV.1 | 0.8181 | 0.1818 | 0 |
| IV.2 | 0.5000 | 0 | 0.5000 |
| IV.3 | 0 | 0.1818 | 0.8181 |
| V | 0.4000 | 0.2000 | 0.4000 |
| V.1 | 0.6666 | 0.3333 | 0 |
| V.2 | 0.5000 | 0 | 0.5000 |
| V.3 | 0 | 0.3333 | 0.6666 |

másica y la viscosidad dinámica de las mezclas binarias analizadas. Adicionalmente, en esta tabla se muestran los resultados para estas mezclas del coeficiente de termodifusión obtenidos mediante la técnica termogravitacional.

La tabla 3.16 por otra parte, muestra los resultados obtenidos en las mezclas ternarias. En esta tabla se muestran los datos obtenidos en la medida de la densidad, el coeficiente de expansión térmica y la viscosidad dinámica de las mezclas. Adicionalmente, se proporcionan los datos medidos mediante la técnica termogravitacional del coeficiente de termodifusión de los componentes de la mezcla. Estos valores representan el valor medio de los resultados obtenidos mediante las dos columnas planas. En el apéndice K se muestran los ensayos realizados mediante estas columnas. En este caso, se da el valor obtenido de este coeficiente para el componentes más denso

(THN) y menos denso de la mezcla ($nC_{12}$).

Los valores experimentales obtenidos para el coeficiente de termodifusión serán contrastados con los obtenidos mediante otras técnicas, tanto en condiciones terrestres como de microgravedad.

Tabla 3.15: Propiedades termofísicas y coeficiente de termodifusión a una temperatura de 25 °C y diferentes concentraciones másicas de las mezclas binarias estudiadas.

| Mezcla $nC_i$-$nC_j$ | Conc. Másica $nC_i$ | $\rho$ (kg/m$^3$) | $\alpha \times 10^{-3}$ (K$^{-1}$) | $\beta$ | $\mu \times 10^{-3}$ (Pa· s) | $D_T^1 \times 10^{-12}$ (m$^2$/s · K) |
|---|---|---|---|---|---|---|
| THN-IBB | 0.1111 | 861.007 | 9.433 | 0.129 | 1.054 | 3.66 |
| | 0.5000 | 904.514 | 8.876 | 0.128 | 1.363 | 2.84 |
| | 0.6666 | 924.032 | 8.630 | 0.129 | 1.500 | 2.77 |
| | 0.8181 | 942.275 | 8.442 | 0.131 | 1.729 | 2.43 |
| | 0.8889 | 951.097 | 8.347 | 0.130 | 1.813 | 2.50 |
| THN-$nC_{12}$ | 0.1111 | 764.580 | 9.561 | 0.236 | 1.380 | 5.97 |
| | 0.5000 | 841.241 | 8.950 | 0.257 | 1.502 | 6.21 |
| | 0.8889 | 934.359 | 8.368 | 0.287 | 1.815 | 6.18 |
| IBB-$nC_{12}$ | 0.1111 | 754.940 | 9.694 | 0.119 | 1.288 | 3.20 |
| | 0.1818 | 761.368 | 9.678 | 0.121 | 1.223 | 3.28 |
| | 0.3333 | 775.664 | 9.641 | 0.125 | 1.165 | 3.58 |
| | 0.5000 | 792.355 | 9.612 | 0.130 | 1.108 | 3.93 |
| | 0.8889 | 835.454 | 9.590 | 0.144 | 1.008 | 5.28 |

Tabla 3.16: Propiedades termofísicas y coeficiente de termodifusión de la mezcla ternaria THN-IBB-$nC_{12}$ a diferentes concentraciones másicas y a una temperatura de 25°C.

| Mezcla | $c_1$ | $c_3$ | $\rho$ (kg/m$^3$) | $\alpha \times 10^{-3}$ (K$^{-1}$) | $\mu \times 10^{-3}$ (Pa · s) | $\mathbf{D}_T^1 \times 10^{-13}$ (m$^2$/s · K) | $\mathbf{D}_T^3 \times 10^{-13}$ (m$^2$/s · K) |
|---|---|---|---|---|---|---|---|
| THN-IBB-$nC_{12}$ | 0.1000 | 0.8000 | 771.944 | 9.542 | 1.314 | 5.01 | -7.75 |
| | 0.1000 | 0.1000 | 847.553 | 9.470 | 1.053 | 3.31 | -4.84 |
| | 0.4000 | 0.4000 | 842.524 | 9.054 | 1.266 | 13.84 | -14.70 |
| | 0.4500 | 0.4500 | 841.822 | 9.004 | 1.440 | 14.03 | -14.76 |
| | 0.8000 | 0.1000 | 924.348 | 8.483 | 1.719 | 7.72 | -5.39 |

**Sistema Tol-$nC_6$-$nC_{12}$**

El segundo sistema estudiado a lo largo de esta tesis ha sido el compuesto por Tol-$nC_6$-$nC_{12}$. En este sistema se han estudiado 4 mezclas ternarias a diferentes composiciones y sus correspondientes mezclas binarias (Tabla 3.17). El análisis de estas mezclas se ha realizado en colaboración con el grupo de la Prof. Wiegand, del centro de investigación de Jülich. Este grupo utiliza la técnica TDFRS, la cual ha permitido determinar adicionalmente los coeficientes de difusión molecular, termodifusión y Soret en las mezclas binarias, pudiendo de este modo hacer una comparación con los resultados obtenidos mediante la técnica termogravitacional y la técnica *sliding symmetric tubes*.

Tabla 3.17: Concentración másica de cada uno de los componentes en las mezclas ternarias estudiadas y sus correspondientes mezclas binarias.

| Mezcla | Concentración Másica | | |
|---|---|---|---|
| | tolueno (Tol) | *n*-hexano ($nC_6$) | *n*-dodecano ($nC_{12}$) |
| I | 0.2642 | 0.2471 | 0.4885 |
| I.1 | 0.5167 | 0.4832 | 0 |
| I.2 | 0.3510 | 0 | 0.6489 |
| I.3 | 0 | 0.3359 | 0.6640 |
| II | 0.2413 | 0.1367 | 0.6218 |
| II.1 | 0.6405 | 0.3594 | 0 |
| II.2 | 0.2787 | 0 | 0.7212 |
| II.3 | 0 | 0.1781 | 0.8218 |
| III | 0.2920 | 0.3807 | 0.3272 |
| III.1 | 0.4331 | 0.5668 | 0 |
| III.2 | 0.4741 | 0 | 0.5258 |
| III.3 | 0 | 0.5413 | 0.4586 |
| IV | 0.3333 | 0.3333 | 0.3333 |
| IV.1 | 0.5000 | 0.5000 | 0 |
| IV.2 | 0.5000 | 0 | 0.5000 |
| IV.3 | 0 | 0.5000 | 0.5000 |

Las mediciones de las mezclas binarias se han llevado a cabo tanto a 25 °C como a 35 °C, lo que ha permitido hacer un análisis del efecto de la temperatura en las propiedades de transporte de las mezclas binarias. Las mezclas ternarias, por otra parte, únicamente han sido estudiadas a una temperatura media de 25 °C. Las tablas 3.18, 3.19 y 3.20 muestran las diferentes propiedades termofísicas determinadas en las mezclas tanto binarias como ternarias estudiadas a ambas temperaturas.

Tabla 3.18: Propiedades termofísicas a una temperatura de 25 °C y diferentes concentraciones másicas de las mezclas binarias de los compuestos Tol, $nC_6$ y $nC_{12}$ estudiadas.

| Mezcla $nC_i$-$nC_j$ | Conc. Másica $nC_i$ | $\rho$ (kg/m$^3$) | $\alpha \times 10^{-3}$ (K$^{-1}$) | $\beta$ | $\mu \times 10^{-3}$ (Pa· s) | $(\partial n/\partial c)$ | $(\partial n/\partial T)$ $\times 10^{-4}$ |
|---|---|---|---|---|---|---|---|
| Tol-$nC_6$ | 0.053 | 663.583 | 1.369 | 0.243 | 0.324 | - | - |
| | 0.2630 | 699.368 | 1.305 | 0.257 | 0.344 | - | - |
| | 0.4331 | 731.425 | 1.255 | 0.268 | 0.369 | 0.1210 | -5.4800 |
| | 0.5000 | 744.757 | 1.231 | 0.273 | 0.385 | 0.1210 | -5.4800 |
| | 0.5167 | 748.213 | 1.230 | 0.275 | 0.386 | 0.1210 | -5.4900 |
| | 0.6405 | 774.495 | 1.200 | 0.284 | 0.416 | 0.1210 | -5.5000 |
| Tol-$nC_{12}$ | 0.2787 | 772.611 | 1.000 | 0.135 | 0.949 | 0.0691 | -4.6300 |
| | 0.3510 | 780.306 | 1.008 | 0.141 | 0.881 | 0.0691 | -4.6600 |
| | 0.4741 | 793.966 | 1.022 | 0.144 | 0.786 | 0.0691 | -4.8900 |
| | 0.5000 | 796.902 | 1.023 | 0.145 | 0.769 | 0.0691 | -4.9000 |
| $nC_{12}$-$nC_6$ | 0.4586 | 695.112 | 1.174 | 0.129 | 0.524 | 0.0471 | -4.8318 |
| | 0.5000 | 698.780 | 1.158 | 0.128 | 0.564 | 0.0471 | -4.7869 |
| | 0.6640 | 713.777 | 1.094 | 0.129 | 0.712 | 0.0471 | -4.6120 |
| | 0.8218 | 728.268 | 1.035 | 0.129 | 0.940 | 0.0471 | -4.4955 |

Tabla 3.19: Propiedades termofísicas a una temperatura de 35 °C y diferentes concentraciones másicas de las mezclas binarias de los compuestos Tol, $nC_6$ y $nC_{12}$ estudiadas.

| Mezcla $nC_i$-$nC_j$ | Conc. Másica $nC_i$ | $\rho$ (kg/m$^3$) | $\alpha \times 10^{-3}$ (K$^{-1}$) | $\mu \times 10^{-3}$ (Pa· s) | $(\partial n/\partial c)$ | $(\partial n/\partial T)$ $\times 10^{-4}$ |
|---|---|---|---|---|---|---|
| Tol-$nC_6$ | 0.0530 | 654.407 | 1.415 | 0.298 | - | - |
| | 0.2630 | 690.160 | 1.345 | 0.316 | - | - |
| | 0.4331 | 722.131 | 1.287 | 0.337 | 0.1205 | -5.5400 |
| | 0.5000 | 735.573 | 1.260 | 0.352 | 0.1205 | -5.5400 |
| | 0.5167 | 735.944 | 1.256 | 0.353 | 0.1205 | -5.5500 |
| | 0.6405 | 765.235 | 1.216 | 0.378 | 0.1205 | -5.5700 |
| Tol-$nC_{12}$ | 0.2787 | 764.853 | 1.017 | 0.837 | 0.0676 | -4.5800 |
| | 0.3510 | 772.411 | 1.024 | 0.765 | 0.0676 | -4.6600 |
| | 0.4741 | 785.827 | 1.038 | 0.686 | 0.0676 | -4.8200 |
| | 0.5000 | 788.715 | 1.040 | 0.674 | 0.0676 | -4.8800 |
| $nC_{12}$-$nC_6$ | 0.4586 | 686.825 | 1.203 | 0.466 | 0.0480 | -4.9042 |
| | 0.5000 | 690.604 | 1.185 | 0.496 | 0.0480 | -4.8704 |
| | 0.6640 | 706.090 | 1.113 | 0.622 | 0.0480 | -4.6661 |
| | 0.8218 | 720.818 | 1.090 | 0.806 | 0.0480 | -4.5180 |

Tabla 3.20: Propiedades termofísicas de la mezcla ternaria Tol-$nC_6$-$nC_{12}$ a diferentes concentraciones másicas y a una temperatura de 25 °C.

| Mezcla | $c_1$ | $c_2$ | $c_3$ | $\rho$ (kg/m$^3$) | $\alpha \times 10^{-3}$ (K$^{-1}$) | $\mu \times 10^{-3}$ (Pa · s) |
|---|---|---|---|---|---|---|
| Tol-$nC_6$-$nC_{12}$ | 0.2642 | 0.2471 | 0.4885 | 754.713 | 1.047 | 0.753 |
| | 0.2413 | 0.1367 | 0.6218 | 746.337 | 1.091 | 0.624 |
| | 0.2920 | 0.3807 | 0.3272 | 736.305 | 1.151 | 0.513 |
| | 0.3333 | 0.3333 | 0.3333 | 744.643 | 1.137 | 0.524 |

En la tabla 3.21 se muestran los valores obtenidos para el coeficiente de difusión molecular, obtenidos experimentalmente mediante la técnica TDFRS y para el caso de la mezcla $nC_{12}$-$nC_6$ mediante la técnica SST. Adicionalmente en esta tabla se muestran los valores de este coeficiente para la mezcla $nC_{12}$-$nC_6$ determinados mediante la ecuación (3.10) desarrollada en [84].

Tabla 3.21: Resultados para el coeficiente de difusión molecular a temperaturas de 25 y 35 °C para las mezclas binarias Tol-$nC_6$, Tol-$nC_{12}$ y $nC_{12}$-$nC_6$ medidos mediante la técnica TDFRS y los obtenidos para la mezcla $nC_{12}$-$nC_6$ determinados mediante la técnica SST y la ecuación (3.10) desarrollada en [84].

| Mezcla $nC_i$-$nC_j$ | Conc. Másica $nC_i$ | $D \times 10^{-9}$ (m$^2$/s) 25°C | | | 35°C | |
|---|---|---|---|---|---|---|
| | | TDFRS | SST | Corr. D [84] | TDFRS | Corr. D [84] |
| Tol-$nC_6$ | 0.4331 | 2.99 | - | - | 3.63 | - |
| | 0.5000 | 2.94 | - | - | 3.34 | - |
| | 0.5167 | 2.85 | - | - | 3.29 | - |
| | 0.6405 | 2.49 | - | - | 2.80 | - |
| Tol-$nC_{12}$ | 0.2787 | 1.34 | - | - | 1.45 | - |
| | 0.3510 | 1.40 | - | - | 1.64 | - |
| | 0.4741 | 1.44 | - | - | 1.59 | - |
| | 0.5000 | 1.47 | - | - | 1.75 | - |
| $nC_{12}$-$nC_6$ | 0.4586 | 2.54 | 2.26 | 2.15 | 2.89 | 2.44 |
| | 0.5000 | 2.13 | 2.13 | 2.09 | 2.75 | 2.38 |
| | 0.6640 | 2.24 | 1.93 | 1.87 | 2.59 | 2.12 |
| | 0.8218 | 1.79 | 1.73 | 1.65 | 2.17 | 1.88 |

En el caso del coeficiente de termodifusión, en la tabla 3.22, se presentan los resultados obtenidos mediante la técnica TDRFS y los determinados utilizando la técnica termogravitacional. Los resultados de la técnica termogravitacional representan una media de los valores obtenidos mediante la columna de configuración plana y configuración cilíndrica. El coeficiente de termodifusión de la mezcla $nC_{12}$-$nC_6$ también ha sido determinado por medio de la expresión (3.3), desarrollada en [83].

La tabla 3.23 muestra los resultados obtenidos para el coeficiente Soret en las mezclas binarias estudiadas tanto a 25 °C como a 35 °C. Por un lado se muestran los resultados obtenidos mediante la técnica TDFRS, mientras que para la mezcla $nC_{12}$-$nC_6$ se muestran adicionalmente los datos determinados utilizando la combinación de las técnicas termogravitacional y *sliding symmetric tubes*.

Tabla 3.22: Resultados para el coeficiente de termodifusión a temperaturas de 25 y 35 °C para las mezclas binarias Tol-$nC_6$, Tol-$nC_{12}$ y $nC_{12}$-$nC_6$ medidos mediante la técnica TDFRS y los obtenidos para la mezcla $nC_{12}$-$nC_6$ determinados mediante la expresión (3.3) desarrollada en [83].

| Mezcla $nC_i$-$nC_j$ | Conc. Másica $nC_i$ | $D_T \times 10^{-12}$ ($m^2/s \cdot K$) 25°C TDFRS | TC | Corr. $D_T$ [83] | 35°C TDFRS | TC | Corr. $D_T$ [83] |
|---|---|---|---|---|---|---|---|
| Tol-$nC_6$ | 0.0530 | - | 12.80 | - | - | 13.08 | - |
| | 0.2630 | - | 12.77 | - | - | 13.71 | - |
| | 0.4331 | 12.61 | 13.38 | - | 14.09 | 14.36 | - |
| | 0.5000 | 13.75 | 13.51 | - | 14.68 | 14.44 | - |
| | 0.5167 | 13.73 | 13.70 | - | 14.79 | 14.59 | - |
| | 0.6405 | 13.94 | 14.09 | - | 14.65 | 14.82 | - |
| Tol-$nC_{12}$ | 0.2787 | 1.61 | 1.95 | - | 1.74 | 2.41 | - |
| | 0.3510 | 2.06 | 2.38 | - | 2.41 | 2.88 | - |
| | 0.4741 | 2.97 | 3.14 | - | 3.29 | 3.64 | - |
| | 0.5000 | 3.37 | 3.39 | - | 3.96 | 3.87 | - |
| $nC_{12}$-$nC_6$ | 0.4586 | 8.39 | 8.02 | 7.72 | 9.01 | 8.46 | 8.91 |
| | 0.5000 | 6.81 | 7.67 | 7.38 | 8.26 | 7.97 | 8.58 |
| | 0.6640 | 5.54 | 6.69 | 6.54 | 7.09 | 7.12 | 7.61 |
| | 0.8218 | 5.60 | 5.79 | 5.53 | 6.36 | 6.61 | 6.80 |

El coeficiente de termodifusión en las mezclas ternarias ha sido únicamente determinado en este caso mediante la técnica termogravitacional. Se ha medido el coeficiente de termodifusión de dos de los tres componentes de la mezcla. En este caso han sido el componente más denso (tolueno) y el menos denso ($n$-hexano). Los resultados obtenidos para este coeficiente se muestran en la tabla 3.24.

Tabla 3.23: Resultados para el coeficiente Soret a temperaturas de 25 y 35 °C para las mezclas binarias Tol-$nC_6$, Tol-$nC_{12}$ y $nC_{12}$-$nC_6$ obtenidos mediante la técnica TDFRS y los obtenidos para la mezcla $nC_{12}$-$nC_6$ determinados mediante combinación de las técnicas TC y SST.

| Mezcla $nC_i$-$nC_j$ | Conc. Másica $nC_i$ | $S_T \times 10^{-3}$ ($K^{-1}$) 25 °C TDFRS | SST-TC | 35 °C TDFRS |
|---|---|---|---|---|
| Tol-$nC_6$ | 0.4331 | 4.22 | - | 3.88 |
| | 0.5000 | 4.67 | - | 4.39 |
| | 0.5167 | 4.82 | - | 4.49 |
| | 0.6405 | 5.59 | - | 5.23 |
| Tol-$nC_{12}$ | 0.2787 | 1.20 | - | 1.20 |
| | 0.3510 | 1.47 | - | 1.47 |
| | 0.4741 | 2.06 | - | 2.06 |
| | 0.5000 | 2.29 | - | 2.27 |
| $nC_{12}$-$nC_6$ | 0.4586 | 3.31 | 3.54 | 3.11 |
| | 0.5000 | 3.20 | 3.60 | 3.00 |
| | 0.6640 | 2.48 | 3.46 | 2.74 |
| | 0.8218 | 3.12 | 3.34 | 2.93 |

Tabla 3.24: Resultados obtenidos mediante la técnica TC para la mezcla ternaria Tol-$nC_6$-$nC_{12}$ a una temperatura de 25 °C y a diferentes concentraciones másicas y los obtenidos mediante la expresión (3.29) [17].

| Mezcla | Conc. Másica $c_1$ | $c_2$ | $c_3$ | $\mathbf{D}_T \times 10^{-12}$ ($m^2/s \cdot K$) Exp. $\mathbf{D}_T^1$ | $\mathbf{D}_T^2$ | Corr. (3.29) $\mathbf{D}_T^1$ | $\mathbf{D}_T^2$ | Dif. (%) $\mathbf{D}_T^1$ | $\mathbf{D}_T^2$ |
|---|---|---|---|---|---|---|---|---|---|
| Tol-$nC_6$-$nC_{12}$ | 0.2642 | 0.2471 | 0.4885 | 0.57 | -0.70 | 0.58 | -0.83 | -0.9 | -16.1 |
| | 0.2413 | 0.1367 | 0.6218 | 0.90 | -1.47 | 0.93 | -1.41 | -3.8 | 4.1 |
| | 0.2920 | 0.3807 | 0.3272 | 1.55 | -2.02 | 1.48 | -2.07 | 4.6 | -2.7 |
| | 0.3333 | 0.3333 | 0.3333 | 1.63 | -2.01 | 1.60 | -1.98 | 1.8 | 1.6 |

### 3.1.3. Discusión

Los resultados obtenidos en las dos mezclas ternarias analizadas, muestran como en todos los casos, el componente más denso se dirige hacia la zona fría, mientras que el componente menos denso se dirige hacia la caliente. Este comportamiento está de acuerdo con el observado en mezclas ternarias por otros grupos [122].

Sin embargo, a la hora de la realización de los ensayos mediante la columna termogravitacional plana de menor longitud, se ha podido comprobar durante el análisis de las muestras, que la separación de los componentes dentro de la columna es menor en el caso de algunas concentraciones de las mezclas ternarias, lo que muestra que el proceso de análisis es muy sensible, comparado con el caso de las mezclas binarias.

Adicionalmente, se ha podido comprobar cómo, para este tipo de muestras el proceso de calibración tiene una gran importancia. Se ha observado que para las mezclas analizadas existe un cierto comportamiento lineal entre la densidad y el índice de refracción con la concentración (ver apéndice L). A mayor linealidad mayor es la dificultad para determinar la concentración de los componentes de las mezclas ternarias en base al ajuste de calibración. Un comportamiento similar ya había sido observado en [156], donde se apreciaba que ciertas concentraciones de los componentes en mezclas ternarias eran más idóneas que otras a la hora de determinar la separación de cada componente mediante técnicas ópticas.

Por esta razón, y con el fin de subsanar la sensibilidad en la lectura de la concentración en el estado estacionario a partir de las medidas de densidad e índice de refracción, se ha utilizado la nueva columna termogravitacional plana de mayor longitud. Esta cualidad hace que la separación de los componentes dentro de la columna sea mayor (casi el doble: 1.96 veces mayor), y por lo tanto también aumenta la sensibilidad de la medida. Se repitieron los ensayos en las mezclas ternarias analizadas en este estudio, pudiendo comprobar que aunque se mejoraba la calidad de los resultados obtenidos mediante esta nueva columna, las diferencias con respecto a la columna de menor longitud no eran importantes. Teniendo en cuenta estos resultados y considerando la influencia del proceso de calibración en la medida, se ha determinado que para estas mezclas y mediante este procedimiento de análisis, no se puede obtener un error experimental mejor que el 10 %.

Con el fin de analizar la influencia de la concentración de la mezcla en el coeficiente de termodifusión de cada componente para este tipo de mezclas, los datos obtenidos para la mezcla THN-IBB-$nC_{12}$ se han añadido a los medidos para esta misma mezcla en [17]. En la figura 3.12 se muestran los resultados del coeficiente de termodifusión de los componentes THN y $nC_{12}$ en función de la concentración. Estos datos muestran cómo el coeficiente de termodifusión para esta mezcla alcanza

su máximo valor cuando la concentración de los componentes es similar.

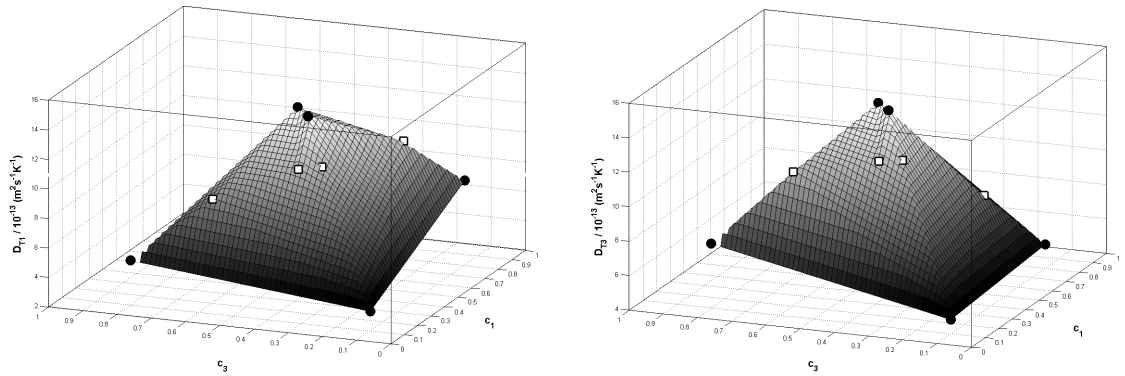


(a) (b)

Figura 3.12: Valores del coeficiente de termodifusión de los compuestos de la mezcla THN-IBB-$nC_{12}$ a diferentes concentraciones y una temperatura media de 25 °C: (a) Valores para el componente THN; (b) Valores para el componente $nC_{12}$.

Adicionalmente, los resultados obtenidos han servido para comprobar la eficiencia de varias correlaciones para la determinación de las propiedades de transporte en mezclas binarias y ternarias [17, 83, 84]. En el caso de las correlaciones propuestas en [83] y [84] se puede observar cómo los valores determinados para el coeficiente de difusión molecular (Tabla 3.21) y termodifusión (Tabla 3.22) de las mezclas binarias están en buen acuerdo con los determinados experimentalmente.

En el caso de la correlación propuesta en [17], esta permite la predicción del coeficiente de termodifusión en mezclas ternarias a partir de los coeficientes de termodifusión de las correspondientes mezclas binarias (apéndice A). La correlación propuesta, la cuál está basada en un regla aditiva desarrollada en [117], está definida por la expresión (3.29).

$$\mathbf{D}_T^i \frac{\nu_i}{\alpha_i} = D_T^{ij} c_i c_j \frac{\nu_{ij}}{\alpha_{ij}} + D_T^{ik} c_i c_k \frac{\nu_{ik}}{\alpha_{ik}} \tag{3.29}$$

Gracias a que se dispone de los datos de las mezclas ternarias y de sus correspondientes mezclas binarias, se ha podido aplicar la ecuación (3.29) a las dos mezclas ternarias estudiadas. Se ha podido comprobar el buen funcionamiento de esta correlación con diferencias, en general, entorno al 10 % de media. En la tabla 3.24, se muestran los datos para el coeficiente de termodifusión en la mezcla Tol-$nC_6$-$nC_{12}$ determinados de forma experimental y mediante la correlación propuesta. En la tabla

3.25 se muestra esta misma comparación para la mezcla THN-IBB-$nC_{12}$, incluyéndose los datos de las diferencias encontradas en la determinación de este coeficiente para cada componente mediante los dos métodos.

Tabla 3.25: Comparación entre los datos experimentales y los obtenidos mediante la ecuación (3.29) desarrollada en [17] para el coeficiente de termodifusión de la mezcla ternaria THN-IBB-$nC_{12}$ a diferentes concentraciones y una temperatura de 25 °C.

| Mezcla | Conc. Másica | | | $\mathbf{D}_T \times 10^{-13}$ ($m^2/s \cdot K$) | | | | | |
|---|---|---|---|---|---|---|---|---|---|
| | | | | Exp. | | Corr. (3.29) | | Dif. (%) | |
| | $c_1$ | $c_2$ | $c_3$ | $\mathbf{D}_T^1$ | $\mathbf{D}_T^2$ | $\mathbf{D}_T^1$ | $\mathbf{D}_T^2$ | $\mathbf{D}_T^1$ | $\mathbf{D}_T^2$ |
| THN-IBB-$nC_{12}$ | 0.1000 | 0.1000 | 0.8000 | 5.01 | -7.75 | 5.32 | -7.65 | 7.0 | -1.3 |
| | 0.1000 | 0.8000 | 0.1000 | 3.31 | -4.84 | 3.84 | -5.00 | -15.8 | 3.3 |
| | 0.4000 | 0.2000 | 0.4000 | 13.84 | -14.70 | 14.46 | -14.63 | 4.5 | -0.5 |
| | 0.4500 | 0.1000 | 0.4500 | 14.03 | -14.76 | 14.47 | -14.50 | 3.1 | -1.7 |
| | 0.8000 | 0.1000 | 0.1000 | 7.72 | -5.69 | 7.17 | -5.50 | -7.2 | 2.1 |

Como se ha comentado anteriormente, la determinación experimental con precisión del coeficiente de termodifusión en mezclas ternarias es sumamente complicada. Por un lado se tiene la influencia de la calibración sobre la determinación de las concentraciones, y sobre todo, de la magnitud de la separación estacionaria de cada componente.

## 3.2. Mezclas Acuosas

Tal y como se ha comentado en la sección 1, el estudio experimental de las mezclas acuosas es de gran interés, debido a los escasos datos bibliográficos existentes y a las dificultades que presenta su medición. En esta tesis doctoral se han analizado mezclas binarias de este tipo, compuestas por agua e isopropanol. Más concretamente se han realizado medidas en esta mezcla abarcando todo el rango de concentración y a una temperatura media de 25 °C, comparando los resultados obtenidos con los determinados mediante las técnicas *Optical Beam Deflection*, utilizada por el grupo del Prof. Köhler, de la universidad de Bayreuth (UB), y *Optical Digital Interferometry*, utilizada por el grupo de la Prof. Shevtsova, de la universidad Libre de Bruselas (ULB). Adicionalmente se han comparado los datos obtenidos con los medidos por la Prof. Shevtsova para esta misma mezcla en un entorno de microgravedad en el experimento IVIDIL.

### 3.2.1. Propiedades Termofísicas y Factores de Contraste

La determinación de las propiedades de transporte mediante las técnicas utilizadas en este estudio requiere de la medida previa de varias de las propiedades de las mezclas. En el caso de las medidas realizadas en el laboratorio de fluidos de Mondragon Goi Eskola Politeknikoa, se hace necesaria la medida de la viscosidad dinámica ($\mu$), el coeficiente de expansión térmica ($\alpha$) y el coeficiente de expansión másica ($\beta$) de las mezclas estudiadas (ver tabla 3.26). Estos coeficientes se han medido utilizando la metodología descrita en el apartado 2.

Tabla 3.26: Propiedades termofísicas de la mezcla agua-isopropanol a diferentes concentraciones másicas medidas a una temperatura de 25 °C.

| $c$, agua | $\mu \times 10^{-3}$ (Pa · s) | $\alpha \times 10^{5}$ ($K^{-1}$) | $\beta \times 10^{2}$ | $\rho$ (kg/m$^3$) |
|---|---|---|---|---|
| 0.990 | 0.946 | 25.64 | 18.56 | 995.16 |
| 0.950 | 1.126 | 27.70 | 16.24 | 988.35 |
| 0.900 | 1.416 | 33.34 | 14.37 | 980.89 |
| 0.850 | 1.748 | 42.79 | 14.28 | 974.96 |
| 0.800 | 2.093 | 55.64 | 16.44 | 966.55 |
| 0.750 | 2.390 | 67.23 | 19.92 | 957.89 |
| 0.700 | 2.604 | 75.05 | 22.53 | 947.75 |
| 0.650 | 2.801 | 80.35 | 23.99 | 936.92 |
| 0.600 | 2.927 | 84.44 | 25.24 | 925.60 |
| 0.500 | 3.056 | 90.04 | 26.06 | 902.37 |
| 0.400 | 3.015 | 95.23 | 27.17 | 878.74 |
| 0.300 | 2.816 | 100.49 | 27.89 | 855.03 |
| 0.200 | 2.521 | 106.10 | 28.90 | 831.15 |
| 0.100 | 2.172 | 110.48 | 30.63 | 806.89 |

Adicionalmente, las técnicas ópticas requieren de la medición de los factores de contraste de las mezclas, los cuales se pueden ver en la tabla 3.27. Para este estudio, los valores para estos coeficientes han sido determinados en la UB por el grupo del Prof. Köhler.

Tabla 3.27: Variación del índice de refracción en función de la temperatura, $(\partial n/\partial T)_{p,c}$, y la concentración, $(\partial n/\partial c)_{p,T}$, para la mezcla agua-isopropanol a diferentes concentraciones másicas y a $T = 25$ °C.

| $c$, agua | $(\partial n/\partial T) \times 10^{-4}$ ($K^{-1}$) | $(\partial n/\partial c) \times 10^{-2}$ |
|---|---|---|
| 0.000 | -4.266 | - |
| 0.052 | -4.369 | 0.336 |
| 0.100 | -4.324 | -0.517 |
| 0.150 | -4.241 | -1.02 |
| 0.200 | -4.138 | -1.45 |
| 0.250 | -4.033 | -1.86 |
| 0.300 | -3.921 | -2.25 |
| 0.351 | -3.809 | -2.62 |
| 0.409 | -3.681 | -3.01 |
| 0.451 | -3.585 | -3.30 |
| 0.500 | -3.474 | -3.64 |
| 0.547 | -3.359 | -4.02 |
| 0.600 | -3.217 | -4.56 |
| 0.650 | -3.062 | -5.22 |
| 0.700 | -2.854 | -6.04 |
| 0.747 | -2.574 | -6.97 |
| 0.800 | -2.127 | -8.18 |
| 0.854 | -1.653 | -8.99 |
| 0.899 | -1.343 | -9.23 |
| 0.926 | - | -9.14 |
| 0.950 | -1.135 | -8.91 |
| 0.975 | - | -8.49 |
| 1.000 | -1.060 | -7.89 |

### 3.2.2. Resultados de las Técnicas Termogravitacional y *Sliding Symmetric Tubes*

En primer lugar se muestran los resultados obtenidos para el coeficiente Soret en la mezcla agua-isopropanol, determinados utilizando una combinación de la técnicas termogravitacional y técnica *sliding symmetric tubes*.

Se ha utilizado la técnica termogravitacional (TC) de configuración plana para

la medición del coeficiente de termodifusión en la mezcla de agua-isopropanol en todo el rango de concentraciones. Por otro lado, las medidas del coeficiente de difusión molecular se han realizado utilizando la técnica *sliding symmetric tubes* (SST). Posteriormente se han utilizado los resultados obtenidos para estos coeficientes para calcular el coeficiente Soret de las mezclas por medio de la expresión (1.1). En la tabla 3.28 se muestran los resultados obtenidos para el coeficiente de difusión, coeficiente de termodifusión y coeficiente Soret de las mezclas estudiadas.

Tabla 3.28: Coeficientes de difusión, termodifusión y Soret medidos mediante las técnicas termogravitacional y *sliding symmetric tubes* a una temperatura de 25 °C.

| $c$, agua | $D \times 10^{-10}$ ($m^2/s$) | $D_T \times 10^{-13}$ ($m^2/s \cdot K$) | $S_T \times 10^{-3}$ ($K^{-1}$) |
|---|---|---|---|
| 0.100 | 6.13 | 4.72 | 0.77 |
| 0.200 | 3.50 | 8.44 | 2.41 |
| 0.300 | 2.45 | 10.10 | 4.13 |
| 0.400 | 1.80 | 10.45 | 5.80 |
| 0.500 | 1.68 | 9.88 | 5.89 |
| 0.600 | 1.89 | 8.83 | 4.67 |
| 0.650 | 2.08 | 7.54 | 3.62 |
| 0.700 | 2.47 | 5.27 | 2.13 |
| 0.750 | 3.62 | 4.01 | 1.11 |
| 0.800 | 5.03 | - | - |
| 0.850 | 5.51 | - | - |
| 0.900 | 7.29 | - | - |
| 0.950 | 8.77 | - | - |
| 0.990 | 9.66 | - | - |

El sistema estudiado, presenta un cambio de signo del coeficiente Soret en función de la concentración. Esto quiere decir que el componente más denso (agua) se dirige a la zona caliente en vez de hacerlo hacia la zona fría. En el caso de la técnica termogravitacional esto conlleva al problema de estabilidad termohidrodinámica, el cual distorsiona la separación de los componentes. Debido a este efecto, ha sido imposible la determinación del coeficiente de termodifusión mediante la técnica termogravitacional para las mezclas de agua-isopropanol con concentración másica superior a 0.75 de agua. Esto a su vez a impedido el cálculo del coeficiente Soret, ya que para este rango de concentraciones, únicamente se disponían de los datos del coeficiente de difusión molecular obtenidos mediante la técnica *sliding symmetric tubes*.

### 3.2.3. Resultados *Optical Beam Deflection*

El sistema agua-isopropanol también ha sido estudiado por parte del grupo del Prof. Köhler. Este grupo ha utilizado la técnica *optical beam deflection* para llevar a cabo las medidas de las propiedades de transporte. En este caso, el sistema de medida y análisis de esta técnica permite la medición de los tres coeficientes ($D$, $D_T$ y $S_T$).

Gracias a las dimensiones de la célula de medición utilizada por este grupo, con una altura de $H$ =1.022±0.002 mm, el dispositivo puede utilizarse para la medición de mezclas que presenten Soret negativo. Para ello, al aplicar el gradiente de temperatura, es la placa inferior la que se encuentra a mayor temperatura. Seleccionando un gradiente de temperatura adecuado, se consiguen valores pequeños del número de Rayleigh, lo que permite realizar la medida en este tipo de mezclas [91].

En la tabla 3.29 se presentan los resultados obtenidos mediante esta técnica para el sistema agua-isopropanol en todo el rango de concentración a una temperatura media de 25 °C.

### 3.2.4. Resultados *Optical Digital Interferometry*

El grupo de la Prof. Shevtsova ha realizado medidas en el sistema agua-isopropanol, pero en esta ocasión utilizando la técnica *optical digital interferometry*. Mediante esta técnica se han determinado el coeficiente de difusión molecular y el coeficiente Soret de las mezclas, obteniéndose el coeficiente de termodifusión usando la relación $D_T = D \cdot S_T$.

En las mezclas que presentan Soret negativo, debido a las dimensiones de la célula utilizada ($18 \times 18 \times 6{,}5$ mm), se genera una inestabilidad convectiva complicada de eliminar. Esto impide la medida de los coeficientes de difusión molecular y Soret en dichos rangos de concentración. El grupo de la Prof. Shevtsova, ha conseguido estimar el valor del coeficiente Soret en uno de estos puntos alrededor de la concentración en la que se produce el cambio de signo del coeficiente Soret (±0,75 en concentración másica de agua). Esto se ha conseguido por medio de la extrapolación de datos positivos del coeficiente Soret medidos próximos a la concentración en la que se produce el cambio de signo. La tabla 3.30 muestra los datos medidos mediante esta técnica así como el dato estimado para el coeficiente Soret negativo.

Dentro del experimento IVIDIL [129, 130], se han llevado a cabo diferentes medidas en condiciones de microgravedad en la mezcla agua-isopropanol a varias concentraciones utilizando una técnica similar al método *optical digital interferometry* [129]. Las condiciones en las que se han realizado algunas de estas mediciones las hacen adecuadas para su comparación con los resultados obtenidos por el resto de

Tabla 3.29: Coeficientes de difusión, termodifusión y Soret medidos en la mezcla agua-isopropanol por la UB en todo el rango de concentración y a una temperatura T = 25 °C.

| $c$, agua | $D \times 10^{-10}$ ($m^2/s$) | $D_T \times 10^{-13}$ ($m^2/s \cdot K$) | $S_T \times 10^{-3}$ ($K^{-1}$) |
|---|---|---|---|
| 0.200 | 3.71 | 13.2 | 3.55 |
| 0.250 | 3.05 | 12.7 | 4.16 |
| 0.300 | 2.60 | 11.7 | 4.51 |
| 0.351 | 2.08 | 11.2 | 5.37 |
| 0.409 | 1.89 | 10.6 | 5.62 |
| 0.451 | 1.79 | 10.6 | 5.91 |
| 0.500 | 1.64 | 9.57 | 5.83 |
| 0.547 | 1.58 | 9.04 | 5.72 |
| 0.600 | 1.67 | 8.84 | 5.30 |
| 0.650 | 1.96 | 8.29 | 4.24 |
| 0.700 | 2.43 | 5.97 | 2.46 |
| 0.747 | 3.25 | -0.61 | -0.19 |
| 0.800 | 4.98 | -18.3 | -3.67 |
| 0.854 | 6.42 | -43.9 | -6.83 |
| 0.900 | 7.49 | -66.4 | -8.87 |
| 0.950 | 8.95 | -90.7 | -10.14 |

laboratorios incluidos en este estudio. Los valores determinados en el experimento IVIDIL para los diferentes coeficientes se muestran en la tabla 3.31.

Tabla 3.30: Coeficientes de difusión, termodifusión y Soret medidos en la mezcla agua-isopropanol por la ULB a diversas concentraciones másicas y a una temperatura de 25 °C.

| $c$, agua | $D \times 10^{-10}$ ($m^2/s$) | $D_T \times 10^{-13}$ ($m^2/s \cdot K$) | $S_T \times 10^{-3}$ ($K^{-1}$) |
|---|---|---|---|
| 0.200 | 3.15 | 10.7 | 3.39 |
| 0.300 | 2.48 | 10.8 | 4.37 |
| 0.401 | 1.81 | 10.2 | 5.64 |
| 0.500 | 1.72 | 10.1 | 5.89 |
| 0.600 | 1.76 | 9.39 | 5.32 |
| 0.700 | 2.35 | 5.52 | 2.35 |
| 0.720 | 2.94 | 3.97 | 1.35 |
| 0.750 | - | - | -0.26 |

Tabla 3.31: Coeficientes de difusión, termodifusión y Soret medidos en un entorno de microgravedad (IVIDIL) para las mezclas agua-isopropanol a una temperatura de 25 °C.

| $c$, agua | $D \times 10^{-10}$ ($m^2/s$) | $D_T \times 10^{-13}$ ($m^2/s \cdot K$) | $S_T \times 10^{-3}$ ($K^{-1}$) |
|---|---|---|---|
| 0.900 | 6.55 | -45.9 | -7.01 |
| 0.500 | 1.62 | 9.51 | 5.87 |

### 3.2.5. Discusión

Los resultados obtenidos para los coeficientes de difusión molecular ($D$), termodifusión ($D_T$) y Soret ($S_T$) mediante las diferentes técnicas experimentales muestran un buen acuerdo entre ellas. Estos resultados se pueden ver en las figuras 3.13, 3.14 y 3.15. En estas figuras también se incluyen algunos datos para estos coeficientes en la bibliografía. Se han añadido valores para el coeficiente de difusión molecular, medidos mediante la técnica de dispersion de Taylor [157], y datos para el coeficiente Soret determinados mediante la célula de flujo [158].

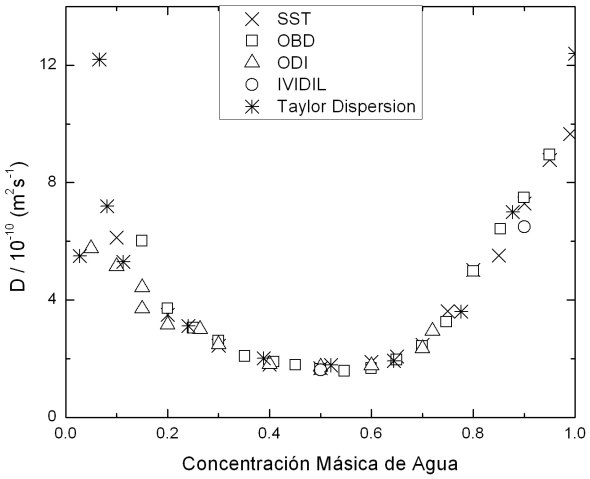


Figura 3.13: Coeficiente de difusión molecular para la mezcla agua-isopropanol en todo el rango de concentración a una temperatura media de 25 °C. (∗) Datos para este coeficiente de la Ref. [157].

Un análisis de los datos obtenidos permite diferenciar tres zonas en función de la concentración en esta mezcla. Por un lado se tiene una zona de alta concentración de agua ($c$ >0.75). Se ha confirmado que para esta mezcla, en este rango de concentración, el valor del coeficiente Soret es negativo. Es decir, el componente más denso, agua, se dirige hacia la zona caliente mientras que el menos denso, isopropanol, se desplaza hacia la zona fría. Para esta región se observa cómo al aumentar la concentración de agua se produce un incremento del valor absoluto del coeficiente $D_T$. Del mismo modo, el valor del coeficiente $D$ crece al aumentar la concentración, pero no con la misma proporción. Esto se traduce en un aumento del valor absoluto del coeficiente Soret conforme crece la concentración de agua en la mezcla.

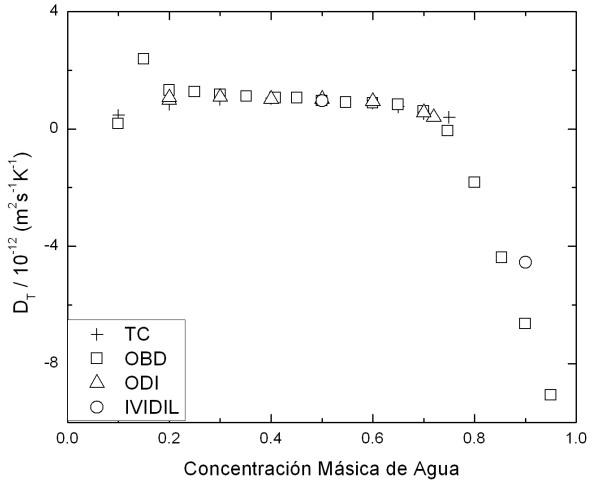


Figura 3.14: Coeficiente de termodifusión para la mezclas agua-isopropanol en todo el rango de concentración a una temperatura media de 25 °C.

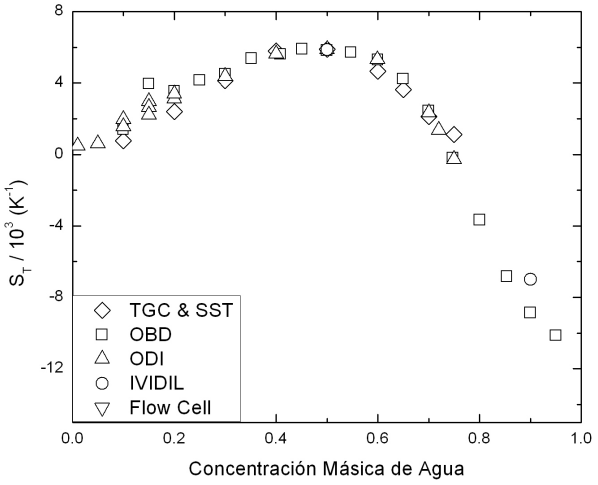


Figura 3.15: Coeficiente Soret para la mezclas agua-isopropanol en todo el rango de concentración a una temperatura media de 25 °C. ($\bigtriangledown$) Datos para este coeficiente de la Ref. [158].

Otra de las zonas diferenciadas comprende los valores intermedios del rango de concentración de agua ($0.2< c <0.75$). Esta zona es la mejor caracterizada, ya que todas las técnicas son capaces de proporcionar valores fiables de las propiedades de transporte. En esta zona se puede apreciar que el coeficiente $D_T$ está poco influenciado por la concentración y mantiene un valor aproximadamente constante. Por otra parte tanto el coeficiente $D$ como $S_T$, toman una forma parabólica en este tramo, con un extremo en ambos casos a una concentración másica de 0.50 de agua.

Se puede distinguir otra tercera zona, correspondiente a la zona de baja concentración de agua ($c <0.25$). En esta zona los valores de los factores de contraste decrecen rápidamente, lo que impide obtener datos fiables mediante las técnicas ópticas. Es por ello que esta zona únicamente se ha podido caracterizar utilizando las medidas obtenidas mediante la TC y SST. En este caso se puede observar que tanto el valor del coeficiente $S_T$, como el de $D_T$ decrecen al disminuir la concentración de agua en la mezcla. El coeficiente $D$, por otro lado, aumenta su valor con la disminución de la concentración de agua. En la literatura existen medidas experimentales [158], que sugieren que se podría dar un segundo cambio de signo del coeficiente Soret en este rango de concentración para la mezcla agua-isopropanol. Sin embargo, los datos obtenidos en este estudio no dan indicios de que este segundo cambio de signo suceda. Los valores experimentales obtenidos, incluyendo los medidos con técnicas ópticas, proporcionan valores positivos del coeficiente Soret para toda esta zona.

Entre los resultados del proyecto IVIDIL, llevados a cabo en condiciones de microgravedad y en ausencia de la convección, se han medido dos mezclas del sistema agua-isopropanol. Uno de los puntos que se ha medido es en la zona con coeficiente Soret positivo (concentración másica de agua $c =0.50$), mientras que el otro, en la zona del coeficiente Soret negativo (concentración másica de agua $c =0.90$). Esto ha permitido la comparación de los puntos medidos en el espacio con los determinados en condiciones terrestres. En ambos casos se ha podido comprobar que existe un gran acuerdo entre los valores obtenidos, tal y como se puede apreciar en la figura 3.15.

De acuerdo con los datos obtenidos, para los valores de los coeficientes de difusión, termodifusión y Soret de la mezcla agua-isopropanol a una temperatura de 25 °C, se ha propuesto un benchmark, utilizando para definir sus valores los datos determinados por diferentes grupos y mediante diferentes técnicas, y condiciones terrestres y de microgravedad. De entre estos valores se han utilizado únicamente los datos con alta fiabilidad y coincidentes en más de una técnica (es por ello, que únicamente se incluyen valores a concentraciones másicas de agua superiores a $c >0.20$). Los valores propuestos para los diferentes coeficientes se presentan en la tabla 3.32.

Tabla 3.32: Valores del benchmark para el coeficiente de difusión, termodifusión y Soret en la mezcla agua-isopropanol a diferentes concentraciones másicas y a una temperatura media de 25 °C.

| $c$, agua | $D \times 10^{-10}$ ($m^2/s$) | $D_T \times 10^{-13}$ ($m^2/s \cdot K$) | $S_T \times 10^{-3}$ ($K^{-1}$) |
|---|---|---|---|
| 0.20 | $3{,}45 \pm 0{,}2$ | $10{,}66 \pm 2$ | $3{,}09 \pm 0{,}5$ |
| 0.25 | $2{,}87 \pm 0{,}2$ | $11{,}38 \pm 1$ | $3{,}96 \pm 0{,}4$ |
| 0.30 | $2{,}46 \pm 0{,}1$ | $11{,}30 \pm 0{,}5$ | $4{,}60 \pm 0{,}4$ |
| 0.35 | $2{,}16 \pm 0{,}1$ | $10{,}96 \pm 0{,}5$ | $5{,}08 \pm 0{,}2$ |
| 0.40 | $1{,}93 \pm 0{,}1$ | $10{,}53 \pm 0{,}5$ | $5{,}47 \pm 0{,}2$ |
| 0.45 | $1{,}73 \pm 0{,}1$ | $10{,}04 \pm 0{,}5$ | $5{,}81 \pm 0{,}2$ |
| 0.50 | $1{,}60 \pm 0{,}1$ | $9{,}57 \pm 0{,}5$ | $5{,}99 \pm 0{,}3$ |
| 0.55 | $1{,}59 \pm 0{,}2$ | $9{,}31 \pm 0{,}5$ | $5{,}85 \pm 0{,}3$ |
| 0.60 | $1{,}75 \pm 0{,}2$ | $9{,}21 \pm 0{,}5$ | $5{,}25 \pm 0{,}3$ |
| 0.65 | $2{,}14 \pm 0{,}3$ | $8{,}63 \pm 0{,}5$ | $4{,}02 \pm 0{,}2$ |
| 0.70 | $2{,}79 \pm 0{,}3$ | $5{,}85 \pm 0{,}5$ | $2{,}10 \pm 0{,}2$ |
| 0.75 | $3{,}67 \pm 0{,}3$ | $-1{,}33 \pm 3$ | $-0{,}36 \pm 0{,}2$ |
| 0.80 | $4{,}71 \pm 0{,}3$ | $-14{,}62 \pm 5$ | $-3{,}10 \pm 0{,}5$ |
| 0.85 | $5{,}87 \pm 0{,}4$ | $-34{,}58 \pm 6$ | $-5{,}89 \pm 0{,}9$ |
| 0.90 | $7{,}11 \pm 0{,}4$ | $-60{,}16 \pm 10$ | $-8{,}47 \pm 1{,}5$ |
| 0.95 | $8{,}35 \pm 0{,}4$ | $-88{,}53 \pm 8$ | $-10{,}60 \pm 2{,}0$ |

## 3.3. Mezclas de Polímeros

Otro de los tipos de mezclas con los que se ha trabajado a lo largo de esta tesis han sido las disoluciones de polímeros. En este caso, el análisis realizado se ha centrado en las disoluciones de poliacrilamida (PAAm) en agua. El trabajo se ha realizado en colaboración con el grupo del Prof. Doumenc, de la universidad de *Pierre et Marie Curie* de Paris, se han estudiado diferentes propiedades de esta mezcla, como son la adsorción isotérmica, la transición vítrea y la difusión (para más información ver apéndice F).

La determinación del coeficiente de difusión de las mezcla agua-PAAm en este trabajo se ha realizado por medio de dos técnicas. La técnica gravimétrica y la técnica *sliding symmetric tubes* (sección 2.5). En la técnica gravimétrica, para la determinación de este coeficiente, se preparan unas muestras en forma de discos de la disolución, y se analiza la evolución de su masa al depositarlas en un lugar con

atmósfera controlada. El análisis del cambio de masa de la muestra permite obtener el coeficiente de difusión.

Sin embargo, el procedimiento para obtener el valor del coeficiente de difusión, es sólo válido en el caso de que al menos una parte de la cinética de adsorción esté regida por la difusión polimero/solvente. Esto limita la utilización de esta técnica solamente en el régimen concentrado de la disolución. Por contra, el sistema de análisis mediante la técnica SST es más adecuado para su uso en los regímenes diluido y semi-diluido de este tipo de mezclas. Por lo tanto, el uso conjunto de estas dos técnicas permite realizar un estudio del coeficiente de difusión en todo el rango de concentración y en sus tres regímenes (concentrado, diluido y semi-diluido).

La poliacrilamida (PAAm), se puede encontrar con diferentes propiedades. En este caso, se ha estudiado una PAAm con una masa molecular de 22.4 $kg \cdot mol^{-1}$. Se ha determinado el coeficiente de difusión de la mezcla agua-PAAm, a diferentes fracciones volumétricas de polímero ($\overline{\varphi}_p$), correspondientes tanto a los regímenes diluido y semi-diluido, como al régimen concentrado, a una temperatura media de 25 °C. Los resultados obtenidos para los tres regímenes estudiados mediante ambas técnicas se muestran en la tabla 3.33.

Tabla 3.33: Coeficiente de difusión molecular de la mezcla agua-PAAm a diferentes concentraciones volumétricas de polímero y a una temperatura media de 25 °C.

| Régimen Diluido/ Semi-diluido | | Régimen Concentrado | |
|---|---|---|---|
| $\overline{\varphi}_p$ | $D_{mut}$ /m$^2$s$^{-1}$ | $\overline{\varphi}_p$ | $D_{mut}$ /m$^2$s$^{-1}$ |
| 0.0346 | $2{,}47 \times 10^{-10}$ | 0.8423 | $2{,}7 \times 10^{-13}$ |
| 0.1072 | $2{,}09 \times 10^{-10}$ | 0.8448 | $2{,}3 \times 10^{-13}$ |
| 0.1848 | $1{,}90 \times 10^{-10}$ | 0.8682 | $7{,}4 \times 10^{-14}$ |
| 0.2526 | $1{,}91 \times 10^{-10}$ | 0.8653 | $9{,}6 \times 10^{-14}$ |

Los resultados obtenidos muestran una tendencia de disminución del coeficiente de difusión molecular al aumentar la concentración de PAAm en la mezcla. Se puede apreciar un cambio de varios ordenes de magnitud en este coeficiente en función de la concentración, encontrando que estos cambios son más acentuados en los extremos del rango de concentración (Figura 3.16). En los regímenes diluido y semi-diluido, se puede observar un decrecimiento pronunciado del coeficiente de difusión al cambiar de régimen.

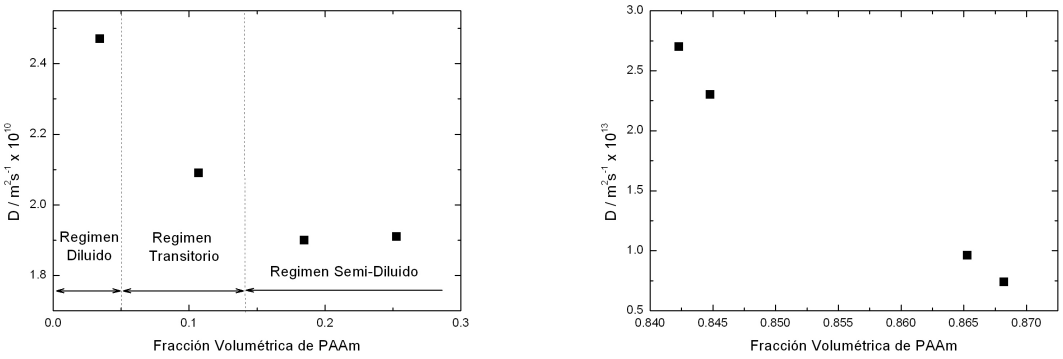


(a) (b)

Figura 3.16: Valores del coeficiente de difusión en función de la concentración volumétrica de PAAm a una temperatura de 25 °C (a) Regímenes Diluido y Semidiluido (b) Régimen Concentrado.

## 3.4. Mezclas a Altas Presiones

Cabe mencionar, que durante la realización de esta tesis doctoral también se han realizado avances en el campo de las medidas a altas presiones. En Mondragon Goi Eskola Politeknikoa, se dispone de una instalación termogravitacional cilíndrica, la cual está diseñada para la determinación del coeficiente de termodifusión a presiones de hasta 500 bar [132]. Este dispositivo ya ha sido utilizado con éxito para la medición del coeficiente de termodifusión en varias mezclas binarias de hidrocarburos a altas presiones (ver apéndice H).

Adicionalmente a los objetivos propuestos en la tesis, se planteó el uso de este dispositivo para la determinación del coeficiente de termodifusión en mezclas binarias de alcanos normales a altas presiones. Para ello, en primer lugar, se propuso el diseño y puesta a punto de varios dispositivos que permitiesen la determinación de las diversas propiedades termofísicas (viscosidad, densidad y coeficientes de expansión másica y térmica) a altas presiones.

Con este fin, se ha puesto en funcionamiento una célula Anton Paar DMA512P, la cual permite realizar mediciones de la densidad en fluidos a presiones de hasta 500 bar (Figura 3.17). Adicionalmente se ha adquirido un viscosímetro Viscolab PVT High Pressure Regulating Bath System, el cual permite realizar mediciones de la viscosidad dinámica de fluidos a presiones de hasta 1370 bar (Figura 3.17). Estos dispositivos permiten obtener las propiedades termofísicas de los fluidos requeridas

para la obtención del coeficiente de termodifusión mediante la técnica termogravitacional.


(a) (b)

Figura 3.17: Dispositivos para el estudio de las propiedades de transporte a altas presiones (a) célula Anton Paar DMA512P y (b) viscosímetro Viscolab PVT High Pressure Regulating Bath System.

De esta forma, se ha completado a lo largo de esta tesis la instalación a altas presiones para analizar los fenómenos de transporte en mezclas líquidas. No obstante, se ha encontrado que las juntas de presión de la columna termogravitacional se han degradadado debido a su uso, lo que provoca caídas de presión cuando se realizan ensayos a altas presiones. Este incidente ha frenado el avance de las actividades experimentales propuestas, las cuales han quedado inconclusas y no se han podido presentar en esta memoria.

# Capítulo 4

# Conclusiones

De acuerdo con el objetivo principal de esta tesis doctoral, se han logrado los siguientes resultados:

- Se han determinado diferentes propiedades termofísicas como densidad, viscosidad, coeficiente de expansión másica y coeficiente de expansión térmica en mezclas líquidas tanto binarias como ternarias a diferentes temperaturas.

- Se han determinado los coeficientes de difusión molecular, termodifusión y Soret mediante la técnica *sliding symmetric tubes* y la técnica termogravitacional para tres series de alcanos normales ($nC_6$-$nC_i$, $nC_{10}$-$nC_i$ y $nC_{12}$-$nC_i$) tanto equimolares como equimásicas, a una temperatura media de 25 °C.

- Se han determinado las propiedades de transporte en la mezcla agua-isopropanol en colaboración con el grupo del Prof. Köhler, de la universidad de Bayreuth y el grupo de la Prof. Shevtsova, de la universidad Libre de Bruselas, contribuyendo a ofrecer valores de referencia para los coeficientes de difusión molecular, termodifusión y Soret en esta mezcla.

- Se ha combinado la técnica *sliding symmetric tubes* con la técnica gravimétrica para el estudio del coeficiente de difusión molecular en la mezcla agua-poliacrilamida para todo el rango de concentración y en sus tres regímenes: concentrado, semi-diluido y diluido.

- Se han realizado medidas del coeficiente de termodifusión en dos mezclas ternarias de hidrocarburos (tetrahidronaftalina-isobutilbenceno-*n*dodecano y tolueno-*n*hexano-*n*dodecano) y en sus correspondientes mezclas binarias.

- Se han desarrollado tres nuevas correlaciones cuantitativas para la determinación de las propiedades de transporte:
  - Una de estas correlaciones se ha desarrollado para la determinación del coeficiente de termodifusión en mezclas binarias de alcanos normales a cualquier concentración, a partir de los datos de las masas moleculares de los componentes y del coeficiente de expansión térmica y la viscosidad de la mezcla.
  - La segunda de estas correlaciones permite la determinación, también en mezclas binarias de alcanos normales, del coeficiente de difusión molecular para cualquier concentración utilizando los datos de la viscosidad de la mezcla equimásica, la masa molecular de los componentes de la mezcla y la concentración de cada componente en la mezcla.
  - La última de estas correlaciones utiliza los datos de la viscosidad dinámica y el coeficiente de expansión térmica de los componentes puros de la mezcla y de la densidad de la mezcla equimolar para la determinación del coeficiente Soret de mezclas binarias de alcanos normales a cualquier concentración.

Los resultados obtenidos en esta tesis doctoral, han permitido avanzar en el campo de las propiedades de transporte en mezclas líquidas, especialmente en las mezclas binarias de alcanos normales, mezclas acuosas, mezclas de polímeros y mezclas multicomponentes.

## 4.1. Publicaciones y participaciones en Congresos

Los resultados obtenidos a lo largo de esta tesis han sido publicados en revistas indexadas, además han sido expuestos en diversos congresos de carácter nacional e internacional. En los anexos se pueden encontrar los artículos publicados.

### 4.1.1. Artículos

Los resultados obtenidos han sido publicados en formato de artículos en las siguientes revistas indexadas:

1. S. Srinivasan, D. Alonso de Mezquia, M.M. Bou-Ali y M.A. Saghir. *Thermodiffusion and Molecular Diffusion in binary n-alkane mixtures: Experiments and Numerical Analysis*. Philosophical Magazine, **91**, 4332-4344, (2011).

2. D. Alonso de Mezquia, F. Doumenc y M.M. Bou-Ali. *Sorption Isotherm, Glass transition, and diffusion coefficients of polyacrylamide/water solutions*. Journal of Chemical and Engineering Data, **57**, 776-783, (2012).

3. D. Alonso de Mezquia, M.M. Bou-Ali, M. Larrañaga, J.A. Madariaga y C. Santamaría. *Determination of Molecular Diffusion Coefficient in n-alkane binary mixtures: Empirical Correlations*. Journal of Physical Chemistry B, **116**, 2814-2819, (2012).

4. A. Mialdun, V. Yasnou, V. Shevtsova, A. Königer, W. Köhler, D. Alonso de Mezquia y M.M. Bou-Ali. *A comprehensive Study of Diffusion, Thermodiffusion and Soret Coefficients of Water-Isopropanol Mixtures*. Journal of Chemical Physics, **136**, 244512, (2012).

5. D. Alonso de Mezquia, E. Lapeira, M.M. Bou-Ali, M. Klein, Z. Wang y S. Wiegand. *Thermodiffusion, Molecular Diffusion and Soret Coefficient for Some Binary and Ternary Mixtures*. En preparación.

6. D. Alonso de Mezquia, M.M. Bou-Ali, J.A. Madariaga y C. Santamaría. *et al.. Soret coefficient in n-alkane binary mixtures: empirical correlations of composition dependence*. En preparación.

7. D. Alonso de Mezquia, M.M. Bou-Ali, J.A. Madariaga, C. Santamaría y J.K. Platten. *et al.. Determination of the thermodiffusion coefficient in THN-IBB-$nC_{12}$ ternary mixture using the thermogravitational column: contribution to ground experiments of DCMIX*. En preparación.

### 4.1.2. Participaciones en Congresos

Los resultados obtenidos a lo largo de esta tesis doctoral han sido presentados en forma de comunicación oral o escrita en los siguientes congresos nacionales e internacionales:

1. D. Alonso de Mezquia, P. Blanco, M.M. Bou-Ali y P. Urteaga. *Determination of Molecular Diffusion Coefficients in Liquid Mixtures by the "Sliding Symmetric Tubes"technique*. $9^{eme}$ Congrés de Mécanique, Marrakech (Marruecos), 21-24 Abril 2009. Comunicación Oral.

2. D. Alonso de Mezquia, P. Blanco, M.M. Bou-Ali y A. Zebib. *New technique for measuring the molecular diffusion coefficients of binary liquid mixture*. Thermodynamics of phase changes Conference (EUROTHERM), Namur (Bélgica), 24-27 Mayo 2009. Comunicación Oral.

3. D. Alonso de Mezquia, M.M. Bou-Ali, P. Blanco, J.K. Platten, J.A. Madariaga y C. Santamaría. *Measurements of Thermal Diffusion Coefficients of THN-IBB-$nC_{10}$ and THN-IBB-$nC_{12}$ Liquid Mixtures with mass fraction $c_i = 1/3$ at 25°C.* Second International Conference on Energy Conversion and Conservation (CICME10), Hammamet (Túnez), 22-25 Abril 2010. Comunicación Oral.

4. D. Alonso de Mezquia, M.M. Bou-Ali y P. Blanco. *Measurements of Molecular Diffusion Coefficient in some Binary Liquid Mixtures by the "Sliding Symmetric Tubes"Technique.* Second International Conference on Energy Conversion and Conservation (CICME10), Hammamet (Túnez), 22-25 Abril 2010. Comunicación Oral.

5. D. Alonso de Mezquia, M.M. Bou-Ali y P. Blanco, J.A. Madariaga y C. Santamaría. *Thermal Diffusion Coefficient Measurements of THN-IBB-$nC_{10}$ and THN-IBB-$nC_{12}$ Mixtures with Mass Fraction $c_i = 1/3$ at 25 °C.* $5^{th}$ International Conference on Thermal Engineering: Theory and Applications (ICTEA2010), Marrakesh (Marruecos), 10-14 Mayo 2010. Comunicación Oral.

6. D. Alonso de Mezquia, M.M. Bou-Ali, J.A. Madariaga, C. Santamaría y P. Urteaga. *New Correlation for the Determination of Thermal Diffusion Coefficient in n-Alkane binary Mixtures.* $9^{th}$ International Meeting on Thermodiffusion (IMT9), Toulouse (Francia), 7-11 Junio 2010. Comunicación Escrita.

7. D. Alonso de Mezquia y M.M. Bou-Ali. *Soret Coefficient values for $H_2O$-Isopropanol Mixtures at 25 °C.* $9^{th}$ International Meeting on Thermodiffusion (IMT9), Toulouse (Francia), 7-11 Junio 2010. Comunicación Escrita.

8. G. Galliero, D. Alonso de Mezquia y M.M. Bou-Ali. *Experimental and Numerical Analysis of the Soret Coefficient in Normal Alkanes Mixtures $nC_i/nC_{12}$.* $9^{th}$ International Meeting on Thermodiffusion (IMT9), Toulouse (Francia), 7-11 Junio 2010. Comunicación Escrita.

9. D. Alonso de Mezquia, M.M. Bou-Ali, J.A. Madariaga, C. Santamaría y M. Larrañaga. *Thermodiffusion and Molecular Diffusion Coefficient values for n-Alkane binary mixtures at 25 °C.* Joint European Thermodynamics Conference (JECT11), Chemnitz (Alemania), 27 Junio-1 Julio 2011. Comunicación Escrita.

10. D. Alonso de Mezquia, M.M. Bou-Ali, J.A. Madariaga, C. Santamaría, P. Urteaga y M. Larrañaga. *Determination of Thermal Diffusion and Molecular Diffusion Coefficients in n-Alkane Binary Mixtures* $19^{th}$. European Conference on

Thermophysical Properties (ECTP), Tesalónica (Grecia), 28 Agosto-1 Septiembre 2011. Comunicación Oral.

11. S. Srinivasan, D. Alonso de Mezquia, M.M. Bou-Ali y M.A. Saghir. *Experimental and Numerical Analysis of Molecular and Thermal Diffusion in Binary n-Alkane Mixtures*. International Symposium on Multiphase flow and Transport Phenomena (MFTP2012), Agadir (Marruecos), 22-25 Abril 2012. Comunicación Oral.

12. D. Alonso de Mezquia, M.M. Bou-Ali, M. Larrañaga, J.A. Madariaga y C. Santamaría. *Experimental and Analytical Determination of Molecular Diffusion Coefficient in alkane binary mixtures at 50 wt %*. Sixth International Conference on Thermal Engineering: Theory and Applications (ICTEA2012), Estambul (Turquía), 29 Mayo-1 Junio 2012. Comunicación Oral.

13. D. Alonso de Mezquia, M.M. Bou-Ali, M. Klein y S. Wiegand. *Determination of Soret Coefficient of Binary Mixtures Measured by Different Experimental Techniques*. $10^{th}$ International Meeting on Thermodiffusion (IMT10), Bruselas (Bélgica), 4-8 Junio 2012. Comunicación Escrita.

14. D. Alonso de Mezquia, M.M. Bou-Ali, J.K. Platten, J.A. Madariaga y C. Santamaría. *Determination of Thermal Diffusion in Binary and Ternary Hydrocarbon Mixtures by Thermogravitational Technique*. $10^{th}$ International Meeting on Thermodiffusion (IMT10), Bruselas (Bélgica), 4-8 Junio 2012. Comunicación Escrita.

15. A. Mialdun, V. Yasnou, V. Shevtsova, A. Königer, W. Köhler, D. Alonso de Mezquia, and M.M. Bou-Ali. *Measurements of diffusion, thermodiffusion, and Soret coefficients in water-isopropanol mixtures by different techniques*. $10^{th}$ International Meeting on Thermodiffusion (IMT10), Bruselas (Bélgica), 4-8 Junio 2012. Comunicación Escrita.

16. D. Alonso de Mezquia, M.M. Bou-Ali, M. Larrañaga, J.A. Madariaga y C. Santamaría. *Determination of the Molecular Diffusion Coefficient in binary n-Alkane Mixtures*. $10^{th}$ International Meeting on Thermodiffusion (IMT10), Bruselas (Bélgica), 4-8 Junio 2012. Comunicación Oral.

Además, a lo largo de la tesis doctoral y durante la estancia en el laboratorio de fluidos de MGEP, se ha participado en los siguientes trabajos:

### 4.1.3. Artículos en los que se ha colaborado

1. J.A. Madariaga, C. Santamaría, M.M. Bou-Ali, P. Urteaga y D. Alonso de Mezquia. *Measurement of Thermodiffusion Coefficient in n-alkane binary mixtures: Composition dependence*. Journal of Physical Chemistry B, **114**, 6937-6942, (2010).

2. P. Blanco, M.M. Bou-Ali, J.K. Platten, D. Alonso de Mezquia, J.A. Madariaga y C. Santamaría. *Thermodiffusion coefficients of Binary and Ternary Hydrocarbon Mixtures*. Journal of Chemical Physics, **132**, 114506, (2010).

3. A. Martin, M.M. Bou-Ali, H. Barrutia y D. Alonso de Mezquia. *Microfluidic Separation process by the Soret effect in biological fluids*. Comptes Rendus Mecanique, **339**, 342-348, (2011).

4. P. Urteaga, M.M. Bou-Ali, D. Alonso de Mezquia, J. Santamaría, C. Santamaría, J.A. Madariaga y H. Bataller. *Measurement of Thermodiffusion Coefficient of Hydrocarbon Binary Mixtures Under Pressure with the Thermogravitational Technique*. Review of Scientific Instruments, **339**, 074903,(2012).

### 4.1.4. Participaciones en congresos en las que se ha colaborado

1. P. Blanco, M.M. Bou-Ali, J.K. Platten, D. Alonso de Mezquia, P. Urteaga, J. A. Madariaga y C. Santamaría. *The thermodiffusion coefficients in the ternary mixture THN-IBB-n$C_{12}$ with mass fraction $c_i = 1/3$ and molar fraction $x_i = 1/3$ at 25 °C*. International Meeting on Thermodiffusion (IMT8), Bonn (Alemania), 9-13 Junio 2008. Comunicación Escrita.

2. P. Blanco, M.M. Bou-Ali, J.K. Platten, D. Alonso de Mezquia y P. Urteaga. *Remarks on the analysis method for determining the mass fractions in ternary mixtures of alkanes*. International Meeting on Thermodiffusion (IMT8), Bonn (Alemania), 9-13 Junio 2008. Comunicación Escrita.

3. P. Blanco, M.M. Bou-Ali, P. Urteaga, D. Alonso de Mezquia y J.K. Platten. *Determinación de propiedades termofísicas y de transporte en mezclas líquidas*. X Congreso Nacional de Materiales (CNM08), Donostia-San Sebastián (España), 18-20 Junio 2008. Comunicación Oral.

4. P. Blanco, M.M. Bou-Ali, P. Urteaga, D. Alonso de Mezquia y J.K. Platten. *Sliding Symmetric Tubes: New technique for the molecular diffusion coefficients*

*determination of liquid mixtures*. $18^{th}$ European Conference on Thermophysical Properties (ECTP08), Pau (Francia), 31 Agosto-04 Septiembre 2008. Comunicación Escrita.

5. P. Urteaga, M.M. Bou-Ali y D. Alonso de Mezquia. *New experimental method for thermodiffusion coefficient at high pressure*. $9^{eme}$ Congrés de Mécanique, Marrakech (Marruecos), 21-24 Abril 2009. Comunicación Oral.

6. P. Blanco, D. Alonso de Mezquia, M.M. Bou-Ali, J.A. Madariaga, C. Santamaría y J.K. Platten. *Thermal Diffusion Coefficients in Multicomponent Mixtures: Comparison between experimental and empirical values*. Joint European Thermodynamics Conference (JETC10), Copenhagen (Dinamarca), 22-24 Junio 2009. Comunicación Escrita.

7. M.M. Bou-Ali y D. Alonso de Mezquia. *Détermination expérimentale du coefficient de thermodiffusion et de diffusion moléculaire pour les mélanges liquides binaires et ternaires*. $1^{er}$ Congrès de l'Association Marocaine de Thermique (AMT2010), Settat (Marruecos), 6-7 Mayo 2010. Comunicación Oral.

8. A. Martin, M.M. Bou-Ali, D. Alonso de Mezquia y H. Barrutia. *Soret Effect Separation Processes In Biological Mixtures: Focused to Microfluidics*. $5^{th}$ International Conference on Thermal Engineering: Theory and Applications (ICTEA2010), Marrakesh (Marruecos), 10-14 Mayo 2010. Comunicación Escrita.

9. P. Blanco, M.M. Bou-Ali, J.K. Platten, D. Alonso de Mezquia, J.A. Madariaga y C. Santamaría. *Determination of Thermal Diffusion Coefficients for THN-IBB-$nC_{10}$ and THN-IBB-$nC_{12}$ Liquid Ternary Mixtures*. $9^{th}$ International Meeting on Thermodiffusion (IMT9), Toulouse (Francia), 7-11 Junio 2010. Comunicación Oral.

10. A. Martin, M.M. Bou-Ali, H. Barrutia y Alonso de Mezquia. *Microfluidic Separation Process by Soret Effect in Biological Fluids*. $9^{th}$ International Meeting on Thermodiffusion (IMT9), Toulouse (Francia), 7-11 Junio 2010. Comunicación Escrita.

11. A. Martin, M.M. Bou-Ali y D. Alonso de Mezquia. *Microfluidic Separation Process by Thermohidrodinamic Effect in Biological Fluids*. CIC microGUNE Cooperation Session, Arrasate-Mondragon (España), 14 Junio 2011. Comunicación Escrita.

# Capítulo 5

# Bibliografía


[1] R. Piazza and A. Parola. Thermophoresis in colloidal suspensions. *Journal of Physics: Condensed Matter*, 20(15):153102, 2008.

[2] M. Eslamian. Advances in thermodiffusion and thermophoresis (Soret effect) in liquid mixtures. *Frontiers in Heat and Mass Transfer*, 2(4):1 – 20, 2011.

[3] M. Eslamian and M.Z. Saghir. A critical review of thermodiffusion models: Role and significance of the heat of transport and the activation energy of viscous flow. *Journal of Non-Equilibrium Thermodynamics*, 34(2):97 – 131, 2009.

[4] S. Srinivasan and M.Z. Saghir. Experimental approaches to study thermodiffusion - A review. *International Journal of Thermal Sciences*, 50:1125–1137, 2011.

[5] C. Soret. Au point de vue de sa concentration une dissolution saline primitevement homogéne dont deux parties sont portées a des températures différentes. *Archives des Sciences Physiques et Naturelles de Geneve*, 2:48–61, 1879.

[6] C. Soret. Influence de la tempèrature sur la distribution des sels dans leurs solutions. *C R Academie Scientifique*, 91(5):289–290, 1880.

[7] C. Soret. Sur l'etat déquilibre que prend, au point de vue de sa concentration, une dissolution saline primitivement homogéne dont deux parties sont portées á des températures différentes. *Annales de chimie et physique*, 22:293–297, 1881.

[8] C. Ludwig. Diffusion zwischen ungleich erwärmten orten gleich zusammengesetzter lösungen. *Sitz. Ber. Akad. Wiss. Wien Math.-Naturw. Kl.*, 20:539, 1856.

[9] J.M. Kincaid and B. Hafskjold. Thermal diffusion factors for the lennard-jones/spline system. *Molecular Physics*, 82(6):1099 – 114, 1994.

[10] S. Wiegand. Thermal diffusion in liquid mixtures and polymer solutions. *Journal of Physics: Condensed Matter*, 16:R357–R379, February 2004.

[11] P. Blanco, M.M. Bou-Ali, J.K. Platten, J.A. Madariaga, P. Urteaga, and C. Santamaria. Thermodiffusion coefficient for binary liquid hydrocarbon mixtures. *J. Non-Equilib. Thermodyn.*, 32:309–317, 2007.

[12] A. Leahy-Dios, L. Zhuo, and A. Firoozabadi. New thermal diffusion coefficient measurements for hydrocarbon binary mixtures: Viscosity and composition dependency. *J. Phys. Chem. B*, 112:6442–6447, 2008.

[13] P. Polyakov, F. Müller-Plathe, and S. Wiegand. Reverse nonequilibrium molecular dynamics calculation of the Soret coefficient in liquid heptane/benzene mixtures. *Journal of Physical Chemistry B*, 112(47):14999 – 15004, 2008.

[14] A. Abbasi, M.Z. Saghir, and M. Kawaji. A new proposed approach to estimate the thermodiffusion coefficients for linear chain hydrocarbon binary mixtures. *Journal of Chemical Physics*, 131(1):014502, 2009.

[15] T.J. Jaber, Y. Yan, S. Pan, and M.Z. Saghir. Theoretical prediction of thermal diffusion coefficients for ternary hydrocarbon mixtures based on the irreversible thermodynamics theory. *Acta Astronautica*, 65(7-8):1158 – 1161, 2009.

[16] S. Van Vaerenbergh, S. Srinivasan, and M.Z. Saghir. Thermodiffusion in multicomponent hydrocarbon mixtures: experimental investigations and computational analysis. *Journal of Chemical Physics*, 131(11):114505, 2009.

[17] P. Blanco, M.M. Bou-Ali, J.K. Platten, D. A. De Mezquia, J.A. Madariaga, and C. Santamaria. Thermodiffusion coefficients of binary and ternary hydrocarbon mixtures. *Journal of Chemical Physics*, 132(11), 2010.

[18] K. Ghorayeb, A. Firoozabadi, and T. Anraku. Interpretation of the unusual fluid distribution in the Yufutsu gas-condensate field. *SPE Journal*, 8 (2):114–123, 2003.

[19] F. Montel, J. Bickert, A. Lagisquet, and G. Galliero. Initial state of petroleum reservoirs: A comprehensive approach. *Journal of Petroleum Science and Engineering*, 58(3-4):391 – 402, 2007.

[20] M. Touzet, G. Galliero, V. Lazzeri, M.Z. Saghir, F. Montel, and J.C. Legros. Thermodiffusion: From microgravity experiments to the initial state of petroleum reservoirs. *Comptes Rendus Mecanique*, 339:318–323, 2011.

[21] F. Montel. Importance de la thermodiffusion en exploration et production pétroliéres. *Entropie*, 184/185:86–93, 1994.

[22] S. Van Vaerenbergh, A. Shapiro, G. Galliero, F. Montel, J.C. Legros, J.P. Caltagirone, J.L. Daridon, and Z.M. Saghir. Multicomponent processes in crudes. *European Space Agency, Special Publication, ESA SP*, 1290(1290):202–213, 2005.

[23] D.V. Nichita, L. Goual, and A. Firoozabadi. Wax precipitation in gas condensate mixtures. *SPE Production and Facilities*, 16(4):250 – 259, 2001.

[24] H. Hoteit, R. Banki, and A. Firoozabadi. Wax deposition and aging in flowlines from irreversible thermodynamics. *Energy and Fuels*, 22(4):2693 – 2706, 2008.

[25] H. Hoteit and A. Firoozabadi. Numerical modeling of diffusion in fractured media for gas-injection and -recycling schemes. *SPE Journal*, 14(2):323 – 337, 2009.

[26] H. Nasrabadi, A. Firoozabadi, and T. Ahmed. Complex flow and composition path in CO2 injection schemes from density effects in 2 and 3D. In *SPE Annual Technical Conference and Exhibition Proceedings*, volume 5, pages 3183 – 3202, New Orleans, USA, 2009.

[27] J. Moortgat, S. Sun, and A. Firoozabadi. Compositional modeling of three-phase flow with gravity using higher-order finite element methods. *Water Resources Research*, 47(5), 2011.

[28] J.R. Petit, J. Jouzel, D. Raynaud, N.I. Barkov, J.M. Barnola, I. Basile, M. Bender, J. Chappellaz, M. Davis, G. Delaygue, M. Delmotte, V.M. Kotlyakov, M. Legrand, V.Y. Lipenkov, C. Lorius, C. Pépin, E. Saltzmand, and M. Stievenard. Climate and atmospheric history of the past 420,000 years from the Vostok ice core, Antarctica. *Nature*, 399(6735):429 – 436, 1999.

[29] S. I. Plasynski, J. T. Litynski, H. G. McIlvried, and R. D. Srivastava. Progress and new developments in carbon capture and storage. *Critical Reviews in Plant Sciences*, 28(3):123–138, 2009.

[30] S. Bouquet, A. Gendrin, D. Labregere, I. Le Nir, T. Dance, J. Xu, and Y. Cinar. CO2CRC otway project, Australia: Parameters influencing dynamic modeling of CO2 injection into a depleted gas reservoir. In *Offshore Europe Conference Proceedings*, volume 2, pages 752 – 770, Aberdeen, United kingdom, 2009.

[31] A.M. Grachev and J.P. Severinghaus. Laboratory determination of thermal diffusion constants for 29N2/28N2 in air at temperatures from -60 to 0 °C for reconstruction of magnitudes of abrupt climate changes using the ice core fossil-air paleothermometer. *Geochimica et Cosmochimica Acta*, 67(3):345 – 60, 2003.

[32] A.M. Grachev and J.P. Severinghaus. Determining the thermal diffusion factor for 40Ar/36Ar in air to aid paleoreconstruction of abrupt climate change. *Journal of Physical Chemistry A*, 107(23):4636 – 42, 2003.

[33] R.L. Kaffel, A.K. Mojtabi, and M. Safi. A linear stability study of the gradient zone of a solar pond with non-constant diffusivities. In M.M. Bou-Ali and J.K. Platten, editors, *Thermodiffusion: Basics and Applications (IMT7)*, pages 197–205. Mondragon Unibertsitateko Zerbitzu Editoriala, 2006.

[34] F.H. Shehadi, M. Mseddi, and M. Baccar. Numerical investigation of heat transfer and fluid flow in a salt gradient pond. In M.M. Bou-Ali and J.K. Platten, editors, *Thermodiffusion: Basics and Applications (IMT7)*, pages 325–334. Mondragon Unibertsitateko Zerbitzu Editoriala, 2006.

[35] J. Spelling, D. Favrat, A. Martin, and G. Augsburger. Thermoeconomic optimization of a combined-cycle solar tower power plant. *Energy*, 41(1):113 – 120, 2012.

[36] G.R. Longhurst. Soret effect and its implications for fusion reactors. *Journal Of Nuclear Materials*, 131(1):61–69, 1985.

[37] C. Guy and J. Schot. Modelling of Soret diffusion in radioactive waste glass. *Applied Geochemistry*, 7(Suppl):33 – 40, 1992.

[38] G. Gautier, L. Ventura, R. Jerisian, S. Kouassi, C. Leborgne, B. Morillon, and M. Roy. Deep trench etching combining aluminum thermomigration and electrochemical silicon dissolution. *Applied Physics Letters*, 88(21):212501, 2006.

[39] R.A. Normann, K.W. Rousche, P.J. Horch, and S.P. Schmidt. Impact inserter mechanism for implantation of a biomedical device. *U.S. Patent, US005361760A*, 1994.

[40] K. Clusius and G. Dickel. New process for separation of gas mixtures and isotopes. *Naturwissenschaften*, 26:546, 1938.

[41] T. Debroy, K. Tankala, and W.A. Yarbrough. Role of heat transfer and fluid flow in the chemical vapor deposition of diamond. *Journal Of Applied Physics*, 68(5):2424–2432, 1990.

[42] S.A. Gokoglu, M. Kuczmarski, and L.C. Veitch. Prediction of chemical vapor deposition rates on monofilaments and its implications for fiber properties. *Journal of Materials Research*, 7(11):3023 – 3031, 1992.

[43] W. Huang and K.S.C. Chiu. Soret, Dufour and heat by chemical reaction effects in a chemical vapor deposition optical fiber coating process. In *ASME Conference Proceedings*, volume 3, pages 393 – 397, San Francisco, CA, United States, 2005.

[44] S. L. Brimhall, M.N. Myers, K.D. Caldwell, and J.C. Giddings. Separation of polymers by flow field-flow fractionation. *Journal of Polymer Science*, 22(6):339–345, 1984.

[45] M.E. Schimpf and J.C. Giddings. Characterization of thermal diffusion in polymer solutions by thermal field-flow fractionation: Dependence on polymer and solvent parameters. *Journal of Polymer Science Part B: Polymer Physics*, 27 (6):1317–1332, 1989.

[46] J.C. Giddings. Field-flow fractionation. analysis of macromolecular, colloidal, and particulate materials. *Science*, 260(5113):1456 – 1456, 1993.

[47] S. Odenbach and T.T. Völker. Thermal convection in a ferrofluid supported by thermodiffusion. *Journal of Magnetism and Magnetic Materials*, 289:122 – 5, 2005.

[48] T. Völker and S. Odenbach. Thermodiffusion in magnetic fluids. *Journal of Magnetism and Magnetic Materials*, 289:289–291, 2005.

[49] C. Scherer and A. M. Figueiredo Neto. Ferrofluids: Properties and applications. *Brazilian Journal of Physics*, 35(3A):718–727, 2005.

[50] P. Baaske, F.M. Weinert, S. Duhr, K.H. Lemke, M.J. Russell, and D. Braun. Extreme accumulation of nucleotides in simulated hydrothermal pore systems. In H. Brenner, editor, *Proceedings of the National Academy of Sciences of the United States of America*, volume 104, pages 9346 – 9351, USA, 2007.

[51] S. Duhr, S. Arduini, and D. Braun. Thermophoresis of DNA determined by microfluidic fluorescence. *European Physical Journal E*, 15(3):277–286, 2004.

[52] A. Martin, M.M. Bou-Ali, H. Barrutia, and D. Alonso de Mezquia. Microfluidic separation process by the Soret effect in biological fluids. *Comptes Rendus Mecanique*, 339:342–348, 2011.

[53] A. Abbasi, M.Z. Saghir, and M. Kawaji. A new approach to evaluate the thermodiffusion factor for associating mixtures. *Journal of Chemical Physics*, 130(6):064506, 2009.

[54] L.J.T.M. Kempers. A thermodynamic theory of the Soret effect in a multicomponent liquid. *Journal of Chemical Physics*, 90(11):6541–6548, 1989.

[55] L.J.T.M. Kempers. A comprehensive thermodynamic theory of the Soret effect in a multicomponent gas, liquid, or solid. *Journal of Chemical Physics*, 115(14):6330–6341, 2001.

[56] R. Haase. *Thermodynamics of Irreversible Processes*. Addison-Wesley Publishing Company, 1969.

[57] K. Shukla and A. Firoozabadi. New model of thermal diffusion coefficients in binary hydrocarbon mixtures. *Industrial and Engineering Chemistry Research*, 37(8):3331 – 3342, 1998.

[58] A. Firoozabadi, K. Ghorayeb, and K. Shukla. Theoretical model of thermal diffusion factors in multicomponent mixtures. *AIChE*, 46(5):892–900, 2000.

[59] L.J. Tichacek, W.S. Kmak, and H.G. Drickamer. Thermal diffusion in liquids; the effect of non-ideality and association. *The Journal Of Physical Chemistry*, 60(5):660–665, 1956.

[60] M. Eslamian and M. Ziad Saghir. Dynamic thermodiffusion model for binary liquid mixtures. *Physical Review E*, 80(1):011201, 2009.

[61] E. Bringuier. Gauge-invariant approach to thermodiffusion in a liquid binary mixture. *Physica A: Statistical Mechanics and its Applications*, 390:1861 – 75, 2011.

[62] W.M. Rutherford and H.G. Drickamer. Theory of thermal diffusion in liquids and the use of pressure to invesgate the theory. *Journal of Chemical Physics*, 22(7):1157–1165, 1954.

[63] E.I. Dougherty and H.G. Drickamer. Thermal diffusion and molecular motion in liquids. *Journal of Physical Chemistry*, 59:443–449, 1955.

[64] W.M. Rutherford and J.G. Roof. Thermal diffusion in methane-n-butane mixtures in the critical region. *Journal of Physical Chemistry*, 63:1506–1511, 1959.

[65] R.G. Mortimer and H. Eyring. Elementary transition state theory of the Soret and Dufour effects. *Proc. Natl. Acad. Sci.*, 77:1728–1731, 1980.

[66] S.N. Semenov and M.E. Schimpf. Molecular thermodiffusion (thermophoresis) in liquid mixtures. *Physical Review E (Statistical, Nonlinear, and Soft Matter Physics)*, 72(4):41202–1, 2005.

[67] H. Brenner. Elementary kinematical model of thermal diffusion in liquids and gases. *Physical Review E*, 74(3):036306, 2006.

[68] I. Prigogine, L. Brouckere, and R. Amand. Recherches sur la thermodiffusion en phase liquide. *Physica XVI*, 7-8:577–598, 1950.

[69] P.A. Artola, B. Rousseau, and G. Galliero. A new model for thermal diffusion: Kinetic approach. *Journal of the American Chemical Society*, 130(33):10963 – 10969, 2008.

[70] J.M. Kincaid, E.G.D. Cohen, and M. Lopez de Haro. The Enskog theory for multicomponent mixtures. iv. thermal diffusion. *Journal of Chemical Physics*, 86(2):963 – 75, 1987.

[71] A.A. Shapiro. Fluctuation theory for transport properties in multicomponent mixtures: thermodiffusion and heat conductivity. *Physica A*, 332:151–175, 2004.

[72] K.I. Morozov. Soret effect in molecular mixtures. *Physical Review E - Statistical, Nonlinear, and Soft Matter Physics*, 79(3):031204, 2009.

[73] M. Schoen and C. Hoheisel. The mutual diffusion coefficient D12 in binary liquid model mixtures. molecular dynamics calculations based on Lennard-Jones (12-6) potentials I. the method of determination. *Molecular Physics*, 52(1):33 – 56, 1984.

[74] M. Schoen and C. Hoheisel. The mutual diffusion coefficient D12 in liquid model mixtures - A molecular dynamics study based on Lennard-Jones (12-6) potentials II. Lorentz-Berthelot mixtures. *Molecular Physics*, 52(5):1029 – 1042, 1984.

[75] D. MacGowan and D. J. Evans. Heat and matter transport in binary liquid mixtures. *Physical Review A*, 34(3):2133–2142, 1986.

[76] G. V. Paolini and G. Ciccotti. Cross thermotransport in liquid mixtures by nonequilibrium molecular dynamics. *Phys. Rev. A*, 35:5156, 1987.

[77] A. Perronace, G. Ciccotti, F. Leroy, A.H. Fuchs, and B. Rousseau. Soret coefficient for liquid argon-krypton mixtures via equilibrium and nonequilibrium molecular dynamics: a comparison with experiments. *Physical Review E (Statistical, Nonlinear, and Soft Matter Physics)*, 66(3):31201–31201, 2002.

[78] B. Rousseau, P.A. Artola, C. Nieto-Draghi, and J. Bonet-Avalos. Thermal diffusion in aqueous and non-ideal mixtures using non-equilibrium molecular dynamics. In M.M. Bou-Ali and J.K. Platten, editors, *Thermodiffusion: Basics and Applications (IMT7)*. Mondragon Unibertsitateko Zerbitzu Editoriala, 2006.

[79] P.A. Artola and B. Rousseau. Microscopic interpretation of a pure chemical contribution to the Soret effect. *Physical Review Letters*, 98(12):125901, 2007.

[80] G. Galliero, M. Bugel, B. Duguay, and F. Montel. Mass effect on thermodiffusion using molecular dynamics. *Journal of Non-Equilibrium Thermodynamics*, 32(3):251 – 258, 2007.

[81] G. Galliero and S. Volz. Thermodiffusion in model nanofluids by molecular dynamics simulations. *Journal of Chemical Physics*, 128(6):064505, 2008.

[82] P. Blanco, M.M. Bou-Ali, J.K. Platten, P. Urteaga, J.A. Madariaga, and C. Santamaria. Determination of thermal diffusion coefficient in equimolar n-alkane mixtures: empirical correlations. *Journal of Chemical Physics*, 129(17):174504, 2008.

[83] J.A. Madariaga, C. Santamaria, M. M. Bou-Ali, P. Urteaga, and D. Alonso de Mezquia. Measurement of thermodiffusion coefficient in n -alkane binary mixtures: Composition dependence. *Journal of Physical Chemistry B*, 114(20):6937 – 6942, 2010.

[84] D. Alonso de Mezquia, M. M. Bou-Ali, M. Larranaga, J.A. Madariaga, and C. Santamaria. Determination of molecular diffusion coefficient in n -alkane binary mixtures: Empirical correlations. *Journal of Physical Chemistry B*, 116(9):2814 – 2819, 2012.

[85] A. Würger. Is Soret equilibrium an equilibrium effect? In S. Vitaliy and V. Shevtsova, editors, *10th International Meeting on Thermodiffusion Proceedings*, page 51, Brussels, Belgium, 2012.

[86] P. Costeseque, T. Pollak, J.K. Platten, and M. Marcoux. Transient-state method for coupled evaluation of soret and pick coefficients, and related tortuosity factors, using free and porous packed thermodiffusion cells: Application to CuSO4 aqueous solution (0.25 m). *European Physical Journal E*, 15(3):249–253, 2004.

[87] J.K. Platten. The soret effect: A review of recent experimental results. *Journal of Applied Mechanics, Transactions ASME*, 73(1):5–15, 2006.

[88] S. Wiegand, H. Ning, and R. Kita. To the warm or to the cold? thermal diffusion in aqueous systems. In M.M. Bou-Ali and J.K. Platten, editors, *Thermodiffusion:Basics and Applications(IMT7)*. Mondragon Unibertsitateko Zerbitzu Editoriala, 2006.

[89] R.C. Schechter, M.G. Velarde, and J.K. Platten. The two-component Bènard problem. *Advances in Chemical Physics*, 26:265–301, 1974.

[90] D. Vigolo, G. Brambilla, and R. Piazza. Thermophoresis of microemulsion droplets: Size dependence of the Soret effect. *Physical Review E - Statistical, Nonlinear, and Soft Matter Physics*, 75(4):040401, 2007.

[91] A. Königer, B. Meier, and W. Köhler. Measurement of the Soret, diffusion, and thermal diffusion coefficients of three binary organic benchmark mixtures and of ethanol-water mixtures using a beam deflection technique. *Philosophical Magazine*, 89(10):907 – 923, 2009.

[92] A. Mialdun and V. Shevtsova. Measurement of the Soret and diffusion coefficients for benchmark binary mixtures by means of digital interferometry. *The Journal Of Chemical Physics*, 134:044524, 2011.

[93] A. Mialdun, V. Yasnou, V. Shevtsova, A. Königer, W. Köhler, D. Alonso de Mezquia, and M.M. Bou-Ali. A comprehensive study of diffusion, thermodiffusion, and Soret coefficients of water-isopropanol mixtures. *J. Chem. Phys.*, 136:244512, 2012.

[94] W. Köhler and B. Müller. Soret and mass diffusion coefficients of toluene/ n-hexane mixtures. *Journal of Chemical Physics*, 103(10):4367–4370, 1995.

[95] S. Wiegand and W. Köhler. *Thermal Nonequilibrium Phenomena in Fluid Mixtures*, chapter Measurements of Transport Coefficients by an Optical Grating Technique, pages 36–43. Number 2002. Springer, Berlin, 2002.

[96] B. Arlt, S. Datta, T. Sottmann, and S. Wiegand. Soret effect of n-octyl -D-glucopyranoside (C8G 1) in water around the critical micelle concentration. *Journal of Physical Chemistry B*, 114(6):2118 – 2123, 2010.

[97] S. Wiegand, H. Ning, and H. Kriegs. Thermal diffusion forced rayleigh scattering setup optimized for aqueous mixtures. *Journal of Physical Chemistry B*, 111(51):14169 – 14174, 2007.

[98] H. Cabrera, L. Marti-Lopez, E. Sira, K. Rahn, and M. Garcia-Sucre. Thermal lens measurement of the Soret coefficient in acetone/water mixtures. *Journal of Chemical Physics*, 131(3), 2009.

[99] P.S. Arora, I.R. Shankland, T.N. Bell, M.A. Yabsley, and P.J. Dunlop. Use of precise binary diffusion coefficients to calibrate two-bulb cells instead of using the standard end correction for the connecting tube. *Review of Scientific Instruments*, 48(6):673–674, 1977.

[100] H. Davarzani, M. Marcoux, P. Costeseque, and M. Quintard. Experimental measurement of the effective diffusion and thermodiffusion coefficients for binary gas mixture in porous media. *Chemical Engineering Science*, 65(18):5092 – 5104, 2010.

[101] W.L. Taylor and P.T. Pickett. Noble gas-carbon dioxide thermal diffusion factors: anomalous behavior for Ar/CO2. *International Journal of Thermophysics*, 7(4):837 – 49, 1986.

[102] J.K. Platten, M.M. Bou-Ali, and J.F. Dutrieux. Enhanced molecular separation in inclined thermogravitational columns. *Journal of Physical Chemistry B*, 107(107):11763–11767, 2003.

[103] B. Elhajjar, A. Mojtabi, P. Costeseque, and M.C. Charrier-Mojtabi. Separation in an inclined porous thermogravitational cell. *International Journal of Heat and Mass Transfer*, 53(21-22):4844 – 51.

[104] O. Ecenarro, J.A. Madariaga, J.L. Navarro, and C.M. Santamaria. Mass transport coefficients from liquid thermal diffusion columns. *Berichte der Bunsengesellschaft fuer Physikalische Chemie*, 94(3):377–378, 1990.

[105] O. Ecenarro, J.A. Madariaga, J. Navarro, C.M. Santamaria, J.A. Carrion, and J.M. Saviron. Fickian and thermal diffusion coefficients from liquid thermogravitational columns. *Journal of Physics: Condensed Matter*, 2(9):2289–2296, 1990.

[106] J.F. Dutrieux, J.K. Platten, G. Chavepeyer, and M.M. Bou-Ali. On the measurement of positive Soret coefficients. *Journal of Physical Chemistry B*, 106(23):6104–6114, 2002.

[107] A. Zebib and M.M. Bou-Ali. Inclined layer Soret instabilities. *Physical Review E*, 79(5):056305, 2009.

[108] M.M. Bou-Ali, O. Ecenarro, J.A. Madariaga, and C.M. Santamaria. Stability of convection in a vertical binary fluid layer with an adverse density gradient. *Physical Review E*, 59:1250–1252, 1999.

[109] M.M. Bou-Ali, O. Ecenarro, J.A. Madariaga, C.M. Santamaria, and J.J. Valencia. Measurements of negative Soret coefficients in a vertical fluid layer with an adverse density gradient. *Physical Review E*, 62(1):1420–1423, 2000.

[110] I. Prigogine. *Etude Thermodinamique Des Phénoménes Irréversibles*. Desoer, Paris, 1947.

[111] J.K. Platten, M.M. Bou-Ali, P. Costeséque, J.F. Dutrieux, W. Köhler, C. Leppla, S. Wiegand, and G. Wittko. Benchmark values for the Soret, thermal diffusion and diffusion coefficients of three binary organic liquid mixtures. *Philosophical Magazine*, 83:1965–1971, 2003.

[112] P. Costesèque and J.C. Loubet. Measuring the Soret coefficient of binary hydrocarbon mixtures in packed thermogravitational columns (contribution of toulouse university to the benchmark test). *Philosophical Magazine*, 83(17-18):2017–2022, 2003.

[113] M.M. Bou-Ali, J.J. Valencia, J.A. Madariaga, C. Santamaria, O. Ecenarro, and J.F. Dutrieux. Determination of the thermodiffusion coefficient in three binary organic liquid mixtures by the thermogravitational method (contribution of the universidad del País Vasco, Bilbao, to the benchmark test). *Pilosophical Magazine*, 83(0):2011–2015, 2003.

[114] J.K. Platten, M.M. Bou-Ali, and J.F. Dutrieux. Precise determination of the Soret, thermodiffusion and isothermal diffusion coefficients of binary mixtures of dodecane, isobutylbenzene and 1,2,3,4-tetrahydronaphthalene (contribution of the university of mons to the benchmark test). *Pilosophical Magazine*, 83(17-18):2001–2010, 2003.

[115] C. Leppla and S. Wiegand. Investigation of the Soret effect in binary liquid mixtures by thermal-diffusion-forced Rayleigh scattering (contribution to the benchmark test). *Pilosophical Magazine*, 83:1989–1999, 2003.

[116] G. Wittko and W. Köhler. Precise determination of the Soret, thermal diffusion and mass diffusion coefficients of binary mixtures of dodecane, isobutylbenzene and 1,2,3,4-tetrahydronaphthalene by a holographic grating technique. *Philosophical Magazine*, 83(17-18):1973–1987, 2003.

[117] J.P. Larre, J.K. Platten, and G. Chavepeyer. Soret effects in ternary systems heated from below. *Int.J.Heat Mass Transfer*, 40(3):545–555, 1997.

[118] K. Ghorayeb and A. Firoozabadi. Modeling multicomponent diffusion and convection in porous media. *SPE Journal*, 5(2):158–171, 2000.

[119] M.M. Bou-Ali and J.K. Platten. Metrology of the thermodiffusion coefficients in a ternary system. *Journal of non-equilibrium thermodynamics*, 30 (4):385–399, 2005.

[120] A. Leahy-Dios, M.M. Bou-Ali, J.K. Platten, and A. Firoozabadi. Measurements of molecular and thermal diffusion coefficients in ternary mixtures. *The Journal Of Chemical Physics*, 122 (23):234502.1–234502.12, 2005.

[121] S. Srinivasan and M. Saghir. Experimental data on thermodiffusion in ternary hydrocarbon mixtures. *Journal of Chemical Physics*, 131:114505, 2009.

[122] A. Königer, H. Wunderlich, and W. Köhler. Measurement of diffusion and thermal diffusion in ternary fluid mixtures using a two-color optical beam deflection technique. *J. Chem. Phys.*, 132:174506, 2010.

[123] M. Marcoux and M.C. Charrier-Mojtabi. Résolution analytique du probléme de la diffusion thermogravitationnelle dans un mélange ternaire. *Entropie*, 35(218):13–17, 1999.

[124] S. Van Vaerenbergh, J.C. Legros, and J.C. Dupin. First results of Soret coefficient measurement experiment. *Advances in Space Research*, 16(8):69 – 81, 1995.

[125] J. Bert and J. Dupuy-Philon. Microgravity measurement of the Soret effect in a molten salts mixture. *Journal of Physics: Condensed Matter*, 9(50):11045 – 11060, 1997.

[126] S. Van Vaerenbergh and J.C. Legros. Soret coefficients of organic solutions measured in the microgravity SCM experiment and by the flow and benard cells. *Journal of Physical Chemistry B*, 102(22):4426–4431, 1998.

[127] S. Srinivasan, M. Eslamian, and M.Z. Saghir. Estimation of the thermodiffusion coefficients for dodecane/n-butane/ methane mixtures and comparison with experimental data from FOTON M3 mission. In *60th International Astronautical Congress Proceedings*, volume 1, pages 617 – 619, Daejeon, Republic of Korea, 2009.

[128] Y.P. Razi, K. Maliwan, M.C. Charrier Mojtabi, and A. Mojtabi. Importance of direction of vibration on the onset of Soret-driven convection under gravity or weightlessness. *European Physical Journal E*, 15(3):335–341, 2004.

[129] V. Shevtsova. IVIDIL experiment onboard the ISS. *Advances in Space Research*, 46(5):672 – 679, 2010.

[130] V. Shevtsova, T. Lyubimova, Z.M. Saghir, D. Melnikov, Y. Gaponenko, V. Sechenyh, J.C. Legros, and A. Mialdun. IVIDIL: On-board g-jitters and diffusion controlled phenomena. volume 327, 2011.

[131] F. Croccolo, F. Plantier, G. Galliero, G. Pijaudier-Cabot, M.Z. Saghir, F. Dubois, S. Van Vaerenbergh, F. Montel, and H. Bataller. Note: Temperature derivative of the refractive index of binary mixtures measured by using a new thermodiffusion cell. *Review of Scientific Instruments*, 82(12):126105, 2011.

[132] P. Urteaga, M.M. Bou-Ali, D. Alonso de Mezquia, J. Santamaría, C. Santamaría, J.A. Madariaga, and H. Bataller. Measurement of thermodiffusion coefficient of hydrocarbon binary mixtures under pressure with the thermogravitational technique. *Review of Scientific Instruments*, 83:074903, 2012.

[133] E. Leonardi, B. D'Aguanno, and C. Angeli. Temperature and composition dependence of the Soret coefficient in Lennard-Jones mixtures presenting consolute critical phenomena. *Journal of Chemical Physics*, 132(12):124512, 2010.

[134] M.M. Bou-Ali, O. Ecenarro, J.A. Madariaga, C.M. Santamaria, and J.J. Valencia. Thermogravitational measurement of the Soret coefficient of liquid mixtures. *Journal of Physics: Condensed Matter*, 10:3321–3331, 1998.

[135] W.H. Furry, R.C. Jones, and L. Onsager. On the theory of isotope separation by thermal diffusion. *Physical Review E*, 55:1083–1095, 1939.

[136] S.D. Majumdar. The theory of the separation of isotopes by thermal diffusion. *Physical Review E*, 81:844–848, 1951.

[137] P. Urteaga, M.M. Bou-Ali, J.A. Madariaga, C. Santamaria, P. Blanco, and J.K. Platten. Themogravitational column for high pressure. In M.M. Bou-Ali and J.K. Platten, editors, *Thermodiffusion: Basics and Applications*, page 449. Mondragon Unibertsitateko Zerbitzu Editoriala, 2006.

[138] P. Blanco. *Desarrollo De Técnicas Experimentales Para La Determinación De Los Coeficientes De Difusion Termica, Difusion Molecular Y Soret De Mezclas Multicomponente*. PhD thesis, Mondragon Goi Eskola Politeknikoa, 2008.

[139] J.J. Valencia, M.M. Bou-Ali, O. Ecenarro, J.A. Madariaga, and C.M. Santamaria. Validity limits of the FJO thermogravitational column theory. In W.Köhler and Simone Wiegand, editors, *Thermal Nonequilibrium Phenomena in Fluid Mixtures*, pages 233–249. Springer Berlin / Heidelberg, 2002.

[140] J.A. Madariaga, C. Santamaría, H. Barrutia, M.M. Bou-Ali, O. Ecenarro, and J.J. Valencia. Validity limits of the FJO thermogravitational column theory: Experimental and numerical analysis. *Comptes Rendus Mecanique*, 339:292–296, 2011.

[141] P. Blanco, M. M. Bou-Ali, and P. Urteaga. Columna termogravitacional a altas y bajas presiones. *Patente ES 2330905 (A1)*, 2009.

[142] P. Blanco, P. Polyakov, M.M. Bou-Ali, and S. Wiegand. Thermal diffusion and molecular diffusion values for some alkane mixtures: a comparison between thermogravitational column and thermal diffusion forced rayleigh scattering. *Journal of Physical Chemistry B*, 112(28):8340 –8345, 2008.

[143] Y. Yan, P. Blanco, M.Z. Saghir, and M.M. Bou-Ali. An improved theoretical model for thermal diffusion coefficient in liquid hydrocarbon mixtures: Comparison between experimental and numerical results. *Journal of Chemical Physics*, 129(19):194507, 2008.

[144] A. Leahy-Dios and A. Firoozabadi. A unified model for nonideal multicomponent molecular diffusion coefficients. *AIChE Journal*, 53(11):2932 – 2939, 2007.

[145] S. Semenov and M. Schimpf. Thermophoresis of dissolved molecules and polymers: Consideration of the temperature induced macroscopic pressure gradient. *Physical Review*, 69:011201, 2004.

[146] D. Stadelmaier and W. Köhler. Thermal diffusion of dilute polymer solutions: The role of chain flexibility and the effective segment size. *Macromolecules*, 42(22):9147 – 9152, 2009.

[147] M. Hartung, J. Rauch, and W. Kohler. Thermal diffusion of dilute polymer solutions: The role of solvent viscosity. *Journal of Chemical Physics*, 125(21):214904, 2006.

[148] D. L. Bidlack and D.K. Anderson. Mutual diffusion in the liquid system hexane-hexadecane. *Journal of Physical Chemistry*, 68:206–208, 1964.

[149] J.C. Shieh and P.A. Lyons. Tranport properties of liquid n-alkanes. *Journal Of Physical Chemistry*, 73:3258, 1969.

[150] H.Y. Lo. Diffusion coefficients in binary liquid n-alkane systems. *Chemical and Engineering Data Series*, 19:236–241, 1974.

[151] L. Van Geet and W. Adamson. Diffusion in liquid hydrocarbon mixtures. *Journal of Physical Chemistry*, 68:238, 1964.

[152] A.A. Alizadeh and W.A. Wakeham. Mutual diffusion coefficients for binary mixtures of normal alkanes. *International Journal of Thermophysics*, 3(4):307 – 323, 1982.

[153] C. Debuschewitz and W. Köhler. Molecular origin of thermal diffusion in benzene + cyclohexane mixtures. *Physical Review Letters*, 87(5):055901, 2001.

[154] G. Wittko and W. Köhler. Universal isotope effect in thermal diffusion of mixtures containing cyclohexane and cyclohexane-d12. *Journal of Chemical Physics*, 123(1):14506–1, 2005.

[155] S. Hartmann, W. Köhler, and K.I. Morozov. The isotope Soret effect in molecular liquids: A quantum effect at room temperatures. *Soft Matter*, 8(5):1355 – 1360, 2012.

[156] V. Shevtsova, V. Sechenyh, A. Nepomnyashchy, and J.C. Legros. Analysis of the application of optical two-wavelength techniques to measurement of the Soret coefficients in ternary mixtures. *Philosophical Magazine*, 91(26):3498 – 3518, 2011.

[157] K.C. Pratt and W.A. Wakeham. The mutual diffusion coefficient for binary mixtures of water and the isomers of propanol. *Proceedings of the Royal Society of London, Series A (Mathematical and Physical Sciences)*, 342(1630):401 – 19, 1975.

[158] P. Poty, J.C. Legros, and G. Thomaes. Thermal diffusion in some binary liquid mixtures by the flowing cell method. *Zeitschrift fur Naturforschung A (Astrophysik, Physik und Physikalische Chemie)*, 29a(12):1915 – 16, 1974.

# Índice de figuras

# Índice de tablas

# Apéndices

# Apéndice A

# Coeficiente de Termodifusión en Mezclas Binarias y Ternarias de Hidrocarburos

# Thermodiffusion coefficients of binary and ternary hydrocarbon mixtures

Pablo Blanco,[1,a),b)] M. Mounir Bou-Ali,[1,a)] J. Karl Platten,[1,2] David A. de Mezquia,[1] Jose A. Madariaga,[3] and Carlos Santamaría[3]
[1]*Department of Manufacturing, Mondragon Goi Eskola Politeknikoa (MGEP), Loramendi 4, Apartado 23, 20500 Mondragon, Spain*
[2]*University of Mons-Hainaut, 7000 Mons, Belgium*
[3]*Department of Applied Physics II, University of Basque Country, Apartado 644, 48080 Bilbao, Spain*

(Received 9 November 2009; accepted 14 February 2010; published online 16 March 2010)

In this study, we have measured the thermodiffusion coefficients of six hydrocarbon liquid ternary mixtures at 25 °C using the thermogravitational technique. Mixtures of 1,2,3,4-tetrahydronaphthalene-isobutylbenzene-n-dodecane at four different concentrations and 1,2,3,4-tetrahydronaphthalene-isobutylbenzene-n-decane at two concentrations have been considered. We have used a plane-thermogravitational column with a small gap dimension to improve the accuracy of the recently reported data. The obtained results have been confirmed by measurements in a cylindrical column. We have also measured the thermodiffusion coefficients of 13 binary mixtures between the different components of ternaries in order to analyze the validity of the additive rule proposed in the literature to determine thermodiffusion coefficients of ternary mixtures from binary thermodiffusion data. A new correlation based on column separation, which reproduces the data within the experimental error, is proposed. © *2010 American Institute of Physics*. [doi:10.1063/1.3354114]

## I. INTRODUCTION

Most of the experimental thermodiffusion studies in liquids have been performed only in binary mixtures, as there is a lack of accurate experimental methods for multicomponent mixtures. There are a few experimental studies focused on the determination of mass separation[1,2] or concentration profiles[3] in multicomponent mixtures but without providing the thermodiffusion coefficients. However, there are very few experimental studies in ternary liquid mixtures where the thermodiffusion coefficients are determined. Using the thermal diffusion forced Rayleigh scattering (TDFRS) technique, Gans *et al.*[4,5] and Kita *et al.*[6] measured the Soret coefficient of a dilute polymer and a colloid in a mixed water-ethanol solvent at different concentrations and temperatures. By means of the TDFRS technique, Sugaya *et al.*[7] analyzed the consequences of adding urea to dextran-water solutions in the thermodiffusion properties. Leaist and Hui[8] determined the Soret coefficients in a ternary electrolyte mixture of water-sodium chloride-sodium hydroxide by means of a conductometric technique. More recently, Bou-Ali and Platten[9] proposed a new methodology to determine the thermodiffusion coefficients in ternary liquid mixtures using the thermogravitational column technique. These authors[9] and Leahy-Dios *et al.*[10] measured the thermodiffusion coefficients in the ternary mixture 1,2,3,4-tetrahydronaphthalene (THN), isobutylbenzene (IBB), and normal dodecane ($nC_{12}$) with an equal mass fraction for all components at 25 °C. They analyzed the validity of the additive rule proposed by Larre *et al.*[11] to estimate the thermodiffusion coefficients in a ternary mixture from those in the corresponding binary mixtures at the same mass fraction ratio; the results show that the values given by the additive rule are in fair agreement with the experimental data at least for the only case that was investigated. Leahy-Dios *et al.*[10] also provided the thermodiffusion coefficients of the components in the ternary mixtures composed of normal octane ($nC_8$), normal decane ($nC_{10}$), and 1-methylnaphthalene with mass fraction ratios of 1:1:1 and 1:1:4 at 22.5 °C. They pointed out that for the mixture with mass fraction ratio of 1:1:4 the additive rule does not work. At least, in these last experimental studies[9,10] the potentiality of the thermogravitational technique to determine thermodiffusion coefficients in ternary mixtures has been established.

In the past few years the interest in transport properties of ternary mixtures has increased, especially in the oil industry,[12,13] and the demand for experimental results has grown in order to verify numerical codes[14,15] and theories.[9] In fact, different formalisms[11] and theories[16,17] exist in literature to describe the thermodiffusion effect in multicomponent mixtures. For these reasons, we present in this study the experimental results of the thermodiffusion coefficients in six ternary liquid mixtures. In order to check the validity of the above-mentioned additive rule we have also measured the thermodiffusion coefficients of 13 binary mixtures between the components of the ternaries at the same mass ratio. The studied mixtures are listed in Tables I and II. One of the reasons for having chosen these ternary mixtures is that they are representative of a hydrocarbon reservoir mixture containing a normal alkane and two aromatics, one with one ring and the other with two rings.[18] Moreover, we could compare the previously reported data of thermodiffusion coefficients

[a)]Authors to whom correspondence should be addressed. Electronic addresses: p.blanco@fz-juelich.de and mbouali@eps.mondragon.edu.
[b)]Present address: Forschungszentrum Jülich GmbH, IFF Weiche Materie, D-52428 Jülich, Germany.

 

TABLE I. Mass fraction ratio of components and relevant thermophysical properties of the ternary mixtures studied at 25 °C. The ratio in parentheses is the molar ratio.

| Mixture | Mass ratio (molar ratio) | $\rho$ (kg/m$^3$) | $\alpha$ ($10^{-4}$ K$^{-1}$) | $\mu$ ($10^{-3}$ Pa s) |
|---|---|---|---|---|
| THN-IBB-$n$C$_{12}$ | 1:1:1 | 843.541 | 9.142 | 1.289 |
| | 1:1:3 | 800.875 | 9.367 | 1.287 |
| | 3:1:1 | 888.788 | 8.747 | 1.484 |
| | (1:1:1) | 833.888 | 9.188 | 1.274 |
| THN-IBB-$n$C$_{10}$ | 1:1:1 | 835.806 | 9.366 | 1.076 |
| | 3:1:1 | 883.900 | 8.949 | 1.325 |

for the mixture THN-IBB-$n$C$_{12}$ at a mean fraction ratio of 1:1:1 with those measured in this study using two columns of different configurations with smaller gap dimensions to improve the accuracy of the measurements.

This article is organized as follows. In Sec. II the experimental method is described starting with the description of the equipment, the experimental installation, and the studied mixtures, followed by the working equations. In Sec. III, the results and discussions are presented, and finally the conclusions of this study are provided in Sec. IV.

## II. EXPERIMENTAL

### A. Installations, equipments, and materials

We have designed and constructed a new plane-parallel thermogravitational column of length $L_z=50\pm0.1$ cm, gap dimension $L_x=0.1\pm0.001$ cm, and width $L_y=5\pm0.1$ cm. The column is provided with five extracting points equidistantly separated along the column.

To confirm the results obtained in the plane column we have also used a cylindrical column designed to operate at high pressures and that has been used extensively in previous studies.[19–21] Both columns have been validated with measurements using the standard mixtures of the benchmark of Fontainebleau.[18]

An Anton Paar DMA 5000 vibrating quartz U-tube densimeter having a repeatability of $1\times10^{-6}$ g/cm$^3$ and an Anton Paar RXA 156 refractometer with a repeatability of $2\times10^{-5}$ nD have been used to determine simultaneously the density and refractive index of the studied mixtures and the extracted samples along the column in order to have the vertical composition profiles. From the density measurements we have determined the thermal expansion and the mass expansion coefficients of the mixtures. A Haake falling ball viscosimeter with ±1% precision has been used to determine the dynamic viscosity of the mixtures. A digital scale balance (capacity of 310 g and accuracy of 0.0001 g) has been used to prepare the mixtures to fill the plane column. Another digital scale balance (capacity of 4500 g and accuracy of 0.01 g) has been used to prepare the mixtures for the cylindrical column, as the necessary volume of liquid is much greater in this last case. All the products used were from Merck with purity better than 99%.

Tables I and II show the measured thermophysical properties of the binary and ternary mixtures considered.

### B. Working equations

In a multicomponent mixture the mass diffusion flux is given by[9,10]

$$J_i = -\rho\left(\sum_{k=1}^{n-1} D_{ik}\nabla c_k + \mathbf{D}_T^{\,i}\nabla T\right) \quad i=1,2,\ldots(n-1), \tag{1}$$

where $\rho$ is the density, $c_k$ the mass fraction of the component $k$, $D_{ik}$ denotes the molecular diffusion coefficients, and $\mathbf{D}_T^{\,i}$ the thermodiffusion coefficient of the $i$ component. In this study we shall determine the values of $\mathbf{D}_T^{\,i}$ from the column separation measurements. The theory of the thermogravitational column was first developed by Furry *et al.*[22] for binary mixtures. A summary of this theory can be found in Ref. 23. Later Marcoux and Charrier-Mojtabi[24] extended the theory to ternary mixtures and Haugen and Firoozabadi[25] made a generalization for multicomponent mixtures. Considering that for the dimensions of our columns the vertical diffusion can be neglected, the column theory gives for the vertical concentration gradient at the steady state

TABLE II. Mass fraction ratio and relevant thermophysical properties of the binary mixtures at 25 °C. Component 1 is the first named component. The ratios in parentheses are molar ratios.

| Mixture | Mass ratio (molar ratio) | $\rho$ (kg/m$^3$) | $\alpha$ ($10^{-4}$ K$^{-1}$) | $\beta$ | $\mu$ ($10^{-3}$ Pa s) | $D_T^1$ ($10^{-12}$ m$^2$/s K) |
|---|---|---|---|---|---|---|
| THN-$n$C$_{12}$ | 1:1 | 841.248 | 8.950 | 0.257 | 1.523 | 6.17 |
| | 3:1 | 898.957 | 5.583 | 0.274 | 1.680 | 6.03 |
| | 1:3 | 790.380 | 9.350 | 0.241 | 1.431 | 6.19 |
| | (1:1) | 827.947 | 9.053 | 0.253 | 1.499 | 5.93 |
| THN-IBB | 1:1 | 904.514 | 8.876 | 0.128 | 1.374 | 2.92 |
| | 3:1 | 934.216 | 8.555 | 0.130 | 1.708 | 2.53 |
| | (1:1) | 904.069 | 8.860 | 0.127 | 1.374 | 2.98 |
| IBB-$n$C$_{12}$ | 1:1 | 792.355 | 9.612 | 0.130 | 1.133 | 3.85 |
| | 1:3 | 767.714 | 9.670 | 0.122 | 1.217 | 3.42 |
| | (1:1) | 786.400 | 9.626 | 0.130 | 1.105 | 4.20 |
| THN-$n$C$_{10}$ | 1:1 | 829.823 | 9.299 | 0.284 | 1.150 | 8.12 |
| | 3:1 | 892.747 | 8.742 | 0.302 | 1.443 | 7.50 |
| IBB-$n$C$_{10}$ | 1:1 | 781.753 | 9.995 | 0.156 | 0.866 | 6.01 |

TABLE III. Constant parameters of calibration planes of Eqs. (5) and (6) for studied ternary mixtures. Component $i$ is THN. Component $j$ is $n\mathrm{C}_{12}$ or $n\mathrm{C}_{10}$. The ratios in parentheses are molar ratios.

| Mixture | Mass ratio (molar ratio) | $k_0$ (kg/m$^3$) | $k_1$ (kg/m$^3$) | $k_2$ (kg/m$^3$) | $k_0'$ | $k_1'$ | $k_2'$ |
|---|---|---|---|---|---|---|---|
| THN-IBB-$n\mathrm{C}_{12}$ | 1:1:1 (1:1:1) | 848.056 | 101.957 | −115.443 | 1.483 119 | 0.047 282 | −0.071 593 |
| | 1:1:3 | 843.946 | 95.009 | −103.380 | 1.480 316 | 0.043 599 | −0.063 707 |
| | 3:1:1 | 848.249 | 111.566 | −131.806 | 1.483 840 | 0.052 267 | −0.082 077 |
| THN-IBB-$n\mathrm{C}_{10}$ | 1:1:1 | 848.308 | 101.537 | −138.909 | 1.483 277 | 0.047 144 | −0.084 067 |
| | 3:1:1 | 848.026 | 111.787 | −155.911 | 1.483 854 | 0.052 217 | −0.094 888 |

$$\frac{\partial c_i}{\partial z} = -\frac{504}{gL_x^4}\frac{\mathbf{D}_T^i \nu}{\alpha} \quad i = 1,2,\ldots(n-1), \tag{2}$$

where $z$ is the vertical coordinate, $L_x$ is the gap dimension, $\nu$ the kinematic viscosity of the mixture, $\alpha$ the thermal expansion coefficient, and $g$ the gravity acceleration. Equation (2) helps to determine the thermodiffusion coefficient of the components of a mixture from the concentration measurements along the column.

According to Eq. (1) for $\mathbf{D}_T^i > 0$, the thermodiffusion flux of the $i$ component goes to the cold side. Then from Eq. (2) $\partial c_i/\partial z$ is negative, and thus this component concentrates at the bottom of the column. On the contrary for $\mathbf{D}_T^i < 0$, the thermodiffusion flux of the $i$ component goes to the hot and it concentrates at the top of the column.

In the case of binary mixtures the vertical concentration gradient is determined from the calibration curve for density as a function of composition near the concentration of interest. From this curve the mass expansion coefficient $\beta_i = 1/\rho(\partial\rho/\partial c_i)$ is obtained. The measurements show that this coefficient is constant in the range of the concentrations considered. Considering that the vertical variations of composition are small, the concentration gradient is given by

$$\frac{\partial c_i}{\partial z} = \frac{1}{\beta\rho}\frac{\partial \rho}{\partial z}, \tag{3}$$

where $\partial\rho/\partial z$ is the vertical density gradient along the column. It is obtained from the measurements of the density of samples taken from five sampling outlets distributed along the column's high. In all the mixtures considered the variation in density with height is linear.

In binary mixtures it is customary to define the thermodiffusion coefficient $D_T^i$ which relates to $\mathbf{D}_T^i$ by

$$\mathbf{D}_T^i = c_i c_j D_T^i, \tag{4}$$

where $c_i$ and $c_j$ are the mass fractions of the two components. In what follows, we shall take $D_T^i$ as the thermodiffusion coefficient of a binary mixture.

In ternary mixtures we have two independent concentrations, and therefore according to Eq. (2), the determination of the corresponding concentration gradients is needed to obtain the two independent thermodiffusion coefficients. The composition is determined from the calibration planes of density and refractive index as a function of the concentrations. More details can be found in Refs. 9 and 26. Summarizing, for small variations in concentrations around their initial values, this calibration planes can be written as

$$\rho = k_0 + k_1 c_i + k_2 c_j, \tag{5}$$

$$n = k_0' + k_1' c_i + k_2' c_j, \tag{6}$$

where $\rho$ and $n$ are the mixture density and refractive index, and $c_i$ and $c_j$ the mass fractions of the components THN and $n\mathrm{C}_{12}$ (or $n\mathrm{C}_{10}$), respectively. $k_0$, $k_1$, $k_2$, $k_0'$, $k_1'$, and $k_2'$ are the constant parameters given in Table III for the mixtures considered. They are determined from the measurement of $\rho$ and $n$ for many mixtures of known concentration near the mixture of interest. As an example the calibration planes of $\rho$ and $n$ for the equimolar and equal mass fraction mixtures of THN-IBB-$n\mathrm{C}_{12}$ are shown in Figs. 1 and 2, respectively.

To determine the concentration gradients we measured both the density and refractive index of five samples taken along the column. In all considered ternary mixtures the density and refractive index were both linear functions of the column height, as shown in Fig. 3, for the mixture THN-IBB-$n\mathrm{C}_{12}$ with a mass fraction of 1:1.3 at 25 °C. Subsequently, taking into account that the variations in concentration along the column are small, Eqs. (5) and (6) help to determine the vertical concentration gradient of the components of the mixture.

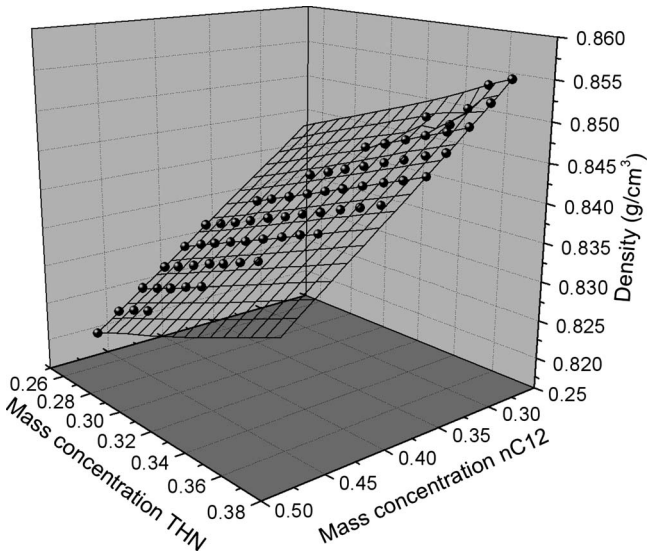


FIG. 1. Calibration plane of density for the mixture THN-IBB-$n\mathrm{C}_{12}$ at the mass fraction ratio of 1:1:1.

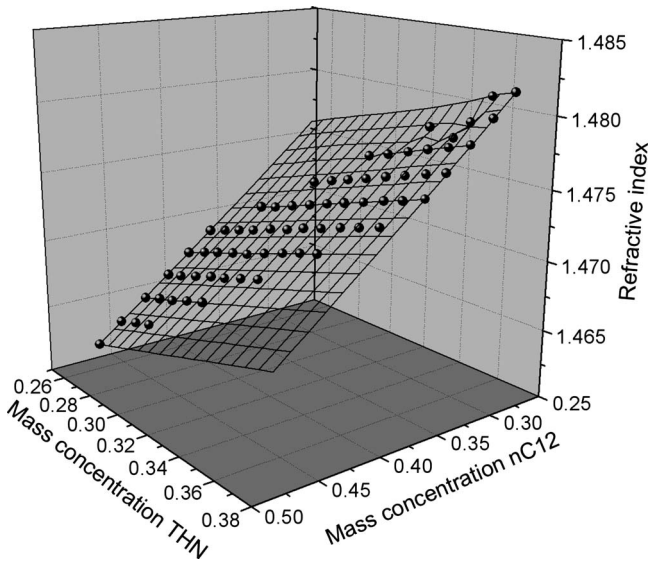


FIG. 2. Calibration plane of refractive index for the mixture THN-IBB-$n$C$_{12}$ at the mass fraction ratio of 1:1:1.

## III. RESULTS AND DISCUSSION

Table IV shows the measured thermodiffusion coefficients for three of the ternary mixtures considered using the plane and cylindrical columns. As can be seen, the two sets of values agree within a few percent. This coincidence between data extracted from columns with a different geometry gives a great support to the results presented in this study. In view of this agreement we have used the plane column for the remaining of the mixtures because it requires a lesser quantity of mixture in each experiment and it is easier to handle than the cylindrical column.

Table V gives the measured thermodiffusion coefficients for all the ternary mixtures studied. The coefficients for THN and $n$C$_{12}$ have been obtained from column measurements and the one for IBB has been calculated from the condition that the sum of the three thermodiffusion coefficients is zero.

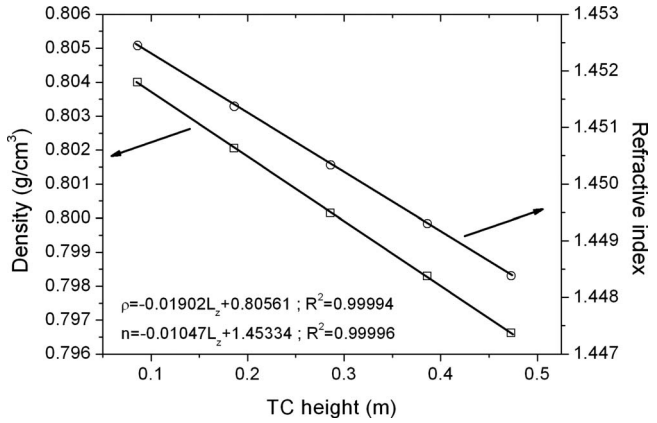


FIG. 3. Density $\rho$ and refractive index $n$ of the ternary mixture THN-IBB-$n$C$_{12}$ with mass fraction ratio of 1:1:3 at 25 °C as a function of the height of the plane column.

TABLE IV. Thermodiffusion coefficients of ternary mixtures at 25 °C obtained from plane thermogravitational column (PTC) and cylindrical thermogravitational column (CTC). Component 1 is THN and component 3 is $n$C$_{12}$ or $n$C$_{10}$.

| | | | $\mathbf{D}_T^1$ ($10^{-12}$ m$^2$/s K) | | $\mathbf{D}_T^3$ ($10^{-12}$ m$^2$/s K) | |
|---|---|---|---|---|---|---|
| Mixture | $c_1$ | $c_3$ | PTC | CTC | PTC | CTC |
| THN-IBB-$n$C$_{12}$ | 0.333 | 0.333 | 1.09 | 1.11 | −1.25 | −1.20 |
| | 0.303 | 0.390[a] | 1.09 | 1.08 | −1.24 | −1.21 |
| THN-IBB-$n$C$_{10}$ | 0.333 | 0.333 | 1.39 | 1.34 | −1.59 | −1.55 |

[a]Equimolar mixture.

As can be seen in Table V, the thermodiffusion coefficient of the denser component (THN) is always positive and for the less dense component ($n$C$_{12}$ or $n$C$_{10}$) it is negative. Therefore, THN goes to the cold side and then is advected to the bottom of the column and $n$C$_{12}$ or $n$C$_{10}$ migrates to the hot side and thus concentrates at the top.

The thermodiffusion coefficient of IBB is in absolute values much smaller than the other two, being positive for a concentration of about 0.30, and at the concentration of 0.20 it is positive or negative depending on the concentrations of the other two components. This behavior has also been observed in other ternary mixtures. According to Kita *et al.*,[6] the thermodiffusion of the polymer polyethylene oxide in mixed water/ethanol solvent changes the sign, being positive for high water concentrations and negative for low water concentration.

Table VI shows the measured thermodiffusion coefficients for the ternary mixture THN-IBB-$n$C$_{12}$ at equal mass fractions for the components and the reported values from Refs. 9 and 10. As can be seen, relative differences of about 25% exist between the two sets of data. These differences may be due to the method of analysis (separate measurements of density and refractive index in previous studies instead of simultaneous determinations used here) and to the gap dimension of the plane column used in this study. As the separation is proportional to the inverse fourth power of the gap, the column used here ($L_x$=1 mm) produces a mass separation between the column ends that is six times higher than in the column employed in previous studies[9,10] ($L_x$=1.59 mm), and therefore the accuracy of the measurements is much higher.

Table II shows the measured thermodiffusion coefficient for the binary mixtures studied. These coefficients have been measured in both cylindrical and plane columns, obtaining coincident results within the experimental error, that is, on the order of 5%. The reference component is the denser one (the first named component in the binary mixture), which in all cases goes to the cold side and concentrates at the bottom of the column. Thus, $D_T^1 > 0$ for this component.

Larre *et al.*[11] proposed the following additive rule to determine the thermodiffusion coefficient of any component in a ternary mixture from those in the corresponding binary mixtures:

$$\mathbf{D}_T^{\,i} = D_T^{ij} c_i c_j + D_T^{ik} c_i c_k, \tag{7}$$

TABLE V. Thermodiffusion coefficients of ternary mixtures at 25 °C. Component 1 is THN, component 2 is IBB, and component 3 is $n$C$_{12}$ or $n$C$_{10}$.

| Mixture | $c_1$ | $c_2$ | $c_3$ | $\mathbf{D}_T^1$ ($10^{-12}$ m$^2$/s K) | $\mathbf{D}_T^2$ ($10^{-12}$ m$^2$/s K) | $\mathbf{D}_T^3$ ($10^{-12}$ m$^2$/s K) |
|---|---|---|---|---|---|---|
| THN-IBB-$n$C$_{12}$ | 0.333 | 0.333 | 0.333 | 1.10 | 0.13 | −1.23 |
| | 0.200 | 0.200 | 0.600 | 0.90 | 0.28 | −1.18 |
| | 0.600 | 0.200 | 0.200 | 1.14 | −0.23 | −0.91 |
| | 0.303 | 0.307 | 0.390[a] | 1.09 | 0.14 | −1.23 |
| THN-IBB-$n$C$_{10}$ | 0.333 | 0.333 | 0.333 | 1.36 | 0.24 | −1.57 |
| | 0.600 | 0.200 | 0.200 | 1.34 | −0.16 | −1.18 |

[a]Equimolar mixture.

where $\mathbf{D}_T^i$ is the thermodiffusion coefficient of component $i$ in the ternary mixture; $c_i$, $c_j$, and $c_k$ are the mass fractions of components $i$, $j$, and $k$ in the ternary mixture; and $D_T^{ij}$ and $D_T^{ik}$ are the thermodiffusion coefficients of component $i$ in the binaries $i+j$ or $i+k$ with mass fraction ratios $c_i/c_j$ and $c_i/c_k$.

We have checked this correlation with all the ternary mixtures dealt with in this study. In Table VII, we compare the measured thermodiffusion coefficients with those obtained using this additive rule. As can be seen the empirical correlation reproduces the experimental data within 7% on an average, with maximum deviations of 11%, which is quite good considering the sum of experimental errors of thermodiffusion coefficients in the binary and ternary mixtures.

We have observed from column data that the separation of one component in a ternary mixture is nearly equal to the sum of the separations of the corresponding binaries. Thus, a better correlation can be obtained when the above additive rule is applied to the separations instead of the thermodiffusion coefficient. Then, taking into account Eq. (2) for the separation, we can write

$$\mathbf{D}_T^i \frac{\nu_i}{\alpha_i} = D_T^{ij} c_i c_j \frac{\nu_{ij}}{\alpha_{ij}} + D_T^{ik} c_i c_k \frac{\nu_{ik}}{\alpha_{ik}}, \tag{8}$$

where the subscripts of $\nu$ and $\alpha$ have the same meaning than those for $D_T$.

Table VII shows the obtained values of the thermodiffusion coefficients using this correlation. As can be seen, Eq. (8) reproduces the experimental data with an average difference of 3%, being the maximum difference of 6%. These differences are within the experimental error of the measurements. We have also found in a previous experimental study[27] some regularities for the column separation in n-alkane binary mixtures, which lead a quantitative correlation where the thermodiffusion coefficient was proportional to the ratio $\alpha/\nu$.

TABLE VI. Thermodiffusion coefficients for the system THN-IBB-$n$C$_{12}$ at 25 °C and mass fraction ratio of 1:1:1. Component 1 is THN, component 3 is $n$C$_{12}$.

| $\mathbf{D}_T^{i\,a}$ | $\mathbf{D}_T^{i\,b}$ |
|---|---|
| $\mathbf{D}_T^1 = +0.874 \times 10^{-12}$ m$^2$/s K | $\mathbf{D}_T^1 = +1.10 \times 10^{-12}$ m$^2$/s K |
| $\mathbf{D}_T^3 = -1.021 \times 10^{-12}$ m$^2$/s K | $\mathbf{D}_T^3 = -1.23 \times 10^{-12}$ m$^2$/s K |

[a]References 9 and 10.
[b]This study.

## IV. CONCLUSION

In this study we have measured the thermodiffusion coefficients of six hydrocarbon ternary mixtures and 13 binary mixtures between the components of the ternaries at the same mass fraction ratio. The present data for the mixture THN-IBB-$n$C$_{12}$ at equal mass fraction for all components are 25% higher compared with the recently published data.[9,10] The reason for this discrepancy is that we have used here a plane column with a smaller gap dimension than the one used in these references. The smaller gap increases the accuracy of determining the column separation. Moreover, the obtained results have been confirmed by measurements in a cylindrical column. Differences smaller than 4% have been found between the data measured in both columns.

The measurements performed show that the additive rule proposed by Larre *et al.*[11] reproduces the thermodiffusion of all the ternary mixtures with a 7% difference on an average. A better correlation is obtained when the additive rule is applied to the column separation. This correlation reproduces the experimental data of the ternary mixtures within the experimental error of the measurements.

## ACKNOWLEDGMENTS

In memory of Professor A. Zebib, we are grateful to him for his collaboration. This article presents results partly obtained in the framework of the following projects: GOVSORET (Grant No. PI2008-14) of the Basque Government and TESBLUR (Grant No. CTQ2005/09389/C02/01/PPQ) of the Spanish Government. We also thank the Department of Education, Universities and Investigation of Basque Government for the grants (BFI05.449 and BFI08188.0)

TABLE VII. Comparison between experimental thermodiffusion coefficients and correlations (7) and (8). Component 1 is THN and component 3 is $nC_{12}$ or $nC_{10}$.

| | | | $\mathbf{D}_T^1$ ($10^{-12}$ m$^2$/s K) | | | $\mathbf{D}_T^3$ ($10^{-12}$ m$^2$/s K) | | |
|---|---|---|---|---|---|---|---|---|
| Mixture | $c_1$ | $c_3$ | Expt. | Eq. (7) | Eq. (8) | Expt. | Eq. (7) | Eq. (8) |
| THN-IBB-$nC_{12}$ | 0.333 | 0.333 | 1.10 | 1.01 | 1.16 | −1.23 | −1.11 | −1.21 |
| | 0.200 | 0.200 | 0.90 | 0.86 | 0.95 | −1.18 | −1.15 | −1.23 |
| | 0.600 | 0.200 | 1.14 | 1.03 | 1.17 | −0.91 | −0.88 | −0.95 |
| | 0.303 | 0.390[a] | 1.09 | 0.98 | 1.13 | −1.23 | −1.20 | −1.28 |
| THN-IBB-$nC_{10}$ | 0.333 | 0.333 | 1.36 | 1.23 | 1.39 | −1.57 | −1.57 | −1.52 |
| | 0.600 | 0.200 | 1.34 | 1.20 | 1.39 | −1.18 | −1.14 | −1.15 |

[a]Equimolar mixture.


[1] A. L. Jones and E. C. Milberger, Ind. Eng. Chem. **45**, 2689 (1953).
[2] M. El Maâtaoui, Ph.D. thesis, Université Paul Sabatier, Toulouse, France, 1986.
[3] P. Costesèque, D. Fargue, and Ph. Jamet, in *Thermal Nonequilibrium Phenomena in Fluid Mixtures*, Lecture Notes in Physics Vol. 584, edited by W. Köhler and S. Wiegand (Springer, Berlin, 2002), p. 389.
[4] B. de Gans, R. Kita, S. Wiegand, and J. Luettmer-Strathmann, Phys. Rev. Lett. **91**, 245501 (2003).
[5] B. de Gans, R. Kita, B. Müller, and S. Wiegand, J. Chem. Phys. **118**, 8073 (2003).
[6] R. Kita, S. Wiegand, and J. Luettmer-Strathmann, J. Chem. Phys. **121**, 3874 (2004).
[7] R. Sugaya, B. A. Wolf, and R. Kita, Biomacromolecules **7**, 435 (2006).
[8] D. G. Leaist and L. Hui, J. Phys. Chem. **94**, 447 (1990).
[9] M. M. Bou-Ali and J. K. Platten, J. Non-Equilibrium Thermodyn. **30**, 385 (2005).
[10] A. Leahy-Dios, M. M. Bou-Ali, J. K. Platten, and A. Firoozabadi, J. Chem. Phys. **122**, 234502 (2005).
[11] J. Larre, J. K. Platten, and G. Chavepeyer, Int. J. Heat Mass Transfer **40**, 545 (1997).
[12] P. Georis, F. Montel, S. Van Vaerenbergh, Y. Decroly, and J. Legros, Proceedings of the European Petroleum Conference, 1998 (unpublished), Vol. 1, p. 57.
[13] S. Van Vaerenbergh, A. Shapiro, G. Galliero, F. Montel, J. Legros, J. Caltagirone, J. Daridon, and Z. Saghir, Eur. Space Agency, [Spec. Publ.] ESA SP **1290**, 202 (2005).
[14] A. Firoozabadi, K. Ghorayeb, and K. Shukla, AIChE J. **46**, 892 (2000).
[15] M. Khawaja, C. G. Jiang, S. Van Vaerenbergh, and M. Saghir, J. Non-Equilibrium Thermodyn. **30**, 359 (2005).
[16] L. Kempers, J. Chem. Phys. **90**, 6541 (1989).
[17] K. Ghorayeb and A. Firoozabadi, AIChE J. **46**, 883 (2000).
[18] J. K. Platten, M. M. Bou-Ali, P. Costesèque, J. Dutrieux, W. Köhler, C. Leppla, S. Wiegand, and G. Wittko, Philos. Mag. **83**, 1965 (2003).
[19] P. Blanco, P. Polyakov, M. M. Bou-Ali, and S. Wiegand, J. Phys. Chem. B **112**, 8340 (2008).
[20] P. Blanco, M. M. Bou-Ali, J. K. Platten, J. A. Madariaga, P. Urteaga, and C. Santamaria, J. Non-Equilibrium Thermodyn. **32**, 309 (2007).
[21] J. K. Platten, M. M. Bou-Ali, P. Blanco, J. A. Madariaga, and C. Santamaría, J. Phys. Chem. B **111**, 11524 (2007).
[22] W. H. Furry, R. C. Jones, and L. Onsager, Phys. Rev. **55**, 1083 (1939).
[23] J. Dutrieux, J. K. Platten, G. Chavepeyer, and M. M. Bou-Ali, J. Phys. Chem. B **106**, 6104 (2002).
[24] M. Marcoux and M. C. Charrier-Mojtabi, Entropie **218**, 13 (1999).
[25] K. H. Haugen and A. Firoozabadi, J. Phys. Chem. B **110**, 17678 (2006).
[26] P. Blanco, M. M. Bou-Ali, J. K. Platten, D. Alonso de Mezquia, and P. Urteaga, in *Thermal Nonequilibrium*, edited by S. Wiegand, W. Köhler, and J. K. G. Dhont (Forschungszentrum Jülich, Jülich, 2008), p. 141.
[27] P. Blanco, M. M. Bou-Ali, J. K. Platten, P. Urteaga, J. A. Madariaga, and C. Santamaría, J. Chem. Phys. **129**, 174504 (2008).

# Apéndice B

# Medida del Coeficiente de Termodifusión en Mezclas Binarias de $n$-Alcanos: Dependencia con la Composición

# Measurement of Thermodiffusion Coefficient in *n*-Alkane Binary Mixtures: Composition Dependence

**J. A. Madariaga,[†] C. Santamaría,[†] M. Mounir Bou-Ali,*[,‡] P. Urteaga,[‡] and D. Alonso De Mezquia[‡]**

*Department of Applied Physics II, University of Basque Country, Apdo. 644, 48080 Bilbao, Spain, and Mechanical and Manufacturing Department, Engineering Faculty of Mondragon Unibertsitatea, Loramendi 4 Apdo. 23, 20500 Mondragon, Spain*

*Received: November 13, 2009; Revised Manuscript Received: March 20, 2010*

In this work, we have measured the thermodiffusion coefficient of different *n*-alkane binary mixtures at several concentrations using the thermogravitational technique. In particular, we have studied the *n*-dodecane/*n*-heptane system as a function of composition and other systems covering a large range of mass differences and concentration at 25 °C and 1 atm. The results show that for any concentration the thermodiffusion coefficient of *n*-alkane mixtures is proportional to the mass difference between the components and to the ratio of the thermal expansion coefficient and viscosity of the mixture. The obtained equation allows us to determine the infinite dilution values of the thermodiffusion coefficient. We compare these values with recent experimental results in dilute polymer solutions and analyze the Brenner theory of thermodiffusion. Finally, it is shown that the thermodiffusion coefficient depends linearly with the mass fraction, and it can be calculated from the viscosity and thermal expansion of the pure components.

## I. Introduction

In an isothermal mixture, there is a transport of matter created by temperature gradients. This transport phenomenon is known as thermodiffusion or in particular for condensed systems as the Soret effect. According to nonequilibrium thermodynamics the mass flux of one component is given by

$$\vec{J} = -\rho D \nabla c - \rho D_T c(1 - c)\nabla T \qquad (1)$$

where $\rho$ is the density; $c$ is the mass fraction of the reference component; $T$ is the temperature; $D$ is the Fickian diffusion coefficient; and $D_T$ is the thermodiffusion coefficient.

A survey of the literature over the past decade shows an increasing interest in thermodiffusion. However, there is still no microscopic theory to explain the thermodiffusion in liquids. According to Wiegand,[1] the main features that determine the thermodiffusion in nonpolar fluids are the mass, moment of inertia, and size of the molecules as well as their interactions. Debuschewiz and Kölher[2] investigated the contribution of mass and moment of inertia differences by measurements in isotopic mixtures of benzene and cyclohexane. The influence of the molecular structure was analyzed by Polyakov et al.[3] in mixtures of benzene with normal and branched *n*-alkanes, and Artola et al.[4] determined by molecular dynamic simulations the chemical contribution to thermodiffusion. Finally, the influence of chain length in dilute polymer solution has been investigated by Stadelmaier and Köhler[5] and rationalized by the theory developed by Würger.[6]

A number of studies have focused on the nonpolar *n*-alkane mixtures. These ideal mixtures have normal thermodiffusion behavior: the heavier component migrates always to the cold side. Measurements of the thermodiffusion coefficient for different *n*-alkane mixtures have been recently performed using different techniques. Blanco et al.[7,8] investigated the series $nC_i/nC_6$, $nC_i/nC_{10}$, $nC_i/nC_{12}$, and $nC_i/nC_{18}$ at a molar fraction $x = 0.5$ and $nC_i/nC_{18}$ a mass fraction $c = 0.5$. Leahy-Dios et al.[9,10] studied the series $nC_i/nC_{10}$ at decane mass fractions of $c = 0.25$, 0.50, and 0.75. Yu Yan et al.[11] analyzed the series $nC_i/nC_{12}$ at $c = 0.5$. All these authors employed the thermogravitational method. Finally, Blanco et al.[12] analyzed the system $nC_5/nC_{10}$ at different molar fractions and the series $nC_i/nC_{10}$ at a mass fraction of $c = 0.5$. They used both the thermogravitational and the thermodiffusion forced Rayleigh scattering techniques and obtained a good agreement between these two methods.

For equimolar mixtures it has been recently reported[7] that for each of the above-mentioned series mass difference is the only parameter that determines the thermodiffusion coefficient. On the other hand, a quantitative correlation was found between the thermodiffusion coefficient, the mass difference, and the ratio of the thermal expansion coefficient and viscosity of the mixture.

In the present work, we shall extend this correlation to nonequimolar binary mixtures of *n*-alkanes and analyze the dependence of $D_T$ with composition. Finally, we compare the obtained results with the Brenner[13] theory of thermodiffusion and with the recent experimental results of Stadelmaier and Köhler[5] for dilute polymer solutions.

## II. Experimental Method

**A. Equipment.** The thermogravitational column used in this study is a conventional stainless steel concentric tube column, closed at both ends. It has been described in detail in earlier publications; for example, see ref 8 and references therein. The total length of the column is 0.49 m; the distance between the two sampling ports near the ends is 0.40 m; and the annular gap dimension is 1.2 mm. The temperature difference across the column is 10 °C with an average temperature of 25 °C.

* Corresponding author. E-mail: mbouali@eps.mondragon.edu.
[†] University of Basque Country.
[‡] Engineering Faculty of Mondragon Unibertsitatea.

10.1021/jp910823c 
Published on Web 04/29/2010

**TABLE 1: Mixtures Considered, the Difference of Molecular Masses, and His Thermophysical Properties: Density ($\rho$), Thermal Expansivity ($\alpha$), and Dynamic Viscosity ($\mu$) at 25°C[a]**

| mixture | $\Delta M$ $10^{-3}$kg/mol | $\rho$ kg/m$^3$ | $\alpha$ $10^{-3}$K$^{-1}$ | $\mu$ $10^{-3}$Pa s | $D_T$ $10^{-12}$m$^2$/sK | $D_T$(calcd) $10^{-12}$m$^2$/sK | $\delta$ % |
|---|---|---|---|---|---|---|---|
| | | | $x_1 = 0.80$ | | | | |
| $nC_{10}-nC_7$ | 42.08 | 719.021 | 1.071 | 0.772 | 3.02 | 2.92 | 3.3 |
| $nC_{12}-nC_7$ | 70.13 | 736.409 | 1.005 | 1.118 | 3.69 | 3.59 | 2.6 |
| $nC_{15}-nC_8$ | 98.19 | 757.129 | 0.937 | 2.022 | 2.70 | 2.77 | −2.7 |
| $nC_{16}-nC_7$ | 126.24 | 760.652 | 0.928 | 2.334 | 3.55 | 3.56 | −0.4 |
| | | | $x_1 = 0.40$ | | | | |
| $nC_{10}-nC_7$ | 42.08 | 702.601 | 1.151 | 0.580 | 4.00 | 3.75 | 6.3 |
| $nC_{12}-nC_8$ | 56.11 | 721.000 | 1.060 | 0.807 | 3.39 | 3.31 | 2.4 |
| $nC_{17}-nC_{12}$ | 70.12 | 759.557 | 0.938 | 2.213 | 1.35 | 1.33 | 1.2 |
| $nC_{16}-nC_{10}$ | 84.17 | 747.768 | 0.960 | 1.520 | 2.37 | 2.39 | −0.7 |
| $nC_{18}-nC_{11}$ | 98.20 | 757.000 | 0.933 | 2.220 | 1.89 | 1.85 | 1.9 |
| $nC_{18}-nC_7$ | 154.30 | 740.200 | 0.994 | 1.385 | 5.52 | 5.32 | 3.6 |
| | | | $x_1 = 0.30$ | | | | |
| $nC_{12}-nC_7$ | 70.13 | 706.600 | 1.125 | 0.611 | 5.30 | 5.38 | −1.6 |
| $nC_{13}-nC_6$ | 98.18 | 700.261 | 1.142 | 0.610 | 7.71 | 7.49 | 2.8 |
| $nC_{14}-nC_6$ | 112.21 | 705.405 | 1.132 | 0.656 | 7.97 | 7.91 | 0.8 |
| $nC_{18}-nC_{10}$ | 112.22 | 748.413 | 0.964 | 1.584 | 2.83 | 2.83 | 0.0 |
| $nC_{15}-nC_6$ | 126.24 | 705.000 | 1.115 | 0.707 | 8.16 | 8.10 | 0.7 |
| $nC_{16}-nC_6$ | 140.27 | 708.000 | 1.110 | 0.745 | 8.37 | 8.15 | 2.6 |
| $nC_{18}-nC_8$ | 140.27 | 738.000 | 1.011 | 1.250 | 4.70 | 4.68 | 0.4 |
| $nC_{18}-nC_7$ | 154.30 | 727.000 | 1.030 | 1.044 | 6.34 | 6.20 | 2.2 |
| | | | $x_1 = 0.20$ | | | | |
| $nC_{12}-nC_7$ | 70.13 | 698.661 | 1.159 | 0.530 | 5.82 | 5.87 | −0.9 |
| $nC_{18}-nC_{12}$ | 84.16 | 754.246 | 0.946 | 1.808 | 1.65 | 1.76 | −6.5 |
| $nC_{18}-nC_{10}$ | 112.22 | 741.925 | 0.985 | 1.311 | 3.07 | 3.16 | −3.1 |
| $nC_{18}-nC_7$ | 154.30 | 716.475 | 1.083 | 0.796 | 7.28 | 7.08 | 2.7 |

[a] $x_1$ is the molar fraction of the heavier component; $D_T$ is the measured thermodiffusion coefficient; and $D_T$(calcd) that calculated with eq 5.

In *n*-alkane mixtures, the heavier component always goes to the cold wall and thus concentrates at the bottom of the column. Thus, according to eq 1 $D_T > 0$ for this component. Further, in this article, we take the heavier component as the reference component, and it is denoted by subscript 1. The lighter component is denoted by subscript 2.

The theory of the thermogravitational columns, which was proposed by Furry−Jones−Onsager,[14−16] establishes a relation between the steady separation and the thermodiffusion coefficient $D_T$ as follows

$$\Delta c_1 = \varphi c_1 c_2 \frac{\mu D_T}{\rho \alpha} \tag{2}$$

where $\varphi$ is a geometrical factor: $\varphi = (504L_z)/(gL_x^4)$, $L_z$ being the column length, $L_x$ the annular gap dimension, $g$ the gravity acceleration, $c_1$ and $c_2$ the initial mass fractions of the heavier and lighter components, respectively, $\Delta c_1$ the steady separation between the column ends, $\alpha$ the thermal expansion coefficient, $\mu$ the dynamic viscosity; and $\rho$ the density of the mixture.

To determine the separation $\Delta c_1$, we measure the index of refraction of the two samples extracted from the sampling ports using a Pulfrich-type refractometer with a nominal accuracy of $5 \times 10^{-6}$. The composition of each sample is then determined from a calibration curve of refractive index as a function of concentration. Each experimental test is repeated three times for each mixture under consideration. To ensure that the stationary state is reached, we work at operation times that are considerably longer than the estimated relaxation time of the separation process.[16] The other required thermophysical properties, $\rho$, $\alpha$, and $\mu$, at 25 °C were also measured by us. A vibrating-quartz U-tube densimeter manufactured by Anton Paar (DMA 5000) was used with an accuracy of $5 \times 10^{-6}$ g/cm$^3$ to measure the density $\rho$ of the different mixtures at the mean temperature of 25 °C. By repeating the density measurements at different temperatures (24, 24.5, 25, 25.5, and 26 °C), the thermal expansion coefficient was determined. Dynamic viscosity $\mu$ was measured using the falling ball viscosimeter of Haake with an estimated error of ±1%.

**B. Studied Mixtures.** All the products used in this study were purchased from Merck and Aldrich with purity higher than 99%. The mixtures have been prepared by introducing the less volatile component first, i.e., the alkane with higher molecular weight. Then the corresponding amount of second alkane is added. The concentrations of the binary mixtures are adjusted by weighing both components separately using a balance with an accuracy of 0.001 g. The sample volume needed to run an experiment is approximately 30 cm$^3$.

We have prepared the mixtures that appear in Table 1 at the molar fractions of the heavier component $x_1 = 0.2$, $x_1 = 0.3$, $x_1 = 0.4$, and $x_1 = 0.8$. For each concentration, the mixtures cover a large range of mass difference to analyze the influence of this difference on the thermodiffusion coefficient. In this table, the values of the thermophysical properties $\alpha$, $\rho$, and $\mu$ and the obtained values of $D_T$ for each of the mixtures are displayed.

We have also studied the *n*-dodecane/*n*-heptane mixture at different molar fractions to determine the dependence of $D_T$ with composition for a given mass difference. The measured values of the relevant thermophysical properties and $D_T$ for each molar fraction appear in Table 2.

## III. Discussion

**A. Correlation of $D_T$ with Other Physical Properties.** In a previous work[7] we found that for equimolar binary mixtures of *n*-alkanes the column separation is proportional to the mass

**TABLE 2: Density ($\rho$), Thermal Expansion Coefficient ($\alpha$), and Dynamic Viscosity ($\mu$) for the System $n$C$_{12}$/$n$C$_7$ ($\Delta M = 70$) at 25 °C and Different Molar Fractions ($x_1$) of $n$-Dodecane[a]**

| $x_1$ | $\rho$ (kg/m$^3$) | $\alpha$ ($10^{-3}$K$^{-1}$) | $\mu$ ($10^{-3}$Pa s) | $D_T$ ($10^{-12}$m$^2$/sK) | $D_T$(calcd) ($10^{-12}$m$^2$/sK) | $\delta$ % |
|---|---|---|---|---|---|---|
| 0.10 | 689.767 | 1.202 | 0.475 | 6.34 | 6.20 | 2.2 |
| 0.20 | 698.661 | 1.158 | 0.530 | 5.82 | 5.87 | −0.9 |
| 0.30 | 706.600 | 1.124 | 0.611 | 5.30 | 5.39 | −1.7 |
| 0.37 | 711.000 | 1.102 | 0.682 | 5.08 | 5.00 | 1.6 |
| 0.50 | 720.378 | 1.066 | 0.807 | 4.50 | 4.49 | 0.2 |
| 0.70 | 731.471 | 1.023 | 1.004 | 3.86 | 3.89 | −0.7 |
| 0.80 | 736.409 | 1.004 | 1.118 | 3.69 | 3.59 | 2.7 |
| 0.90 | 740.949 | 0.990 | 1.234 | 3.35 | 3.31 | 1.1 |

[a] $D_T$ is the measured thermodiffusion coefficient, and $D_T$(calcd) is that calculated from eq 5.

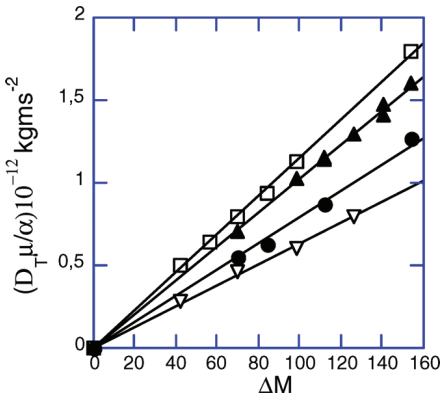


**Figure 1.** $\mathscr{D}_T\mu/\alpha\mathscr{D}_T = \mathscr{D}_T c_1 c_2$ ($\mathscr{D}_T = \mathscr{D}_T c_1 c_2$) values of the systems in Table 1 as a function of the molecular weight difference, $\Delta M = M_1 - M_2$, for the molar fractions: ●, $x_1 = 0.20$; ▲, $x_1 = 0.30$; □, $x_1 = 0.40$; ▽, $x_1 = 0.80$. Solid straight lines are a fit of experimental data.

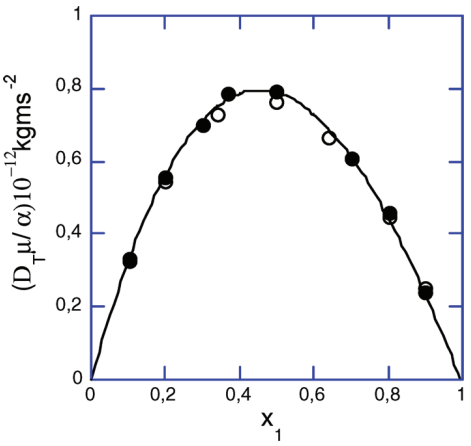


**Figure 2.** $\mathscr{D}_T\mu/\alpha$ values as a function of the molar fraction of the heavier component $x_1$. ●, $n$-dodecane/$n$-heptane. Solid line is a fit of experimental data. For comparison, we have shown the values for $n$-decane/$n$-pentane from ref 12 (○).

difference, $\Delta M = M_1 - M_2$, between the components of the mixture. According to eq 2, that means that this proportionality holds for the quantity $(\mathscr{D}_T\mu)/(\alpha)$, where $\mathscr{D}_T$ is the coefficient of the thermal gradient in eq 1 ($\mathscr{D}_T = D_T c_1 c_2$). In what follows and based on column separation data, we shall show that this proportionality can be extended to nonequimolar mixtures.

In Figure 1, the values of $(\mathscr{D}_T\mu)/(\alpha)$ are plotted as a function of $\Delta M$ for the $n$-alkane mixtures in Table 1 for molar fractions $x_1 = 0.2$, 0.3, 0.4, and 0.8. As shown in the figure, these values for each composition lie on a straight line through the origin. Therefore, one can tentatively write the following correlation

$$\frac{\mathscr{D}_T\mu}{\alpha} = k(x_1)\Delta M \tag{3}$$

where $k(x_1)$ only depends on the molar fraction. Being independent of $\Delta M$, it can be conveniently determined from experimental data of $(\mathscr{D}_T\mu)/(\alpha)$ at different molar fraction for a reference $n$-alkane binary system. With regard to this, we have taken the $n$-dodecane/$n$-heptane system, where the mass difference between the components is $\Delta M = 0.070$ kg/mol. The thermophysical properties at the different concentrations considered are shown in Table 2.

In Figure 2, $(\mathscr{D}_T\mu)/(\alpha)$ for this system versus the concentration is shown. As can be seen, the data fit to a parabolic line. Then, $k(x_1)$ is given by the equation of the fitted line divided by the mass difference. In this way, the following is obtained

$$k(x_1) = (5.34x_1 - 7.00x_1^2 + 1.65x_1^3)10^{-11} \tag{4}$$

For $x_1 = 0.5$, $k(x_1) = 1.15 \times 10^{-11}$ m s$^{-2}$, and this is in agreement with the value obtained for equimolar mixtures in a previous work.[7]

In Figure 2, the data of $(\mathscr{D}_T\mu)/(\alpha)$ for the $n$-decane/$n$-pentane system at several concentrations, taken from ref 12, are also shown. The mass difference between the components is $\Delta M = 0.070$ kg/mol, which is the same as that for the $n$-heptane/$n$-dodecane system. Thus, according to eq 3, $(\mathscr{D}_T\mu)/(\alpha)$ is the same for each concentration in both systems. As shown in Figure 2, the experimental points for $n$-decane/$n$-pentane lie on the curve corresponding to $n$-dodecane/$n$-heptane, which is in agreement with eq 3.

According to the results obtained above, we can use for $\mathscr{D}_T$ the following correlation

$$\mathscr{D}_T = k(x_1)(M_1 - M_2)\frac{\alpha}{\mu} \tag{5}$$

where $k(x_1)$ is given by eq 4. To confirm the validity of this correlation, we have determined the values of $D_T = \mathscr{D}_T/c_1c_2$ from eq 5 for the mixtures given in Tables 1 and 2. As shown in these tables, the agreement between the obtained values and the experimental ones is within the error of the measurements.

As an additional test of eq 5 we have used the experimental $D_T$ values for the mixtures $n$C$_{10}$/$n$C$_i$ ($i = 5$, 6, 7, 15, 16, 17, 18, and 20) at the mass fraction $c_1 = 0.5$ as reported in ref 12. We have also used $D_T$ values for the mixtures $n$C$_{18}$/$n$C$_i$ ($i = 5$, 6, 7, 8, 9, 10, 11, 12, and 13) and $n$C$_{12}$/$n$C$_i$ ($i = 5$, 6,7, 8, 9, 17, and 18) at $c_1 = 0.5$ from ref 8 and 11, respectively. In Figure 3 the values of $D_T$ determined using eq 5 are plotted against the

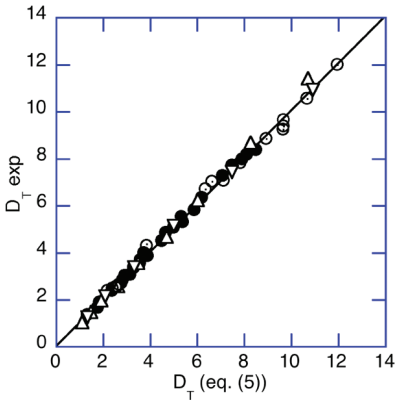


**Figure 3.** Comparison of experimental and calculated thermodiffusion coefficients of the mixtures from eq 5: ●, in this work; △, in ref 12; ○, in ref 7; ▽, in ref 11. Solid straight line is a fit of data.

experimental ones for each mixture. As seen here, all the data lie on a straight line through the origin with slope unity. Therefore, we can conclude that eq 5 helps in determining the accurate values of the thermodiffusion coefficient for any *n*-alkane binary mixture from viscosity and thermal expansion data of the mixture.

**B. Dilute Solutions.** For the purpose of comparison with recent theories[13−17] and experimental results,[5] it is convenient to determine $D_T$ in the dilute region. Taking into account that for a dilute solution of the heavier component as solute ($x_1 \rightarrow 0$) is

$$c_1c_2 \approx c_1 \text{ and } c_1 \approx \frac{M_1}{M_2}x_1$$

and further $k(x_1)$ reduces to

$$k(x_1) = 5.34 \times 10^{-11}x_1$$

we obtain from eq 5 for the infinite dilution value of $D_T$

$$D_T(x_1 \rightarrow 0) = 5.34 \times 10^{-11}\left(\frac{\alpha_2}{\mu_2}\right)M_2\left(1 - \frac{M_2}{M_1}\right) \quad (6)$$

where $M_2$, $\alpha_2$, and $\mu_2$ are the molar mass, the thermal expansion coefficient, and the viscosity of the lighter component (the solvent). $M_1$ is the molar mass of the heavier component (the solute), and $D_T$ is the thermodiffusion coefficient of this component. Thus, $M_1 > M_2$ and $D_T > 0$.

As can be seen, $D_T$ depends on the ratio $\alpha_2/\mu_2$. This dependence is predicted by the two theories of thermodiffusion of Semenov and Shimpf[17] and Brenner.[13] The dependence of $D_T$ with inverse viscosity of the solvent has also been experimentally confirmed by Hartung et al.[18] for dilute polymer solutions.

Equation 6 can be written in the form

$$D_T(x_1 \rightarrow 0) = \bar{D}_T\left(1 - \frac{M_2}{M_1}\right) \text{ where } \bar{D}_T = 5.34 \times 10^{-11}\left(\frac{\alpha_2}{\mu_2}\right)M_2 \quad (7)$$

which shows that $D_T$ increases with the molecular mass of solute and extrapolating to large $M_1$ reaches for $M_1 \gg M_2$ a solute molar mass independent plateau $D^-_T$. The deviation of $D_T$ from the asymptotic plateau shows an $M_1^{-1}$ dependence, and the plateau value is inversely proportional to the solvent viscosity. A similar behavior has been observed in a recent paper of Stadelmaier and Köhler[5] for dilute polymer and *n*-alkane solutions in different solvents. The theory developed by Würger[6] explains this dependence of $D_T$ with the molecular mass of solute. Moreover, if we consider for instance the dilute mixtures of *n*-alkanes in *n*-pentane as solvent, the plateau value according to eq 7, $D^-_T = 0.62 \times 10^{-14}/\mu_2$, in agreement with the expression proposed by Stadelmaier and Köhler[5] for dilute polymer solutions.

As the Semenov and Shimpf theory[17] includes parameters that are difficult to assign to *n*-alkane mixtures, in what follows we will compare our results to the theory of thermal diffusion developed by Brenner.[13] According to this theory, the thermodiffusion coefficient in the dilute region for solute large molecules compared with those of the solvent is given by

$$D_T = \lambda\alpha_2 D_s \quad (8)$$

where $D_s$ is the self-diffusion coefficient of the solvent and $\lambda$ is an unknown nondimensional parameter of O(1) independent of the nature of solute that becomes unity for ideal mixtures.

To test the validity of eq 7, we consider the dilute solutions of *n*-decane and *n*-octadecane in the solvent *n*-pentane. The needed thermophysical properties of *n*-pentane are $D_s = 5.5 \times 10^{-9}$ m$^2$/s (ref 19) and $\mu_2 = 0.224 \times 10^{-3}$ Pa s. Thus, $\mu_2 D_s = 1.23 \times 10^{-12}$ kg m/s$^2$, and comparing eqs 6 and 8, we obtain for $\lambda$

$$\lambda = 43.4M_2\left(1 - \frac{M_2}{M_1}\right) \quad (9)$$

which depends on the molecular mass of solute $M_1$ in disagreement with Brenner's model. For the solute, *n*-decane is $\lambda = 1.54$ and *n*-octadecane is $\lambda = 2.24$, and thus $\lambda$ is of O(1) although it differs from unity despite the ideality of the mixtures. Therefore, the Brenner formulation with $\lambda = 1$ can be used for a rough estimation of $D_T$. Similar results have been recently obtained by Hartung et al.[18] for dilute mixtures of polystyrene in different solvents.

Finally, we shall determine the limiting value of $D_T$ for $x_1 \rightarrow 1$ ($x_2 \rightarrow 0$), i.e., when the heavier component is the solvent. We have for $D_T(x_2 \rightarrow 0)$ from eqs 4 and 5

$$D_T(x_2 \rightarrow 0) = 3.71 \times 10^{-11}\left(\frac{\alpha_1}{\mu_1}\right)M_1\left(\frac{M_1}{M_2} - 1\right) \quad (10)$$

where $\alpha_1$ and $\mu_1$ are the thermal expansion and viscosity of the solvent.

**C. Dependence of $D_T$ with Concentration.** In Figure 4 the values of $D_T$ plotted against the mass fraction of the lighter component, $c_2$, for the *n*-dodecane/*n*-heptane (Table 1) and *n*-decane/*n*-pentane (ref 10) systems are shown. As can be seen, $D_T$ data for each system fit to a straight line of positive slope which shows that $D_T$ increases linearly with the mass fraction of the lighter component. Therefore, we can write for $D_T$ the following linear equation

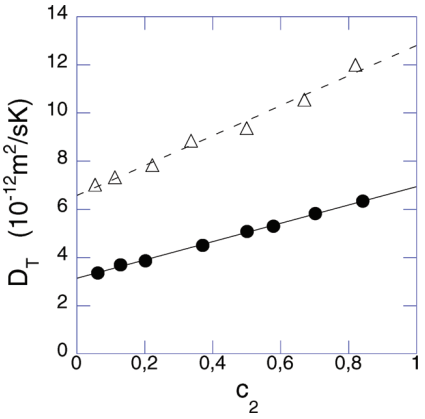


**Figure 4.** Thermodiffusion coefficient as a function of the mass fraction, $c_2$, of the lighter component. ●, *n*-dodecane/*n*-heptane; Δ, *n*-decane/*n*-pentane.

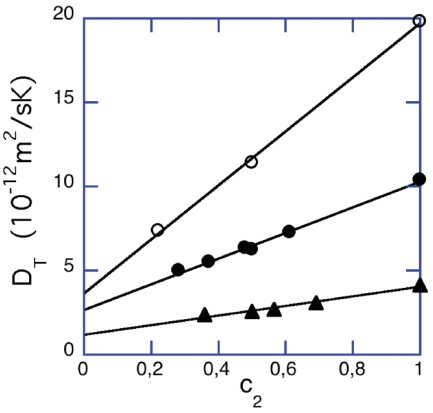


**Figure 5.** Thermodiffusion coefficient as a function of the mass fraction, $c_2$, of the lighter component. ○, *n*-octadecane/*n*-pentane; ●, *n*-octadecane/*n*-heptane; ▲, *n*-octadecane/n-decane.

$$D_T = c_1 D_T(c_2 \rightarrow 0) + c_2 D_T(c_1 \rightarrow 0) \qquad (11)$$

where $D_T(c_1 \rightarrow 0)$ and $D_T(c_2 \rightarrow 0)$ are the limiting values of $D_T$ for $c_1 \rightarrow 0$ and $c_2 \rightarrow 0$, respectively. According to this equation, the limiting values of $D_T$ determine $D_T$ in all the concentration ranges.

By using eq 6 and eq 10, one can calculate the limiting $D_T$ values from viscosity and thermal expansion coefficient data of the pure components. These data measured by us for all liquid *n*-alkanes appear in Table 3. Then, eq 11 allows us to predict $D_T$ for the full range of concentrations.

We have checked the validity of eqs 6, 10, and 11 for all the mixtures of *n*-alkanes in the references quoted above. The results show that these equations allow us to predict $D_T$ with the same accuracy as eq 5. For instance, these equations reproduce the $D_T$ data for all the mixtures in ref 7 and Table 1 with deviations smaller than 5%. As another example, in Figure 5, $D_T$ data for the mixtures of *n*-octadecane with *n*-heptane, *n*-decane, and *n*-pentane versus the mass fraction of the lighter component are plotted. The solutions of *n*-octadecane/*n*-pentane present the higher mass difference of *n*-alkanes studied. The data for equimolar and equimass mixtures are taken from ref 8 and for other concentrations from Table 1. We have also represented the limiting values for $c_1 \rightarrow 0$. The other limiting value when $c_2 \rightarrow 0$ cannot be calculated because the *n*-octadecane is solid at 25 °C. As can be seen, the experimental points and the calculated ones for $D_T(c_1 \rightarrow 0)$ are in a straight line. It can also be observed that the increase of $D_T$ with the concentration of the lighter component is enhanced with increasing mass difference between the two alkanes. This behavior has also been observed for Lennard-Jones mixtures by molecular dynamics simulation.[20]

**TABLE 3: Molar Masses ($M$), Density ($\rho$), Thermal Expansion Coefficient ($\alpha$), and Dynamic Viscosity ($\mu$) at 25°C for the *n*-Alkanes Used in This Work**

| solvent | $M$ ($10^{-3}$kg/mol) | $\rho$ (kg/m$^3$) | $\alpha$ ($10^{-3}$K$^{-1}$) | $\mu$ ($10^{-3}$Pa s) |
|---|---|---|---|---|
| pentane | 72.15 | 621.77 | 1.61 | 0.224 |
| hexane | 86.18 | 655.12 | 1.38 | 0.300 |
| heptane | 100.20 | 679.78 | 1.24 | 0.387 |
| octane | 114.23 | 698.76 | 1.16 | 0.508 |
| nonane | 128.25 | 713.96 | 1.09 | 0.665 |
| decane | 142.28 | 726.09 | 1.04 | 0.838 |
| undecane | 156.30 | 736.74 | 1.00 | 1.098 |
| dodecane | 170.34 | 745.15 | 0.971 | 1.383 |
| tridecane | 184.36 | 752.89 | 0.951 | 1.724 |
| tetradecane | 198.39 | 759.34 | 0.930 | 2.128 |
| pentadecane | 212.42 | 765.36 | 0.920 | 2.570 |
| hexadecane | 226.45 | 770.21 | 0.910 | 3.032 |
| heptadecane | 240.26 | 774.52 | 0.905 | 3.690 |

## IV. Conclusions

In this study, we have measured the thermodiffusion coefficient of several *n*-alkane mixtures at different concentrations by the thermogravitational method. We have found a linear universal correlation between the thermodiffusion coefficient, the mass difference, and the ratio of the thermal expansion coefficient and viscosity. This correlation helps to determine quantitatively the thermodiffusion coefficient of any binary mixture of *n*-alkanes. In particular, the infinite dilution values of $D_T$ can be calculated.

We have shown that in dilute solutions of *n*-alkanes $D_T$ increases with the molar mass of solute reaching a molar mass independent plateau, in accordance with recent studies for dilute polymer solutions. Moreover, we have checked the Brenner theory of thermodiffusion.

Finally, we have found that the thermodiffusion coefficient in *n*-alkane mixtures depends linearly on the mass fraction. This result allows us to determine accurate $D_T$ values from viscosity and thermal expansion coefficient of the pure components.

**Acknowledgment.** This paper presents results that were partly obtained in the framework of the following projects: GOVSORET (PI2008-14) of Basque Government and TESBLUR (CTQ2005/09389/C02/01/PPQ) of Spanish Government.

## References and Notes

(1) Wiegand, S. *J. Phys.: Condens. Matter* **2004**, *16*, R357.
(2) Debuschewitz, C.; Köhler, W. *Phys. Rev. Lett.* **2001**, *87*, 055901.
(3) Polyakov, P.; Luettmer-Strathmann, J.; Wiegand, S. *J. Phys. Chem. B* **2006**, *110*, 26215.
(4) Artola, P.-A.; Rousseau, B. *Phys. Rev. Lett.* **2007**, *98*, 125901.
(5) Stadelmaier, D.; Köhler, W. *Macromolecules* **2009**, *42*, 9147–9152.
(6) Würger, A. *Phys. Rev. Lett.* **2009**, *102*, 078302.
(7) Blanco, P.; Bou-Ali, M. M.; Platten, J. K.; Urteaga, P.; Madariaga, J. A.; Santamaría, C. *J. Chem. Phys.* **2008**, *129*, 174504.
(8) Blanco, P.; Bou-Ali, M. M.; Platten, J. K.; Madariaga, J. A.; Urteaga, P.; Santamaría, C. *J. Non-Equilib. Thermodyn.* **2007**, *32*, 309–317.
(9) Leahy-Dios, A.; Zhou, L.; Firoozabadi, A. *J. Phys. Chem. B* **2007**, *111*, 191.
(10) Leahy-Dios, A.; Zhou, L.; Firoozabadi, A. *J. Phys. Chem. B* **2008**, *112*, 6442.
(11) Yan, Y.; Blanco, P.; Saghir, M. Z.; Bou-Ali, M. M. *J. Chem. Phys.* **2008**, *129*, 194507.
(12) Blanco, P.; Polyakov, P.; Bou-Ali, M. M.; Wiegand, S. *J. Phys. Chem. B* **2008**, *112*, 8340.

(13) Brenner, H. *Phys. Rev. E* **2006**, *74*, 036306.
(14) Furry, W. H.; Jones, R. C.; Onsager, L. *Phys. Rev.* **1939**, *55*, 1083.
(15) Jones, R. C.; Furry, W. H. *Rev. Mod. Phys.* **1946**, *18*, 151.
(16) Valencia, J.; Bou-Ali, M. M.; Ecenarro, O.; Madariaga, J. A.; Santamaría, C. M. *Thermal Nonequilibrium Phenomena in Fluid Mixtures*; Köhler, W., Wiegand, S., Eds.; Springer: Berlin, 2002; pp 233−249.
(17) Semenov, S.; Schimpf, M. *Phys. Rev. E* **2004**, *69*, 011201.
(18) Hartung, M.; Rauch, J.; Köhler, W. *J. Chem. Phys.* **2006**, *125*, 214904.
(19) Fishman, E. *J. Chem. Phys.* **1955**, *592*, 469.
(20) Galliero, G.; Duguay, B.; Caltagirone, J.-P.; Montel, F. *Philos. Mag.* **2003**, *83*, 2097.

JP910823C

# Apéndice C

# Procedimiento de Separación Microfluídica por el Efecto Soret en Fluidos Biológicos

C. R. Mecanique 339 (2011) 342–348

Contents lists available at ScienceDirect

Comptes Rendus Mecanique

www.sciencedirect.com

Thermodiffusion and coupled phenomena / Thermodiffusion et phénomènes couplés

# Microfluidic separation process by the Soret effect in biological fluids

Alain Martin, M. Mounir Bou-Ali *, Haritz Barrutia, David Alonso de Mezquia

*MGEP Mondragon Goi Eskola Politeknikoa, Mechanical and Industrial Manufacturing Department, Loramendi 4, Apdo. 23, 20500 Mondragon, Spain*

ARTICLE INFO

*Article history:*
Available online 22 April 2011

*Keywords:*
Microfluidics
Molecular diffusion
Biotechnology
Soret effect
Microseparation

ABSTRACT

In this article the thermophysical and transport properties of mixtures composed of glucose and sucrose in dimethylsulfoxide (DMSO) are determined. The studied mass concentrations are 5%, 10%, 15%, 20% and 25% of glucose or sucrose in DMSO at an average temperature of 25 °C. The properties studied experimentally are the dynamic viscosity, density, mass and thermal expansion coefficient and thermodiffusion coefficient. The thermogravitational technique in flat configuration is used in order to obtain the thermodiffusion coefficients. Once these properties are known, the work is focused on the numerical study of applying a temperature gradient in microdevices in order to optimize the extraction of DMSO using the CFD Ansys Fluent software. The results show an improvement even of 35% on microfluidic separation techniques that are based on a purely diffusive regime.



## 1. Introduction

For over a decade, numerous studies have demonstrated the importance of miniaturization in biotechnology [1], since it can perform multiple assays simultaneously in a short period of time and uses less sample and reagent, among others. To this end, microfluidic platforms are used, where the flows are laminar. Because of this, the mix of components, in many cases, is limited by molecular diffusion. This makes the analysis of transport properties essential to determine the efficiency of the mixture.

Within this context, one of the applications that have been attributed to microfluidic devices is the cleaning of cryopreserved cells, removing the cryoprotectant by molecular diffusion [2–4]. However, the microdevices submitted for this purpose are too large or too complicated geometrically. This article presents the possibility of improving the efficiency of these microdevices by the application of temperature gradients. These temperature gradients increase the separation through the Soret effect [5].

One of the cryoprotectants employed is DMSO, which is used to cryopreserve cells, tissues or organs [6]. Some studies have shown that its power of cryopreservation, is improved by adding sugars such as glucose [7]. Although DMSO provides a protective benefit to cells during freezing, a long-term exposure can result in cell death because of its toxicity [4]. Therefore, before implanting the cells it is necessary to clean them. The usual technique is the centrifugation cleaning, however, this technique can damage up to 30% of the cells [8].

This article demonstrates the importance of determining the transport properties in biological mixtures in order to improve on a microscopic scale the separation process without damaging the cells. To determine the transport properties, specifically the thermodiffusion coefficient, the thermogravitational column technique is used [9]. The experimental results are used in the numerical software Ansys Fluent, where the benefits of the Soret effect at the micro-scale is observed, optimizing the microdevices for DMSO extraction.

* Corresponding author.
*E-mail address:* mbouali@eps.mondragon.edu (M.M. Bou-Ali).

1631-0721/$ – see front matter 
doi:10.1016/j.crme.2011.03.012

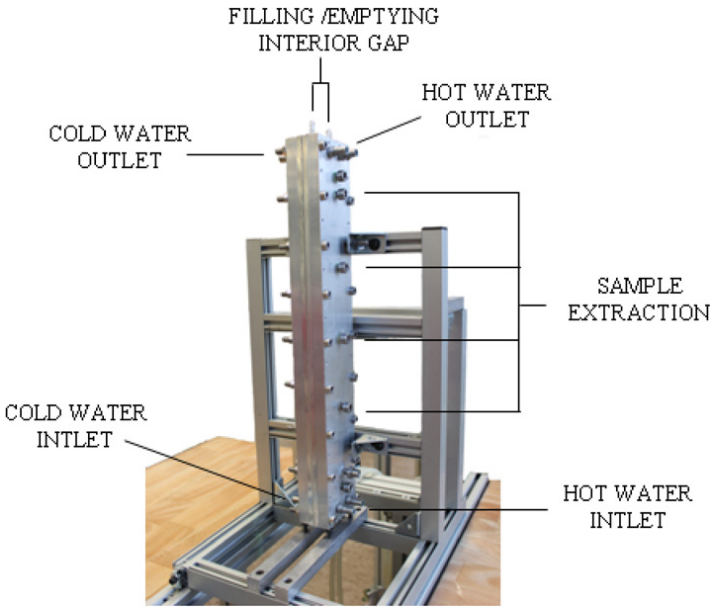


**Fig. 1.** Thermogravitational column configuration.

The determined properties correspond to biological mixtures of sucrose–DMSO and glucose–DMSO at mass concentrations of 5%, 10%, 15%, 20% and 25% of sucrose and glucose. Similarly, the thermophysical and transport properties for a mass concentration of 10% of DMSO in phosphate buffered saline (PBS) is determined, to discuss the results of work [3] and demonstrate the effectiveness of the Soret effect in separation microdevices in biological mixtures.

## 2. Experimental procedure

To determine the thermodiffusion coefficient, the thermogravitational column (TC) technique is used. In this case a flat configuration with four-point sample extraction is used (Fig. 1). For more details around the experimental procedure of this technique the reader is invited to consult [10] where is fully explained.

The thermodiffusion coefficient can be determined by measuring the change in the density of samples at steady state along the column, as shown in Eq. (1) [11]:

$$D_T = -\frac{gL_X^4}{504}\frac{\alpha}{c_0(1-c_0)\beta\eta}\frac{\partial\rho}{\partial z} \tag{1}$$

where $L_x$ is the gap of the TC, $c_0$ the initial mass fraction of the reference component in the initial homogeneous mixture, $\alpha = -\frac{1}{\rho}\frac{\partial\rho}{\partial T}$ the thermal expansion coefficient, $\beta = \frac{1}{\rho}\frac{\partial\rho}{\partial c}$ the mass expansion coefficient, $\rho$ the density of the mixture, $\frac{\partial\rho}{\partial z}$ the density gradient along TC, $\upsilon$ the kinetic viscosity, $g$ the gravitational acceleration and $\eta$ the dynamic viscosity.

## 3. Experimental results

All experiments are performed at an average temperature of 25 °C. All measurements were repeated at least 4 times. In all cases the deviation was less than 4%. Table 1 shows the thermophysical and transport properties determined for mixtures of sucrose–DMSO, glucose–DMSO and DMSO–PBS at different mass concentrations at an average temperature of 25 °C. Fig. 2 shows the thermal diffusion coefficient versus the mass concentration of sucrose (Fig. 2a) and glucose.

Fig. 2 shows how the thermodiffusion coefficient decreases linearly as the solute concentration increases. At solute concentrations on the order of 30% of sucrose and glucose it is expected that the thermal diffusion coefficient changes sign, i.e. in these concentrations the denser component is directed toward the warmest wall. Therefore, at higher concentration of sugars in DMSO, the thermodiffusion coefficient is negative which will mean readjusting the sense of the temperature gradient depending on the range of solute concentration in the mixture in order to optimize the separation.

## 4. Numerical simulation

Through numerical studies performed in a finite volume method (FVM) based fluid flow solver [12], the possibility of optimizing the separation process in the microdevices by Soret effect is analyzed [13]. To this purpose, the geometry proposed by other researchers is used [3], which separates the DMSO only by molecular diffusion. This device shown in Fig. 3 is composed mainly of a central cavity of constant rectangular section where the separation occurs by diffusion of

**Table 1**
Thermophysic and transport properties of sucrose–DMSO, glucose–DMSO and DMSO–PBS mixtures at an average temperature of 25 °C.

| % Sucrose | Density (kg/m$^3$) | $\alpha$ (°C$^{-1}$) ($10^{-4}$) | $\beta$ ($10^{-1}$) | $\eta$ (kg/m s) ($10^{-3}$) |
|---|---|---|---|---|
| 5 | 1113.85 | 8.87 | 3.404 | 2.73 |
| 10 | 1132.89 | 8.57 | 3.41 | 4.05 |
| 15 | 1152.37 | 8.28 | 3.438 | 6.4 |
| 20 | 1172.38 | 8.03 | 3.449 | 10.95 |
| 25 | 1192.70 | 7.72 | 3.532 | 20.59 |
| % Sucrose | Density (kg/m$^3$) | $\alpha$ (°C$^{-1}$) ($10^{-4}$) | $\beta$ ($10^{-1}$) | $\eta$ (kg/m s) ($10^{-3}$) |
| 5 | 1114.08 | 8.86 | 3.405 | 2.93 |
| 10 | 1133.12 | 8.56 | 3.402 | 4.06 |
| 15 | 1152.62 | 8.30 | 3.4 | 6.34 |
| 20 | 1172.36 | 8.01 | 3.399 | 10.55 |
| 25 | 1192.41 | 7.69 | 3.386 | 18.73 |
| % PBS | Density (kg/m$^3$) | $\alpha$ (°C$^{-1}$) ($10^{-4}$) | $\beta$ ($10^{-1}$) | $\eta$ (kg/m s) ($10^{-3}$) |
| 10 | 1070.64 | 3.97 | 0.706 | 1.345 |

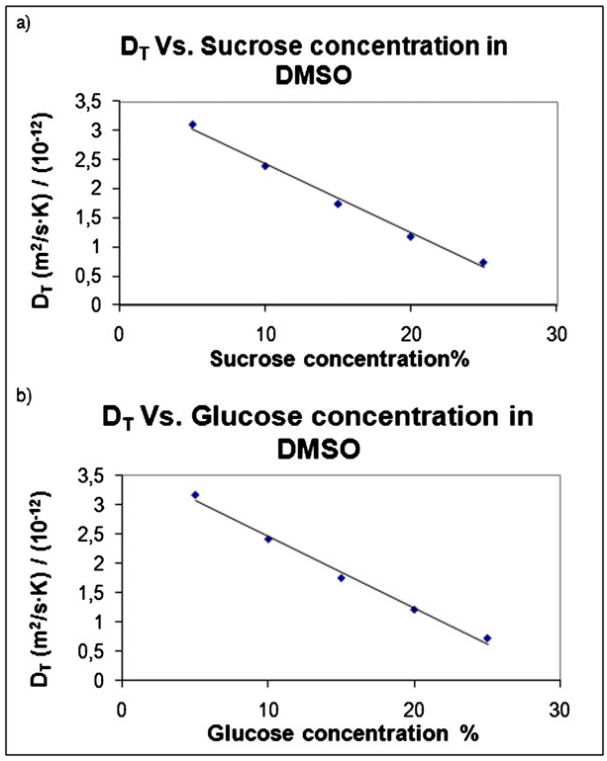


**Fig. 2.** Variation of the thermal diffusion coefficient in mixtures of a) sucrose–DMSO, b) glucose–DMSO versus the mass concentration and at a temperature of 25 °C.

DMSO. The flows are introduced through two opposing inlets. These two flows are separated by a splitter plate that redirects the flow and prevents the mixing between them, so that they flow in parallel to the central cavity. The flow extraction is performed by two outputs identical to the inlet design. From the top entry cleaning liquid is introduced, which in this case is PBS, while from the bottom entry a mixture of 10% DMSO in PBS is introduced.

The model used in the numerical simulation represents the main parts of the device, i.e. the central cavity and the transition to outlets. The central cavity consists of two flat plates that generate a constant rectangular cavity. The dimensions of it are exactly those used in [3], 25 mm wide, 500 μm high and 75 mm long. Downstream of this section, constant area geometry is used as transition to outlets. The overall length from the beginning of the central cavity to the outlets, is $L = 111$ mm. In Fig. 4a can be appreciated the two inputs coupled to the central cavity in order to achieve fully developed flow in the cavity. In Fig. 4b the whole geometry can be seen, where the transition from the central cavity to the outlets is shown.

A 3-D incompressible implicit numerical method is used. For higher accurate results double precision option is used and to avoid instabilities second order discretization for pressure, density, momentum, mass flux and energy is used too.

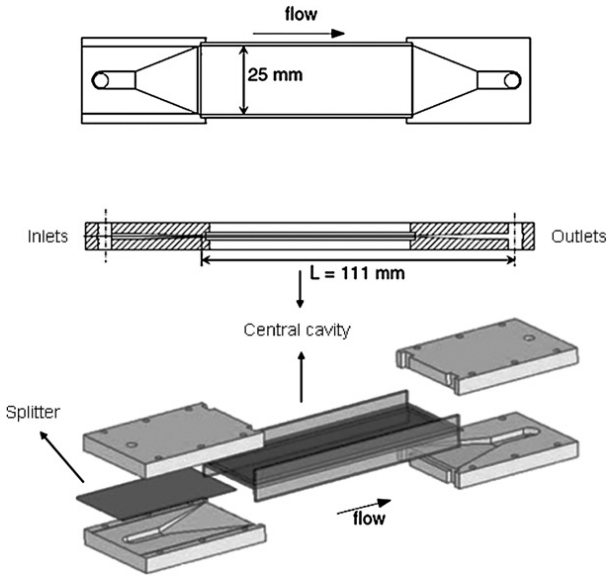


**Fig. 3.** Diagram of the experimental device used in [3].

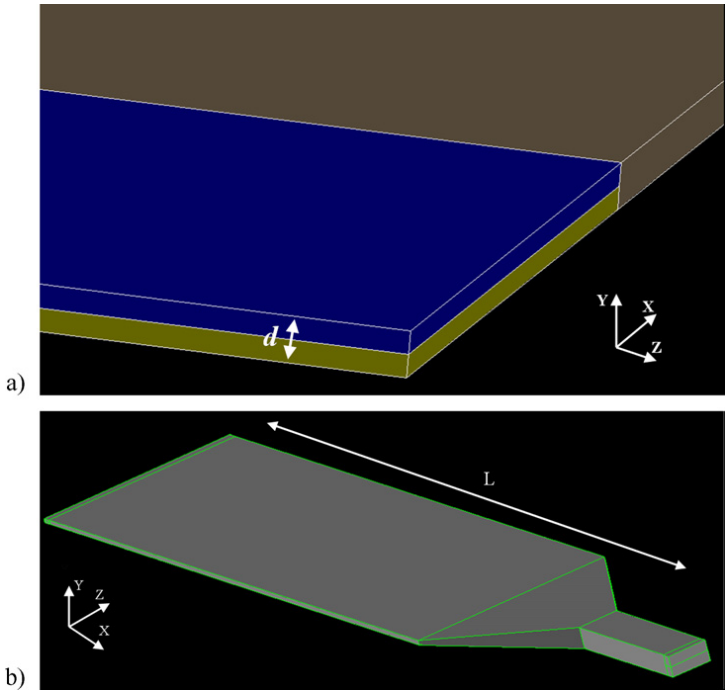


**Fig. 4.** Model used. a) Detail of the entrance area of the flow, b) general view of the device model.

A fourteen order of magnitude residual level drop is selected to convergence in this study to be sure that the system reaches the steady state. The final mesh configuration consists of 416 000 hexahedral cells.

### *4.1. Governing equations*

The fully developed flow in a microchannel is governed by the Navier–Stokes equations (Eq. (2)) for the geometrical model of the channel depicted in Fig. 4:

$$\frac{\partial^2 u}{\partial x^2} + \frac{\partial^2 u}{\partial y^2} + \frac{\partial^2 u}{\partial z^2} = \frac{1}{\eta}\frac{\mathrm{d}p}{\mathrm{d}x}$$

**Table 2**
Comparison of the separation ratio with and without Soret effect for DMSO–PBS mixture with a mass fraction of 10% DMSO at $T = 25\,^{\circ}\mathrm{C}$.

| $f_q$ | $q_t$ ($m^3$/min) ($10^{-8}$) | $c_c/c_0$ [3] | $c_c/c_0$ (Soret) | Improvement (%) |
|---|---|---|---|---|
| 0.1 | 3.3 | 0.13 | 0.08 | 35.84 |
| 0.1 | 5.4 | 0.17 | 0.13 | 25.12 |
| 0.1 | 7.5 | 0.20 | 0.17 | 17.20 |
| 0.1 | 13.3 | 0.26 | 0.24 | 8.13 |
| 0.15 | 3.3 | 0.20 | 0.15 | 26.40 |
| 0.15 | 5.4 | 0.25 | 0.21 | 15.92 |
| 0.15 | 7.5 | 0.29 | 0.26 | 10.72 |
| 0.15 | 13.3 | 0.37 | 0.35 | 5.68 |
| 0.23 | 3.3 | 0.30 | 0.25 | 15.63 |
| 0.23 | 5.4 | 0.36 | 0.33 | 7.72 |
| 0.23 | 7.5 | 0.41 | 0.39 | 4.22 |
| 0.23 | 13.3 | 0.52 | 0.50 | 3.85 |
| 0.37 | 3.3 | 0.46 | 0.42 | 9.61 |
| 0.37 | 5.4 | 0.53 | 0.50 | 5.23 |
| 0.37 | 7.5 | 0.59 | 0.57 | 3.39 |
| 0.37 | 13.3 | 0.69 | 0.67 | 2.62 |

$$\frac{\partial^2 v}{\partial x^2} + \frac{\partial^2 v}{\partial y^2} + \frac{\partial^2 u}{\partial z^2} = \frac{1}{\eta}\frac{\mathrm{d}p}{\mathrm{d}y}$$
$$\frac{\partial^2 \omega}{\partial x^2} + \frac{\partial^2 \omega}{\partial y^2} + \frac{\partial^2 \omega}{\partial z^2} = \frac{1}{\eta}\frac{\mathrm{d}p}{\mathrm{d}z} \tag{2}$$

where $u$, $v$ and $\omega$ are the velocity components and $p$ is the pressure. To study the molecular diffusion between streams "Species Transport" model is necessary. To know the contribution of the temperature gradient the "thermodiffusion" option is enabled too. Mass transport is formulated in Eq. (3) [14]:

$$\vec{J} = -\rho D \nabla c_0 - \rho D_T c_0 (1 - c_0) \nabla T \tag{3}$$

where $D$ is the molecular diffusion coefficient and $T$ is the temperature. For molecular diffusion, not having this property the value of order $\sim 10^{-9}$ $m^2/s$ used also in [3] has been chosen. To analyze the effect of thermodiffusion, the properties of the mixture determined experimentally are used. Jointly a temperature difference is imposed between the top and the bottom walls of the dispositive. As the DMSO is the heaviest component and the mixture of 10% of DMSO in PBS has a positive Soret effect, the bottom wall is heated and the top wall cooled. This will boost the DMSO to the washing stream (PBS) enhancing the separation. The chosen working temperature difference is 10 K.

As we analyze different density fluid streams and due to diffusion the density varies, the Boussinesq approximation (Eq. (4)) to account those changes in density is used:

$$\rho = \rho_0\big(1 - \alpha(T - T_0) - \beta(c - c_0)\big) \tag{4}$$

where $\rho_0$ is the density for 10% of DMSO in PBS. User defined function (UDFs) are written in C++ programming language and are successfully incorporated into the present model to account for the changes in density.

### 4.2. Boundary conditions

No-slip boundary conditions are imposed at walls, which mean: $u = v = \omega = 0$. Outflow 0.5 outlet condition is applied at both outlets in order to have same volumetric flow rate conditions at the outlets.

### 4.3. Numerical results

Table 2 provides a comparison of results obtained in [3] and those obtained in this study using the Soret effect. Sixteen different cases were analyzed in total. At Table 2 the dimensionless variable dependent on the concentration of the bottom plate is represented $c_c/c_0$, where $c_0$ is the initial mass concentration of DMSO (10%) and $c_c$ the mass concentration of DMSO in the output. In the same way it is represented a fraction of the inflows, defined in Eq. (5):

$$f_q = \frac{q_c}{q_t} \tag{5}$$

where $q_c$ is the flow of the mixture DMSO–PBS and $q_t$ the total input flow. The inlet flow of PBS is $q_w$ and therefore $q_t = q_c + q_w$.

As can be seen, the results of Table 2 show a clear improvement in the separation process by the Soret effect, which can reach up to 35% for a total volumetric flow of $3{,}33 \times 10^{-8}$ $m^3/s$. In the same way the results are shown in a neutral diagram (Fig. 5) of the dimensionless variable dependent $c_c/c_0$ as a function of $(1/P_e) \times (L/d)$, where $P_e$ is the Peclet number, and

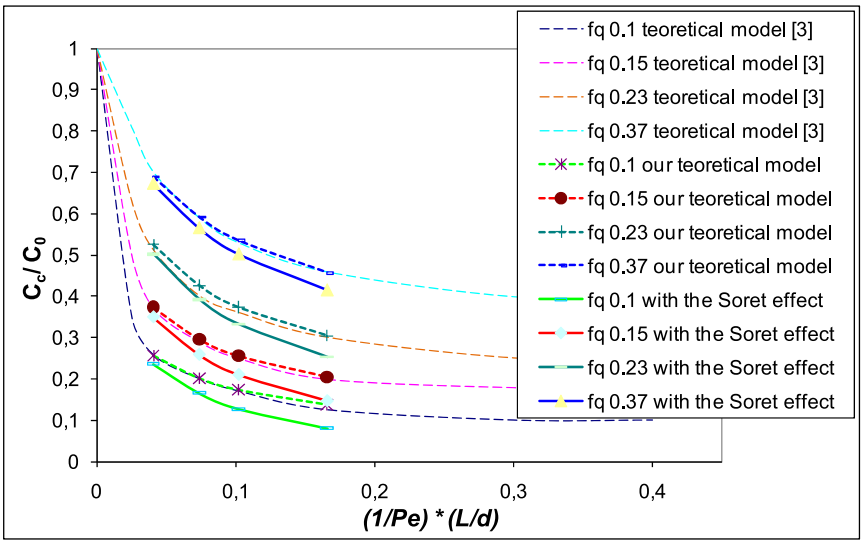


**Fig. 5.** DMSO extraction fraction $c_c/c_0$ as a function of $(1/P_e) \times (L/d)$.

$L$ and $d$ are the length and height of the diffusion zone, respectively. The Peclet number is represented as $P_e = U \cdot d/D$, where $U$ is the characteristic velocity. These variables are parameterized by $f_q$, where the results of [3] are compared with this work diffusion and Soret effect model.

As shown in Fig. 5, the results obtained for the diffusion model of this work are in well agree with those of [3]. Even the amount of DMSO diffused into the cleaning flow (PBS) is higher due to the temperature gradient applied. As shown in Table 2, the lower the difference between inflows best results are obtained. In the same way, the lower the flow velocity best results are obtained. Thus, for all tested flows an improvement in separation by the Soret effect is achieved.

## 5. Conclusions

This work has highlighted the importance of the transport properties in microfluidics, as well as its applications in biotechnological mixtures. Similarly, it has reflected the importance of experimental data in the numerical study. In this case, we have explored the possibility of the removal of DMSO by molecular diffusion and proposed an improvement by implementing the Soret effect. The results showed an improvement in the process of extracting up to 35%. In this way we can reduce the final size of the device and the extraction time. Therefore, we propose a more efficient and lower cost microdevice due to the decrease in extraction channel length and extraction time.

## Acknowledgements

This study was realized with the grants from the LOCUS project of R+D+I national plan of the Department of Education and Science of the Spanish Government and with GOVSORET, MIVDIRA, DIRAMINA and MICNOFLU projects of the Basque Government.

## References

[1] J. Köhler, M.T. Henkel, Chip devices for miniaturized biotechnology, Appl. Microbiol. Biotechno. 69 (2005) 113–125.
[2] K.K. Fleming, E.K. Longmire, A. Hubel, Numerical characterization of diffusion-based extraction in cell-laden flow through a microfluidic channel, Journal of Biomechanical Engineering 129 (2007) 703–711.
[3] C. Mata, E.K. Longmire, D.H. McKenna, K.K. Glass, A. Hubel, Experimental study of diffusion-based extraction from a cell suspension, Microfluid Nanofluid 5 (2008) 529–540.
[4] K.K. Fleming, E.K. Longmire, A. Hubel, Optimization of a microfluidic device for diffusion-based extraction of DMSO from a cell suspension, International Journal of Heat and Mass Transfer 51 (2008) 5749–5757.
[5] J.K. Platten, M.M. Bou-Ali, P. Blanco, J.A. Madariaga, C.J. Santamaria, Phys. Chem. B 111 (2007) 11524–11530.
[6] A. Torreggiani, M. Di Foggia, I. Manco, S.A. Markarian, S. Bonora, Effect of sulfoxides on the thermal denaturation of hen lysozyme: A calorimetric and Raman study, Journal of Molecular Structure 891 (2008) 115–122.
[7] N.H. Chao, C.P. Chiang, H.W. Hsu, C.T. Tsai, T.T. Lin, Toxicity tolerance of oyster embryos to selected cryoprotectants, Aquat. Living Resour. 7 (1994) 99–104.
[8] V. Antonenas, K. Bradstock, P. Shaw, Effect of washing procedures on unrelated cord blood units for transplantation in children and adults, Cytotherapy 4 (2002) 16.
[9] J.K. Platten, M.M. Bou-Ali, P. Costeseque, J.K. Dutrieux, W. Köhler, C. Leppla, S. Wiegand, G. Wittko, Benchmark values for the Soret, thermal diffusion and diffusion coefficients of three binary organic liquid mixtures, Philosophical Magazine 83 (2003) 1965–1971.
[10] M.M. Bou-Ali, J.J. Valenciaga, J.A. Madariaga, C. Santamaría, O. Ecenarro, J.K. Dutrieux, Determination of the thermodiffusion coefficient in three binary organic liquid mixtures by the thermogravitational method, Philosophical Magazine 83 (2003) 2011–2015.

[11] M.M. Bou-Ali, O. Ecenarro, J.A. Madariaga, C.M. Santamaría, J.J. Valencia, Thermogravitational measurement of the Soret coefficient of liquid mixtures, Journal of Physics 10 (1998) 3321–3331.
[12] Fluent, Fluent Inc., Version 6.3.26, 2006.
[13] H. Barrutia, A. Martin, A. Zebib, M.M. Bou-Ali, Thermal diffusion effects in T-shaped micromixers, in: 1st European Conference on Microfluidics, Bologna, 2008.
[14] S.R. De Groot, P. Mazur, Non-Equilibrium Thermodynamics, North-Holland Pub. Co., Amsterdam, 1962.

# Apéndice D

# Termodifusión y Difusión Molecular en Mezclas Binarias de $n$-Alcanos: Experimentos y Análisis Numérico

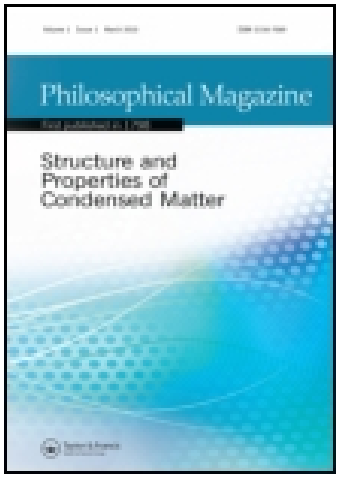


Philosophical Magazine
Publication details, including instructions for authors and subscription information:
http://www.tandfonline.com/loi/tphm20

# Thermodiffusion and molecular diffusion in binary *n*-alkane mixtures: experiments and numerical analysis

S. Srinivasan [a] , D. Alonso de Mezquia [b] , M.M. Bou-Ali [b] & M.Z. Saghir [a]

[a] Department of Mechanical Industrial Engineering, Ryerson University, Toronto, Ontario M5B 2K3, Canada

[b] Manufacturing Department, Mondragon Unibertsitatea, Loramendi, 4 Apartado, 20500 Mondragon, Spain

Available online: 31 Oct 2011

To cite this article: S. Srinivasan, D. Alonso de Mezquia, M.M. Bou-Ali & M.Z. Saghir (2011): Thermodiffusion and molecular diffusion in binary *n*-alkane mixtures: experiments and numerical analysis, Philosophical Magazine, 91:34, 4332-4344

To link to this article: http://dx.doi.org/10.1080/14786435.2011.617716

*Philosophical Magazine*
Vol. 91, No. 34, 1 December 2011, 4332–4344



# Thermodiffusion and molecular diffusion in binary *n*-alkane mixtures: experiments and numerical analysis

S. Srinivasan[a]*, D. Alonso de Mezquia[b], M.M. Bou-Ali[b] and M.Z. Saghir[a]

[a]*Department of Mechanical Industrial Engineering, Ryerson University, Toronto, Ontario M5B 2K3, Canada;* [b]*Manufacturing Department, Mondragon Unibertsitatea, Loramendi, 4 Apartado, 20500 Mondragon, Spain*

(*Received 17 May 2011; final version received 22 August 2011*)

New experimental data on the thermodiffusion and molecular diffusion coefficients of nine non-equimolar binary mixtures of $nC_6 - nC_i$ ($i = 10, \ldots, 18$) at 298 K and 1 atm have been reported. The data have been obtained using a combination of the thermogravitational column and the sliding symmetric tubes technique, respectively. It was found that with an increase in the disparity between the two components, the Soret effect becomes more dominant. Further, the stronger Soret effect weakens the molecular diffusion process. These trends are observed in the form of an increase in magnitude of the thermodiffusion coefficient and a decrease in the magnitude of the molecular diffusion coefficient. Numerical analysis was also performed using the principles of non-equilibrium thermodynamics. The model was able to predict the experimental data as well as the trends fairly accurately.

**Keywords:** experiments; thermodiffusion; molecular diffusion; hydrocarbons; numerical simulation



## 1. Introduction

*Thermodiffusion* or the *Ludwig–Soret effect* or simply the *Soret effect*, is a phenomenon in which an applied temperature gradient induces a concentration gradient in the mixture [1,2]. However, the onset of a concentration gradient almost immediately initiates a counter-force in the form of Fickian diffusion. Thus, in a binary mixture, one can write the net mass flux, $J$, under the influence of these two opposing forces as

$$J = -\rho D \nabla c - \rho D_T c(1 - c) \nabla T, \tag{1}$$

where $D_T$ is the thermodiffusion coefficient, $D$ is the molecular diffusion coefficient, $\rho$ is the mixture density, $c$ is the mass fraction of the reference species and $T$ is the temperature. At equilibrium, the net concentration gradient will depend on the Fickian and thermodiffusion coefficients, which can be experimentally determined.

While the mass transfer phenomenon has been the subject of many investigations because of its importance in areas such as medicine and physiology [3],

*Corresponding author. Email: seshasai.srinivasan@ryerson.ca

ISSN 1478–6435 print/ISSN 1478–6443 online

http://dx.doi.org/10.1080/14786435.2011.617716
http://www.tandfonline.com

thermodiffusion is speculated to play a role in natural processes such as solar ponds [4], ocean demographics [5], convection in stars [6], etc. In industrial applications, it is the mechanism employed for separation and characterization in thermal field-flow fractionation devices [7].

Among other avenues, thermodiffusion is known to affect the distribution of the components of hydrocarbons in an underground oil reservoir [8]. This has prompted theoretical [9–16] as well as experimental investigations [17–20] on thermodiffusion in hydrocarbon mixtures. While a theoretical formulation exists for multi-component mixtures [21], due to the complexity of the problem, experiments are often undertaken on binary [18,22,23] and ternary [24–26] hydrocarbon mixtures. Recently, a four-component mixture has also been studied by Van Vaerenbergh et al. [27].

Various experimental techniques have been devised over the years to understand thermodiffusion. A comparison of a subset of these methods was presented by Platten et al. [28] in which binary mixtures of dodecane, isobutylbenzene and 1,2,3,4-tetrahydronaphthalene were investigated using several experimental approaches. From the results of these experiments, the Fontainebleau benchmark values of thermodiffusion coefficient for these mixtures were established [23,29–32]. A detailed review of all the methods has been published recently by Srinivasan and Saghir [33]. Likewise, several devices have been developed to analyze and determine the molecular diffusion coefficient. Modern techniques include Open Ended Capillary (OEC) [34] and Thermal Diffusion Forced Rayleigh Scattering (TDFRS) [35].

While the composition distribution in an underground oil reservoir is influenced by the combined effect of thermodiffusion and molecular diffusion, there is a limited amount of experimental data even for binary hydrocarbon mixtures. As a result, our understanding of the thermodiffusion process is very limited and has consequently hampered the formulation of an accurate thermodiffusion model. Hence, as a primary objective, in this study a thermogravitational column (TGC) and the sliding symmetric tubes technique have been used to determine the thermodiffusion and the molecular diffusion coefficients, respectively, in several binary *n*-alkane mixtures at 298 K and atmospheric pressure. Specifically, mixtures of hexane ($nC_6$) and $nC_i$ ($i = 10, \ldots, 18$) have been studied. The mixtures have also been studied theoretically using a computational model that is based on the principles of non-equilibrium thermodynamics.



## 2. Experiments

### 2.1. *Thermodiffusion*

The experiments of this study have been carried out using a thermogravitational column. Specifically, a cylindrical thermogravitational column that is capable of handling mixture pressures of up to 500 bars was used [36]. The column has a height of $L_z = 0.5 \pm 0.001$ m and a gap of $L_x = 1 \times 10^{-3} \pm 5 \times 10^{-6}$ m. The behavior of this apparatus has been validated with respect to the experimental data of binary mixtures [37]. The validation has also been made with respect to the cylindrical and parallelepipedic versions of the thermogravitational column for alkane mixtures [18].

The working principles of a TGC are as follows. With the application of a horizontal temperature gradient, the denser component separates to the cold side

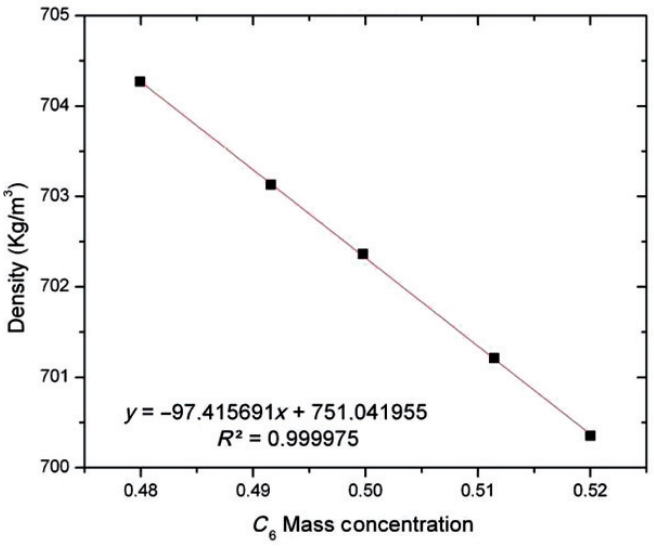


Figure 1. Density of $nC_6 - nC_{13}$ mixture for different concentrations of $nC_6$ in the mixture at 298 K.



and advects to the bottom of the column. In other words, a vertical concentration gradient is established along the height of the TGC. The developed theory of TGC relates this steady state separation and $D_T$ for a reference component as [34]

$$\Delta c = -\frac{504 L_z}{g L_x^4} \frac{D_T \nu}{\alpha} c_0(1 - c_0), \tag{2}$$

where $\nu$ and $\alpha$ are the kinematic viscosity and thermal expansion coefficient, respectively. Further, $\alpha$ is related to the mixture density as $\alpha = -(1/\rho)(\partial\rho/\partial T)$. Knowing $\Delta c$, $\nu$ and $\alpha$, $D_T$ of the reference species can be derived. These quantities have been determined as discussed below.

A preliminary calibration curve was generated to relate the mass fraction with the density of the mixture (cf. Figure 1). This calibration is made by measuring the density of several mixtures of known composition. In this study, these small compositions were made by a 310 g capacity balance with an accuracy of 0.0001 g. Further, the mass fractions of the mixtures are close to the original mass fraction, i.e., $c_0 \pm 0.02$. For measuring the density, an Anton Paar DMA 5000 vibrating quartz U-tube densimeter with a repeatability of $1 \times 10^{-6}$ g/cm$^3$ was used. Also, from the calibration curve of density and concentration, observing the linear relation between the two, the slope of the line in Figure 1 is used to calculate the mass expansion coefficient ($\beta$) via the following relation

$$\beta = \frac{1}{\rho} \frac{\partial \rho}{\partial c}. \tag{3}$$

To measure the concentration gradient, samples extracted from five equidistant sampling points along the height of the column were analyzed to

determine the density of the mixture. The concentration gradient was then determined as

$$\Delta c = \frac{L_z}{\beta\rho}\frac{\partial\rho}{\partial z}. \tag{4}$$

Now, comparing Equations (2) and (4) we can express $D_T$ as

$$D_T = -\frac{gL_x^4}{504}\frac{\alpha}{c_0(1-c_0)\beta\eta}\frac{\partial\rho}{\partial z}, \tag{5}$$

where $\eta$ is the dynamic viscosity of the mixture that is experimentally determined using a Haake falling-ball viscometer with a precision of $\pm 1\%$. It must be noted that as per the above equation $D_T > 0$ when the denser component migrates to the cold side, i.e., advects to the bottom of the column.

Experiments were performed on binary mixtures of $nC_6 - nC_i$, $i = 10, 11, \ldots, 18$, at 298 K and atmospheric pressure. All the components used in this study were Merck products with purity better than 99%. The mixtures were prepared by adding the more volatile component to the less volatile one. The mixture was then shaken to ensure a homogeneous composition. For the experiments, 300 $cm^3$ of mixture was needed in a TGC. Hence, mixtures were prepared using a balance with a capacity of 4500 g and an accuracy of 0.01 g. Following the mixture preparation, its density was measured and compared with the calibration curve to ensure the correct composition. The composition of $nC_6$ in each mixture and the mixture properties are summarized in Table 1.

For each binary mixture the experiment was repeated three times. To ensure that a stationary state has been reached, experiments were conducted for a much longer duration than the *relaxation time*, $t_r$, that is given as

$$t_r = \frac{9!(l_z\nu)^2 D}{(g\pi\alpha\Delta T L_x^3)^2}, \tag{6}$$

Table 1. Thermophysical properties of each $nC_6 - nC_i$ mixture at 298 K and 1 atm.

| $nC_i$ | $x_{nC_6}$ | $\rho$ (kg/m$^3$) | $\alpha\times10^3$ (K$^{-1}$) | $\beta$ | $\eta\times10^3$ (Pa s) |
|---|---|---|---|---|---|
| $nC_{10}$ | 0.623 | 689.823 | 1.20 | 0.103 | 470.4 |
| $nC_{11}$ | 0.645 | 694.886 | 1.178 | 0.118 | 531.2 |
| $nC_{12}$ | 0.664 | 698.803 | 1.159 | 0.128 | 558.1 |
| $nC_{13}$ | 0.681 | 702.374 | 1.142 | 0.139 | 610.3 |
| $nC_{14}$ | 0.697 | 705.405 | 1.132 | 0.147 | 655.6 |
| $nC_{15}$ | 0.711 | 708.106 | 1.120 | 0.155 | 693.8 |
| $nC_{16}$ | 0.724 | 710.322 | 1.110 | 0.161 | 744.6 |
| $nC_{17}$ | 0.736 | 712.325 | 1.106 | 0.167 | 773.7 |
| $nC_{18}$ | 0.747 | 714.123 | 1.090 | 0.172 | 826.5 |

where $\Delta T$ is the applied temperature difference, 6°C in the present experiments. While the duration of the experiments was $t = 5t_r$, in one of the trials the experimental duration was $t = 15t_r$. This was done to ensure that a stationary state with maximum possible separation has been reached.

The thermodiffusion coefficients of these mixtures are summarized in Table 2 with an experimental error of less than 5%. The negative sign of $D_T$ indicates that $nC_6$, the lighter component, migrates to the hot side, i.e., collects at the top of the TGC. It can be seen that the magnitude of the thermodiffusion coefficient increases as the disparity between the two participating components increases. This trend is graphically represented in Figure 2, where the disparity between the molecules is represented by the difference in the molecular weight of the two components. As can be seen in this figure, there is a linear relationship between $D^T$ and $\Delta M$. This linear



Table 2. Experimental values of the thermodiffusion, molecular diffusion and the Soret coefficient of each $nC_6 - nC_i$ mixture at 298 K and 1 atm.

| $nC_i$ | $D_T^{\text{expt}} \times 10^{12}$ ($m^2$/s K) | $D^{\text{expt}} \times 10^9$ ($m^2$/s) | $S_T^{\text{expt}} \times 10^3$ (1/K) |
|---|---|---|---|
| $nC_{10}$ | −6.71 | 2.54 | −2.65 |
| $nC_{11}$ | −6.65 | 2.27 | −2.93 |
| $nC_{12}$ | −7.45 | 2.09 | −3.57 |
| $nC_{13}$ | −7.57 | 1.96 | −3.86 |
| $nC_{14}$ | −7.95 | 1.76 | −4.50 |
| $nC_{15}$ | −8.28 | 1.59 | −5.22 |
| $nC_{16}$ | −8.37 | 1.50 | −5.58 |
| $nC_{17}$ | −8.57 | 1.40 | −6.11 |
| $nC_{18}$ | −8.9 | 1.37 | −6.49 |

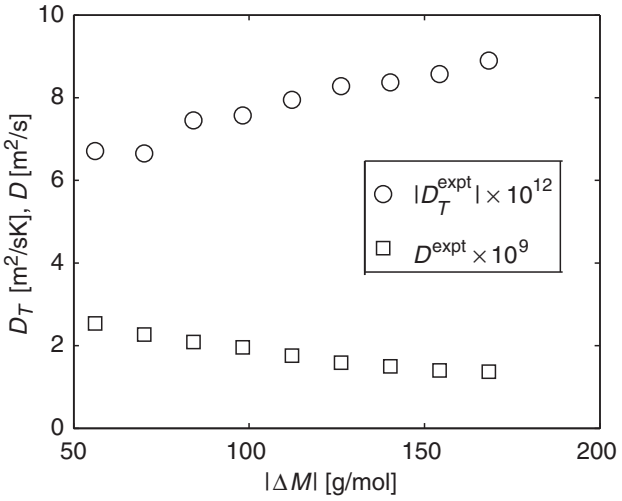


Figure 2. $D_T^{\text{expt}}$ and $D^{\text{expt}}$ plotted against the difference between the molecular weights of the components ($\Delta M = M_{nC_6} - M_{nC_i}$).

trend is in agreement with the observations of Blanco et al. [36] and Madariaga et al. [38] for binary *n*-alkane mixtures.

### 2.2. *Molecular diffusion*

For the determination of the molecular diffusion coefficient, the *sliding symmetric tubes* technique, validated with the experimental data of several binary mixtures [28,39–42], was used. This method consists of several sets of two identical vertical tubes of length $L$ each containing a mixture with slightly different mass concentrations. The mixture with the higher concentration of the denser component is placed in the lower tube in order to eliminate convection.

At the beginning of the experiment, several sets (typically 10) in their separated configuration are placed in a water bath that is at a constant temperature until they all reach the working temperature. The sets are then changed to the faced configuration allowing the diffusion to start. At specified instants of time the sets are changed one by one back to the separated configuration to stop the mass transfer. The densities of the mixtures are measured and the average concentration inside each tube is determined from the calibration data. Thus, the change of the average concentration with time is obtained for both tubes.

From the mathematical point of view, the mass transport in one direction ($z$) obeys the equation

$$\frac{\partial c}{\partial t} = D\frac{\partial^2 c}{\partial z^2}. \tag{7}$$

The associated boundary conditions are

$$c(z,0) = \begin{cases} c^{\text{top}} & z > 0 \\ c^{\text{bot}} & z < 0 \end{cases}$$

$$\frac{\partial c(z,t)}{\partial z} = 0, \text{ at } z = \pm L \text{ and } t > 0.$$

In the above equations, $c^{\text{top}}$ and $c^{\text{bot}}$ are the concentrations at the top and bottom tube, respectively. Solving for $c$, the following expressions are obtained for the average concentrations at the top ($\overline{c^{\text{top}}}$) and bottom ($\overline{c^{\text{bot}}}$) tubes

$$\overline{c^{\text{top}}(t)} - \frac{c^{\text{top}} + c^{\text{bot}}}{2} = \frac{8}{\pi^2}\left(c_i^{\text{top}} - \frac{c_i^{\text{top}} + c_i^{\text{bot}}}{2}\right)\Phi, \tag{8}$$

$$\overline{c^{\text{bot}}(t)} - \frac{c^{\text{top}} + c^{\text{bot}}}{2} = -\frac{8}{\pi^2}\left(c_i^{\text{top}} - \frac{c_i^{\text{top}} + c_i^{\text{bot}}}{2}\right)\Phi, \tag{9}$$

where

$$\Phi = \sum_{n=0}^{\infty} \frac{e^{-(n+0.5)^2(\pi^2/L^2)Dt}}{(2n+1)^2}. \tag{10}$$

By measuring the concentration as a function of time, the molecular diffusion coefficient can be obtained from Equations (8) and (9).

The molecular diffusion coefficients of these mixtures are summarized in Table 2. The uncertainty in the experimental data is less than 2%. The table also includes the Soret coefficient ($S_T^{\text{expt}}$) which is the ratio of the thermodiffusion and molecular diffusion coefficients, i.e., $S_T^{\text{expt}} = D_T^{\text{expt}}/D^{\text{expt}}$. As seen in the table, the molecular diffusion coefficient decreases linearly in magnitude as the disparity between the molecules increases (cf. Figure 2). This is because with an increase in the difference between the molecules, the thermodiffusion process gains strength and this impinges on the molecular diffusion process. In other words, molecular diffusion decreases in magnitude.



## 3. Evaluation from the non-equilibrium thermodynamic model

The experimental mixtures have also been studied using the principles of non-equilibrium thermodynamics that has been used to present a formalism for thermodiffusion theory in multicomponent mixtures. According to this theory [21,43], when a $n$-component mixture in mechanical equilibrium is subjected to a thermal gradient, there is a segregation of the components of the mixture. The molar diffusion flux, $J_i$, of the $i$th component in the mixture, with respect to the molar average velocity, can be expressed as

$$J_i = -\sum_{k=1}^{n-1} L_{ik}\left[\frac{(Q_k^* - Q_n^*)}{T}\nabla T + \sum_{j=1}^{n-1}\frac{\partial \mu_k}{\partial x_j}\nabla x_j\right], \tag{11}$$

where $x_i$ is the mole fraction of the $i$th component, $T$ is the temperature, $\mu_i$ is the chemical potential, $Q_i^*$ is the net heat of transport of the $i$th component and $L_{ik}$ are the phenomenological coefficients.

On the other hand, Equation (1) for an $n$-component mixture can be written as

$$J_i = -\chi\left(\sum_{j=1}^{n-1} D_{ij}\nabla x_j + D_{T,i}\nabla T\right), \tag{12}$$

where $\chi$ is the total mole density, $D_{ij}$ are the Fickian diffusion coefficients and $D_{T,i}$ is the thermodiffusion coefficient. Comparing Equations (11) and (12) we can write the expression for the thermodiffusion coefficients as:

$$D_{T,i} = \frac{L_{iq}}{\chi T}, \tag{13}$$

where $L_{iq}$ is

$$L_{iq} = \sum_{k=1}^{n-1}(Q_k^* - Q_n^*)L_{ik}. \tag{14}$$

Thus, the key aspect of the thermodiffusion calculation is the estimate of the net heat of transport and the phenomenological coefficients. The calculation of these factors is discussed next.

$Q_i^*$ is the net amount of energy which must be absorbed by the region per mole of a component while diffusing out in order to maintain the constancy in the temperature and pressure of the mixture [12]. Further, as suggested by Denbigh [44] $Q_i^*$ can be expressed in terms of the energy needed to detach a molecule $i$ from its neighbors and the energy given out when a molecule fills the hole. Dougherty and Drickamer [45] suggested the use of viscous energy as a good approximation of the energy needed to detach a molecule and proposed an expression for the thermodiffusion factor in a binary mixture. Firoozabadi and co-workers [21] extended the work of Dougherty and Drickamer to multicomponent mixtures and they proposed the following equation for the net heat of transport that is also employed in this study

$$Q_i^* = \frac{U_i}{\tau_i} + \left( \sum_{j=1}^{n} x_j U_j \Big/ \tau_j \right) \frac{V_j}{\sum_{k=1}^{n} x_k V_k}, \tag{15}$$

where $\tau_i$ is the ratio of the cohesive and viscous energy of component $i$. $U_i$ and $V_i$ are the partial molar internal energy and partial molar volume, respectively, that are calculated using the Peng–Robinson equation of state (PR EOS) [46,47]. The parameters that are used by PR EOS for these calculations are summarized in Table 3, whereas the detailed calculation procedure using these data is outlined in [46,47].

The performance of PR EOS with respect to hydrocarbon mixtures has been validated by Galliero et al. [11]. The superior performance of PR EOS has also been demonstrated by Srinivasan and Saghir [12] for several hydrocarbon mixtures, where the authors have shown that compared to an equation of state like the Perturbed Chain Statistical Associating Fluid Theory (PCSAFT), PR EOS performs better due to a more accurate calculation of the density and chemical potential for a thermodiffusion model.

Table 3. Parameters and properties associated with the pure components of the mixture that are used by PR EOS to calculate various quantities of the thermodiffusion/molecular diffusion models. These include the molecular weight ($M$), the acentric factor ($\omega$), the critical temperature ($T_c$), the critical pressure ($P_c$), the critical volume ($V_c$), the molar volume at normal boiling point ($V_b$) and the ratio of cohesive and viscous energies ($\tau$).

| $nC_i$ | $M$ (g/mol) | $\omega$ | $T_c$ (K) | $P_c$ (MPa) | $V_c$ ($m^3/kg$) $\times 10^3$ | $V_b$ ($m^3/mol$) $\times 10^3$ | $\tau$ |
|---|---|---|---|---|---|---|---|
| $nC_6$ | 86.175 | 0.298 | 507.889 | 3.028 | 4.33 | 0.140 | 0.303 |
| $nC_{10}$ | 142.282 | 0.488 | 617.700 | 2.110 | 4.22 | 0.235 | 0.303 |
| $nC_{11}$ | 156.308 | 0.530 | 638.700 | 1.940 | 4.25 | 0.262 | 0.298 |
| $nC_{12}$ | 170.335 | 0.571 | 658.300 | 1.810 | 4.23 | 0.288 | 0.297 |
| $nC_{13}$ | 184.361 | 0.609 | 676.200 | 1.680 | 4.20 | 0.316 | 0.294 |
| $nC_{14}$ | 198.388 | 0.644 | 693.200 | 1.570 | 4.17 | 0.342 | 0.287 |
| $nC_{15}$ | 212.415 | 0.692 | 706.800 | 1.470 | 4.14 | 0.370 | 0.287 |
| $nC_{16}$ | 226.441 | 0.731 | 720.600 | 1.380 | 4.11 | 0.399 | 0.282 |
| $nC_{17}$ | 240.468 | 0.762 | 733.400 | 1.290 | 4.06 | 0.426 | 0.277 |
| $nC_{18}$ | 254.494 | 0.792 | 745.300 | 1.210 | 4.02 | 0.457 | 0.272 |

To obtain the phenomenological coefficients, $L$, the following relation derived by Firoozabadi et al. [9] is used

$$\sum_{l=1}^{n-1}\sum_{k=1}^{n-1}\frac{M_k x_k + M_n x_n \delta_{kl}}{M_k}\frac{\partial \ln f_k}{\partial x_j}\Big|_{x_j,T,P} L_{li} = \frac{\rho_m M_n x_n}{R} D_{ij}, \tag{16}$$

where $f_k$ and $M_k$ are the fugacity and the molecular weight of the $k$th component, respectively. In this equation, fugacity is calculated using PR EOS.

For calculating $D_{ij}$, the following expression for the diffusion coefficients in an $n$-component mixture as presented by Leahy-Dios and Firoozabadi [48] has been used

$$\mathbf{D} = \left(\mathbf{B^M}\right)^{-1}\mathbf{\Gamma}, \tag{17}$$

where $\mathbf{D}$ is the $(n-1)\times(n-1)$ matrix of diffusion coefficients, and $\mathbf{B^M}$ is a matrix that has elements

$$\begin{aligned} B^M_{ii} &= \frac{x_i}{\mathcal{D}_{in}} + \sum_{k=1,i\neq k}^{n}\frac{x_k}{\mathcal{D}_{ik}}, \quad i = 1,\ldots,n-1, \\ B^M_{ij} &= -x_i\left(\frac{1}{\mathcal{D}_{ij}} - \frac{1}{\mathcal{D}_{in}}\right), \quad i,j = 1,\ldots,n-1, i\neq j, \end{aligned} \tag{18}$$

where $\mathcal{D}_{ij}$ are the Stefan–Maxwell diffusion coefficients for each $i$-$j$ binary pair in the mixture that are calculated using the infinite dilution coefficients as discussed by Leahy-Dios and Firoozabadi [48]. Finally, $\mathbf{\Gamma}$ is a matrix with elements

$$\Gamma_{ij} = x_i\frac{\partial \ln f_i}{\partial x_j}\Big|_{x_j,T,P}, \quad i,j = 1,\ldots,n-1, \tag{19}$$

and is computed using the PR EOS. Further details of the calculation of $\mathbf{D}$ are presented in the work of Leahy-Dios and Firoozabadi [48].

The molecular diffusion coefficient computed by the non-equilibrium thermodynamic model (NE) is summarized in Table 4. These calculated values of $D$ agree well with the experimental data (cf. Figure 3), the errors being less than 5%.

Table 4. Thermodiffusion, molecular diffusion and the Soret coefficient of each $nC_6 - nC_i$ mixture at 298 K and 1 atm using the non-equilibrium thermodynamic theory. In the table, $S_T^{NE1} = D_T^{NE1}/D^{expt}$ and $S_T^{NE2} = D_T^{NE2}/D^{NE}$.

| $nC_i$ | $D^{NE}\times 10^9$ ($m^2$/s) | $D_T^{NE1}\times 10^{12}$ ($m^2$/s K) | $D_T^{NE2}\times 10^{12}$ ($m^2$/s K) | $S_T^{NE1}\times 10^3$ (1/K) | $S_T^{NE2}\times 10^3$ (1/K) |
|---|---|---|---|---|---|
| $nC_{10}$ | 2.50 | −6.75 | −6.65 | −2.66 | −2.66 |
| $nC_{11}$ | 2.26 | −7.92 | −7.89 | −3.49 | −3.49 |
| $nC_{12}$ | 2.06 | −8.31 | −8.21 | −3.98 | −3.98 |
| $nC_{13}$ | 1.92 | −8.65 | −8.48 | −4.41 | −4.41 |
| $nC_{14}$ | 1.75 | −9.79 | −9.72 | −5.55 | −5.55 |
| $nC_{15}$ | 1.65 | −9.25 | −9.64 | −5.83 | −5.83 |
| $nC_{16}$ | 1.52 | −10.56 | −10.71 | −7.04 | −7.04 |
| $nC_{17}$ | 1.42 | −10.12 | −10.26 | −7.22 | −7.23 |
| $nC_{18}$ | 1.33 | −10.48 | −10.21 | −7.64 | −7.65 |

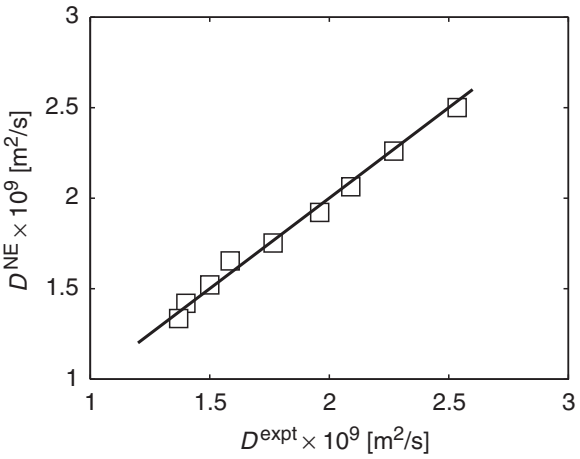


Figure 3. Comparison of the experimental ($D^{expt}$) and calculated molecular diffusion coefficient ($D^{NE}$) of the binary mixtures of $nC_6 - nC_i$ at 298 K and 1 atm. $D^{NE}$ is computed using the theory of non-equilibrium thermodynamics. The solid straight line is a fit of the data.

To calculate the thermodiffusion coefficients, the molecular diffusion coefficients from the experiments as well as the values calculated by the model were used. This was done to understand the sensitivity of the model to the variations in the molecular diffusion coefficients. The thermodiffusion coefficients from these two sets of $D$ are also presented in Table 4. $D_T^{NE1}$ represents the values obtained by using the experimental $D$, and $D_T^{NE2}$ is the result using the value of $D$ from the model ($D^{NE}$). Specifically, these are calculated as follows:

- For calculating $D_T^{NE1}$, experimental values of $D$ are used in Equation (16) to obtain the phenomenological coefficients. Using these values of $L_{ik}$ and calculating $Q_k^*$ from Equation (15), we can estimate $D_T^{NE1}$ via Equation (13).
- For calculating $D_T^{NE2}$, instead of using the experimental values of the molecular diffusion coefficient, the model of Leahy-Dios and Firoozabadi is employed [48] (cf. Equation 17) and the value $D^{NE}$ is used in Equation (16) to obtain the phenomenological coefficients. Next, using these values of $L_{ik}$ and the calculated value of $Q_k^*$ from Equation (15), $D_T^{NE2}$ is estimated via Equation (13).

The corresponding Soret coefficients are $S_T^{NE1} = D_T^{NE1}/D^{expt}$ and $S_T^{NE2} = D_T^{NE2}/D^{NE}$, respectively. A comparison of the thermodiffusion coefficients in Tables 2 and 4 shows that the direction of separation of the components is predicted accurately by non-equilibrium thermodynamic theory. Also, in Table 4 the thermodiffusion coefficients in columns three and four are nearly the same. This indicates that thermodiffusion is not very sensitive to small variations in $D$.

The Soret coefficients, $S_T^{NE1}$ and $S_T^{NE2}$, are equal and are summarized in the last two columns of Table 4. As in the experiments, the magnitude of the Soret coefficient increases with the increasing disparity between the molecules. In other words, the separation is stronger when the molecules are very different. A comparison of these Soret coefficients with the experimental value of $S_T$ is shown in Figure 4.

While the overall prediction of the NE model is fairly good, the disagreement increases with the increasing difference between the two components. This is perhaps

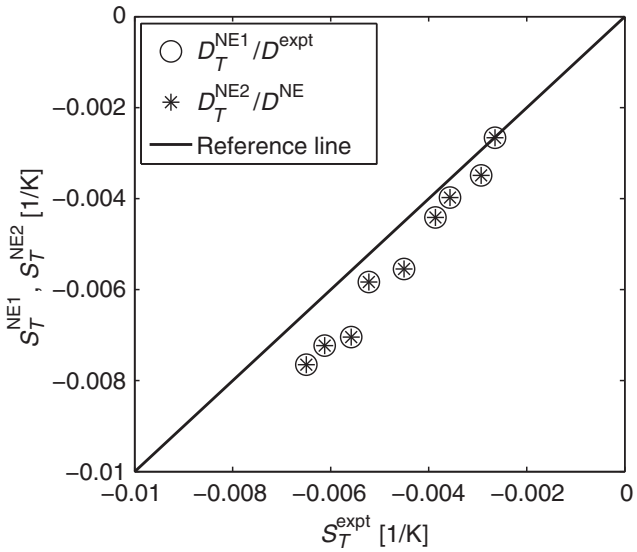


Figure 4. Comparison of the experimental ($S_T^{expt}$) and calculated ($S_T^{NE1}$, $S_T^{NE2}$) Soret coefficient of $nC_6$ for binary mixtures of $nC_6 - nC_i$ at 298 K and 1 atm. $S_T^{NE1} = D_T^{NE1}/D^{expt}$ and $S_T^{NE2} = D_T^{NE2}/D^{NE}$. The calculated values are obtained using the theory of non-equilibrium thermodynamics. The reference line with slope = 1 indicates agreement between the model and the experimental data.

an indicator that the disparity between the components must be represented more aggressively in the model. Nevertheless, we can conclude that the non-equilibrium thermodynamic theory is able to predict the thermodiffusion process fairly accurately using the concept of net heat of transport.

## 4. Conclusions

The thermodiffusion and molecular diffusion coefficients of nine non-equimolar binary mixtures of $nC_6 - nC_i$ ($i = 10, \ldots, 18$) have been experimentally determined. All mixtures were at 298 K and atmospheric pressure. For the thermodiffusion experiments, a previously validated cylindrical thermogravitational column was used. For measuring the molecular diffusion coefficients, the sliding symmetric tubes technique was employed. It was found that as the disparity between the two components increases, the thermodiffusion process becomes stronger, i.e., the magnitude of the thermodiffusion coefficient increases. This in turn impedes the molecular diffusion process as a result of which the molecular diffusion coefficient becomes smaller.

Numerical analysis has also been done for these mixtures using the theory of non-equilibrium thermodynamics. The theoretical model was able to predict these experimental trends fairly accurately. Specifically, it was found that the model can predict the molecular diffusion coefficients fairly accurately. A similar conclusion was made for the thermodiffusion coefficients. Finally, it was noted that the errors for the Soret coefficient was slightly higher when the dissimilarity between the

components greatly increases. This favors a stronger representation of the difference between the molecules in the numerical model.

**Acknowledgments**

The authors would like to acknowledge the financial support of the Canadian Space Agency, NSERC and the Basque Government (grants – Research Groups (IT557-10), GOVSORET3 (PI2011-22) and MICBIO2).

**References**

[1] C. Ludwig, Sitz. Ber. Akad. Wiss. Wien Math-Naturw 20 (1856) p.539.
[2] C. Soret, Acad. Sci. Paris 91 (1880) p.289.
[3] E. Cussler, *Diffusion Mass Transfer in Fluid Systems*, 3rd ed., Cambridge Press, Cambridge, 2009.
[4] W. Weinberger, Solar Energy 8 (1964) p.45.
[5] M. Gregg, Sci. Amer. 228 (1973) p.65.
[6] E.A. Spiegel, Ann. Rev. Astron. Astrophys. 10 (1972) p.261.
[7] J. Janča, I.A. Ananieva, J. Sobota and J. Dupák, Int. J. Poly. Anal. Charact. 13 (2008) p.232.
[8] F. Montel, J. Bickert, A. Lagisquet and G. Galliero, J. Petrol. Sci. Eng. 58 (2007) p.391.
[9] A. Firoozabadi, K. Ghorayeb and K. Shukla, AIChE J. 46 (2000) p.892.
[10] G. Galliero, M. Bugel, B. Duguay and F. Montel, J. Non-Equilib. Thermodyn. 32 (2007) p.251.
[11] G. Galliero, S. Srinivasan and M.Z. Saghir, High Temp. High Press. 38 (2010) p.315.
[12] S. Srinivasan and M.Z. Saghir, High Temp. High Press. 39 (2010) p.65.
[13] S. Srinivasan, M. Dejmeck and M.Z. Saghir, Int. J. Therm. Sci. 49 (2010) p.1613.
[14] S. Srinivasan and M.Z. Saghir, J. Non-Equilib. Thermodyn. (2011), doi: 10.1515/JNETDY.2011.015.
[15] S. Pan, Y. Yan, T.J. Jaber, M. Kawaji and M.Z. Saghir, J. Non-Equilib. Thermodyn. 32 (2007) p.241.
[16] M. Khawaja, C.G. Jiang, S. Van Vaerenbergh and M.Z. Saghir, J. Non-Equilib. Thermodyn. 30 (2005) p.359.
[17] P. Blanco, M. Bou-Ali, J.K. Platten, D.A. Mezquiade, J.A. Madariaga and C. Santamaria, J. Chem. Phys. 132 (2010) p.114506.
[18] P. Blanco, M. Bou-Ali, J.K. Platten, J.A. Madariaga, P. Urteaga and C. Santamaria, J. Non-Equilib. Thermodyn. 32 (2007) p.309.
[19] P. Blanco, P. Polyakov, M. Bou-Ali and S. Wiegand, J. Phys. Chem. 112 (2008) p.8340.
[20] A. Königer, B. Meier and W. Köhler, Phil. Mag. 89 (2009) p.907.
[21] K. Ghorayeb and A. Firoozabadi, AIChE J. 46 (2000) p.883.
[22] A. Leahy-Dios and A. Firoozabadi, J. Phys. Chem. B 112 (2008) p.6442.
[23] M.M. Bou-Ali, J.J. Valencia, J.A. Madariaga, C.M. Santamaria, O. Ecennaro and J.F. Dutrieux, Phil. Mag. 83 (2003) p.2011.
[24] A. Leahy-Dios, M.M. Bou-Ali, J.K. Platten and A. Firoozabadi, J. Chem. Phys. 122 (2005), article ID: 234502.
[25] M.M. Bou-Ali and J.K. Platten, J. Non-Equilib. Thermodyn. 30 (2005) p.385.
[26] S. Srinivasan and M.Z. Saghir, J. Chem. Phys. 131 (2009), article ID: 124508.
[27] S. Van Vaerenbergh, S. Srinivasan and M.Z. Saghir, J. Chem. Phys. 131 (2009), article ID: 114505.

[28] J.K. Platten, M.M. Bou-Ali, P. Costeséque, J. Dutrieux, W. Köhler, C. Leppla, S. Wiegand and G. Wittko, Phil. Mag. 83 (2003) p.1965.
[29] P. Costeséque and J.C. Loubet, Phil. Mag. 83 (2003) p.2017.
[30] C. Leppla and S. Wiegand, Phil. Mag. 83 (2003) p.1989.
[31] G. Wittko and W. Köhler, Phil. Mag. 83 (2003) p.1973.
[32] J.K. Platten, M.M. Bou-Ali and J. Dutrieux, Phil. Mag. 83 (2003) p.2001.
[33] S. Srinivasan and M.Z. Saghir, Int. J. Therm. Sci. 50 (2011) p.1125.
[34] J.F. Dutrieux, J.K. Platten, G. Chavepeyer and M.M. Bou-Ali, J. Phys. Chem. 106 (2002) p.6104.
[35] W. Köhler and S. Wiegand, *Thermal Nonequilibrium Phenomena in Fluid Mixtures*, Springer, Berlin, 2002.
[36] P. Blanco, M. Bou-Ali, J.K. Platten, P. Urteaga, J.A. Madariaga and C. Santamaria, J. Chem. Phys. 129 (2008) p.174504.
[37] P. Urtaega, M. Bou-Ali, J. Madariaga, C. Santamaria, P. Blanco and J. Platten, M.M. Bou-Ali and J. Platten, eds., *Mondragon Unibertsitateko Zerbitzu Editoriala*, Mondragon, Spain, 2006, p.449.
[38] J.A. Madariaga, C. Santamaria, M. Bou-Ali, P. Urteaga and D.A. De, Mezquia, J. Phys. Chem. B 114 (2010) p.6937.
[39] M.M. Bou-Ali, O. Ecennaro, J.A. Madariaga, C.M. Santamaria and J.J. Valencia, J. Phys. Condens. Matter 10 (1998) p.3321.
[40] W. Köhler and B. Muller, J. Chem. Phys. 103 (1995) p.4367.
[41] P. Kolodner, H. Williams and C. Moe, J. Chem. Phys. 88 (1988) p.6512.
[42] K.J. Zhang, M.E. Briggs, R.W. Gammon and J.V. Sengers, J. Chem. Phys. 104 (1996) p.6881.
[43] S.R. Grootde and P. Mazur, *Non-Equilibrium Thermodynamics*, Dover Publications, New York, 1984.
[44] K.G. Denbigh, Trans. Faraday Soc. 48 (1952) p.1.
[45] E.L. Dougherty and H.G. Drickamer, J. Phys. Chem. 59 (1955) p.443.
[46] D. Peng and D.B. Robinson, Ind. Eng. Chem. Fundam. 15 (1976) p.59.
[47] M. Chacha, D. Faruque, M.Z. Saghir and J.C. Legros, Int. J. Therm. Sci. 41 (2002) p.899.
[48] A. Leahy-Dios and A. Firoozabadi, AIChE J. 53 (2007) p.2932.

# Apéndice E

# Determinación del Coeficiente de Difusión Molecular en Mezclas Binarias de $n$-Alcanos: Correlaciones Empíricas

THE JOURNAL OF PHYSICAL CHEMISTRY B

Article

pubs.acs.org/JPCB

# Determination of Molecular Diffusion Coefficient in *n*-Alkane Binary Mixtures: Empirical Correlations

D. Alonso De Mezquia,[†] M. Mounir Bou-Ali,*[,†] M. Larrañaga,[†] J. A. Madariaga,[‡] and C. Santamaría[‡]

[†]Mechanical and Manufacturing Department, Engineering Faculty, Mondragon Unibertsitatea, Loramendi 4 Apdo. 23, 20500 Mondragon, Spain

[‡]Department of Applied Physics II, University of Basque Country, Apdo. 644, 48080 Bilbao, Spain

**ABSTRACT:** In this work we have measured the molecular diffusion coefficient of the *n*-alkane binary series $nC_i$-$nC_6$, $nC_i$-$nC_{10}$, and $nC_i$-$nC_{12}$ at 298 K and 1 atm and a mass fraction of 0.5 by using the so-called sliding symmetric tubes technique. The results show that the diffusion coefficient at this concentration is proportional to the inverse viscosity of the mixture. In addition, we have also measured the diffusion coefficient of the systems $nC_{12}$-$nC_6$, $nC_{12}$-$nC_7$, and $nC_{12}$-$nC_8$ as a function of concentration. From the data obtained, it is shown that the diffusion coefficient of the n-alkane binary mixtures at any concentration can be calculated from the molecular weight of the components and the dynamic viscosity of the corresponding mixture at 50% mass fraction.

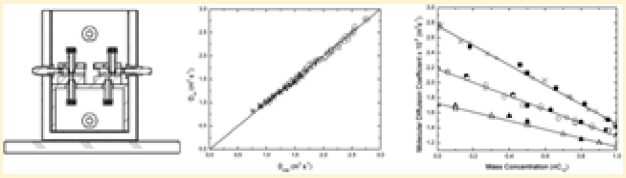

## I. INTRODUCTION

A concentration gradient within a mixture results in a mass transport of its components from the zones of a higher concentration to those of a lower concentration. This phenomenon, known as molecular diffusion, has generated great interest since its discovery in the nineteenth century when, first in gases and later on in liquids, it was studied with the aim of understanding the atom's behavior.

It was in 1855 when Fick[1] established the first quantitative relation for the molecular diffusion phenomenon, known nowadays as Fick's law. Since then, interest in this transport property has increased, discovering a great number of fields in which the molecular diffusion coefficient has a huge influence, such as medicine or phisiology.[2]

As a consequence of this interest, there have appeared a great number of apparatus designed for the determination of the molecular diffusion coefficient. There are, for example, techniques that employ the principle of Taylor dispersion[3] or other techniques such as open ended capillary (OEC)[4] or thermal diffusion forced Rayleigh scattering (TDFRS)[5] developed for the study of the molecular diffusion coefficient in liquid mixtures. The different techniques used for the determination of the molecular diffusion coefficient can be found elsewhere.[2,6−9]

Some of these techniques, such as the OEC, have already been satisfactorily used in several studies earlier.[4,10] With the aim of correcting some of the limitations of this technique, the sliding symmetric tubes (SST) technique has been developed. This new technique takes out perturbations that appeared in the OEC technique, especially in aspects such as evaporations or manipulation of the apparatus, reducing, at the same time, the liquid quantity needed to carry out a measurement. In this work a complete description of the SST technique will be done, including the improvements obtained compared with the OEC technique, and the validation process used to validate this new technique.

On the other hand, nowadays, there exist several models developed for the estimation of the molecular diffusion coefficient.[11,12] In order to check the validity of these models, it is necessary to compare the theoretical values obtained with the experimental ones. On some occasions, the procedure that checks these models requires a huge number of experimental values, which, at the same time, requires a great experimental effort. In this work, a new correlation, which is capable of predicting the molecular diffusion coefficient in normal alkane binary mixtures, is presented. The use of this correlation may help in the development of new theories or could be useful in verifying the existing ones.

This article is organized as follows: In section II, the SST technique is presented, and a complete description of the experimental installation and its analytical resolution is done. In this section, the process used to validate the technique is also included. In section III, the results obtained in the measurement of the molecular diffusion coefficient in several normal alkane mixtures are presented, to continue with the discussion and the development of new correlations for the prediction of the molecular diffusion coefficient ($D_{12}$) in normal alkane mixtures. In section IV, the conclusions obtained are based on the study carried out in this work.

## II. SST TECHNIQUE

**A. SST Technique Description.** The SST technique consists of several sets of two identical vertical tubes. Each set has two positions: "faced tubes" (Figure 1a), in which the

**Received:** October 13, 2011
**Revised:** January 12, 2012

   dx.doi.org/10.1021/jp209838m | *J. Phys. Chem. B* XXXX, XXX, XXX−XXX

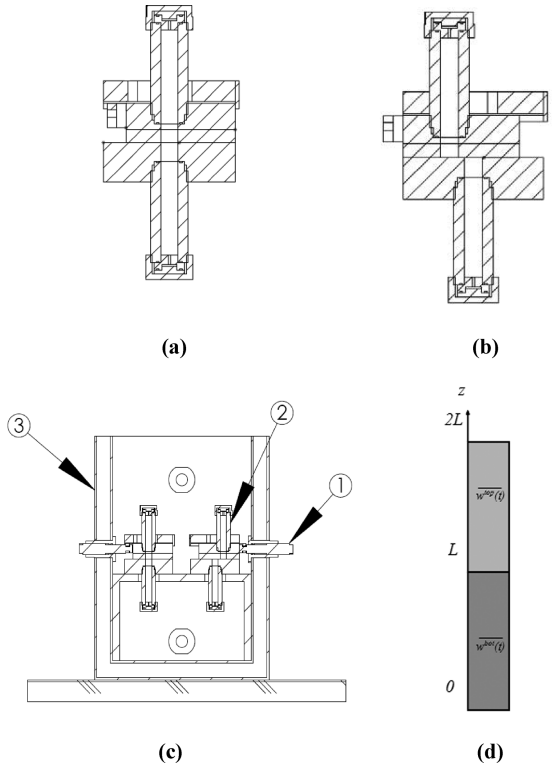


**Figure 1.** (a) Scheme of the sets of the SST technique on "faced tubes" configuration. (b) Scheme of the sets of the SST technique on "separated tubes" configuration. (c) Scheme of the SST sets (2) inside the water bath (3) in both their configurations: "faced tubes" position (left) and "separated tubes" position (right) and the screws (1) used to make the tubes slide. (d) Scheme of SST technique. $\overline{w^{top}}(t)$ and $\overline{w^{bot}}(t)$ are the mass fractions of component $i$ in the top and bottom recipient, respectively.

mass transfer between both tubes is permitted, and "separated tubes" (Figure 1b). In this position, the content of the tubes is isolated. At the beginning of an experiment, the studied mixture with a slight difference of mass fraction of its components is introduced in each of the tubes. The mixture with a higher mass fraction of the denser component is introduced in the bottom tube, and the upper tube is filled with the mixture with a less concentration of the denser component so that the convective instability is avoided.

The SST technique introduces some improvements compared with the OEC technique on which it is based. For example, since the mixture is contained inside closed tubes, evaporations are eliminated, which gives the advantage of using this technique with volatile mixtures without reducing its efficiency. Another fact that has been improved has been the mixture quantity needed to carry out an essay. The OEC technique requires a huge quantity of mixture (400 $cm^3$ approximately). This quantity is highly reduced in the SST technique, as it only needs around 100 $cm^3$ of mixture in each experiment. One more improvement has been done related to the setup handling. In the OEC technique, whenever it is needed to analyze the experiment evolution, it is necessary to manipulate the setup. This fact affects the results of the experiment, which are highly influenced by the experimenter's expertise. However, in the SST technique, thanks to its design, all of these influences have been eliminated.

**B. Analytical Solution.** Assuming Fick's second law in one dimension ($z$: vertical direction), the following can be written:

$$\frac{\partial w}{\partial t} = D_{12}\frac{\partial^2 w}{\partial z^2} \tag{1}$$

where $D_{12}$ is the molecular diffusion coefficient, which is considered constant for small mass fraction ($w$) changes. The formulation can be implemented as can be seen in Figure 1d considering the following boundary conditions:

$$w(z, 0) = \begin{cases} w^{bot} & 0 \le z < L \\ w^{top} & L < z \le 2L \end{cases} \tag{2}$$

$$\frac{\partial w(z, t)}{\partial t} = 0 \text{ at } z = 0,\ 2L \text{ and } t > 0 \tag{3}$$

where $w^{bot}$ and $w^{top}$ are the mass fractions of the bottom and upper tube, respectively, and $L$ is the tube length. Solving eqs 1−3, we have

$$w(z, t) = \frac{w^{top} + w^{bot}}{2} - \frac{2(w^{top} - w^{bot})}{\pi} \sum_{n=0}^{\infty} \frac{(-1)^n e^{\phi} \cos\left(\frac{2n+1}{2}\pi\frac{z}{L}\right)}{2n+1} \tag{4}$$

where $\varphi = -((2n + 1)/2)^2(\pi/L)^2 D_{12}t)$. Therefore, at the middle point between both the tubes, we have

$$w(L, t) = \frac{w^{top} + w^{bot}}{2} \tag{5}$$

The change of mass fraction in each tube in function of time can be obtained using the following equations:

$$\overline{w^{top}(t)} = \frac{1}{L}\int_{L}^{2L} w(z, t)\, dz = \frac{w^{top} + w^{bot}}{2} + \frac{4(w^{top} - w^{bot})}{\pi^2} \sum_{n=0}^{\infty} \frac{e^{\phi}}{(2n+1)^2} \tag{6}$$

$$\overline{w^{bot}(t)} = \frac{1}{L}\int_{0}^{L} w(z, t)\, dz = \frac{w^{top} + w^{bot}}{2} - \frac{4(w^{top} - w^{bot})}{\pi^2} \sum_{n=0}^{\infty} \frac{e^{\phi}}{(2n+1)^2} \tag{7}$$

where $\overline{w^{top}}$ and $\overline{w^{bot}}$ are the mean mass fractions in the upper and bottom tube, respectively. The solution of the inverse problem posed by eqs 6 and 7 to obtain the molecular diffusion coefficient ($D_{12}$) is solved by the least-squares method using *Matlab* software. Solving expressions 6 and 7 when $n = 0$, an initial guess of the molecular diffusion coefficient $D_{12}$ is obtained. This initial value is then used for obtaining the $D_{12}$ coefficient iterating the eqs 10 times and using terms on the summation up to $n = 1000$. The more experimental points used, the more accurate the estimated value of the molecular


dx.doi.org/10.1021/jp209838m | J. Phys. Chem. B XXXX, XXX, XXX−XXX

diffusion coefficient. Typically up to 11 points are used in each experiment. This tactic allows the use of experimental points from the very beginning of the experiment, which does not happen in other similar techniques that require some initial experimental time before beginning the analysis of experimental data.[3,8]

**C. Equipment and Procedure.** We have used the SST equipment designed and constructed in Mondragon Goi Eskola Politeknikoa and described elsewhere.[13−15] The two tubes with which each set of the device is provided have the same dimensions (length of 60 ± 0.01 mm and diameter of 9 ± 0.01 mm).

The experimental procedure starts with the preparation of two mixtures of 50 $cm^3$ with a mass fraction difference (±4−6 wt %) so that the mean concentration of both mixtures corresponds with the one of the mixture to be studied. The tubes of several sets (typically 10) in their "separated tubes" position are filled with the mixtures, next introducing the sets in the water bath (Figure 1d) so that the mixture obtains the working temperature ($T$ = 298 K). The temperature of the water in this bath is controlled by a thermostatic bath, which has a temperature control of 0.1 K. In order to make sure that the studied mixture is in the working temperature, the sets in their "separated tubes" configuration are introduced in the bath no less than 48 h before the beginning of the experiment.

Once the mixture has reached the working temperature, all the sets in the bath are changed to their "faced tubes" configuration, starting the diffusion process in this manner. With the aim of making this transition, the bath has some external screws (Figure 1c) that make sliding of the tubes possible in a controlled way.

In determined time intervals, the position of the sets is changed one by one using the screws back to the "separated tubes position." The time intervals in which the set's positions are changed are between 6, 12, or 24 h, depending on the speed at which sensitive concentration changes occur in the tubes. After stopping the mass transfer process between the tubes, the sets are extracted from the bath, and the concentration in each of them is analyzed. This allows obtaining the concentration change in the tubes in function of time.

The SST technique was validated[13,14] using five binary mixtures: the three binary mixtures composed of pairwise combinations of tetrahydronaphtalene, normal dodecane, and isobutylbenzene at 298 K and 50 wt % of each component used in a benchmark test[16] to compare various experimental techniques and the binary mixtures: water−ethanol at 298 K and 60.88 wt % water and toluene-n hexane at 298 K and 51.67 wt % toluene, which have been widely studied in the literature.[17−20] The experimental test was repeated at least twice. The reproducibility of the experimental results of the SST technique is within 3% of deviation. In general, the differences with published data are, on an average, below 3%.

The determination of the mass fraction of a mixture is essential to determine molecular diffusion coefficients. In binary mixtures, the mass fraction is related to one physical property of the mixture (the density in this experimental study). An Anton Paar DMA 5000 vibrating quartz U-tube densimeter having an accuracy of $\pm 5 \times 10^{-6}$ g/$cm^3$ is used to determine the density of the mixture. Since we are working with small mass fraction differences, it can be supposed that

$$\rho = a w_i \tag{8}$$

where $\rho$ is the density of the mixture, $w_i$ is the mass fraction of component i in the binary mixture, and $a$ is a constant parameter. To determine the constant parameter, $a$, five mixtures of known concentration are prepared by weighing and then, the density of each mixture is measured. Thus, we

**Table 1. Values of Viscosity ($\mu$) and Molecular Diffusion Coefficient ($D_{12}$) for the $nC_6$-$nC_i$, $nC_{10}$-$nC_i$, and $nC_{12}$-$nC_i$ Series at 50 wt % and 298 K[a]**

| system | $\mu$ mPa s | $D_{12}$ $10^{-9}$ $m^2$ $s^{-1}$ | $(\overline{D_{12}})_{cc}$ $10^{-9}$ $m^2$ $s^{-1}$ | $\delta$ (%) |
|---|---|---|---|---|
| | | set 1: $nC_i$-$nC_6$ | | |
| $nC_{10}$-$nC_6$ | 0.4704 | 2.53 | 2.51 | 0.8 |
| $nC_{11}$-$nC_6$ | 0.5312 | 2.27 | 2.22 | 2.1 |
| $nC_{12}$-$nC_6$ | 0.5581 | 2.09 | 2.11 | −1.2 |
| $nC_{13}$-$nC_6$ | 0.6103 | 1.96 | 1.93 | 1.4 |
| $nC_{14}$-$nC_6$ | 0.6556 | 1.76 | 1.80 | −2.3 |
| $nC_{15}$-$nC_6$ | 0.6938 | 1.62 | 1.68 | −3.7 |
| $nC_{16}$-$nC_6$ | 0.7446 | 1.54 | 1.58 | −2.6 |
| $nC_{17}$-$nC_6$ | 0.7737 | 1.46 | 1.52 | −4.1 |
| $nC_{18}$-$nC_6$ | 0.8265 | 1.39 | 1.43 | −2.9 |
| | | set 1: $nC_i$-$nC_{10}$ | | |
| $nC_5$-$nC_{10}$ | 0.3993 | 3.03 | 2.96 | 2.3 |
| $nC_6$-$nC_{10}$ | 0.4704 | 2.54 | 2.51 | 1.2 |
| $nC_7$-$nC_{10}$ | 0.5633 | 2.09 | 2.09 | −0.0 |
| $nC_{14}$-$nC_{10}$ | 1.2929 | 0.913 | 0.915 | −0.2 |
| $nC1_5$-$nC_{10}$ | 1.3972 | 0.819 | 0.845 | −3.1 |
| $nC_{16}$-$nC_{10}$ | 1.5150 | 0.756 | 0.779 | −3.0 |
| $nC_{17}$-$nC_{10}$ | 1.6337 | 0.702 | 0.722 | −2.8 |
| $nC_{18}$-$nC_{10}$ | 1.7780 | 0.656 | 0.664 | −1.2 |
| | | set 1: $nC_i$-$nC_{12}$ | | |
| $nC_5$-$nC_{12}$ | 0.4551 | 2.57 | 2.59 | −0.9 |
| $nC_6$-$nC_{12}$ | 0.5581 | 2.09 | 2.11 | −1.2 |
| $nC_7$-$nC_{12}$ | 0.6823 | 1.70 | 1.73 | −1.7 |
| $nC_8$-$nC_{12}$ | 0.8071 | 1.49 | 1.46 | 1.9 |
| $nC_9$-$nC_{12}$ | 0.9452 | 1.24 | 1.25 | −0.8 |
| $nC_{16}$-$nC_{12}$ | 2.0335 | 0.589 | 0.580 | 1.5 |
| $nC_{17}$-$nC_{12}$ | 2.2323 | 0.547 | 0.529 | 3.2 |
| $nC_{18}$-$nC_{12}$ | 2.3945 | 0.503 | 0.493 | 2.0 |

[a] $(\overline{D_{12}})_{cc}$ is the diffusion coefficient calculated from eq 9, and $\delta$ is the relative deviation between $D_{12}$ and $D_{cc}$.

**Table 2. Diffusion Coefficient ($D_{12}$) in the $nC_{12}$-$nC_6$, $nC_{12}$-$nC_7$, and $nC_{12}$-$nC_8$ Systems for Different Mass Fractions of $nC_{12}$ ($w_1$) at 298 K[a]**

| mixture | $w_1$ | $D_{12}$ $10^{-9}$ $m^2$ $s^{-1}$ | $(D_{12})_{cc}$ $10^{-9}$ $m^2$ $s^{-1}$ | $\delta$ (%) |
|---|---|---|---|---|
| $nC_{12}$-$nC_6$ | 0.18 | 2.48 | 2.55 | −3.0 |
| | 0.46 | 2.24 | 2.17 | 3.1 |
| | 0.50 | 2.13 | 2.11 | 0.7 |
| | 0.66 | 1.93 | 1.88 | 2.2 |
| | 0.82 | 1.72 | 1.67 | 2.9 |
| | 0.95 | 1.51 | 1.49 | 1.0 |
| $nC_{12}$-$nC_7$ | 0.16 | 2.09 | 2.04 | 2.6 |
| | 0.42 | 1.84 | 1.80 | 2.2 |
| | 0.50 | 1.70 | 1.73 | −1.7 |
| | 0.63 | 1.64 | 1.61 | 1.6 |
| | 0.80 | 1.48 | 1.46 | 1.2 |
| | 0.94 | 1.37 | 1.33 | 2.9 |
| $nC_{12}$-$nC_8$ | 0.10 | 1.70 | 1.69 | 0.6 |
| | 0.40 | 1.56 | 1.52 | 2.5 |
| | 0.50 | 1.49 | 1.46 | 2.0 |
| | 0.80 | 1.25 | 1.28 | −2.4 |

[a] $(D_{12})_{cc}$ is the diffusion coefficient calculated from eq 19, and $\delta$ is the relative deviation between calculated and measured diffusion coefficient.


dx.doi.org/10.1021/jp209838m | J. Phys. Chem. B XXXX, XXX, XXX−XXX

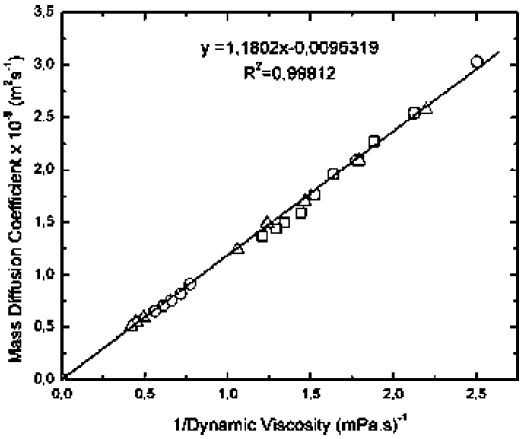


**Figure 2.** Diffusion coefficient as a function of the inverse of the dynamic viscosity for the systems $nC_6$-$nC_i$ (□), $nC_{10}$-$nC_i$ (○), and $nC_{12}$-$nC_i$ (Δ), at 50 wt % and 298 K.

determined the mass fraction with a deviation around wt % ± 0.01.

The dynamic viscosity ($\mu$) of the studied mixtures has been measured with an Anton Paar AMVn falling ball Micro-viscosimeter with reproducibility better than 0.1%. All the measurements were done at 298 K.

## III. RESULTS AND DISCUSSION

**A. Studied Mixtures.** All of the products used in this study were purchased from Merck with a purity better than 99%. The studied mixtures have been prepared by weight using a Gram VXI-310 digital scale with a precision of 0.001 g. and introducing first the less volatile component and then the corresponding amount of the second component; the mixture is finally shaken to ensure homogeneity. After the preparation, the density of the mixture was measured to confirm that the composition deduced from the calibration curve coincides with the prepared one. This was always the case.

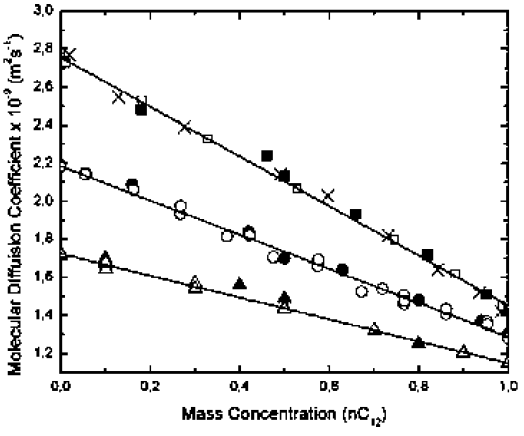


**Figure 3.** Diffusion coefficient as a function of the mass fraction of the denser component ($nC_{12}$) for the mixtures, $nC_{12}$-$nC_6$, $nC_{12}$-$nC_7$, and $nC_{12}$-$nC_8$ at 298 K. ■, $nC_{12}$-$nC_6$ this work; □, $nC_{12}$-$nC_6$ ref 22; ×, $nC_{12}$-$nC_6$ ref 24; ●, $nC_{12}$-$nC_7$ this work; ○, $nC_{12}$-$nC_7$ ref 23; ▲, $nC_{12}$-$nC_8$ this work; Δ, $nC_{12}$-$nC_8$ ref 21. The continuous lines represent a linear fit to the data.

In this study, 25 mixtures at 50 wt % have been prepared corresponding to the *n*-alkane series

$$nC_6 - nC_i \; i = 10, 11, 12, 13, 14, 15, 16, 17, 18$$

$$nC_{10} - nC_i \; i = 5, 6, 7, 14, 15, 16, 17, 18$$

**Table 3. Values of the Limiting Diffusion Coefficient ($D_1^0$ and $D_2^0$) Taken from Refs 3 and 23[a]**

| system | $D_1^0$ | $D_2^0$ | $D_1^0/D_2^0$ | $M_1/M_2$ | $\delta$(%) |
|---|---|---|---|---|---|
| $nC_{16}$-$nC_6$ | 2.21 | 0.85 | 2.60 | 2.62 | 0.7 |
| $nC_{12}$-$nC_6$ | 2.74 | 1.42 | 1.93 | 1.97 | 2.5 |
| $nC_{12}$-$nC_7$ | 2.19 | 1.30 | 1.69 | 1.70 | 0.6 |
| $nC_{12}$-$nC_8$ | 1.71 | 1.15 | 1.49 | 1.49 | 0.0 |
| $nC_{16}$-$nC_{12}$ | 0.67 | 0.49 | 1.36 | 1.33 | −2.2 |
| $nC_7$-$nC_8$ | 2.80[b] | 2.43[b] | 1.15 | 1.14 | −1.7 |

[a] $M_1$ and $M_2$ are the molecular masses of the components, and $\delta$ is the relative deviation between the ratios $D_1^0/D_2^0$ and $M_1/M_2$. [b] Interpolated from ref 3.

$$nC_{12} - nC_i \; i = 5, 6, 7, 8, 9, 16, 17, 18$$

The measured values at 298 K for dynamic viscosity ($\mu$) and mass diffusion coefficients for these mixtures are summarized in Table 1.

In addition, this study has been completed measuring the molecular diffusion coefficient of the systems $nC_{12}$-$nC_6$, $nC_{12}$-$nC_7$, and $nC_{12}$-$nC_8$ at 298 K at different concentrations. For this end, the following mixtures were prepared:

$$nC_{12} - nC_6 \; w_1 = 0.18, 0.46, 0.50, 0.66, 0.82, 0.95.$$

$$nC_{12} - nC_7 \; w_1 = 0.16, 0.42, 0.50, 0.63, 0.80, 0.94.$$

$$nC_{12} - nC_8 \; w_1 = 0.10, 0.40, 0.50, 0.80.$$

where $w_1$ is the mass fraction of dodecane.

In Table 2, the measured values of the diffusion coefficients of these systems at the concentrations considered are shown.

These systems were chosen, as hydrocarbon mixtures are quite regular in their properties. It was hoped that at least some general and useful empirical relationship would be found.

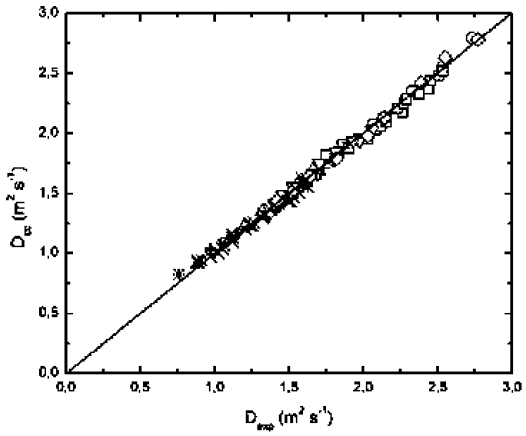


**Figure 4.** Experimental diffusion coefficient versus calculated from eq 19 diffusion coefficient. ×, $nC_{10}$-$nC_7$ ref 23; ○, $nC_{12}$-$nC_6$ ref 22; ◊, $nC_{12}$-$nC_6$ ref 24; ∇, $nC_{12}$-$nC_7$ ref 23; Δ, $nC_{12}$-$nC_8$ ref 21; +, $nC_{14}$-$nC_7$ ref 23; ×, $nC_{14}$-$nC_8$ ref 23; *, $nC_{16}$-$nC_7$ ref 22.


dx.doi.org/10.1021/jp209838m | J. Phys. Chem. B XXXX, XXX, XXX–XXX

**B. Correlation between Diffusion and Viscosity.** In what follows, we shall analyze the relation between the diffusion coefficient and the dynamic viscosity for mixtures at a mass fraction equal to 50 wt % (equimass mixtures).

In Figure 2, the values of $D_{12}$ as a function of the inverse of dynamic viscosity for the equimass mixtures in Table 1 are represented. As can be seen, the data fit well to a straight line, which passes through the origin and, thus, the following linear relation can be written:

$$\overline{D_{12}} = k\frac{1}{\bar{\mu}} \tag{9}$$

where $\overline{D_{12}}$ and $\bar{\mu}$ are the diffusion coefficient and the dynamic viscosity at $w_1 = 0.5$, respectively. The proportionality constant $k$ is $k = 1.18 \times 10^{-12}$ kg m/s$^2$.

In Table 1, the values of $\overline{D_{12}}$ calculated using eq 9 for each mixture are also shown and in the last column, the relative deviations with the measured values are given. As can be seen, these deviations are smaller than 3% in all the cases. Thus, we can conclude that the product $\overline{D_{12}}\mu$ for equimass mixtures is a universal constant for *n*-alkane mixtures.

**D. Dependence of the Diffusion Coefficient with Composition.** According to Darken equation for thermodynamic ideal mixtures, the diffusion coefficient should be a linear function of the molar fraction. However, as was suggested in an earlier work by van Geet and Adamson,[21] the diffusion coefficient in n-alkane mixtures is linear with the mass fraction but not with the mole fraction. To closely analyze the diffusion composition dependence we have measured the diffusion coefficient as a function of composition for the three systems: $nC_{12}$-$nC_6$, $nC_{12}$-$nC_7$, and $nC_{12}$-$nC_8$. The results obtained appear in Table 2. In Figure 3, these data as a function of the mass fraction of the heavier component, $w_1$, are plotted. As can be seen, the ordinary diffusion coefficient is for each system a linear function of the mass fraction and decreases with the concentration of the heavier component. In this figure, the diffusion data in the literature for the systems considered[21−24] are also shown. These data coincide with our measurements within the experimental error.

Thus, the dependence of $D_{12}$ with composition can be written as follows:

$$D_{12} = w_2 D_1^0 + w_1 D_2^0 \tag{10}$$

where $w_1$ and $w_2$ are the mass fraction of heavier and lighter components, respectively, and $D_1^0$ and $D_2^0$ are the limiting diffusion coefficients defined by

$$D_1^0 = \lim_{w_1 \to 0} D_{12} \tag{11}$$

$$D_2^0 = \lim_{w_2 \to 0} D_{12} \tag{12}$$

In Table 3, the values of $D_1^0$ and $D_2^0$ for some selected mixtures reported in the literature[3,23] covering a large range of mass ratio for liquid n-alkanes are given. As can be seen in this table, the ratio $D_1^0/D_2^0$ is always close to the ratio of the molecular masses $M_1/M_2$ of the two alkanes involved. Thus, we have

$$\frac{D_1^0}{D_2^0} = \frac{M_1}{M_2} \tag{13}$$

Introducing eq 13 in eq 10, one obtains

$$D_{12} = D_1^0\left(w_2 + \frac{M_2}{M_1}w_1\right) \tag{14}$$

For $w_1 = w_2 = 0.5$, the corresponding diffusion coefficient $\overline{D_{12}}$ will be

$$\overline{D_{12}} = \frac{D_1^0}{2}\left(\frac{M_1 + M_2}{M_1}\right) \tag{15}$$

and then, eq 14 in terms of $\overline{D_{12}}$ can be written as

$$D_{12} = 2\overline{D_{12}}\left(\frac{M_1 w_2 + M_2 w_1}{M_1 + M_2}\right) \tag{16}$$

In particular, the infinite dilution values $D_1^0$ and $D_2^0$ will be

$$D_1^0 = 2\overline{D_{12}}\frac{M_1}{M_1 + M_2} \tag{17}$$

$$D_2^0 = 2\overline{D_{12}}\frac{M_2}{M_1 + M_2} \tag{18}$$

Finally, using eq 9, the diffusion coefficient can be written as

$$D_{12} = \frac{2k}{\bar{\mu}}\left(\frac{M_1 w_2 + M_2 w_1}{M_1 + M_2}\right) \tag{19}$$

where $k = 1.18 \times 10^{-12}$ kg m/s$^2$.

Equation 16 allows determining $D_{12}$ from $\overline{D_{12}}$ measurements, which, in turn, can be calculated using eq 9 from viscosity measurements.

To confirm the validity of this correlation, we have determined the values of $D_{12}$ from eq 19 for the mixtures given in Table 2. As shown in the last column of this table, the relative deviations between these values and the experimental ones are inferior to the experimental error.

As an additional test of eq 19, we have taken the experimental $D_{12}$ values as a function of concentration reported in the literature[21−24] for different *n*-alkane systems. In Figure 4, the values of $D_{12}$ calculated using eq 19 are plotted against the corresponding experimental ones. As seen here, all data lie on a straight line through the origin with slope unity.

From what has been just mentioned, we can conclude that the diffusion coefficient of *n*-alkane mixtures at any concentration can be calculated from the data of dynamic viscosity for equimass mixtures.

## IV. CONCLUSIONS

In this work, the diffusion coefficient of several *n*-alkane mixtures at 50 wt % has been measured by using the SST technique. From the results obtained, it is shown that the product of the diffusion coefficient and the dynamic viscosity for these mixtures is a universal constant independent of the alkane involved.

In addition, the diffusion coefficient of the systems $nC_{12}$-$nC_6$, $nC_{12}$-$nC_7$, and $nC_{12}$-$nC_8$ in the whole concentration range has also been measured. We have obtained for each system a linear correlation between the diffusion coefficient and the mass fraction. This correlation allows determining the diffusion coefficient at any concentration from the molecular weight of the components of a mixture and the dynamic viscosity of the mixture at 50 wt %.


dx.doi.org/10.1021/jp209838m | J. Phys. Chem. B XXXX, XXX, XXX−XXX

## AUTHOR INFORMATION

### Corresponding Author

*E-mail: mbouali@mondragon.edu.

### Notes

The authors declare no competing financial interest.

## ACKNOWLEDGMENTS

This article presents results that were partly obtained in the framework of the following projects: GOVSORET3 (PI2011-22), MIBIO, and Research Groups (IT557-10) of Basque Government and DCMIX from the European Space Agency.

## REFERENCES

(1) Fick, A. *Poggendorff's Ann. Phys.* **1855**, *94*, 59.
(2) Cussler, E. *Diffusion Mass Transfer in Fluid Systems*; Cambridge Univesity Press: New York, 1997.
(3) Alizadeh, A. A.; Wakeham, W. A. *Int. J. Themophys.* **1982**, *3* (4), 307.
(4) Dutrieux, J.; Platten, J. K.; Chavepeyer, G.; Bou-Ali, M. M. *J. Phys. Chem. B* **2002**, *106*, 6104.
(5) Wiegand, S.; Köhler, W. *Thermal Nonequilib. Phenom. Fluid Mixt.*; Springer: Berlin, 2002; pp 36−43.
(6) Taylor, R.; Krishna, R. *Multicomponent mass transfer*; John Wiley & Sons Inc.: New York, 1993.
(7) Cussler, E. *Multicomponent diffusion*; Elsevier Scientific Publishing Company: Amsterdam, 1976.
(8) Rutten, P. W. M. *Diffusion in liquids*; Delft University Press: Delft, 1992.
(9) Tyrrell, J. V. Harris, K. R. *Diffusion in liquids*; Butterworth & Co., Ltd.: London, 1984.
(10) Leahy-Dios, A.; Bou-Ali, M. M.; Platten, J. K.; Firoozabadi, A. *J. Chem. Phys.* **2005**, *122*, 234502.
(11) Ghorayeb, K.; Firoozabadi, A. *AIChE J.* **2000**, *46*, 883−891.
(12) Polyakov, P.; Müller-Plathe, F.; Wiegand, S. *J. Phys. Chem. B* **2008**, *112*, 14999.
(13) Blanco P.; Bou-Ali M. M.; Urteaga P.; Alonso de Mezquia D.; Platten J. K. Sliding Symmetric Tubes: new technique for the molecular diffusion coefficients determination of liquid mixtures. 18th European Conference on Thermophysical Properties, Pau, France, 2008.
(14) Alonso de Mezquia D.; Blanco, P.; Bou-Ali M. M.; Zebib A. New Technique for Measuring the Molecular Diffusion Coefficients of Binary Liquid Mixtures. *European Thermodynamics Seminar EUROTHERM* 84, Namur, Belgium, **2009**.
(15) Blanco P., Bou-Ali M. M., Urteaga P.; *Tubos Simétricos Deslizantes*, Patente P200700132/2, 2008.
(16) Platten, J. K.; Bou-Ali, M. M.; Costesèque, P.; Dutrieux, J.; Köhler, W.; Leppla, C.; Wiegand, S.; Wittko, G. *Philos. Mag.* **2003**, *83*, 1965.
(17) Leahy-Dios, A.; Firoozabadi, A. *J. Phys. Chem. B* **2007**, *111*, 191.
(18) Zhang, K. J.; Briggs, M. E.; Gammon, R. W.; Sengers, J. V. *J. Chem. Phys.* **1996**, *104*, 6881.
(19) Kolodner, P.; Williams, H.; Moe, C. *J. Chem. Phys.* **1988**, *88*, 6512.
(20) Köhler, W.; Müller, B. *J. Chem. Phys.* **1995**, *103*, 4367.
(21) Van Geet, L. A.; Adamson, W. A. *J. Phys. Chem.* **1964**, *68* (2), 238.
(22) Bidlack, D. L.; Anderson, D. K. *J. Phys. Chem.* **1964**, *68*, 3790.
(23) Lo, H. Y. *Chem. Eng. Data Ser.* **1974**, *19* (3), 236−241.
(24) Shieh, J. J. C.; Lyons, P. A. *J. Phys. Chem.* **1969**, *73*, 3258.

# Apéndice F

# Sorción Isotérmica, Transición Vítrea y Coeficiente de Difusión de Soluciones de Poliacrilamida/Agua

JOURNAL OF CHEMICAL & ENGINEERING DATA

Article

pubs.acs.org/jced

# Sorption Isotherm, Glass Transition, and Diffusion Coefficient of Polyacrylamide/Water Solutions

David Alonso de Mezquia,[†] Frédéric Doumenc,*[,‡] and M. Mounir Bou-Ali[†]

[†]Mechanical and Manufacturing Department, Engineering Faculty of Mondragon Unibertsitatea, Loramendi 4 Apdo. 23, 20500 Mondragon, Spain

[‡]UPMC Université Paris 06, Université Paris-Sud, CNRS, Laboratoire FAST, Bâtiment 502, Campus Universitaire, Orsay F-91405, France

**ABSTRACT:** The sorption isotherm, the glass transition, and the mutual diffusion coefficient of polyacrylamide/water solutions are obtained experimentally. All of these parameters are measured in the concentrated regime by gravimetric experiments. The mutual diffusion coefficient is also measured at high solvent concentrations by the sliding symmetric tubes technique. Three different polyacrylamide batches differing in their molar mass have been characterized. The results are expressed in terms of simple empirical correlations, suitable for use in process modelization or numerical simulations.

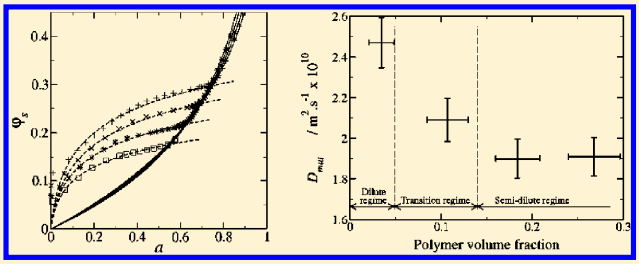


## INTRODUCTION

Thermodynamic properties of polymer solutions are of great interest for both industrial processes and fundamental research. For example, the saturated vapor pressure and mutual diffusion coefficient, which strongly depend on solvent concentration, are needed for the design of industrial dryers used in the coating industry[1−3] or for membranes formation processes.[4] More fundamental issues like hydrodynamic instabilities[5] or wetting phenomena[6,7] in drying polymer solutions also require such characteristics.

The present article is dedicated to the characterization of polyacrylamide (PAAm)/water solutions. Gravimetric experiments allowing swelling and deswelling of a polymer film in a controlled solvent vapor are used for the investigation of the saturated vapor pressure as a function of concentration and temperature. The solvent activity and the polymer volume fraction at glass transition are deduced from the desorption isotherm at several temperatures. Data obtained in the rubbery regime allow the determination of the polymer−solvent interaction parameter, using the well-known Flory−Huggins model. This model is then modified to take into account the effect of viscoelastic stress on the solvent activity in the glassy regime.

Finally, the mutual diffusion coefficient is measured at room temperature, on one hand in the concentrated regime using the same experimental setup and on the other hand at high solvent concentrations using a different experimental technique called the sliding symmetric tube technique.

## SYSTEM CHARACTERIZATION

**Pure Polymer.** Characteristics of polyacrylamide (PAAm) used in the present study are listed in Table 1. The three batches differ in their molar mass. The weight average molar mass $M_w$ has been obtained from the manufacturer for batches 2 and 3. The polydispersity is defined as $M_w/M_n$, $M_n$ being the number average molar mass. The polydispersity of batch 2 comes from ref 8. For batch 1, $M_w$ and $M_n$ have been measured by gel permeation chromatography (GPC) at Laboratory PMMD (ESPCI, France). This laboratory also measured the glass transition temperature $T_g$ of pure polymers by differential scanning calorimetry. There are no significant differences between the three polymers, the uncertainty in $T_g$ being ± 7 K, and these glass transition temperatures are close to the value $T_g$ = 461 K reported in *Polymer Data Handbook*.[9]

**Table 1. Characteristics of PAAm (NA Stands for Not Available)**

| batch no. | 1 | 2 | 3 |
|---|---|---|---|
| supplier | Sigma-Aldrich | Polysciences, Inc. | Biovalley |
| catalog no. | 434949 | 19901 | 02806 |
| product form | 50 wt % aqueous solution | 10 wt % aqueous solution | powder |
| $M_w$/kg·mol$^{-1}$ | 22.4 | 600−1000 | 5000−6000 |
| $M_w/M_n$ | 3.5 | 11 | NA |
| $T_g$/K | 449 | 451 | 460 |
| $\varphi^*_p$ | 0.049−0.14 | NA | 0.0054−0.0094 |
| $[\mu]$/m$^3$·kg$^{-1}$ | 0.014 | NA | 6.7 |

**Aqueous Solutions.** The theta temperature of aqueous solutions is 235 K,[9] so they are stable in the whole range of temperature investigated in this study, (283 to 328) K. Crystallization is not expected (amorphous system)[9] and has not been detected in our experiments.

**Received:** September 5, 2011
**Accepted:** January 30, 2012
**Published:** February 15, 2012





dx.doi.org/10.1021/je200777d | *J. Chem. Eng. Data* 2012, 57, 776−783

The solvent mass fraction $\omega_s$ is defined as the ratio of the solvent mass $M_s$ over the total mass of the solution: $\omega_s = M_s/(M_s + M_p)$ with $M_p$ as the mass of polymer. $\omega_p = (1 - \omega_s)$ is the polymer mass fraction. The solution specific volume $\overline{v}$ has been measured as a function of $\omega_p$ by an Anton Paar 5000 vibrating tube densimeter with a relative uncertainty of $5{\cdot}10^{-6}$ (temperature $T$ = 298 K, polymer from batch 1). The relative uncertainty on $\omega_p$ due to sample preparation is lower than $3{\cdot}10^{-5}$. Figure 1 shows that $\overline{v}$ varies linearly with $\omega_p$. This result

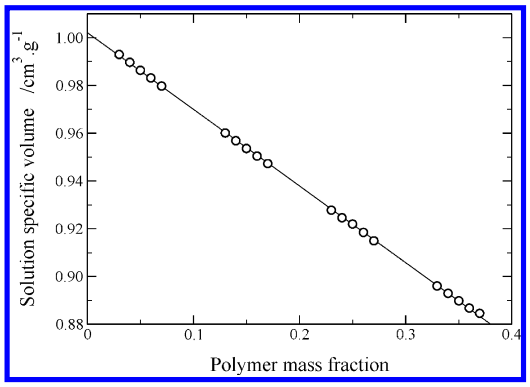


**Figure 1.** Solution specific volume $\overline{v}$ as a function of polymer mass fraction $\omega_p$ at $T$ = 298 K (polymer from batch 1). ○, experimental points; solid line, linear fit.

supports the assumption of constant partial specific volumes $\overline{v}_s$ and $\overline{v}_p$ (respectively of solvent and polymer) since $\overline{v}$ is given by

$$\overline{v} = \overline{v}_s - \omega_p(\overline{v}_s - \overline{v}_p) \quad (1)$$

A linear fit performed on data of Figure 1 gives $\overline{v}_s$ = 1.0021 cm$^3$·g$^{-1}$ and $\overline{v}_p$ = 0.681 cm$^3$·g$^{-1}$. The value of $\overline{v}_s$ is very close from the value 1.0030 cm$^3$·g$^{-1}$ reported for water,[10] and the value of $\overline{v}_p$ is consistent with the data collected from the literature,[9] ranging from 0.674 cm$^3$·g$^{-1}$ to 0.716 cm$^3$·g$^{-1}$.

The solvent volume fraction $\varphi_s$ is derived from the solvent mass fraction $\omega_s$ assuming volume additivity:

$$\varphi_s = \frac{\omega_s \overline{v}_s/\overline{v}_p}{1 - \omega_s(1 - \overline{v}_s/\overline{v}_p)} \quad (2)$$

Variations of the ratio $\overline{v}_s/\overline{v}_p$ with temperature and polymer molar mass are neglected. The polymer volume fraction $\varphi_p$ is given by $\varphi_p = 1 - \varphi_s$.

Using solutions of various concentrations, the polymer volume fraction at critical entanglement $\varphi^*_p$ and the intrinsic viscosity $[\mu]$ have been obtained from viscosity measurements performed with a low shear 30 rheometer at room temperature (see values in Table 1). Due to high polydispersity of polymers used in this study, we are not able to provide a single value of $\varphi^*_p$, but a concentration range corresponding to the transition between the dilute and the semidilute regimes. It is well-known that the intrinsic viscosity dependence on the polymer molar mass can be described by a power law. In the case of batch 1, using the value of $[\mu]$ in Table 1 and the sets of coefficients reported by Scholtan,[11] Klein and Conrad,[12] or Munk et al.,[13] we obtain molar mass estimations of (15, 21, or 9.2) kg·mol$^{-1}$, respectively, which are rather close from the value $M_w$ = 22.4 kg·mol$^{-1}$ measured by GPC. On the contrary, the same method applied to batch 3 leads to molar mass estimations 10 times higher than the value provided by the manufacturer. Anyway, this batch is only used in experiments which are expected to be weakly sensitive to the molar mass (sorption isotherm or diffusion coefficient in the concentrated regime). This weak dependency is systematically checked by comparison with results from batch 2.

## EXPERIMENTAL SETUP

**Gravimetric Experiments.** *Setup Characteristics.* The sorption isotherm and the diffusion coefficient in the concentrated regime are obtained using an experimental setup which consists of an accurate balance coupled with a vapor chamber whose temperature and pressure are controlled. The sample is hung in the chamber, and changing the solvent vapor pressure allows for swelling or drying of the polymer film. The gravimetric setup is a Hiden IGA system based on a precise balance. The chamber is a stainless steel cylinder with a diameter of 34.5 mm and a height of 300 mm. The temperature is regulated with a fluid circulating in the outer wall of the chamber from a thermostatted bath. The temperature is measured by a platinum resistance thermometer (Pt 100) located near the sample. The uncertainty in the temperature measurement is ± 0.1 K, and the temperature stability is better than ± 0.05 K. The chamber is connected through various valves to a vacuum pump on one hand and to a solvent tank on the other hand, where liquid solvent is in equilibrium with its vapor at 328 K. The pressure is regulated with a PID controller, and the pressure stability is better than 2 Pa. The solvent vapor is the only gas present in the chamber, so the total pressure and the solvent vapor pressure are the same. The pressure is measured with a manometer (relative error 0.3 %). The mass measurement noise is about 1 μg, and the reproducibility (same measurement performed at various times) is about 10 μg.

*Determination of Solvent Activity.* The saturated vapor pressure of pure water has been estimated from Antoine's law:

$$P_{vs0} = \exp\left(A - \frac{B}{T - C}\right) \quad (3)$$

with $P_{vs0}$ in Pa, $T$ the absolute temperature in K, $A$ = 23.5334, $B$ = 4023.44, and $C$ = 38.076 (coefficients obtained from the Hiden microbalance software). We tested this relation by comparison with data reported by Riddick et al.[14] and found a relative error lower than 0.4 % in the temperature range from (273 to 373) K. Assuming that water vapor behaves like an ideal gas, the water activity is given by the classical relation $a = (P_{vs}/P_{vs0})$, with $P_{vs}$ the vapor pressure measured above the solution. The relative error in the activity due to the uncertainty in $P_{vs}$ and $P_{vs0}$ is lower than 1.4 %.

*Sample Preparation.* For gravimetric experiments, aqueous solutions were prepared using ultrapure water (resistivity 18.2 MΩ.cm). Then polymer films of uniform thickness were obtained by slow drying of the aqueous solution in glass dishes. The drying time (typically a few days) was controlled by putting the dish in a box, with a small aperture to allow slow vapor diffusion outside the box. The initial concentration was chosen to get a solution initial viscosity in the range from (0.1 to 1) Pa·s. Indeed, a too-large viscosity induces formation of air bubbles, while hydrodynamic instabilities leading to wrinkle formation[5] are promoted by a too-small viscosity (for the highest molar mass, good results were obtained with an initial polymer mass fraction approximately equal to 0.01). The initial thickness (typically from 1 mm to a few centimeters) is adjusted to get the desired dried sample thickness. After drying,


dx.doi.org/10.1021/je200777d | J. Chem. Eng. Data 2012, 57, 776–783

the film is taken off from the dish, and a disk of diameter $D$ = 20.0 ± 0.1 mm is cut with a hollow punch. This operation is performed in an atmosphere of 80 % humidity to prevent formation of cracks. Then the sample is hung horizontally in the balance chamber, its two sides being exposed to solvent vapor. After the end of experiments, complete drying of the sample is achieved by placing it in an oven under vacuum during at least 10 h at 423 K. Then the film is weighed on a Sartorius balance to get the polymer mass $M_p$ (absolute uncertainty: ± 0.1 mg). Finally, the sample dry thickness $h_{dry}$ is estimated by the relation $h_{dry} = \bar{v}_p M_p/(\pi D^2/4)$.

The polymer mass $M_p$, the dry thickness $h_{dry}$, and the higher bound of the absolute error in $\omega_s$ (estimated from the errors in $M_p$ and $M_s$) of the three samples used in gravimetric experiments are given in Table 2. The relative uncertainty on $h_{dry}$ is estimated at ± 7 %.

**Table 2. Characteristics of Samples Used in Gravimetric Experiments (See Table 1 for Batch Characteristics)**

| sample | 1 | 2 | 3 |
|---|---|---|---|
| batch | 2 | 3 | 3 |
| $M_p$/mg | 9.5 | 16.8 | 217.5 |
| $h_{dry}/\mu$m | 21 | 36 | 470 |
| $\Delta\omega_s$ | $\leq 5{\cdot}10^{-3}$ | $\leq 2{\cdot}10^{-3}$ | $\leq 1{\cdot}10^{-4}$ |

**Sliding Symmetric Tubes Technique.** *Setup Characteristics.* The determination of the mutual diffusion coefficient $D_{mut}$ at high solvent concentrations has been carried out by the sliding symmetric tubes (SST) technique, which has been developed recently at Mondragon Unibertsitatea for the determination of mutual diffusion coefficient of binary systems in the liquid phase. This technique has been validated by measuring the mutual diffusion coefficient of several well-documented systems.[15] The difference with data from literature was less than 3 %.

The SST technique consists of two identical vertical tubes (length: 60 ± 0.01 mm, diameter: 9 ± 0.01 mm), each containing a solution with slightly different concentrations (the concentration difference between the tubes has to be small enough to make the variation of diffusion coefficient negligible). The solution with higher density is placed in the lower tube to eliminate convection. The temperature of the tubes is controlled by introducing them in a water bath, regulated by a Lauda RCS thermostatic bath. All of the walls of the bath are thermally insulated so that the temperature variations inside the bath are lower than 0.1 K. A couple of tubes can be set in two positions: the "faced" configuration allows mass transfer between tubes, while the "separated" configuration interrupts it (in the latter case, each tube is closed impermeably).

*Measurement of Average Concentration as a Function of Time.* In these experiments, we used batch 1 polymer, purchased as an aqueous solution of 0.50 polymer mass fraction. The desired concentration is obtained by adding the appropriate amount of bidistilled water, using a 10 mg precision microbalance. At the beginning of the experiment, 10 couples of tubes are placed in the water bath in a "separated" configuration. We first wait a time long enough to be sure that thermal equilibrium is reached (typically 48 h), and then the tubes are switched to the "faced" configuration by an external screw, allowing the diffusion to begin. The couples of tubes are then switched back to the "separated" configuration, one after the other, at different times (see Figure 2). After homogenization of the concentration field by shaking, the

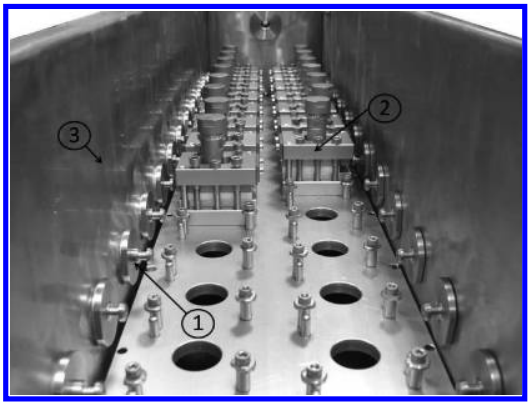


**Figure 2.** Photograph of the chamber containing the sets of tubes. (1) Screws used to switch between "faced" and "separated" positions, (2) sets of sliding tubes, (3) insulated walls.

density of the solution is measured by the Anton Paar 5000 densimeter, which allows us to know the average solution density in each tube (maximum solution viscosity allowed with this densimeter: 70 mPa·s). Finally, the average concentration inside each tube is determined from density measurements (see data in Figure 1). This gives the average polymer concentration in each tube at the time corresponding to the interruption of mass transfer between the tubes.

## ■ SORPTION ISOTHERM

As already mentioned, sorption isotherms are obtained from gravimetric experiments. The experimental protocol must take into account that dry PAAm is glassy at temperatures investigated in this study. To erase history effects,[16,17] we always start the experiments at a vapor pressure high enough to bring the sample above the glass transition, in a state of thermodynamic equilibrium (rubbery regime). Then we perform a series of decreasing differential steps of solvent vapor pressure. When the sample is still in the rubbery regime, the asymptotic value reached at the end of the step gives the equilibrium solvent concentration in the film, corresponding to the imposed solvent vapor pressure. Below the glass transition (i.e., in the glassy regime), a steady state can no longer be reached in a reasonable time. In that case, the duration of each step is fixed at three hours, and the desorption isotherm is built using the mass at the end of each step.

The experimental desorption isotherms obtained for the different temperatures are represented in Figure 3. The glass transition corresponds to the sudden change of slope in the function $\varphi_s(a)$. The glassy regime is characterized by an excess of solvent, compared to thermodynamic equilibrium. The extension of the glassy regime is reduced when the temperature is increased.

The rubbery domain can be described by the classical Flory–Huggins law:[18]

$$a = (1 - \varphi_p)\exp(\varphi_p + \chi\varphi_p^2) \quad (4)$$

where $\chi$ is the Flory–Huggins interaction parameter which characterizes the affinity between the solvent and the polymer. To determine $\chi$ as a function of $\varphi_s$ and $T$, we first make a rough determination of $\varphi_{sg}$ and $a_g$ (with $\varphi_{sg}$ and $a_g$ the solvent volume


dx.doi.org/10.1021/je200777d | J. Chem. Eng. Data 2012, 57, 776–783

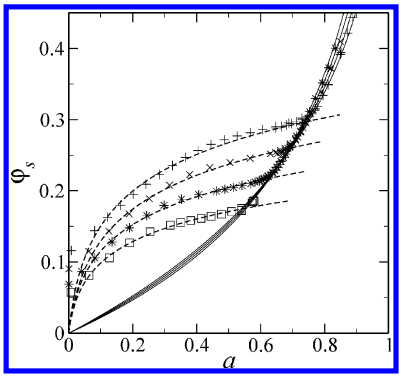


**Figure 3.** Desorption isotherm: solvent volume fraction $\varphi_s$ as a function of activity $a$ (sample 2). +, 283 K; ×, 298 K; ∗, 313 K; □, 328 K; solid lines, fit of the equilibrium regime (eq 4); dashed lines, fit of the glassy regime (eq 6).

fraction and the activity at glass transition, respectively), based on the change of slope in the function $\varphi_s(a)$. Then $\chi$ is fitted using the data such that $\varphi_s > \varphi_{sg}$. Assuming that $\chi$ varies linearly with $\varphi_s$ and $T$ gives a good description of experimental data. We obtain:

$$\chi(\varphi_s, T) = 0.482 - 0.150\varphi_s + 3.3\cdot10^{-3}(T - 298) - 1.44\cdot10^{-2}\varphi_s(T - 298) \quad (5)$$

This empirical law is valid in the rubbery regime and in the parameter range covered in the experiments, that is, $a_g \leq a \leq 0.9$ and 283 K $\leq T \leq$ 328 K. In this validity domain, the Flory–Huggins interaction parameter varies from 0.32 to 0.48. Polymer of batch 3 was used in the experiments, but we do not expect any significant effect of molar mass on $\chi$ in that concentration range. Indeed, we checked that eqs 4 and 5 predict in a very satisfactory way, at $T$ = 298 K, the rubbery regime of a solution made from batch 2 polymer.

We can account for the excess of solvent in the glassy regime by using the simple model developed by Leibler and Sekimoto.[19] This model relates the excess of solvent to elastic properties in glassy regime. The elastic energy associated with the sample deformation under volume variation is taken into account via an osmotic bulk modulus $K_g$, which is assumed to be constant. This leads to a modified Flory–Huggins equation, valid below the glass transition:

$$a = (1 - \varphi_p)\exp\left[\varphi_p + \chi\varphi_p^2 - \frac{\bar{v}^\circ_s K_g}{RT}\log\left(\frac{\varphi_p}{\varphi_{pg}}\right)\right] \quad (6)$$

with $\bar{v}^\circ_s$ as the solvent molar volume, $R$ as the ideal gas constant, and $\varphi_{pg}$ as the polymer volume fraction at glass transition.

Parameters $K_g$ and $\varphi_{pg}$ are fitted using eq 6 and the experimental data in the glassy regime. Then the activity at glass transition $a_g$ is obtained by setting $\varphi_p = \varphi_{pg}$ in eq 6 (this leads to a slightly more accurate estimation of $\varphi_{pg}$ and $a_g$ than the values previously obtained by slope inspection). We can see in Figure 3 that the fit is quite good, except at very low solvent volume fractions. It is worthwhile to note that a constant value of $K_g$ gives a good agreement with the experimental data over a wide range of solvent volume fraction $\varphi_s$, so a direct dependence of $K_g$ on $\varphi_s$ cannot be established in a straightforward way. As already pointed out by Saby-Dubreuil et al.,[20] the value of $K_g$ obtained from this method is an average value which corresponds to the concentration range of the fit and depends strongly on the polymer matrix state.

The results are presented in Table 3. By comparing samples 1 and 2 at $T$ = 298 K, we see that the effect of the molar mass

**Table 3. Activity $a_g$ and Solvent Volume Fraction $\varphi_{sg}$ at Glass Transition, with Osmotic Bulk Modulus $K_g$ in a Glassy Regime, as a Function of Temperature (The Relative Uncertainty in $K_g$ Is of the Order of 10 %)**

| temperature/K | 283 | 298 | 298 | 313 | 328 |
|---|---|---|---|---|---|
| sample | 2 | 2 | 1 | 2 | 2 |
| $\varphi_{sg}$ | 0.30 | 0.26 | 0.28 | 0.22 | 0.18 |
| $a_g$ | 0.75 | 0.69 | 0.72 | 0.62 | 0.54 |
| $K_g$/GPa | 1.08 | 1.25 | 1.04 | 1.65 | 2.22 |

on $\varphi_{sg}$, $a_g$, and $K_g$ is very weak, at the limit of the uncertainty ranges. On the other hand, increasing the temperature from (283 to 328) K induces a significant effect on these parameters. We observe that the higher the temperature, the lower $\varphi_{sg}$ and $a_g$, as expected. At the contrary, $K_g$ increases significantly with the temperature (it is multiplied by 2 when the temperature goes up by 45 K). This means that the system stiffness in the glassy regime increases with temperature. This nontrivial behavior can be related to observations made by Saby-Dubreuil et al.[20] on the desorption isotherm of PMMA-PnBMA statistical copolymers in toluene (similar protocol than the present study). These authors found that, at a fixed temperature, increasing the amount of the monomer with the lowest glass transition temperature (nBMA) leads to a decrease of $\varphi_{sg}$ and $a_g$, but to an increase of $K_g$, while the opposite behavior was noticed on annealed samples (decrease of $K_g$ when increasing the nBMA amount). This observation confirms that $K_g$ is not an intrinsic property of the system but also depends on its history.

## ■ DIFFUSION COEFFICIENT

**Concentrated Regime.** The time evolution of the mass of the film in response to an imposed step of the solvent vapor pressure gives access to the mutual diffusion coefficient, through a suitable model of the swelling kinetics. This method of measurement of mutual diffusion coefficients of polymer solutions has been widely used in the literature, for rubbery systems[21,22] as well as glassy systems.[23−27] This method can only be used if at least a part of the sorption kinetics is driven by polymer/solvent mutual diffusion. This is not the case at high vapor pressure, since it has been shown that in this regime the kinetics are dominated by thermal effects.[28] This is why the measurement of polymer/solvent diffusivity by gravimetry is usually restricted to the concentrated regime. Moreover, in the case of glassy systems, the model must take into account viscoelastic relaxation, coupled with diffusion. Like for sorption isotherms, we always perform decreasing vapor pressure steps, starting from thermodynamic equilibrium. However, the step duration is not fixed but adapted to be much longer than the diffusion time. This condition is necessary to distinguish the mass evolution due to diffusion from the effect of viscoelastic stress relaxation.[29] For the thickest samples at low vapor pressure, the step duration can go to several days.

The sample being glassy in the concentration range covered by the experiments, the variation of mass after the pressure step is due to the coupling between solvent diffusion and polymer


dx.doi.org/10.1021/je200777d | J. Chem. Eng. Data 2012, 57, 776–783

matrix relaxation. Indeed, in the glassy regime, viscoelastic relaxation involves characteristic times of the same order of the experiment duration and must be incorporated into the modeling of kinetics. We therefore used the classical model by Long and Richman,[30] which takes into account the relaxation of polymer matrix through its effect on solvent solubility at the film−vapor interface. After the pressure step, the solvent concentration at the interface is assumed to vary in the following way:

$$\Delta c_{int}(t) = \Delta c_d + (\Delta c_\infty - \Delta c_d)[1 - \exp(-t/\tau_r)] \quad (7)$$

where $\Delta c_{int}(t)$ is the variation of solvent concentration at the interface as a function of time $t$, $\Delta c_d$ is the "quasi-equilibrium" concentration variation (the asymptotic concentration variation if the only mechanism is diffusion), $\Delta c_\infty$ the equilibrium concentration variation, and $\tau_r$ the relaxation characteristic time. The solvent transport inside the film is described by the Fick equation. If the pressure step is small enough, the solvent contents varies very little, so the mutual diffusion coefficient $D_{mut}$ and the sample thickness $h$ can be considered as constant. The diffusion equation thus reads:

$$\frac{\partial \Delta c}{\partial t} = D_{mut}\frac{\partial^2 \Delta c}{\partial x^2} \qquad \text{for} \quad 0 < x < h/2 \quad (8)$$

where $\Delta c$ is the local solvent concentration variation since the pressure step and $x$ the distance from the symmetry plane in the center of the sample. The second boundary condition results from symmetry:

$$\frac{\partial \Delta c}{\partial x} = 0 \qquad \text{for} \quad x = 0 \quad (9)$$

and the initial condition is $\Delta c = 0$. Finally, the variation of solvent mass can be obtained by integration over the sample thickness:

$$\Delta m_s(t) = \int_0^{h/2} c(x, t)\mathrm{d}x \quad (10)$$

Equations 7 to 10 can be solved analytically by use of the Laplace transform.[29] The parameters $D_{mut}$, $\tau_r$, $\Delta c_d$, and $\Delta c_\infty$ are then estimated by least-squares optimization (Levenberg−Marquardt algorithm), to minimize the differences between the theoretical and the experimental mass variations.

The Long and Richman model is well-known to reproduce in a very satisfactory way the shape of the different types of kinetics encountered in the glassy regime,[26,30] with the advantage of simplicity and low computational time. Its drawback is the naive representation of viscoelastic relaxation, based on a unique characteristic time. Indeed, the relaxation of the polymer matrix in the glassy regime involves a broad distribution of characteristic times, running on several decades.[31] In a previous study,[26] we showed that changing the exponential in eq 7 into a stretched exponential to introduce a time distribution into the relaxation model leads to different values of $\Delta c_\infty$ and $\tau_r$ but does not alter significantly the estimated values of $\Delta c_d$ and $D_{mut}$. Although oversimplified, this modeling of relaxation succeeds in separating the effect of diffusion from the effect of relaxation and therefore is consistent with our aim which is the determination of $D_{mut}$. The parameter $\tau_r$ having no physical sense, we do not present it in the following (in fact, it reflects the part of the time distribution which is observable during the experiments, so its value is always of order of the experimental time $\tau_{exp}$; see ref 27 for details).

The typical kinetics is presented in Figure 4. The absolute value of mass variation is plotted as a function of square root of time. The change of slope around $(t)^{1/2} \approx 50\ s^{1/2}$ delimits two regimes: the first one is dominated by diffusion, the second one by viscoelastic relaxation. The very good fit observed in that figure is representative of all of the experiments.

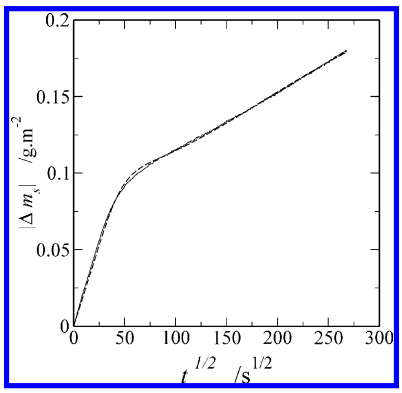


**Figure 4.** Drying kinetics at 298 K. Sample 2, $h_{dry}$ = 36 mm, $\varphi_{si}$ = 0.142, $\varphi_{sf}$ = 0.135, $D_{mut}$ = 1.6·10$^{-13}$ m$^2$·s$^{-1}$, $\tau_r$ = 6.9·10$^4$ s, $\tau_{exp}$ = 7.2·10$^4$ s. Solid line, experimental data; dashed line, numerical simulation (fit).

The same procedure has been repeated for various initial and final vapor pressures and different sample thicknesses. The values obtained for $D_{mut}$ are presented in Table 4, as a function of $\varphi_{si}$ and $\varphi_{sf}$, the initial and final polymer volume fraction averaged on the sample thickness, respectively.

**Table 4. Mutual Diffusion Coefficient $D_{mut}$ in the Concentrated Regime (Relative Uncertainty: ± 15 %)**

| Sample 1, $h_{dry}$ = 21 $\mu$m | | | |
|---|---|---|---|
| | | | $D_{mut}$ |
| $\overline{\varphi}_s$ | $\varphi_{si}$ | $\varphi_{sf}$ | m$^2$·s$^{-1}$ |
| 0.1347 | 0.1393 | 0.1301 | 9.6·10$^{-14}$ |
| 0.1318 | 0.1301 | 0.1334 | 7.4·10$^{-14}$ |
| 0.1552 | 0.1541 | 0.1563 | 2.3·10$^{-13}$ |
| 0.1577 | 0.1613 | 0.1541 | 2.7·10$^{-13}$ |
| Sample 2, $h_{dry}$ = 36 $\mu$m | | | |
| | | | $D_{mut}$ |
| $\overline{\varphi}_s$ | $\varphi_{si}$ | $\varphi_{sf}$ | m$^2$·s$^{-1}$ |
| 0.1125 | 0.1207 | 0.1043 | 4.6·10$^{-14}$ |
| 0.1278 | 0.1346 | 0.1209 | 8.9·10$^{-14}$ |
| 0.1411 | 0.1400 | 0.1421 | 1.4·10$^{-13}$ |
| 0.1384 | 0.1421 | 0.1346 | 1.6·10$^{-13}$ |
| 0.1449 | 0.1501 | 0.1396 | 2.4·10$^{-13}$ |
| Sample 3, $h_{dry}$ = 470 $\mu$m | | | |
| | | | $D_{mut}$ |
| $\overline{\varphi}_s$ | $\varphi_{si}$ | $\varphi_{sf}$ | m$^2$·s$^{-1}$ |
| 0.1766 | 0.1845 | 0.1687 | 1.7·10$^{-12}$ |
| 0.1897 | 0.1949 | 0.1845 | 5.0·10$^{-12}$ |
| 0.1981 | 0.2013 | 0.1949 | 7.0·10$^{-12}$ |


dx.doi.org/10.1021/je200777d | J. Chem. Eng. Data 2012, 57, 776−783

These data have been fitted to get the following empirical relation:

$$\log_{10}(D_{mut}) = 27.23\varphi_s - 16.624 \quad \text{for} \quad 0.11 \le \varphi_s \le 0.20 \tag{11}$$

The experimental values of $D_{mut}$ are plotted in Figure 5 as a function of solvent volume fraction $\varphi_s$. $D_{mut}$ increases by more

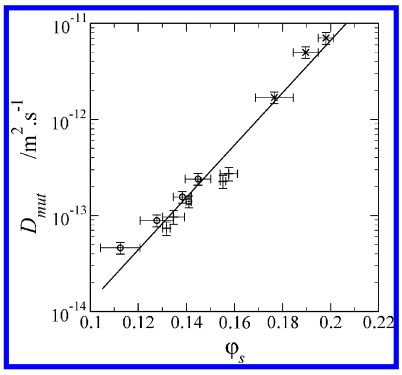


**Figure 5.** Mutual diffusion coefficient in the concentrated regime as a function of solvent volume fraction, at $T$ = 298 K. Symbols, experimental values (horizontal error bars represent $\varphi_{si}$ and $\varphi_{sf}$; vertical error bars represent the uncertainty on $D_{mut}$); solid line, linear fit (eq 11).

than two orders of magnitude when $\varphi_s$ goes up by approximately 0.1. This strong sensitivity of $D_{mut}$ on $\varphi_s$ is characteristic of polymer solutions in the concentrated regime.

**Semidilute and Dilute Regimes.** The mutual diffusion coefficient at high concentration of solvent has been measured by the SST technique at $T$ = 298 K, for polymers of batch 1. Figure 6 shows the time evolution of the average polymer

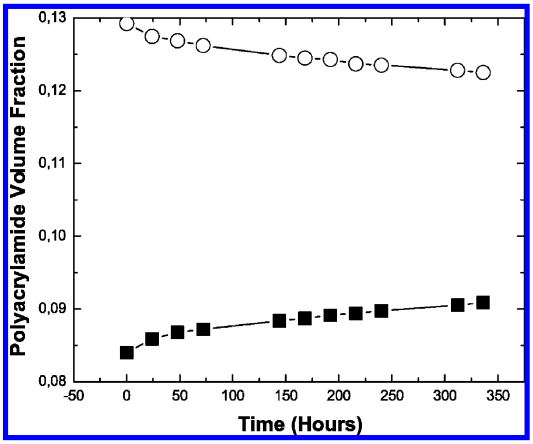


**Figure 6.** Time evolution of polymer volume fraction in both tubes for $\overline{\varphi}_p$ = 0.1072. ■, top tube; ○, bottom tube; solid lines represent fits by eqs 12 and 13 ($T$ = 298 K, polymer from batch 1).

volume fraction in each tube (upper and bottom). The polymer volume fraction averaged over both tubes $\overline{\varphi}_p$ is a constant and is equal to 0.1072 during the entire experiment.

We assume that mass transfer inside the tubes is purely diffusive (convection has been canceled by placing the heavier fluid in the bottom tube) and obey the classical Fick's law (solvent concentration being far above the glass transition, the effect of viscoelastic stress on mass transfer can be neglected). In addition, we consider that, before contact at time $t$ = 0, the concentration is uniform in each tube. Solving the diffusion equation with these assumptions leads to the expression of the average concentration in each tube as a function of time:

$$\overline{c^{up}}(t) - \frac{c_i^{up} + c_i^{bot}}{2} = \frac{8}{\pi^2}\left(c_i^{up} - \frac{c_i^{up} + c_i^{bot}}{2}\right) \cdot \sum_{n=0}^{\infty} \frac{\exp\left(-(n+1/2)^2 \frac{\pi^2}{L^2} D_{mut} t\right)}{(2n+1)^2} \tag{12}$$

$$\overline{c^{bot}}(t) - \frac{c_i^{up} + c_i^{bot}}{2} = -\frac{8}{\pi^2}\left(c_i^{up} - \frac{c_i^{up} + c_i^{bot}}{2}\right) \cdot \sum_{n=0}^{\infty} \frac{\exp\left(-(n+1/2)^2 \frac{\pi^2}{L^2} D_{mut} t\right)}{(2n+1)^2} \tag{13}$$

where $\overline{c^{up/bot}}$ (t) are the mean polymer concentrations in the upper and lower tube, $c_i^{up/bot}$ are the initial polymer concentrations in upper and lower tube, respectively, $L$ is the length of the tube, $t$ is the time of the experiment, and $D_{mut}$ is the mutual diffusion coefficient. The mutual diffusion coefficient is obtained by least-squares method (Matlab routine), to minimize the difference between the model and the experimental results (see the fit in Figure 6). Typically up to 11 points are used in each experiment. This allows us to take into account experimental points from the very beginning of the experiment, which is not possible in other similar techniques like the open-ended capillary technique.[32] Another advantage of the SST is that the two tubes give independent results, which can be compared each other. Indeed, in the ideal case where the difference of initial concentrations goes to zero, the two tubes should give the same result. In all cases presented in this article, the difference between the values obtained for $D_{mut}$ in each tube was lower than 5 %. In the following, we present the average value.

Four different polymer volume fractions have been investigated. The first one ($\overline{\varphi}_p$ = 0.0346) is in the dilute regime; the second ($\overline{\varphi}_p$ = 0.1072) is in the transition regime, and the two last ones ($\overline{\varphi}_p$ = 0.1848 and 0.2526) are in the semidilute regime. Results are presented in Table 5 and Figure 7. The order of magnitude of $D_{mut}$ is the same in all cases and corresponds to what is expected for polymer solutions at room temperature in that concentration range. There is no variation of $D_{mut}$ in the semidilute regime, and then it increases by 30 % when the polymer concentration is lowered.

The mutual diffusion coefficient of PAAm/water solutions has been widely investigated in the literature, but at very low polymer volume fractions. Experimental techniques include ultracentrifuge[11] or light scattering.[33,34] The diffusion coefficient $D_0$ in the limit of vanishing polymer volume fraction depends on the polymer molar mass through a power law,

**Table 5. Mutual Diffusion Coefficient as a Function of Polymer Volume Fraction in the Dilute and Semidilute Regimes[a]**

| | | | $\mu$ | $D_{mut}$ |
|---|---|---|---|---|
| $\overline{\varphi}_p$ | $\varphi_p^{up}$ | $\varphi_p^{bot}$ | mPa·s | $m^2 \cdot s^{-1}$ |
| 0.0346 | 0.0206 | 0.0486 | 1.6 | $2.47 \cdot 10^{-10}$ |
| 0.1072 | 0.0844 | 0.1300 | 5.2 | $2.09 \cdot 10^{-10}$ |
| 0.1848 | 0.1606 | 0.2091 | 17 | $1.90 \cdot 10^{-10}$ |
| 0.2526 | 0.2400 | 0.2962 | 68 | $1.91 \cdot 10^{-10}$ |

[a] $\varphi_p^{up}$ and $\varphi_p^{bot}$ are the initial polymer volume fractions in the upper and bottom tubes, respectively. $\overline{\varphi}_p$ is the polymer volume fraction averaged over both tubes. The dynamic viscosity $\mu$ at volume fraction $\overline{\varphi}_p$ is also provided for information ($T$ = 298 K, polymer from batch 1).

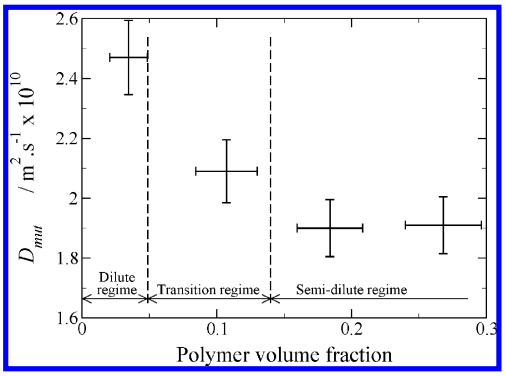


**Figure 7.** Mutual diffusion coefficient $D_{mut}$ as a function of polymer volume fraction $\overline{\varphi}_p$ in the dilute and semidilute regimes ($T$ = 298 K, polymer from batch 1). Horizontal error bars represent $\varphi_p^{up}$ and $\varphi_p^{bot}$; vertical error bars represent the uncertainty on $D_{mut}$.

which coefficients have been experimentally fitted. Using our value $M_w$ = 22.4 kg·mol$^{-1}$, Scholtan's empirical law[11] gives $D_0$ = $0.84 \cdot 10^{-10}$ m$^2$·s$^{-1}$ at 298 K, while the laws proposed by François et al.[33] or Patterson et al.[34] at temperature 293 K both lead to $D_0$ = $0.61 \cdot 10^{-10}$ m$^2$·s$^{-1}$. These values are significantly lower than our results presented in Table 5. Nevertheless, the experimental study performed by Patterson et al.[34] shows a rapid increase of the diffusion coefficient in a very short-range of PAAm volume fraction (from 0 to $10^{-3}$), so there is no inconsistency with our results.

## CONCLUSION

Some thermodynamic properties of polyacrylamide/water solutions have been measured by several techniques. In the concentrated regime, we used gravimetric experiments to obtain the desorption isotherm and the glass transition as a function of temperature from (283 to 328) K. In that range of temperature, the Flory–Huggins interaction parameter in the rubbery regime varies from 0.32 to 0.48, the solvent activity at glass transition from 0.75 to 0.54, and the corresponding solvent volume fraction from 0.30 to 0.18. In the glassy regime, the osmotic bulk modulus $K_g$ increases with temperature, from 1.1 GPa at 283 K to 2.2 GPa at 328 K. The same experimental setup was used to measure the mutual diffusion coefficient at room temperature in the glassy regime. As expected, in this regime, this parameter is strongly dependent on concentration. It increases by two decades and a half when the solvent volume fraction goes up by approximately 0.1 ($D_{mut}$ = $2.4 \cdot 10^{-14}$ m$^2$·s$^{-1}$ to $6.6 \cdot 10^{-12}$ m$^2$·s$^{-1}$ for $\varphi_s$ = 0.11 to 0.20). The diffusion coefficient has also been measured at high solvent concentration. Since gravimetric techniques fail in that case, due to thermal effects induced by latent heat of vaporization, we used another technique called the sliding symmetric tube, which consists in measuring the concentration as a function of time in two tubes in contact each other. The mutual diffusion coefficient keep the same order of magnitude over the whole range of polymer volume fraction investigated (from 0.035 to 0.25), around $2 \cdot 10^{-10}$ m$^2$·s$^{-1}$.

## AUTHOR INFORMATION

### Corresponding Author

*E-mail: frederic.doumenc@upmc.fr.

### Notes

The authors declare no competing financial interest.

## ACKNOWLEDGMENTS

This article presents results that were partly obtained in the framework of the following projects: GOVSORET3 (PI2011-22), MIBIO2, and Research Groups (IT557-10) of the Basque Government, and FP7Marie Curie scheme (grant PITN-GA-2008-214919 (MULTIFLOW)) from the European Union. We also thank Laboratory PPMD (ESPCI, France) for polymer characterization and Béatrice Guerrier (FAST, CNRS, France) for useful discussion.

## REFERENCES

(1) Cairncross, R. A.; Jeyadev, S.; Dunham, R. F.; Evans, K.; Francis, L. F.; Scriven, L. E. Modeling and design of an industrial dryer with convective and radiant heating. *J. Appl. Polym. Sci.* **1995**, *58*, 1279–1290.

(2) Guerrier, B.; Bouchard, C.; Allain, C.; Bénard, C. Drying kinetics of polymer films. *AIChE J.* **1998**, *44*, 791–798.

(3) Allanic, N.; Salagnac, P.; Glouannec, P.; Guerrier, B. Estimation of an effective water diffusion coefficient during infrared-convective drying of a polymer solution. *AIChE J.* **2009**, *55*, 2345–2355.

(4) Altinkaya, S. A.; Ozbas, B. Modeling of asymmetric membrane formation by dry-casting method. *J. Membr. Sci.* **2004**, *230*, 71–89.

(5) Bassou, N.; Rharbi, Y. Role of Bénard-Marangoni Instabilities during Solvent Evaporation in Polymer Surface Corrugations. *Langmuir* **2009**, *25*, 624–632.

(6) Kajiya, T.; Monteux, C.; Narita, T.; Lequeux, F.; Doi, M. Contact-Line Recession Leaving a Macroscopic Polymer Film in the Drying Droplets of Water-Poly(N,N-dimethylacrylamide) (PDMA) Solution. *Langmuir* **2009**, *25*, 6934–6939.

(7) Doumenc, F.; Guerrier, B. Drying of a Solution in a Meniscus: A Model Coupling the Liquid and the Gas Phases. *Langmuir* **2010**, *26*, 13959–13967.

(8) Huraux, K.; Narita, T.; Frétigny, C.; Lequeux, F. Solution Drying and Phase Separation Morphology of Polyacrylamide/Poly(ethylene glycol)/Water System. *Macromolecules* **2007**, *40*, 8336–8341.

(9) Mark, J. E. *Polymer Data Handbook*; Oxford University Press: New York, 1999.

(10) Marcus, Y. *The properties of solvents*; John Wiley and Sons: New York, 1998.

(11) Scholtan, W. Molekulargewichtsbestimmung von Polyacrylamid mittels der Ultrazentrifuge. *Makromol. Chem.* **1954**, *14*, 169–178.

(12) Klein, J.; Conrad, K. D. Molecular weight determination of poly(acrylamide) and poly(acrylamide-co-sodium acrylate). *Makromol. Chem.* **1978**, *179*, 1635–1638.

(13) Munk, P.; Aminabhavi, T.; Williams, P.; Hohhman, D.; Chmelir, M. Some Solutions Properties of Polyacrylamide. *Macromolecules* **1980**, *13*, 871–875.

(14) Riddick, J.; Bunger, W.; Sakano, T. *Organic solvents: physical properties and methods of purification*; John Wiley and Sons: New York, 1986.

(15) Alonso de Mezquia, D.; Blanco, P.; Bou-Ali, M.; Zebib, A. New technique for measuring the molecular diffusion coefficients of binary liquid mixtures.*Proceedings of Eurotherm Seminar 84*, Namur, Belgium, 2009.
(16) Doumenc, F.; Guerrier, B.; Allain, C. Aging and history effects in solvent-induced glass transition of polymer films. *Europhys. Lett.* **2006**, *76*, 630−636.
(17) Doumenc, F.; Bodiguel, H.; Guerrier, B. Physical aging of glassy PMMA/toluene films: Influence of drying/swelling history. *Eur. Phys. J. E* **2008**, *27*, 3−11.
(18) Flory, P. J. *Principles of polymer chemistry*; Cornell University Press: Ithaca, NY, 1995.
(19) Leibler, L.; Sekimoto, K. On the sorption of gases and liquids in glassy polymers. *Macromolecules* **1993**, *26*, 6937−6939.
(20) Saby-Dubreuil, A. C.; Guerrier, B.; Allain, C.; Johannsmann, D. Glass transition induced by solvent desorption for statistical MMA/nBMA copolymers—Influence of copolymer composition. *Polymer* **2001**, *42*, 1383−1391.
(21) Duda, J. L.; Ni, Y. C.; Vrentas, J. S. Toluene diffusion in molten polystyrene. *J. Appl. Polym. Sci.* **1979**, *23*, 947−951.
(22) Doumenc, F.; Guerrier, B.; Allain, C. Mutual diffusion coefficient and vapor-liquid equilibrium data for the system PIB/Toluene. *J. Chem. Eng. Data* **2005**, *50*, 983−988.
(23) Berens, A. Diffusion and relaxation in glassy polymer powders: 1. Fickian diffusion of vinyl chloride in poly(vinyl choride). *Polymer* **1977**, *18*, 697−704.
(24) Sanopoulou, M.; Roussis, P. P.; Petropoulos, J. H. A detailed study of the viscoelastic nature of vapor sorption and transport in a cellulosic polymer. I. Origin and physical implications of deviations from Fickian sorption kinetics. *J. Polym. Sci., Part B: Polym. Phys.* **1995**, *33*, 993−1005.
(25) Dimos, V.; Sanopoulou, M. Anomalous sorption kinetics in the methanol vapor-poly(methyl methacrylate) system. *J. Appl. Polym. Sci.* **2005**, *97*, 1184−1195.
(26) Dubreuil, A.-C.; Doumenc, F.; Guerrier, B.; Johannsmann, D.; Allain, C. Analysis of the solvent diffusion in glassy polymer films using a set inversion method. *Polymer* **2003**, *44*, 377−387.
(27) Dubreuil, A.-C.; Doumenc, F.; Guerrier, B.; Allain, C. Mutual Diffusion in PMMA/PnBMA Copolymer Films: Influence of the Solvent-Induced Glass Transition. *Macromolecules* **2003**, *36*, 5157−5164.
(28) Doumenc, F.; Guerrier, B.; Allain, C. Coupling between mass diffusion and film temperature evolution in gravimetric experiments. *Polymer* **2005**, *46*, 3708−3719.
(29) Doumenc, F.; Guerrier, B. Estimation of the characteristic times of solvent diffusion and polymer relaxation in glassy polymer films by a set inversion method. *Inverse Prob. Sci. Eng.* **2006**, *14*, 747−765.
(30) Long, F.; Richman, D. Concentration gradients for diffusion of vapors in glassy polymers and their relation to time dependant diffusion phenomena. *J. Am. Chem. Soc.* **1960**, *82*, 513−519.
(31) Souche, M.; Long, D. Case-II diffusion and solvent-polymer films drying: A mesoscale model. *Europhys. Lett.* **2007**, *77*, 48002.
(32) Dutrieux, J.; Platten, J.; Chavepeyer, G.; Bou-Ali, M. On the Measurement of Positive Soret Coefficients. *J. Phys. Chem. B* **2002**, *106*, 6104−6114.
(33) Francois, J.; Schwarz, T.; Weill, G. Crossover from the $\theta$ to the Excluded Volume Single Chain Statistics: New Experimental Evidences and a Modified Blob Model. *Macromolecules* **1980**, *13*, 564−570.
(34) Patterson, M.; Jamieson, A. Molecular Weight Scaling of the Transport Properties of Polyacrylamide in Water. *Macromolecules* **1985**, *18*, 266−272.

# Apéndice G

# Estudio Exhaustivo de los Coeficientes de Difusión, Termodifusión y Soret en mezclas de Agua-Isopropanol

# A comprehensive study of diffusion, thermodiffusion, and Soret coefficients of water-isopropanol mixtures

A. Mialdun, V. Yasnou, V. Shevtsova, A. Königer, W. Köhler et al.

Citation: J. Chem. Phys. **136**, 244512 (2012); doi: 10.1063/1.4730306
View online: http://dx.doi.org/10.1063/1.4730306
View Table of Contents: http://jcp.aip.org/resource/1/JCPSA6/v136/i24
Published by the American Institute of Physics.

# A comprehensive study of diffusion, thermodiffusion, and Soret coefficients of water-isopropanol mixtures

A. Mialdun,[1] V. Yasnou,[1] V. Shevtsova,[1,a)] A. Königer,[2] W. Köhler,[2,b)]
D. Alonso de Mezquia,[3] and M. M. Bou-Ali[3,c)]
[1]*MRC, Université Libre de Bruxelles, 50, Av. F.D. Roosevelt - CP-165/62, B-1050, Brussels, Belgium*
[2]*Physikalisches Institut, Universität Bayreuth, D-95440 Bayreuth, Germany*
[3]*Mechanical and Manufacturing Department, MGEP Mondragon Goi Eskola Politeknikoa, Loramendi 4 Apdo. 23, 20500 Mondragon, Spain*

(Received 28 February 2012; accepted 7 June 2012; published online 29 June 2012)

We report on the measurement of diffusion ($D$), thermodiffusion ($D_T$), and Soret ($S_T$) coefficients in water-isopropanol mixtures by three different instrumental techniques: thermogravitational column in combination with sliding symmetric tubes, optical beam deflection, and optical digital interferometry. All the coefficients have been measured over the full concentration range. Results from different instruments are in excellent agreement over a broad overlapping composition (water mass fraction) range $0.2 < c < 0.7$, providing new reliable benchmark data. Comparison with microgravity measurements (SODI/IVIDIL (Selected Optical Diagnostic Instrument/Influence of VIbration on DIffusion in Liquids)) onboard the International Space Station and with literature data (where available) generally gives a good agreement. Contrary to theoretical predictions and previous experimental expectations we have not observed a second sign change of $S_T$ at low water concentrations. © *2012 American Institute of Physics*. [http://dx.doi.org/10.1063/1.4730306]

## I. INTRODUCTION

Diffusion and thermodiffusion correspond to mixing and separation on the molecular level that is essential for a wide range of physical and chemical processes. Important examples include chemical and electrochemical reactions, sedimentation equilibrium (e.g., in crude oil reservoirs), crystal growth, transport across membranes, cell metabolism, and solidification (see Refs. 1–4). Molecular and thermodiffusion processes are quantified by mass and thermodiffusion coefficients, $D$ and $D_T$, respectively. Due to mass conservation, there is only one independent component of a binary mixture. Let us denote the mass fraction of this independent component (solute) as $c$. Then, the mass fraction of the dependent component (solvent) is $(1 - c)$. When pressure diffusion is negligible, the diffusive flux of the independent component is driven by concentration and temperature gradients

$$J = -\rho(D\,\nabla c + D'_T \nabla T), \tag{1}$$

where $\rho$ is the mixture mass density and $T$ is the temperature. The transport coefficients are assumed to be constant in a sufficiently small range of temperature and concentration variations and correspond to the mean temperature $T_0$ and composition $c_0$. Since the diffusive flux must vanish in the two dilute limits $c = 0$ and $c = 1$, the thermodiffusion coefficients can be represented as[5]

$$D'_T = c\,(1 - c)\,D_T. \tag{2}$$

Note that $D_T$ assumes finite values in the two dilute limits but may still depend on concentration. In the linear limit of small concentration changes the approximation $c\,(1 - c) \approx c_0(1 - c_0)$ is used and the diffusive flux can be written as

$$J = -\rho D\,[\nabla c + c_0\,(1 - c_0)\,S_T \nabla T]\,. \tag{3}$$

The Soret coefficient $S_T = D_T/D$ is determined as the ratio of the thermodiffusion and the mass diffusion coefficient. The signs of the Soret coefficient $S_T$ and of the thermodiffusion coefficient $D_T$ depend on the selection of the independent component. For its choice there exist two approaches in the literature: one is based on the molecular mass and the other one on the density of the components. In molecular dynamics simulations the use of molecular mass is appropriate and, as a rule, the component with a higher molecular mass is chosen as the independent one. Hydrodynamic effects become important when liquid mixtures are studied on a macroscopic scale. Correspondingly, it is appropriate to choose the denser component as the independent one, and a positive Soret coefficient implies that this component migrates towards the cold side. In case of a negative Soret coefficient, even heating from above may lead to convective instabilities[6,7] (unstable density stratification). Following the latter convention, we have chosen water (mass fraction $c$) as the independent component for the analysis of water-isopropanol (IPA) mixtures.

The growing interest in the measurement of transport coefficients of multicomponent mixtures at first requires well established and reliable techniques for binary mixtures. Since the discovery of thermodiffusion in the second half of the 19th century,[8,9] a variety of different experimental techniques has been developed, where one or two coefficients among $D$, $D_T$, and $S_T$ can be measured.

Motivated by the need for a pool of reliable data that could serve as a test for existing and novel experimental

a)Electronic mail: vshev@ulb.ac.be.
b)Electronic mail: werner.koehler@uni-bayreuth.de.
c)Electronic mail: mbouali@mondragon.edu.

 

techniques, a concerted effort with the aim to provide reference values for Soret, diffusion, and thermal diffusion coefficients has led to the so-called Fontainebleau benchmark. During this campaign, the transport coefficients of the three symmetric ($c = 0.5$) binary mixtures of 1,2,3,4-tetrahydronaphthalene, isobutylbenzene, and dodecane at $T_0 = 298$ K have been determined. These quasi-ideal hydrocarbon mixtures mimic representative compounds of crude oil that can be modeled with different degrees of success by molecular dynamics simulations.[10] The experimental techniques employed by the five participating laboratories[11–16] covered all methods for measuring the Soret coefficient available at that time, with the exception of diffusion cell experiments. Recently, two teams using different variants of diffusion cell setups, beam deflection technique[17] and optical digital interferometry (ODI),[18] reported the missing benchmark data.

Another type of mixtures of high interest comprises aqueous solutions, for which molecular dynamic simulations are still scarce.[19,20] These mixtures impose a number of experimental difficulties: the Soret coefficient changes sign in a certain concentration range, optical properties exhibit strong variations with concentration, or contrast factors may exhibit extrema at certain compositions. In this class of systems, water-ethanol is one of the most intensively studied binary mixtures and has served as a model system for double-diffusive convection experiments.[21–24] There are speculations that the sign change of $S_T$ might be related to the breakdown of the hydrogen bond network.[23] The idea that some aqueous solutions may exhibit two sign changes[25,26] could not be confirmed for water-ethanol mixtures.[17]

The present study is focused on mass and thermodiffusion coefficients in a less investigated aqueous binary mixture, namely, water-IPA. The data presented in this work cover a wide range of compositions measured by three different techniques in the participating laboratories and, in addition, the coefficients of two compositions measured in the experiment IVIDIL (Influence of VIbration on DIffusion in Liquids) on the International Space Station (ISS). The experimental techniques employed by the three participating laboratories are the thermogravitational column (TGC) and the sliding symmetric tubes (SST) technique (University of Mondragon (UM), Spain), beam deflection (University of Bayreuth (UB), Germany), and optical digital interferometry (University of Brussels (ULB), Belgium). The experimental technique used in the microgravity experiment IVIDIL, which we briefly discuss in support of our comprehensive study, is similar to that developed in Brussels.

This paper is organized as follows: Sec. II presents a short description of all employed experimental techniques. Section III reports on the results of the measurements of contracts factors and transport coefficients. A discussion, the comparison with literature data, and an error estimation are given in Sec. IV. Finally, the conclusions are drawn in Sec. V.

## II. DESCRIPTION OF THE EXPERIMENTAL TECHNIQUES

### A. Thermogravitational column and sliding symmetric tubes

#### 1. Thermodiffusion coefficient

The thermogravitational column (TGC) is the eldest among all the techniques in this study.[27] The here employed plane thermogravitational column has been developed at UM and is characterized by the following parameters: a plane-parallel column has a length of $L_z = (50.0 \pm 0.1)$ cm, gap dimension $L_x = (0.1 \pm 0.001)$ cm, and width $L_y = (5.0 \pm 0.1)$ cm. The critical element of the column is its very uniform thickness $L_x$ over the entire length. The precision in $L_x$ is a reflection of gap uniformity. In the column, a mixture is placed in a narrow slot between two plates with different temperatures (Fig. 1). The imposed horizontal temperature gradient induces horizontal gradients of composition due to the Soret effect. It also results in convective flow driven by buoyancy forces. The flow is strictly vertical, except at the top and bottom ends of the slot. The horizontal separation of components in combination with the vertical convective current

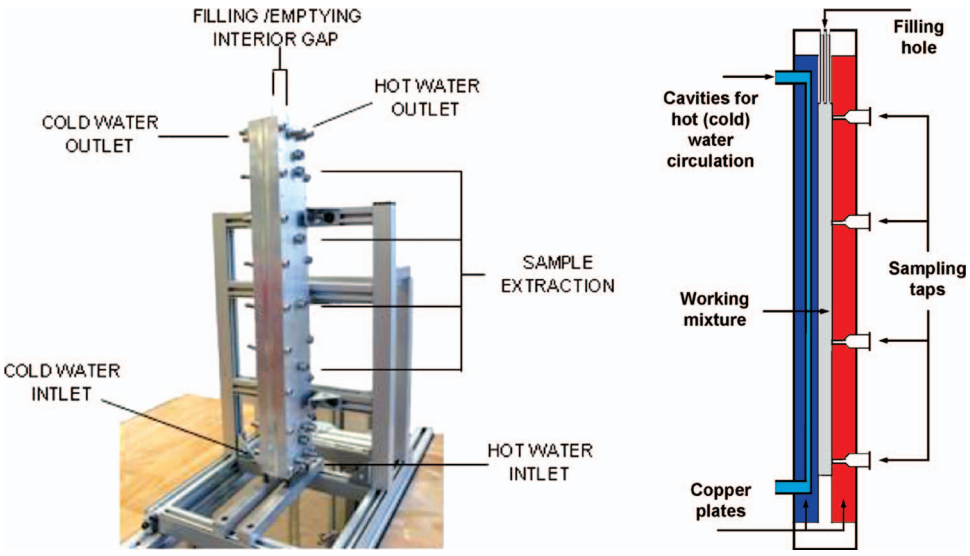


FIG. 1. Thermogravitational column, general view and sketch of cross section.

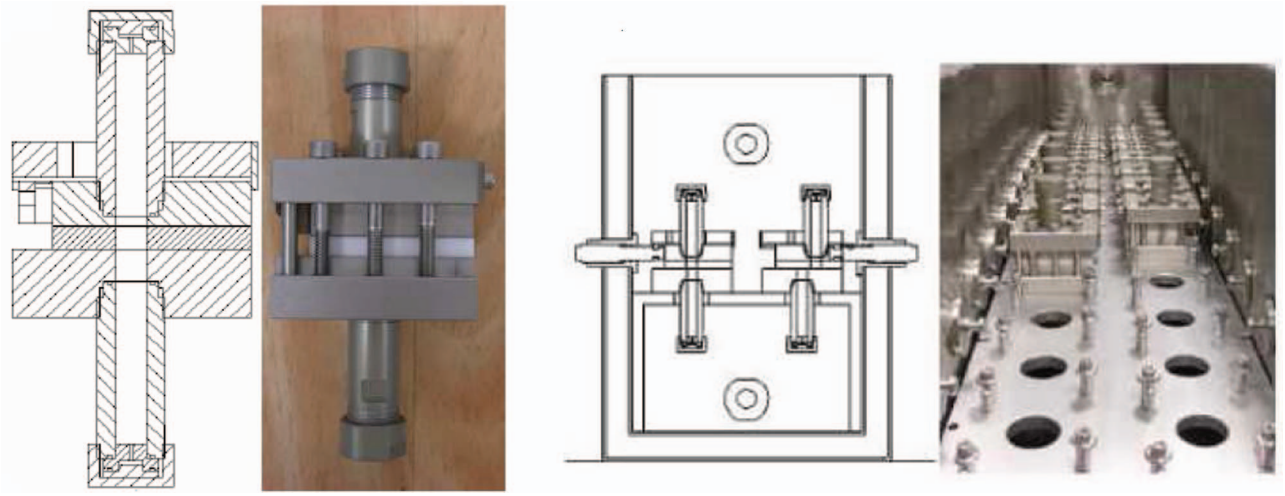

FIG. 2. Sliding symmetric tubes instrument; individual cell (left) and cell array (right).

leads to an enhanced separation between the top and bottom ends. The theories for the column operation and for data extraction are well established and verified for both gaseous and liquid mixtures. The vertical concentration gradient is measured in the steady state by taking samples through sampling taps. The aspect ratio $L_z/L_x = 500$ of the thermogravitational column is very high, which allows for neglecting the vertical diffusion in the steady state. Then, the vertical concentration gradient is given by[28,29]

$$\frac{\partial c}{\partial z} = -c_0\,(1 - c_0)\frac{504}{g\,L_x^4}\frac{D_T\,\nu}{\alpha}, \tag{4}$$

where $x$ and $z$ are the horizontal and vertical coordinates, $\nu$ is the kinematic viscosity of the mixture, $\alpha = \rho^{-1}(\partial\rho/\partial T)_{p,\,c}$ is the thermal expansion coefficient, and $g$ is the gravity acceleration. Equation (4) is used to determine the thermodiffusion coefficient $D_T$ from the concentration measurements along the column. Note that the separation in the column is independent of the temperature difference between the cold and hot plates. The temperature gradient is imposed by heating (cooling) the walls of the thermogravitational column. The two water baths used for stabilizing the temperatures of these lateral walls had a temperature control to within $\pm 0.01$ K.

The thermal expansion coefficient of the mixture is obtained by measuring the density of the fluid at five different temperatures between 297 and 299 K centered around the working temperature of $T = 298$ K. The thermal expansion coefficient is determined from a linear fit to the temperature dependence of the density of the mixture.

The vertical concentration gradient is determined from a previously obtained calibration curve for the density as a function of composition near the concentration of interest, from which the mass expansion coefficient $\beta_c = \rho^{-1}(\partial\rho/\partial c)_{p,\,T}$ is obtained. This coefficient is constant in the typical range of the concentration variation over the column. Considering that this vertical variation of composition is small, the concentration gradient is given by $dc/dz = (\beta_c\,\rho)^{-1}(d\rho/dz)$. The vertical density gradient along the column $d\rho/dz$ is directly obtained from the measurements of the density of four samples taken at evenly spaced elevations. In a narrow mass fraction range, the variation of $\rho$ with height is linear.

An Anton Paar DMA 5000 vibrating quartz $U$-tube densimeter with a precision of $1 \times 10^{-6}$ g/cm$^3$ and an accuracy of $5 \times 10^{-6}$ g/cm$^3$ has been used to determine the density of the extracted samples along the column as well as the mass and thermal expansion coefficients $\beta_c$ and $\alpha$ of the mixtures. An Anton Paar AMVn falling ball microviscometer with an accuracy of better than 2% has been used to determine the dynamic viscosity $\mu$ of the mixtures. A digital balance with a capacity of 310 g and accuracy of 0.0001 g has been used to prepare the mixtures. All the chemicals used were purchased from Merck with a purity of better than 99%.

### 2. Diffusion coefficient

The TGC experiments provide only the thermodiffusion coefficient $D_T$. In order to obtain the Soret coefficient, supplementary measurements of the diffusion coefficient $D$ are required. For this purpose a new apparatus, called sliding symmetric tubes, has been developed and validated at UM.[30] It is a modification of the open ended capillary method.[29] In this technique, two liquid mixtures ($c_{0,\,t}$, $c_{0,\,b}$) with slightly different concentrations around the point of interest ($c_0 \pm 3\%$) are placed into two tubular containers (subscripts $t$ and $b$ stand for top and bottom). In the experiment, typically 10 sets of such two-tube cells, with the same initial concentration of the mixtures, are used (see Fig. 2). To prevent convection, the mixture with the higher concentration of the denser component is placed in the bottom tube. The sets are then introduced into a water bath and given time to equilibrate at the working temperature, which is controlled with a precision of 0.1 K. All pairs of tubes are then simultaneously brought into contact with each other and the diffusion process starts. From this point on, the initial concentration difference between the corresponding tubes gradually decreases by diffusion.

Separating different pairs of tubes, one by one with a certain time step, the mean concentrations in the top and bottom parts $\overline{c}_t$, $\overline{c}_b$ are determined at successive moments of time. The

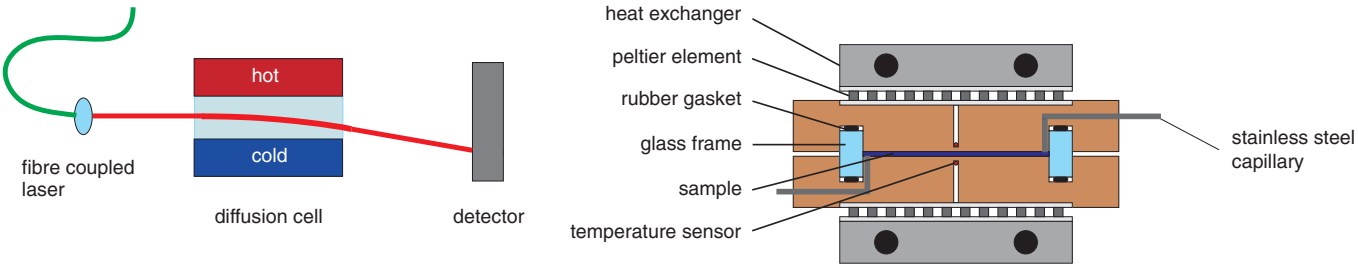


FIG. 3. Optical beam deflection setup: principle (left) and cross section of the cell (right).

diffusion coefficient is extracted by fitting the experimentally obtained concentration profile with the solution of the diffusion equation[30]

$$\bar{c}_t = \frac{1}{L}\int_L^{2L} c(z,t)dz = \frac{c_{0,t}-c_{0,b}}{2} + \frac{4(c_{0,t}-c_{0,b})}{\pi^2}\sum_{n=0}^{\infty}\left(\frac{2}{2n+1}\right)^2 \times \exp\left[-\frac{\left(\frac{2n+1}{2}\right)^2\pi^2}{L^2}Dt\right], \quad (5)$$

$$\bar{c}_b = \frac{1}{L}\int_0^{L} c(z,t)dz = \frac{c_{0,t}-c_{0,b}}{2} - \frac{4(c_{0,t}-c_{0,b})}{\pi^2}\sum_{n=0}^{\infty}\left(\frac{2}{2n+1}\right)^2 \times \exp\left[-\frac{\left(\frac{2n+1}{2}\right)^2\pi^2}{L^2}Dt\right]. \quad (6)$$

### B. Optical beam deflection (OBD)

The optical beam deflection technique has recently been used by different teams for the measurement of the Soret effect.[17,22,31] Advantages of the technique are the short duration of a typical experiment, a relative simplicity of the setup, and a well established theory. The method utilizes the classical Soret cell, but often relatively small in height (typically 1 mm). The setup used in this benchmark at UB has thoroughly been tested against reference data for water-ethanol and the Fontainebleau benchmark mixtures and is described in detail in Ref. 17.

The cell is formed by a rectangular glass frame with an internal optical path length of 40 mm. This glass frame is clamped between chromium-plated copper plates with two Viton O-rings for sealing. The vertical spacing between the plates defines the diffusion length of the experiment and is fixed by two spacers to $H = 1.022 \pm 0.002$ mm. The entire cell is sandwiched between two Peltier elements, which are connected to digital proportional-integral-derivative (PID) temperature controllers for maintaining the temperatures of the two plates with residual fluctuations of $\pm 1$ mK. Feedback to the controllers is provided by calibrated thermistors inserted into the copper plates close to the copper/liquid interface. Filling of the cell is accomplished with syringes via two stainless steel capillaries ending in two opposite corners of the cell. Figure 3 shows a sketch of the OBD setup and a cross section of the diffusion cell.

A fiber coupled diode laser with reduced coherence length operating at $\lambda = 637$ nm is used as light source. The beam is weakly focused into the diffusion cell with a beam waist of 244 $\mu$m (FWHM) and detected 1.5 m behind the cell by a line scan CCD camera. The position of the laser spot on the camera can be measured very precisely with a sub-pixel resolution by fitting a Gaussian function to the measured intensity profile. All components are mounted on a profile rail reducing the beam drift at the detector to typically 11 nm/h.

In a typical experiment, the plate temperatures are set to the same value for at least ten diffusion times, $\tau_D = H^2/(\pi^2 D)$, in order to allow the system to reach thermal equilibration. Then, a sudden temperature gradient is applied by symmetrically rising and lowering the two plate temperatures. Depending on the sign of the Soret coefficient, the sign of the temperature gradient is chosen to avoid convection. For a positive Soret coefficient of the denser component, heating is done from above to ensure a stable density profile. In the case of a negative Soret coefficient, heating is done from below to guarantee a stratified stationary state. A thermal Rayleigh number below the critical threshold ensures a convection free intermediate state between the temperature step and mass diffusion.

Values of refractive index variation with temperature and concentration, $(\partial n/\partial T)_{p,c}$ and $(\partial n/\partial c)_{p,T}$ (the so-called contrast factors), are required for conversion of the deflection signals into concentration changes. These values were determined by refractive index measurements over a wide range of temperatures and concentrations. Concentration dependent measurements have been carried out with an Abbe refractometer (Anton Paar Abbemat WR-MW) with an accuracy of $4 \times 10^{-5}$. For temperature dependence, an interferometer has been employed.[12] The isopropanol (99.9%) was obtained by BDH Prolabo and used without further purification. The water used in this work was deionized with a Milli-Q system.

The laser beam deflection is proportional to the refractive index gradient

$$\frac{\partial n}{\partial z} = \left(\frac{\partial n}{\partial T}\right)_{p,c}\frac{\partial T}{\partial z} + \left(\frac{\partial n}{\partial c}\right)_{p,T}\frac{\partial c}{\partial z}. \quad (7)$$

The transport coefficients are determined by numerically fitting a mathematical model of the experiment to the time dependent measured beam deflection angle using the plate

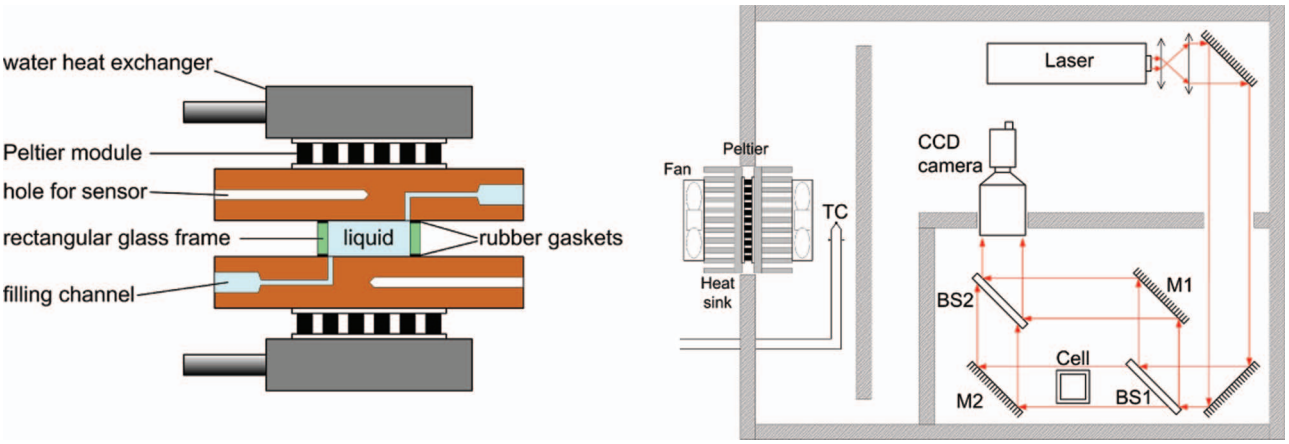


FIG. 4. Optical digital interferometry setup; cross section of the cell (left) and top view of the entire setup (right).

temperatures as time dependent boundary conditions. Even minute effects, like the time constants of the thermistors, the heat conduction in the copper plates, and the tiny temperature fluctuations of the order of 1 mK, are taken into account. Detail of the procedure can be found in Ref. 17. All quantities of interest, the Soret, diffusion, and thermodiffusion coefficients, are determined in the fitting routine simultaneously.

### C. Optical digital interferometry

#### 1. Laboratory setup

A setup for the measurement of the Soret effect by ODI has been developed at ULB and recently tested against the Fontainebleau benchmark mixtures.[18] A classical thermodiffusion cell has also been adopted for this setup but, when compared to OBD, with a relatively large height (Fig. 4(a)). Similarly to the OBD cell, a rectangular glass frame is clamped between two nickel-plated copper blocks with special seals of high thermal conductivity and thickness of either 0.08 mm (in case of epoxy glue) or 0.15 mm (in case of rubber). The cell used for these experiments has an inner volume of $18 \times 18 \times 6.5\,\text{mm}^3$ and is custom made from optical quality fused silica with a wall thickness of 2 mm. Each copper block is thermostabilized by Peltier elements driven independently by PID controllers that allow for a temperature stability of $\pm 0.002$ K. The temperature gradient applied across the cell was close to 1 K/mm in all measurements. The chemicals used were purchased from Fisher Scientific (isopropanol) and Acros Organic (water) with a purity of better than 99%.

The concentration variation within the liquid mixtures is observed by means of a Mach-Zehnder interferometer. The light source is a He-Ne laser with the wavelength of $\lambda = 632.8$ nm. An expanded and collimated laser beam is split into a reference and an objective arm, with the cell assembly placed within the latter. Then, both beams are deflected by mirrors and merged at the second beam splitter. One of the beams is inclined with respect to the other in order to create a narrow fringe pattern. The resulting interferogram is recorded by a CCD camera with a sensor of $1280 \times 1024$ pixels. The resolution of the imaging system is about 50 pixels/mm. In order to reconstruct a wave front (spatial distribution of optical phase), the Fourier transform method is applied to obtain the phase distribution from a single interferogram. To be precise, two interferograms are used in processing, as the interference pattern of interest is always processed against a reference interferogram taken before the refractive index change.

To ensure the thermal stability of the interferometer during the course of an experiment (up to 2–3 days), the whole setup, including a bearing bench plate, is placed inside a box of thermal insulation material, see Fig. 4(b). The box is equipped with air-to-air cooling/heating assembly based on a Peltier element and driven by a dedicated PID controller. A set of shields is inserted in the box to prevent air motion over optical paths. The temperature inside the box was kept equal to the mean temperature of the liquid with residual fluctuations of $\pm 0.02$ K. With this stabilization, the optical phase variations due to the instability of interferometer do not exceed 0.1−0.2 rad. More details about the setup can be found in Ref. 18.

The unique feature of this method is that it traces the *transient* path of the system over the *entire* two-dimensional cross section of the cell. The quantity obtained after processing an interferogram is a spatial phase distribution $\Delta\varphi(x, z, t)$, which is transferred into a concentration distribution by the equation

$$\frac{\lambda}{2\pi H}\Delta\varphi(x,z,t) = \left(\frac{\partial n}{\partial c}\right)_{p,T} \Delta c(x,z,t) + \left(\frac{\partial n}{\partial T}\right)_{p,c} \Delta T(x,z,t), \quad (8)$$

where the second term is defined during the initial step of the experiment.[18] Consequently, Soret and diffusion coefficients are simultaneously extracted by fitting of $\Delta c(x, z, t)$ from Eq. (8), averaged in x-direction, with the 1D analytical solution[33]

$$c(z,t) = c_0 + c_0(1-c_0)\,S_T\,\Delta T\left[\frac{1}{2} - \frac{z}{H} - \frac{4}{\pi^2}\sum_{n,odd}^{\infty}\frac{1}{n^2}\cos\left(\frac{n\pi z}{H}\right)\exp\left(-\frac{n^2\pi^2}{H^2}D\,t\right)\right]. \quad (9)$$

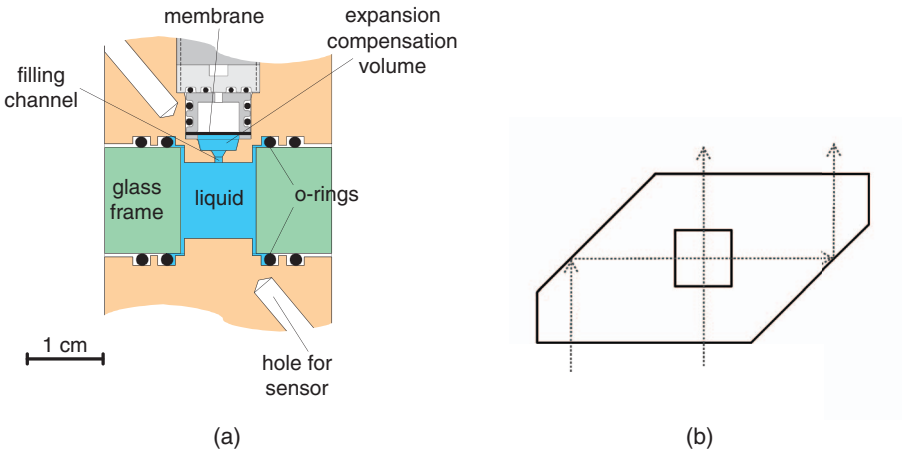


FIG. 5. Microgravity setup: Cross section of the IVIDIL cell housing and top view of the cell with the path of the objective beam.

### 2. Setup inside the SODI instrument on the ISS

The IVIDIL experimental objectives were manifold (for details see Refs. 34 and 35). A few experimental runs without imposed vibrations enabled measurements of the Soret coefficient of water-isopropanol mixtures at two specific compositions, namely, $c = 0.50$ and $c = 0.90$ mass fraction of water. It is valuable to compare these unique measurements with ground results.

The sketch of the IVIDIL cell housing is shown in Fig. 5(a) and the top view of the cell in Fig. 5(b). The cell geometry is different from the laboratory one: the IVIDIL cell had a cubic inner volume of $10 \times 10 \times 10\,\text{mm}^3$. The external walls of the cell are shaped in the form of two prisms to allow optical observation in two perpendicular directions. The beam paths through the cell are shown by the arrows in Fig. 5(b). The coherent light source was a laser diode emitting at $\lambda = 670$ nm wavelength. Temperature differences applied to the cell were 5, 10, or 15 K with a typical stability of $\pm 0.02$ K. The resolution of the imaging system is about 77 pixels/mm. In spite of the same type of probing (Mach-Zehnder interferometer), the instrument had many peculiarities when compared with its ground analogue.

Along with the housekeeping data, the interferograms are the only source of scientific information provided by the IVIDIL experiment. An example of an interference pattern in front view of the cell is shown in Fig. 6(a). For a quick examination of running experiments, 283 digital images were downloaded for each run via telemetry. In total 653 images per run have been recorded, and they have returned to Earth on flash disks a few months later.

The data extraction procedure was basically the same as for the ground experiments. Due to time constraints, the duration of the microgravity experiments was relatively short: 12 h of thermodiffusion separation followed by 6 h of diffusion relaxation. Consequently, the analysis of the data relies on the transient behaviour. The concentration field in the

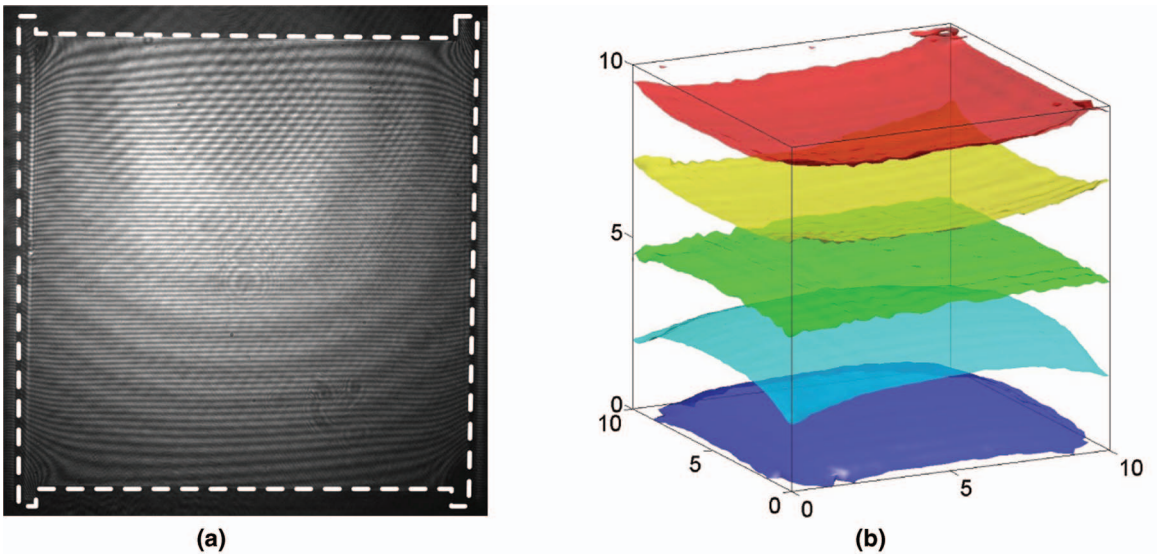


FIG. 6. Microgravity experiment. (a) Typical interference pattern of the cell in front view. White line depicts the volume filled with liquid. (b) Surfaces of the equal concentration after 12 h of the Soret separation in water-IPA mixture when $c_0 = 0.9$.

IVIDIL cell is shown in Fig. 6(b) after $t = 12$ h of separation. The isosurfaces of equal concentrations are shown by different colors for the mixture with negative Soret coefficient. The mid-surface (green) corresponds to the initial concentration $c_0 = 0.9$ and the following surfaces are separated by $\Delta c = 6 \times 10^{-4}$. This 3D concentration field demonstrates the possibility of optical digital interferometry using two perpendicular views and shows that ODI is capable to follow a component separation $\Delta c$ of less than 1% from the initial value.

## III. EXPERIMENTAL RESULTS

Following the discussion in the Introduction, the mass fraction of water $c$ is selected as the independent concentration. Correspondingly, the mass fraction of IPA is $(1 - c)$. When taking the concentration of IPA as the independent one, the signs of $S_T$, $D_T$, and $(\partial n/\partial c)_{p,T}$ must be inverted.

### A. Physical properties of the mixtures

The Soret coefficient of water-IPA mixtures displays a sign change as a function of concentration. In a non-uniform temperature field in the presence of gravity the mixture develops fingering and instabilities, which renders it an attractive system for theoretical and numerical analysis. These studies require the knowledge of all relevant physical properties of the system, including viscosity, thermal and mass expansion coefficients, and density. Some of these data can be found from different sources in literature, e.g., Ref. 32, but they are scattered and correspond to various mean temperatures. Thus, we have measured these properties along with diffusion and Soret coefficients in order to provide all necessary information for theoretical studies of this system and their comparison with experimental observations. Furthermore, the determination of the thermodiffusion coefficient by the thermogravitational technique (Eq. (4)) requires knowledge of thermophysical properties of the mixture such as dynamic viscosity, thermal expansion coefficient, mass expansion coefficient, and density. Table I summarizes these properties for different concentrations measured at UM at $T = 298$ K.

TABLE I. Physical properties of the water-IPA mixture measured at $T = 298$ K.

| $c$, water | $\mu \times 10^2$ mPa × s | $\alpha \times 10^5$ $K^{-1}$ | $\beta_C \times 10^2$ | $\rho$ kg/m$^3$ |
|---|---|---|---|---|
| 0.990 | 94.57 | 25.64 | 18.56 | 995.16 |
| 0.950 | 112.60 | 27.70 | 16.24 | 988.35 |
| 0.900 | 141.57 | 33.34 | 14.37 | 980.89 |
| 0.850 | 174.75 | 42.79 | 14.28 | 974.96 |
| 0.800 | 209.26 | 55.64 | 16.44 | 966.55 |
| 0.750 | 239.03 | 67.23 | 19.92 | 957.89 |
| 0.700 | 260.42 | 75.05 | 22.53 | 947.75 |
| 0.650 | 280.06 | 80.35 | 23.99 | 936.92 |
| 0.600 | 292.68 | 84.44 | 25.24 | 925.60 |
| 0.500 | 305.56 | 90.04 | 26.06 | 902.37 |
| 0.400 | 301.47 | 95.23 | 27.17 | 878.74 |
| 0.300 | 281.63 | 100.49 | 27.89 | 855.03 |
| 0.200 | 252.06 | 106.10 | 28.90 | 831.15 |
| 0.100 | 217.22 | 110.48 | 30.63 | 806.89 |

### B. Contrast factors

Beam deflection and optical digital interferometry require precise knowledge of the contrast factors $(\partial n/\partial T)_{p,c}$ and $(\partial n/\partial c)_{p,T}$, whose accuracy directly determines the accuracy of the Soret and the thermodiffusion coefficient. These values were measured at UB from 288 K to 308 K and in the full concentration range for a wavelength of $\lambda = 633$ nm. The measured values for the temperature dependence $(\partial n/\partial T)_{p,c}$ were obtained by an interferometric technique. Details of the interferometer and the data evaluation can be found in Ref. 12. The measurement error is typically below 0.5%.

The concentration derivative has been determined by refractive index measurements at different concentrations and differentiation of an approximating polynomial fitted to a small concentration range. All contrast factors are summarized in Table II and presented in Figs. 7 and 8. The symbols in the figures indicate the measured points and the curves outline the trend.

At low water concentration the contrast factor $(\partial n/\partial c)_{p,T}$ changes its sign. Near this point, concentration changes in the sample cannot be detected by optical techniques. In the vicinity, where the contrast factor is low, an optical measurement of the transport properties is difficult and subject to large errors.

TABLE II. Variation of refractive index with temperature, $(\partial n/\partial T)_{p,c}$, and concentration, $(\partial n/\partial c)_{p,T}$, for water-IPA.

| $c$, water | $(\partial n/\partial T)_{p,c}/10^{-4}$ $K^{-1}$ | | | $(\partial n/\partial c)_{p,T}/10^{-2}$ | | |
|---|---|---|---|---|---|---|
| $T =$ | 288 K | 298 K | 308 K | 288 K | 298 K | 308 K |
| 0.000 | − 4.141 | − 4.266 | − 4.420 | | | |
| 0.052 | − 4.243 | − 4.369 | − 4.505 | 0.260 | 0.336 | 0.399 |
| 0.100 | − 4.185 | − 4.324 | | − 0.564 | − 0.517 | |
| 0.150 | − 4.125 | − 4.241 | − 4.372 | − 1.14 | − 1.02 | − 0.746 |
| 0.200 | | − 4.138 | | | − 1.45 | |
| 0.250 | − 3.919 | − 4.033 | − 4.156 | − 2.09 | − 1.86 | − 1.67 |
| 0.300 | | − 3.921 | − 4.040 | | − 2.25 | − 2.01 |
| 0.351 | − 3.705 | − 3.809 | − 3.922 | − 2.83 | − 2.62 | − 2.42 |
| 0.409 | − 3.570 | − 3.681 | − 3.784 | − 3.26 | − 3.01 | − 2.79 |
| 0.451 | | − 3.585 | | | − 3.30 | |
| 0.500 | − 3.398 | − 3.474 | − 3.560 | − 3.89 | − 3.64 | − 3.47 |
| 0.547 | | − 3.359 | | | − 4.02 | |
| 0.600 | − 3.155 | − 3.217 | − 3.294 | − 4.84 | − 4.56 | − 4.38 |
| 0.650 | | − 3.062 | | | − 5.22 | |
| 0.700 | − 2.782 | − 2.854 | − 2.943 | − 6.42 | − 6.04 | − 5.35 |
| 0.747 | | − 2.574 | | | − 6.97 | |
| 0.800 | − 1.863 | − 2.127 | − 2.347 | − 9.15 | − 8.18 | − 7.30 |
| 0.854 | − 1.389 | − 1.653 | − 1.974 | − 9.84 | − 8.99 | − 8.13 |
| 0.899 | − 0.9801 | − 1.343 | − 1.652 | − 9.92 | − 9.23 | − 8.72 |
| 0.926 | | | − 1.540 | | − 9.14 | |
| 0.950 | − 0.7687 | − 1.135 | − 1.439 | − 9.20 | − 8.91 | − 8.43 |
| 0.975 | | | | | − 8.49 | |
| 1.000 | − 0.7200 | − 1.060 | − 1.350 | | − 7.89 | |

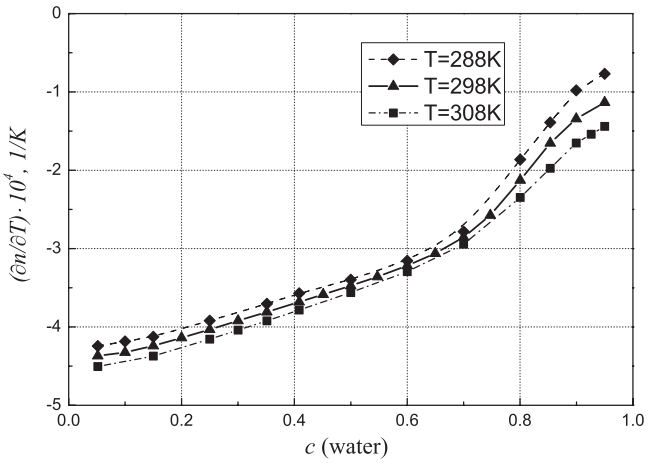


FIG. 7. Contrast factors $(\partial n/\partial T)_{p,\,c}$ versus the mass fraction of water at different mean temperatures.

### C. Soret, diffusion, and thermodiffusion coefficients

#### 1. Thermogravitational column and sliding symmetric tubes

The thermodiffusion coefficients $D_T$ were measured in a thermogravitational column and the mass diffusion coefficient $D$ in the separate SST instrument at UM. The Soret coefficients $S_T$ have been calculated as $S_T = D_T/D$. All results are summarized in Table III. Data on thermodiffusion coefficients are missing for $c > 0.75$, as in this region the thermodiffusion coefficient changes sign and instabilities developing in the column prohibit correct measurements. Consequently, also the Soret coefficient cannot be determined in this concentration range.

#### 2. Optical beam deflection

Soret, diffusion, and thermodiffusion coefficients were measured directly in the OBD experiments at UB. The measurements were performed at three different temperatures of 288, 298, and 308 K, and the data evaluation yields all three coefficients $D$, $D_T$, and $S_T$. The results are summarized in Table IV.

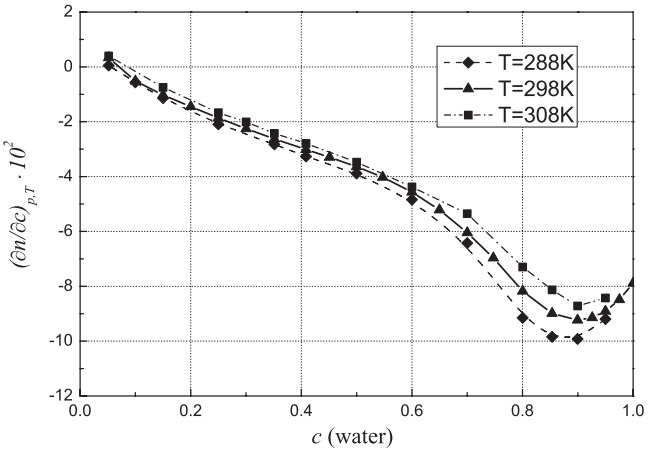


FIG. 8. Contrast factors $(\partial n/\partial c)_{p,\,T}$ versus the mass fraction of water at different temperatures.

TABLE III. Diffusion, thermodiffusion, and Soret coefficients measured by TGC and SST at $T = 298$ K.

| $c$, water | $D/10^{-10}$ m$^2$s$^{-1}$ | $D_T/10^{-13}$ m$^2$s$^{-1}$K$^{-1}$ | $S_T/10^{-3}$ K$^{-1}$ |
|---|---|---|---|
| 0.100 | 6.13 | 4.72 | 0.77 |
| 0.200 | 3.50 | 8.44 | 2.41 |
| 0.300 | 2.45 | 10.10 | 4.13 |
| 0.400 | 1.80 | 10.45 | 5.80 |
| 0.500 | 1.68 | 9.88 | 5.89 |
| 0.600 | 1.89 | 8.83 | 4.67 |
| 0.650 | 2.08 | 7.54 | 3.62 |
| 0.700 | 2.47 | 5.27 | 2.13 |
| 0.750 | 3.62 | 4.01 | 1.11 |
| 0.800 | 5.03 | | |
| 0.850 | 5.51 | | |
| 0.900 | 7.29 | | |
| 0.950 | 8.77 | | |
| 0.990 | 9.66 | | |

#### 3. Optical digital interferometry

Similar to OBD, all three coefficients $S_T$, $D$, and $D_T$ are directly obtained from the experiment by performing the data evaluation based on the two independent coefficients $S_T$ and $D$ and calculating $D_T = D\,S_T$. The results for the three coefficients obtained at ULB are summarized in Table V. Near the sign change region the measurements of $S_T$ were performed while increasing the concentration by small steps. The first point at which weak instability was observed in the cell (i.e., negative Soret) corresponds to $c = 0.75$. The extrapolation of the curve $S_T(c)$ to the region of negative Soret coefficient within a small range of $c$ allowed us to determine the concentration when $S_T = 0$ and estimate a negative value of $S_T$ for $c = 0.75$.

#### 4. Results from microgravity experiment

$D$, $D_T$, and $S_T$ have been determined in the IVIDIL microgravity experiment in analogy to the ground based ODI experiment. The results are summarized in Table VI. Note that in previous publications[35,36] the Soret coefficient from the IVIDIL experiment was given 5% lower for $c = 0.9$, based on contrast factors taken from the literature. The new value has been calculated with the improved contrast factors $(\partial n/\partial c)_{p,\,T}$ from Table II.

## IV. DISCUSSION

The results for $D$, $S_T$, and $D_T$ from Tables III–VI are plotted in Figs. 9–11. Also shown in gray are some less reliable values at low water concentrations that are not listed in the tables and that have been excluded from the data evaluation. These problematic data will be discussed in more detail below.

In addition to the here measured and tabulated data, Fig. 9 contains also literature data for the diffusion coefficient as measured by the Taylor dispersion technique.[37] Figure 10 shows supplemental literature results for the Soret coefficient

TABLE IV. Diffusion, thermodiffusion, and Soret coefficients measured by OBD.

| $c$, water | $D/10^{-10}$ m$^2$s$^{-1}$ | | | $D_T/10^{-13}$ m$^2$s$^{-1}$K$^{-1}$ | | | $S_T/10^{-3}$ K$^{-1}$ | | |
|---|---|---|---|---|---|---|---|---|---|
| $T=$ | 288 K | 298 K | 308 K | 288 K | 298 K | 308 K | 288 K | 298 K | 308 K |
| 0.200 | | 3.71 | | | 13.2 | | | 3.55 | |
| 0.250 | 1.23 | 3.05 | | 4.82 | 12.7 | | 3.92 | 4.16 | |
| 0.300 | | 2.60 | | | 11.7 | | | 4.51 | 3.74 |
| 0.351 | 0.87 | 2.08 | | 5.04 | 11.2 | 19.3 | 5.80 | 5.37 | 3.98 |
| 0.409 | 1.06 | 1.89 | 2.88 | 7.19 | 10.6 | 12.4 | 6.81 | 5.62 | 4.30 |
| 0.451 | | 1.79 | | | 10.6 | | | 5.91 | |
| 0.500 | 1.04 | 1.64 | 2.35 | 8.19 | 9.57 | 9.53 | 7.87 | 5.83 | 4.05 |
| 0.547 | | 1.58 | | | 9.04 | | | 5.72 | |
| 0.600 | 1.15 | 1.67 | 1.95 | 8.83 | 8.84 | 8.60 | 7.69 | 5.30 | 4.41 |
| 0.650 | | 1.96 | | | 8.29 | | | 4.24 | |
| 0.700 | 1.73 | 2.43 | 3.16 | 6.31 | 5.97 | 3.67 | 3.65 | 2.46 | 1.16 |
| 0.747 | | 3.25 | | | − 0.61 | | | − 0.19 | |
| 0.800 | 3.62 | 4.98 | 5.51 | − 14.4 | − 18.3 | − 18.0 | − 3.97 | − 3.67 | − 3.27 |
| 0.854 | 4.73 | 6.42 | 7.86 | − 36.9 | − 43.9 | − 46.6 | − 7.80 | − 6.83 | − 5.93 |
| 0.900 | | 7.49 | | | − 66.4 | | − 9.83 | − 8.87 | |
| 0.950 | 6.51 | 8.95 | 11.9 | − 72.0 | − 90.7 | − 109.9 | − 11.05 | − 10.14 | − 9.28 |

measured about 35 years ago by a flow cell technique[38] using a very thin fluid layer with $d \approx 0.2$ mm. Both these $D$ and $S_T$ literature data show a reasonable to good agreement with our results. In particular at intermediate and high water concentrations the agreement is convincing.

From a first inspection it is immediately evident that the overall concentration range can be divided into three regimes: The region with negative thermal diffusion and Soret coefficients at high water content ($c > 0.75$) is fully characterized only by the OBD technique. For the broad range of intermediate concentrations ($0.20 < c < 0.75$) with positive Soret coefficients there are ample and consistent data. Finally, there is the region of low water content ($c < 0.2$), where the optical techniques become less reliable, whereas the TGC/SST data still show a smooth behaviour. In the following we will discuss these three regimes in more detail.

### A. Region with negative Soret effect; water rich mixture, $c > 0.75$

Measuring negative Soret coefficients in the gravity field may lead to different types of instabilities, depending on the experimental technique. Theoretical studies[39–41] show that mixtures with a positive Soret effect can become convectively unstable in TGC when the temperature difference between its lateral walls exceeds some critical value. At the onset of instability a long stationary vortex is broken into a series of smaller ones. In mixtures with negative Soret effect there is a convective instability for any finite temperature difference due to accumulation of the heavier components at the top of the column. It occurs in form of a transversal wave propagating perpendicular to the vertical axis of the column and the applied temperature gradient. Convective instabilities in TGC necessarily lead to incorrect measurements.

In the ODI instrument the separation starts to develop with a negative Soret effect until a sufficient amount of a denser component is accumulated at the top of the cell.[7] The density stratification becomes unstable and at some moment the flow is initiated in form of large plumes, which convectively transport the heavier liquid downward. Due to the large differences among the viscous, thermal, and diffusion time scales, the system has a tendency towards these fingering buoyant instabilities. The advantage of the ODI technique is that it traces the transient path of the system in the entire two-dimensional cross section of a cell. Thus, it allows for studying both diffusive transport mechanisms and convection. Figure 12 shows a typical example for the development of convection in the water-IPA mixture containing 80% of water.

Approaching the point of sign change, $S_T \to 0$, the measurements by the ODI technique have been conducted with small increments in the mass fraction. Since the ODI technique allows for a reliable detection of the instability, the

TABLE V. Soret, thermodiffusion, and diffusion coefficients measured by ODI at $T = 298$ K.

| $c$, water | $D/10^{-10}$ m$^2$s$^{-1}$ | $D_T/10^{-13}$ m$^2$s$^{-1}$K$^{-1}$ | $S_T/10^{-3}$ K$^{-1}$ |
|---|---|---|---|
| 0.200 | 3.15 | 10.7 | 3.39 |
| 0.300 | 2.48 | 10.8 | 4.37 |
| 0.401 | 1.81 | 10.2 | 5.64 |
| 0.500 | 1.72 | 10.1 | 5.89 |
| 0.600 | 1.76 | 9.39 | 5.32 |
| 0.700 | 2.35 | 5.52 | 2.35 |
| 0.720 | 2.94 | 3.97 | 1.35 |
| 0.750 | | | − 0.26 |

TABLE VI. Diffusion, thermodiffusion, and Soret coefficients measured in IVIDIL experiment in microgravity, $T = 298$ K.

| $c$, water | $D/10^{-10}$ m$^2$s$^{-1}$ | $D_T/10^{-13}$ m$^2$s$^{-1}$K$^{-1}$ | $S_T/10^{-3}$ K$^{-1}$ |
|---|---|---|---|
| 0.900 | 6.55 | − 45.9 | − 7.01 |
| 0.500 | 1.62 | 9.51 | 5.87 |

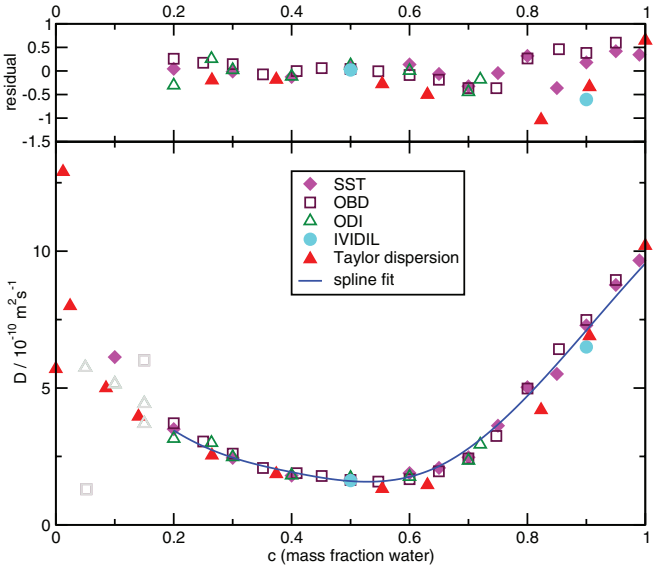


FIG. 9. Diffusion coefficients $D$ for water/IPA. Own measurements and literature data from Ref. 37 measured by Taylor dispersion.

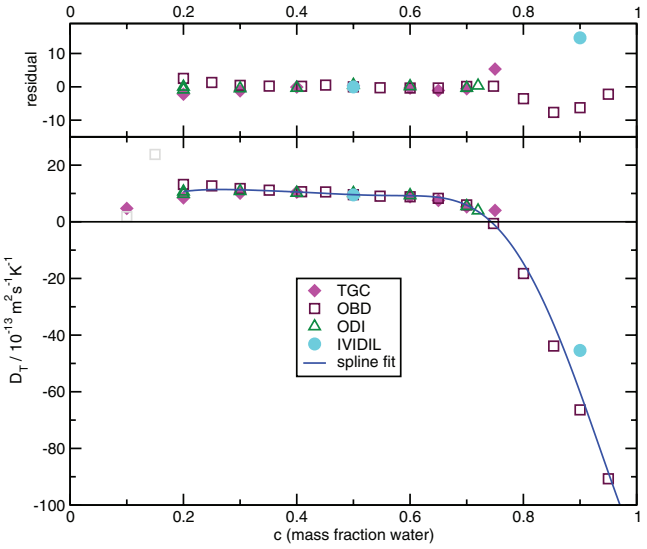


FIG. 11. Thermodiffusion coefficients $D_T$ for water/IPA. Own measurements.

concentration at which $S_T$ changes sign has been established rather precisely, $S_T = 0$ at $c = 0.745$. This value is in good agreement with the one determined by the OBD technique.

Because of the small size of the cell in the OBD technique and the resulting small Rayleigh numbers, also systems with negative Soret coefficients can be investigated.[42] In the case of unstable density stratification special changes are introduced in the experimental protocol. In particular, an inverse temperature gradient (heating from below) is applied to the OBD cell. The temperature difference is chosen in such a way that the Rayleigh number does not exceed the instability threshold. So, the essential advantage of OBD is its capability to measure the Soret effect independently of its sign. In the limit $c \to 1$ the OBD data for $S_T(c)$ show a decreasing slope, which resembles the behaviour of the Soret coefficient of ethanol/water.[17,21]

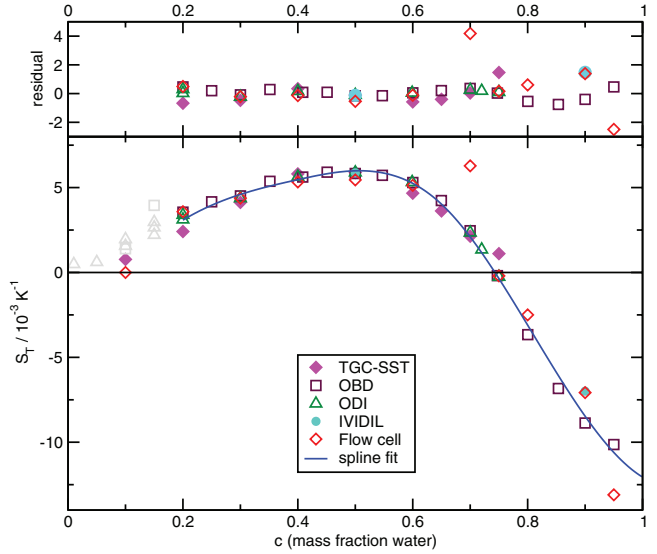


FIG. 10. Soret coefficients $S_T$ for water/IPA. Own measurements and literature data from Ref. 38 measured by flow cell technique at $T = 297$ K.

Both Soret and diffusion coefficients measured in microgravity (IVIDIL) at $c_0 = 0.9$ are in satisfactory agreement with the ones measured by OBD and the $S_T$ value coincides with that measured about 35 years ago by a flow cell technique.[38]

### B. Intermediate concentration regime, 0.2 < *c* < 0.75

This is the region where all techniques provide reliable and consistent data for all the quantities $S_T$, $D$, and $D_T$. The Soret coefficients display a parabolic concentration dependence with a maximum at $c \approx 0.5$. The thermodiffusion coefficient $D_T$ in this region depends only weakly on concentration, varying from $0.8 \times 10^{-12}$ to $1.1 \times 10^{-12}$ m$^2$/s$^{-1}$K$^{-1}$. It is worth noting that, despite of the good agreement among the three main techniques TGC/SST, ODB, and ODI, there are slightly different trends towards low water concentrations. According to OBD there is a very slight increase of $D_T$ with decreasing $c$, whereas the TGC data show a slight decrease. The ODI results are in between and approximately constant. The microgravity data at $c = 0.5$ are in an excellent agreement with all three ground based measurements. Also most literature data for $D$, measured by Taylor dispersion,[37] and for $S_T$, measured by a flow cell technique,[38] are in perfect agreement with our results. There is one pronounced exception: the Soret coefficient reported by Poty *et al.*[38] for $c = 0.7$ deviates significantly from all other data and seems to be too high.

### C. Region with low water content, *c* < 0.2

This region is difficult to explore by optical means. The concentration contrast factor $(\partial n/\partial c)$ vanishes at approximately $c = 0.07$ (see Table II), which means that concentration variations become invisible for optical techniques. The common opinion based on experience is that optical measurements become very noisy and inaccurate in this region.

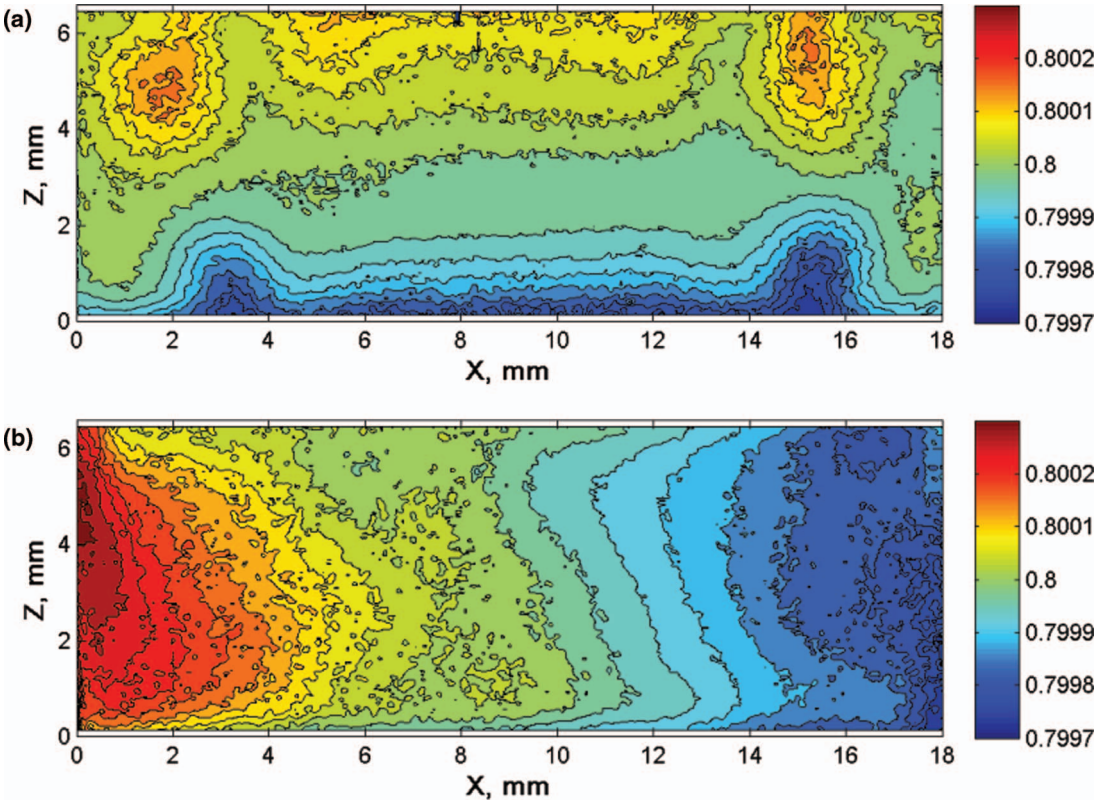


FIG. 12. Concentration field experimentally observed by ODI during Soret separation in mixture of $c_0 = 0.80$. (a) Fifteen minutes after applying $\Delta T$ and beginning of separation. (b) A few hours later.

The results of measurements in the region $c < 0.2$ by OBD and ODI are not given in Tables IV and V as they are considered non-reliable. TGC is not affected in the same way as the optical techniques from a vanishing refractive index contrast factor at low water concentration. The relevant contrast factor for the composition analysis, $\beta_c = \rho^{-1}(\partial\rho/\partial c)_{p,T}$ (Table I), remains finite over the entire composition range. Thus, we expect the coefficients measured for $c = 0.1$ by the combination of TGC and SST as still being reliable. Unfortunately, also the Taylor dispersion literature values for $D$ scatter significantly in the limit of low water content. The previous measurements by Poty *et al.*[38] give a hint to a possible sign change of $S_T$ at $c = 0.1$, but this trend is not confirmed by the new results. Our measurements using three different techniques provide positive Soret coefficients at $c = 0.1$, although the results are scattered ($0.77 \times 10^{-3}\,\mathrm{K}^{-1} < S_T < 1.96 \times 10^{-3}\,\mathrm{K}^{-1}$). In particular the positive $D_T(c = 0.1)$ as measured by TGC should be sufficiently reliable to exclude a sign change of $D_T$ and $S_T$ for water concentrations down to a few percent. A unique extrapolation to zero water concentration based on all available data still appears not feasible.

### D. Benchmark values

In summary, there are good and sufficient data for the intermediate concentration range and for high water content. For low water concentrations the situation is less clear and not satisfactory. Thus, we have extracted suggested benchmark values only for water concentrations $c > 0.2$. These benchmark values have been obtained from fits of approximating spline functions to all available data (Figs. 9–11).

The fit functions have been constructed such that two independent spline approximations $s_D$ and $s_{S_T}$ have been formulated for $D$ and $S_T$ as independent coefficients. The fit function $s_{D_T}$ for the dependent coefficient $D_T$ has been defined as $s_{D_T} = s_D s_{S_T}$. Both $s_D$ and $s_{S_T}$ are implemented as cubic splines with nodes at $c = 0.2$, 0.4, 0.65, and 1.0. The fit procedure simultaneously minimizes the sum of the squared residues for all three coefficients in Figs. 9–11 and determines the ordinates of the nodes and the derivatives at the two boundaries $c = 0.2$ and $c = 1.0$ as fit parameters.

Where appropriate, we have not only incorporated our own data, but also the available literature values. Since the accuracies of the different experimental techniques are comparable and since a precise determination of the error bars of the individual measurements is rather difficult and unclear, or not available, we have not introduced individual weight factors. The thus determined final benchmark values for all coefficients $D$, $D_T$, and $S_T$ are tabulated in Table VII. The error bars have been estimated from the scattering of the residues in the vicinity of the respective concentrations. A more detailed discussion of experimental errors will be given in Sec. IV E.

### E. Error estimation

The estimation of the errors of the transport coefficients is a delicate task. The statistical errors can be obtained in

TABLE VII. Benchmark values for diffusion, thermal diffusion, and Soret coefficients at $T = 298\,\mathrm{K}$ as calculated from the spline approximations in Figs. 9–11.

| $c$, water | $D/10^{-10}$ $\mathrm{m^2 s^{-1}}$ | $D_T/10^{-13}$ $\mathrm{m^2 s^{-1} K^{-1}}$ | $S_T/10^{-3}$ $\mathrm{K^{-1}}$ |
|---|---|---|---|
| 0.20 | $3.45 \pm 0.2$ | $10.66 \pm 2$ | $3.09 \pm 0.5$ |
| 0.25 | $2.87 \pm 0.2$ | $11.38 \pm 1$ | $3.96 \pm 0.4$ |
| 0.30 | $2.46 \pm 0.1$ | $11.30 \pm 0.5$ | $4.60 \pm 0.4$ |
| 0.35 | $2.16 \pm 0.1$ | $10.96 \pm 0.5$ | $5.08 \pm 0.2$ |
| 0.40 | $1.93 \pm 0.1$ | $10.53 \pm 0.5$ | $5.47 \pm 0.2$ |
| 0.45 | $1.73 \pm 0.1$ | $10.04 \pm 0.5$ | $5.81 \pm 0.2$ |
| 0.50 | $1.60 \pm 0.1$ | $9.57 \pm 0.5$ | $5.99 \pm 0.3$ |
| 0.55 | $1.59 \pm 0.2$ | $9.31 \pm 0.5$ | $5.85 \pm 0.3$ |
| 0.60 | $1.75 \pm 0.2$ | $9.21 \pm 0.5$ | $5.25 \pm 0.3$ |
| 0.65 | $2.14 \pm 0.3$ | $8.63 \pm 0.5$ | $4.02 \pm 0.2$ |
| 0.70 | $2.79 \pm 0.3$ | $5.85 \pm 0.5$ | $2.10 \pm 0.2$ |
| 0.75 | $3.67 \pm 0.3$ | $-1.33 \pm 3$ | $-0.36 \pm 0.2$ |
| 0.80 | $4.71 \pm 0.3$ | $-14.62 \pm 5$ | $-3.10 \pm 0.5$ |
| 0.85 | $5.87 \pm 0.4$ | $-34.58 \pm 6$ | $-5.89 \pm 0.9$ |
| 0.90 | $7.11 \pm 0.4$ | $-60.16 \pm 10$ | $-8.47 \pm 1.5$ |
| 0.95 | $8.35 \pm 0.4$ | $-88.53 \pm 8$ | $-10.60 \pm 2.0$ |

a straightforward manner from the uncertainties of the measured quantities and material parameters that enter the working equations. Examples of such parameters are the slit width and the dynamic viscosity in TGC, the cell height and the optical path length in OBD and ODI, and the derivatives of the density and the refractive index with respect to concentration and temperature. Typically, these quantities are known to within 0.1% to 1%. The accumulated error is obtained either analytically according to standard error propagation or, since the partial derivatives are sometimes not easily manageable, from a Monte Carlo analysis. It is obvious that parameters that enter the working equations with a high power, like the fourth power of the gap width $L_x$ in TGC (Eq. (4)), play a crucial role and need to be known as accurate as possible.

Depending on the technique and the respective transport coefficient, such a procedure results in relative statistical errors ranging from less than one up to a few percent under otherwise optimum conditions with sufficiently large contrast factors and Soret coefficients as observed around $c = 0.5$. In case of vanishing $S_T$, around $c = 0.75$, the absolute error of the Soret coefficient stays approximately constant but its relative error naturally diverges for $S_T = 0$. Since a non-vanishing concentration signal is required for the measurement of the diffusion coefficient by optical means, also the error of $D$ as measured by OBD and ODI increases in this concentration region.

Even more critical than the location of the sign change of $S_T$ is the isopropanol-rich region around a water mass fraction of $c = 0.07$. Here, the contrast factor $(\partial n/\partial c)_{p,\,T}$ vanishes and, consequently, not only the relative but also the absolute errors of the transport coefficients obtained from the optical techniques diverges.

Experience tells that there are often additional unknown sources of error beyond the statistical and known systematic errors discussed above. These errors are very difficult to quantify and may stem from unaccounted-for minor experimental details like non-uniform boundary conditions, small temperature inhomogeneities, or stability problems. Naturally, these unknown conditions are not included in the mathematical model of the experiment used for data evaluation. Such unknown systematic errors can only be estimated from repeated measurements on the same or similar samples, from systematic variations of experimental parameters like the employed temperature difference, and from long term practical experience with the respective experimental setups. Additional complications arise from correlations between errors of the different coefficients. For this reason, the error of, e.g., $S_T = D_T/D$ cannot easily be obtained from the individual errors of $D$ and $D_T$. As an example, the errors of $D$ and $D_T$ may be significant, but, nevertheless, the Soret coefficient can be determined with a high accuracy, since it is entirely encoded in the stationary amplitude of the OBD signal. A rough estimation of the errors can also be obtained, without complicated assumptions, from the fluctuations of the data points for different concentrations around a smooth interpolating curve. The errors given for the benchmark values have been estimated to the best of our knowledge and also contain, besides the easily quantifiable errors, realistic estimates of these additional error sources, where possible.

## V. CONCLUSIONS

Soret ($S_T$), thermodiffusion ($D_T$), and diffusion ($D$) coefficients of water-isopropanol mixtures have been measured by three different techniques over the full concentration range. Additionally, the coefficients for two compositions, one with positive and the other with negative Soret effect, have been measured in microgravity in the IVIDIL experiment on the ISS. The thermodiffusion coefficients $D_T$ have directly been measured in TGC and combined with diffusion coefficient measurements by SST in order to obtain $S_T$. From the optical methods OBD and ODI all three coefficients $S_T$, $D_T$, and $D$ could be obtained simultaneously. Although the benchmark quantities were measured at $T_0 = 298\,\mathrm{K}$, the OBD data are also provided for two additional mean temperatures: $T_0 = 288\,\mathrm{K}$ and $308\,\mathrm{K}$.

An excellent agreement between all the results is observed over a broad range of water concentrations, $0.2 < c < 0.70$, proving that all the techniques are capable to provide reliable and consistent data. The benchmark values have been elaborated for this concentration region along with an estimation of the errors. Because of the sign change of $S_T$ at $c = 0.745$ from positive to negative, the system becomes gravitationally unstable. Thus, the measurements in water rich area ($c > 0.70$) were conducted only by the OBD technique and in microgravity. In the region with low water content ($c < 0.2$) the optical measurements are difficult due to the small absolute value of the contrast factor $(\partial n/\partial c)_{p,\,T}$. It leads to the scattering of the results in this region. Within the accuracy of our experiments we did not observe a tendency for a second sign change of the Soret coefficient. Except for certain concentrations, the available literature data are in a satisfactory agreement with our benchmark values.

## ACKNOWLEDGMENTS

This work has been supported by the PRODEX programme of the Belgian Federal Science Policy Office and ESA (European Space Agency). The authors (ULB) are indebted to Professor J. C. Legros (ULB, Brussels) for valuable discussions. The experiments at UB have been supported by the Deutsche Forschungsgemeinschaft (DFG) (KO1541/9 and Research Unit FOR608/TP4). Authors from UM would like to thank the support of GOVSORET3 (Grant No. PI2011-22) and Research Groups (Grant No. IT557-10) of Basque Government.

[1] F. Montel, Entropie **86**, 184 (1994).
[2] J. P. Severinghaus, T. Sowers, E. J. Brook, R. Alley, and M. Bender, Nature (London) **391**, 141 (1998).
[3] D. V. Alexandrov and D. L. Aseev, J. Fluid Mech. **527**, 57 (2005).
[4] C. B. Mast and D. Braun, Phys. Rev. Lett. **104**, 188102 (2010).
[5] S. R. de Groot and P. Mazur, *Non-Equilibrium Thermodynamics* (North-Holland, Amsterdam, 1962).
[6] M. M. Bou-Ali, O. Ecenarro, J. Madariaga, and C. Santamaría, Phys. Rev. E **59**, 1250 (1999).
[7] V. Shevtsova, D. E. Melnikov, and J. C. Legros, Phys. Rev. E **73**, 047302 (2006).
[8] C. Soret, Arch. Sci. Phys. Nat. **2**, 48 (1879).
[9] L. Sitzber, Akad. Wiss. Wien Math.-Naturwiss. Kl. **20**, 539 (1856).
[10] K. Harstad, Ind. Eng. Chem. Res. **48**, 6907 (2009).
[11] J. K. Platten, M. M. Bou-Ali, P. Costesèque *et al.*, Philos. Mag. **83**, 1965 (2003).
[12] G. Wittko and W. Köhler, Philos. Mag. **83**, 1973 (2003).
[13] C. Leppla and S. Wiegand, Philos. Mag. **83**, 1989 (2003).
[14] M. M. Bou-Ali, J. J. Valencia, J. A. Madariaga *et al.*, Philos. Mag. **83**, 2011 (2003).
[15] J. K. Platten, M. M. Bou-Ali, and J. F. Dutrieux, Philos. Mag. **83**, 2001 (2003).
[16] P. Costesèque and J. C. Loubet, Philos. Mag. **83**, 2017 (2003).
[17] A. Königer, B. Meier, and W. Köhler, Philos. Mag. **89**, 907 (2009).
[18] A. Mialdun and V. Shevtsova, J. Chem. Phys. **134**, 044524 (2011).
[19] C. Nieto-Draghi, J. B. Avalos, and B. Rousseau, J. Chem. Phys. **122**, 114503 (2005).
[20] B. Rousseau, C. Nieto-Draghi, and J. B. Avalos, Europhys. Lett. **67**, 976 (2004).
[21] P. Kolodner, H. Williams, and C. Moe, J. Chem. Phys. **88**, 6512 (1988).
[22] K. J. Zhang, M. E. Briggs, R. W. Gammon, and J. V. Sengers, J. Chem. Phys. **104**, 6881 (1996).
[23] R. Kita, P. Polyakov, and S. Wiegand, Macromolecules **40**, 1638 (2007).
[24] Y. Yu, C. L. Chan, and C. F. Chen, J. Fluid Mech. **589**, 183 (2007).
[25] P.-A. Artola and B. Rousseau, Phys. Rev. Lett. **98**, 125901 (2007).
[26] P.-A. Artola, B. Rousseau, and G. Galliero, J. Am. Chem. Soc. **130**, 10963 (2008).
[27] K. Clusius and G. Dickel, Kurze Originalmitteilungen Naturwiss. **26**, 546 (1938).
[28] M. M. Bou-Ali, O. Ecenarro, J. A. Madariaga, C. M. Santamaria, and J. J. Valencia, J. Phys.: Condens. Matter **10**, 3321 (1998).
[29] J. F. Dutrieux, J. K. Platten, G. Chavepeyer, and M. M. Bou-Ali, J. Phys. Chem. B **106**, 6104 (2002).
[30] D. Alonso De Mezquia, M. M. Bou-Ali, M. Larrañaga, J. A. Madariaga, and C. Santamaría, J. Phys. Chem. B **116**(9), 2814–2819 (2012).
[31] D. Vigolo, G. Brambilla, and R. Piazza, Phys. Rev. E **75**, 040401 (2007).
[32] *CRC Handbook of Chemistry and Physics*, 56th ed., edited by R. C. Weast (CRC, Cleveland, Ohio), pp. 1975–1976.
[33] A. Mialdun and V. Shevtsova, Int. J. Heat Mass Transfer **51**, 3164 (2008).
[34] V. Shevtsova, Adv. Space Res. **46**, 672 (2010).
[35] V. Shevtsova, A. Mialdun, D. Melnikov, I. Ryzhkov, Y. Gaponenko, Z. Saghir, T. Lyubimova, and J. C. Legros, C. R. Mec. **339**, 310–317 (2011).
[36] V. Shevtsova, T. Lyubimova , Z. Saghir, D. Melnikov, Y. Gaponenko, V. Sechenyh, J. C. Legros, and A. Mialdun, J. Phys.: Conf. Ser. **327**, 012031 (2011).
[37] K. C. Pratt and W. A. Wakeham, Proc. R. Soc. London, Ser. A **342**, 401 (1975).
[38] P. Poty, J. C. Legros, and G. Thomaes, Z. Naturforsch. **29A**, 1915 (1974).
[39] A. Zebib, J. Non-Equil. Thermodyn. **32**, 211 (2007).
[40] A. Zebib, J. Chem. Phys. **129**, 134711 (2008).
[41] I. Ryzhkov and V. Shevtsova, Phys. Rev. E **79**, 026308 (2009).
[42] J. K. Platten and J. C. Legros, *Convection in Liquids* (Springer, Berlin, 1984).

# Apéndice H

# Medidas del Coeficiente de Termodifusión en Mezclas Binarias de Hidrocarburos Bajo Presión mediante la Técnica Termogravitacional

AIP | Review of Scientific Instruments

# Measurement of thermodiffusion coefficient of hydrocarbon binary mixtures under pressure with the thermogravitational technique

P. Urteaga, M. M. Bou-Ali, D. Alonso de Mezquia, J. Santamaría, C. Santamaría et al.

Citation: Rev. Sci. Instrum. **83**, 074903 (2012); doi: 10.1063/1.4737628
View online: http://dx.doi.org/10.1063/1.4737628
View Table of Contents: http://rsi.aip.org/resource/1/RSINAK/v83/i7
Published by the American Institute of Physics.

# Measurement of thermodiffusion coefficient of hydrocarbon binary mixtures under pressure with the thermogravitational technique

P. Urteaga,[1] M. M. Bou-Ali,[1,a)] D. Alonso de Mezquia,[1] J. Santamaría,[1] C. Santamaría,[2] J. A. Madariaga,[2] and H. Bataller[3]
[1]*Mechanical and Manufacturing Department, Engineering Faculty, Mondragon Unibertsitatea, Loramendi 4 Apdo. 20500 Mondragon, Spain*
[2]*Department of Applied Physics II, University of Basque Country UPV/EHU, Apdo. 644. 48080 Bilbao, Spain*
[3]*Laboratoire des Fluides Complexes – UMR 5150, Université de Pau et des Pays de l'Adour, BP 1155, 64013 Pau, France*

(Received 9 May 2012; accepted 2 July 2012; published online 19 July 2012)

It was designed and constructed a new thermogravitational column able to operate at high pressures (up to 50 MPa). This new thermogravitational column is of the cylindrical type with closed ends. It is made of stainless steel. The length of the column is 0.5 m and the gap between its two walls is variable. First, the column was validated at atmospheric pressure by means of measurements of the thermodiffusion coefficient of well-known binary mixtures. Then, this new thermogravitational column was used to measure the thermodiffusion coefficient of the binary mixtures 1,2,3,4-tetrahydronaphtalene/isobutylbenzene, 1,2,3,4-tetrahydronaphtalene/n-dodecane, and isobutylbenzene/n-dodecane at high pressures and within the pressure range between 0.1 and 20 MPa at a mean temperature of 25 °C. We have found a linear dependence between the thermodiffusion coefficient and the pressure. © *2012 American Institute of Physics*. [http://dx.doi.org/10.1063/1.4737628]

## I. INTRODUCTION

The processes of transport of matter in liquids due to thermodiffusion have acquired a considerable interest in very different problems like: hydrodynamics instability analysis,[1] the transport of matter in living creatures,[2,3] or in some practical problems, like polymer division[4,5] and modeling oil fields for optimal exploitation.[6] Nowadays, the use of thermal diffusion also is of great interest in environmental problems, like aerosol deposition or thermophoresis.[7,8] From the industrial point of view, the importance of thermodiffusion in oil field exploitation lies in the knowledge of composition variations of fluids that imbue the reservoir.[9] It is important to analyze the influence of the pressure on the transport properties of dense mixtures. This is done in order to improve the description of the initial state of a reservoir, i.e., the initial distribution of the components within a reservoir.[10,11] At depths near 4000 m, the fluids are often close to critic conditions, and consequently they are very sensitive to applied forces such as gravity, temperature, and pressure gradients.[12,13] The experimental data of transport properties like thermodiffusion coefficient, ordinary diffusion coefficient, and Soret coefficient of fluid mixtures (liquid and liquefied) under pressure would help when numerical models are applied in order to predict and optimize the exploitation of oil fields.[14,15] Some experimental work has been done for fluids in the critical region, which shows a considerable dependence between thermal diffusion factor and pressure.[16,17] Additionally, results for the thermodiffusion coefficient at high pressures measured in microgravity conditions have been recently published.[12,18] However, the lack of experimental data for these coefficients under the conditions at which the fluids are found in the oil fields still represents an additional difficulty for further development in the industrial sector from the theoretical, numerical, and experimental point of view.[19]

In a recently carried out benchmark[20] for values of thermodiffusion, molecular diffusion, and Soret coefficients of binary mixtures, the efficiency of the thermogravitational technique and the corresponding experimental method for determining the transport properties of liquid mixtures have been demonstrated. The thermogravitational effect is the result of a thermodiffusion (due to a thermal gradient) and convection effect in the gravitational field. Up to now, the thermogravitational technique has been used only at atmospheric pressure. Nevertheless, the conditions in which the hydrocarbons are found in oilfields, depending on the systems, imply high pressure. All this has encouraged us to get involved in a project to design and build a new thermogravitational column that allows us to experimentally determine the thermodiffusion coefficient at several pressures, up to 50 MPa, for both liquid and liquefied mixtures (Patent No. ES 2 330 905 B1).

## II. THE NEW EXPERIMENTAL DEVICE

The built setup has a new structure and methodology, which makes possible to carry out experimental measurements of stationary separation of the components in fluid mixtures under high pressures.

The described installation, which is able of working with pressures within the range of 0.1–50 MPa, allows using all type of fluids–liquid phase and liquefied gases. Moreover, the installation allows an easy assembling and disassembling of its components. Also, it is possible to vary the width of the gap where the liquid mixture is located by changing the inner

a)Electronic mail: mbouali@mondragon.edu.

 

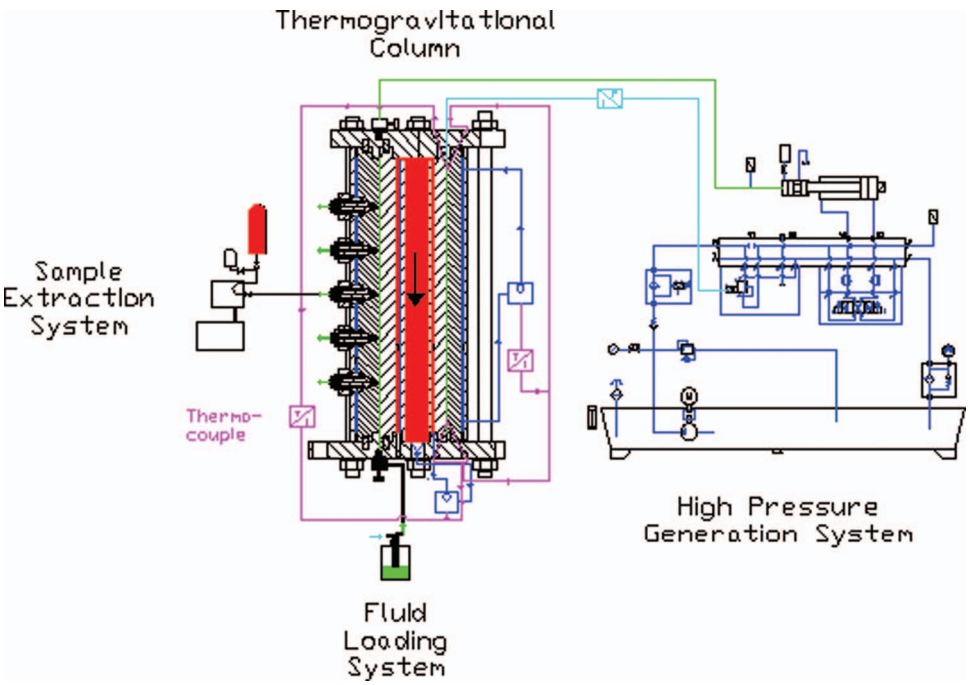


FIG. 1. High-pressure thermogravitational column setup.

cylinder of the column. Another advantage of this device is that sampling method allows extraction of the samples at the same pressure as they are inside the gap (isobar extraction).

The new high-pressure thermogravitational setup (TGC-HP) is constituted of 4 different modules as can be seen in Figure 1: thermogravitational column, fluid loading system, high-pressure generation system, and the sample extraction system. The different modules that make up the installation are described in the following paragraphs.

The thermogravitational column is composed by two coaxial cylinders. The distance between the inner and the outer cylinder is the gap. Each cylinder is thermo-regulated by a water thermostatic bath (Lauda T-1200) in order to produce the necessary temperature gradient between the walls of the gap. The main factors to consider when designing and manufacturing a thermogravitational column are: the dimensional, geometric and surface finish tolerances, compatibility of materials, sealing for the entire range of pressures up to 50 MPa and to be detachable and easy to handle throughout the whole experimental process. Extensive structural calculations of the column under pressure have been done. The column is constructed in stainless steel and the height is 500 mm, having five equidistant sample extraction taps along it. The gap width for this study is 1.000 $\pm$ 0.005 mm (we have used only one inner cylinder). When designing a thermogravitational column, it is important to considerer the validity limits of the Furry, Jones and Onsager (FJO) theory.[21,22] In order to do this, we have to know the real temperature gradient between the two walls of the gap. To collect reliable information about the gap's outer and inner walls temperatures, the previously described installation has four "J" type thermocouples, of 1 mm diameter. Two of them are in the top and the other two in the bottom of the column. These thermocouples allow measuring the horizontal temperature gradient with an accuracy of 0.01 °C. In addition, the device has a pressure transducer in the top part of the column in order to know the pressure of the fluid inside the gap. To guarantee a totally hermetic closing of the gap, single acting, spring-energized, PTFE seals are used. The spring supplies the load required for sealing at low pressure while when pressure increases the "U" shaped jacket allows fluid pressure to energize the sealing lips, so total sealing pressure rises. Once the steady state is reached the extraction of the samples for being analyzed can be done across the valves, which are integrated in the outer tube of the column. Thanks to the valves design the extraction can be done, both, at atmospheric pressure and at high pressure. The valves ensure hermetic closing while they eliminate all the possible dead volumes.

The loading module allows the introduction of the fluid mixtures inside the thermogravitational column from the bottom of the column at controlled speed. The fluid is forced inside the column by means of compressed air's pressure. Filling the column from the bottom reduces the possibility of death volumes inside the gap.

The operation pressure is achieved by means of the pressure generation system, see Figure 1. This system is able to generate pressures up to 50 MPa in the fluid inside the column. This module is composed of a pressure intensifier which has a pressure relation of 1–5 and a fluid storage capacity of 120 $cm^3$. The intensifier is driven by a hydraulic system with proportional valves that make it possible to control the pressure in the gap, as well as the sample extraction speed and volume.

In the sample extraction system, the extracted volume of liquid is controlled by means of cylinder displacement. In order to do this, the hydraulic cylinder has a displacement transducer which provides continuous information about the cylinder's position. The sample extraction and analysis have to be

made without any change on pressure throughout the whole process. This is possible thanks to the fact that the whole system is preloaded up to the process pressure, and afterwards all the installation is maintained at constant process temperature gradient and pressure. The sample extraction system allows two different options for the analysis of the samples. One possibility is to analyze the sample without any pressure loss, connecting the thermogravitational column directly to the analysis system (see Figure 1). Another possibility, which can only be used when working with liquids, is to decrease the pressure of the fluid down to atmospheric pressure and carry out the analysis of the samples at this pressure. This procedure has minor influence in the obtained results as pressure decrease is not done until the separation process is completed. On the other hand, this second option has the advantage of being less time consuming. In this study, the last option has been used in the measurements.

## III. WORKING EQUATIONS

The theory of the thermogravitational column, which was proposed by FJO,[23] establishes a relation between the steady separation of the components and the thermodiffusion coefficient $D_T$ as follows:[24]

$$\Delta c = \frac{504}{g}\frac{L_z}{L_x^4}c_i(1-c_i)\frac{\nu}{\alpha}D_T, \tag{1}$$

where $\Delta c$ is the mass fraction difference between the top and the bottom of the column, $L_x$ is the annular gap dimension, $L_z$ is the total length of the column, $g$ is the gravity acceleration, $c_i$ is the mass fraction of the reference component in the initial homogeneous mixture, $\alpha$ is the thermal expansion coefficient, and $\nu$ is the kinematic viscosity ($\nu = \mu/\rho$), being $\mu$ the dynamic viscosity and $\rho$ the density of mixture.

In thermogravitational column, we measure the variation of the density along the column's height $\partial\rho/\partial z$. The mass separation at the steady state $\Delta c$ is determined by means of the following equation:[25,26]

$$\Delta c = \frac{L_z}{\beta\cdot\rho}\frac{\partial\rho}{\partial z}, \tag{2}$$

where $\beta$ and $\rho$ are, respectively, the mass expansion coefficient and the density of the studied mixture.

The time necessary to reach the stationary state in a thermogravitational column is typically five times the relaxation time ($t_r$), given by the following expression:[24]

$$t_r = \frac{9(L_z\nu)^2 D}{\left(g\pi\alpha\Delta T L_x^3\right)^2}, \tag{3}$$

where $D$ is the molecular diffusion coefficient and $\Delta T$ is the applied temperature gradient. The effect of pressure in the value of $t_r$ is mainly represented through the viscosity, as it is this property the one which is more influenced by the pressure.

As the molecular diffusion coefficient $D$ of studied mixtures at high pressures in this article is unknown, an upper bound value ($10^{-9}$ m$^2$/s) is taken to estimate the order of magnitude of the relaxation time corresponding to each mixture. Nevertheless, by using the Leffler-Cullinan relation[27] it is possible to make an evaluation of the molecular diffusion coefficient $D$ as a function of the pressure

$$D \times \mu \approx \text{constant}, \tag{4}$$

where $\mu$ is the dynamic viscosity of the fluid. Generally, the viscosity increases with the pressure, so a decrease in the value of the molecular diffusion coefficient $D$ is expected.

Each experimental test was repeated three times for each mixture, and at least in one of them the time of the experiment was 15 times the relaxation time. This assures that the stationary state has been reached. The reproducibility in the obtained values of the separation of the components in all the tests was lower than 5%.

## IV. EXPERIMENTAL RESULTS

### A. Setup validation

The validation of the new column was performed at atmospheric pressure by means of test with liquid binary mixtures which transport properties are sufficiently verified in the bibliography. The binary mixtures selected were: toluene/n-hexane, water/ethanol, and the three binary mixtures composed of pairwise combinations of 1,2,3,4-tetrahydronaphtalene, isobutylbenzene, and n-dodecane. The toluene/n-hexane and water/ethanol mixtures have been widely studied[21,24,25,28–33,35] at temperatures close to 25 °C and the three last binary mixtures have been used in the benchmark test of Fontainebleau[20] to compare various experimental techniques. From here on, 1,2,3,4-tetrahydronaphtalene will be referred to as THN, isobutylbenzene as IBB, n-dodecane as $nC_{12}$, water as $H_2O$, ethanol as ETH, toluene as TOL, and n-hexane as $nC_6$. Measurements were performed at 25 °C and 0.1 MPa. The composition of mixtures was 50 wt. % except for the mixtures $H_2O$-ETH ($c_0$ = 60.88 wt. % water) and TOL-$nC_6$ ($c_0$ = 51.67 wt. % toluene).

All the components used in this study were purchased from Merck and Aldrich with purity higher than 99%; and were used without further purification. The mixtures have been prepared by weight by introducing the less volatile component first, and then adding the corresponding amount of second component. Finally, the mixtures were shacked to ensure a homogeneous mixture. Approximately 300 cm$^3$ were used in this study to make each experimental test in the TGC-HP setup. After the preparation, the density of the mixture was measured to confirm that the composition deduced from a previously done calibration curve agrees with the prepared one. This was always the case.

A vibrating-quartz U-tube densimeter manufactured by Anton Paar (DMA 5000) with an estimated temperature fluctuation of ±0.005 °C and accuracy of 5 × $10^{-6}$ g/cm$^3$ was used to measure the density $\rho$ of the samples at atmospheric pressures. By repeating the density measurements at different temperatures (24, 24.5, 25, 25.5, and 26 °C), the thermal expansion coefficient $\alpha = -(1/\rho)(\partial\rho/\partial T)$ was determined. Similarly, the mass expansion coefficient can be calculated from a calibration. The calibration is made measuring the density of several mixtures of known composition. The mass fraction

TABLE I. Thermophysical properties ($\rho$, density; $\beta$, mass expansion coefficient; $\alpha$, thermal expansion coefficient; $\mu$, dynamic viscosity) at 25 °C and 0.1 MPa for the mixtures used for validation of experimental setup and procedure in this work.

| System $c_i$-$c_j$ | Mass fraction of component $i$ ($c_i$) | $\rho$ (kg/m$^3$) | $\beta$ | $\alpha$ ($10^{-3}$ K$^{-1}$) | $\mu$ ($10^{-3}$ Pa s) |
|---|---|---|---|---|---|
| THN-IBB | 50 wt. % | 904.5 | 0.128 | 0.8876 | 1.374 |
| IBB-n$C_{12}$ | 50 wt. % | 792.3 | 0.130 | 0.9612 | 1.133 |
| THN-n$C_{12}$ | 50 wt. % | 841.2 | 0.257 | 0.8950 | 1.523 |
| $H_2O$-ETH | 60.88 wt. % $H_2O$ | 935.8 | 0.220 | 0.7892 | 2.380 |
| TOL-HEX | 51.67 wt. % TOL | 748.4 | 0.275 | 1.2280 | 0.386 |

of these mixtures is always close to the mass fraction of the studied one ($c_0 \pm 0.02$). In all the cases, a linear relationship between the density and the mass fraction is observed. From the obtained calibration line, we determine the mass expansion coefficient $\beta = (1/\rho)(\partial\rho/\partial c)$.[26]

Dynamic viscosity of the mixtures at 0.1 MPa has been determined by a Haake falling-ball viscometer with an accuracy of ±1%. The value for the viscosity $\mu$ of the mixtures used in the study corresponds to the mean value of three independent measurements.

Table I shows the density, mass expansion coefficient, thermal expansion coefficient, and dynamic viscosity at 0.1 MPa of the binary mixtures used in the validation process.

Generally, a good agreement exists between our data and the data set reported in literature for these mixtures.[28,34,35] Especially, the data measured by Leahy-Dios and A. Firoozabadi,[28] which has also been measured using the thermogravitational technique but in its plane configuration, are in excellent agreement with the data obtained by us.

The vertical density gradient $\partial\rho/\partial z$ along the column is determined by measuring the density of the samples taken at stationary state, from five sampling outlets uniformly distributed throughout the column height. The average temperature of the fluids in the measurements was of 25 °C and the difference of temperatures between the walls of the gap was $\Delta T = 6$ °C. Table II shows the results obtained for the density gradient for the mixtures analyzed in the validation process.

With the values of thermophysical properties shown in Table I and the data obtained for the density gradient, we can determine the thermal diffusion coefficient using Eqs. (1) and (2). Table II shows our results for the thermal diffusion coefficient $D_T$ along with the values taken from the literature[20,21,24,25,28–33,35] of the mixtures used in the validation process. The agreement between our results and those in the literature can be considered excellent if we consider the experimental error.

On the other hand, Eq. (1) predicts that $D_T$ does not depend on the temperature gradient established between the walls of the column. Experimental measurements of separation of the components of the mixtures in the TGC-HP at different temperature gradients between cold and hot walls have been made for the mixtures, toluene-n hexane ($c_0 = 51.67$ wt. % toluene) and water-ethanol ($c_0 = 60.88$ wt. % water) at 25 °C. As can be seen in Figure 2, the values found for the stationary separation were identical, within the experimental error, in all the cases. This result is another factor that let us to figure out that the construction of the new column is adequate.

With the validation results shown here, we are confident that the new TGC-HP can be used to measure $D_T$ with reliability and accuracy.

### B. Dependence of thermodiffusion coefficient with pressure

With purpose to determine the thermodiffusion coefficient, it is required to previously know the values of $\rho$, $\alpha$, and $\mu$ to the pressure at which the measurements have been

TABLE II. Thermodiffusion coefficient $D_T$ for binary mixtures TOL-n$C_6$ (51.67 wt. % toluene), $H_2O$-ETH (60.88 wt. % $H_2O$), THN-IBB (50 wt. %), THN-n$C_{12}$ (50 wt. %), and IBB-n$C_{12}$ (50 wt. %) at 25 °C, 0,1 MPa and $\Delta T = 6$ °C. $\partial\rho/\partial z$ is the vertical density gradient along the thermogravitational column.

| System | $-\frac{\partial\rho}{\partial z}$ (kg/m$^4$) | $D_T \times 10^{-12}$ (m$^2$ s$^{-1}$ K$^{-1}$) $10^{-12}$ (m$^2$/s K) (this work) | $D_T \times 10^{-12}$ (m$^2$ s$^{-1}$ K$^{-1}$) $10^{-12}$ (m$^2$/s K) (literature) |
|---|---|---|---|
| TOL-n$C_6$ | 15.1 | 13.6 | 13.6 (Ref. 29)<br>13.2 (Ref. 24)<br>13.6 (Ref. 31)<br>13.5 (Ref. 33)<br>13.3 (Ref. 21 and 35) |
| $H_2O$-ETH | 11.0 | 1.35 | 1.37 ± 0.01 (Ref. 25)<br>1.34 ± 0.01 (Ref. 28)<br>1.32 (Ref. 30)<br>1.36 (Ref. 31)<br>1.35 (Ref. 32)<br>1.46 (Ref. 29) |
| THN-IBB | 7.40 | 2.8 | 2.8 ± 0.1 (Ref. 20)<br>2.81 ± 0.13 (Ref. 28) |
| THN-n$C_{12}$ | 33.93 | 6.0 | 5.9 ± 0.3 (Ref. 20)<br>5.88 ± 0.2 (Ref. 28) |
| IBB-n$C_{12}$ | 7.58 | 3.8 | 3.7 ± 0.2 (Ref. 20)<br>3.85 ± 0.15 (Ref. 28) |

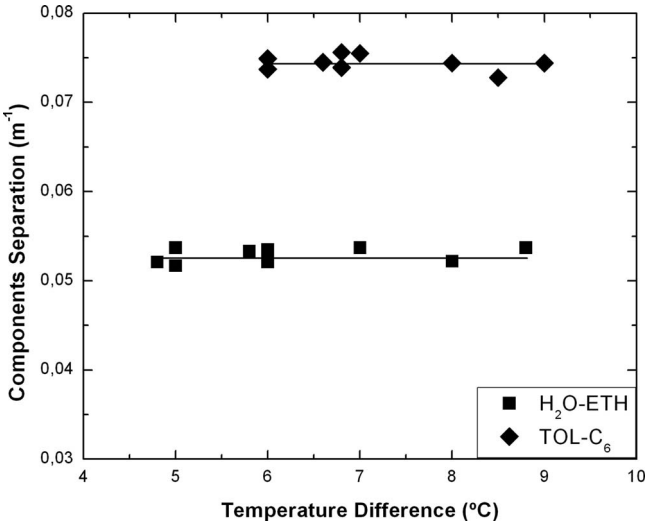


FIG. 2. Dependence of the vertical gradient of concentration with the difference of temperatures between the walls of the column ΔT. ■: $H_2$0-ETH; ■: TOL-n$C_6$.

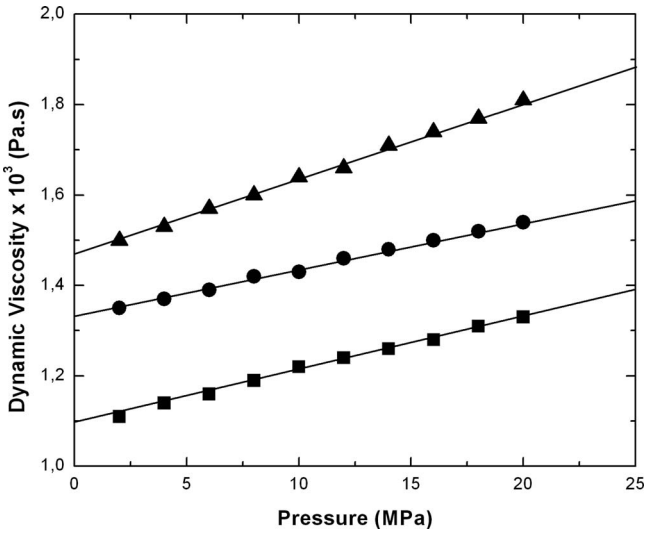


FIG. 3. Dynamic viscosity of the mixture versus pressure at 25 °C. Experimental results: ●: THN-IBB; ▲: THN-n$C_{12}$; ■: IBB-n$C_{12}$.

performed. The density and dynamic viscosity of the mixtures at high pressures were determined in the Laboratoire des Fluides Complexes of the University of Pau by means of a DMA HPM Anton Paar densimeter equipped with a mPDS-200V3 unit and a falling body viscometer (semi-automatic Stony Brook Scientific HPHTV-viscosimeter). The complete experimental assembly has been described in detail in Ref. 36. The mixtures analyzed were the corresponding to the benchmark of Fontenaibleau,[20] THN-IBB, THN-n$C_{12}$, and IBB-n$C_{12}$ at $c_0 = 50$ wt. % and 25 °C. Table III shows the measured values of density, thermal expansion coefficient, and dynamic viscosity variation for different pressures (up to 20 MPa). It can be observed that thermal expansion coefficient goes down slightly as the working pressure rises. On the contrary, the dynamic viscosity rises when working pressure increases. An analysis of these data shows how the dependence of the dynamic viscosity with the pressure is lineal (Figure 3).

The stationary separation of the components in function of working pressure has been measured in the TGP-HP at an average temperature of 25 °C and a temperature difference between cold and hot walls of $\Delta T = 6$ °C. As example, Figure 4 shows the variation of density of the mixture among the height of the TGC-HP for THN-n$C_{12}$ mixture at 10 MPa. The variation of the density with the height of the column is linear as it should be from Furry-Jones-Onsager theory for a small separation between the top and the bottom of the column when the spacing between the two walls is larger than, say 1 mm.[37] The value of its slope allows us to know the value of the gradient $\partial\rho/\partial z$. The density decreases with elevation as it should because $D_T > 0$, and therefore, the lighter component migrates to the hot wall and concentrates in the top of the column. The relative pressure range at which the tests have been carried out is between 2 and 20 MPa. In addition to the well-known obtained value at atmospheric pressure, 10 more tests have been made at the following pressures 2, 4, 6, 8, 10, 12, 14, 16, 18, 20 MPa. Now, from the density gradient $\partial\rho/\partial z$, we calculate the difference between the mass fraction at the top and the bottom part of the column from Eq. (2). Each

TABLE III. Thermophysical properties ($\alpha$, thermal expansion coefficient; $\beta$, mass expansion coefficient, and $\mu$, dynamic viscosity) for THN-IBB, THN-n$C_{12}$, and IBB-n$C_{12}$ at $c_0 = 0.5$ (mass fraction), 25 °C (average temperature), and pressures up to 20 MPa.

| | Pressure (MPa) | | | | | | | | | |
|---|---|---|---|---|---|---|---|---|---|---|
| Thermophysical properties | 2 | 4 | 6 | 8 | 10 | 12 | 14 | 16 | 18 | 20 |
| THN-IBB | | | | | | | | | | |
| $\rho$ (kg/m$^3$) | 904.8 | 906.1 | 907.5 | 908.6 | 910.1 | 911.3 | 912.5 | 913.9 | 914.9 | 916.1 |
| $\alpha \times 10^{-3}$ (K$^{-1}$) | 0.86 | 0.85 | 0.84 | 0.85 | 0.85 | 0.84 | 0.84 | 0.82 | 0.81 | 0.81 |
| $\mu$ (mPa s) | 1.35 | 1.37 | 1.39 | 1.42 | 1.43 | 1.46 | 1.48 | 1.50[a] | 1.52[a] | 1.54[a] |
| THN-n$C_{12}$ | | | | | | | | | | |
| $\rho$ (kg/m$^3$) | 842.7 | 843.4 | 845.0 | 846.5 | 847.1 | 848.8 | 850.0 | 851.1 | 852.3 | 853.0 |
| $\alpha \times 10^{-3}$ (K$^{-1}$) | 0.85 | 0.83 | 0.82 | 0.84 | 0.84 | 0.82 | 0.81 | 0.79 | 0.79 | 0.80 |
| $\mu$ (mPa s) | 1.50 | 1.53 | 1.57 | 1.60 | 1.64 | 1.66 | 1.71 | 1.74[a] | 1.77[a] | 1.81[a] |
| IBB-n$C_{12}$ | | | | | | | | | | |
| $\rho$ (kg/m$^3$) | 792.9 | 794.5 | 795.7 | 796.9 | 798.6 | 799.6 | 800.7 | 801.9 | 803.4 | 805.1 |
| $\alpha \times 10^{-3}$ (K$^{-1}$) | 0.90 | 0.89 | 0.88 | 0.90 | 0.90 | 0.89 | 0.88 | 0.87 | 0.85 | 0.86 |
| $\mu$ (mPa s) | 1.11 | 1.14 | 1.16 | 1.19 | 1.22 | 1.24 | 1.26 | 1.28[a] | 1.31[a] | 1.33[a] |

[a]Extrapolated values.

TABLE IV. Stationary separation ($\Delta c$) and thermal diffusion coefficient ($D_T$) for THN-IBB (50 wt. %), THN-$nC_{12}$ (50 wt. %), and IBB-$nC_{12}$ (50 wt. %) at 25 °C and pressures up to 20 MPa.

| | THN-IBB | | | THN-$nC_{12}$ | | | IBB-$nC_{12}$ | | |
|---|---|---|---|---|---|---|---|---|---|
| Pressure (MPa) | $\partial\rho/\partial z$ (kg/m$^4$) | $\Delta c$ | $D_T$ ($10^{-12}$ m$^2$/sK) | $\partial\rho/\partial z$ (kg/m$^4$) | $\Delta c$ | $D_T$ ($10^{-12}$ m$^2$/sK) | $\partial\rho/\partial z$ (kg/m$^4$) | $\Delta c$ | $D_T$ ($10^{-12}$ m$^2$/sK) |
| 2 | 6.87 | 0.0295 | 2.65 | 33.76 | 0.0781 | 5.80 | 7.76 | 0.0375 | 3.77 |
| 4 | 7.09 | 0.0305 | 2.67 | 33.00 | 0.0764 | 5.43 | 7.77 | 0.0376 | 3.64 |
| 6 | 7.05 | 0.0304 | 2.59 | 32.70 | 0.0757 | 5.19 | 7.70 | 0.0372 | 3.51 |
| 8 | 7.06 | 0.0304 | 2.57 | 32.38 | 0.0749 | 5.18 | 7.54 | 0.0365 | 3.43 |
| 10 | 6.86 | 0.0295 | 2.48 | 31.85 | 0.0737 | 4.97 | 7.62 | 0.0370 | 3.39 |
| 12 | 6.94 | 0.0299 | 2.44 | 31.54 | 0.0730 | 4.76 | 7.51 | 0.0364 | 3.25 |
| 14 | 6.94 | 0.0298 | 2.40 | 31.11 | 0.0720 | 4.51 | 7.46 | 0.0361 | 3.15 |
| 18 | 6.74 | 0.0289 | 2.19 | 30.65 | 0.0709 | 4.19 | 7.40 | 0.0360 | 2.91 |
| 20 | 6.64 | 0.0285 | 2.13 | 30.73 | 0.0711 | 4.17 | 7.35 | 0.0359 | 2.89 |

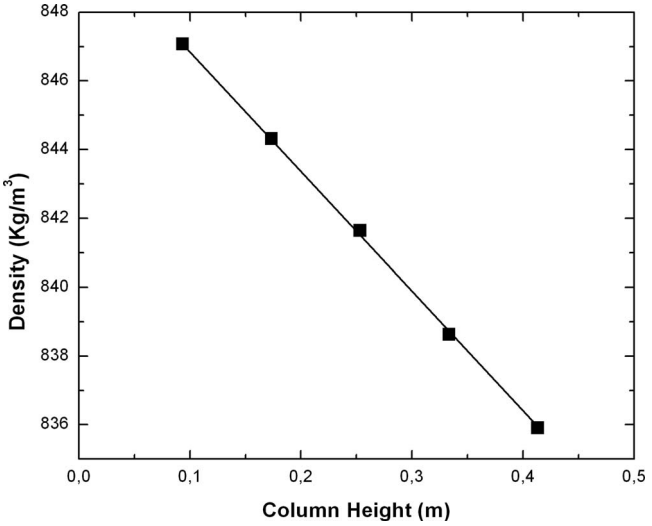


FIG. 4. Density variation through the height of column for THN-$nC_{12}$ with $c_0 = 0.5$ at mean temperature of 25 °C and pressure of 10 MPa.

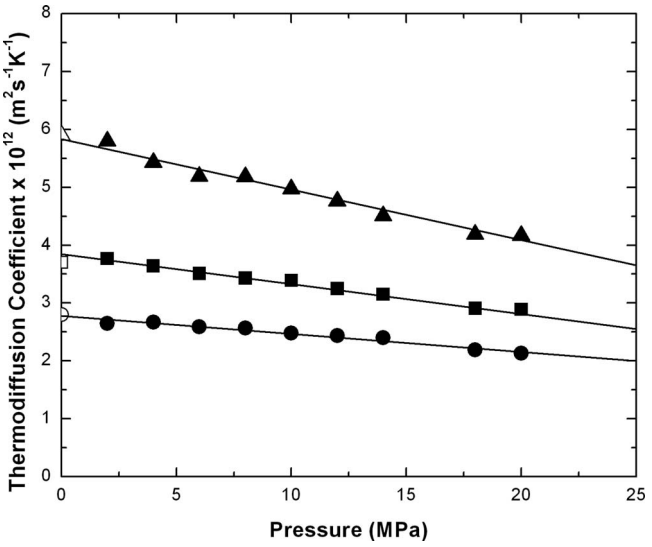


FIG. 5. Thermal diffusion coefficient versus pressure at 25 °C. Experimental results: ▲: THN-$nC_{12}$; ■: IBB-$nC_{12}$; ●: IBB-THN. Data of benchmark:[20] △: THN-$nC_{12}$; □: IBB-$nC_{12}$; ○: IBB-THN.

experimental test is repeated 3 times for each mixture and in the entire test we ensure that the separation has reached the stationary state. In Table IV, the mean values of the vertical density gradient $\partial\rho/\partial z$ and the separation $\Delta c$ for the different pressures are shown. It can be observed that the obtained gradient, i.e., the separation, decreases slightly when the working pressure rises. In the systems THN-IBB and IBB-$nC_{12}$, the influence of the pressure on the stationary separation is light and practically we can consider, within the experimental error, that its value does not depend on the pressure (at least until 20 MPa). Nevertheless, for the mixture THN-$nC_{12}$, the pressure in the column sensibly affects the stationary separation.

Thermodiffusion coefficient $D_T$ has been determined for the binary liquid mixtures THN-IBB, THN-$nC_{12}$, IBB-$nC_{12}$ at mass fraction of 50%, mean temperature of 25 °C and working relative pressures up to 20 Mpa. The obtained values for $D_T$ are shown in Table IV. From Table IV, it can be stated that for all the mixtures studied the variation of $D_T$ with working pressure fits rather well to a linear variation and it decreases as working pressure rises. This linear dependence is fundamentally due to the dependence of viscosity with pressure, which is also lineal (Figure 4). The values of $D_T$ generated by these straight lines for 0.1 MPa agree excellently with the proposed ones in the benchmark of Fontainebleau (see Fig. 5). This agreement indicates the consistency of our values for the thermal diffusion coefficient to pressures superior to the atmospheric one.

A diminution in the value of the thermodiffusion coefficient when increasing the pressure also was found by Rutherford *et al.*[16] in the system methane-n butane between 9.65 and 20.69 MPa.

## V. CONCLUSIONS

In this work, we have designed and constructed a new thermogravitational column for the determination of thermodiffusion coefficient under high pressures. The new thermogravitational column constructed is a conventional stainless steel concentric tube column, closed at both ends. The working pressure is generated by a pressure intensifier and is driven by a hydraulic system with proportional valves that makes possible to control pressure in the gap, as well as the sample extraction speed. Measurements of thermodiffusion

coefficient in fluids at pressures up to 50 MPa can be performed with this new thermogravitational column (Patent No. ES 2 330 905 B1).

This thermogravitational column was validated by several experimental test realized at atmospheric pressure for binary mixtures whose transport properties are sufficiently verified in the bibliography and widely used in the literature.

Additionally, we have measured the thermodiffusion coefficient under different pressures (up to 20 MPa) of the binary mixtures THN-IBB, THN-$nC_{12}$, and IBB-$nC_{12}$. We have found a linear dependence between the thermodiffusion coefficient and the working pressure.

## ACKNOWLEDGMENTS

This article presents results that were partly obtained in the framework of the following projects: GOVSORET3 (PI2011-22) and Research Groups (IT557-10) of Basque Government, DCMIX form the European Space Agency.

[1]J. K. Platten and J. C. Legros, *Convection in Liquids* (Springer-Verlag, Berlin, 1984).
[2]F. J. Bonner and L. O. Sundelöf, Z. Naturforsch. **39**, 656 (1984).
[3]D. Braun and A. Libchaber, Phys. Biol. **1**, 1 (2004).
[4]O. Ecenarro, J. A. Madariaga, J. Navarro, C. Santamaría, J. A. Carrión, and J. M. Savirón, Macromolecules **27**, 4968 (1994).
[5]R. Kita, S. Wiegand, and J. Luettmer-Strathmann, J. Chem. Phys. **121**, 3874 (2004).
[6]A. Firoozabadi, *Thermodynamics of Hydrocarbon Reservoirs* (McGraw-Hill, 1999).
[7]M. M. Williams, J. Phys. D: Appl. Phys. **19**, 1631 (1986).
[8]R. Rusconi, L. Isa, and R. Piazza, J. Opt. Soc. Am. B **21**, 605 (2004).
[9]F. Montel, Entropie **184/185**, 86 (1994).
[10]K. Ghorayeb, A. Firoozabadi, and T. Anraku, SPE J. **8**, 114 (2003).
[11]F. Montel, J. Bickert, A. Lagisquet, and G. Galliéro, J. Pet. Sci. Eng. **58**, 391 (2007).
[12]M. Touzet, G. Galliéro, V. Lazzeri, M. Saghir, F. Montel, and J. Legros, C. R. Mec. **339**, 318 (2011).
[13]K. Ghorayeb and A. Firoozabadi, AIChE J. **46**, 883 (2000).
[14]F. Montel, Entropie **214**, 7 (1998).
[15]B. Wilbois, G. Galliero, J. P. Caltagirone, and F. Montel, Philos. Mag. **83**, 17 (2003).
[16]W. M Rutherford and J. G. Roof, J. Phys. Chem. **63**, 1506 (1959).
[17]S. Srinivasan and M. Z. Saghir, J. Chem. Phys. **131**, 124508 (2009).
[18]S. Van Vaerenbergh, S. Srinivasan, and M. Saghir, J. Chem. Phys. **131**, 114505 (2009).
[19]S. Van Vaerenbergh, A. Shaphiro, G. Galliero, F. Montel, J. Legros, J. P. Caltagirone, J. Daridod, and Z. Shagir, Eur. Space Agency, [Spec. Publ.] ESA SP **1290**, 202 (2005).
[20]J. K. Platten, M. M. Bou-Ali, P. Costesèque, J. F. Dutrieux, W. Köhler, C. Leppla, S. Wiegand, and G. Wittko, Philos. Mag. **83**, 1965 (2003).
[21]J. J. Valencia, M. M. Bou-Ali, O. Ecenarro, J. A. Madariaga, and C. Santamaría, *Thermal Nonequilibrium Phenomena in Fluid Mixtures* (Springer, Berlin, 2002).
[22]J. A. Madariaga, C. Santamaría, H. Barrutia, M. M. Bou-Ali, O. Ecenarro, and J. J. Valencia, C. R. Mec. **339**, 292 (2011).
[23]W. H. Furry, R. C. Jones, and L. Onsanger, Phys. Rev. **55**, 1083 (1939).
[24]M. M. Bou- Ali, O. Ecenarro, J. A. Madariaga, C. Santamaría, and J. Valencia, J. Phys.: Condens. Matter **10**, 3321 (1998).
[25]J. F. Dutrieux, J. K. Platten, G. Chavepeyer, and M. M. Bou-Ali, J. Phys. Chem, B **106**, 6104 (2002).
[26]P. Blanco, M. M. Bou-Ali, J. K. Platten, D. Alonos de Mezquia, J. A. Madariaga, and C. Santamaría, J. Chem. Phys. **132**, 114506 (2010).
[27]J. Leffler and H. T. Cullinan Jr., Ind. Eng. Chem. Fundam. **9**, 84 (1970).
[28]A. Leahy-Dios and A. Firoozabadi, J. Phys. Chem. B **111**, 191 (2007).
[29]K. J. Zhang, M. E. Briggs, R. W. Gammon, and J. V. Sengers, J. Chem. Phys. **104**, 6881 (1996).
[30]P. Kolodner, H. Williams, and C. Moe, J. Chem. Phys. **88**, 6512 (1998).
[31]W. Köhler and B. Müller, J. Chem. Phys. **103**, 4367 (1995).
[32]M. M. Bou-Ali, O. Ecenarro, J. A. Madariaga, C. Santamaría, and J. Valencia, Entropie **218**, 5 (1999).
[33]O. Ecenarro, J. A. Madariaga, C. Santamaría, M. M. Bou-Ali, and J. Valencia, Entropie **198/199**, 71 (1996).
[34]J. K. Platten, M. M. Bou-Ali, and J. F. Dutrieux, Philos. Mag. **83**, 2001 (2003).
[35]J. J. Valencia, M. M. Bou-Ali, J. K. Platten, O. Ecenarro, J. A. Madariaga, and C. Santamaría, J. Non-Equilib. Thermodyn. **32**, 299 (2007).
[36]H. Bataller, C. Miqueu, F. Plantier, J. L. Daridon, T. J. Jaber, A. Abbasi, Z. Saghir, and M. M. Bou-Ali, J. Chem. Eng. Data. **54**, 1710 (2009).
[37]G. Chavepeyer and J. K. Platten, Entropie **198–199**, 25 (1996).

# Apéndice I

# Coeficiente Soret en Mezclas Binarias de $n$-Alcanos: Correlación Empírica de la Dependencia de la Composición (En preparación)

Soft Matter

Dynamic Article Links ►

Cite this: DOI: 10.1039/c0xx00000x

www.rsc.org/xxxxxx

PAPER

# Soret Coefficient in *n*-alkane Binary Mixtures: empirical correlation of composition dependence

**David Alonso de Mezquia[a], M. Mounir Bou-Ali*[a], Jose Antonio Madariaga[b] and Carlos Santamaría[b]**

***Received (in XXX, XXX) Xth XXXXXXXXX 20XX, Accepted Xth XXXXXXXXX 20XX***

**DOI: 10.1039/b000000x**

In this work, the results obtained for the Soret coefficient in *n*-alkane equimolar binary mixtures are presented. The Soret coefficient has been determined by an indirect method by means of the experimental results obtained for the thermodiffusion coefficient by the thermogravitational technique, and for the molecular diffusion coefficient by the sliding symmetric tubes technique (SST). Additionally, a new correlation for the determination of the Soret coefficient in normal alkane binary mixtures is presented. This correlation is able of determining the value of this coefficient for any concentration of the components, using the data of the thermal expansion coefficient and the dynamic viscosity of the pure substances in the mixture and the density of the equimolar mixture.

## A Introduction

When a thermal gradient is applied to a binary liquid mixture, a separation process of the components in the mixture is induced, which causes a diffusion process due to the concentration gradient generated within the mixture. This phenomenon, which is known as Soret effect[1-4], generates a flux of matter that can be quantified by the following expression:

$$J_i = -\rho D \frac{\partial c}{\partial x} - \rho D_T c_0 (1 - c_0) \frac{\partial T}{\partial x} \quad (1)$$

The first term on the right side of this equation represents the Fick´s law[5] of diffusion, being $c$ the mass fraction of the reference component $i$, and $D$ the molecular diffusion coefficient. The second term of this equation describes the thermodiffusive effect, which is proportional to the temperature gradient, being $D_T$ the thermodiffusion coefficient. This second term of eq. (1) describes the mass separation due to the thermal gradient, and the first summation term refers to the homogenization of the mixture by the molecular diffusion. Both terms are of opposite sign, and when they become equal, a stationary state, in which the flux ($J$) neglects, is reached. In this situation the following can be written:

$$\frac{\partial c}{\partial x} = -\frac{D_T}{D} c_0 (1 - c_0) \frac{\partial T}{\partial x} \quad (2)$$

The efficiency of the separation in the stationary state can be judged by the ratio,

$$S_T = \frac{D_T}{D} \quad (3)$$

which is known as the Soret coefficient.

This coefficient can be positive or negative depending on the sign of $D_T$, i.e., the direction of the migration of the reference component to the cold wall or to the warm wall.

When the mixture is composed by gases, the thermal diffusion factor ($\alpha_T$) is more commonly used to describe this phenomenon. This factor is defined as:

$$\alpha_T = S_T \cdot T = -\frac{T}{C_0(1-c_0)} \frac{\nabla C_0}{\nabla T} \quad (4)$$

At low pressures, the thermal diffusion factor of gaseous mixtures is almost independent with composition. The kinematic theory of gases predicts that $\alpha_T$ can be almost determined by the molecular weights or the size relation of the species of the mixture[6-7].

The absolute value of this coefficient for organic mixtures is small, in the order of $S_T$ =$10^{-3}$-$10^{-2}$ $K^{-1}$. Nevertheless, the Soret effect has huge influence in several phenomena. It has been demonstrated how the Soret effect has many influence in the initial distribution of the components in oil reservoirs[8-10], as well as in their exploitation[11]. It has also been checked how this phenomenon can be used in separation processes of biologic mixtures[12], and it has been considered too as an important mechanism in the origin of life[13].

Even nowadays, the experimental results of this coefficient for a mixture obtained using different experimental techniques, are scattered[14]. Apart from this, the few existing microscopic theories are not completely in agreement with the experimental data[15]. This is why the experimental determination of the Soret coefficient has gained renewed interest.

For these reasons, in this study the Soret coefficient of 23 different equimolar mixtures of *n*-alkanes at 25ºC has been determined. These mixtures correspond to the following three series: $n$C$_6$-$n$C$_i$, $n$C$_{10}$-$n$C$_i$, and $n$C$_{12}$-$n$C$_i$. To determine the thermodiffusion coefficient the thermogravitational technique has been used while the determination of the molecular diffusion coefficient has been done by the sliding symmetric tubes (SST) technique.

The obtained results make the study of the influence in the Soret coefficient of the molecular weight and the density of *n*-alkanes possible.

The Soret coefficient of 20 mixtures of the systems $nC_{10}$-$nC_5$, $nC_{12}$-$nC_6$, and $nC_{12}$-$nC_8$ in different compositions has also been determined in order to conduct a study on the dependence of $S_T$ with the molar fraction of the mixtures.

## B Equipment and procedure

### B.1 Studied mixtures

In this work, 23 *n*-alkane binary mixtures at 50% molar fraction have been prepared, corresponding to the series:

$nC_6$-$nC_i$ with $i$=10, 11, 12, 13, 14, 15, 16, 17, 18;
$nC_{10}$-$nC_i$ with $i$=5, 6, 7, 14, 15, 16;
$nC_{12}$-$nC_i$ with $i$=5, 6, 7, 8, 9, 16, 17, 18.

In addition, this work has been completed studying the influence of composition in Soret coefficient in the systems $nC_{12}$-$nC_6$, $nC_{12}$-$nC_7$, $nC_{12}$-$nC_8$ and $nC_{10}$-$nC_5$. For this end the following mixtures have been prepared:

$nC_{12}$-$nC_6$ ($x_1$=0.10, 0.30, 0.34, 0.50, 0.70, 0.90);
$nC_{12}$-$nC_7$ ($x_1$=0.10, 0.30, 0.37, 0.50, 0.70, 0.90);
$nC_{12}$-$nC_8$ ($x_1$=0.07, 0.31, 0.40, 0.50, 0.73);
$nC_{10}$-$nC_5$ ($x_1$=0.10, 0.20, 0.34, 0.50, 0.64, 0.80).

where $x_1$ is the molar fraction of the first component.

All the products used in this study were purchased from Merck with purity better than 99%. The mixtures have been prepared by weight using a Gram VXI-310 digital scale with a precision of 0.001g, introducing first the less volatile component and then adding the corresponding amount of the second component.

An Anton Paar DMA 5000 vibrating quartz U-tube densimeter, having an accuracy of $5 \cdot 10^{-6}$ g/cm$^3$, has been used to determine the density of the mixtures. Since we are working with small mass fraction differences, it can be supposed that $\rho = ac_i$, where $\rho$ is the density of the mixture, $c_i$ is the mass fraction of component $i$ in the binary mixture, and $a$ is a constant parameter. To determine the constant parameter, $a$, five mixtures of known concentration are prepared by weighting and then, the density of each mixture is measured. Thus, we determine the mass fraction with a deviation around ±0.01 wt %.

The dynamic viscosity ($\mu$) of the studied mixtures has been measured with an Anton Paar AMVn falling ball microviscometer, with reproducibility better than 0.1%.

The thermophysical properties, density ($\rho$), thermal expansion coefficient ($\alpha$) and dynamic viscosity ($\mu$) were measured in this work and also taken from ref. 16, 17 and ref. 18. These values are detailed in Table I and Table II. All the measurements were done at 298 K.

**Table I** Values of the density ($\rho$), thermal expansion coefficient ($\alpha$), dynamic viscosity ($\mu$) and relative mass ($\delta M$) for the equimolar binary mixtures ($x$=0.5) used in this work at 298 K.

| Mixture | $\rho$ (g/cm$^3$) | $\alpha$ $10^{-3}$ (K$^{-1}$) | $\mu$ $10^{-3}$ (Pa s) | $\delta M$ | $\rho^4\delta$M (g$^4$/cm$^{12}$) |
|---|---|---|---|---|---|
| $nC_{10}$-$nC_6$ | 0.698508 | 1.159 | 0.538 | 0.24556 | 0.058457 |
| $nC_{11}$-$nC_6$ | 0.706712 | 1.124 | 0.623 | 0.28918 | 0.072133 |
| $nC_{12}$-$nC_6$ | 0.713792 | 1.095 | 0.730 | 0.32808 | 0.085167 |
| $nC_{13}$-$nC_6$ | 0.720307 | 1.068 | 0.831 | 0.36290 | 0.097693 |
| $nC_{14}$-$nC_6$ | 0.726124 | 1.047 | 0.945 | 0.39431 | 0.109630 |
| $nC_{15}$-$nC_6$ | 0.731762 | 1.025 | 1.108 | 0.42277 | 0.121220 |
| $nC_{16}$-$nC_6$ | 0.736556 | 1.009 | 1.260 | 0.44868 | 0.132010 |
| $nC_{17}$-$nC_6$ | 0.741007 | 0.991 | 1.432 | 0.47200 | 0.142310 |
| $nC_{18}$-$nC_6$ | 0.745086 | 0.976 | 1.715 | 0.49407 | 0.152270 |
| $nC_{10}$-$nC_5$ | 0.689961 | 1.203 | 0.486 | 0.32705 | 0.074117 |
| $nC_{10}$-$nC_7$ | 0.706677 | 1.122 | 0.608 | 0.17354 | 0.043280 |
| $nC_{14}$-$nC_{10}$ | 0.745410 | 0.976 | 1.410 | 0.16470 | 0.050850 |
| $nC_{15}$-$nC_{10}$ | 0.749433 | 0.960 | 1.582 | 0.19774 | 0.062379 |
| $nC_{16}$-$nC_{10}$ | 0.752850 | 0.952 | 1.762 | 0.22827 | 0.073330 |
| $nC_{12}$-$nC_5$ | 0.706503 | 1.126 | 0.671 | 0.40492 | 0.100890 |
| $nC_{12}$-$nC_7$ | 0.720338 | 1.066 | 0.807 | 0.25926 | 0.069804 |
| $nC_{12}$-$nC_8$ | 0.726279 | 1.043 | 0.892 | 0.19717 | 0.054861 |
| $nC_{12}$-$nC_9$ | 0.731708 | 1.021 | 0.992 | 0.14096 | 0.040407 |
| $nC_{16}$-$nC_{12}$ | 0.759300 | 0.930 | 2.113 | 0.14141 | 0.047004 |
| $nC_{17}$-$nC_{12}$ | 0.759557 | 0.922 | 2.389 | 0.17029 | 0.056679 |
| $nC_{18}$-$nC_{12}$ | 0.761665 | 0.909 | 2.665 | 0.19810 | 0.067814 |

[a] Footnote text.

### B.2 Determination of Soret coefficient

For the determination of the Soret coefficient and as defined by eq. (3), it is necessary to know the value of the thermodiffusion coefficient and the molecular diffusion coefficient. In the following, the process followed to determine these coefficients will be described.

### B.3 Determination of molecular diffusion coefficient.

The molecular diffusion coefficient was determined by the sliding symmetric tubes (SST) technique.

The SST technique consists of several sets of two identical vertical tubes. Each set has two positions: "faced tubes" in which the mass transfer between both tubes is permitted, and "separated tubes". In this position, the content of the tubes is isolated. At the beginning of an experiment, the studied mixtures with a slight difference of mass fraction of its components (c±3%) are introduced in each of the tubes. The mixture with a higher mass fraction of the denser component is introduced in the bottom tube, and the upper tube is filled with the mixture with less concentration of the denser component so that the convective instability is avoided. The two tubes with which each set of the device is provided have the same dimensions (length of 60±0.01 mm and diameter of 9±0.01 mm).

The tubes in their "separated tubes" position are filled with the mixtures, next introducing the sets in a water bath so that the mixture obtains the working temperature (T=298 K). Once the mixture has reached the working temperature, all the sets in the bath are changed to their "faced tubes" configuration, starting in this manner the diffusion process.

Cite this: DOI: 10.1039/c0xx00000x

www.rsc.org/xxxxxx

# ARTICLE TYPE

**Table II** Values of the density ($\rho$), thermal expansion coefficient ($\alpha$), dynamic viscosity ($\mu$) and relative mass ($\delta M$) at 298 K for $nC_{12}$-$nC_6$, $nC_{12}$-$nC_7$, $nC_{12}$-$nC_8$ and $nC_{10}$-$nC_5$ systems, at different molar fractions of the first component.

| $x$ | $\rho$ (g/cm$^3$) | $\alpha$ $10^{-3}$ (K$^{-1}$) | $\mu$ $10^{-3}$ (Pa s) |
|---|---|---|---|
| | Set 1: $nC_{12}$-$nC_6$ | | |
| 0.10 | 0.671330 | 1.240 | 0.360 |
| 0.30 | 0.696530 | 1.560 | 0.523 |
| 0.34 | 0.700130 | 1.159 | 0.558 |
| 0.50 | 0.713792 | 1.098 | 0.730 |
| 0.70 | 0.728940 | 1.030 | 0.963 |
| 0.90 | 0.740650 | 0.990 | 1.255 |
| | Set 2: $nC_{12}$-$nC_7$ | | |
| 0.10 | 0.689767 | 1.202 | 0.475 |
| 0.30 | 0.706600 | 1.124 | 0.611 |
| 0.37 | 0.711000 | 1.102 | 0.682 |
| 0.50 | 0.720338 | 1.066 | 0.807 |
| 0.70 | 0.731471 | 1.023 | 1.004 |
| 0.90 | 0.740949 | 0.990 | 1.234 |
| | Set 3: $nC_{12}$-$nC_8$ | | |
| 0.07 | 0.703400 | 1.146 | 0.555 |
| 0.31 | 0.717320 | 1.101 | 0.734 |
| 0.40 | 0.721960 | 1.060 | 0.807 |
| 0.50 | 0.726279 | 1.043 | 0.892 |
| 0.73 | 0.735870 | 1.022 | 1.105 |
| | Set 3: $nC_{10}$-$nC_5$ | | |
| 0.10 | 0.637718 | 1.495 | 0.277 |
| 0.20 | 0.652835 | 1.399 | 0.333 |
| 0.34 | 0.670325 | 1.297 | 0.403 |
| 0.50 | 0.689961 | 1.203 | 0.486 |
| 0.64 | 0.700261 | 1.150 | 0.586 |
| 0.80 | 0.711864 | 1.098 | 0.690 |

[a] Footnote text.

In determined time intervals, the position of the sets is changed one by one back to the "separated tubes" position. After stopping the mass transfer process between the tubes the concentration in each of them is analyzed. This allows obtaining the concentration change in the tubes in function of time and consequently the molecular diffusion coefficient can be obtained from eqs. (5) and (6).

$$\overline{c^{top}(t)} = \frac{c^{top}+c^{bot}}{2} + \frac{4(c^{top}-c^{bot})}{\pi^2}\sum_{n=0}^{\infty}\frac{e^{\varphi}}{(2n+1)^2} \quad (5)$$

$$\overline{c^{bot}(t)} = \frac{c^{top}+c^{bot}}{2} - \frac{4(c^{top}-c^{bot})}{\pi^2}\sum_{n=0}^{\infty}\frac{e^{\varphi}}{(2n+1)^2} \quad (6)$$

where,

$$\varphi = -\left(\left(\frac{2n+1}{2}\right)^2\left(\frac{\pi}{L}\right)^2 Dt\right) \quad (7)$$

and $\overline{c^{top}(t)}$ and $\overline{c^{bot}(t)}$ are the mean mass fractions in the upper and bottom tube, respectively. $L$ is the tube length and $t$ is the test time.

The solution of the inverse problem posed by eqs. (5) and (6) to obtain the molecular diffusion coefficient is solved by the least-squares method using *Matlab* software.

The procedure has been described in detail in an earlier publication[19].

**B.4 Thermodiffusion coefficient determination.**

The thermodiffusion coefficients for equimolar *n*-alkanes mixtures were previously determined experimentally by our group[16] by the thermogravitational technique. The thermogravitational column used was a stainless steel concentric tube column, closed at both ends. The geometrical parameters of the column were the height $L_z$= 0.5±0.001 m and a gap $L_x$= 1x10$^{-3}$±5x10$^{-6}$ m. The temperature difference across the column was 10 K with an average temperature of 298 K.

The determination of the thermodiffusion coefficient by this technique is done by the analysis of the separation of the components in the stationary state[17]. The value of the thermodiffusion coefficient is obtained using the following expression:

$$D_T = \frac{g\cdot\alpha\cdot L_x^4}{504\cdot\beta\cdot\mu\cdot c_0\cdot(1-c_0)}\frac{\partial\rho}{\partial z} \quad (9)$$

where $g$ is the acceleration of gravity, $L_z$ is the distance between the warm and cold walls of the thermogravitational column, $\mu$ is the dynamic viscosity of the mixture and $c_0$ is the mass concentration of the reference component.

The term $\alpha = -1/\rho_0\,(\partial\rho/\partial T)$, corresponds to the thermal expansion coefficient, while $\beta = 1/\rho_0\,(\partial\rho/\partial c)$ is the mass expansion coefficient. The former of these coefficients is obtained by analyzing the density of the mixture to be studied in function of temperature, while the latter is determined by the analysis of the density of 5 mixtures of known concentration close to the reference one.

The density variation of the components along the thermogravitational column $(\partial\rho/\partial z)$ is determined by the analysis of the density of samples extracted from ports situated at different heights of the columns. More details of this experimental procedure can be seen in ref. 18.

The thermodiffusion coefficients, $D_T$, for these mixtures of *n*-alkanes can also be calculated from the correlation obtained in ref. 16 and 17. This correlation shows that the thermodiffusion coefficient is proportional to the mass difference between the components and to the ratio of the thermal expansion coefficient and viscosity of the mixture. In all cases the difference between the experimental data and the one calculated from this correlation is less than 4%.

## C Results and discussion

**C.1 Experimental results for equimolar mixtures.**

In Table III are summarized the values of the diffusion coefficients measured in this work for the equimolar mixtures ($x$=0.5) of the systems described above. The reproducibility of the experimental results for $D$ coefficient in the SST technique is within 3% of deviation. Each experimental test was repeated, at

least, 2 times for each mixture.

**Table III** Comparison of experimental data of the Soret coefficient, $S_T$ (exp) with results derived from Eq (33), $S_T$ (cc) for each series $n$C$_i$-$n$C$_j$ with molar fraction x=0.5 at 298 K. $D_T$ stands for the thermodiffusion coefficient and $D$ for the molecular diffusion coefficient; $\delta$ is de relative difference.

| Mixture | $D_T$ | $D$ | $S_T$ (exp) | $S_T$ (cc) | δ (%) |
|---|---|---|---|---|---|
| | $10^{-12}$ m$^2$/sK | $10^{-9}$ m$^2$/s | $10^{-3}$ K$^{-1}$ | $10^{-3}$ K$^{-1}$ | |
| Set 1: $n$C$_i$-$n$C$_6$ | | | | | |
| $n$C$_{10}$-$n$C$_6$ | 6.08 | 2.53 | 2.40 | 2.47 | -2.5 |
| $n$C$_{11}$-$n$C$_6$ | 6.40 | 2.14 | 2.99 | 2.97 | 0.7 |
| $n$C$_{12}$-$n$C$_6$ | 6.45 | 1.93 | 3.34 | 3.43 | -2.5 |
| $n$C$_{13}$-$n$C$_6$ | 6.61 | 1.67 | 3.96 | 3.84 | 3.0 |
| $n$C$_{14}$-$n$C$_6$ | 6.68 | 1.54 | 4.34 | 4.21 | 2.9 |
| $n$C$_{15}$-$n$C$_6$ | 6.47 | 1.48 | 4.37 | 4.56 | -4.1 |
| $n$C$_{16}$-$n$C$_6$ | 6.38 | 1.26 | 5.06 | 4.86 | 4.2 |
| $n$C$_{17}$-$n$C$_6$ | 6.10 | 1.24 | 4.92 | 5.13 | -4.1 |
| $n$C$_{18}$-$n$C$_6$ | 5.90 | 1.12 | 5.27 | 5.38 | -2.0 |
| Set 2: $n$C$_i$-$n$C$_{10}$ | | | | | |
| $n$C$_{10}$-$n$C$_5$ | 8.78 | 2.96 | 2.97 | 3.04 | -2.5 |
| $n$C$_{10}$-$n$C$_6$ | 6.08 | 2.53 | 2.40 | 2.47 | -2.5 |
| $n$C$_{10}$-$n$C$_7$ | 3.90 | 2.07 | 1.88 | 1.87 | 0.6 |
| $n$C$_{14}$-$n$C$_{10}$ | 1.84 | 0.88 | 2.09 | 2.17 | -3.7 |
| $n$C$_{15}$-$n$C$_{10}$ | 2.15 | 0.78 | 2.76 | 2.61 | 5.5 |
| $n$C$_{16}$-$n$C$_{10}$ | 2.23 | 0.72 | 3.10 | 3.01 | 2.8 |
| Set 3: $n$C$_i$-$n$C$_{12}$ | | | | | |
| $n$C$_{12}$-$n$C$_5$ | 8.81 | 2.20 | 4.00 | 3.94 | 1.6 |
| $n$C$_{12}$-$n$C$_6$ | 6.45 | 1.93 | 3.34 | 3.43 | -2.5 |
| $n$C$_{12}$-$n$C$_7$ | 4.74 | 1.70 | 2.79 | 2.89 | -3.4 |
| $n$C$_{12}$-$n$C$_8$ | 3.23 | 1.45 | 2.23 | 2.33 | -4.3 |
| $n$C$_{12}$-$n$C$_9$ | 2.15 | 1.26 | 1.71 | 1.76 | -2.9 |
| $n$C$_{16}$-$n$C$_{12}$ | 1.16 | 0.58 | 2.00 | 2.02 | -0.1 |
| $n$C$_{17}$-$n$C$_{12}$ | 1.29 | 0.54 | 2.39 | 2.40 | -0.4 |
| $n$C$_{18}$-$n$C$_{12}$ | 1.33 | 0.48 | 2.77 | 2.81 | -1.4 |

[a] Footnote text.

Table III also shows the values of the thermal diffusion coefficient previously obtained by our group[16] and determined in this work for the equimolar $n$-alkane binary mixtures.

With these values of $D_T$ and $D$ the Soret coefficients for these mixtures can be directly calculated. These values are shown in Table III.

### C.2 Dependence of the Soret coefficient with density for equimolar mixtures.

The kinetic theory provides expressions that adequately describe the behavior of thermal diffusion factor in the case of low density systems. Thus, it is found that in isotopic mixtures of hard-spheres $\alpha_T$ exhibits a relative simple dependence on $x_1$ and $M_1/M_2$, where $M_1$ and $M_2$ are the masses of the components of mixture. Chapman[7] showed that in the Boltzman limit it is possible to expand $\alpha_T$ in powers of $\delta M=(M_1-M_2)/(M_1+M_2)$.

$$\alpha_T = \alpha_0 \delta M + \ldots \quad (10)$$

On the other hand, Kincaid *et al.*[20] found using numerical calculation that the thermal diffusion factor of isotopic mixtures of hard-spheres can be accurately represented,

$$\alpha_T = \alpha_0 \delta M (1 - \gamma (x_1 - x_2) \delta M + \ldots) \quad (11)$$

where $\alpha_0$ and $\gamma$ are independent of the composition but increase and decrease with increasing density, respectively[20].

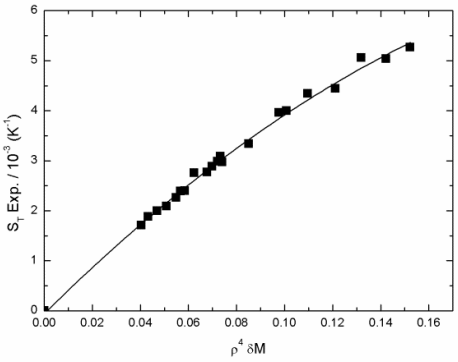


**Fig. 1** Soret coefficient in function of the $\rho^4 \delta M$ factor, for the binary equimolar mixtures

Eq. (7) describes qualitatively, and in some cases quantitatively, the dependence of $\alpha_T$ on $\delta M$ for all values of $\delta M$. Moreover, new expressions for the Soret coefficient have been developed in several works[21-24]. These expressions are based on the concept that this coefficient can be expressed by the contribution done by several factors, such us the molecular mass of the components, their inertia and the interactions between molecules.

In other works[24], the Soret coefficient has been expressed taking into account the dispersion forces, and the influence of the composition of the mixtures in the Soret coefficient has been analyzed.

In equimolar mixtures, Eq. (7) reduces to:

$$\alpha_T = \alpha_0 \delta M \quad (12)$$

that for a fixed temperature can be written as:

$$S_T = \alpha_0 \delta M \quad (13)$$

Galliero *et al.*[25] analyzed the validity of such relation for dense systems from molecular dynamics simulations and found that $\alpha_0$ has a strong dependence on density but a weak one on temperature.

In view of these results, in Fig. 1 the Soret coefficient values obtained in this work for equimolar mixtures versus the group, $\rho^4 \delta M$ are plotted. Here, $\rho$ represents the density of mixture. The values used for the density of the equimolar mixtures are shown in Table I. As can be seen, the data fit to a quadratic curve given by:

$$S_T = 46.44(\rho^4 \delta M)[1 - 1.57(\rho^4 \delta M)] \quad (14)$$

In Table III the Soret coefficients calculated from this expression together with the experimental values are shown. The agreement between the two sets is excellent. The last column of Table I shows the relative differences between the two sets of values. These differences are lower than the experimental error.

Eq. (10) allows a quantitative prediction of the Soret coefficient of an equimolar two $n$-alkane mixture if the molecular weights and the density are known.

### C.1 Experimental results for binary mixtures of *n*-alkanes.

Cite this: DOI: 10.1039/c0xx00000x

www.rsc.org/xxxxxx

# ARTICLE TYPE

**Table IV** Comparison of experimental data of the Soret coefficient, $S_T$ (exp) with results derived from Eq (30), $S_T$ (cc) for several series in the whole molar fraction concentration at 298 K. $D_T$ stands for the thermodiffusion coefficient and $D$ for the molecular diffusion coefficient; $\delta$ is the relative difference.

| Mixture | $x_1$ | $D_T$ | $D$ | $S_T$ (exp) | $S_T$ (cc) | δ (%) |
|---|---|---|---|---|---|---|
| | | $10^{-12}$ m$^2$/sK | $10^{-9}$ m$^2$/s | $10^{-3}$ K$^{-1}$ | $10^{-3}$ K$^{-1}$ | |
| $n$C$_{12}$-$n$C$_6$ | 0.10 | 9.14 | 2.48 | 3.69 | 3.70 | -0.4 |
| | 0.30 | 7.62 | 2.24 | 3.40 | 3.56 | -4.5 |
| | 0.34 | 7.45 | 2.13 | 3.50 | 3.54 | 1.1 |
| | 0.50 | 6.45 | 1.93 | 3.34 | 3.43 | -2.5 |
| | 0.70 | 5.37 | 1.72 | 3.12 | 3.21 | -5.1 |
| | 0.90 | 4.50 | 1.51 | 2.98 | 3.15 | -5.3 |
| $n$C$_{12}$-$n$C$_7$ | 0.10 | 6.34 | 2.09 | 3.03 | 3.22 | -5.8 |
| | 0.30 | 5.30 | 1.84 | 2.88 | 3.05 | -5.6 |
| | 0.37 | 5.08 | 1.70 | 2.99 | 2.99 | 0.0 |
| | 0.50 | 4.74 | 1.70 | 2.79 | 2.89 | -3.4 |
| | 0.70 | 3.86 | 1.48 | 2.61 | 2.72 | -4.1 |
| | 0.90 | 3.35 | 1.37 | 2.45 | 2.55 | -4.3 |
| $n$C$_{12}$-$n$C$_8$ | 0.07 | 4.34 | 1.70 | 2.55 | 2.67 | -4.4 |
| | 0.31 | 3.62 | 1.56 | 2.32 | 2.48 | -6.4 |
| | 0.40 | 3.39 | 1.49 | 2.28 | 2.41 | -5.5 |
| | 0.50 | 3.23 | 1.45 | 2.23 | 2.33 | -4.3 |
| | 0.73 | 2.64 | 1.25 | 2.11 | 2.15 | 1.5 |
| $n$C$_{10}$-$n$C$_5$ | 0.10 | 11.90 | 3.75 | 3.17 | 3.14 | 1.0 |
| | 0.20 | 10.36 | 3.36 | 3.08 | 3.12 | -1.1 |
| | 0.34 | 9.37 | 3.03 | 3.09 | 3.08 | 0.4 |
| | 0.50 | 8.76 | 2.96 | 2.96 | 3.04 | -2.7 |
| | 0.64 | 7.56 | 2.48 | 3.05 | 3.01 | 1.4 |
| | 0.80 | 6.92 | 2.20 | 3.15 | 2.97 | 6.0 |

[a] Footnote text.

In Table IV the diffusion coefficient values obtained in this work for different concentrations of the $n$C$_{10}$-$n$C$_5$ system are shown. The diffusion coefficient values for the rest of mixtures shown in this table were taken from ref. 19.

On the other hand, the thermodiffusion coefficients for the $n$C$_{12}$-$n$C$_6$ and $n$C$_{12}$-$n$C$_8$ systems at different concentrations were determined in this work. $D_T$ coefficient values for *n*-decane/*n*-pentane system were taken from ref. 20 and for *n*-dodecane/*n*-heptane system from ref. 17. The values corresponding to $D_T$ for concentrations of $x$=0.5 and $c$=0.5 were previously measured by our group[16], [26-27].

With these values for $D_T$ and $D$, the Soret coefficients of these mixtures can be calculated. These values are listed in Table IV.

### C.3 Dependence of the Soret coefficient with composition.

In ref. 17 it was concluded that the thermal diffusion factor is a lineal function with mass concentration, so accordingly we can write $D_T$, as:

$$D_T = D_{T1}^0 c_2 + D_{T2}^0 c_1 \qquad (15)$$

where $D_{T1}^0$ y $D_{T2}^0$ are the limiting values of $D_T$ for $c_1 \to 0$ and $c_2 \to 0$, respectively.

This equation can be expressed in terms of the molar fraction. For doing so, one must remember that the mass fraction is $c_1=x_iM_i/(c_1M_1+c_2M_2)$, and consequently eq. (15) takes the form:

$$D_T = \frac{D_{T1}^0 M_2 x_2 + D_{T2}^0 M_1 x_1}{M_1 x_1 + M_2 x_2} = D_T(x_1) \qquad (16)$$

On the other hand, in ref. 19 it was concluded that the diffusion coefficient shows also a linear dependence with mass concentration, i.e..

$$D = D_1^0 c_2 + D_2^0 c_1 = \frac{D_1^0 M_2 x_2 + D_2^0 M_1 x_1}{M_1 x_1 + M_2 x_2} = D(x_1) \qquad (17)$$

where, $D_1^0$ and $D_2^0$ are the limiting diffusion coefficients, defined by:

$$D_1^0 = lim_{c_1 \to 0} D \qquad (18)$$

$$D_2^0 = lim_{c_2 \to 0} D \qquad (19)$$

Accordingly, the Soret coefficient can be written as:

$$S_T(x_1) = \frac{D_T}{D} = \frac{D_{T1}^0 M_2 x_2 + D_{T2}^0 M_1 x_1}{D_1^0 M_2 x_2 + D_2^0 M_1 x_1} \qquad (20)$$

It is also known[19] that the mass ratio, $M_1/M_2$, corresponds approximately to the ratio between the limiting diffusion coefficients,

$$\frac{D_1^0}{D_0^2} = \frac{M_1}{M_2} \qquad (21)$$

together with:

$$x_1 + x_2 = 1 \qquad (22)$$

and if we have defined $S_{T1}^0$ and $S_{T2}^0$ as:

$$S_{T1}^0 = \frac{D_{T1}^0}{D_1^0} \;\; and \;\; S_{T2}^0 = \frac{D_{T2}^0}{D_2^0} \qquad (23)$$

**Table V** Values of the thermal expansion coefficient ($\alpha$) and dynamic viscosity ($\mu$) for the pure components of $n$C$_{10}$-$n$C$_5$, $n$C$_{12}$-$n$C$_6$, $n$C$_{12}$-$n$C$_7$ and $n$C$_{12}$-$n$C$_8$ mixtures. $D^0_{T1}$ and $D^0_{T2}$ are the limiting values of $D_T$ for $c_i$=0.

| Mixture | $\alpha_1$ $10^{-3}$ | $\mu_1$ $10^{-3}$ | $\alpha_2$ $10^{-3}$ | $\mu_2$ $10^{-3}$ | $D^0_{T1}$ $10^{-12}$ | $D^0_{T2}$ $10^{-12}$ | $\lambda$ |
|---|---|---|---|---|---|---|---|
| | K$^{-1}$ | Pa s | K$^{-1}$ | Pa s | m$^2$/sK | m$^2$/sK | |
| $n$C$_{10}$-$n$C$_5$ | 1.040 | 0.838 | 1.61 | 0.224 | 13.65 | 6.37 | 0.041 |
| $n$C$_{12}$-$n$C$_6$ | 0.971 | 1.383 | 1.38 | 0.300 | 10.46 | 4.34 | 0.100 |
| $n$C$_{12}$-$n$C$_7$ | 0.971 | 1.383 | 1.24 | 0.387 | 7.06 | 3.11 | 0.144 |
| $n$C$_{12}$-$n$C$_8$ | 0.971 | 1.383 | 1.16 | 0.508 | 4.59 | 2.18 | 0.171 |

[a] Footnote text.

It is easy to obtain that:

$$S_T(x_1) = S_{T1}^0 x_2 + S_{T2}^0 x_1 \qquad (24)$$

What means that the Soret coefficient is a lineal function of the molar fraction.

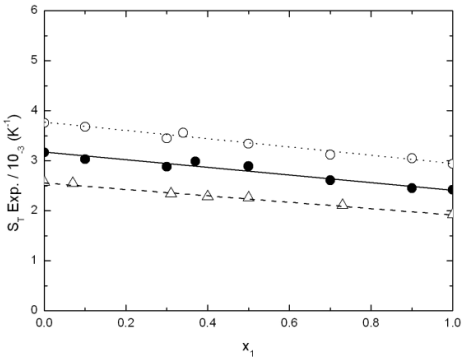


**Fig. 2** Soret coefficient in function of the molecular concentration for the mixtures "○" $n$C$_{12}$-$n$C$_6$, "●" $n$C$_{12}$-$n$C$_7$ and "Δ" $n$C$_{12}$-$n$C$_8$ at 298 K

In Fig. 2, the Soret coefficient,obtained in this work for the $n$C$_{12}$-$n$C$_6$, $n$C$_{12}$-$n$C$_7$ and $n$C$_{12}$-$n$C$_8$ systems as a function of the molar fraction of the mixture are represented. As one can see, the Soret coefficient fits well to a straight line in accordance with eq. (17).

In equimolar mixtures ($x_1$=0.5),

$$S_T(x = 0.5) = \frac{S_{T1}^0 + S_{T2}^0}{2} = \overline{S_T} \quad (25)$$

The linearity of $S_T$ with molar fraction allows obtaining the limit values of $S_T$ for $x$=0 and $x$=1:

$$S_{T1}^0 = \overline{S_T} + \Delta S_T \quad (26)$$

$$S_{T2}^0 = \overline{S_T} - \Delta S_T \quad (27)$$

$$\Delta S_T = \frac{S_{T1}^0 - S_{T2}^0}{2} \quad (28)$$

Therefore,

$$S_T(x_1) = \overline{S_T} + \Delta S_T(x_2 - x_1) = \overline{S_T}\left[1 - \frac{\Delta S_T}{\overline{S_T}}(x_1 - x_2)\right] \quad (29)$$

$$S_T(x_1) = \overline{S_T}\left[1 - \frac{S_{T1}^0 - S_{T2}^0}{S_{T1}^0 + S_{T2}^0}(x_1 - x_2)\right] \quad (30)$$

$$S_T(x_1) = \overline{S_T}\left[1 - \frac{\frac{S_{T1}^0}{S_{T1}^0} - 1}{\frac{S_{T1}^0}{S_{T1}^0} + 1}(x_1 - x_2)\right] \quad (31)$$

Bearing in mind that

$$\frac{S_{T1}^0}{S_{T2}^0} = \frac{D_1^0}{D_2^0}\frac{D_{T1}^0}{D_{T2}^0} = \frac{M_2}{M_1}\frac{D_{T1}^0}{D_{T2}^0} \quad (32)$$

The Soret coefficient can be written as:

$$S_T(x_1) = \overline{S_T}[1 - \lambda(x_1 - x_2)] \quad (33)$$

where λ is:

$$\lambda = \frac{D_{T1}^0 M_2 - D_{T2}^0 M_1}{D_{T1}^0 M_2 + D_{T2}^0 M_1} \quad (34)$$

$D_{T1}^0$ and $D_{T2}^0$ values can be calculated from expressions obtained in ref. (17) and given by:

$$D_{T1}^0 = D_T(x_1 \to 0) = 5.34 \cdot 10^{-11}\left(\frac{\alpha_2}{\mu_2}\right) M_2\left(1 - \frac{M_2}{M_1}\right) \quad (35)$$

$$D_{T2}^0 = D_T(x_2 \to 0) = 3.71 \cdot 10^{-11}\left(\frac{\alpha_1}{\mu_1}\right) M_1\left(\frac{M_1}{M_2} - 1\right) \quad (36)$$

where $\alpha_i$ and $\mu_i$ are the thermal expansion coefficient and the dynamic viscosity of the pure components. In Table V values of α and μ for the pure components corresponding to binary mixtures of Table IV are displayed. In this Table V the values obtained for $\lambda$ and the limiting values of $D_T$ calculated from eq. (34), (35) and (36) respectively are also shown.

Table IV shows the results obtained from eq. (33) for the Soret coefficients for different concentrations of the mixtures. These results agree reasonably well with those determined experimentally and the relative difference (last column in Table IV) in all cases is less than estimated experimental error.

This equation (33) also reproduces, within experimental error, the Soret coefficients calculated from experimental measurements of $D_T$ and $D$ previously obtained [18,19,26,27] for mixtures of $n$-alkanes at 50 wt%.

Furthermore, eq. (33) shows that the dependence of Soret coefficient with composition is governed by the factor $\lambda$. Large values of $\lambda$ mean a strong dependence of $S_T$ with $x$. For example, the $\lambda$ value for $n$C$_{10}$-$n$C$_5$ system is $\lambda$ =0.040 indicating that $S_T$ is practically independent of the composition, however for $n$C$_{12}$-$n$C$_8$ system, $\lambda$ takes the value $\lambda$ = 0.171, pointing out a significant dependence with the molar fraction. These results are corroborated by our experimental results (see Table II and Fig. 2).

So, for $n$C$_{10}$-$n$C$_5$ system the Soret coefficient measured in this work are, within the experimental error, independent of the composition of the mixture.

Finally, considering that the Soret coefficient ($S_T$) for equimolar mixtures is given by eq. (14), the expression of $S_T$ can be written as:

$$S_T = 46.44\rho^4\delta M[1 - 1.57\rho^4\delta M][1 - \lambda(x_1 - x_2)] \quad (37)$$

In conclusion, the Soret coefficient of binary mixtures of $n$-alkanes may be calculated if the dynamic viscosity, the thermal expansion coefficient of the pure component and the density of the equimolar mixture are known.

On the other hand, the equation for the Soret coefficient, eq. (37), can be written as:

$$S_T = A\delta M + B\delta M^2 \quad (38)$$

where $A$ and $B$ coefficients are function of the density and the molar fraction of the mixture. This expression agrees with the first terms of the expansion of $\alpha_T$ in powers of $\delta M$ proposed by Chapman[7] for isotopic mixtures of hard-spheres.

Moreover, eq (33) derived in this work for $S_T$ in $n$-alkanes binary mixtures is similar to that proposed by Kincaid *et al.*[20] for the thermal diffusion factor in isotopic mixtures.

$$\alpha_T = \alpha_0\delta M(1 - \gamma(x_1 - x_2)\delta M + \cdots) \quad (39)$$

Namely, the experimental results obtained in this work for the Soret coefficient suggests that the microscopic behaviour of the $n$-alkane binary mixtures (quasi-ideal systems) is similar to the theoretically deduced one for isotopic mixtures of hard-spheres.

Cite this: DOI: 10.1039/c0xx00000x

www.rsc.org/xxxxxx

# ARTICLE TYPE

## Conclusions

In this work values of the Soret coefficient of 23 equimolar *n*-alkane binary mixtures have been presented. The results obtained for the Soret coefficient have been determined by the measurement of thermodiffusion and molecular diffusion coefficients of these binary mixtures. The thermodiffusion coefficients were measured by the thermogravitational technique and the molecular diffusion coefficients by the sliding symmetric tubes technique.

Additionally, the Soret coefficients of four binary mixtures in the whole range of concentration have been determined. The experimental results obtained have been used to develop a new correlation for the determination of the Soret coefficient in normal alkane binary mixtures at any concentration, using the data of the viscosity and thermal expansion coefficient of the pure components of the mixture, and the density of the equimolar mixture. The good agreement between the experimental data and the one obtained with this correlation has been checked

## Acknowledgements

Authors would like to thank GOVSORET3 (PI2011-22) and Research Groups (IT557-10) projects of the Basque Government, and DCMIX from the European Space Agency for the financial support.

## Notes and references

[a] *Mechanical and Manufacturing Department, Engineering Faculty, Mondragon Unibertsitatea, Loramendi 4 Apdo. 23, 20500 Mondragon, Spain. Fax: +34 943 79 15 36; Tel:+34 943 79 47 00; E-mail: mbouali@mondragon.edu*

[b] *Department of Applied Physics II, University of Basque Country, (UPV/EHU) Apdo. 644, 48080 Bilbao, Spain.*

† Electronic Supplementary Information (ESI) available: [details of any supplementary information available should be included here]. See DOI: 10.1039/b000000x/

‡ Footnotes should appear here. These might include comments relevant to but not central to the matter under discussion, limited experimental and spectral data, and crystallographic data.

1 C. Soret, *Archives des Sciences Physiques es Naturelles de Geneve*, 1879, **2**, 48.

2 C. Soret, *C.R. Academie Scientificque*, 1880, **91**, 289.

3 C. Soret, *Annales de Chimie et Physique*, 1881, **22**, 293.

4 C. Ludwig, *Sitz. Ber. Akad. Wiss. Wien Math.-Naturw. Kl.*, 1856, **20**, 539.

5 A. Fick, *Annalen der Physik*, 1855, **170**, 59

6 W.H. Furry, R.C. Jones and L. Onsager, *Physical Review E*, 1939, **55**, 1083.

7 S. Chapman, *Proc. R. Soc. Lond.*, 1940, **177**, 38.

8 F. Montel, J. Bickert, A. Lagisquet and G. Galliero, *Journal of Petroleum Science and Egineering*, 2007, **58**, 391.

9 M. Touzet, G. Galliero, V. Lazzeri, M.Z. Saghir, F. Montel and J.C. Legros, *Comptes Rendus Mecanique*, 2011, **339**, 318.

10 K. Ghorayeb, A. Firoozabadi and T. Anraku, *SPE Journal*, 2003, **8**, 114.

11 F. Montel, *Entropie*, 1994, **184**, 86.

12 S. Duhr, S. Arduini and D. Braun, *European Physical Journal E*, 2004, **15**, 277.

13 P. Baaske, F.M. Weinert, S. Duhr, K.H. Lemke, M.J. Russell and D. Braun, *Proceedings of the National Academy of Sciences of the United States of America*, 2007, **104**, 9346.

14 A. Mialdun, V. Yasnou, V. Shevtsova, A. Königer, W. Köhler, D. Alonso de Mezquia and M.M. Bou-Ali, *J. Chem. Phys.*, 2012, **136**, 244515.

15 M. Eslamian and M.Z. Saghir, *Journal of Non-Equilibrium Thermodynamics*, 2009, **34**, 97.

16 P. Blanco, M.M. Bou-Ali, J.K. Platten, P. Urteaga, J.A. Madariaga and C. Santamaría, *Journal of Chemical Physics*, 2008, **129**, 174504.

17 J.A. Madariaga, C. Santamaría, M.M. Bou-Ali, P. Urteaga and D. Alonso de Mezquia, *Journal of Physical Chemistry B*, 2010, **114**, 6937.

18 P. Blanco, P. Polyakov, M.M. Bou-Ali and S. Wiegand, *Journal of Physical Chemistry B*, 2008, **112**, 8340.

19 D. Alonso de Mezquia, M.M. Bou-Ali, M. Larrañaga, J.A. Santamaría and C. Santamaría, *Journal of Physical Chemistry B*, 2012, **116**, 2814.

20 J.M. Kincaid, E.G.D. Cohen and M. Lopez de Haro, *Journal of Chemical Physics*, 1987, **86**, 963.

21 C. Debuschewitz and W. Köhler, *Physical Review Letters*, 2001, **87**, 055901-1.

22 G. Wittko and W. Köhler, *Journal of Chemical Physics*, 2005, **123**, 14506.

23 S. Hartmann, W. Köhler and K.I. Morozoz, *Soft Matter*, 2012, **8**, 1355.

24 Y. Leroyer and A. Würger, *Journal of Chemical Physics*, 2011, **135**, 054102.

25 G. Galliero, M. Bugel, B. Duguay and F. Montel, *Journal of Non-Equilibrium Thermodynamics*, 2007, **32**, 251.

26 Y. Yan, P. Blanco, M.Z. Saghir and M.M. Bou-Ali, *Journal of Chemical Physics*, 2008, **129**, 194507.

27 S. Srinivasan, D. Alonso de Mezquia, M.M. Bou-Ali and M.Z. Saghir, Philosophical Magazine, 2011, 91, 4332.

# Apéndice J

# Determinación del Coeficiente de Termodifusión en la mezcla ternaria THN-IBB-$nC_{12}$ Mediante la Columna Termogravitacional: Contribución a los Experimentos Terrestres del DCMIX (En preparación)

# Determination of the thermodiffusion coefficient in THN-IBB-$n$C$_{12}$ ternary mixtures using the thermogravitational column: contribution to ground experiments of DCMIX

*David Alonso de Mezquia*[1], *M. Mounir Bou-Ali*[1*], *J. Antonio Madariaga*[2], *Carlos Santamaría*[2] *and J. Karl Platten*[1]

[1]Mechanical and Manufacturing Department, Engineering Faculty of Mondragon Unibertsitatea, Loramendi 4 Apdo. 23, 20500 Mondragon, Spain

[2]Department of Applied Physics II, University of Basque Country, Apdo 644, 48080 Bilbao, Spain

*Corresponding Author. E-mail: mbouali@mondragon.edu

ABSTRACT

In this work, the thermodiffusion coefficient of five ternary mixtures composed by tetrahydronaphthalene, isobutylbenzene and *n*-decane and their corresponding binary mixtures at a mean temperature of 25 ºC have been determined. The experimental measurements have been carried out by the thermogravitational technique using two parallelepiped thermogravitational columns and another one with a cylindrical configuration. The influence of concentration of the components of the mixtures in the thermodiffusion coefficient has been analyzed both for the binary and ternary mixtures. The obtained results for the ternary mixtures have been compared with the ones determined by means of two correlations that are able of predicting the thermodiffusion coefficient of a component of a ternary mixture from the combination of the thermodiffusion coefficient of the corresponding binary mixtures. A good agreement between the experimental data and the one calculated with the correlations has been found.

KEYWORDS

Thermodiffusion Coefficient, Alkane Mixtures, Ternary Mixtures, DCMIX.

## I. INTRODUCTION

When applying a temperature gradient within a liquid mixture, this undergoes a separation of its components due to Soret effect[1,2,3,4]. This effect causes a flux ($J$) of the components in the mixture that can be quantified as:

$$J_i = -\rho\left(\sum_{k=1}^{n-1} D_{ik}\nabla c_k + \mathcal{D}_T^i \nabla T\right) \; i = 1,2,\dots(n-1) \tag{1}$$

Where ρ is the density of the mixture, $c$ stands for the mass concentration of the components, $T$ is the temperature and $D$ and $\mathcal{D}_T$ refer to the molecular diffusion coefficient and the thermodiffusion coefficient respectively.

In oil reservoirs exploitation[5,6] and recovery[7] is where these fluxes became very important. The models developed for the recovery of the fields work in scales of decades, and in most of the cases, the operational scenario is predicted using very few data. A similar situation can be found when predicting the initial state of the oil reservoirs[8,9]. This initial state prediction is important when estimating the economic return to be obtained from the oil field, and for sizing the installations needed for its exploitation. The different models developed for doing this have proved that the Soret effect is an important factor in all these processes.

The existing data for the thermodiffusion coefficient on hydrocarbon mixtures that can be found in the literature are scarce. It is in binary mixtures where one can find the most number of studies in this field[10,11,12,13,14]. In these mixtures, studies like the Benchmark of Fontainebleau[15] have been conducted, in which different experimental techniques were used in order to establish some reference values for the transport properties in several binary mixtures. In the case of

ternary mixtures, there exist very few experimental data for the thermodiffusion coefficient[16,17,18,19,20,21], not being completely in agreement with each other.

Due to the importance that the Soret effect has, and the few data available, DCMIX project has been recently created for the study of the transport properties in ternary mixtures. One of the objectives of this project is to study several ternary mixtures in a terrestrial environment using different techniques, as well as in a microgravity environment in experiments onboard the International Space Station (ISS).

One of the mixtures to be studied in the framework of this project is the ternary mixture of the compounds tetrahydronaphthalene (THN), isobutylbenzene (IBB) and *n*-dodecane ($nC_{12}$) at different concentrations. These compounds have been chosen because they can be used to model the elements that can be found in an oil field, having two rings, one ring and a linear chain respectively.

In this work, the results obtained in the measurement of the thermodiffusion coefficient at 25 ºC on five ternary mixtures of these compounds by the thermogravitational technique are presented. To complete the study, the thermodiffusion coefficient of the corresponding binary mixtures has also been measured. Additionally, the experimental results of the thermodiffusion coefficient obtained for the ternary mixtures have been compared with the ones determined using the correlations developed in ref. 17 and ref. 22.

The document is organized as follows: in section II the different devices used are presented, as well as the correlation used for the determination of the thermodiffusion coefficient in ternary mixtures. In section III, the obtained results, both for the binary and ternary mixtures, are presented and discussed, to finish with the conclusions of this work in section IV.

## II. EXPERIMENTAL SECTION

### A. Equipment and Materials

The materials used in this work have been purchased from Merck, with purity better than 99%. The mixtures have been prepared by weight using the gravimetric deposition method by two high precision digital scales. Two Gram digital scales with a precision of $1x10^{-4}$ g and $1x10^{-2}$ g have been used, using one or the other depending on the quantity of mixture to be prepared. When small volumes are required, the first scale is used while when the volume needed is greater, the second scale is used. The volume to be prepared depends on the experimental procedure to be carried out. In the case of the cylindrical thermogravitational column, around 230 cc. are needed, whereas in the case of the plane columns only 35 cc and 65 cc are required. For the determination of the thermophysical properties of the mixture such as the thermal expansion coefficient, the mass expansion coefficient, the viscosity or the calibration process, the quantity of fluid required is below 10 cc.

The density of the mixtures has been measures by an Anton Paar DMA 5000 densimeter. This apparatus has a precision of $1x10^{-6}$ g/cm$^3$ in the determination of the density, having a precision in the temperature in which the measurement in carried out of $1x10^{-3}$ K thanks to the Peltier elements incorporated to the device.

In the case of ternary mixtures, it is necessary to measure also the refractive index of the mixtures. For doing this, an Anton Paar RXA 156 refractometer, having a precision of $2x10^{-5}$ nD, is used. These two devices can be connected, so data for the density and the refractive index of a mixture can be measured at the same time.

The viscosity of the mixtures has been measured using an Anton Paar falling ball micro-viscometer. This apparatus has a repeatability over 99% and a temperature control during the measurement of $1x10^{-2}$ K.

B. Thermogravitational Technique

The determination of the thermodiffusion coefficient has been done by means of the thermogravitational technique[12,17]. In his technique, the mixture to be analyzed is introduced within two vertical walls at different temperatures. The horizontal temperature gradient applied to the mixture causes a horizontal separation of the components, creating at the same time a diffusive flux in the opposite direction due to the molecular diffusion. The horizontal differentiation of the components is amplified between the extremes of the column by the effect of convection, generating, in the case of positive Soret effect, an enrichment of the less dense component in the top of the column and of the denser component in the bottom of it.

According to the theory developed by Furry, Jones and Onsager[23], and extended for liquid mixtures by Majumdar[24], the thermodiffusion coefficient can be determined from the measurements at stationary states by the following equation:

$$\frac{\partial c_i}{\partial z} = -\frac{504}{g L_x^4}\frac{\mathcal{D}_T^i \nu}{\alpha} \quad i = 1,2,\dots(n-1) \tag{2}$$

Where $L_x$ is the gap distance between the warm and the cold walls, $g$ is the gravity acceleration, $\alpha = -(1/\rho)(\partial\rho/\partial T)$ is the thermal expansion coefficient of the mixture and $\nu$ stands for the kinematic viscosity. The $(\partial c_i/\partial z)$ factor refers to the concentration variation of the

reference component along the column, while $\mathcal{D}_T^i$ refers to the phenomenological thermodiffusion coefficient of component *i* in multicomponent mixtures.

In binary mixtures, the concentration of the components in the mixture can be related with the density by using the mass expansion coefficient $\beta = (1/\rho)(\partial\rho/\partial c)$. Additionally, in binary mixtures the thermodiffusion coefficient must be defined as $\mathcal{D}_T^i = c_i c_j D_T^i$, so combining this with expression (2), the following can be written:

$$D_T^i = -\frac{gL_x^4}{504}\frac{\alpha}{c_i c_j \beta \eta}\frac{\partial \rho}{\partial x} \tag{3}$$

where $\eta$ is the dynamic viscosity of the mixture.

In the case of ternary mixtures, for the determination of the concentration of the components of a mixture, an analysis method which uses the data of the density and the refractive index is used. For each of the ternary mixtures studied in the thermogravitational column, it is necessary to analyze and determine the density and the refractive index of at least 25 ternary mixtures of concentration close to the one to be anlyzed[17]. This process allows determining the calibration and adjusting equations 4 and 5.

$$\rho = k_0 + k_1 c_i + k_2 c_j \tag{4}$$

$$n = k_0' + k_1' c_i + k_2' c_j \tag{5}$$

Table 1 shows the values for the constants of the two calibration planes of the five ternary mixtures analyzed in this study. In addition, in Fig. 1 and Fig. 2 the calibration planes constructed for the density and the refractive index for one of the mixtures studied can be seen.

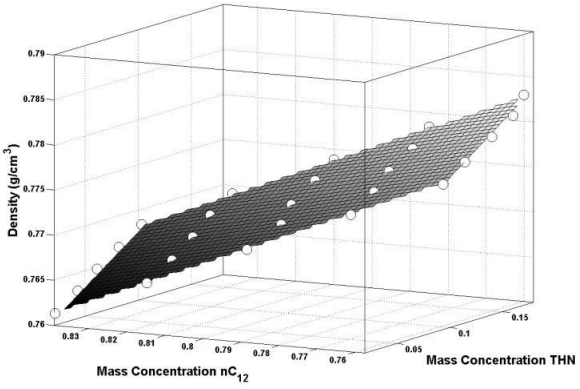


FIG. 1. Calibration plane of density for the mixture THN-IBB-*n*$C_{12}$ at mass concentration of 0.10-0.10-0.80 measured at 25 ºC.

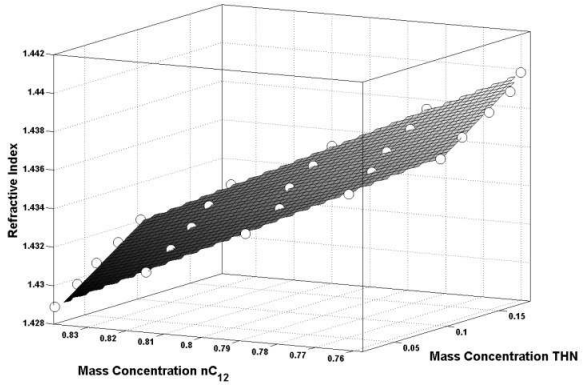


FIG. 2. Calibration plane of refractive index for the mixture THN-IBB-*n*$C_{12}$ at mass concentration of 0.10-0.10-0.80 measured at 25 ºC.

In this study three different thermogravitational columns have been used, being two of them of plane geometry and the other one of cylindrical configuration. In all these columns, the *gap* distance is of $L_x$= 1x10$^{-3}$ m. The cylindrical column and one of the plane thermogravitational columns have a height of $L_z$= 0.50 m, while this distance for the last plane column is of $L_z$= 0.98x10$^{-3}$ m. The width of the gap for both plane thermogravitational columns is of $L_y$= 5x10$^{-2}$ m.

C. Empirical Correlation

The experimental results obtained for the thermodiffusion coefficient in ternary mixtures have been compared with the ones deduced with two different correlations. One of these correlations is the one developed in Ref. 17. This correlation gives the chance of calculating the thermodiffusion coefficient of the components of hydrocarbon ternary mixtures at any concentration using the data of the kinematic viscosity, thermal expansion coefficient and concentration of the components of the ternary mixture as well as the kinematic viscosity, thermal expansion coefficient and thermodiffusion coefficient of the corresponding binary mixtures. This correlation is written as:

$$\mathcal{D}_T^i \frac{\nu_i}{\alpha_i} = D_T^{ij} c_i c_j \frac{\nu_{ij}}{\alpha_{ij}} + D_T^{ik} c_i c_k \frac{\nu_{ik}}{\alpha_{ik}} \tag{6}$$

Additionally, and with the aim of verifying the previous expression, the thermodiffusion coefficients of the analyzed mixtures have also been calculated using equation 7, which was developed by Larre *et el*.[22]. Note that this correlation was used as a starting point for the development of equation 6.

$$\mathcal{D}_T^i = D_T^{ij} c_i c_j + D_T^{ik} c_i c_k \tag{7}$$

III. RESULTS AND DISCUSSION

A. Studied Mixtures

Five ternary mixtures at different mass concentrations of the components tetrahydronaphthalene (THN), isobutylbenzene (IBB) y *n*-dodecane ($nC_{12}$) have been studied. Additionally, the properties of the corresponding binary mixtures have been also analyzed. In Table 2 the 20 binary and ternary mixtures analyzed and their concentrations are listed.

B. Binary Mixtures

Table 3 shows both the results obtained for the thermophysical properties and the thermodiffusion coefficient at a temperature of 25 ºC for the binary mixtures analyzed. The results presented for the thermodiffusion coefficient correspond to the mean values of the results obtained with both thermogravitational columns.

For the three mixtures analyzed, THN-IBB, THN-$nC_{12}$ and IBB-$nC_{12}$, the thermodiffusion coefficient at 13 concentrations and at T=25 ºC has been determined. In Fig. 3 it can be appreciated a linear behavior of the thermodiffusion coefficient in function of the concentration of the denser component. It must be noticed that the thermodiffusion coefficient for the mixture THN-$nC_{12}$ is almost constant in the whole range of concentration, while in the case of IBB-$nC_{12}$ mixture, this coefficient increases in function of the concentration of the denser component (IBB). In the case of THN-IBB mixture, the thermodiffusion coefficient decreases in function of the concentration of the denser component (THN).

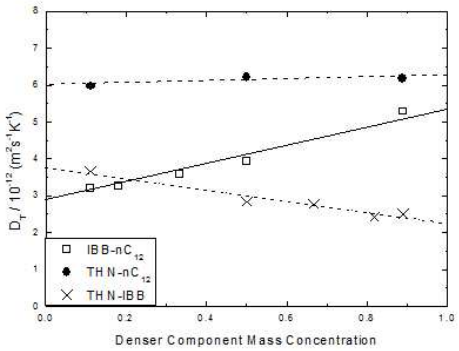


FIG. 3. Thermodiffusion coefficient values for (□) IBB-*n*$C_{12}$, (•) THN-*n*$C_{12}$ and (x) THN-IBB binary mixture at 25 ºC in the whole range of concentration.

C. Ternary Mixtures

The results obtained for the density, the thermal expansion coefficient and the dynamic viscosity in the ternary mixtures are shown in Table 4. This table also shows the results for the thermodiffusion coefficient for these mixtures. For the determination of the thermodiffusion coefficients in ternary mixtures two plane thermogravitational columns have been used. During the analysis of the extracted samples in the experiments using the shorter column, it has been checked that the separation of the components inside the column for some concentrations in the ternary mixtures is smaller, what makes the analysis process in these mixtures very sensitive compared to the case of binary mixtures.

Additionally, it has been seen how, for these kinds of mixtures, the calibration process becomes very important. Up to some point, a linear behavior of the density and the refractive index in function of the concentration has been observed. The higher this linear behavior, the more difficult becomes the process to determine the concentration of the components in the

ternary mixtures by the data of the calibration adjust. A similar behavior had already been seen in ref. 25, where it was seen that some certain concentrations of the components were better than others for the measurement of separation of the components by optical techniques.

For this reason and with the aim of improving the sensibility in the lecture of the concentration in the stationary state from the data of the density and the refractive index of the mixtures, a new longer plane thermogravitational column has been constructed. The fact of being longer makes the separation of the components inside the column to increase (it is almost twice: 1.96), increasing at the same time the sensibility of the measurement process. This new column has been validated by binary mixtures of the Benchmark of Fontainebleau[15]. For all the mixtures analyzed the error found has been below 5%, so this way one can say that this new column is validated.

Once this column has been validated, the measurements on the ternary mixtures analyzed in this study were repeated. This new measurements show that the quality of the results obtained with this new column improves, but the differences with the shorter column are not significant. Taking into account these results and considering the influence of the calibration process on the measurements, it can be concluded that for this mixtures, and with the actual experimental procedures, an experimental error better than 10% cannot be obtained. In Table 4, the mean value of the thermodiffusion coefficients of each component measured with both columns are presented.

The obtained results show how, for the analyzed cases, the denser component (THN), migrates to the cold wall, while the lighter component ($n$C$_{12}$) goes towards the warm wall. With the aim of analyzing the influence of the concentration of the components of the mixture in the thermodiffusion coefficient, figure 4 and figure 5 show the results obtained for this coefficient

for THN and nC12 components in function of concentration. This figures show how the thermodiffusion coefficient has a maximum values when the concentration of the three components of the mixture is similar.

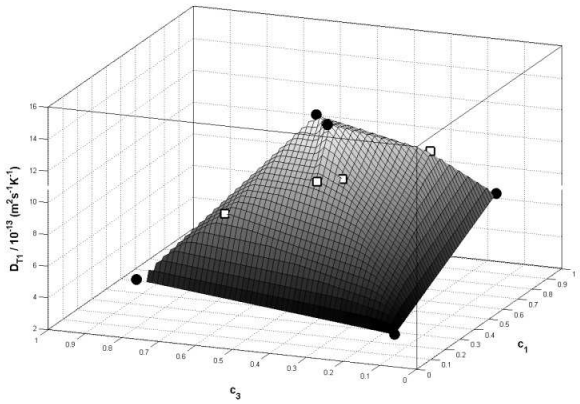


FIG. 2. Thermodiffusion coefficient of component 1 (THN) in function of the mass concentration of components 1 (THN) and 3 ($n$C$_{12}$) for the ternary mixture THN-IBB-$n$C$_{12}$ in the whole range of concentration at 25 ºC. "•" Data from this work; "□"Data from Ref. [17].

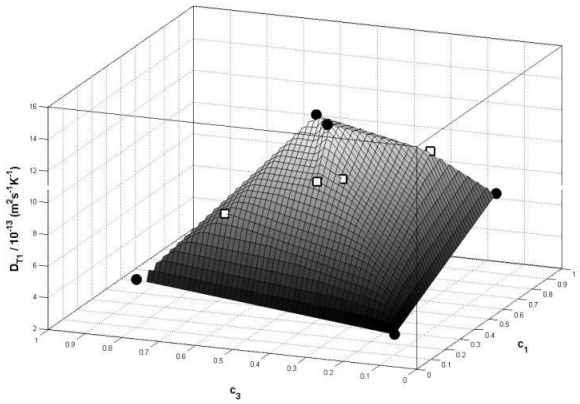


FIG. 3. Thermodiffusion coefficient of component 3 (THN) in function of the mass concentration of components 1 (THN) and 3 ($n$C$_{12}$) for the ternary mixture THN-IBB-$n$C$_{12}$ in the whole range of concentration at 25 ºC. "•" Data from this work; "□"Data from Ref. [17].

The obtained experimental data for the thermodiffusion coefficient can be compared with the ones calculated with the correlations developed in Ref. 17 and Ref. 22. Table 5 shows a comparison between the obtained experimental data and the one calculated using these correlations. It can be observed that the agreement between the experimental data and the calculated ones is good, with differences around 10 %. Nevertheless, a slight improvement in the data obtained with the correlation in ref. 17 is observed, while the expression developed in ref. 22, on the other side, is simpler, as does not need the data of the viscosity and the thermal expansion coefficient of the analyzed mixtures.

## IV. CONCLUSIONS

In this work the thermodiffusion coefficient and the thermophysical properties (density, viscosity, thermal expansion coefficient and mass expansion coefficient) of 20 mixtures, both binary and ternary mixtures, of the tetrahydronaphthalene, isobutylbenzene and *n*-dodecane compounds at different concentrations and a mean temperature of 25 ºC have been determined.

In the measurements carried out in the binary mixtures it has been checked how the thermodiffusion coefficient is influenced by the concentration of the components in the mixture.

In the case of ternary mixtures, the thermodiffusion coefficient of the components of these mixtures has been determined, and it has been observed that the thermodiffusion coefficient in ternary mixtures has its maximum value in the region where the concentrations of the three components of the mixture are similar.

To finish with, the good agreement between the data for the thermodiffusion coefficient of each component at different concentrations obtained experimentally and the ones obtained using

the correlations developed in Ref. 17 and Ref. 22, which used the data of the binary mixtures, has been checked. It has been observed that the obtained differences are around 10 %.

## V. ACKNOWLEDGMENT

This article presents results that were partly obtained in the framework of the following projects: GOVSORET3 (PI2011-22) and Research Groups (IT557-10) of Basque Government, and DCMIX from the European Space Agency.

REFERENCES

[1] C. Soret. Au point de vue de sa concentration une dissolution saline primitevement homogéne dont deux parties sont portées a des temepératures différentes. Archives des Sciences Physiques et Naturelles de Geneve, 2, 1879, 48-61.

[2] C. Soret. Influence de la température sur la distribution des sels dans leurs solutions. C. R. Academie Scientifique, 91, 1880, 289-290.

[3] C. Soret. Sur l´etat déquilibre que pend, au point de vue de sa concentration, une dissolution saline primitivement homogéne don't deux parties sont portées á des températures différentes. Annales de chimie et physique, 22, 1881, 293-297.

[4] C. Ludwig. Diffusion zwischen ungleich erwärmten orten gleich zusammengesetzter. Sitz. Ber. Akad. Wiss. Wien Math.-Naturw. Kl, 20, 1856, 539.

[5] F. Montel. Importance de la thermodiffusion en esploration et production pétroliéres. Entropie, 185, 1994, 86-93.

[6] S. Van Vaerenbergh, A. Shapiro, G. Galliero, F. Montel, J.C. Legros, J.P. Caltagarione, J.L. Darion and Z. Saghir. Multicomponent processes in crudes. European Space Agency, Special Publication, ESA SP, 1290, 2005, 202-213.

[7] H. Nasrabadi, A. Firoozabadi and T. Ahmed. Complex flow and composition path in CO2 injection schemes from density effects in 2 and 3D. SPE Annual Technical Conference and Exhibition, 2009.

[8] F. Montel, J. Bickert, A. Lagisquet and G. Galliero. Initial state of petroleum reservoirs: A comprehensive approach. Journal of Petroleum Science and Engineering, 58, 2007, 391-402.

[9] M. Touzet, G. Galliero, V. Lazzeri, M.Z. Saghir, F. Montel and J.C. Legros. Thermodiffusion: From microgravity experiments to the initial state of petroleum, Comptes Rendus Mecanique, 339, 2011, 318-323.

[10] A. Abbasi, M.Z. Saghir and M. Kawaji. Theoretical and experimental comparison of the Soret effect for binary mixtures of toluene and n-hexane, and benzene and n-heptane. Journal of Non-Equilibrium Thermodynamics. 35, 2010, 1-14.

[11] Y. Leroyer and A. Würger. Soret motion in non-ioninc binary molecular mixtures. Journal of Chemical Physics. 135, 2011, 054107.

[12] P. Blanco, M.M. Bou-Ali, J.K. Platten, J.A. Madariaga, P. Urteaga and C. Santamaría. Thermodiffusion Coefficient for Binary Liquid Hydrocarbon Mixtures. J. Non-Equilib. Thermodyn., 32, 2007, 309-317.

[13] P. Polyakov, M. Zhang, F. Müller-Plathe and S. Wiegand. Thermal diffusion measurements and simulations of binary mixtures of spherical molecules. Journal of Chemical Physics, 127, 2007, 014502.

[14] A. Mialdun, V. Yasnou, V. Shevtsova, A. Königer, W. Köhler, D. Alonso de Mezquia and M.M. Bou-Ali. A comprehensive Study of diffusion, thermodiffusion and Soret coefficients of Water-Isopropanol Mixtures.

[15] J.K. Platten, M.M. Bou-Ali, P. Costeséque, J.F. Dutrieux, W. Köhler, c. Leppla, S. Wiegand and G. Wittko. Benchmark values for the Soret, thermal diffusion and diffusion coefficients of three binary organic liquid mixtures. Philosophical Magazine, 83, 2003, 1965-1971.

[16] S. Van Vaerenbergh, S Srinivasan and M.Z. Saghir. Thermodiffusion in multicomponent hydrocarbon mixtures: experimental investigations and computational analysis. Journal of Chemical Physics, 131, 2009, 114505.

[17] P. Blanco, M.M. Bou-Ali, J.K. Platten, D. A. De Mezquia, J.A. Madariaga and C. Santamaría. Thermodiffusion coefficients of binary and ternary hydrocarbon mixtures. Journal of Chemical Physics, 132, 2010.

[18] M.M. Bou-Ali and J.K. Platten. Metrology of the thermodiffusion coefficients in a ternary system. Journal of Non-equilibrium thermodynamics, 30, 2005, 385-399.

[19] A. Leahy-Dios, M.M. Bou-Ali, j.K. Platten and A. Firoozabadi. Measurements of molecular and thermal diffusion coefficients in ternary mixtures. Journal of Chemical Physics, 122, 2005, 234502.1-234502.12.

[20] S. Srinivasan and M.Z. Saghir. Experimental data on thermodiffusion in ternary hydrocarbon mixtures. Journal of Chemical Physics, 134, 2009, 114505.

[21] A. Königer, H. Wunderlich and W. Köhler. Measurement of diffusion and thermal diffusion in ternary fluid mixtures using a two-color optical beam deflection technique. J. Chem. Phys., 132, 2010, 174506.

[22] J. Larre, J.K. Platten and G. Chavepeyer, Soret Effects in Ternary Systems Heated from Below .International Journal of Heat and Mass Transfer, 40, 1997, 545-555.

[23] W.H. Furry, R,C. Jones and L. Onsager. On the theory of isotope separation by thermal diffusion. Physical Review E, 55, 1939, 1083-1095.

[24] S.D. Majumdar. The theory of the separation of isotopes by thermal diffusion. Physical Review E. 81, 1951, 844-848.

[25] V. Shevtsova, V. Sechenyh, A. Nepomnyashchy and J.C. Legros. Analysis of the application of optical two-wavelength techniques to measurement of the Soret coefficients in ternary mixtures. Philosophical Magazine, 91 (26), 2011, 3498-3518.

**Table 1.** Coefficients of the calibration planes of the studied ternary mixtures.

| Mixture | $c_1$ | $c_3$ | $k_0$ (kg/m$^3$) | $k_1$ (kg/m$^3$) | $k_2$ (kg/m$^3$) | $k_0^{`}$ | $k_1^{`}$ | $k_2^{`}$ |
|---|---|---|---|---|---|---|---|---|
| THN-IBB-$n$C$_{12}$ | 0.1000 | 0.8000 | 0.849052 | 0.105245 | -0.122807 | 1.483803 | 0.048842 | -0.077341 |
| | 0.1000 | 0.1000 | 0.838380 | 0.089227 | -0.094189 | 1.476349 | 0.040406 | -0.056139 |
| | 0.4000 | 0.4000 | 0.848077 | 0.102365 | -0.116189 | 1.482923 | 0.047269 | -0.071804 |
| | 0.4500 | 0.4500 | 0.847995 | 0.101875 | -0.115505 | 1.483093 | 0.046719 | -0.071311 |
| | 0.8000 | 0.1000 | 0.848940 | 0.105608 | -0.121782 | 1.483748 | 0.049959 | -0.076553 |

**Table 2.** Mass concentration of each component in the ternary mixtures studied and their corresponding binary mixtures.

| Mixture | Mass Concentration | | |
|---|---|---|---|
| | **THN** | **IBB** | ***n*C$_{12}$** |
| I | 0.1000 | 0.1000 | 0.8000 |
| I.1 | 0.5000 | 0.5000 | 0 |
| I.2 | 0.1111 | 0 | 0.8888 |
| I.3 | 0 | 0.1111 | 0.8888 |
| II | 0.1000 | 0.8000 | 0.1000 |
| II.1 | 0.1111 | 0.8888 | 0 |
| II:2 | 0.5000 | 0 | 0.5000 |
| II.3 | 0 | 0.8888 | 0.1111 |
| III | 0.8000 | 0.1000 | 0.1000 |
| III.1 | 0.8888 | 0.1111 | 0 |
| III.2 | 0.8888 | 0 | 0.11111 |
| III.3 | 0 | 0.5000 | 0.5000 |
| IV | 0.4500 | 0.1000 | 0.4500 |
| IV.1 | 0.8181 | 0.1818 | 0 |
| IV.2 | 0.5000 | 0 | 0.5000 |
| IV.3 | 0 | 0.1818 | 0.8181 |
| V | 0.4000 | 0.2000 | 0.4000 |
| V.1 | 0.6666 | 0.3333 | 0 |
| V.2 | 0.5000 | 0 | 0.5000 |
| V.3 | 0 | 0.3333 | 0.6666 |

**Table 3.** Results on the thermophysical properties and thermodiffusion coefficient at 25 ºC for the binary mixtures studied.

| **Mixture** | **Mass Concentration** $c_i$ | **ρ** **(kg/m$^3$)** | **α /10$^{-3}$** **K$^{-1}$** | **β** | **μ** **mPa·s** | $D_T$ **/10$^{-12}$** **m$^2$s$^{-1}$K$^{-1}$** |
|---|---|---|---|---|---|---|
| THN-IBB | 0.1111 | 861.007 | 9.433 | 0.129 | 1.054 | 3.66 |
| | 0.5000 | 904.514 | 8.876 | 0.128 | 1.363 | 2.84 |
| | 0.6666 | 924.032 | 8.630 | 0.129 | 1.500 | 2.77 |
| | 0.8181 | 942.275 | 8.442 | 0.131 | 1.729 | 2.43 |
| | 0.8889 | 951.097 | 8.347 | 0.130 | 1.813 | 2.50 |
| THN-$n$C$_{12}$ | 0.1111 | 764.580 | 9.561 | 0.236 | 1.380 | 5.97 |
| | 0.5000 | 842.241 | 8.950 | 0.257 | 1.502 | 6.21 |
| | 0.8889 | 934.359 | 8.368 | 0.287 | 1.815 | 6.18 |
| IBB-$n$C$_{12}$ | 0.1111 | 754.940 | 9.694 | 0.119 | 1.288 | 3.20 |
| | 0.1818 | 761.368 | 9.678 | 0.121 | 1.223 | 3.28 |
| | 0.3333 | 775.664 | 9.641 | 0.125 | 1.165 | 3.58 |
| | 0.5000 | 792.355 | 9.612 | 0.130 | 1.108 | 3.93 |
| | 0.8889 | 835.454 | 9.590 | 0.144 | 1.008 | 5.28 |

**Table 4.** Results on the thermophysical properties and thermodiffusion coefficient at 25 ºC for the ternary mixtures studied.

| Mixture | $c_1$ | $c_3$ | ρ (kg/m$^3$) | α /10$^{-3}$ K$^{-1}$ | μ mPa·s | $D_T^1$ /10$^{-13}$ m$^2$s$^{-1}$K$^{-1}$ | $D_T^3$ /10$^{-13}$ m$^2$s$^{-1}$K$^{-1}$ |
|---|---|---|---|---|---|---|---|
| THN-IBB-*n*C$_{12}$ | 0.1000 | 0.8000 | 771.944 | 9.542 | 1.314 | 5.01 | -7.75 |
| | 0.1000 | 0.1000 | 847.553 | 9.470 | 1.053 | 3.31 | -4.84 |
| | 0.4000 | 0.4000 | 842.524 | 9.054 | 1.266 | 13.84 | -14.70 |
| | 0.4500 | 0.4500 | 841.822 | 9.004 | 1.440 | 14.03 | -14.76 |
| | 0.8000 | 0.1000 | 924.348 | 8.483 | 1.719 | 7.72 | -5.39 |

**Table 5.** Comparison between the experimental data and the one determined using equations 6 and 7.

| Mixture | $c_1$ | $c_3$ | $D_T^1$ /$10^{-12}$ $m^2s^{-1}K^{-1}$ | | | | | $D_T^3$ /$10^{-12}$ $m^2s^{-1}K^{-1}$ | | | | |
|---|---|---|---|---|---|---|---|---|---|---|---|---|
| | | | **Exp.** | **Eq. 6** | **δ(%)** | **Eq. 7** | **δ(%)** | **Exp.** | **Eq. 6** | **δ(%)** | **Eq. 7** | **δ(%)** |
| THN-IBB-$n$C$_{12}$ | 0.1000 | 0.8000 | 5.01 | 5.32 | 5.74 | 5.06 | 0.91 | -7.75 | -7.65 | -1.33 | -7.41 | -4.60 |
| | 0.1000 | 0.1000 | 3.31 | 3.84 | 13.65 | 3.55 | 6.55 | -4.84 | -5.00 | 3.19 | -4.85 | -0.19 |
| | 0.4000 | 0.4000 | 13.84 | 14.46 | 4.26 | 12.16 | -13.86 | -14.70 | -14.63 | -0.51 | -12.80 | -14.86 |
| | 0.4500 | 0.4500 | 14.03 | 14.47 | 3.03 | 13.67 | -2.60 | -14.76 | -14.50 | -1.77 | -14.05 | -5.04 |
| | 0.8000 | 0.1000 | 7.72 | 7.17 | -7.67 | 6.88 | -12.09 | -5.39 | -5.50 | 2.09 | -5.34 | -0.94 |

# Apéndice K

# Resultados en los ensayos mediante las Columnas Termogravitacionales para la Mezcla Ternaria THN-IBB-$nC_{12}$

| Mezcla | C. masica. | C. molar | Tª media | DT (ºC) | Tiempo |
|---|---|---|---|---|---|
| THN-IBB-$C_{12}$ | 0,1000 | | 25º | 5,7 | 25h |

| | |
|---|---|
| Tª bainu hotza | 21,7 |
| Tªbainu beroa | 28,7 |
| Tª arriba hotza | 22,4 |
| Tª abajo hotza | 22 |
| Tª arriba beroa | 27,7 |
| Tª abajo beroa | 28,1 |
| TªGAPhotza | 22,2 |
| TªGAPberoa | 27,9 |
| $\Delta$Tª | 5,70 |
| Tªmedia | 25,05 |
| $\Delta$Tª vertical hotza | 0,4 |
| $\Delta$Tª vertical beroa | -0,4 |

| Medidas Columna | |
|---|---|
| Longitud (cm) | 98 |
| Ancho (cm) | 5 |
| gap (cm.) | 0,10 |

| Calibración | |
|---|---|
| a | 0,838380235 |
| b | 0,089226696 |
| c | -0,094188936 |
| a' | 1,47634910 |
| b' | 0,040405754 |
| c' | -5,76E-02 |

| | |
|---|---|
| T. Relajación (s.): | 29218 |
| T. Equilibrio (min): | **2434,8** |
| T. Equilibrio (h): | **40,6** |
| D | 1,00E-09 |

| | | | |
|---|---|---|---|
| Viscosidad cin. | 1,70E-03 | | |
| gap | 1,0E-03 | | |
| Gravedad | 9,81 | | |
| $C_0$ | 0,1000 | | |
| Densidad Inicial | 0,771989 | | |
| nD Inicial | 1,434378 | | |
| Alfa | 9,54E-04 | | |
| Viscosidad Din. | 1,314E-03 | | |
| Pendiente c/z | -0,0419911 | 0,0612661 | -0,019275 |
| Delta c | -0,041151278 | 0,060040778 | -0,0188895 |
| ***$D_T$*** | ***5,259E-13*** | ***-7,673E-13*** | ***2,414E-13*** |

| Tomas | Altura toma (cm) | Cantidad (c.c.) | Altura real (m) | Densidad (g/cm$^3$) | nD | THN c | $C_{12}$ c | IBB c |
|---|---|---|---|---|---|---|---|---|
| 1ª | 75,4 | 4 | 0,7926 | 0,76899 | 1,432711 | 0,084185194 | 0,816463214 | 0,099351593 |
| 2ª | 57,8 | 4,1 | 0,6176 | 0,770574 | 1,433583 | 0,091022822 | 0,806123347 | 0,102853831 |
| 3ª | 40,2 | 4,2 | 0,4426 | 0,772249 | 1,434500 | 0,098612826 | 0,795530075 | 0,1058571 |
| 4ª | 22,6 | 4 | 0,2646 | 0,773932 | 1,435418 | 0,106477543 | 0,785112108 | 0,108410349 |
| 5ª | 5 | 4,2 | 0,0906 | 0,775672 | 1,436385 | 0,113345005 | 0,773144258 | 0,113510737 |

NOTAS:

$$\rho = a + cTHN \times b + cC_{12} \times c$$
$$n = a' + cTHN \times b' + cC_{12} \times c'$$

THN-IBB-C12 c=10-10-80

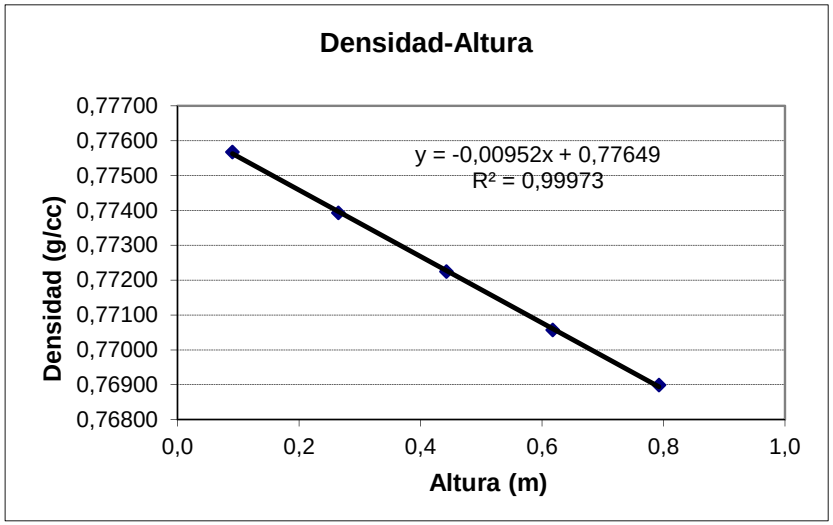


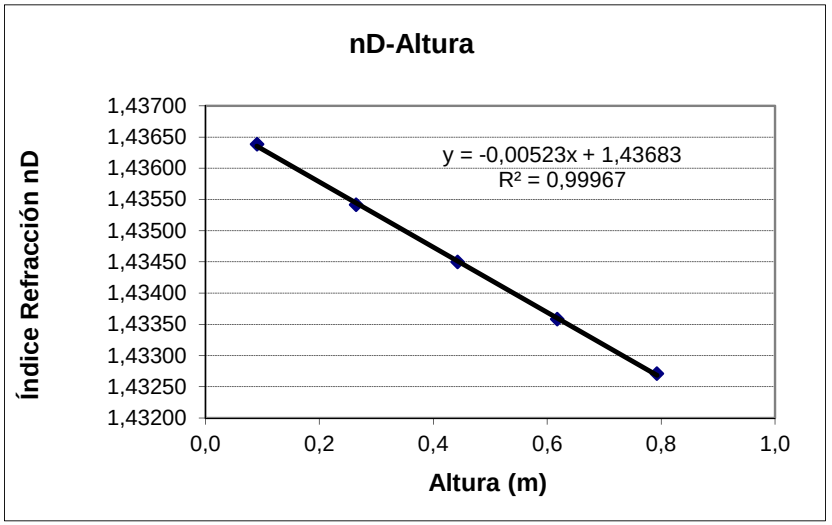


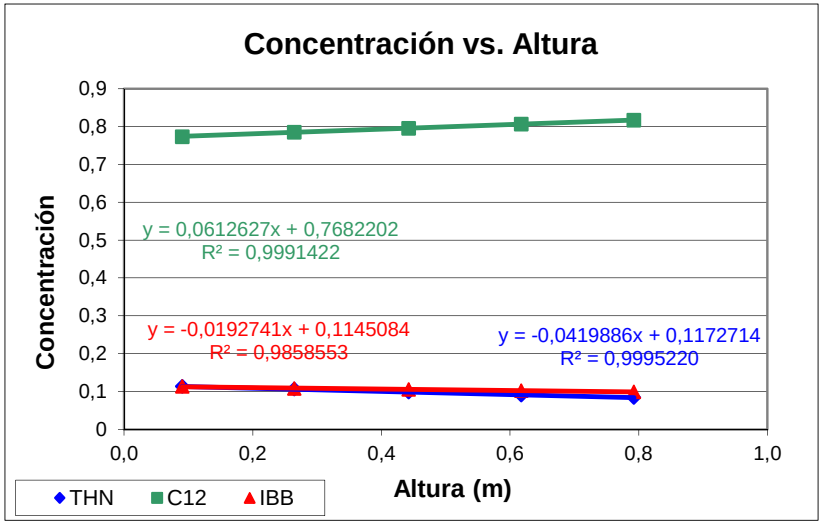

| Mezcla | C. masica. | C. molar | Tª media | DT (ºC) | Tiempo |
|---|---|---|---|---|---|
| THN-IBB-$C_{12}$ | 0,1000 | | 25º | 5,7 | 45h 15` |

| | |
|---|---|
| T. Relajación (s.): | 29225 |
| T. Equilibrio (min): | 2435 |
| T. Equilibrio (h): | **40,6** |
| D | 1,00E-09 |

| | |
|---|---|
| Tª bainu hotza | 21,7 |
| Tªbainu beroa | 28,7 |
| Tª arriba hotza | 22,4 |
| Tª abajo hotza | 22 |
| Tª arriba beroa | 27,7 |
| Tª abajo beroa | 28,1 |
| TªGAPhotza | 22,2 |
| TªGAPberoa | 27,9 |
| $\Delta T^a$ | 5,70 |
| Tªmedia | 25,05 |
| $\Delta T^a$ vertical hotza | 0,4 |
| $\Delta T^a$ vertical beroa | -0,4 |

| Medidas Columna | |
|---|---|
| Longitud (cm) | 98 |
| Ancho (cm) | 5 |
| gap (cm.) | 0,10 |

| Calibración | |
|---|---|
| a | 0,838380235 |
| b | 0,089226696 |
| c | -0,094188936 |
| a' | 1,47634910 |
| b' | 0,040405754 |
| c' | -5,76E-02 |

| | | | |
|---|---|---|---|
| Viscosidad cin. | 1,70E-03 | | |
| gap | 1,0E-03 | | |
| Gravedad | 9,81 | | |
| $C_0$ | 0,1000 | | |
| Densidad Inicial | 0,771897 | | |
| nD Inicial | 1,434324 | | |
| Alfa | 9,54E-04 | | |
| Viscosidad Din. | 1,314E-03 | | |
| Pendiente c/z | -0,0443455 | 0,064034 | -0,0196885 |
| Delta c | -0,04345859 | 0,06275332 | -0,01929473 |
| ***$D_T$*** | ***5,554E-13*** | ***-8,019E-13*** | ***2,466E-13*** |

| Tomas | Altura toma (cm) | Cantidad (c.c.) | Altura real (m) | Densidad ($g/cm^3$) | nD | THN c | $C_{12}$ c | IBB c |
|---|---|---|---|---|---|---|---|---|
| 1ª | 75,4 | 4,1 | 0,7936 | 0,768768 | 1,432600 | 0,082435792 | 0,817162942 | 0,100401266 |
| 2ª | 57,8 | | | | | 67,98377718 | 73,30317438 | -140,2869516 |
| 3ª | 40,2 | 4,1 | 0,4416 | 0,772223 | 1,434494 | 0,097914039 | 0,795144144 | 0,106941817 |
| 4ª | 22,6 | 3,9 | 0,2637 | 0,774006 | 1,435474 | 0,105720087 | 0,783608902 | 0,110671011 |
| 5ª | 5 | 4,1 | 0,0896 | 0,775815 | 1,436467 | 0,11373102 | 0,77199171 | 0,11427727 |

NOTAS:

$$\rho = a + cTHN \times b + cC_{12} \times c$$
$$n = a' + cTHN \times b' + cC_{12} \times c'$$

THN-IBB-C12 c=10-10-80

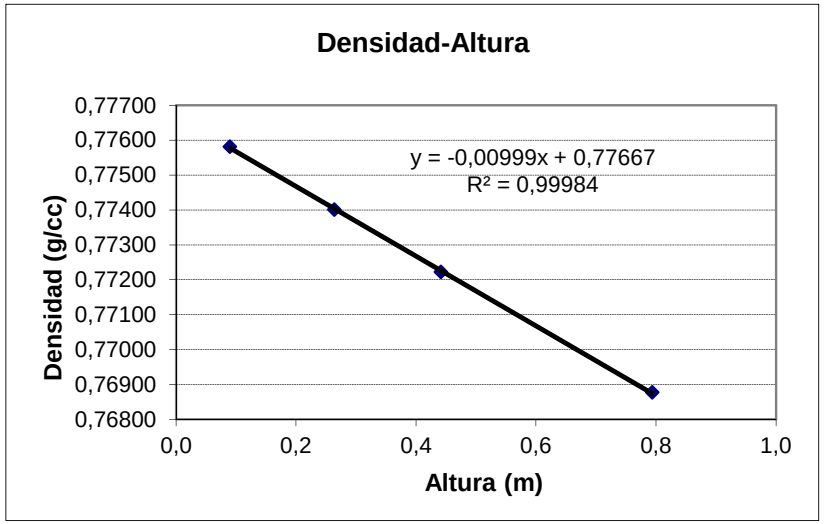


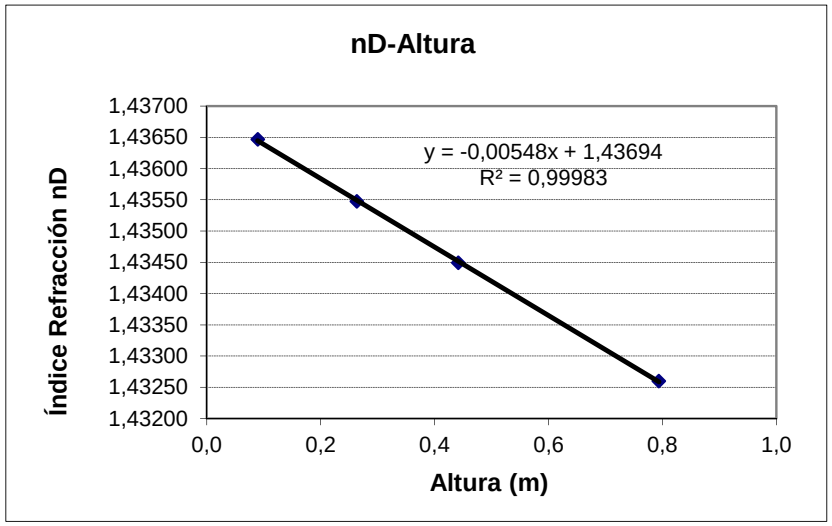


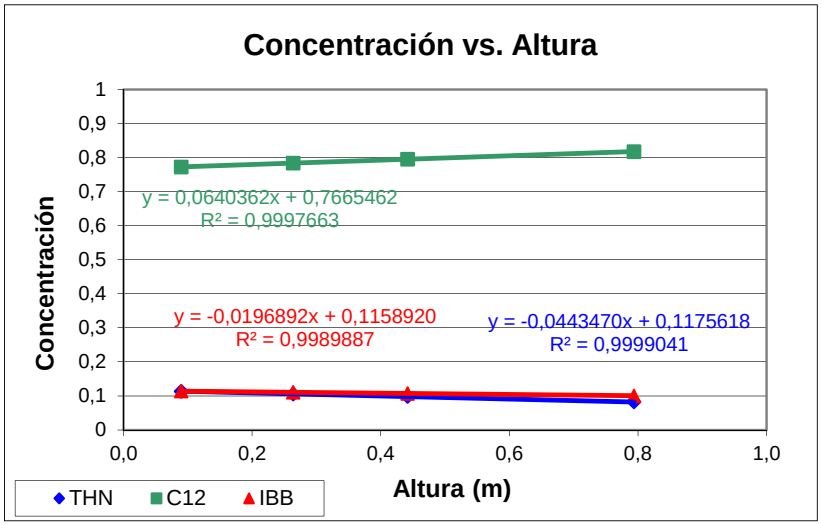

| Mezcla | C. masica. | C. molar | Tª media | DT (ºC) | Tiempo |
|---|---|---|---|---|---|
| THN-IBB-$C_{12}$ | 0,1000 | | 25º | 5,0 | 5h |

| | |
|---|---|
| T. Relajación (s.): | 12400 |
| T. Equilibrio (min): | 1033 |
| T. Equilibrio (h): | **17,2** |
| D | 1,00E-09 |

| | |
|---|---|
| Tª bainu hotza | 22 |
| Tªbainu beroa | 28 |
| Tª arriba hotza | 22,6 |
| Tª abajo hotza | 22,4 |
| Tª arriba beroa | 27,4 |
| Tª abajo beroa | 27,5 |
| TªGAPhotza | 22,5 |
| TªGAPberoa | 27,5 |
| ΔTª | 4,95 |
| Tªmedia | 24,98 |
| ΔTª vertical hotza | 0,2 |
| ΔTª vertical beroa | -0,1 |

| Medidas Columna | |
|---|---|
| Longitud (cm) | 50 |
| Ancho (cm) | 5 |
| gap (cm.) | 0,100 |

| Calibración | |
|---|---|
| a | 0,838380235 |
| b | 0,089226696 |
| c | -0,094188936 |
| a' | 1,47634910 |
| b' | 0,040405754 |
| c' | -5,76E-02 |

| | |
|---|---|
| Viscosidad cin. | 1,70E-03 |
| gap | 1,00E-03 |
| Gravedad | 9,81 |
| $C_0$ | 0,1000 |
| Densidad Inicial | 0,771886 |
| nD Inicial | 1,434254 |
| Alfa | 9,54E-04 |
| Viscosidad Din. | 1,314E-03 |
| Pendiente c/z | -0,0440387 |
| Delta c | -0,02201935 |
| $D_T$ | ***4,806E-13*** |

| | | |
|---|---|---|
| 0,0728411 | -0,0288024 | |
| 0,03642055 | -0,0144012 | |
| ***-7,949E-13*** | ***3,143E-13*** | |

| Tomas | Altura toma (cm) | Cantidad (c.c.) | Altura real (m) | Densidad (g/cm$^3$) | nD | THN c | $C_{12}$ c | IBB c |
|---|---|---|---|---|---|---|---|---|
| 1ª | | | | | | | | |
| 2ª | 35 | 3,8 | 0,3880 | 0,772454 | 1,434683 | 0,094548395 | 0,789503298 | 0,115948307 |
| 3ª | 25 | 3,8 | 0,2880 | 0,77354 | 1,435289 | 0,098661165 | 0,781869374 | 0,119469461 |
| 4ª | 15 | 3,7 | 0,1870 | 0,774581 | 1,435852 | 0,103865752 | 0,77574751 | 0,120386738 |
| | | | | | | | | |

NOTAS:

$$\rho = a + cTHN \times b + cC_{12} \times c$$
$$n = a' + cTHN \times b' + cC_{12} \times c'$$

THN-IBB-C12 c=10-10-80

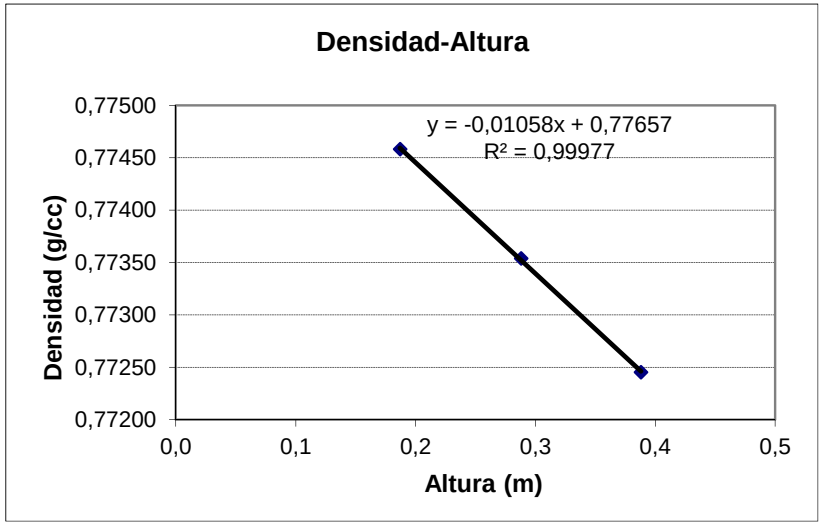


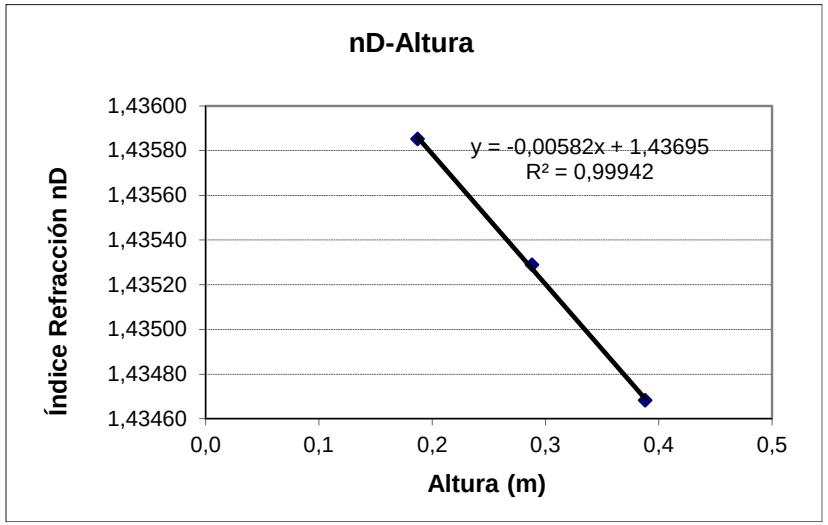


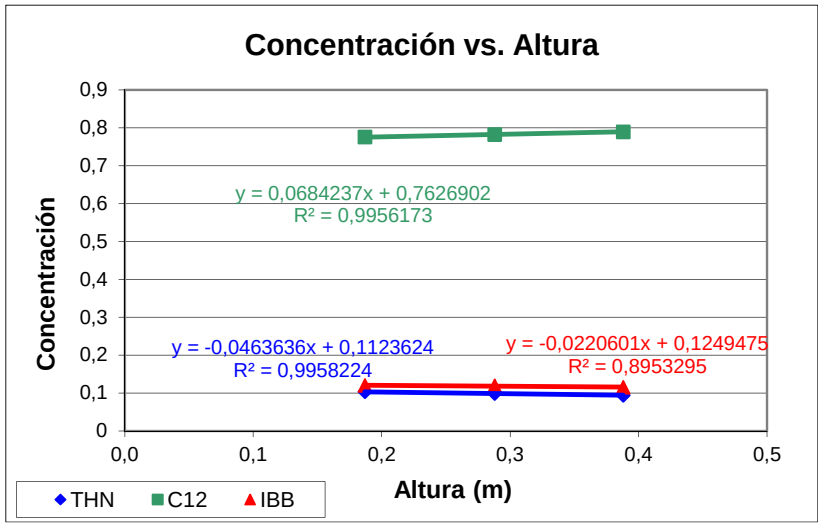

| Mezcla | C. masica. | C. molar | Tª media | DT (ºC) | Tiempo |
|---|---|---|---|---|---|
| THN-IBB-$C_{12}$ | 0,1000 | | 25º | 5,0 | 16h |

| | |
|---|---|
| T. Relajación (s.): | 12400 |
| T. Equilibrio (min): | 1033 |
| T. Equilibrio (h): | **17,2** |
| D | 1,00E-09 |

| | |
|---|---|
| Tª bainu hotza | 22 |
| Tªbainu beroa | 28 |
| Tª arriba hotza | 22,6 |
| Tª abajo hotza | 22,4 |
| Tª arriba beroa | 27,4 |
| Tª abajo beroa | 27,5 |
| TªGAPhotza | 22,5 |
| TªGAPberoa | 27,5 |
| ΔTª | 4,95 |
| Tªmedia | 24,98 |
| ΔTª vertical hotza | 0,2 |
| ΔTª vertical beroa | -0,1 |

| Medidas Columna | |
|---|---|
| Longitud (cm) | 50 |
| Ancho (cm) | 5 |
| gap (cm.) | 0,100 |

| Calibración | |
|---|---|
| a | 0,838380235 |
| b | 0,089226696 |
| c | -0,094188936 |
| a' | 1,47634910 |
| b' | 0,040405754 |
| c' | -5,76E-02 |

| | |
|---|---|
| Viscosidad cin. | 1,70E-03 |
| gap | 1,00E-03 |
| Gravedad | 9,81 |
| $C_0$ | 0,1000 |
| Densidad Inicial | 0,771886 |
| nD Inicial | 1,434254 |
| Alfa | 9,54E-04 |
| Viscosidad Din. | 1,314E-03 |
| Pendiente c/z | -0,0435332 |
| Delta c | -0,0217666 |
| $D_T$ | ***4,751E-13*** |

| | | |
|---|---|---|
| 0,067335 | -0,0238018 | |
| 0,0336675 | -0,0119009 | |
| ***-7,348E-13*** | ***2,598E-13*** | |

| Tomas | Altura toma (cm) | Cantidad (c.c.) | Altura real (m) | Densidad (g/cm$^3$) | nD | THN c | $C_{12}$ c | IBB c |
|---|---|---|---|---|---|---|---|---|
| 1ª | | | | | | | | |
| 2ª | 35 | 3,7 | 0,3870 | 0,7711 | 1,433890 | 0,092063276 | 0,801524466 | 0,106412258 |
| 3ª | 25 | 3,8 | 0,2880 | 0,772088 | 1,434434 | 0,096321033 | 0,795068353 | 0,108610614 |
| 4ª | 15 | 3,8 | 0,1880 | 0,773135 | 1,435012 | 0,100726213 | 0,788125496 | 0,111148291 |
| | | | | | | | | |

NOTAS:

$$\rho = a + cTHN \times b + cC_{12} \times c$$
$$n = a' + cTHN \times b' + cC_{12} \times c'$$

THN-IBB-C12 c=10-10-80

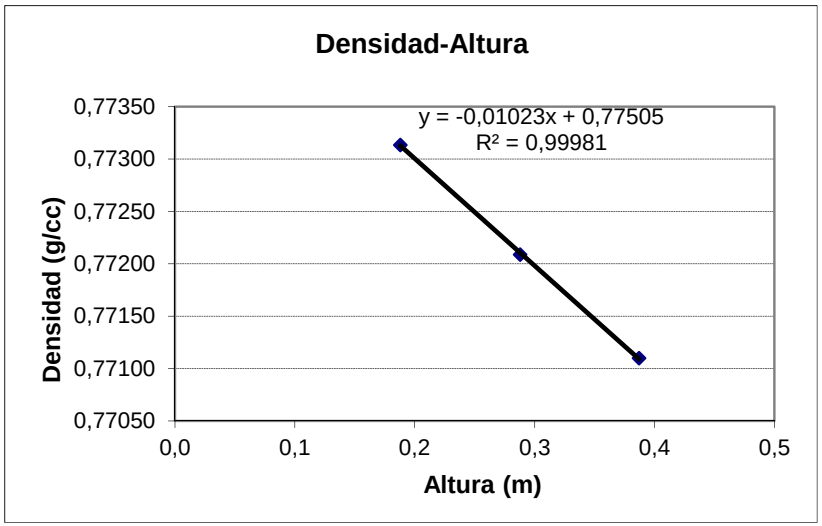


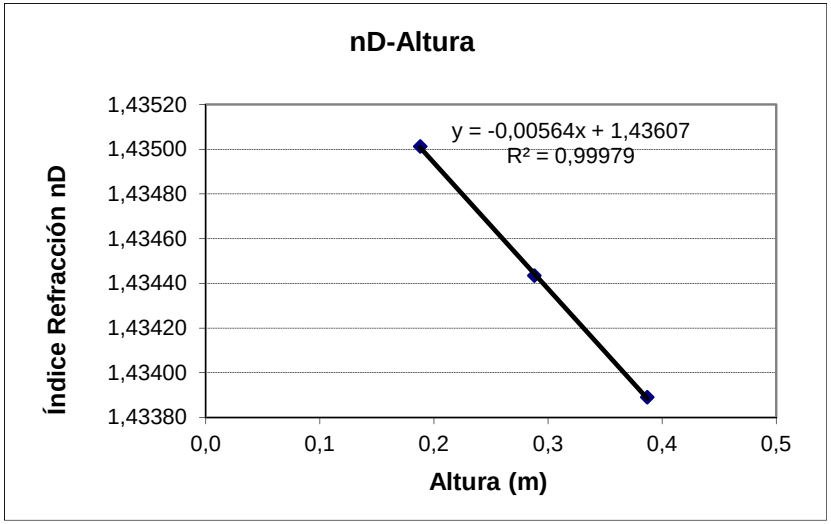


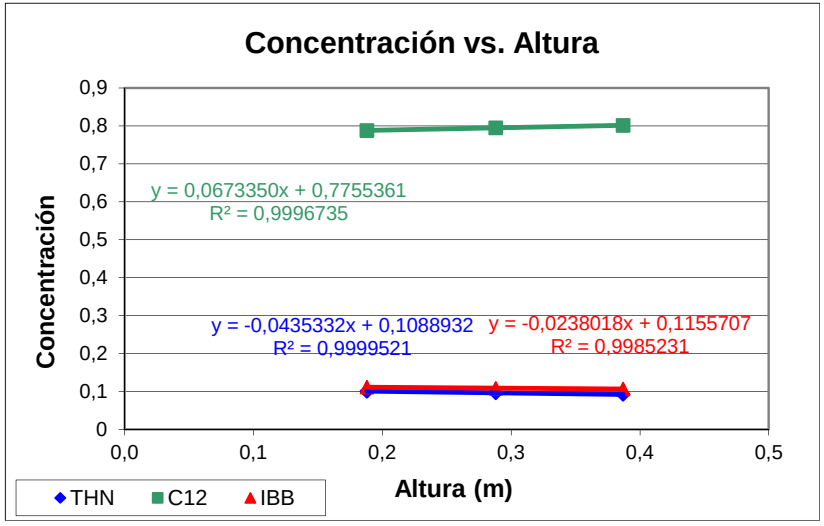

| Mezcla | C. masica. | C. molar | Tª media | DT (ºC) | Tiempo |
|---|---|---|---|---|---|
| THN-IBB-$C_{12}$ | 0,1000 | | 25º | 6,9 | 16h |

| | |
|---|---|
| T. Relajación (s.): | 6476 |
| T. Equilibrio (min): | 540 |
| T. Equilibrio (h): | **9,0** |
| D | 1,00E-09 |

| | |
|---|---|
| Tª bainu hotza | 21 |
| Tªbainu beroa | 29,3 |
| Tª arriba hotza | 21,4 |
| Tª abajo hotza | 21,7 |
| Tª arriba beroa | 28,3 |
| Tª abajo beroa | 28,5 |
| TªGAPhotza | 21,6 |
| TªGAPberoa | 28,4 |
| $\Delta T^a$ | 6,85 |
| Tªmedia | 24,98 |
| $\Delta T^a$ vertical hotza | -0,3 |
| $\Delta T^a$ vertical beroa | -0,2 |

| Medidas Columna | |
|---|---|
| Longitud (cm) | 50 |
| Ancho (cm) | 5 |
| gap (cm.) | 0,10 |

| Calibración | |
|---|---|
| a | 0,838380235 |
| b | 0,089226696 |
| c | -0,09418894 |
| a' | 1,47634910 |
| b' | 0,040405754 |
| c' | -5,76E-02 |

| | | | |
|---|---|---|---|
| Viscosidad cin. | 1,70E-03 | | |
| gap | 1,0E-03 | | |
| Gravedad | 9,81 | | |
| $C_0$ | 0,1000 | | |
| Densidad Inicial | 0,771861 | | |
| nD Inicial | 1,434251 | | |
| Alfa | 9,54E-04 | | |
| Viscosidad Din. | 1,314E-03 | | |
| Pendiente c/z | -0,0394112 | 0,0702224 | -0,0308112 |
| Delta c | -0,0197056 | 0,0351112 | -0,0154056 |
| $D_T$ | ***4,301E-13*** | ***-7,663E-13*** | ***3,362E-13*** |

| Tomas | Altura toma (cm) | Cantidad (c.c.) | Altura real (m) | Densidad (g/cm$^3$) | nD | THN c | $C_{12}$ c | IBB c |
|---|---|---|---|---|---|---|---|---|
| 1ª | | | | | | | | |
| 2ª | 35 | 3,7 | 0,3870 | 0,771625 | 1,434216 | 0,091719981 | 0,795625354 | 0,112654665 |
| 3ª | 25 | 3,7 | 0,2870 | 0,772641 | 1,434782 | 0,095633925 | 0,788546266 | 0,115819809 |
| 4ª | 15 | 3,8 | 0,1880 | 0,773641 | 1,435338 | 0,0995629 | 0,781651289 | 0,118785811 |
| | | | | | | | | |

NOTAS:

$$\rho = a + cTHN \times b + cC_{12} \times c$$
$$n = a' + cTHN \times b' + cC_{12} \times c'$$

THN-IBB-C12 c=10-10-80

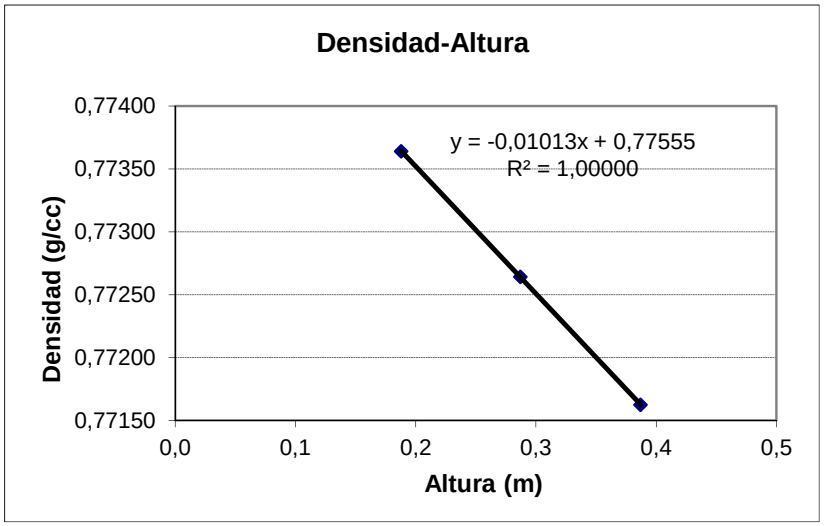


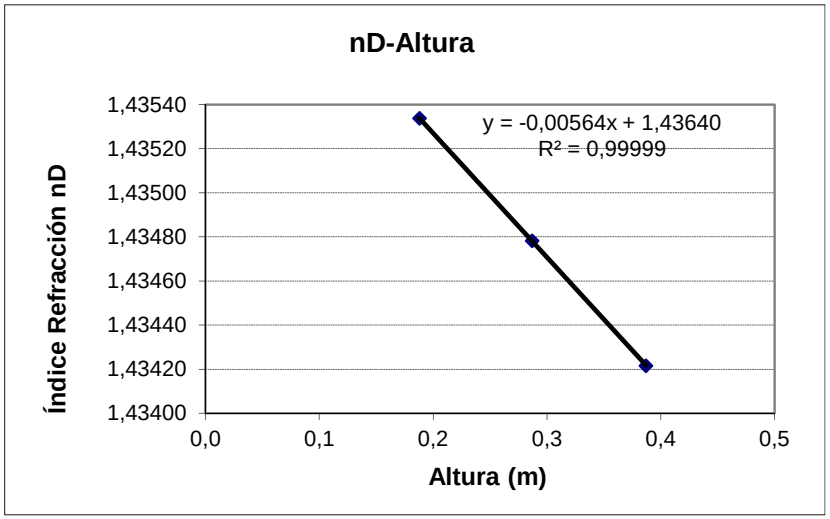


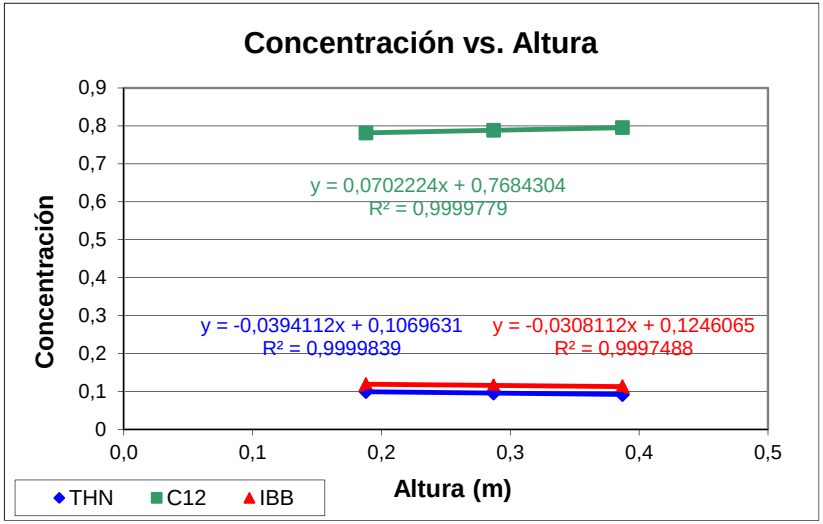

| Mezcla | C. masica. | C. molar | Tª media | DT (ºC) | Tiempo |
|---|---|---|---|---|---|
| THN-IBB-$C_{12}$ | 0,1000 | | 25º | 5,7 | 69h 45´ |

| | |
|---|---|
| T. Relajación (s.): | 15834 |
| T. Equilibrio (min): | 1319 |
| T. Equilibrio (h): | **22,0** |
| D | 1,00E-09 |

| | |
|---|---|
| Tª bainu hotza | 21,7 |
| Tªbainu beroa | 28,7 |
| Tª arriba hotza | 22,4 |
| Tª abajo hotza | 22 |
| Tª arriba beroa | 27,7 |
| Tª abajo beroa | 28,1 |
| TªGAPhotza | 22,2 |
| TªGAPberoa | 27,9 |
| ΔTª | 5,70 |
| Tªmedia | 25,05 |
| ΔTª vertical hotza | 0,4 |
| ΔTª vertical beroa | -0,4 |

| Medidas Columna | |
|---|---|
| Longitud (cm) | 98 |
| Ancho (cm) | 5 |
| gap (cm.) | 0,10 |

| Calibración | |
|---|---|
| a | 0,849052122 |
| b | 0,105244882 |
| c | -0,122806935 |
| a' | 1,48380286 |
| b' | 0,048841964 |
| c' | -7,73E-02 |

| | | | |
|---|---|---|---|
| Viscosidad cin. | 1,24E-03 | | |
| gap | 1,0E-03 | | |
| Gravedad | 9,81 | | |
| $C_0$ | 0,1000 | | |
| Densidad Inicial | 0,847223 | | |
| nD Inicial | 1,480983 | | |
| Alfa | 9,47E-04 | | |
| Viscosidad Din. | 1,053E-03 | | |
| Pendiente c/z | -0,0204043 | 0,0299735 | -0,0095692 |
| Delta c | -0,019996214 | 0,02937403 | -0,009377816 |
| $D_T$ | ***3,472E-13*** | ***-5,100E-13*** | ***1,628E-13*** |

| Tomas | Altura toma (cm) | Cantidad (c.c.) | Altura real (m) | Densidad (g/cm$^3$) | nD | THN c | $C_{12}$ c | IBB c |
|---|---|---|---|---|---|---|---|---|
| 1ª | 75,4 | 4,2 | 0,7946 | 0,845258 | 1,479866 | 0,088733071 | 0,106938778 | 0,804328151 |
| 2ª | 57,8 | 4,2 | 0,6186 | 0,846346 | 1,480492 | 0,092127672 | 0,100988499 | 0,806883829 |
| 3ª | 40,2 | 4,2 | 0,4426 | 0,847414 | 1,481093 | 0,096233582 | 0,095810664 | 0,807955754 |
| 4ª | 22,6 | 4,2 | 0,2666 | 0,848414 | 1,481658 | 0,099948132 | 0,090851151 | 0,809200718 |
| 5ª | 5 | 4,2 | 0,0906 | 0,849353 | 1,482200 | 0,102778657 | 0,085630747 | 0,811590596 |

NOTAS:

$$\rho = a + cTHN \times b + cC_{12} \times c$$
$$n = a' + cTHN \times b' + cC_{12} \times c'$$

THN-IBB-C12 c=10-80-10

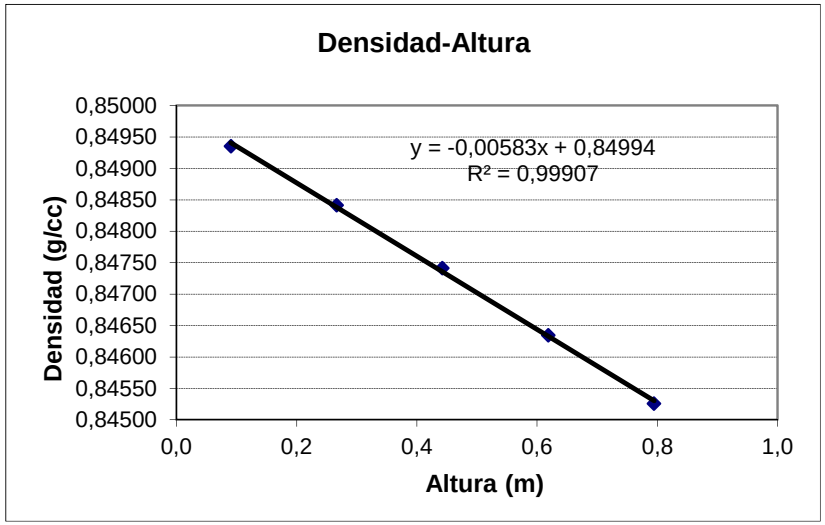


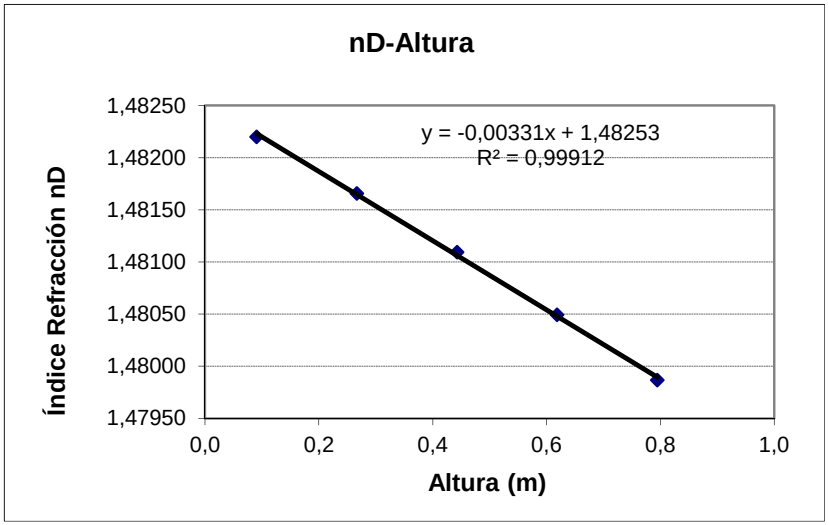


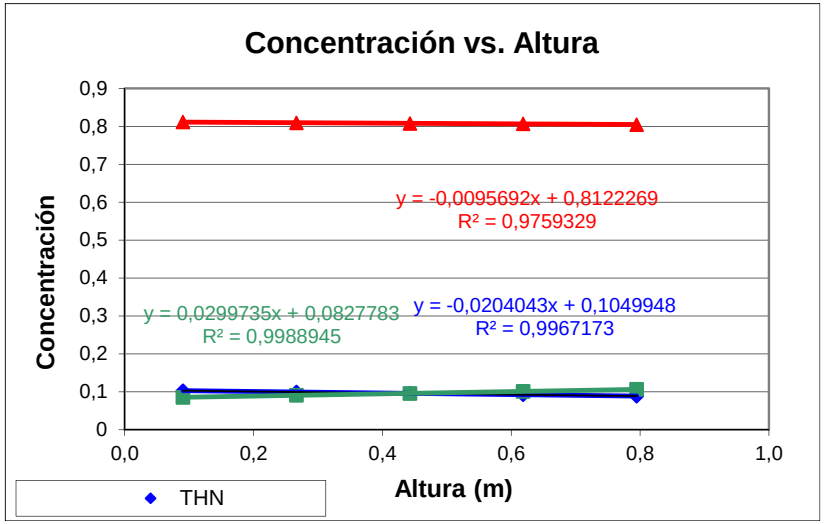

| Mezcla | C. masica. | C. molar | Tª media | DT (ºC) | Tiempo |
|---|---|---|---|---|---|
| THN-IBB-$C_{12}$ | 0,1000 | | 25º | 6,5 | 5h |

| | |
|---|---|
| Tª bainu hotza | 21 |
| Tªbainu beroa | 29,3 |
| Tª arriba hotza | 21,8 |
| Tª abajo hotza | 21,4 |
| Tª arriba beroa | 28 |
| Tª abajo beroa | 28,2 |
| TªGAPhotza | 21,6 |
| TªGAPberoa | 28,1 |
| $\Delta T^a$ | 6,50 |
| Tªmedia | 24,85 |
| $\Delta T^a$ vertical hotza | 0,4 |
| $\Delta T^a$ vertical beroa | -0,2 |

| Medidas Columna | |
|---|---|
| Longitud (cm) | 98 |
| Ancho (cm) | 5 |
| gap (cm.) | 0,10 |

| Calibración | |
|---|---|
| a | 0,849052122 |
| b | 0,105244882 |
| c | -0,122806935 |
| a' | 1,48380286 |
| b' | 0,048841964 |
| c' | -7,73E-02 |

| | |
|---|---|
| T. Relajación (s.): | 12173 |
| T. Equilibrio (min): | 1014 |
| T. Equilibrio (h): | **16,9** |
| D | 1,00E-09 |

| | |
|---|---|
| Viscosidad cin. | 1,24E-03 |
| gap | 1,0E-03 |
| Gravedad | 9,81 |
| $C_0$ | 0,1000 |
| Densidad Inicial | 0,847333 |
| nD Inicial | 1,480985 |
| Alfa | 9,47E-04 |
| Viscosidad Din. | 1,053E-03 |

| | | | |
|---|---|---|---|
| Pendiente c/z | -0,0193012 | 0,030759 | -0,0114578 |
| Delta c | -0,018915176 | 0,03014382 | -0,011228644 |
| $D_T$ | ***3,284E-13*** | ***-5,234E-13*** | ***1,950E-13*** |

| Tomas | Altura toma (cm) | Cantidad (c.c.) | Altura real (m) | Densidad ($g/cm^3$) | nD | THN c | $C_{12}$ c | IBB c |
|---|---|---|---|---|---|---|---|---|
| 1ª | 75,4 | 4,1 | 0,7936 | 0,845374 | 1,479931 | 0,089194924 | 0,106390012 | 0,804415064 |
| 2ª | 57,8 | 4 | 0,6166 | 0,846442 | 1,480551 | 0,092211317 | 0,100278467 | 0,807510217 |
| 3ª | 40,2 | 4 | 0,4406 | 0,847537 | 1,481169 | 0,096317455 | 0,094880971 | 0,808801574 |
| 4ª | 22,6 | 4 | 0,2646 | 0,848507 | 1,481720 | 0,099751407 | 0,089925272 | 0,810323321 |
| 5ª | 5 | 4,2 | 0,0906 | 0,849447 | 1,482266 | 0,102388673 | 0,084531104 | 0,813080223 |

NOTAS:

$$\rho = a + cTHN \times b + cC_{12} \times c$$

$$n = a' + cTHN \times b' + cC_{12} \times c'$$

THN-IBB-C12 c=10-80-10

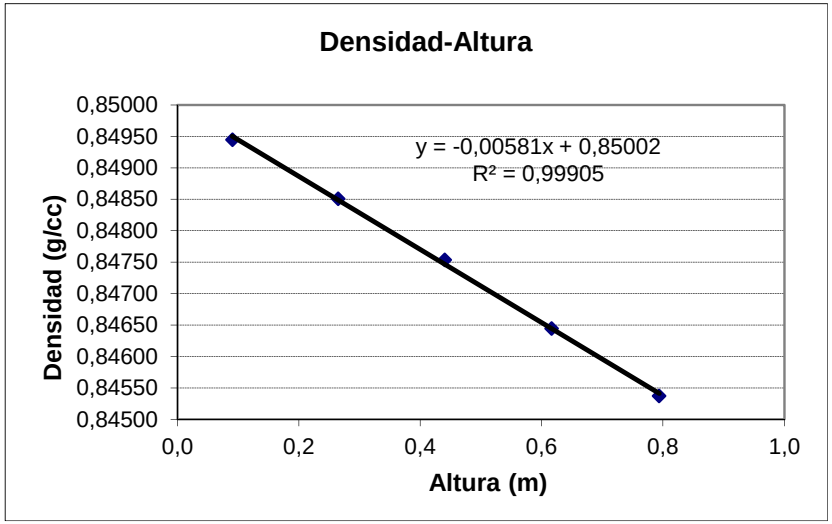


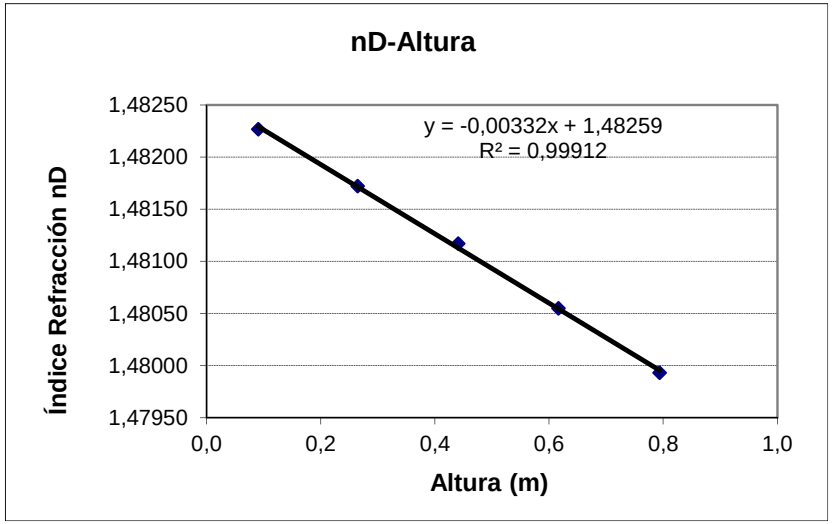


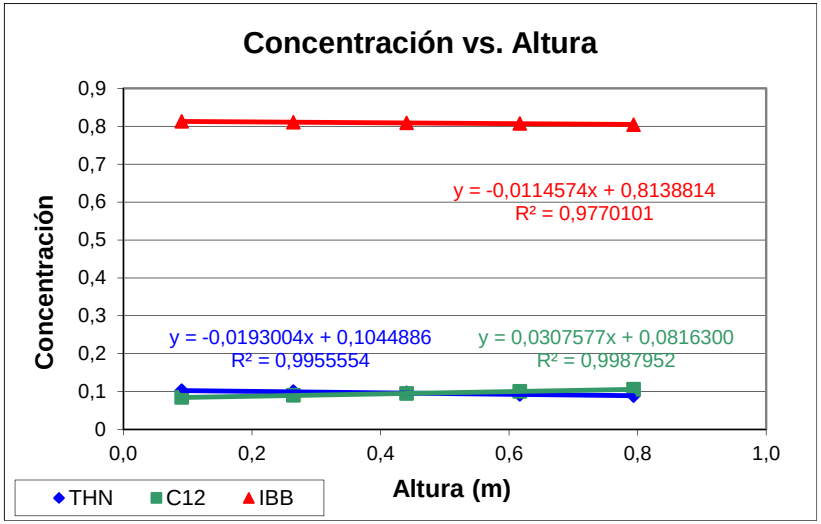

| Mezcla | C. masica. | C. molar | Tª media | DT (ºC) | Tiempo |
|---|---|---|---|---|---|
| THN-IBB-$C_{12}$ | 0,1000 | | 25º | 6,5 | 5h |

| | |
|---|---|
| T. Relajación (s.): | 3895 |
| T. Equilibrio (min): | 325 |
| T. Equilibrio (h): | **5,4** |
| D | 1,00E-09 |

| | |
|---|---|
| Tª bainu hotza | 21 |
| Tªbainu beroa | 29,3 |
| Tª arriba hotza | 21,8 |
| Tª abajo hotza | 21,4 |
| Tª arriba beroa | 28 |
| Tª abajo beroa | 28,2 |
| TªGAPhotza | 21,6 |
| TªGAPberoa | 28,1 |
| $\Delta T^a$ | 6,50 |
| Tªmedia | 24,85 |
| $\Delta T^a$ vertical hotza | 0,4 |
| $\Delta T^a$ vertical beroa | -0,2 |

| Medidas Columna | |
|---|---|
| Longitud (cm) | 50 |
| Ancho (cm) | 5 |
| gap (cm.) | 0,10 |

| Calibración | |
|---|---|
| a | 0,849052122 |
| b | 0,105244882 |
| c | -0,122806935 |
| a' | 1,48380286 |
| b' | 0,048841964 |
| c' | -7,73E-02 |

| | | | |
|---|---|---|---|
| Viscosidad cin. | 1,24E-03 | | |
| gap | 1,0E-03 | | |
| Gravedad | 9,81 | | |
| $C_0$ | 0,1000 | | |
| Densidad Inicial | 0,847333 | | |
| nD Inicial | 1,480985 | | |
| Alfa | 9,47E-04 | | |
| Viscosidad Din. | 1,053E-03 | | |
| Pendiente c/z | -0,0213037 | 0,0300066 | -0,008703 |
| Delta c | -0,01065185 | 0,0150033 | -0,0043515 |
| $D_T$ | ***3,159E-13*** | ***-4,450E-13*** | ***1,291E-13*** |

| Tomas | Altura toma (cm) | Cantidad (c.c.) | Altura real (m) | Densidad (g/cm$^3$) | nD | THN c | $C_{12}$ c | IBB c |
|---|---|---|---|---|---|---|---|---|
| 1ª | | | | | | | | |
| 2ª | 35 | 3,6 | 0,3860 | 0,846289 | 1,480452 | 0,092362932 | 0,101654258 | 0,80598281 |
| 3ª | 25 | 4 | 0,2900 | 0,846879 | 1,480789 | 0,094345214 | 0,098548775 | 0,807106011 |
| 4ª | 15 | 4 | 0,1900 | 0,847451 | 1,481111 | 0,096537602 | 0,095769921 | 0,807692477 |
| | | | | | | | | |

NOTAS:

$$\rho = a + cTHN \times b + cC_{12} \times c$$
$$n = a' + cTHN \times b' + cC_{12} \times c'$$

THN-IBB-C12 c=10-80-10

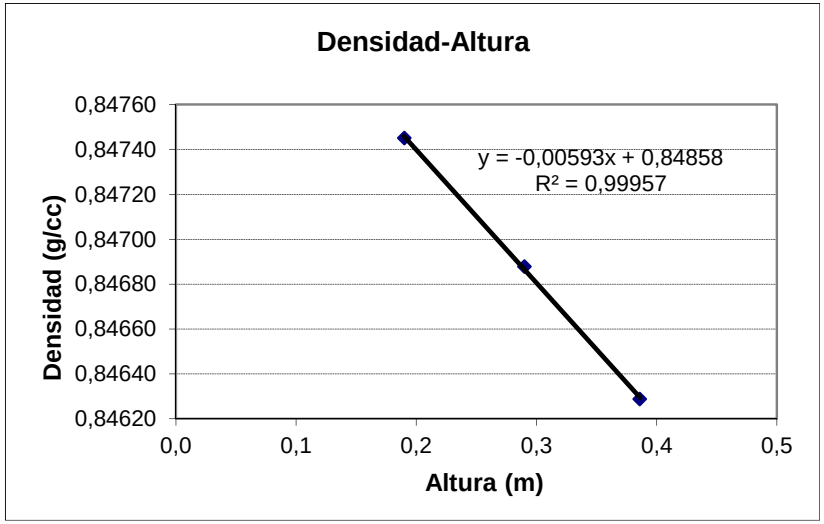


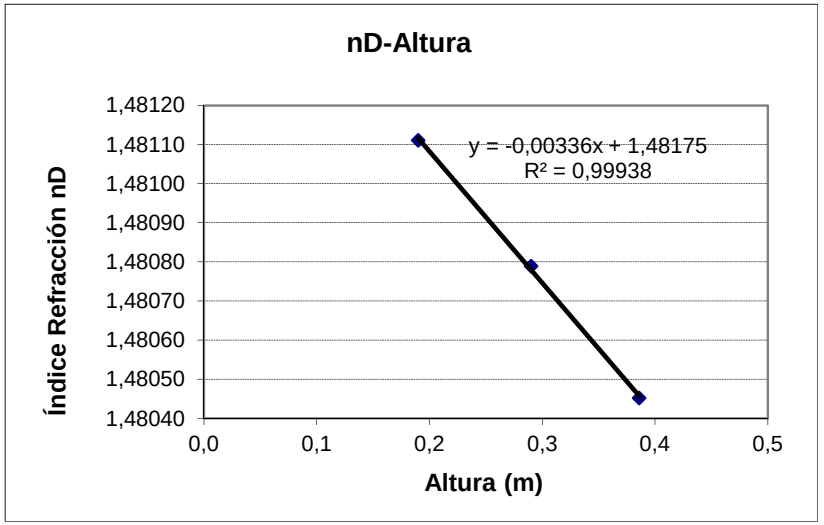


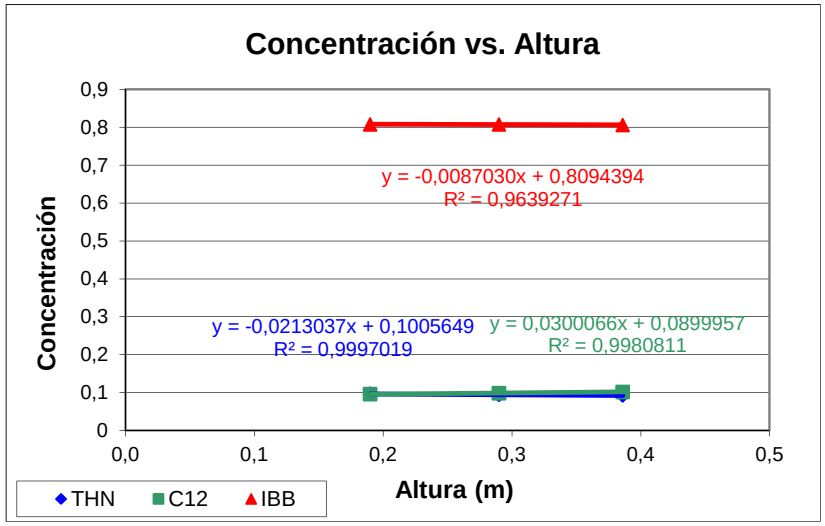

| Mezcla | C. masica. | C. molar | Tª media | DT (ºC) | Tiempo |
|---|---|---|---|---|---|
| THN-IBB-$C_{12}$ | 0,1000 | | 25º | 7,2 | 4h20´ |

| | |
|---|---|
| T. Relajación (s.): | 3175 |
| T. Equilibrio (min): | 265 |
| T. Equilibrio (h): | **4,4** |
| D | 1,00E-09 |

| | |
|---|---|
| Tª bainu hotza | 21 |
| Tªbainu beroa | 29,3 |
| Tª arriba hotza | 21,4 |
| Tª abajo hotza | 21,3 |
| Tª arriba beroa | 28,5 |
| Tª abajo beroa | 28,6 |
| TªGAPhotza | 21,4 |
| TªGAPberoa | 28,6 |
| $\Delta T^a$ | 7,20 |
| Tªmedia | 24,95 |
| $\Delta T^a$ vertical hotza | 0,1 |
| $\Delta T^a$ vertical beroa | -0,1 |

| Medidas Columna | |
|---|---|
| Longitud (cm) | 50 |
| Ancho (cm) | 5 |
| gap (cm.) | 0,10 |

| Calibración | |
|---|---|
| a | 0,849052122 |
| b | 0,105244882 |
| c | -0,122806935 |
| a' | 1,48380286 |
| b' | 0,048841964 |
| c' | -7,73E-02 |

| | | | |
|---|---|---|---|
| Viscosidad cin. | 1,24E-03 | | |
| gap | 1,0E-03 | | |
| Gravedad | 9,81 | | |
| $C_0$ | 0,1000 | | |
| Densidad Inicial | 0,847238 | | |
| nD Inicial | 1,481001 | | |
| Alfa | 9,47E-04 | | |
| Viscosidad Din. | 1,053E-03 | | |
| Pendiente c/z | -0,021364 | 0,0321853 | -0,0108213 |
| Delta c | -0,010682 | 0,01609265 | -0,00541065 |
| ***$D_T$*** | ***3,168E-13*** | ***-4,772E-13*** | ***1,604E-13*** |

| Tomas | Altura toma (cm) | Cantidad (c.c.) | Altura real (m) | Densidad ($g/cm^3$) | nD | THN c | $C_{12}$ c | IBB c |
|---|---|---|---|---|---|---|---|---|
| 1ª | 45 | | | | | | | |
| 2ª | 35 | 4,2 | 0,3920 | 0,846555 | 1,480655 | 0,090328453 | 0,097744719 | 0,811926829 |
| 3ª | 25 | 4,2 | 0,2920 | 0,847177 | 1,481011 | 0,092376845 | 0,09443532 | 0,813187835 |
| 4ª | 15 | 4,3 | 0,1930 | 0,847789 | 1,481358 | 0,094580191 | 0,091340143 | 0,814079665 |
| | | | | | | | | |

NOTAS:

$$\rho = a + cTHN \times b + cC_{12} \times c$$
$$n = a' + cTHN \times b' + cC_{12} \times c'$$

THN-IBB-C12 c=10-80-10

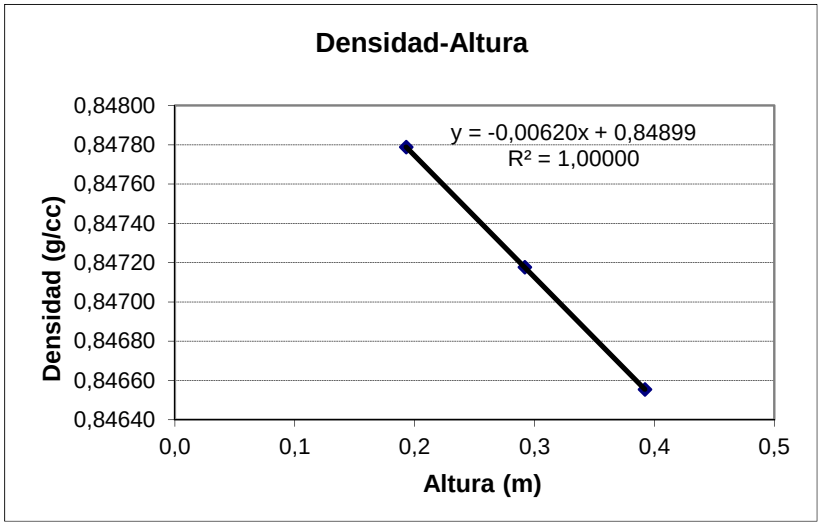


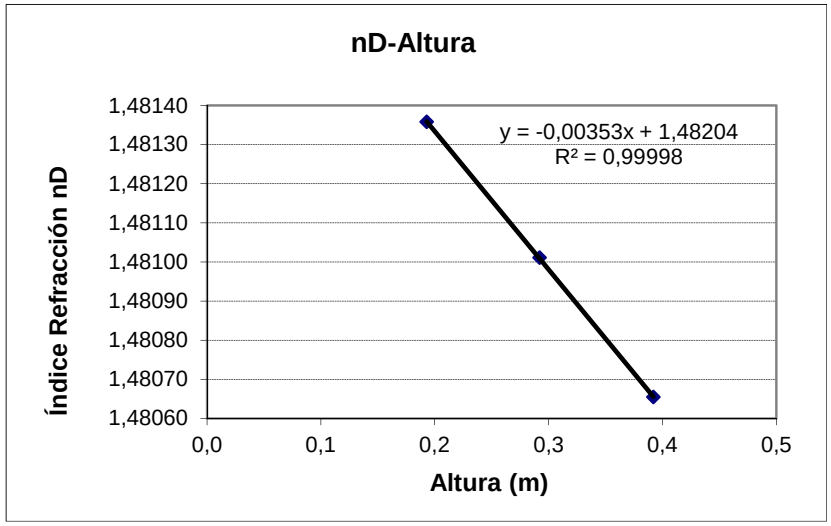


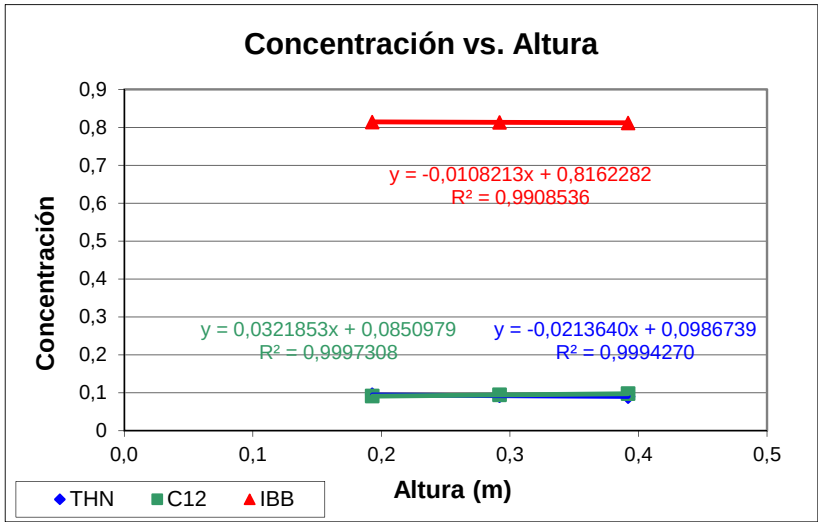

| Mezcla | C. masica. | C. molar | Tª media | DT (ºC) | Tiempo |
|---|---|---|---|---|---|
| THN-IBB-$C_{12}$ | 0,1000 | | 25º | 7,2 | 16h 45` |

| | |
|---|---|
| T. Relajación (s.): | 3175 |
| T. Equilibrio (min): | 265 |
| T. Equilibrio (h): | **4,4** |
| D | 1,00E-09 |

| | |
|---|---|
| Tª bainu hotza | 21 |
| Tªbainu beroa | 29,3 |
| Tª arriba hotza | 21,4 |
| Tª abajo hotza | 21,3 |
| Tª arriba beroa | 28,5 |
| Tª abajo beroa | 28,6 |
| TªGAPhotza | 21,4 |
| TªGAPberoa | 28,6 |
| $\Delta T^a$ | 7,20 |
| Tªmedia | 24,95 |
| $\Delta T^a$ vertical hotza | 0,1 |
| $\Delta T^a$ vertical beroa | -0,1 |

| Medidas Columna | |
|---|---|
| Longitud (cm) | 50 |
| Ancho (cm) | 5 |
| gap (cm.) | 0,10 |

| Calibración | |
|---|---|
| a | 0,849052122 |
| b | 0,105244882 |
| c | -0,122806935 |
| a' | 1,48380286 |
| b' | 0,048841964 |
| c' | -7,73E-02 |

| | | | |
|---|---|---|---|
| Viscosidad cin. | 1,24E-03 | | |
| gap | 1,0E-03 | | |
| Gravedad | 9,81 | | |
| $C_0$ | 0,1000 | | |
| Densidad Inicial | 0,847227 | | |
| nD Inicial | 1,480992 | | |
| Alfa | 9,47E-04 | | |
| Viscosidad Din. | 1,053E-03 | | |
| Pendiente c/z | -0,0231126 | 0,0290909 | -0,0059783 |
| Delta c | -0,0115563 | 0,01454545 | -0,00298915 |
| $D_T$ | ***3,427E-13*** | ***-4,313E-13*** | ***8,864E-14*** |

| Tomas | Altura toma (cm) | Cantidad (c.c.) | Altura real (m) | Densidad ($g/cm^3$) | nD | THN c | $C_{12}$ c | IBB c |
|---|---|---|---|---|---|---|---|---|
| 1ª | 45 | | | | | | | |
| 2ª | 35 | 4 | 0,3900 | 0,846671 | 1,480757 | 0,088668615 | 0,095377674 | 0,815953711 |
| 3ª | 25 | 4,1 | 0,2910 | 0,847261 | 1,481091 | 0,090822926 | 0,092419619 | 0,816757455 |
| 4ª | 15 | 4,2 | 0,1920 | 0,84786 | 1,481426 | 0,093244915 | 0,089617675 | 0,81713741 |
| | | | | | | | | |

NOTAS:

$$\rho = a + cTHN \times b + cC_{12} \times c$$
$$n = a' + cTHN \times b' + cC_{12} \times c'$$

THN-IBB-C12 c=10-80-10

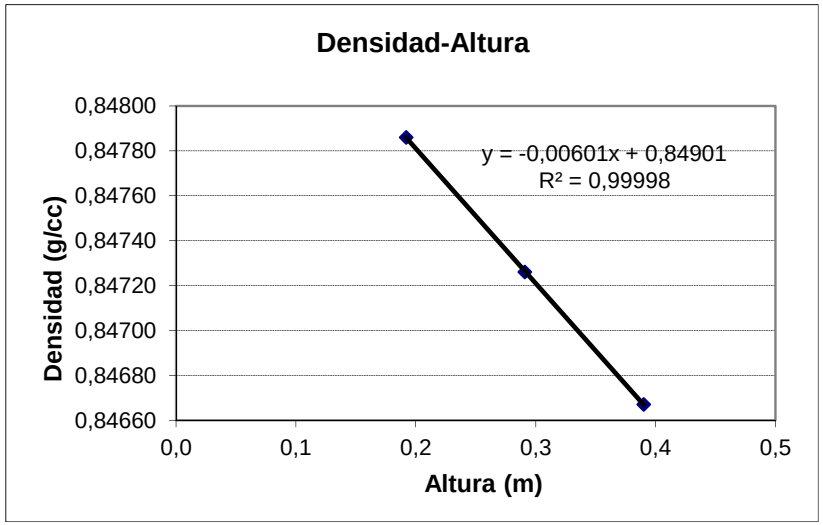


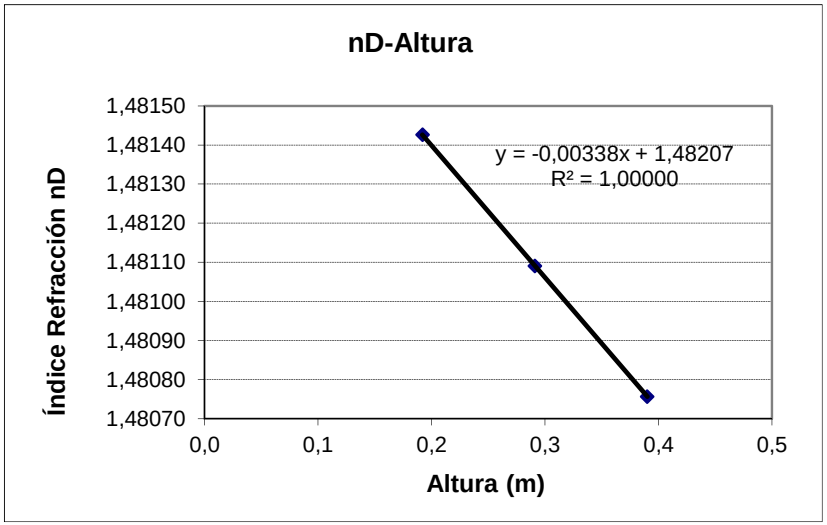


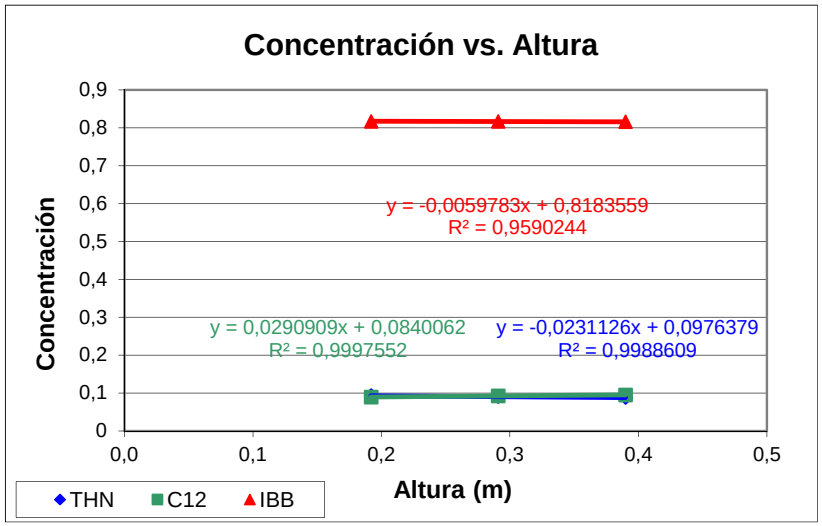

| Mezcla | C. masica. | C. molar | Tª media | DT (ºC) | Tiempo |
|---|---|---|---|---|---|
| THN-IBB-$C_{12}$ | 0,4000 | | 25º | 6,8 | 23h30` |

| | |
|---|---|
| T. Relajación (s.): | 18060 |
| T. Equilibrio (min): | 1505 |
| T. Equilibrio (h): | **25,1** |
| D | 1,00E-09 |

| | |
|---|---|
| Tª bainu hotza | 21 |
| Tªbainu beroa | 29,3 |
| Tª arriba hotza | 21,4 |
| Tª abajo hotza | 21 |
| Tª arriba beroa | 27,7 |
| Tª abajo beroa | 28,2 |
| TªGAPhotza | 21,2 |
| TªGAPberoa | 28,0 |
| ΔTª | 6,75 |
| Tªmedia | 24,58 |
| ΔTª vertical hotza | 0,4 |
| ΔTª vertical beroa | -0,5 |

| Medidas Columna | |
|---|---|
| Longitud (cm) | 98 |
| Ancho (cm) | 5 |
| gap (cm.) | 0,10 |

| Calibración | |
|---|---|
| a | 0,848077002 |
| b | 0,102365167 |
| c | -0,116188581 |
| a' | 1,48292342 |
| b' | 0,047269347 |
| c' | -7,18E-02 |

| | | | |
|---|---|---|---|
| Viscosidad cin. | 1,50E-03 | | |
| gap | 1,0E-03 | | |
| Gravedad | 9,81 | | |
| $C_0$ | 0,4000 | | |
| Densidad Inicial | 0,84247 | | |
| nD Inicial | 1,473198 | | |
| Alfa | 9,05E-04 | | |
| Viscosidad Din. | 1,266E-03 | | |
| Pendiente c/z | -0,1097102 | 0,1124814 | -0,0027712 |
| Delta c | -0,107515996 | 0,110231772 | -0,002715776 |
| ***$D_T$*** | ***1,476E-12*** | ***-1,513E-12*** | ***3,728E-14*** |

| Tomas | Altura toma (cm) | Cantidad (c.c.) | Altura real (m) | Densidad ($g/cm^3$) | nD | THN c | $C_{12}$ c | IBB c |
|---|---|---|---|---|---|---|---|---|
| 1ª | 75,4 | 4 | 0,7926 | 0,834681 | 1,468940 | 0,356720176 | 0,429575111 | 0,213704713 |
| 2ª | 57,8 | | | | | | | |
| 3ª | 40,2 | 4 | 0,4406 | 0,843464 | 1,473726 | 0,396857269 | 0,389344309 | 0,213798422 |
| 4ª | 22,6 | 4 | 0,2646 | 0,847608 | 1,475982 | 0,415928166 | 0,37048011 | 0,213591724 |
| 5ª | 5 | 4,2 | 0,0906 | 0,85173 | 1,478250 | 0,433398529 | 0,350395147 | 0,216206323 |

NOTAS:

$$\rho = a + cTHN \times b + cC_{12} \times c$$
$$n = a' + cTHN \times b' + cC_{12} \times c'$$

THN-IBB-C12 c=40-20-40

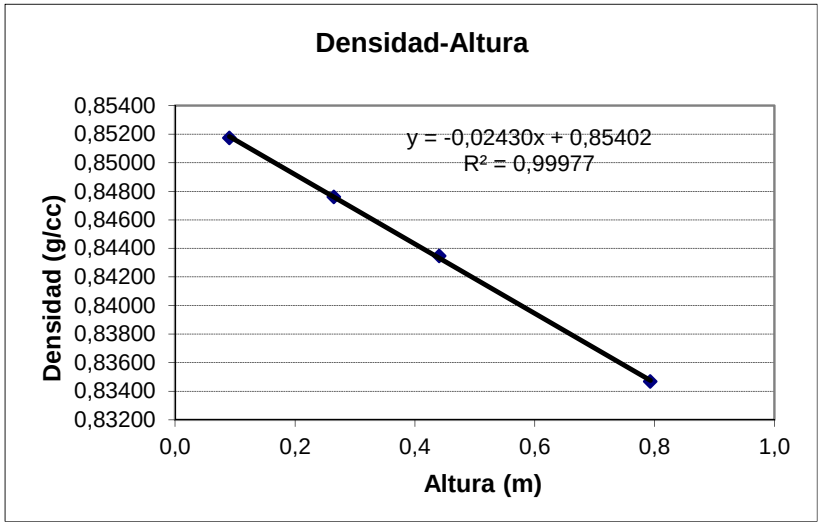


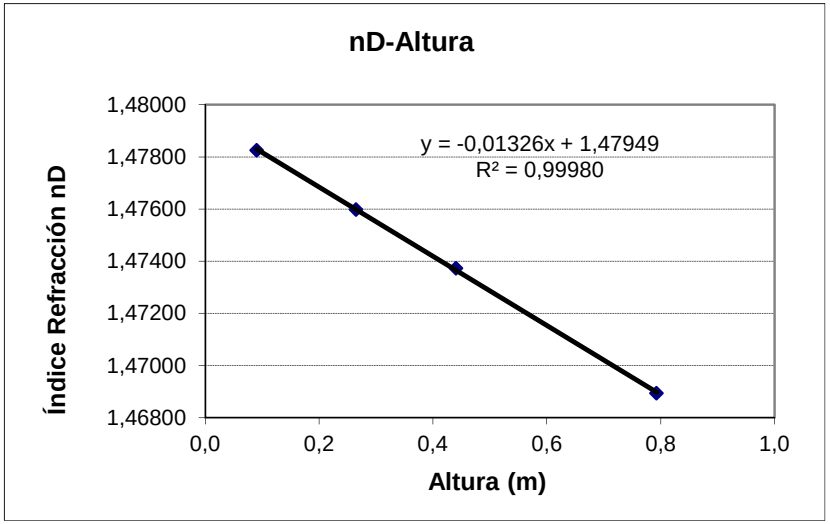


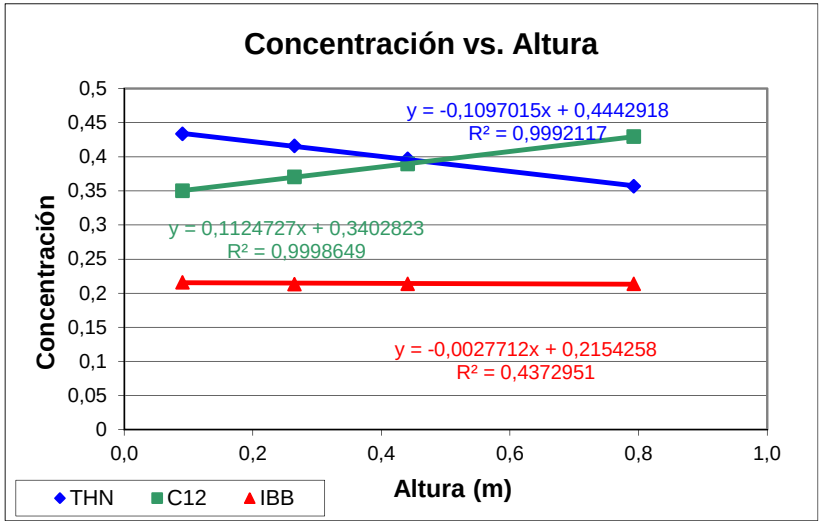

| Mezcla | C. masica. | C. molar | Tª media | DT (ºC) | Tiempo |
|---|---|---|---|---|---|
| THN-IBB-$C_{12}$ | 0,4000 | | 25º | 6,8 | 20h30` |

| | |
|---|---|
| T. Relajación (s.): | 18057 |
| T. Equilibrio (min): | 1505 |
| T. Equilibrio (h): | **25,1** |
| D | 1,00E-09 |

| | |
|---|---|
| Tª bainu hotza | 21 |
| Tªbainu beroa | 29,3 |
| Tª arriba hotza | 21,4 |
| Tª abajo hotza | 21 |
| Tª arriba beroa | 27,7 |
| Tª abajo beroa | 28,2 |
| TªGAPhotza | 21,2 |
| TªGAPberoa | 28,0 |
| $\Delta T^a$ | 6,75 |
| Tªmedia | 24,58 |
| $\Delta T^a$ vertical hotza | 0,4 |
| $\Delta T^a$ vertical beroa | -0,5 |

| Medidas Columna | |
|---|---|
| Longitud (cm) | 98 |
| Ancho (cm) | 5 |
| gap (cm.) | 0,10 |

| Calibración | |
|---|---|
| a | 0,848077002 |
| b | 0,102365167 |
| c | -0,11618858 |
| a' | 1,48292342 |
| b' | 0,047269347 |
| c' | -7,18E-02 |

| | | | |
|---|---|---|---|
| Viscosidad cin. | 1,50E-03 | | |
| gap | 1,0E-03 | | |
| Gravedad | 9,81 | | |
| $C_0$ | 0,4000 | | |
| Densidad Inicial | 0,842531 | | |
| nD Inicial | 1,473214 | | |
| Alfa | 9,05E-04 | | |
| Viscosidad Din. | 1,266E-03 | | |
| Pendiente c/z | -0,106299 | 0,1130535 | -0,0067545 |
| Delta c | -0,10417302 | 0,11079243 | -0,00661941 |
| $D_T$ | ***1,430E-12*** | ***-1,521E-12*** | ***9,087E-14*** |

| Tomas | Altura toma (cm) | Cantidad (c.c.) | Altura real (m) | Densidad ($g/cm^3$) | nD | THN c | $C_{12}$ c | IBB c |
|---|---|---|---|---|---|---|---|---|
| 1ª | 75,4 | 4,2 | 0,7946 | 0,834806 | 1,468990 | 0,358424124 | 0,430000496 | 0,21157538 |
| 2ª | 57,8 | 4,1 | 0,6176 | 0,839132 | 1,471337 | 0,37883791 | 0,410752999 | 0,210409091 |
| 3ª | 40,2 | 4 | 0,4406 | 0,843494 | 1,473732 | 0,397641401 | 0,389776949 | 0,212581651 |
| 4ª | 22,6 | 4 | 0,2646 | 0,847617 | 1,475999 | 0,415212939 | 0,369772516 | 0,215014545 |
| 5ª | 5 | 4 | 0,0886 | 0,851758 | 1,478257 | 0,434042843 | 0,350721817 | 0,215235341 |

NOTAS:

$$\rho = a + cTHN \times b + cC_{12} \times c$$
$$n = a' + cTHN \times b' + cC_{12} \times c'$$

THN-IBB-C12 c=40-20-40

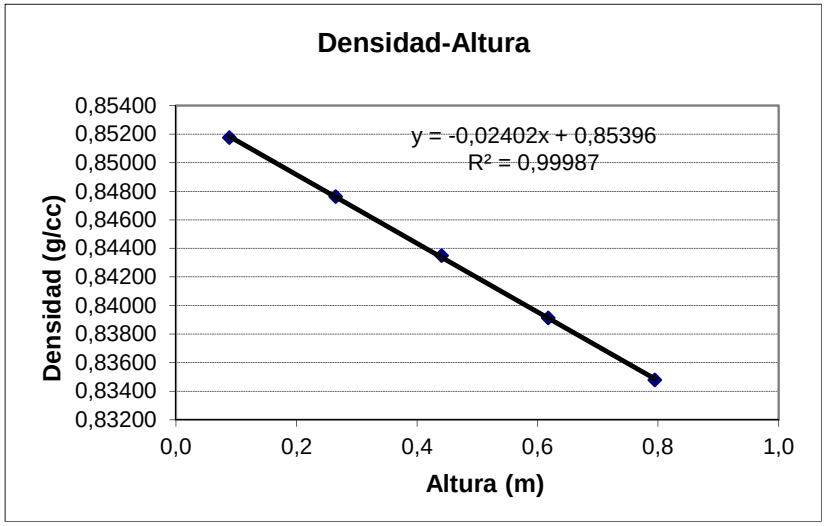


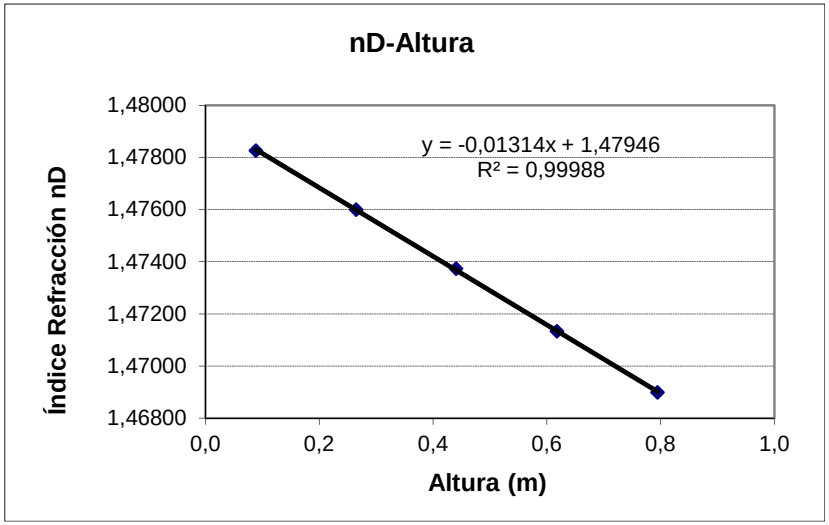


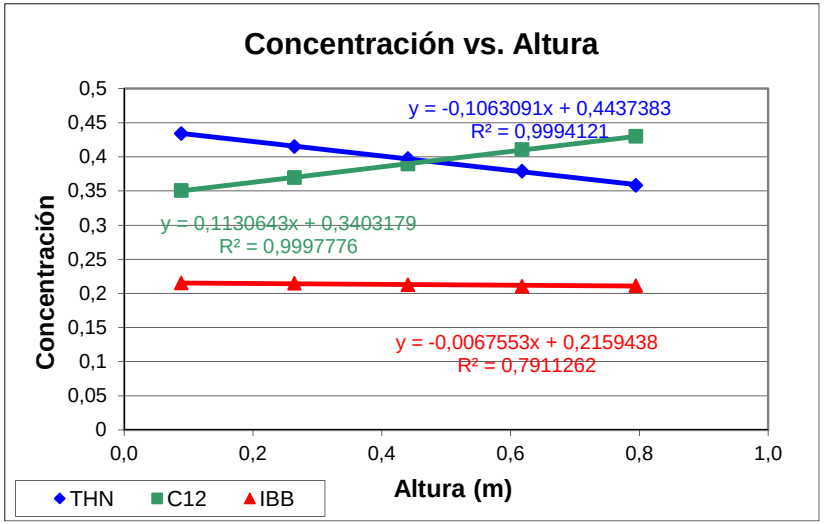

| Mezcla | C. masica. | C. molar | Tª media | DT (ºC) | Tiempo |
|---|---|---|---|---|---|
| THN-IBB-$C_{12}$ | 0,4000 | | 25º | 6,8 | 5h |

| | |
|---|---|
| T. Relajación (s.): | 5778 |
| T. Equilibrio (min): | 482 |
| T. Equilibrio (h): | **8,0** |
| D | 1,00E-09 |

| | |
|---|---|
| Tª bainu hotza | 21 |
| Tªbainu beroa | 29,3 |
| Tª arriba hotza | 21,4 |
| Tª abajo hotza | 21 |
| Tª arriba beroa | 27,7 |
| Tª abajo beroa | 28,2 |
| TªGAPhotza | 21,2 |
| TªGAPberoa | 28,0 |
| ΔTª | 6,75 |
| Tªmedia | 24,58 |
| ΔTª vertical hotza | 0,4 |
| ΔTª vertical beroa | -0,5 |

| Medidas Columna | |
|---|---|
| Longitud (cm) | 50 |
| Ancho (cm) | 5 |
| gap (cm.) | 0,10 |

| Calibración | |
|---|---|
| a | 0,848077002 |
| b | 0,102365167 |
| c | -0,116188581 |
| a' | 1,48292342 |
| b' | 0,047269347 |
| c' | -7,18E-02 |

| | | | |
|---|---|---|---|
| Viscosidad cin. | 1,50E-03 | | |
| gap | 1,0E-03 | | |
| Gravedad | 9,81 | | |
| $C_0$ | 0,4000 | | |
| Densidad Inicial | 0,842518 | | |
| nD Inicial | 1,473142 | | |
| Alfa | 9,05E-04 | | |
| Viscosidad Din. | 1,266E-03 | | |
| Pendiente c/z | -0,1094674 | 0,1215586 | -0,0120912 |
| Delta c | -0,0547337 | 0,0607793 | -0,0060456 |
| $D_T$ | ***1,283E-12*** | ***-1,425E-12*** | ***1,418E-13*** |

| Tomas | Altura toma (cm) | Cantidad (c.c.) | Altura real (m) | Densidad ($g/cm^3$) | nD | THN c | $C_{12}$ c | IBB c |
|---|---|---|---|---|---|---|---|---|
| 1ª | | | | | | | | |
| 2ª | 35 | 3,8 | 0,3880 | 0,838912 | 1,471310 | 0,372024587 | 0,406643758 | 0,221331655 |
| 3ª | 25 | 3,6 | 0,2860 | 0,841587 | 1,472768 | 0,384227153 | 0,394371619 | 0,221401228 |
| 4ª | 15 | 3,9 | 0,1890 | 0,843951 | 1,474076 | 0,393791082 | 0,382451456 | 0,223757462 |
| | | | | | | | | |

NOTAS:

$$\rho = a + cTHN \times b + cC_{12} \times c$$
$$n = a' + cTHN \times b' + cC_{12} \times c'$$

THN-IBB-C12 c=40-20-40

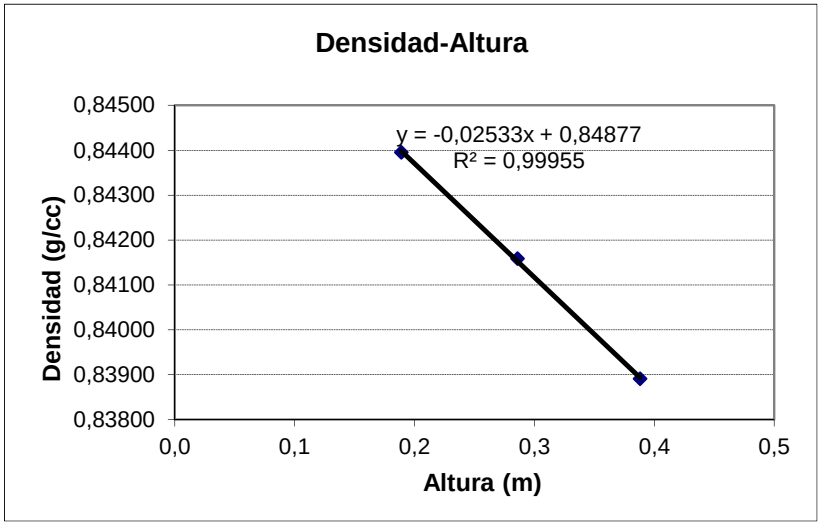


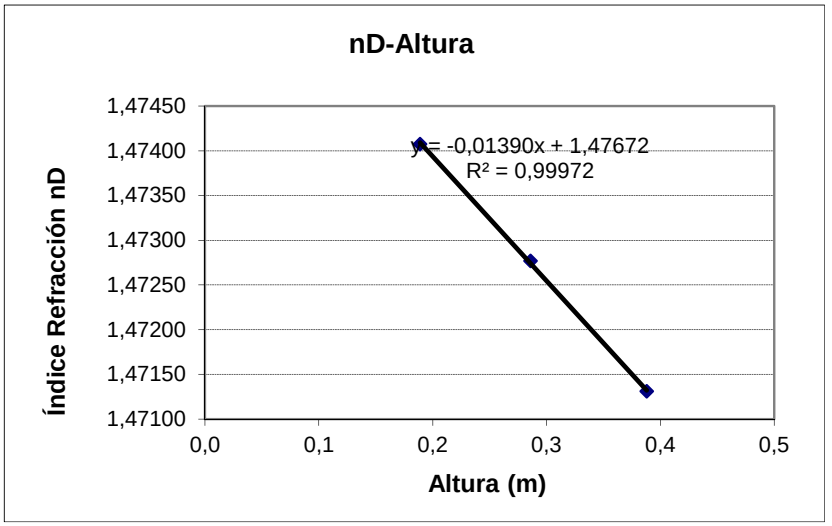


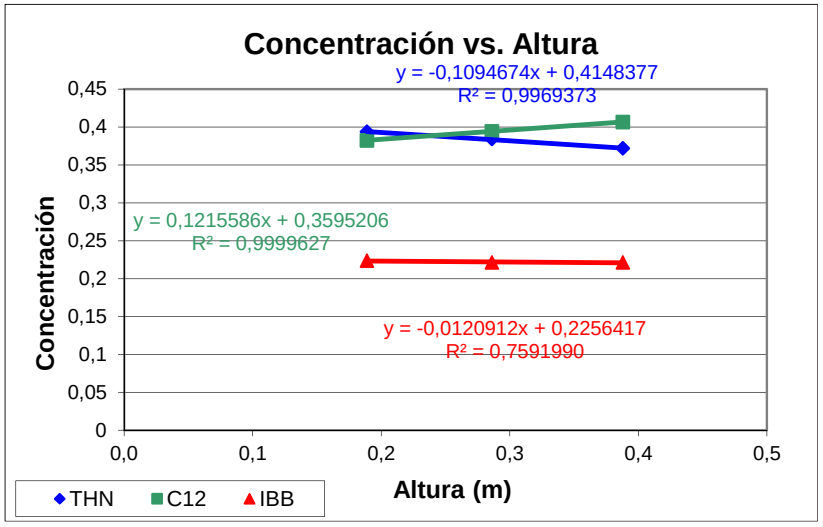

| Mezcla | C. masica. | C. molar | Tª media | DT (ºC) | Tiempo |
|---|---|---|---|---|---|
| THN-IBB-$C_{12}$ | 0,4000 | | 25º | 7,2 | 5h |

| | |
|---|---|
| T. Relajación (s.): | 5079 |
| T. Equilibrio (min): | 423 |
| T. Equilibrio (h): | **7,1** |
| D | 1,00E-09 |

| | |
|---|---|
| Tª bainu hotza | 21 |
| Tªbainu beroa | 29,3 |
| Tª arriba hotza | 21,7 |
| Tª abajo hotza | 21,2 |
| Tª arriba beroa | 28,5 |
| Tª abajo beroa | 28,8 |
| TªGAPhotza | 21,5 |
| TªGAPberoa | 28,7 |
| ΔTª | 7,20 |
| Tªmedia | 25,05 |
| ΔTª vertical hotza | 0,5 |
| ΔTª vertical beroa | -0,3 |

| Medidas Columna | |
|---|---|
| Longitud (cm) | 50 |
| Ancho (cm) | 5 |
| gap (cm.) | 0,10 |

| Calibración | |
|---|---|
| a | 0,848077002 |
| b | 0,102365167 |
| c | -0,116188581 |
| a' | 1,48292342 |
| b' | 0,047269347 |
| c' | -7,18E-02 |

| | | | |
|---|---|---|---|
| Viscosidad cin. | 1,50E-03 | | |
| gap | 1,0E-03 | | |
| Gravedad | 9,81 | | |
| $C_0$ | 0,4000 | | |
| Densidad Inicial | 0,842491 | | |
| nD Inicial | 1,473132 | | |
| Alfa | 9,05E-04 | | |
| Viscosidad Din. | 1,266E-03 | | |
| Pendiente c/z | -0,1127455 | 0,120971 | -0,0082255 |
| Delta c | -0,05637275 | 0,0604855 | -0,00411275 |
| $D_T$ | ***1,322E-12*** | ***-1,418E-12*** | ***9,643E-14*** |

| Tomas | Altura toma (cm) | Cantidad (c.c.) | Altura real (m) | Densidad (g/cm$^3$) | nD | THN c | $C_{12}$ c | IBB c |
|---|---|---|---|---|---|---|---|---|
| 1ª | | | | | | | | |
| 2ª | 35 | 3,8 | 0,3880 | 0,83892 | 1,471306 | 0,372583861 | 0,407067639 | 0,2203485 |
| 3ª | 25 | 3,8 | 0,2880 | 0,8415 | 1,472722 | 0,383741549 | 0,394692572 | 0,221565879 |
| 4ª | 15 | 4 | 0,1900 | 0,843988 | 1,474081 | 0,394908251 | 0,383117264 | 0,221974485 |
| | | | | | | | | |

NOTAS:

$$\rho = a + cTHN \times b + cC_{12} \times c$$
$$n = a' + cTHN \times b' + cC_{12} \times c'$$

THN-IBB-C12 c=40-20-40

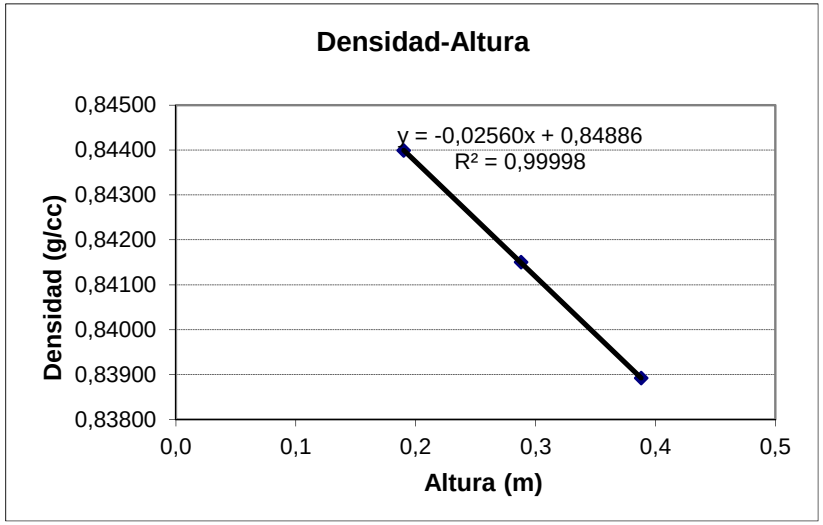


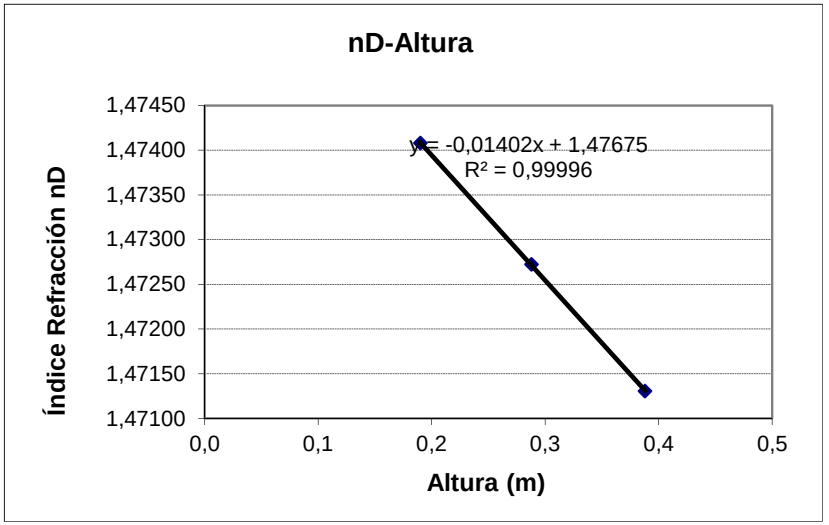


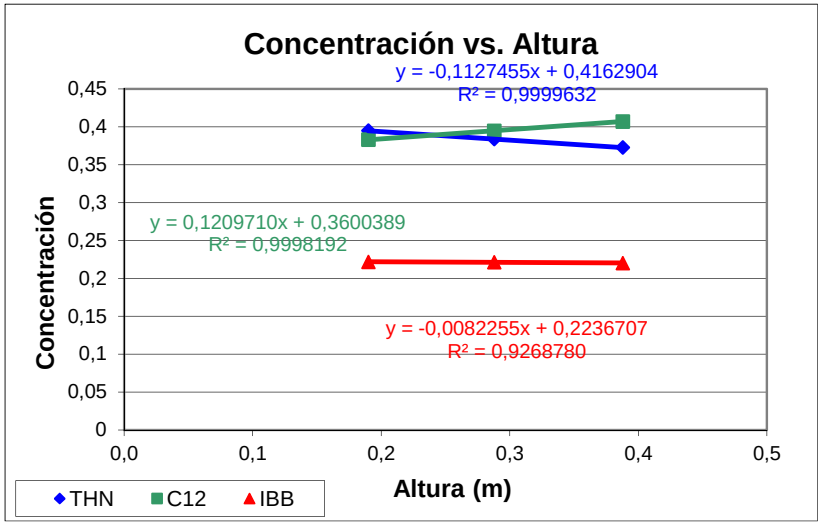

| Mezcla | C. masica. | C. molar | Tª media | DT (ºC) | Tiempo |
|---|---|---|---|---|---|
| THN-IBB-$C_{12}$ | 0,4000 | | 25º | 7,0 | 22h 15` |

| | |
|---|---|
| T. Relajación (s.): | 5451 |
| T. Equilibrio (min): | 454 |
| T. Equilibrio (h): | **7,6** |
| D | 1,00E-09 |

| | |
|---|---|
| Tª bainu hotza | 21 |
| Tªbainu beroa | 29,3 |
| Tª arriba hotza | 21,7 |
| Tª abajo hotza | 21,3 |
| Tª arriba beroa | 28,3 |
| Tª abajo beroa | 28,6 |
| TªGAPhotza | 21,5 |
| TªGAPberoa | 28,5 |
| $\Delta T^a$ | 6,95 |
| Tªmedia | 24,98 |
| $\Delta T^a$ vertical hotza | 0,4 |
| $\Delta T^a$ vertical beroa | -0,3 |

| Medidas Columna | |
|---|---|
| Longitud (cm) | 50 |
| Ancho (cm) | 5 |
| gap (cm.) | 0,10 |

| Calibración | |
|---|---|
| a | 0,848077002 |
| b | 0,102365167 |
| c | -0,116188581 |
| a' | 1,48292342 |
| b' | 0,047269347 |
| c' | -7,18E-02 |

| | | | |
|---|---|---|---|
| Viscosidad cin. | 1,50E-03 | | |
| gap | 1,0E-03 | | |
| Gravedad | 9,81 | | |
| $C_0$ | 0,4000 | | |
| Densidad Inicial | 0,842494 | | |
| nD Inicial | 1,473132 | | |
| Alfa | 9,05E-04 | | |
| Viscosidad Din. | 1,266E-03 | | |
| Pendiente c/z | -0,1144575 | 0,1217458 | -0,0072883 |
| Delta c | -0,05722875 | 0,0608729 | -0,00364415 |
| $D_T$ | ***1,342E-12*** | ***-1,427E-12*** | ***8,544E-14*** |

| Tomas | Altura toma (cm) | Cantidad (c.c.) | Altura real (m) | Densidad ($g/cm^3$) | nD | THN c | $C_{12}$ c | IBB c |
|---|---|---|---|---|---|---|---|---|
| 1ª | | | | | | | | |
| 2ª | 35 | 3,7 | 0,3870 | 0,838922 | 1,471299 | 0,373098864 | 0,407504157 | 0,219396979 |
| 3ª | 25 | 3,6 | 0,2860 | 0,841586 | 1,472757 | 0,384876347 | 0,394952183 | 0,220171471 |
| 4ª | 15 | 3,8 | 0,1880 | 0,844068 | 1,474115 | 0,395873717 | 0,383279328 | 0,220846955 |
| | | | | | | | | |

NOTAS:

$$\rho = a + cTHN \times b + cC_{12} \times c$$
$$n = a' + cTHN \times b' + cC_{12} \times c'$$

THN-IBB-C12 c=40-20-40

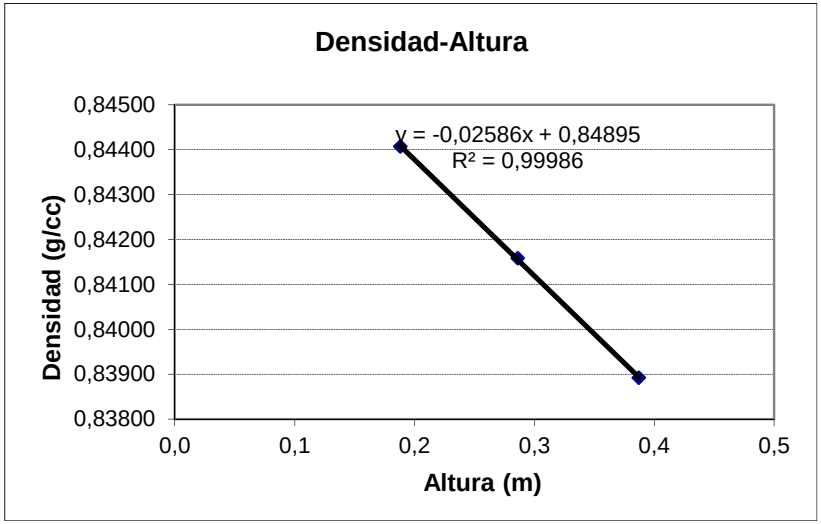


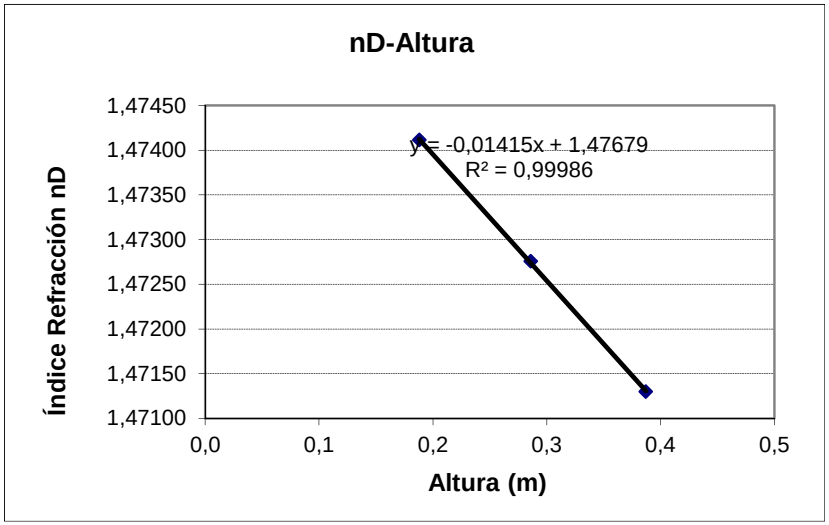


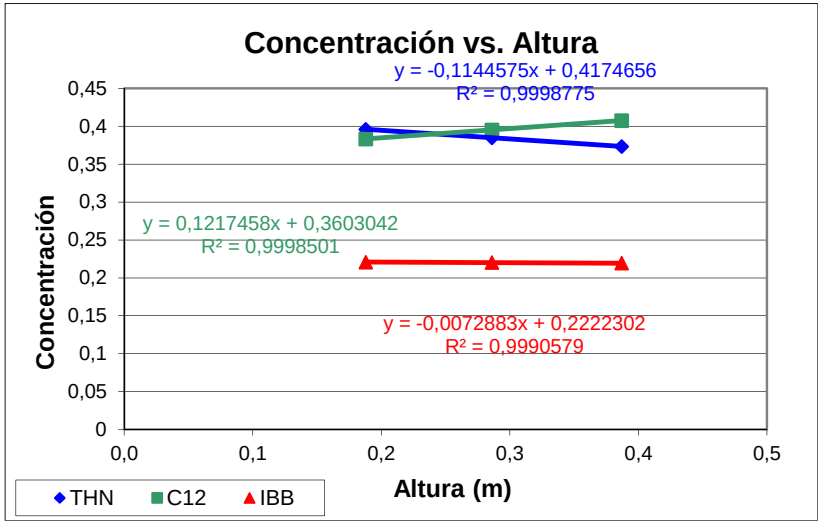

| Mezcla | C. masica. | C. molar | Tª media | DT (ºC) | Tiempo |
|---|---|---|---|---|---|
| THN-IBB-$C_{12}$ | 0,4500 | | 25º | 7,1 | 23h15` |

| | |
|---|---|
| T. Relajación (s.): | 21659 |
| T. Equilibrio (min): | 1805 |
| T. Equilibrio (h): | **30,1** |
| D | 1,00E-09 |

| | |
|---|---|
| Tª bainu hotza | 21 |
| Tªbainu beroa | 29,3 |
| Tª arriba hotza | 21,6 |
| Tª abajo hotza | 21,1 |
| Tª arriba beroa | 28,4 |
| Tª abajo beroa | 28,4 |
| TªGAPhotza | 21,4 |
| TªGAPberoa | 28,4 |
| ΔTª | 7,05 |
| Tªmedia | 24,88 |
| ΔTª vertical hotza | 0,5 |
| ΔTª vertical beroa | 0 |

| Medidas Columna | |
|---|---|
| Longitud (cm) | 98 |
| Ancho (cm) | 5 |
| gap (cm.) | 0,10 |

| Calibración | |
|---|---|
| a | 0,847995152 |
| b | 0,101874647 |
| c | -0,115504805 |
| a' | 1,48309252 |
| b' | 0,046719248 |
| c' | -7,13E-02 |

| | | | |
|---|---|---|---|
| Viscosidad cin. | 1,71E-03 | | |
| gap | 1,0E-03 | | |
| Gravedad | 9,81 | | |
| $C_0$ | 0,4500 | | |
| Densidad Inicial | 0,841817 | | |
| nD Inicial | 1,471966 | | |
| Alfa | 9,00E-04 | | |
| Viscosidad Din. | 1,439E-03 | | |
| Pendiente c/z | -0,1253952 | 0,1282158 | -0,0028206 |
| Delta c | -0,122887296 | 0,125651484 | -0,002764188 |
| $D_T$ | ***1,475E-12*** | ***-1,508E-12*** | ***3,317E-14*** |

| Tomas | Altura toma (cm) | Cantidad (c.c.) | Altura real (m) | Densidad ($g/cm^3$) | nD | THN c | $C_{12}$ c | IBB c |
|---|---|---|---|---|---|---|---|---|
| 1ª | 75,4 | 4,2 | 0,7946 | 0,832961 | 1,467154 | 0,411501266 | 0,493102413 | 0,095396321 |
| 2ª | 57,8 | 4,2 | 0,6186 | 0,837862 | 1,469792 | 0,435474242 | 0,47181532 | 0,092710438 |
| 3ª | 40,2 | 4,4 | 0,4445 | 0,842838 | 1,472508 | 0,457487828 | 0,448150731 | 0,094361441 |
| 4ª | 22,6 | 4,2 | 0,2666 | 0,847587 | 1,475092 | 0,478997831 | 0,426007272 | 0,094994897 |
| 5ª | 5 | 4 | 0,0886 | 0,852429 | 1,477736 | 0,500348143 | 0,402917804 | 0,096734053 |

NOTAS:

$$\rho = a + cTHN \times b + cC_{12} \times c$$
$$n = a' + cTHN \times b' + cC_{12} \times c'$$

THN-IBB-C12 c=45-10-45

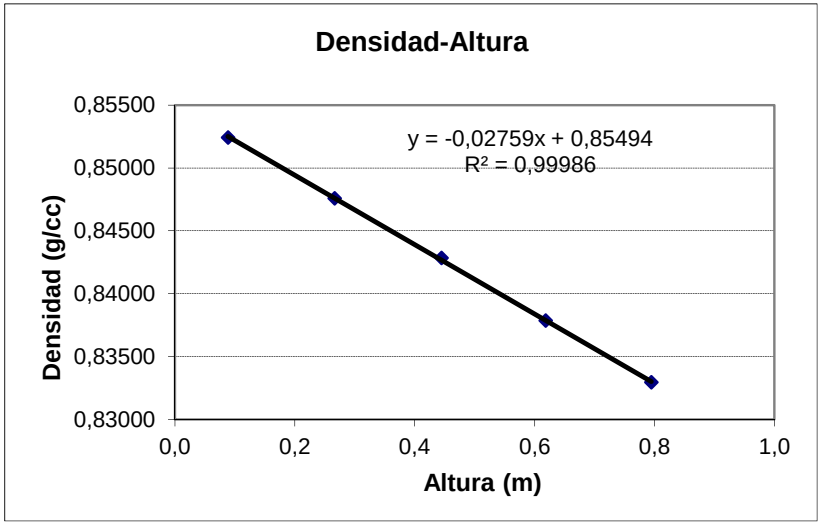


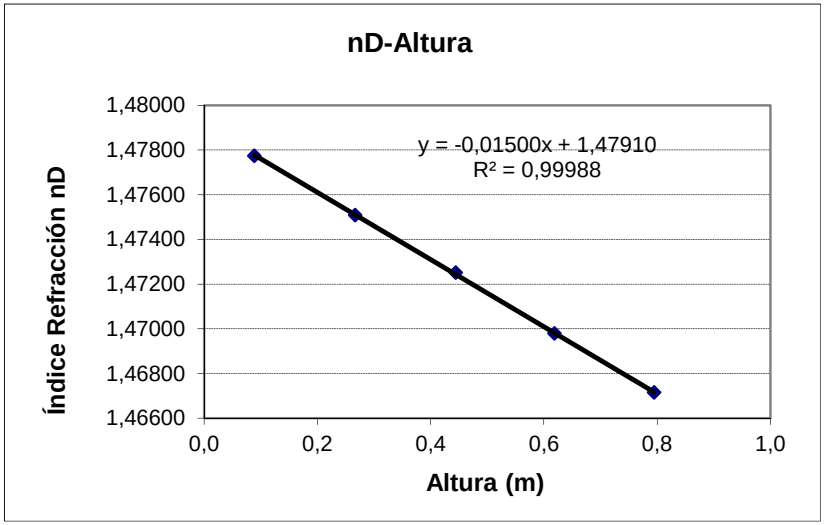


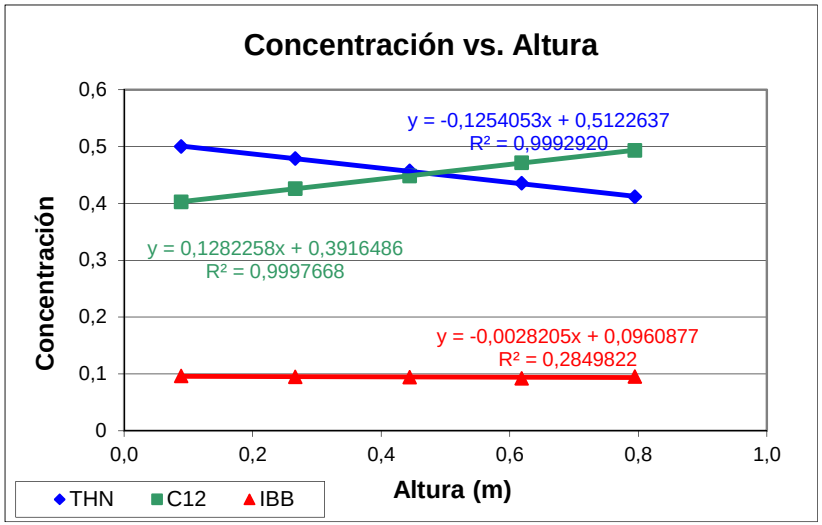

| Mezcla | C. masica. | C. molar | Tª media | DT (ºC) | Tiempo |
|---|---|---|---|---|---|
| THN-IBB-$C_{12}$ | 0,4500 | | 25º | 7,1 | 5h |

| | |
|---|---|
| T. Relajación (s.): | 6931 |
| T. Equilibrio (min): | 578 |
| T. Equilibrio (h): | **9,6** |
| D | 1,00E-09 |

| | |
|---|---|
| Tª bainu hotza | 21 |
| Tªbainu beroa | 29,3 |
| Tª arriba hotza | 21,6 |
| Tª abajo hotza | 21,1 |
| Tª arriba beroa | 28,4 |
| Tª abajo beroa | 28,4 |
| TªGAPhotza | 21,4 |
| TªGAPberoa | 28,4 |
| ΔTª | 7,05 |
| Tªmedia | 24,88 |
| ΔTª vertical hotza | 0,5 |
| ΔTª vertical beroa | 0 |

| Medidas Columna | |
|---|---|
| Longitud (cm) | 50 |
| Ancho (cm) | 5 |
| gap (cm.) | 0,10 |

| Calibración | |
|---|---|
| a | 0,847995152 |
| b | 0,101874647 |
| c | -0,115504805 |
| a' | 1,48309252 |
| b' | 0,046719248 |
| c' | -7,13E-02 |

| | | | |
|---|---|---|---|
| Viscosidad cin. | 1,71E-03 | | |
| gap | 1,0E-03 | | |
| Gravedad | 9,81 | | |
| $C_0$ | 0,4500 | | |
| Densidad Inicial | 0,841817 | | |
| nD Inicial | 1,471912 | | |
| Alfa | 9,00E-04 | | |
| Viscosidad Din. | 1,439E-03 | | |
| Pendiente c/z | -0,1310147 | 0,1426011 | -0,0115864 |
| Delta c | -0,06550735 | 0,07130055 | -0,0057932 |
| $D_T$ | ***1,343E-12*** | ***-1,462E-12*** | ***1,188E-13*** |

| Tomas | Altura toma (cm) | Cantidad (c.c.) | Altura real (m) | Densidad (g/cm$^3$) | nD | THN c | $C_{12}$ c | IBB c |
|---|---|---|---|---|---|---|---|---|
| 1ª | | | | | | | | |
| 2ª | 35 | 3,4 | 0,3840 | 0,83749 | 1,469648 | 0,430178495 | 0,470365143 | 0,099456362 |
| 3ª | 25 | 3,5 | 0,2850 | 0,840496 | 1,471294 | 0,443151407 | 0,455782294 | 0,101066299 |
| 4ª | 15 | 3,7 | 0,1870 | 0,843364 | 1,472857 | 0,45598838 | 0,442274303 | 0,101737317 |
| | | | | | | | | |

NOTAS:

$$\rho = a + cTHN \times b + cC_{12} \times c$$
$$n = a' + cTHN \times b' + cC_{12} \times c'$$

THN-IBB-C12 c=45-10-45

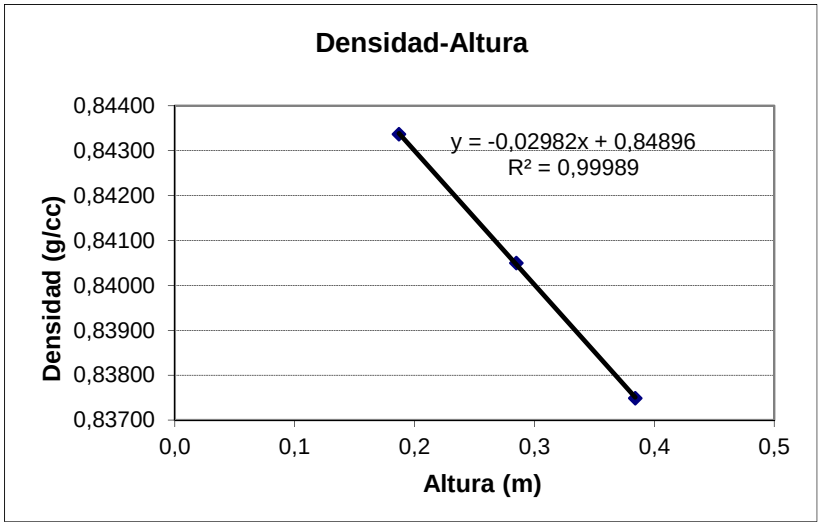


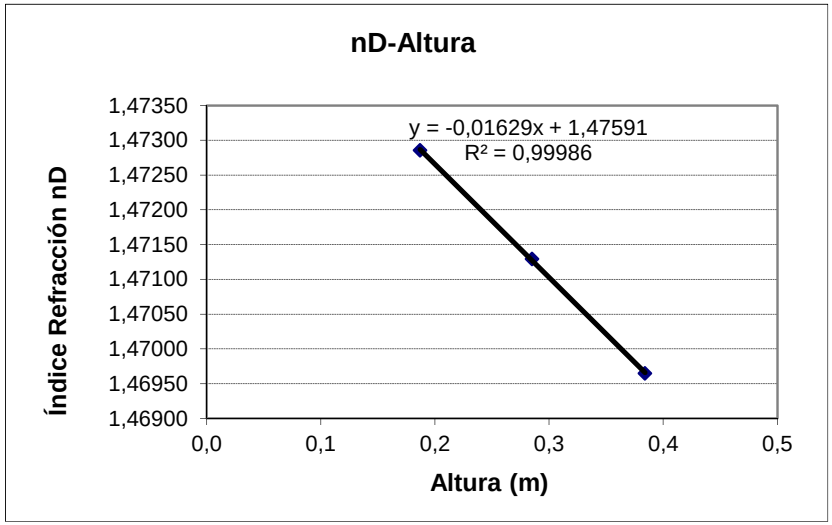


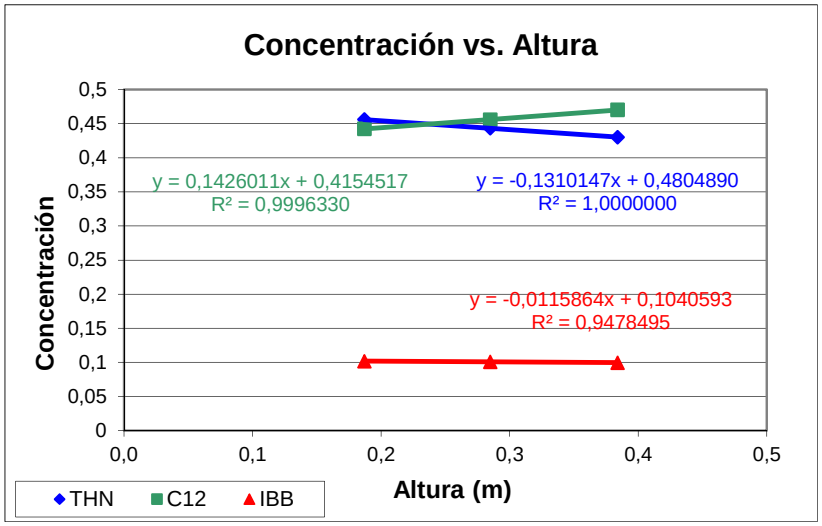

| Mezcla | C. masica. | C. molar | Tª media | DT (ºC) | Tiempo |
|---|---|---|---|---|---|
| THN-IBB-$C_{12}$ | 0,4500 | | 25º | 7,1 | 71h 15` |

| | |
|---|---|
| T. Relajación (s.): | 6931 |
| T. Equilibrio (min): | 578 |
| T. Equilibrio (h): | **9,6** |
| D | 1,00E-09 |

| | |
|---|---|
| Tª bainu hotza | 21 |
| Tªbainu beroa | 29,3 |
| Tª arriba hotza | 21,6 |
| Tª abajo hotza | 21,1 |
| Tª arriba beroa | 28,4 |
| Tª abajo beroa | 28,4 |
| TªGAPhotza | 21,4 |
| TªGAPberoa | 28,4 |
| $\Delta$Tª | 7,05 |
| Tªmedia | 24,88 |
| $\Delta$Tª vertical hotza | 0,5 |
| $\Delta$Tª vertical beroa | 0 |

| Medidas Columna | |
|---|---|
| Longitud (cm) | 50 |
| Ancho (cm) | 5 |
| gap (cm.) | 0,10 |

| Calibración | |
|---|---|
| a | 0,847995152 |
| b | 0,101874647 |
| c | -0,115504805 |
| a' | 1,48309252 |
| b' | 0,046719248 |
| c' | -7,13E-02 |

| | | | |
|---|---|---|---|
| Viscosidad cin. | 1,71E-03 | | |
| gap | 1,0E-03 | | |
| Gravedad | 9,81 | | |
| $C_0$ | 0,4500 | | |
| Densidad Inicial | 0,841798 | | |
| nD Inicial | 1,471912 | | |
| Alfa | 9,00E-04 | | |
| Viscosidad Din. | 1,439E-03 | | |
| Pendiente c/z | -0,1294041 | 0,1405734 | -0,0111693 |
| Delta c | -0,06470205 | 0,0702867 | -0,00558465 |
| $D_T$ | ***1,326E-12*** | ***-1,441E-12*** | ***1,145E-13*** |

| Tomas | Altura toma (cm) | Cantidad (c.c.) | Altura real (m) | Densidad (g/cm$^3$) | nD | THN c | $C_{12}$ c | IBB c |
|---|---|---|---|---|---|---|---|---|
| 1ª | | | | | | | | |
| 2ª | 35 | 3,7 | 0,3870 | 0,837632 | 1,469751 | 0,429230738 | 0,468299841 | 0,102469421 |
| 3ª | 25 | 3,4 | 0,2840 | 0,840728 | 1,471446 | 0,442609458 | 0,453295724 | 0,104094818 |
| 4ª | 15 | 3,8 | 0,1880 | 0,843485 | 1,472948 | 0,454980964 | 0,440338192 | 0,104680843 |
| | | | | | | | | |

NOTAS:

$$\rho = a + cTHN \times b + cC_{12} \times c$$
$$n = a' + cTHN \times b' + cC_{12} \times c'$$

THN-IBB-C12 c=45-10-45

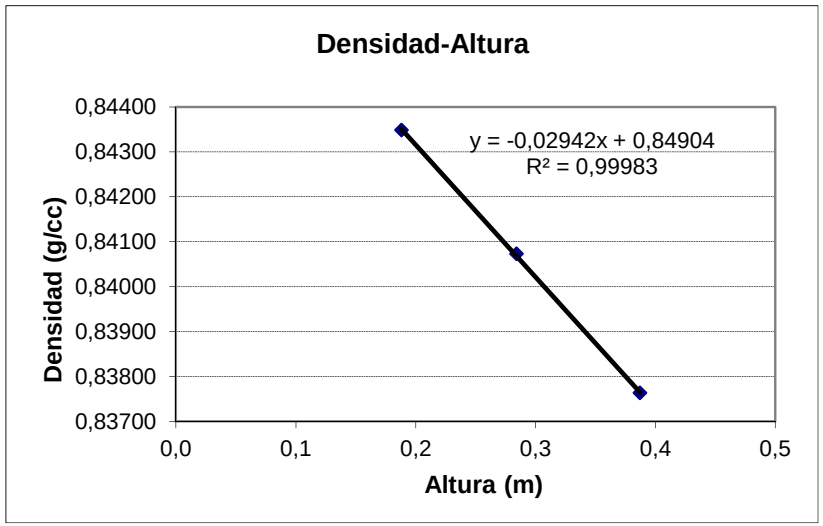


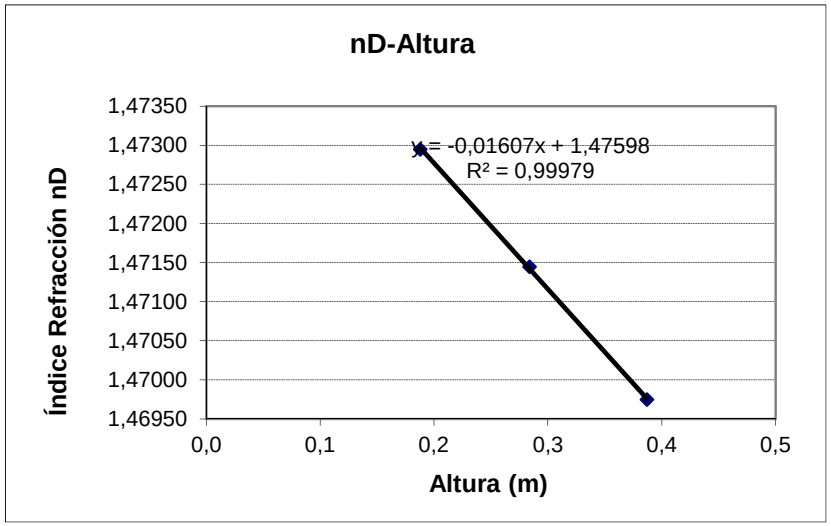


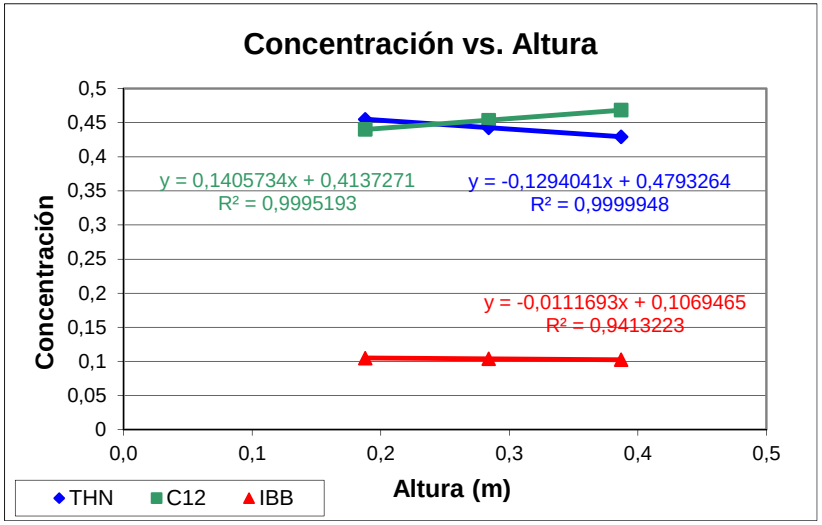

| Mezcla | C. masica. | C. molar | Tª media | DT (ºC) | Tiempo |
|---|---|---|---|---|---|
| THN-IBB-$C_{12}$ | 0,4500 | | 25º | 7,1 | 23h 30` |

| | |
|---|---|
| T. Relajación (s.): | 6931 |
| T. Equilibrio (min): | 578 |
| T. Equilibrio (h): | **9,6** |
| D | 1,00E-09 |

| | |
|---|---|
| Tª bainu hotza | 21 |
| Tªbainu beroa | 29,3 |
| Tª arriba hotza | 21,7 |
| Tª abajo hotza | 21,3 |
| Tª arriba beroa | 28,4 |
| Tª abajo beroa | 28,7 |
| TªGAPhotza | 21,5 |
| TªGAPberoa | 28,6 |
| $\Delta T^a$ | 7,05 |
| Tªmedia | 25,03 |
| $\Delta T^a$ vertical hotza | 0,4 |
| $\Delta T^a$ vertical beroa | -0,3 |

| Medidas Columna | |
|---|---|
| Longitud (cm) | 50 |
| Ancho (cm) | 5 |
| gap (cm.) | 0,10 |

| Calibración | |
|---|---|
| a | 0,847995152 |
| b | 0,101874647 |
| c | -0,115504805 |
| a' | 1,48309252 |
| b' | 0,046719248 |
| c' | -7,13E-02 |

| | | | |
|---|---|---|---|
| Viscosidad cin. | 1,71E-03 | | |
| gap | 1,0E-03 | | |
| Gravedad | 9,81 | | |
| $C_0$ | 0,4500 | | |
| Densidad Inicial | 0,841819 | | |
| nD Inicial | 1,471916 | | |
| Alfa | 9,00E-04 | | |
| Viscosidad Din. | 1,439E-03 | | |
| Pendiente c/z | -0,1290864 | 0,1393058 | -0,0102193 |
| Delta c | -0,0645432 | 0,0696529 | -0,00510965 |
| $D_T$ | ***1,323E-12*** | ***-1,428E-12*** | ***1,047E-13*** |

| Tomas | Altura toma (cm) | Cantidad (c.c.) | Altura real (m) | Densidad (g/cm$^3$) | nD | THN c | $C_{12}$ c | IBB c |
|---|---|---|---|---|---|---|---|---|
| 1ª | | | | | | | | |
| 2ª | 35 | 4 | 0,3900 | 0,837622 | 1,469743 | 0,429343627 | 0,468485985 | 0,102170388 |
| 3ª | 25 | 4 | 0,2900 | 0,840541 | 1,471340 | 0,442025227 | 0,454399415 | 0,103575358 |
| 4ª | 15 | 4,1 | 0,1910 | 0,843441 | 1,472920 | 0,455032588 | 0,440764661 | 0,104202751 |
| | | | | | | | | |

NOTAS:

$$\rho = a + cTHN \times b + cC_{12} \times c$$
$$n = a' + cTHN \times b' + cC_{12} \times c'$$

THN-IBB-C12 c=45-10-45

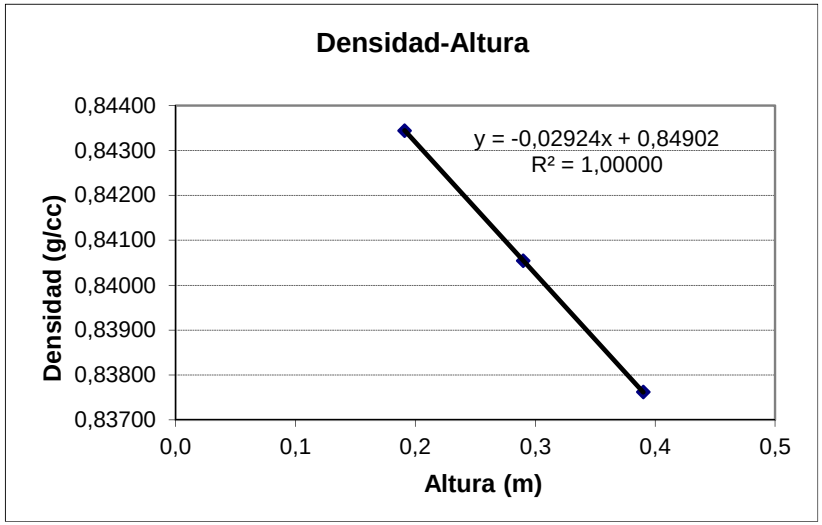


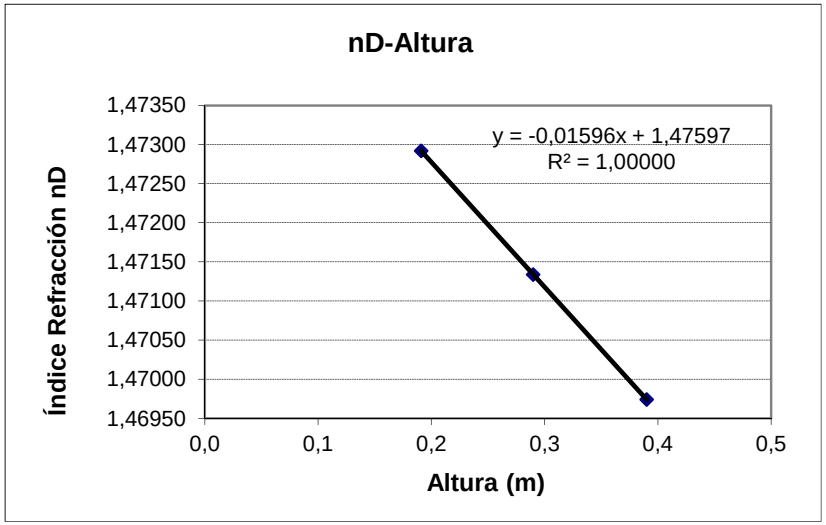


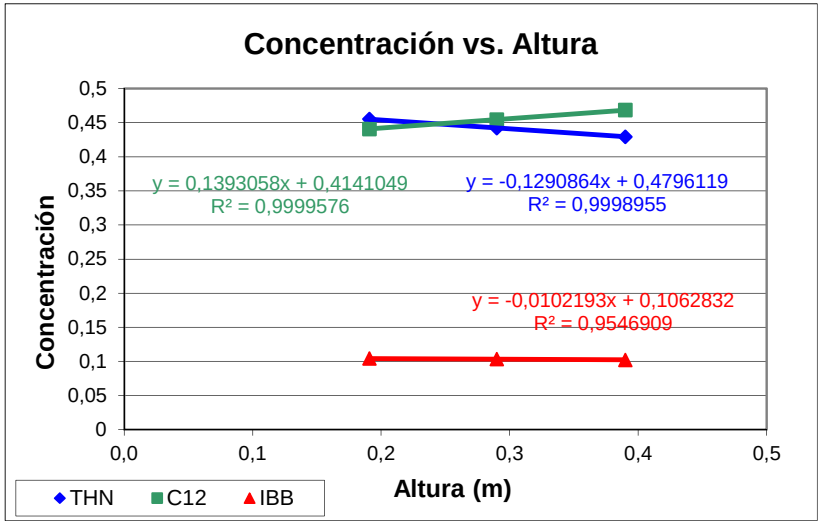

| Mezcla | C. masica. | C. molar | Tª media | DT (ºC) | Tiempo |
|---|---|---|---|---|---|
| THN-IBB-$C_{12}$ | 0,8000 | | 25º | 6,9 | 23h |

| | |
|---|---|
| Tª bainu hotza | 21 |
| Tªbainu beroa | 29,3 |
| Tª arriba hotza | 21,7 |
| Tª abajo hotza | 21,3 |
| Tª arriba beroa | 28,3 |
| Tª abajo beroa | 28,5 |
| TªGAPhotza | 21,5 |
| TªGAPberoa | 28,4 |
| ΔTª | 6,90 |
| Tªmedia | 24,95 |
| ΔTª vertical hotza | 0,4 |
| ΔTª vertical beroa | -0,2 |

| Medidas Columna | |
|---|---|
| Longitud (cm) | 98 |
| Ancho (cm) | 5 |
| gap (cm.) | 0,10 |

| Calibración | |
|---|---|
| a | 0,848940335 |
| b | 0,105608002 |
| c | -0,121781614 |
| a' | 1,48374796 |
| b' | 0,049959033 |
| c' | -7,66E-02 |

| | |
|---|---|
| T. Relajación (s.): | 30049 |
| T. Equilibrio (min): | 2504 |
| T. Equilibrio (h): | **41,7** |
| D | 1,00E-09 |

| | | | |
|---|---|---|---|
| Viscosidad cin. | 1,86E-03 | | |
| gap | 1,0E-03 | | |
| Gravedad | 9,81 | | |
| $C_0$ | 0,8000 | | |
| Densidad Inicial | 0,925505 | | |
| nD Inicial | 1,517867 | | |
| Alfa | 8,48E-04 | | |
| Viscosidad Din. | 1,719E-03 | | |
| Pendiente c/z | -0,0740027 | 0,0549424 | 0,0190602 |
| Delta c | -0,072522646 | 0,053843552 | 0,018678996 |
| $D_T$ | ***7,550E-13*** | ***-5,606E-13*** | ***-1,945E-13*** |

| Tomas | Altura toma (cm) | Cantidad (c.c.) | Altura real (m) | Densidad (g/cm$^3$) | nD |
|---|---|---|---|---|---|
| 1ª | 75,4 | | | | |
| 2ª | 57,8 | 4,3 | 0,6195 | 0,923401 | 1,516713 |
| 3ª | 40,2 | 4,1 | 0,4416 | 0,926259 | 1,518274 |
| 4ª | 22,6 | 4,2 | 0,2666 | 0,928775 | 1,519636 |
| 5ª | 5 | 4,2 | 0,0906 | 0,931081 | 1,520900 |

| | THN | $C_{12}$ | IBB |
|---|---|---|---|
| | c | c | c |
| | 57,83890988 | 57,12842695 | -113,9673368 |
| | 0,842611433 | 0,119277812 | 0,038110755 |
| | 0,856951073 | 0,10824479 | 0,034804138 |
| | 0,870317732 | 0,099176312 | 0,030505956 |
| | 0,881614159 | 0,090036945 | 0,028348896 |

NOTAS:

$$\rho = a + cTHN \times b + cC_{12} \times c$$
$$n = a' + cTHN \times b' + cC_{12} \times c'$$

THN-IBB-C12 c=80-10-10

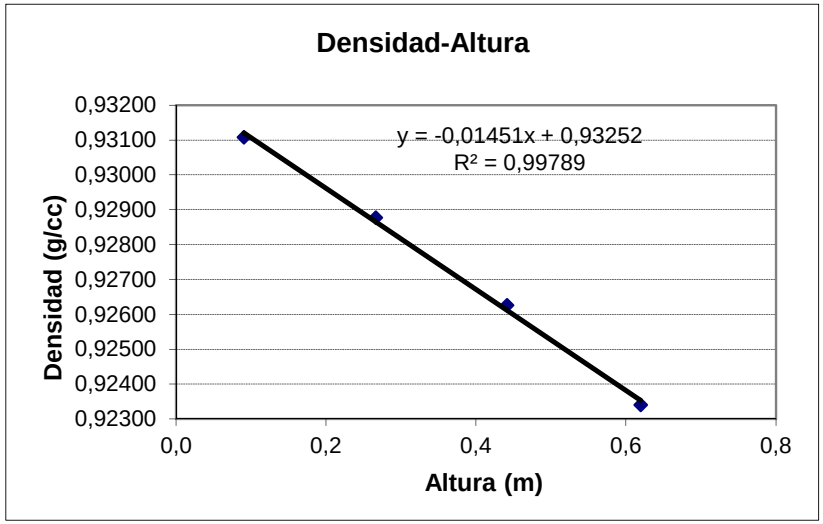


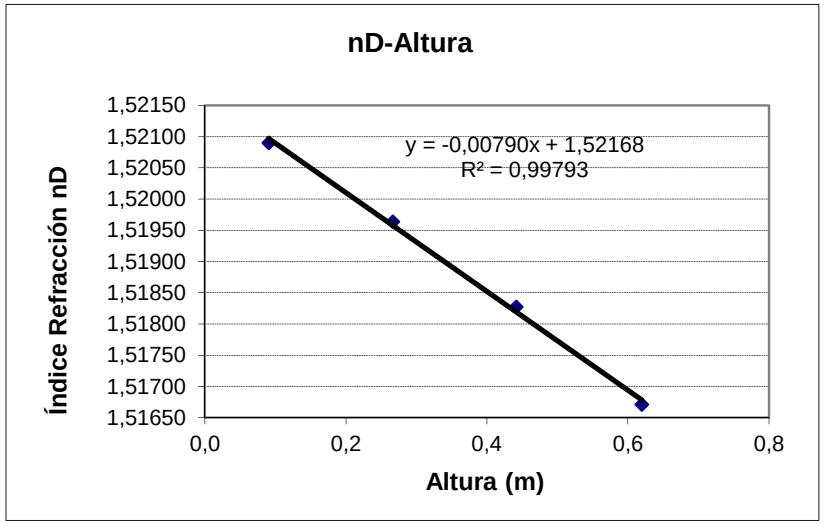


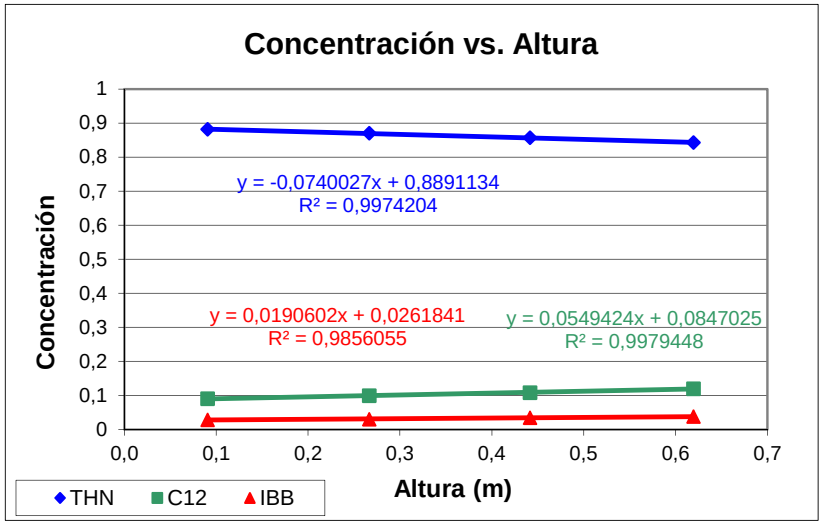

| Mezcla | C. masica. | C. molar | Tª media | DT (ºC) | Tiempo |
|---|---|---|---|---|---|
| THN-IBB-$C_{12}$ | 0,8000 | | 25º | 6,9 | 5h |

| | |
|---|---|
| Tª bainu hotza | 21 |
| Tªbainu beroa | 29,3 |
| Tª arriba hotza | 21,7 |
| Tª abajo hotza | 21,3 |
| Tª arriba beroa | 28,3 |
| Tª abajo beroa | 28,5 |
| TªGAPhotza | 21,5 |
| TªGAPberoa | 28,4 |
| ΔTª | 6,90 |
| Tªmedia | 24,95 |
| ΔTª vertical hotza | 0,4 |
| ΔTª vertical beroa | -0,2 |

| Medidas Columna | |
|---|---|
| Longitud (cm) | 50 |
| Ancho (cm) | 5 |
| gap (cm.) | 0,10 |

| Calibración | |
|---|---|
| a | 0,848940335 |
| b | 0,105608002 |
| c | -0,121781614 |
| a' | 1,48374796 |
| b' | 0,049959033 |
| c' | -7,66E-02 |

| | |
|---|---|
| T. Relajación (s.): | 9618 |
| T. Equilibrio (min): | 802 |
| T. Equilibrio (h): | **13,4** |
| D | 1,00E-09 |

| | |
|---|---|
| Viscosidad cin. | 1,86E-03 |
| gap | 1,0E-03 |
| Gravedad | 9,81 |
| $C_0$ | 0,8000 |
| Densidad Inicial | 0,925359 |
| nD Inicial | 1,517667 |
| Alfa | 8,48E-04 |
| Viscosidad Din. | 1,719E-03 |
| Pendiente c/z | -0,0903241 |
| Delta c | -0,04516205 |
| $D_T$ | ***8,029E-13*** |

| | | | |
|---|---|---|---|
| | | | |
| | -0,0608457 | -0,0294784 | |
| | -0,03042285 | -0,0147392 | |
| | ***-5,409E-13*** | ***-2,620E-13*** | |

| Tomas | Altura toma (cm) | Cantidad (c.c.) | Altura real (m) | Densidad ($g/cm^3$) | nD | THN c | $C_{12}$ c | IBB c |
|---|---|---|---|---|---|---|---|---|
| 1ª | 45 | 2 | 0,4700 | | | | | |
| 2ª | 35 | 3,7 | 0,3870 | 0,921662 | 1,515857 | 0,82817492 | 0,121038248 | 0,050786831 |
| 3ª | 25 | 3,8 | 0,2880 | 0,923394 | 1,516792 | 0,837534306 | 0,11493245 | 0,047533245 |
| 4ª | 15 | 3,8 | 0,1880 | 0,925035 | 1,517682 | 0,846150811 | 0,108929671 | 0,044919518 |
| | | | | | | | | |

NOTAS:

$$\rho = a + cTHN \times b + cC_{12} \times c$$
$$n = a' + cTHN \times b' + cC_{12} \times c'$$

THN-IBB-C12 c=80-10-10

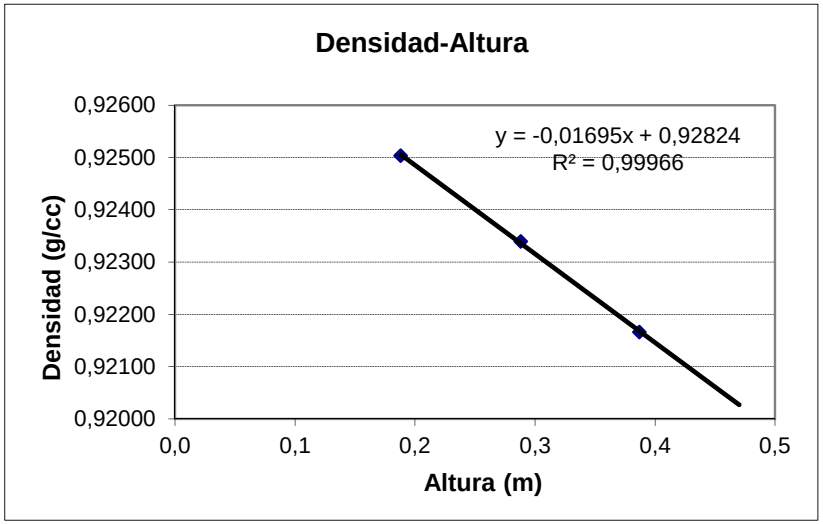


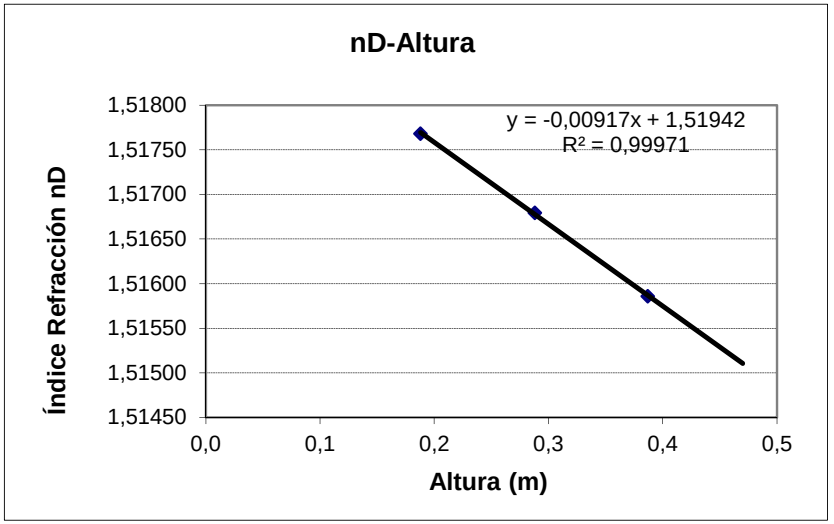


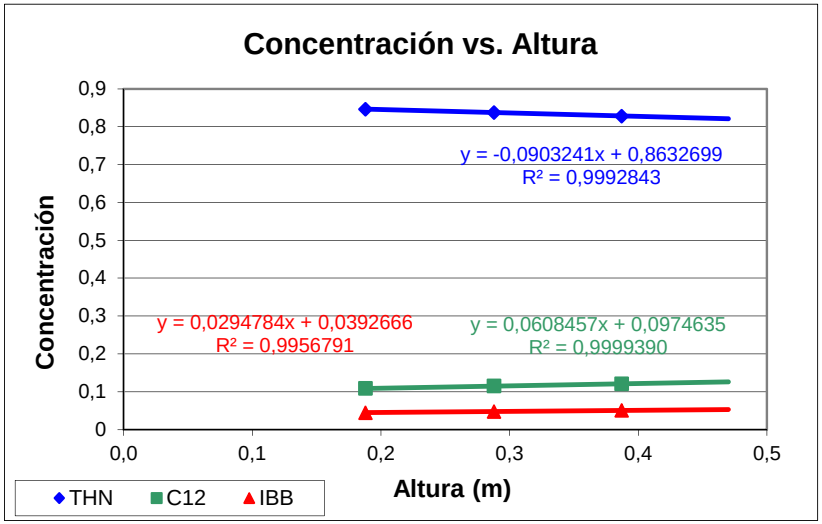

| Mezcla | C. masica. | C. molar | Tª media | DT (ºC) | Tiempo |
|---|---|---|---|---|---|
| THN-IBB-$C_{12}$ | 0,8000 | | 25º | 7,1 | 3h 30` |

| | |
|---|---|
| T. Relajación (s.): | 9213 |
| T. Equilibrio (min): | 768 |
| T. Equilibrio (h): | **12,8** |
| D | 1,00E-09 |

| | |
|---|---|
| Tª bainu hotza | 21 |
| Tªbainu beroa | 29,3 |
| Tª arriba hotza | 21,5 |
| Tª abajo hotza | 21,3 |
| Tª arriba beroa | 28,4 |
| Tª abajo beroa | 28,5 |
| TªGAPhotza | 21,4 |
| TªGAPberoa | 28,5 |
| $\Delta T^a$ | 7,05 |
| Tªmedia | 24,93 |
| $\Delta T^a$ vertical hotza | 0,2 |
| $\Delta T^a$ vertical beroa | -0,1 |

| Medidas Columna | |
|---|---|
| Longitud (cm) | 50 |
| Ancho (cm) | 5 |
| gap (cm.) | 0,10 |

| Calibración | |
|---|---|
| a | 0,848940335 |
| b | 0,105608002 |
| c | -0,121781614 |
| a' | 1,48374796 |
| b' | 0,049959033 |
| c' | -7,66E-02 |

| | | | |
|---|---|---|---|
| Viscosidad cin. | 1,86E-03 | | |
| gap | 1,0E-03 | | |
| Gravedad | 9,81 | | |
| $C_0$ | 0,8000 | | |
| Densidad Inicial | 0,925347 | | |
| nD Inicial | 1,517729 | | |
| Alfa | 8,48E-04 | | |
| Viscosidad Din. | 1,719E-03 | | |
| Pendiente c/z | -0,0874942 | 0,0559596 | 0,0315346 |
| Delta c | -0,0437471 | 0,0279798 | 0,0157673 |
| ***$D_T$*** | ***7,778E-13*** | ***-4,974E-13*** | ***-2,803E-13*** |

| Tomas | Altura toma (cm) | Cantidad (c.c.) | Altura real (m) | Densidad ($g/cm^3$) | nD | THN c | $C_{12}$ c | IBB c |
|---|---|---|---|---|---|---|---|---|
| 1ª | 45 | 1,4 | 0,4640 | 0,921253 | 1,515639 | 0,825794683 | 0,122332597 | 0,051872719 |
| 2ª | 35 | 4,1 | 0,3910 | 0,922561 | 1,516373 | 0,831164918 | 0,116249083 | 0,052585999 |
| 3ª | 25 | | | | | 57,83890988 | 57,12842695 | -113,9673368 |
| 4ª | 15 | 4 | 0,1900 | 0,9256887 | 1,518038 | 0,849494091 | 0,10646113 | 0,044044778 |
| | | | | | | | | |

NOTAS:

$$\rho = a + cTHN \times b + cC_{12} \times c$$
$$n = a' + cTHN \times b' + cC_{12} \times c'$$

THN-IBB-C12 c=80-10-10

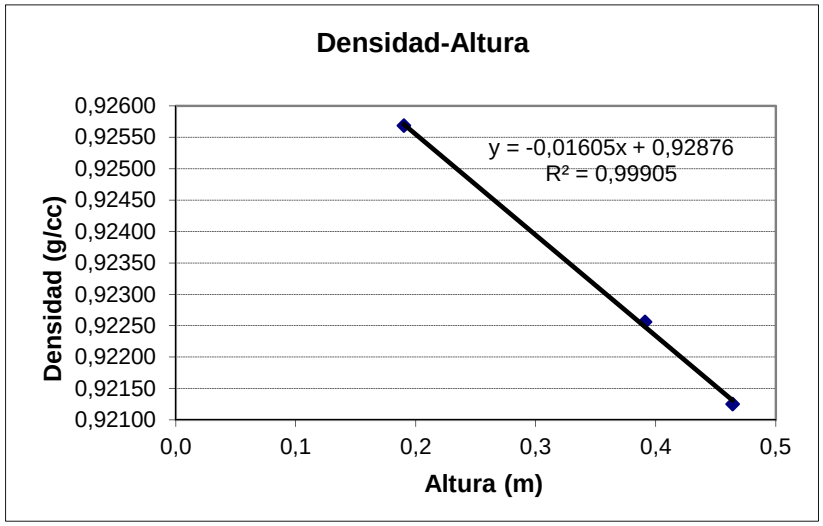


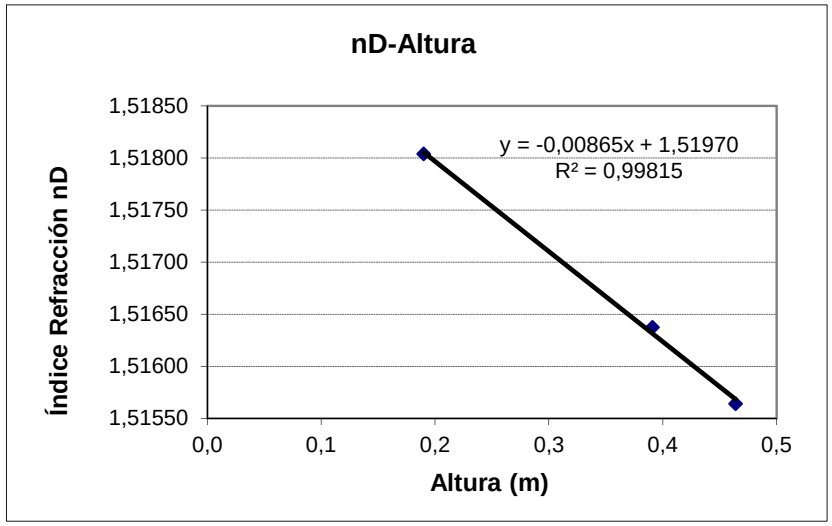


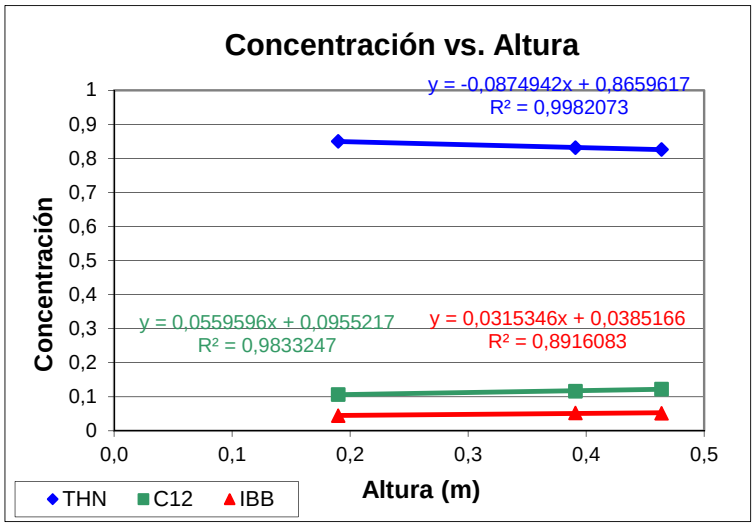

| Mezcla | C. masica. | C. molar | Tª media | DT (ºC) | Tiempo |
|---|---|---|---|---|---|
| THN-IBB-$C_{12}$ | 0,8000 | | 25º | 7,1 | 20h 45` |

| | |
|---|---|
| Tª bainu hotza | 21 |
| Tªbainu beroa | 29,3 |
| Tª arriba hotza | 21,4 |
| Tª abajo hotza | 21,2 |
| Tª arriba beroa | 28,3 |
| Tª abajo beroa | 28,4 |
| TªGAPhotza | 21,3 |
| TªGAPberoa | 28,4 |
| $\Delta T^a$ | 7,05 |
| Tªmedia | 24,83 |
| $\Delta T^a$ vertical hotza | 0,2 |
| $\Delta T^a$ vertical beroa | -0,1 |

| Medidas Columna | |
|---|---|
| Longitud (cm) | 50 |
| Ancho (cm) | 5 |
| gap (cm.) | 0,10 |

| Calibración | |
|---|---|
| a | 0,848940335 |
| b | 0,105608002 |
| c | -0,121781614 |
| a' | 1,48374796 |
| b' | 0,049959033 |
| c' | -7,66E-02 |

| | |
|---|---|
| T. Relajación (s.): | 9213 |
| T. Equilibrio (min): | 768 |
| T. Equilibrio (h): | **12,8** |
| D | 1,00E-09 |
| Viscosidad cin. | 1,86E-03 |
| gap | 1,0E-03 |
| Gravedad | 9,81 |
| $C_0$ | 0,8000 |
| Densidad Inicial | 0,925345 |
| nD Inicial | 1,517828 |
| Alfa | 8,48E-04 |
| Viscosidad Din. | 1,719E-03 |
| Pendiente c/z | -0,0882251 |
| Delta c | -0,04411255 |
| $D_T$ | ***7,843E-13*** |

| | THN | $C_{12}$ | IBB |
|---|---|---|---|
| | c | c | c |
| Pendiente c/z | -0,0882251 | 0,0576382 | 0,0305869 |
| Delta c | -0,04411255 | 0,0288191 | 0,01529345 |
| $D_T$ | ***7,843E-13*** | ***-5,124E-13*** | ***-2,719E-13*** |

| Tomas | Altura toma (cm) | Cantidad (c.c.) | Altura real (m) | Densidad ($g/cm^3$) | nD |
|---|---|---|---|---|---|
| 1ª | 45 | 2 | 0,4700 | | |
| 2ª | 35 | 4 | 0,3900 | 0,922274 | 1,516252 |
| 3ª | 25 | 4 | 0,2900 | 0,924002 | 1,517187 |
| 4ª | 15 | 4,2 | 0,1920 | 0,925508 | 1,517998 |
| | | | | | |

| | THN | $C_{12}$ | IBB |
|---|---|---|---|
| | c | c | c |
| | | | |
| | 0,827548263 | 0,115469427 | 0,05698231 |
| | 0,836754578 | 0,109263733 | 0,053981688 |
| | 0,845014247 | 0,10406005 | 0,050925703 |
| | | | |

NOTAS:

$$\rho = a + cTHN \times b + cC_{12} \times c$$
$$n = a' + cTHN \times b' + cC_{12} \times c'$$

THN-IBB-C12 c=80-10-10

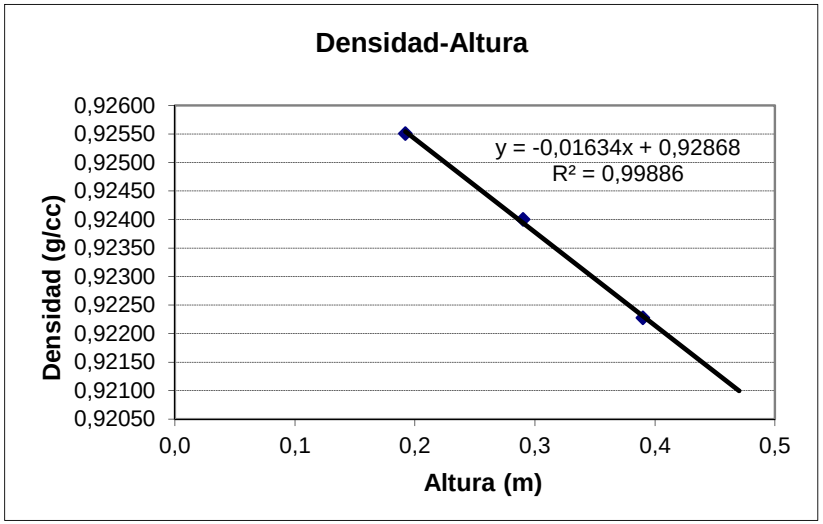


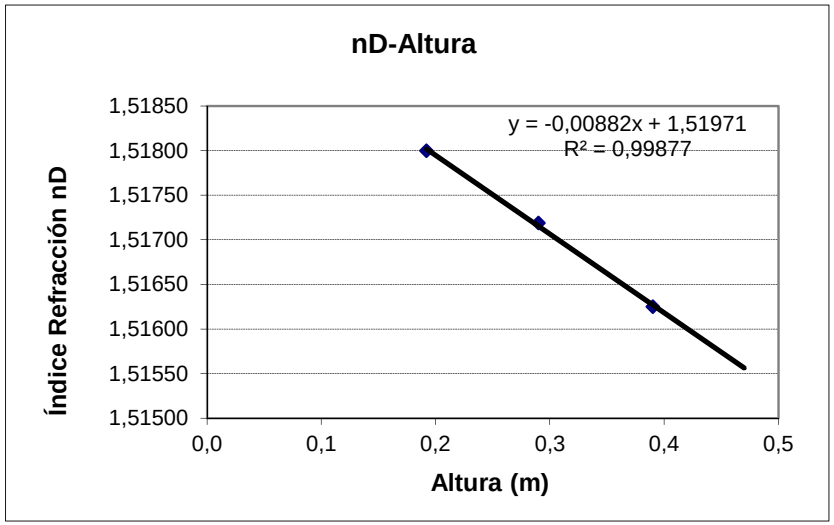


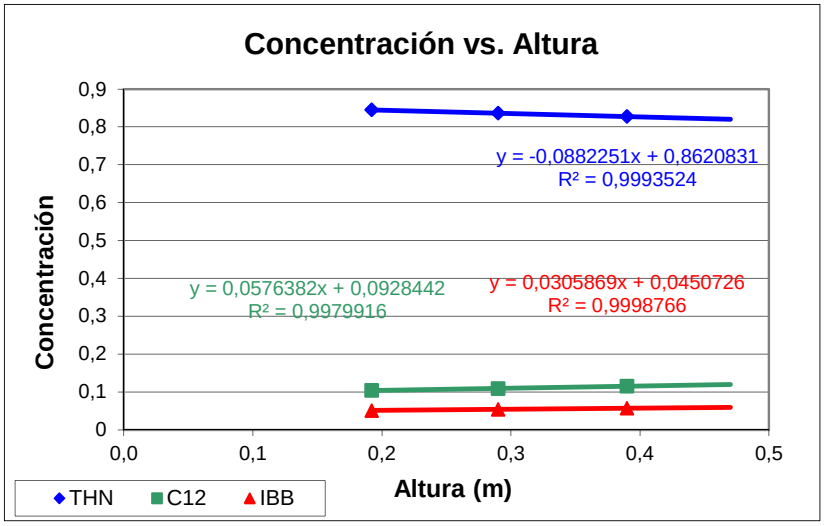

# Apéndice L

# Resultados de los Planos de Calibración para la Mezcla Ternaria THN-IBB-$nC_{12}$

Calibración Mezcla THN-IBB-nC12 (0,10-0,80-0,10)

| CONCENTRACIÓN EXPERIMENTAL | | | | | | | | |
|---|---|---|---|---|---|---|---|---|
| **c THN** | **c IBB** | **c $C_{12}$** | **Densidad** | **Dens ajustada** | **Error** | **nD** | **nD ajustado** | **Error** |
| 0,18064 | 0,75912 | 0,06024 | 0,860791 | 0,860666 | 0,000125 | 1,488130 | 1,487967 | 0,000163 |
| 0,15991 | 0,78004 | 0,06005 | 0,858607 | 0,858506 | 0,000101 | 1,487116 | 1,486968 | 0,000148 |
| 0,14056 | 0,79932 | 0,06012 | 0,856528 | 0,856462 | 0,000066 | 1,486107 | 1,486018 | 0,000089 |
| 0,12076 | 0,81753 | 0,06172 | 0,854200 | 0,854182 | 0,000018 | 1,484977 | 1,484928 | 0,000049 |
| 0,10176 | 0,83812 | 0,06013 | 0,852375 | 0,852377 | 0,000002 | 1,484138 | 1,484122 | 0,000016 |
| 0,15925 | 0,76056 | 0,08018 | 0,856019 | 0,855965 | 0,000053 | 1,485486 | 1,485380 | 0,000106 |
| 0,13960 | 0,77972 | 0,08069 | 0,853835 | 0,853835 | 0,000000 | 1,484443 | 1,484380 | 0,000063 |
| 0,12140 | 0,79897 | 0,07963 | 0,852043 | 0,852050 | 0,000007 | 1,483421 | 1,483574 | 0,000152 |
| 0,10009 | 0,81942 | 0,08049 | 0,849659 | 0,849702 | 0,000042 | 1,482465 | 1,482466 | 0,000001 |
| 0,08108 | 0,83913 | 0,07979 | 0,847747 | 0,847788 | 0,000041 | 1,481589 | 1,481592 | 0,000004 |
| 0,14058 | 0,75877 | 0,10066 | 0,851460 | 0,851485 | 0,000025 | 1,482595 | 1,482884 | 0,000289 |
| 0,11951 | 0,78083 | 0,09966 | 0,849329 | 0,849391 | 0,000062 | 1,481919 | 1,481932 | 0,000013 |
| 0,08344 | 0,83323 | 0,08333 | 0,847553 | 0,847599 | 0,000046 | 1,481303 | 1,481433 | 0,000130 |
| 0,08095 | 0,81885 | 0,10019 | 0,845236 | 0,845268 | 0,000032 | 1,479999 | 1,480008 | 0,000008 |
| 0,06072 | 0,83902 | 0,10026 | 0,843037 | 0,843130 | 0,000094 | 1,478938 | 1,479015 | 0,000077 |
| 0,12269 | 0,75715 | 0,12016 | 0,847170 | 0,847207 | 0,000037 | 1,480533 | 1,480501 | 0,000032 |
| 0,10133 | 0,77816 | 0,12051 | 0,844877 | 0,844917 | 0,000040 | 1,479441 | 1,479431 | 0,000009 |
| 0,08133 | 0,79834 | 0,12033 | 0,842797 | 0,842834 | 0,000037 | 1,478459 | 1,478469 | 0,000009 |
| 0,06057 | 0,81919 | 0,12024 | 0,840723 | 0,840661 | 0,000062 | 1,477513 | 1,477462 | 0,000051 |
| 0,04372 | 0,83673 | 0,11956 | 0,838980 | 0,838970 | 0,000010 | 1,476608 | 1,476691 | 0,000083 |
| 0,10044 | 0,75885 | 0,14070 | 0,842341 | 0,842344 | 0,000003 | 1,477895 | 1,477827 | 0,000068 |
| 0,08105 | 0,77827 | 0,14068 | 0,840324 | 0,840306 | 0,000018 | 1,476925 | 1,476881 | 0,000044 |
| 0,06001 | 0,80015 | 0,13984 | 0,838231 | 0,838194 | 0,000037 | 1,475955 | 1,475918 | 0,000037 |
| 0,04084 | 0,82021 | 0,13895 | 0,836350 | 0,836286 | 0,000064 | 1,475084 | 1,475051 | 0,000033 |
| 0,02246 | 0,83785 | 0,13969 | 0,834376 | 0,834261 | 0,000115 | 1,474135 | 1,474096 | 0,000039 |

| | |
|---|---|
| a = | 0,849052122 |
| b = | 0,105244882 |
| c = | -0,122806935 |

$$\rho = a + cTHN \times b + cC_{12} \times c$$

| | |
|---|---|
| a' = | 1,483802863 |
| b' = | 0,048841964 |
| c' = | -0,077341074 |

$$n = a' + cTHN \times b' + cC_{12} \times c'$$

Calibración Mezcla THN-IBB-nC12 (0,10-0,10-0,80)

**CONCENTRACIÓN EXPERIMENTAL**

| c THN | c IBB | c $C_{12}$ | Densidad | Dens ajustada | Error | nD | nD ajustado | Error |
|---|---|---|---|---|---|---|---|---|
| 0,17971 | 0,06016 | 0,76014 | 0,782874 | 0,782818 | 0,000056 | 1,439839 | 1,439816 | 0,000023 |
| 0,16023 | 0,08218 | 0,75759 | 0,781375 | 0,781321 | 0,000054 | 1,439206 | 1,439176 | 0,000031 |
| 0,14177 | 0,10022 | 0,75802 | 0,779650 | 0,779633 | 0,000017 | 1,438410 | 1,438405 | 0,000005 |
| 0,12025 | 0,12061 | 0,75914 | 0,777595 | 0,777607 | 0,000013 | 1,437458 | 1,437471 | 0,000013 |
| 0,10052 | 0,14017 | 0,75931 | 0,775808 | 0,775830 | 0,000022 | 1,436655 | 1,436664 | 0,000009 |
| 0,16066 | 0,05970 | 0,77964 | 0,779290 | 0,779282 | 0,000008 | 1,437916 | 1,437923 | 0,000007 |
| 0,14125 | 0,08016 | 0,77859 | 0,777634 | 0,777649 | 0,000015 | 1,437186 | 1,437199 | 0,000013 |
| 0,12114 | 0,09963 | 0,77923 | 0,775782 | 0,775795 | 0,000013 | 1,436335 | 1,436350 | 0,000014 |
| 0,10198 | 0,12024 | 0,77778 | 0,774200 | 0,774222 | 0,000022 | 1,435641 | 1,435659 | 0,000018 |
| 0,08171 | 0,14006 | 0,77823 | 0,772362 | 0,772370 | 0,000007 | 1,434812 | 1,434814 | 0,000002 |
| 0,14081 | 0,06005 | 0,79914 | 0,775632 | 0,775675 | 0,000042 | 1,435959 | 1,435997 | 0,000038 |
| 0,12108 | 0,08040 | 0,79852 | 0,774031 | 0,773972 | 0,000059 | 1,435274 | 1,435236 | 0,000038 |
| 0,10084 | 0,10009 | 0,79907 | 0,772070 | 0,772115 | 0,000045 | 1,434455 | 1,434386 | 0,000069 |
| 0,08205 | 0,12137 | 0,79657 | 0,770630 | 0,770673 | 0,000044 | 1,433740 | 1,433771 | 0,000031 |
| 0,06083 | 0,13949 | 0,79967 | 0,768464 | 0,768488 | 0,000024 | 1,432717 | 1,432735 | 0,000017 |
| 0,12020 | 0,05988 | 0,81992 | 0,771824 | 0,771877 | 0,000053 | 1,433934 | 1,433967 | 0,000033 |
| 0,09985 | 0,08002 | 0,82013 | 0,770110 | 0,770043 | 0,000068 | 1,433178 | 1,433133 | 0,000045 |
| 0,08079 | 0,09981 | 0,81940 | 0,768392 | 0,768411 | 0,000018 | 1,432390 | 1,432405 | 0,000015 |
| 0,06025 | 0,12059 | 0,81916 | 0,766581 | 0,766600 | 0,000019 | 1,431573 | 1,431589 | 0,000016 |
| 0,04024 | 0,13961 | 0,82015 | 0,764721 | 0,764722 | 0,000001 | 1,430718 | 1,430723 | 0,000006 |
| 0,10106 | 0,06050 | 0,83844 | 0,768387 | 0,768425 | 0,000038 | 1,432100 | 1,432126 | 0,000026 |
| 0,08070 | 0,08060 | 0,83871 | 0,766557 | 0,766583 | 0,000026 | 1,431277 | 1,431288 | 0,000011 |
| 0,06124 | 0,09976 | 0,83900 | 0,764839 | 0,764820 | 0,000020 | 1,430498 | 1,430485 | 0,000012 |
| 0,04148 | 0,11991 | 0,83861 | 0,763138 | 0,763093 | 0,000044 | 1,429730 | 1,429709 | 0,000021 |
| 0,02097 | 0,14026 | 0,83876 | 0,761328 | 0,761250 | 0,000078 | 1,428897 | 1,428872 | 0,000025 |

| | |
|---|---|
| a = | 0,838380235 |
| b = | 0,089226696 |
| c = | -0,094188936 |

$$\rho = a + cTHN \times b + cC_{12} \times c$$

| | |
|---|---|
| a' = | 1,476349098 |
| b' = | 0,040405754 |
| c' = | -0,057613942 |

$$n = a' + cTHN \times b' + cC_{12} \times c'$$

Calibración Mezcla THN-IBB-nC12 (0,40-0,20-0,40)

| CONCENTRACIÓN EXPERIMENTAL | | | | | | | | |
|---|---|---|---|---|---|---|---|---|
| **c THN** | **c IBB** | **c $C_{12}$** | **Densidad** | **Dens ajustada** | **Error** | **nD** | **nD ajustado** | **Error** |
| 0,47972 | 0,16012 | 0,36016 | 0,855447 | 0,855338 | 0,000109 | 1,479798 | 1,479739 | 0,000059 |
| 0,45973 | 0,18019 | 0,36007 | 0,853369 | 0,853301 | 0,000068 | 1,478844 | 1,478800 | 0,000044 |
| 0,43971 | 0,19998 | 0,36032 | 0,851265 | 0,851223 | 0,000042 | 1,477857 | 1,477836 | 0,000021 |
| 0,41986 | 0,22016 | 0,35997 | 0,849244 | 0,849232 | 0,000012 | 1,476936 | 1,476922 | 0,000014 |
| 0,39993 | 0,24019 | 0,35988 | 0,847187 | 0,847203 | 0,000016 | 1,475991 | 1,475987 | 0,000004 |
| 0,46004 | 0,16006 | 0,37990 | 0,851037 | 0,851030 | 0,000007 | 1,477390 | 1,477391 | 0,000001 |
| 0,43905 | 0,18032 | 0,38063 | 0,848802 | 0,848796 | 0,000006 | 1,476351 | 1,476347 | 0,000004 |
| 0,41971 | 0,20036 | 0,37994 | 0,846875 | 0,846896 | 0,000021 | 1,475459 | 1,475482 | 0,000023 |
| 0,39999 | 0,22009 | 0,37992 | 0,844843 | 0,844879 | 0,000036 | 1,474540 | 1,474551 | 0,000011 |
| 0,37969 | 0,24021 | 0,38009 | 0,842745 | 0,842782 | 0,000037 | 1,473557 | 1,473579 | 0,000022 |
| 0,43991 | 0,16008 | 0,40001 | 0,846589 | 0,846632 | 0,000043 | 1,474960 | 1,474995 | 0,000035 |
| 0,41968 | 0,18069 | 0,39963 | 0,844563 | 0,844606 | 0,000043 | 1,474053 | 1,474067 | 0,000014 |
| 0,39967 | 0,20027 | 0,40007 | 0,842445 | 0,842506 | 0,000061 | 1,473049 | 1,473089 | 0,000040 |
| 0,37947 | 0,21994 | 0,40059 | 0,840325 | 0,840378 | 0,000053 | 1,472066 | 1,472097 | 0,000031 |
| 0,36084 | 0,23965 | 0,39950 | 0,838551 | 0,838597 | 0,000046 | 1,471227 | 1,471294 | 0,000067 |
| 0,41999 | 0,15974 | 0,42027 | 0,842188 | 0,842238 | 0,000050 | 1,472574 | 1,472599 | 0,000025 |
| 0,40005 | 0,18028 | 0,41967 | 0,840224 | 0,840268 | 0,000044 | 1,471679 | 1,471700 | 0,000021 |
| 0,37662 | 0,20706 | 0,41632 | 0,838229 | 0,838259 | 0,000030 | 1,470824 | 1,470833 | 0,000009 |
| 0,36015 | 0,22009 | 0,41976 | 0,836154 | 0,836171 | 0,000017 | 1,469811 | 1,469806 | 0,000005 |
| 0,34035 | 0,23992 | 0,41973 | 0,834161 | 0,834149 | 0,000012 | 1,468883 | 1,468873 | 0,000010 |
| 0,39948 | 0,16005 | 0,44047 | 0,837760 | 0,837791 | 0,000031 | 1,470172 | 1,470179 | 0,000007 |
| 0,38153 | 0,17960 | 0,43887 | 0,836174 | 0,836140 | 0,000034 | 1,469453 | 1,469445 | 0,000008 |
| 0,36048 | 0,19988 | 0,43964 | 0,833950 | 0,833897 | 0,000053 | 1,468415 | 1,468395 | 0,000020 |
| 0,34059 | 0,21977 | 0,43964 | 0,831944 | 0,831860 | 0,000084 | 1,467501 | 1,467455 | 0,000046 |
| 0,32105 | 0,23969 | 0,43926 | 0,830005 | 0,829904 | 0,000101 | 1,466627 | 1,466559 | 0,000068 |

| | |
|---|---|
| a = | 0,848077002 |
| b = | 0,102365167 |
| c = | -0,116188581 |

$$\rho = a + cTHN \times b + cC6 \times c$$

| | |
|---|---|
| a' = | 1,482923423 |
| b' = | 0,047269347 |
| c' = | -0,07180433 |

$$n = a' + cTHN \times b' + cC_{12} \times c'$$

Calibración Mezcla THN-IBB-nC12 (0,45-0,10-0,45)

| CONCENTRACIÓN EXPERIMENTAL | | | | | | | | |
|---|---|---|---|---|---|---|---|---|
| **c THN** | **c IBB** | **c $C_{12}$** | **Densidad** | **Dens ajustada** | **Error** | **nD** | **nD ajustado** | **Error** |
| 0,53003 | 0,06005 | 0,40992 | 0,854766 | 0,854644 | 0,000122 | 1,478699 | 1,478623 | 0,000076 |
| 0,51109 | 0,07980 | 0,40911 | 0,852880 | 0,852807 | 0,000073 | 1,477832 | 1,477796 | 0,000036 |
| 0,48967 | 0,10015 | 0,41018 | 0,850458 | 0,850503 | 0,000045 | 1,476697 | 1,476719 | 0,000022 |
| 0,46881 | 0,12202 | 0,40917 | 0,848493 | 0,848494 | 0,000001 | 1,475830 | 1,475817 | 0,000013 |
| 0,44997 | 0,14011 | 0,40992 | 0,846477 | 0,846488 | 0,000011 | 1,474883 | 1,474883 | 0,000000 |
| 0,50952 | 0,06019 | 0,43029 | 0,850255 | 0,850201 | 0,000054 | 1,476226 | 1,476212 | 0,000014 |
| 0,49004 | 0,08067 | 0,42930 | 0,848344 | 0,848331 | 0,000013 | 1,475374 | 1,475373 | 0,000001 |
| 0,46941 | 0,10051 | 0,43008 | 0,846113 | 0,846139 | 0,000026 | 1,474333 | 1,474353 | 0,000020 |
| 0,44989 | 0,11985 | 0,43027 | 0,844108 | 0,844129 | 0,000021 | 1,473422 | 1,473428 | 0,000006 |
| 0,42972 | 0,14041 | 0,42987 | 0,842097 | 0,842121 | 0,000024 | 1,472494 | 1,472514 | 0,000020 |
| 0,48935 | 0,06076 | 0,44989 | 0,845844 | 0,845883 | 0,000039 | 1,473848 | 1,473872 | 0,000024 |
| 0,46947 | 0,08067 | 0,44987 | 0,843820 | 0,843860 | 0,000040 | 1,472927 | 1,472945 | 0,000018 |
| 0,45027 | 0,10062 | 0,44911 | 0,841948 | 0,841992 | 0,000044 | 1,472073 | 1,472102 | 0,000029 |
| 0,42905 | 0,12018 | 0,45077 | 0,839594 | 0,839638 | 0,000044 | 1,470969 | 1,470993 | 0,000024 |
| 0,40960 | 0,14016 | 0,45023 | 0,837685 | 0,837719 | 0,000034 | 1,470098 | 1,470122 | 0,000024 |
| 0,46942 | 0,06066 | 0,46992 | 0,841487 | 0,841539 | 0,000052 | 1,471488 | 1,471513 | 0,000025 |
| 0,45012 | 0,08010 | 0,46979 | 0,839540 | 0,839588 | 0,000048 | 1,470590 | 1,470621 | 0,000031 |
| 0,42958 | 0,10013 | 0,47030 | 0,837387 | 0,837437 | 0,000050 | 1,469597 | 1,469625 | 0,000028 |
| 0,40969 | 0,12018 | 0,47013 | 0,835416 | 0,835429 | 0,000013 | 1,468708 | 1,468707 | 0,000001 |
| 0,39004 | 0,14017 | 0,46980 | 0,833490 | 0,833466 | 0,000024 | 1,467819 | 1,467813 | 0,000006 |
| 0,44941 | 0,06092 | 0,48967 | 0,837193 | 0,837219 | 0,000026 | 1,469161 | 1,469170 | 0,000009 |
| 0,42941 | 0,08064 | 0,48995 | 0,835158 | 0,835149 | 0,000009 | 1,468223 | 1,468215 | 0,000008 |
| 0,40922 | 0,10056 | 0,49022 | 0,833104 | 0,833062 | 0,000042 | 1,467276 | 1,467253 | 0,000023 |
| 0,38976 | 0,12038 | 0,48986 | 0,831183 | 0,831121 | 0,000062 | 1,466423 | 1,466370 | 0,000053 |
| 0,36964 | 0,14007 | 0,49030 | 0,829140 | 0,829020 | 0,000120 | 1,465449 | 1,465398 | 0,000051 |

| | |
|---|---|
| a = | 0,847995152 |
| b = | 0,101874647 |
| c = | -0,115504805 |

$$\rho = a + cTHN \times b + cC_{12} \times c$$

| | |
|---|---|
| a' = | 1,48309252 |
| b' = | 0,046719248 |
| c' = | -0,071310845 |

$$n = a' + cTHN \times b' + cC_{12} \times c'$$

Calibración Mezcla THN-IBB-nC12 (0,80-0,10-0,10)

**CONCENTRACIÓN EXPERIMENTAL**

| c THN | c IBB | c $C_{12}$ | Densidad | Dens ajustada | Error | nD | nD ajustado | Error |
|---|---|---|---|---|---|---|---|---|
| 0,18012 | 0,75995 | 0,05993 | 0,860780 | 0,860663 | 0,000117 | 1,488221 | 1,488158 | 0,000063 |
| 0,16060 | 0,77910 | 0,06030 | 0,858636 | 0,858558 | 0,000078 | 1,487200 | 1,487155 | 0,000045 |
| 0,13984 | 0,79995 | 0,06021 | 0,856425 | 0,856377 | 0,000048 | 1,486150 | 1,486125 | 0,000025 |
| 0,11998 | 0,81970 | 0,06032 | 0,854260 | 0,854265 | 0,000005 | 1,485119 | 1,485124 | 0,000005 |
| 0,09991 | 0,83956 | 0,06054 | 0,852111 | 0,852119 | 0,000008 | 1,484103 | 1,484105 | 0,000002 |
| 0,15974 | 0,75962 | 0,08064 | 0,856000 | 0,855990 | 0,000010 | 1,485563 | 1,485556 | 0,000007 |
| 0,14113 | 0,77889 | 0,07997 | 0,854074 | 0,854106 | 0,000032 | 1,484665 | 1,484677 | 0,000012 |
| 0,12027 | 0,79940 | 0,08033 | 0,851807 | 0,851858 | 0,000051 | 1,483585 | 1,483607 | 0,000022 |
| 0,10021 | 0,81970 | 0,08009 | 0,849710 | 0,849770 | 0,000060 | 1,482589 | 1,482624 | 0,000035 |
| 0,08036 | 0,83956 | 0,08008 | 0,847624 | 0,847675 | 0,000051 | 1,481612 | 1,481633 | 0,000021 |
| 0,14041 | 0,75882 | 0,10077 | 0,851407 | 0,851496 | 0,000089 | 1,482998 | 1,483048 | 0,000050 |
| 0,12035 | 0,77917 | 0,10047 | 0,849313 | 0,849415 | 0,000102 | 1,482007 | 1,482069 | 0,000062 |
| 0,10006 | 0,79959 | 0,10034 | 0,847206 | 0,847288 | 0,000082 | 1,481025 | 1,481065 | 0,000040 |
| 0,07976 | 0,81940 | 0,10084 | 0,844995 | 0,845083 | 0,000088 | 1,479962 | 1,480013 | 0,000051 |
| 0,07988 | 0,79972 | 0,12039 | 0,843135 | 0,842715 | 0,000420 | 1,478721 | 1,478522 | 0,000199 |
| 0,06377 | 0,81670 | 0,11953 | 0,841077 | 0,841119 | 0,000042 | 1,477762 | 1,477784 | 0,000022 |
| 0,04086 | 0,83959 | 0,11955 | 0,838670 | 0,838696 | 0,000026 | 1,476612 | 1,476637 | 0,000025 |
| 0,09980 | 0,76002 | 0,14018 | 0,842339 | 0,842409 | 0,000070 | 1,477966 | 1,478003 | 0,000037 |
| 0,07926 | 0,78082 | 0,13992 | 0,840219 | 0,840272 | 0,000053 | 1,476967 | 1,476997 | 0,000030 |
| 0,06000 | 0,79789 | 0,14211 | 0,837954 | 0,837970 | 0,000016 | 1,475876 | 1,475866 | 0,000010 |
| 0,03995 | 0,82031 | 0,13974 | 0,836167 | 0,836142 | 0,000025 | 1,475068 | 1,475047 | 0,000021 |
| 0,02082 | 0,83900 | 0,14017 | 0,834146 | 0,834069 | 0,000077 | 1,474102 | 1,474058 | 0,000044 |

| | |
|---|---|
| a = | 0,848940335 |
| b = | 0,105608002 |
| c = | -0,121781614 |

$$\rho = a + cTHN \times b + cC_{12} \times c$$

| | |
|---|---|
| a' = | 1,483747963 |
| b' = | 0,049959033 |
| c' = | -0,076552501 |

$$n = a' + cTHN \times b' + cC_{12} \times c'$$